Investigations on the impact of metaphyllosilicates and calcined common clays on the rheology and early hydration of cements admixed with different superplasticizers

Ricarda Sposito

Vollständiger Abdruck der von der Fakultät für Bauingenieurwesen und Umweltwissenschaften der Universität der Bundeswehr München zur Erlangung des akademischen Grades eines

Doktor-Ingenieurs (Dr.-Ing.)

genehmigten Dissertation.

Gutachter:

1. Univ.-Prof. Dr.-Ing. Karl-Christian Thienel
2. Univ.-Prof. Dr. Johann Plank
3. Prof. PhD Harald Justnes

Die Dissertation wurde am 15.02.2022 bei der Universität der Bundeswehr München eingereicht und durch die Fakultät für Bauingenieurwesen und Umweltwissenschaften am 09.05.2022 genehmigt. Die mündliche Prüfung fand am 09.09.2022 statt.

Danksagung

Diese Dissertation wurde ihm Rahmen meiner Tätigkeit als wissenschaftliche Mitarbeiterin am Institut für Werkstoffe des Bauwesens (IWB) an der Universität der Bundeswehr München (UniBwM) angefertigt.

Mein größter Dank gilt meinem Doktorvater Herrn Professor Dr.-Ing. Karl-Christian Thienel für sein stets offenes Ohr und die engmaschige Betreuung, bei gleichzeitig jeglichem Freiraum zum selbstständigen Arbeiten. Durch seine kontinuierliche Unterstützung habe ich einen Einblick in die internationale Welt der Wissenschaft bekommen, indem ich auf Konferenzen fahren und Kooperationen mit weltweit renommierten Wissenschaftlern begleiten durfte.

Ein Großteil meiner Dissertation entstammt dem durch die Deutsche Forschungsgemeinschaft geförderten Projekt „Ökologische und energetische Optimierung von Betonen: Wechselwirkung strukturell unterschiedlicher Fließmittel mit calcinierten Tonen“ (PL 472/11-1 und TH 1383/3-1), das gemeinsam mit dem Lehrstuhl für Bauchemie, Department für Chemie der Technischen Universität München bearbeitet wurde. Herrn Professor Dr. Johann Plank möchte ich vielmals für die wertvolle Zusammenarbeit, die konstruktive Kritik und die Übernahme des Co-Referates danken. Herrn Professor PhD Harald Justnes danke ich für wertvolle Hilfestellungen zur Beantwortung rheologischer Fragestellungen, seine Denkanstöße und die Übernahme des Co-Referates. Bei Professor Dr.-Ing. Josef Kiendl möchte ich mich für seinen Vorsitz im Promotionsausschuss bedanken.

Meiner lieben Kollegin und wissenschaftlichen Laborleiterin Dr.-Ing. Nancy Beuntner danke ich für ihr unermüdliches Engagement am IWB, motivierende sowie konstruktive Gespräche und ihr stets offenes Ohr. Auch bei meinen sehr geschätzten Kollegen Carola Chucholowksi, Dr. Mathias Köberl, Dr. Matthias Maier, Dr. Sebastian Scherb, Timo Haller, Paul Waibl und Johannes Berger, sowie unseren ehemaligen studentischen Hilfskräften möchte ich mich für die tolle Arbeitsatmosphäre, Unterstützung und die stets kreativen Kaffeerunden bedanken. Prof. Dr.-Ing. Andrea Kustermann und meiner ehemaligen Kollegin Kerstin Anneser möchte ich für unseren Austausch „über die Arbeit hinaus“ in den letzten Jahren danken.

Ich danke all jenen, die mich maßgeblich bei der Laborarbeit unterstützt haben, insbesondere Karola Feldmann für das schier nicht enden wollende Calcinieren der Schichtsilikate und Tone, Thomas Pohl für rheologische und Ultraschall-Messungen und Wolfgang Saur für seine Geduld und Expertise während rasterelektronenmikroskopischer Aufnahmen. Herrn Prof. Dr. Steffen Krause und seinen Mitarbeiterinnen vom Labor für Siedlungswasserwirtschaft (UniBwM) danke ich für zahlreiche Partikelgrößen- und ICP-OES-Messungen.

Marlene Schmid möchte ich für die enge Zusammenarbeit im Rahmen des DFG-Forschungsprojektes danken, insbesondere für das Synthetisieren des amphoteren Fließmittels und die gemeinsamen Konferenzbeiträge, die während dieser Zeit entstanden sind. Für den bilateralen Wissensaustausch zu calcinierten Tonen danke ich unseren argentinischen Kollegen Prof. Edgardo Fabian Irassar, Dr. Alejandra Tironi und Dr. Gisela Cordoba.

Meinem Mann Gianluca, meinen Eltern Wolfgang und Maria Gmür, meinen Schwestern, sowie meinen Schwiegereltern danke ich herzlich für ihre unbeschreibliche Unterstützung in Worten und Taten und ihre bedingungslose Geduld und Liebe.

Ricarda Sposito

Kurzfassung

Im Rahmen dieser Arbeit wird erstmalig das **rheologische Verhalten** von Zementen sowohl unter dem Zusatz calcinierter Schichtsilikate, als auch calcinierter Tongemische untersucht. Die Fließfähigkeit wird durch ihre Zugabe teils stark reduziert, was sich in einer erhöhten Fließgrenze und Viskosität an Messungen von Bindemittelleimen mit dem Rotationsviskometer äußert. Die Untersuchung an reinphasigen Materialien ermöglicht es, den Einfluss der mineralogischen Zusammensetzung der zugrundeliegenden Rohtone, insbesondere deren Gehalt an Kaolinit, Vertretern der Dreischichtsilikate und Quarz herauszuarbeiten. Der Zusammenhang zwischen rheologischem Verhalten und physikalischen Parametern der calcinierten Materialien, wie Partikelgrößenverteilung, Zetapotential, Wasseranspruch und spezifischer Oberfläche wird kritisch beurteilt.

Die **Dispergierwirkung zahlreicher Fließmittel-Vertreter**, wie Ligninsulfonate, eines Polykondensats und verschiedener polycarboxylatbasierter Polymere, wird mittels „mini slump test“ und Rotationsviskometer-Versuchen an Bindemittelleimen untersucht. Der Fließmittelbedarf steigt in Abhängigkeit des Wasseranspruchs, der Mahlfeinheit und des negativen Zetapotentials des jeweiligen calcinierten Tones. Letzterer Parameter wird vom Kaolinitgehalt des Tones dominiert. Ungeachtet des erhöhten Fließmittelbedarfs, ist die Dispergierwirkung von PCE-Fließmitteln in Zementleimen mit calcinierten Tonen ähnlich wie in herkömmlichen Zementleimen am effektivsten. Eine höhere, anionische Ladungsdichte führt hier zu einer besseren, initialen Dispergierwirkung und alle handelsüblichen Makromonomere zu einer guten, teils exzellenten Verflüssigung. Metamuskovit zeichnet sich als einzige Metaphase ab, die sowohl die Wirkungsweise von Fließmitteln reduziert als auch sensibel gegenüber deren Polymerstruktur ist. Die Zugabe calcinierter Tone kann zu einem schnellen **Verlust der Fließfähigkeit** führen. Wie zeitabhängige Messungen zeigen, ist dieser in Anwesenheit von PCE-Fließmitteln stärker ausgeprägt als mit einem NSF Polykondensat. Mit Ligninsulfonaten kann die Fließfähigkeit über die Zeit aufrecht erhalten werden, was jedoch aufgrund einer hohen Dosierung häufig mit einer starken Verzögerung einhergeht. Die Arbeit stellt mit der Einführung von Hydroxyethylmethacrylat in die PCE-Struktur eine mögliche Lösung vor, um einer schnellen Abnahme der Fließfähigkeit vorzubeugen. Dessen Zersetzung im alkalischen Milieu in Ethylenglykol und Carboxylgruppen ermöglicht eine nachträgliche Adsorption letzterer und damit eine länger andauernde Verflüssigung. Dieser Wirkmechanismus wird durch den vorhandenen Gehalt aller Schichtsilikate im Ton, sowie die spezifische Oberfläche des calcinierten Tons entscheidend beeinflusst.

Ergänzend wird die **frühe Hydratation von Kompositzementen mit calcinierten Tonen in Anwesenheit von Fließmitteln** mittels Wärmeflusskalorimetrie sowie selektiv anhand von in situ Röntgenbeugungs- und Ultraschallmessungen untersucht. Sie hängt maßgeblich von den Eigenschaften des calcinierten Tones, sowie der Fließmitteldosis ab. Die Verzögerung in Anwesenheit calcinierter Tone wird als gering eingestuft, was auf die erhöhte Oberfläche und die Bildung früher Hydratationsprodukte trotz der Fließmitteladsorption auf Zement- und vor allem Ettringitoberflächen zurückgeführt wird. Eine verstärkte Ettringitbildung ermöglicht in den meisten Fällen trotz teils hoher Fließmitteldosen eine ungehindert ablaufende Hydratation.

Die Arbeit präsentiert Herausforderungen in Hinblick auf die Wahl geeigneter Fließmittel für ternäre Bindemittelsysteme mit calcinierten Tonen. Dabei zeigt sie Lösungsansätze und kritische Parameter auf, um das rheologische Verhalten mit einer Vielzahl calcinierter Tongemische durch die Zugabe geeigneter Fließmittel gezielt zu steuern und optimieren. So kann die Verwendung calcinierter Tone einen erheblichen Beitrag leisten, dem Bedarf an nachhaltigen Zementersatzstoffen gerecht zu werden und den ökologischen Fußabdruck moderner Betone zu verbessern.

Abstract

This thesis debutes a **systematic study of the rheological behavior** of cements blended with both metaphyllosilicates and calcined common clays. With their addition, the flow resistance, yield stress and viscosity of blended cement pastes increase in parts significantly as shown via rotational viscometer tests. The analysis of single-phase materials reveals the influence of mineralogical composition of raw clays, especially their concentration of kaolinite, different types of 2:1 phyllosilicates, and quartz. The correlation of rheological behavior with physical characteristics of metaphyllosilicates and calcined common clays, such as particle size, zeta potential, water demand, and surface area is evaluated critically.

The **dispersion performance of a broad variety of superplasticizer** (lignosulfonates, NSF polycondensate, polycarboxylate-based co-polymers (PCEs)) is determined via mini slump tests and rotational viscometer tests. The demand for superplasticizer is directly linked to the flow resistance of the respective reference mixture. It increases to different extents depending on the calcined clay added, its water demand, particle fineness, and negative zeta potential; the latter mainly resulting from kaolinite content. Regardless of their increased demand, the performance of superplasticizers in calcined clay blended cements is as efficient as it is in plain cements. In case of PCEs, a higher anionic charge density enables a better initial dispersion. All conventional macromonomers exhibit an overall good to excellent dispersion performance. Metamuscovite is the only phase that perturbs the performance of superplasticizers and is sensitive towards the type of superplasticizer.

The use of calcined clays can lead to rapid slump loss, which is stronger with the addition of conventional PCEs than with NSF polycondensate as time related mini slump tests and rheological tests show. The addition of lignosulfonates may limit this phenomenon, but often goes along with significant retardation effects. This thesis investigates one possible **solution to prevent rapid slump loss**, namely the introduction of hydroxyethyl methacrylate into the PCE polymer. Its decomposition into ethylene glycol and carboxyl groups in alkaline media leads to a later adsorption of the latter and can enable a subsequent dispersion. The study reveals the total phyllosilicate content in clay as well as the specific surface area of the calcined clay as decisive parameters for the functionality of this special type of polymer.

Complementing tests study the **early hydration of calcined clay blended cements in the presence of superplasticizers** via isothermal calorimetry, as well as in situ XRD and ultrasound method on selected samples. The early hydration kinetics depend mainly on the characteristics of the calcined clay as well as on the superplasticizer dosage. Overall, the retardation is minor in calcined clay blended cements. This is related to the increased surface area which favors the formation of early hydration products - despite the adsorption of superplasticizers onto binder particle surfaces. An enhanced ettringite formation of calcined clay blended cements enables an unhindered silicate hydration and transformation of ettringite to hemicarboaluminate, even in the presence of most superplasticizers.

This thesis reveals the **suitability of a wide array of calcined common clays** and their limitations as future SCM regarding their impact on rheological behavior in combination with the correct choice of superplasticizer. A fair assessment and a careful selection provided, their use can meet the high demand for sustainable cementitious materials and help improving the ecological footprint of modern concrete.

Table of contents

Abbreviations and nomenclature

Cement chemistry

A	Al_2O_3
AFm	Monophases, C_4AXH_n
AFm-Hc	Hemicarboaluminate, $C_4A\bar{C}_{0.5}H_{11.5}$
AFm-Mc	Monocarboaluminate, $C_4A\bar{C}_xH_{11}$
AFm-Ms	Monosulfate, $C_4A\$H_{12}$
AFt	Ettringite, $C_6A\$H_{32}$
C	CaO
$\bar{C}$	CO_2
C_2A	Dicalcium aluminate
C_3A	Tricalcium aluminate
C_4AF	Tetracalcium aluminate ferrite
CASH	Calcium aluminate silicate hydrate(s)
CH	Calcium hydroxide, portlandite
C_2S	Dicalcium silicate, belite
C_3S	Tricalcium silicate, alite
CSH	Calcium silicate hydrate(s)
F	Fe_2O_3
H	H_2O
S	SiO_2
$	SO_3

Superplasticizer chemistry (I)

AA	Acrylic acid
AFS	Acetone formaldehyde sulfite
APEG	α-allyl ω-methoxy polyethylen glycol
CSF	Cyclohexane sulfite formaldehyde
DADMAC	Diallyl dimethylammonium chloride
HEMA	Hydroxyethyl methacrylate
HPEG	α-methallyl-ω-methoxy poly(ethylen glycol) / α-methallyl-ω-hydroxy-poly(ethylen glycol)
IPEG	Isoprenyl oxy poly(ethylen glycol) ether
LDH	Layered double hydroxide
MAA	Methacrylic acid
MAPTAC	3-trimethylammonium propyl methacrylamide chloride
MFS	Melamine formaldehyde sulfite

Superplasticizer chemistry (II)

MPEG	ω-methoxy polyethylene glycol methacrylate ester
NSF	Naphthalene sulfonate formaldehyde (-based polycondensate)
OMP	Organo-mineral phases
PAAM	Polyamidoamine-polyethylenglycol
PAH	Poly(allylamine hydrochloride)
PCE	Polycarboxylate ether (based superplasticizer)
PEG	Polyethylene glycol
(P)EO	(Poly)ethylene oxide
PTMEG	Polytetramethylene glycol
SPF	Sulfanilic acid-phenol-formaldehyde (based product)
TMAEMC	2-trimethylammonium ethyl methacrylate chloride

Materials used for the own investigations (chapter 4.1)

AC	Amaltheen clay
amphMPEG	“Amphoteric” MPEG-based PCE with DADMAC as cationic monomer
FUP	Fireclay Upper Palatinate (sedimentary, kaolinite-rich clays from Miocene)
HPEG	α-methallyl-ω-methoxy poly(ethylene glycol) ether type PCE
$H_2O_{dest.}$	Distilled water
IPEG1	Isoprenyl oxy poly(ethylene glycol) ether type PCE consisting of IPEG-AA and an IPEG with hydroxyethyl methacrylate
IPEG2	Isoprenyl oxy poly(ethylene glycol) ether type PCE consisting of IPEG-AA and a vinyloxybutyl polyethylene glycol (VOBPEG)-AA
KUP	Kaolin Upper Palatinate from a primary kaolin deposit, formed in Eocene / Miocene by the weathering of granite
Mg-LS	Lignosulfonate-based superplasticizer with magnesium salt
Mk	Metakaolin
Mi	Metaillite
Mu	Metamuscovite
MURR	Upper Eocene to Upper Miocene sediments from the alpine foreland basin
Na-LS	Lignosulfonate-based superplasticizer with sodium salt
NSF	Naphthalene sulfonate formaldehyde (-based polycondensate)
OPC	Ordinary Portland cement
PLC	Portland limestone cement
QP	Quartz powder
RKUP	Recycling Kaolin Upper Palatinate (kaolinite-rich mine tailing)
SCPS	Synthetic cement pore solution
TG	Tongemisch (*common clay*); Industrial-calcined Amaltheen clay

Further abbreviations (including methods)

ASTM	American Society for Testing and Materials
BET	Brunauer Emmett Teller
CCBC	Calcined clay blended cement
DIN	Deutsches Institut für Normierung (*German Institute for Standardization*)
EN	Europäische Normierung (*European Standardization*)
GGBS	Ground granulated blastfurnace slag
ISO	International Organization for Standardization
LC^3	Limestone calcined clay cement
OPC	Ordinary Portland cement
IEP	Iso-electric point
PLC	Portland limestone cement
Q	Heat of hydration [J/g_{cement}], derived from isothermal calorimetry
$\dot{Q}$	Heat flow [mW/g_{cement}] measured via isothermal calorimetry
SCI(E)	Science Citation Index (Expanded)
SCM(s)	Supplementary cementitious material(s)
SSA	Specific surface area [m^2/g]
$t_{Q,max}$	Time of maximum heat [h], measured with isothermal calorimeter
$t_{Q,min}$	Time of minimum heat [h], measured with isothermal calorimeter
w/b	Water-to-binder ratio
w/c	Water-to-cement ratio

List of figures

1 Background and key content of the thesis

The current construction boom worldwide, especially in emerging countries, requires an **increasing demand for cement**. It is known that cement production is one of the most harmful industries when it comes to carbon dioxide emissions. Key factor is the decarbonation of limestone during clinker production besides the primary energy demand for heating the clinker kiln at high temperature levels (~ 1,450 °C).

For decades, clinker has been partially replaced by supplementary cementitious materials (SCMs). The most established SCMs are fly ash, ground granulated blast-furnace slag (GGBS) and limestone. Pozzolanic fly ash is a by-product from coal combustion. With the trend towards regenerative energies and the gradual shutdown of coal-fired power plants in several countries, the cement industry locally runs out of fly ash. Latent-hydraulic GGBS is also a by-product, a glassy material obtained in the manufacture of pig iron. Iron and steel production, however, are strongly dependent on economic trends. For this reason, and as steel production varies widely from region to region, there is no guarantee that sufficient amounts of GGBS are available long-term. Limestone is abundant worldwide but it does contribute to the properties of concrete in a limited way only or can even jeopardize the durability of concrete. As a consequence, the cement industry is in urgent **need for sustainable, reactive SCMs**.

Calcined clays as reactive, pozzolanic SCM came again into focus of research within the last decade. Among other things it is known that they have a non negligible impact on the workability of fresh concrete and require the use of suitable (super)plasticizers. This present thesis gives in chapter 2.1 an overview of the definition of clays, their thermal activation, pozzolanic properties of calcined clays and their behavior in concrete. Furthermore, it considers the synergy effects with limestone in cement, commonly known as limestone calcined clay cement (LC^3) and challenges that are brought up with the use of calcined clays.

It is no novelty that the use of pozzolanic SCMs requires the addition of **(super) plasticizers**. Already in 1939, E. W. Scriptures stated in his patent that *“pozzuolanic materials, when added to a concrete mix, ordinarily necessitate a substantial increase in the water-cement ratio […]”* (Figure 1-1). He proposed to add lignosulfonates, known as the first plasticizers, so *“the water-cement ratio may be kept low and the advantages of the pozzuolanic material may be obtained without the disadvantages consequent upon an increase in the water-cement ratio”* [1].

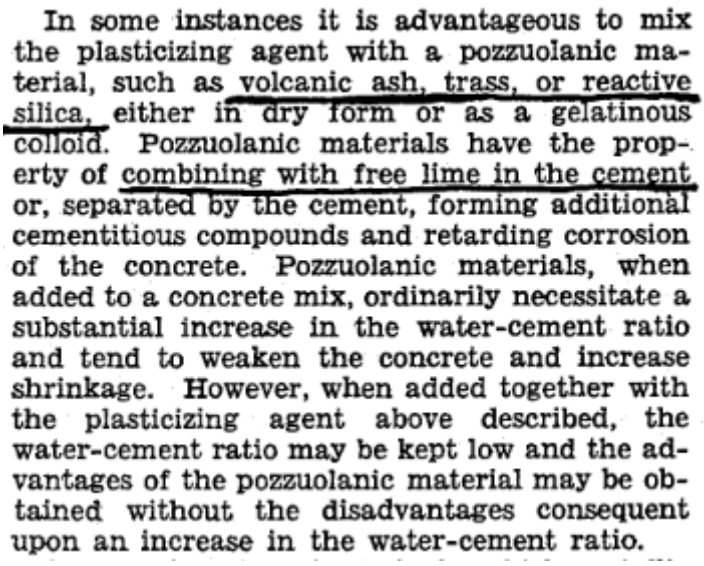

In some instances it is advantageous to mix the plasticizing agent with a pozzuolanic material, such as volcanic ash, trass, or reactive silica, either in dry form or as a gelatinous colloid. Pozzuolanic materials have the property of combining with free lime in the cement or, separated by the cement, forming additional cementitious compounds and retarding corrosion of the concrete. Pozzuolanic materials, when added to a concrete mix, ordinarily necessitate a substantial increase in the water-cement ratio and tend to weaken the concrete and increase shrinkage. However, when added together with the plasticizing agent above described, the water-cement ratio may be kept low and the advantages of the pozzuolanic material may be obtained without the disadvantages consequent upon an increase in the water-cement ratio.

Figure 1-1: Extract of US patent no. 2.169.980 of E. W. Scripture from 1939 [1]

Chapter 2.2 begins with a short overview of superplasticizers. It summarizes characteristics of lignosulfonates, of polycondensate- and polycarboxylate-based superplasticizers. Further it considers the interaction with clay minerals that commonly cause loss of both workability and superplasticizer effectiveness as well as previously known findings towards the interaction of superplasticizers with calcined clays.

Chapter 3 presents aims and open questions that are basis of this thesis. Materials and methods used for the investigations are addressed in chapter 4. The thesis is based on four journal papers as well as four conference contributions that are provided in chapter 7. The main findings of these publications are presented and discussed in chapter 5. It starts with an approach to the rheology of calcined clay blended cement (CCBC) mixtures, with a special focus on the physical and mineralogical parameters of calcined clays. It is followed by the influence of calcined clays on the demand and performance of superplasticizers – regarding also the properties of superplasticizers themselves. Beside discussing the initial dispersion, it does also address the time-dependent behavior. In a last sub-chapter, the early hydration and setting behavior of calcined clays with superplasticizers is presented. The main findings are followed by a brief conclusion as well as a reflection and outlook in chapter 6.

2 State of the art

2.1 Calcined clays as supplementary cementitious materials

2.1.1 Clays – Multicomponent materials with a history

Clays represent about 80 % of all sedimentary rocks, are abundant worldwide and contain primarily mineral particles with diameters smaller than 20 µm. Clay minerals predominate quantitatively in clays. They are mainly hydrous aluminum silicates that origin from weathering processes of silicate rocks ("weathering neoformations"). Clays contain furthermore weathering residues (especially quartz, muscovite, feldspars) and new mineral formations (e.g. carbonates and iron sulfides) [2, p. 1]. They are classified as kaolinite-rich or smectite-rich clays, depending on their mineralogical composition [2, p. 2]. Main phases in common clays are illite, chlorite such as additions of kaolinite, smectites, alternating bearing minerals (e.g. kaolinite-illite or smectite-illite) and accessories (rutile, zircon, apatite). The abundance of the most common clay minerals has been compiled by Ito and Wagai [3] (Figure 2-1).

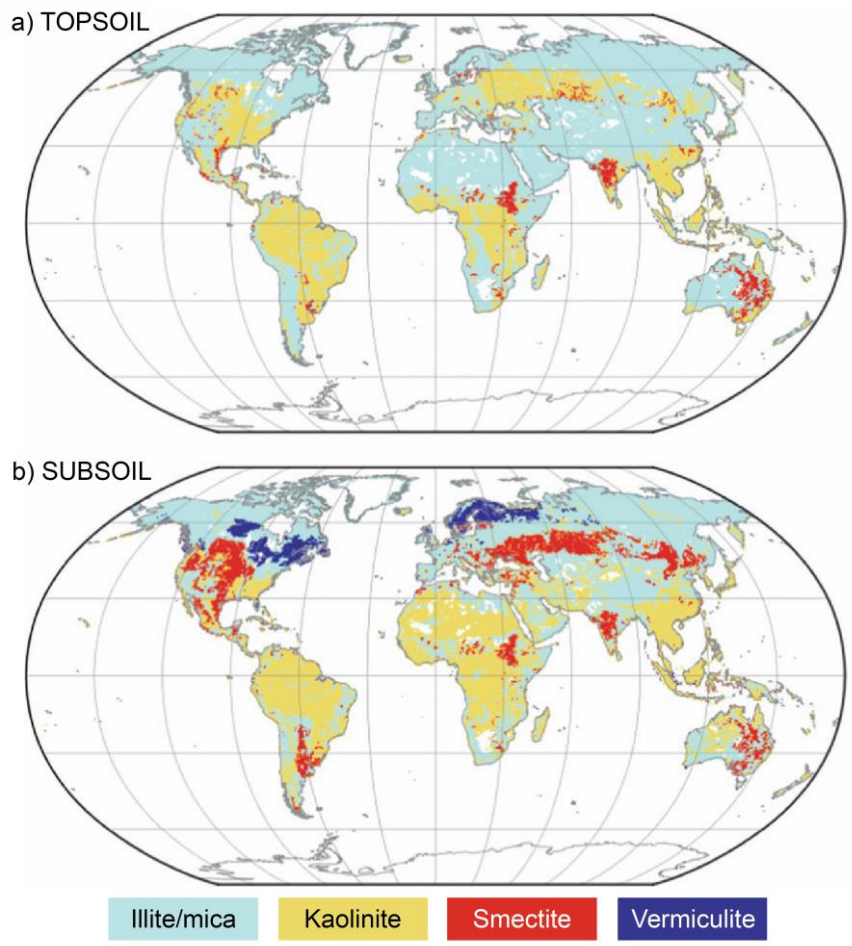

Figure 2-1. Geological world map with the most abundant clay minerals in a) topsoil and b) subsoil (original figure from [3])

Phyllosilicates as main phases in clays are classified according to their arrangement of layers [2, pp. 3-8]. They consist of [SiO_4] tetrahedra and [$M(O,OH)_6$] octahedra. Tetrahedra are bound with joint oxygen ions and form tetrahedral sheets. These tetrahedral sheets are connected in this plane as network consisting of hexagon rings. Each tetrahedral sheet is condensed on an octahedral sheet where the octahedra are connected via edges and two triangular surfaces lay parallelwise to the plane of tetrahedron hexagon rings. Hence, the oxygen ions of tetrahedron tips also belong to the octahedra. Oxygen ions of the octahedral layer, which do not belong to a tetrahedron, have bound a proton (hydroxide ions, OH^-) [2, pp. 3-4]. The 1:1 phyllosilicates are composed of layers with each one tetrahedral and one octahedral sheet. In 2:1 phyllosilicates, another tetrahedral sheet is condensed onto the octahedral sheet. The phyllosilicates relevant for this thesis are described in detail afterwards: *kaolinite, muscovite (representative for mica), illite, smectite*.

Kaolinite ($Al_2[Si_2O_5(OH)_4]$ [4, p. 6]) is the best known 1:1 phyllosilicate. It originates from the decomposition of feldspathic silicate rocks by weathering [2, p. 33]. It forms pseudo hexagonal leaf-like crystallites with median diameters of 0.5 – 4 µm [2, p. 33]. Kaolinite exhibits different grades of structural disorders. Typical disorders concern layer packages regarding a) *b*/3 displacement, b) irregular displacements in *a*-direction, c) rotations against each other, as well as d) incorrect distributions of vacant octahedron places in octahedral layers [2, p. 35].

Mica minerals, such as **muscovite** ($KMg_3[AlSi_3O_{10}(OH,F)_2]$ [2, p. 440]), are 2:1 phyllosilicates that are formed from a sandwich of two tetrahedral layers joined by a layer of Al^{3+} in octahedral coordination [5]. K^+ ions in the interlayer compensate the overall negative charge which is related to the Si for Al tetrahedral substitution. **Illite** is formed either diagenetically from smectites (“illitization” [6, p. 146]) or by the degradation of muscovite. During the latter process, K^+ ions are dissolved out of the interlayers and replaced by Ca^{2+}, Na^+ and H_3O^+ ions [2, p. 171]. This leads to a lower layer charge as compared to muscovite. Mixed-layer illite-smectite tends to swell more with increasing smectite interlayers [6, p. 145]. Phyllosilicates from the **smectite** group are known for innercrystalline swelling and incorporate inorganic or organic cations as well as water molecules. The most abundant smectite mineral is montmorillonite. It can be formed by hydrothermal decomposition of rocks or by weathering of volcanic tuffs / ashes. Rocks with high content in montmorillonite are known as ≪ bentonite ≫ that are mostly conversion products of volcanic tuffs. The approximate structural formula of montmorillonite is $M^+_{0.4}(Al_{1.5}Fe^{3+}_{0.1}Mg_{0.4})_{2.0}[Si_{4.0}O_{10}(OH)_2]$ [2, p. 449].

Their layer arrangements and chemical compositions are typical for individual phyllosilicates. Furthermore, the particle size and shape differ both significantly and depend also on their origins. For instance, the fraction of kaolinite particles < 2 µm (< 0.2 µm) can range from 40 – 95 wt% (5 – 60 wt%) for kaolins from primary kaolin deposits versus kaolin sediments,

respectively [2, p. 12]. Zhang et al. [7] investigated different kaolinite particle sizes and found width-to-thickness ratios (“aspect ratios”) from 0.6 to 5.0, as well as hexagonally shaped particles. The aspect ratio for untreated muscovite, in comparison, was found to be even up to 250, with the major part between 50 and 100 [8]. Their particles are described as overlapping platelets, indicating their lamellar structures, that are yet less stacked than for kaolinite particles, as described e.g. in [9]. As for kaolin, the illite particle morphology mainly depends on the origin of the illite itself. It can range from thin, fibrous particles (thickness of some 100 Å, width = 0.1 – 0.4 µm) over laths to wider platelets, where the laths become thicker and wider with increasing burial depth [10]. Keller et al. [11] described illite further as << flakes >> with << non-uniform edges >>, << ribbed textural pattern >> and << thin, platy crystals >>. For illite/smectite interstratifications, the change in morphology from smectite to illite becomes dominant with 45 wt% and is completed with 30 wt% residual smectite, respectively. The morphology of pure smectite is described as cellular texture that is more open (<< fluffy >>) in the case of Na-montmorillonite than in Ca-montmorillonite. The more open texture is related to an easier hydration of the Na^+ than of the Ca^{2+} interlayer cation [11]. All these parameters lead to major differences in physical and chemical characteristics of phyllosilicates, which are summarized in Table 2-1, and clays / clay minerals. Among other factors, the type and amount of phyllosilicates in clays are indicators for their suitability as pozzolanic SCM, presented in chapter 2.1.2.

Table 2-1. Comparison of selected phyllosilicate characteristics

Parameter	Kaolinite	Muscovite	Illite	Smectite
Specific surface area (BET)	9 – 20 m²/g [12-15]	2 – 14 m²/g [8, 16]	65 – 100 m²/g [17, p. 64]	26 – 330 m²/g [18-20]
Water uptake capacity (Enslin-Neff) [21]	55 – 160 wt%	140 wt% [16], 360 wt%	70 – 140 wt%	140 – > 1000 wt%
Zeta potential at pH = 2.5 – 11	- 24 – 49.5 mV [22]	n.d.	0 - - 42 mV	n.d.
Zeta potential of Na-clays at pH = 7 - 10 [23]	- 35 – 40 mV	n.d.	- 37 – 42 mV	- 39 – 44 mV
Zeta potential of Ca-clays at pH = 7 - 9 [23]	- 22 – 18 mV	n.d.	- 24 – 16 mV	- 30 – 18 mV
Zeta potential at pH = 12.5 [24]	- 30 mV	- 14 mV	n.d.	- 52 mV
Layer charge [2, p. 89]	-	~ 1	0.6 – 0.9	0.2 – 0.4
Layer charge [25]	< 0.01	n.d.	1.4 – 2.0	0.5 – 1.2
Cation exchange capacity [2, p. 89]	0.01 – 0.1 meq/g	< 0.05 meq/g	< 0.35 meq/g	0.5 – 1.2 meq/g

2.1.2 Thermal activation of clays and pozzolanic properties of calcined clays

The thermal activation of phyllosilicates and clays occurs mainly either by flash calcination or by calcination in muffle ovens and rotary kilns ("soak calcination" [26]). During **flash calcination,** finely ground particles are exposed to high temperatures in He or N_2 atmosphere to enable highest dehydroxylation degrees possible at short time periods only [26-28]. Thanks to a rapid cooling down process, there is no further processing of the particles required and the calcined clay can be used as it is [29]. Main differences between flash calcination and **soak calcination** parameters are the initial particle size, holding period and the temperature range. Until now, the majority of calcinations published are on laboratory scale, but several trials show up the feasibility of calcination of clays on industrial scale [30-33]. The latter production takes the use and investigations of calcined clays to a new level as it enables significant larger capacities.

In order to obtain a pozzolanic activity as high as possible, the optimal calcination temperature range can be quickly determined e.g. by thermal analysis to detect dehydroxylation-related mass loss [30, 34-36]. With increasing temperature, there are four stages during calcination as summarized e.g. by Irassar et al. [35] as well as by Garg and Skibsted [37]: I) the dehydration, II) the dehydroxylation, III) the destruction of the structure and IV) a recrystallization / glass formation when surpassing the optimal temperature. The primary effect that is necessary for the thermal activation of phyllosilicates is the process of dehydroxylation – the removal of hydroxyl groups from the phyllosilicate layers [38].

Dehydroxylation of **kaolinite** occurs between 500 and 700 °C [12, 35, 39], where highly ordered kaolinite requires higher calcination temperatures compared to low or medium ordered kaolinite [40]. In [2, p. 38], these temperature ranges are 570 – 600 °C for ordered kaolinite and 540 – 570 °C for disordered kaolinite. Disordered kaolinite dehydroxylates easier as stacking defects do promote twodimensional hydroxyl diffusion processes out of the kaolinite particles, while ordered kaolinite tends to retain its OH bands [41]. By dehydroxylation, the aluminum octahedral and silicon tetrahedral layers collapse and kaolin transforms into disordered / amorphous metakaolin [12, 38]. Between temperatures of 550 and 800 °C, the highest pozzolanic activity is achieved thanks to an increased amount of disordered structure [12]. Disordered kaolinite is more reactive than highly ordered kaolinite as OH bands can dehydroxylate more easily [40, 42]. Lamberov et al. [43] described further that dehydroxylation occurs easier for finer particles than for coarse particles, especially when taking a look at the fraction < 5 µm. At 950 °C, recrystallization takes place and mullite is formed [12, 39].

Compared to kaolin, the temperatures for complete dehydroxylation can differ significantly for **muscovite**. Thermal analysis by Guggenheim et al. [44] revealed that dehydroxylation starts at 475 °C already and is completed at 950 °C. The latter temperature is in accordance with findings of Grim et al. [45] and MacKenzie and Milne [46] that OH bands are removed between 800 and 1100 °C. Other authors described the start of dehydroxylation at T > 770 °C [47] and most of the OH groups are removed at T < 800 - 850 °C [5, 30], where a metastable dehydroxylate phase of muscovite is formed [48]. If dehydroxylation is still incomplete, muscovite is able to rehydroxylate [44]. With higher calcination temperature, this dehydroxylated phase (<< high-temperature modification >>) becomes increasingly disorganized but muscovite maintains its layered structure even until T ~ 1140 °C [5]. At about 1100 °C, further decomposition takes place to a feldspar-like phase and spinel is formed. Higher temperatures lead to the formation of mullite [49].

The temperatures for complete dehydroxylation can differ significantly from **illite** to illite due to interstratifications with other clay minerals. After complete dehydroxylation, illite keeps also its order of structural layers [36]. For the desired pozzolanic activity, illite is commonly calcined at higher temperatures as the amorphization / destruction of layer structure takes place at approximately 800 – 900 °C [37, 50]. According to He et al. [18, 51], the highest pozzolanic activity is achieved at a calcination temperature of ~ 930 °C, which is in agreement with [52]. Nonetheless, calcined illite does usually not achieve the same pozzolanic activity as known from metakaolin as its reactive Al groups are trapped between the Si tetrahedral groups [36]. Compared to kaolinite, the recrystallization occurs at higher temperatures as well (1100 °C) where the formation of spinel phases leads to a loss in pozzolanic reactivity [52, 53].

As $Al^{[VI]}$ groups are placed between the silicon sheets of **montmorillonite**, the Al sites remain largely unaffected by dehydration processes at T < 500 °C. Between 500 and 600 °C, a partial dehydroxylation initiates and the disordered structure of montmorillonite increases continuously until 800 °C, resulting in maximum reactivity [54]. According to He et al. [55], dehydroxylation of Na- and Ca-montmorillonite is completed at 700 °C and 680 °C, respectively, also with the highest pozzolanic activity at 830 °C. Ca-montmorillonite is more reactive than Mg-montmorillonite [40] or Na-montmorillonite [55]. This phenomenon is explained by I) the octahedral occupancy as a cis-vacant montmorillonite requires higher temperatures for complete dehydroxylation than a mixed cis/trans-vacant montmorillonite and consequently obtains a lower reactivity at the same calcination temperature and II) a higher portlandite (CH) consumption of Ca-montmorillonite [40]. At temperatures exceeding 930 °C, Na-montmorillonite decomposes and transforms into spinel. Ca-montmorillonite exhibits high temperature modifications between 850 and 1000 °C with the formation of cristobalite and Mg-

Al-silicate [55]. At 1000 – 1100 °C, the layer structure of montmorillonite collapses and stable crystalline phases are formed [54].

Considering the mineralogical composition of common clays, these dehydroxylation temperatures need to be kept in mind in order to obtain the highest pozzolanic activity possible. Skibsted and Snellings [38] concluded therefore a temperature range of 500 – 800 °C and Beuntner et al. [30] between 550 and 950 °C.

Within the first day of reaction, nearly all SCMs exhibit a **filler effect**: they offer extra space due to a higher, effective water-to-cement ratio (w/c) at same water-to-binder ratio (w/b), as well as nucleation sites that enhance the formation of hydration products [56]. This leads often to an increased amount of CH, which is later on consumed by pozzolanic SCMs in order to form new hydration products. While fly ash is known to react slowly (CH consumption after > 1 week), ultra-fine silica fume is already reactive at very early age. For **Si-rich SCMs**, a decrease in pH value (e.g. by clinker replacement or by incorporation of alkalis in hydrate phases like CSH) means a decrease / slow down of reaction kinetics. As class F fly ash contains 15 – 35 wt% Al_3O_3 and small amounts of sulfate ions only, fly ash blended cement exhibits aluminum-rich hydrate phases. The addition of **Al-rich** metakaolin leads to a rapid consumption of CH with CSH and strätlingite (C_2ASH_8) as main hydrate phases [57]. Wang et al. [58] determined CASH gel as well as crystalline calcium aluminosilicate hydrates and calcium aluminate hydrates (namely C_2ASH_8, C_4AH_{13}, C_3AH_6). With metakaolin-limestone blends, significantly more monocarboaluminate (AFm-Mc) is formed by the introduction of calcium carbonate [59]. The synergy effect of calcined clays with limestone is examined in chapter 2.1.4 in more detail.

Beuntner described the **pozzolanic reaction for calcined clays** depending on the amount of reactive Si and Al ions [60]. According to her findings, the formation of CSH is favored under ambient condition with increasing Si/Al. Released Al ions are incorporated into C(A)SH. Strätlingite can be formed as soon as the capacity for Al ions in CSH is exploited and if the molar ratio of metakaolin and CH is 1, which is not possible at high Si/Al. For metakaolin (Si/Al ~ 1), the formation of CSH is completed within 2 days and does not continue until later ages (> 90 d) when CH is released by modifications of AFm phase content. AFt is formed from sulfate ions originating from calcined clay or sulfate carrier in cement. Depending on the carbonate content, AFt phase is stabilized and the formation of monosulfate (AFm-Ms) is suppressed [61, 62]. With sulfate depletion, AFm carboaluminates are formed, for Al-rich calcined clays especially during early hydration [60]. With these hydration mechanisms, the addition of calcined clays can lead to modified properties in cementitious systems (chapter 2.1.3).

2.1.3 Performance of calcined clays in concrete

The characteristics of clays, clay minerals and the most important phyllosilicates have been described in chapter 2.1.1. After the thermal activation of clays, calcined clays do influence the fresh properties, the mechanical properties as well as the durability of concrete as pozzolanic SCM.

Approaches to characterize the rheological behavior of calcined clay blended cement (CCBC) pastes by Bingham, Herschel-Bulkley or Newton models [63] have been published e.g. in [64-67]. Tregger et al. [68] took the volume fraction into account by using the compressive rheology method and a modified Bingham equation [69]. A modified Krieger & Dougherty model [70] was applied in order to describe non-flocculating suspensions [71] as it takes not only the viscosity and volume fraction into account, but also the maximum packing density of the flocs as well as the shear and yield stress of the suspension [68]. The advantage of this modified model is the consideration of entrapped water into the flocs but also its release from them. According to Blachier et al. [72], the main disadvantage of the Krieger & Dougherty model in context with CCBC is the disregard of non-spherical shaped particles, a morphology that does apply for calcined clays. Instead, they proposed to evaluate the hydrodynamic volume of particles as it considers the aqueous phase entrapped in between the particles [72]. Irassar et al. [73] compared the shear stress of different calcined clay additions and cements at varying shear rates. Ng and Justnes [74] described the rheological behavior of cement paste with calcined marl by using the area under the flow curve, designated as flow resistance.

Calcined clays, shales and marls do significantly affect the fresh properties of cementitious systems. The addition of calcined clays **increases plastic viscosity and both static and dynamic yield stress**, hence causes a loss of workability in concrete [64, 65, 67, 73, 75, 76]. This is due to a large surface area [76, 77], low water film thickness [77], and increased water demand [73, 75], as well as high agglomeration potential [75] and irregular shapes of calcined clay particles [76, 78]. It was found that calcined marl increases the packing density of blended paste [74]. The addition of 60 wt% calcined marl results in no flowability of cement paste (w/b = 0.36) at all and a replacement level of 20 wt% leads to an 1.5 times higher flow resistance compared to neat cement. Over time, a reduction in flow resistance is observed, which is related to wall slipping as the water uptake by calcined marl is irreversible. Calcined clays can increase the degree of thixotropy due to flocculation and high water adsorption [16, 64, 79, 80]. Lorentz et al. [67] described the zeta potential of CCBCs as the decisive parameter for a decreased flowability.

Due to the higher water demand and a lower effective w/c, calcined clay blended concretes reveal beneficial side effects, such as **reduced bleeding** [30] and **lower** plastic **shrinkage** at early age [81].

Long-term shrinkage is also less pronounced compared to plain cement concrete, which is related to the high amount of AFm phases that leads to pore size refinement [81-83]. Contribution to strength development depends on physical properties, disordered / ordered structure and kaolinite content of clays [84], as described already regarding their pozzolanic properties in chapter 2.1.2. An increased amount of disordered kaolinite leads to higher reactivity, provides more Al ions and leads, in consequence, to higher amounts of AFm phases and thus to a **higher compressive strength** [30, 83]. Comparable strength and Young's moduli can also be expected for concretes with up to 30 wt% of low or moderate reactive calcined clays, when the main pozzolanic reaction is completed between 7 and 28 days [30, 85, 86]. Calcined kaolinitic clays can also improve the **interfacial transition zone** [82, 87] and **reduce sorptivity rates** [88, 89] due to their larger specific surface area and the above mentioned pore size refinement. Calcined illitic clays with lower reactivity show up at least comparable performance as plain concrete at later ages (> 90 d) [87, 89]. This affects also the **durability** of calcined clay blended concrete [90, 91].

2.1.4 Synergy effects of calcined clays with limestone in cementitious systems

Limestone is known as filler in cementitious systems [92] and as cement component. Besides grinding, there is no further processing necessary, which designates limestone as an inexpensive and appropriate product in order to reduce carbon dioxide emissions. Limestone powder can improve the packing density and compressive strength thanks to a finer particle size compared to clinker [93]. It provides additional nucleation sites [94] and can lead to an accelerated silicate clinker reaction [95] and thus to a higher degree of hydration [93]. When surpassing a certain amount of limestone, however, the dilution effect dominates and heat of hydration is lowered as well as porosity increases with coarse limestone [96]. Instead of AFm-Ms, carboaluminates are formed from Al ions originating from C_3A and C_4AF with $CaCO_3$ and the AFt phase is stabilized [62, 97, 98]. As the volume of AFt is higher as compared to AFm-Ms, the porosity of the cementitious matrix decreases and the compressive strength is improved. This effect, however, is coupled to the limited amount of Al ions from aluminate clinker phases. This is where the synergy effect of limestone powder and SCMs comes into play as additional Al sources increase the chemical effect [98].

Limestone calcined clay cement (LC^3) is a common blend for clinker replacement with 30 wt% calcined clay and 15 wt% limestone, that stems from the reconsideration of European cement standard DIN EN 197-1 [99]. CEM/II C cement classifications allow future clinker reductions of down to 50 %, but do not consider calcined clays as pozzolanic SCM so far. Current American standard ASTM C595 limits the incorporation of pozzolan and limestone in cement to ≤ 40 wt% and 15 wt% respectively and it requires a minimum clinker content of 45 wt% [100].

Several researchers have conducted investigations on LC^3 regarding its impact on workability [65, 101-103], on hydration [103-107] as well as on microstructure development [108] and durability [59, 109-111]. The **rheological behavior** of LC^3 mixtures is improved with more limestone added, going along with a decrease in compressive strength [65, 101, 102]. On the other hand, the addition of fine limestone increases the packing density and consequently yield stress, while more metakaolin leads to higher yield stress and plastic viscosity due to larger specific surface area [65]. As consequence, these mixtures require more superplasticizer compared to plain cements for an adequate workability [102, 103], where the demand for superplasticizer rises linearly with metakaolin content [103].

The effect of LC^3 on hydration kinetics has been well studied but some aspects are still under discussion. The combination of dilution, filler and pozzolanic effect leads to a higher content of CH at early ages and thus influences the further course of pozzolanic reaction, also with calcined low grade kaolinitic clay [112]. Consumption of CH is increased and carboaluminates and CSH phases are formed [59, 106]. After 1 d, AFt as well as hemicarboaluminate (AFm-Hc) are found as main aluminate phases in LC^3. The amount of AFt is comparable for OPC and LC^3 at this time, whereas the amount of AFt in LC^3 mixtures is higher at later ages despite of a lower sulfate content in the mixture [104].

This **stabilization of AFt** [59, 104, 106] is related to the fast sulfate depletion and a high amount of **AFm-Hc** and **AFm-Mc** that form with Al^{3+} ions from both C_3A and metakaolin and CO_3^{2-} from limestone [59, 104]. The preferred incorporation of CO_3^{2-} into these phases hinders as a consequence the formation of instable **AFm-Ms** [59, 107]. With increased kaolinite content, more Al^{3+} ions are available and AFm-Hc is the dominant phase compared to AFm-Mc [113]. Due to undersulfation and fast aluminate reaction, sulfate depletion occurs fast in blended mixtures and slows down hydration kinetics after approximately 3 d [104, 105]. Afterwards, a continuous formation of CASH takes place with changes in its composition [105]. **Strätlingite** is not detectable before complete consumption of CH, which occurs between 7 and 28 days according to several authors [59, 107] and not even after 90 d according to Avet et al. [104]. The latter authors stated that the formation of strätlingite is thermodynamically possible, but it is hindered by pore size refinement. The pore size refinement stems from the increased amount of AFm phases leading to a denser microstructure [112] without reducing or while even increasing the total porosity, as already presented for CCBCs in chapter 2.1.3. The **pore size refinement** and the associated lower amount of critical pores reduces the permeability and favors the resistance towards harmful ion or fluid transports, improving overall the durability of LC^3 [109, 110, 112].

2.1.5 Challenges for concrete technology

Certain questions arise with the use of calcined clays as SCM. The **access to suitable clays** is an elementary requirement [114]. In the best case, they do not compete with other industries and are therefore also attractive from the economic point of view [30]. So far, mining permits are limited compared to the abundance of clays or limited to the production of clinker or paper, or the ceramic industry.

Along going with the dehydroxylation / structural changes, especially clays dominated by 2:1 phyllosilicates exhibit with increasing calcination temperature a smaller specific surface area (SSA) than raw clays [16, 18, 51, 55, 115]. At the same time, the pozzolanic activity improves with larger SSA [116]. It is commonly assumed that a larger SSA, as determined by the BET method [117], goes along with a higher water demand [18]. Interestingly, some recent findings have shown other trends [16]. However, the large SSA and high water demand of calcined clays compared to cements and other SCMs, like fly ash, lead both to a **reduced workability** of concrete for a given w/b [65, 77].

This holds also for the time-dependent workability as rapid slump loss is often observed in concrete with calcined clays [118-120]. Cassabagnère et al. [121], for instance, found a significant decrease in workability already after 15 minutes. Due to structural build-up, the shear stress increases further between 60 and 90, as well as from 90 to 120 minutes, although the absolute shear stress values differ significantly between CCBC mixtures with different calcined clays [122]. Muzenda et al. [64] stated a large discrepancy between static and dynamic yield stress immediately after water addition, which reflects thixotropy. This effect diminishes due to linking bridges by very early ettringite formation that leads to a sharper increase in static yield stress compared to dynamic yield stress over time. Compared to previous authors, as e.g. [122-124], they stated a slower percentual increase in yield stress in CCBC / LC³ pastes, which they related to the initial dilution effect, slowing down early hydration. Hou et al. [123] and Li et al. [124] instead found a sharper increase in static yield stress and more pronounced **rapid slump loss**, respectively, with increasing clinker replacement. They blamed the faster structural build-up, which is beneficial e.g. for 3D printed concrete, to the calcined clay particles that cause flocculation by their large SSA, particle shape and negative zeta potential. Overall, these observations emphasize the **need for tailor-made superplasticizers**, where the state of the art will be further presented in chapter 2.2.8.

As mentioned in chapter 2.1.3, the pozzolanic reaction of calcined clays contributes to strength especially after 7 days, sometimes only later, depending on the type of calcined clay. In turn, the **early strength is commonly lower** as shown e.g. in [125]. Here, the addition of fine limestone powder or CSH seeds can lead to higher early strength values by enhancing both the silicate and aluminate reactions and compensate the dilution effect in the early age of concrete [125]. Similar to these findings, the addition of CSH-PCE improves the 1 d strength without affecting the strength values at later ages [126].

Although they are not topic of the thesis, **durability aspects** of calcined clay blended concrete must not to be forgotten as they present a further challenge to concrete technology: the consumption of CH during pozzolanic reaction reduces the buffering effect for carbonation process [50]. Here, the denser microstructure might reduce diffusion processes and counteract this problem. A lower chloride threshold has been found for LC^3 concrete due to the consumption of CH and a lower pH value as consequence [127]. However, as (limestone) calcined clay blended concretes show a lower chloride ion migration, this seems to be uncritical if not in favor for the service life of reinforced concretes [110, 128]. Further durability tests revealed a decreased yet sufficient performance towards freeze-thaw resistance [50]. It shall be mentioned that also regarding durability, performance strongly depends on the type of calcined clays and is therefore still under discussion.

2.2 Superplasticizers and their mechanisms in cementitious systems

2.2.1 History and overview of (super)plasticizers

Plasticizers and superplasticizers represent around 80 % of chemical admixtures in Germany [129]. There is no current data available for the European market but the development between 1994 and 2008 revealed similar tendencies compared to the German market, as ~ 85 % of chemical admixtures have been (super)plasticizers [130].

The birth hour of fluidifying admixtures was in the 1930s, when the impact of **lignosulfonates** on concrete was patented by J.G. Mark and E.W. Scripture [1, 131]. **Polycondensates** were described for the first time in the 1930s [132, p. 134]. In 1962, β-naphthalene sulfonate formaldehyde (NSF) was developed by Dr. Kenichi Hattori, Kao Soap company (Japan) [133]. In the same year, melamine formaldehyde sulfite resin (MFS) was invented by Dr. Alois Aignesberger, SKW Trostberg (Germany). In chapter 2.2.4, characteristics of NSF and MFS as main representatives of polycondensate-based superplasticizers are described in detail. Further polycondensates are acetone formaldehyde sulfite resins (AFS), that are in oil well cementing due to their robustness against high salt concentrations and temperatures up to 250 °C [134], sulfanilic acid-phenol-formaldehyde-based products (SPF) [135] and cyclohexane sulfite formaldehyde resins (CSF).

With the trend of high-performance concrete at low w/b and in order to improve the water retention behavior of concrete, **polycarboxylate-based** superplasticizers (PCEs) were developed in the 1980s by Nippon Shokubai (Japan) [136]. Nowadays, PCEs are known to be the most efficient and used superplasticizers. They are classified in “generations” depending on their side chain monomer that are presented in chapter 2.2.5.

Further superplasticizers are

- casein, a biopolymer based on α-, β-, and κ-casein, that is mainly used in self-levelling compounds [137],
- “small molecules” [138] with maximal two anionic anchor groups and a (poly)ethylene oxide ((P)EO) side chain and application in challenging concreting scenarios, e.g. high temperature, pumping and long slump retention [139] as well as
- phosphate comb polymers, where an anionic phosphate group can replace carboxylate groups completely or at least to a certain amount, leading to a better dispersion performance (over time and at lower w/b) and less retardation effects [140, 141].

2.2.2 Interaction mechanisms of (super)plasticizers and parameters affecting them

Three adsorption mechanisms dominate the interaction of (super)plasticizers with cement grains, hydrate phases and further phases:

1. **Monolayer adsorption**: the superplasticizer adsorbs onto the surface of cement grains or early hydration products. In case of anionic polymers, the adsorbed polymer layer converts the complete particle surface to negatively charged that leads to *electrostatic repulsion*. An overlapping of these adsorbed layers leads to *steric forces* and is governed especially by the thickness of the adsorbed layer and the conformation at the interface between cement grains and aqueous phase. [142]
2. **Multilayer adsorption**: the negative surface charge attracts Ca^{2+} ions electrostatically to negatively charged groups of the polymers. The new Ca^{2+} outer layer allows the adsorption of another layer of negatively charged polymers and leads to an additional consumption of polymers. [143-145, 146, p. 194]
3. **Intercalation**: superplasticizers can intercalate e.g. into the layered structure of AFm or CAH phases, or into clay minerals (chapter 2.2.7); layered double hydroxides (LDH) resulting from C_3A reaction, for instance, have positively charged mainlayers consisting of $[Ca_2Al(OH)_6]^+$ with OH^- as counteranions. When insufficient sulfate ions (SO_4^{2-}) are present in the pore solution, anionic superplasticizer molecules can intercalate instead of OH^- and SO_4^{2-}, forming organo-mineral phases (OMP) [147, 148].

Along going with the adsorption of superplasticizer onto binder components and their early hydration products, electrostatic repulsion and steric hindrance are the two most relevant dispersion mechanisms. As shown in Figure 2-2, **electrostatic repulsion** takes place with the particles all negatively charged due to adsorption [142]. This mechanism is detected as the main dispersion mechanism when zeta potential becomes more negative after superplasticizer addition [149].

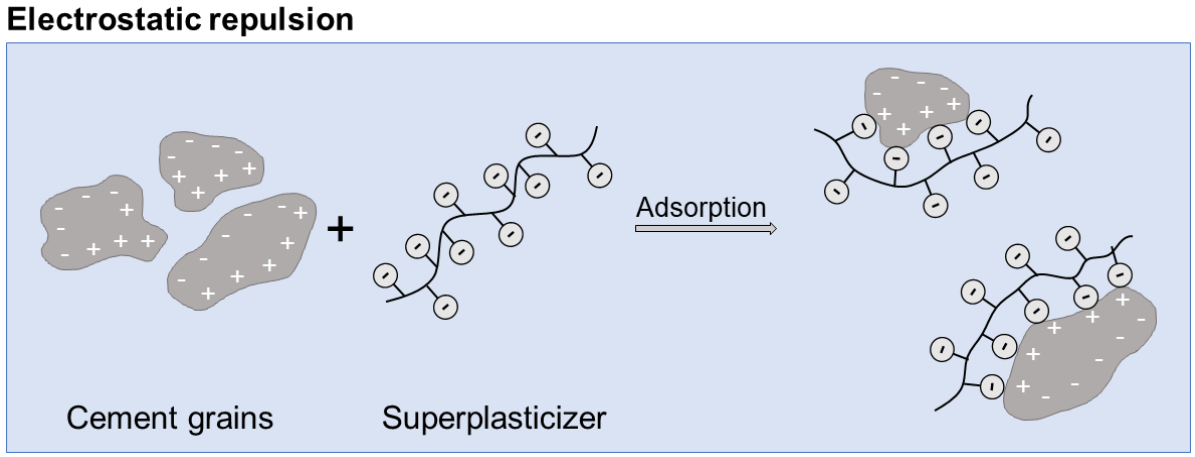

Figure 2-2. Scheme for electrostatic repulsion, drawing based on [150]

Steric hindrance can take place by avoiding an overlapping of the adsorbed layers, or by protruding side chains of PCE into pore solution [147, 151, 152] (Figure 2-3). When zeta potential becomes less negative or even positive, steric hindrance is assumed to be the main dispersion mechanism of a superplasticizer polymer [149].

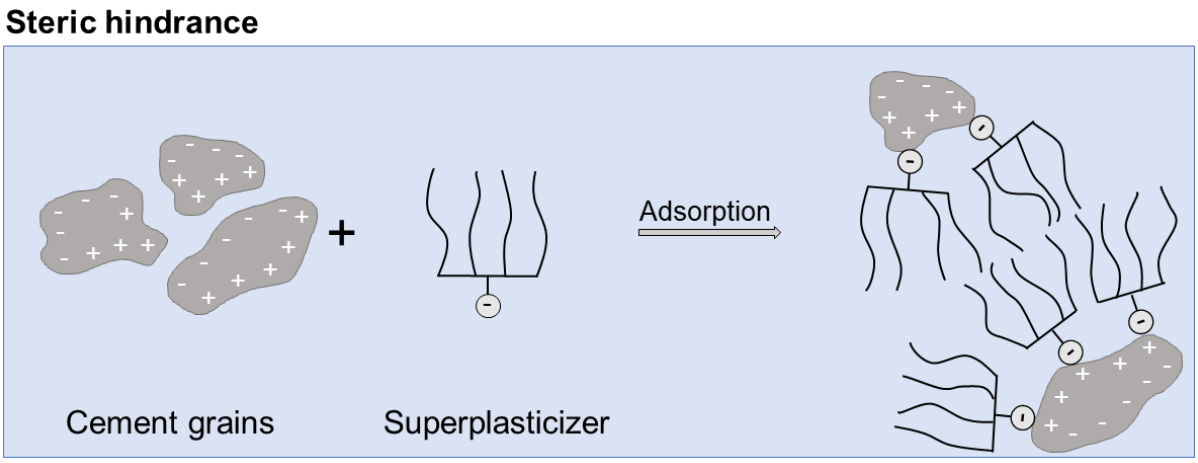

Figure 2-3. Scheme for steric hindrance, modified drawing based on [150]

As the addition of superplasticizer can lead to fragile mixtures, the following overview shall give a short information about commonly known parameters to consider.

Sulfate carrier

- Required optimiziation of sulfate carrier for enhanced fluidity and superplasticizer effectiveness; preferred optimization with SO_3 from calcium sulfate as the effect of SO_3 from alkali sulfates is limited [153].
- Better dispersing performance of PCEs and poly naphthalene sulfonate with higher ratio of hemihydrate to gypsum in cement [153] but higher retardation effects on aluminate reaction with hemihydrate than with gypsum [154].

C_3A - content and reactivity

- Efficiency of superplasticizers is favored with small C_3A to C_4AF ratio [153, 155].
- Adsorption decreases with decreasing C_3A content, especially for PCEs [156].
- Cements with higher C_3A content need more superplasticizer in order to achieve the same workability as cements with lower C_3A content [157, 158].
- Orthorhombic C_3A requires more superplasticizer than cubic C_3A [158].
- Slow C_3A reactivity reduces the consumption of SO_4^{2-}, leading to more SO_4^{2-} in aqueous phase [153].

Pore solution

- Superplasticizers intercalate into interlayer space of CAH crystals and formation of OMP in case of undersulfation [148, 159].
- Sufficient SO_4^{2-} to C_3A molar ratio (0.7 – 2.0) is required in order to avoid intercalation. SO_4^{2-} ions do preferably intercalate due to their higher negative charge density [148].
- Adsorption of PCEs reduces with increased SO_4^{2-} concentration due to competitive adsorption of PCE and SO_4^{2-} onto cement particles, which reduces the fluidity as consequence ([160] in [161]).
- More anions in pore solution, as beforementioned SO_4^{2-} do reduce the adsorption of superplasticizer, especially of PCEs with low anionic charge density [161].
- Preferred complexation of main groups of superplasticizers occurs with cations (e.g. Ca^{2+}) and the adsorption of superplasticizer reduces with high concentrations of cations in pore solution [143].
- In theory: control of sulfate ion concentration in aqueous phase is possible by addition of multivalent charged cations or soluble sulfates [161].

Zeta potential

- Positive zeta potential of binder components or hydrate phases is required for good adsorption of anionic superplasticizers. This is known for C_3A, C_4AF, free CaO as well as AFt and to less extent AFm-Ms [152, 162, 163].
- AFt is negatively charged at a pH value between 11 and 12.9 [164].
- Zeta potential of C_3S and CSH turns positive if enough Ca^{2+} ions (> 3 mmol CaO/l) are present in pore solution that adsorb onto these phases [165].
- Quartz and limestone powder are less negatively or even positively charged with the adsorption of Ca^{2+} ions [166].
- Zeta potential of cement (without or with mineral additions) turns positive or less negative with increasing molar ratio of Ca/SO_4 [166].

Uncalcined clay minerals

- PEO side chains intercalate into layers of clay minerals [167].
- Sorption takes preferably place onto clay minerals instead of cement [167].
- A further literature review is provided in chapter 2.2.7.

Delayed addition of superplasticizers

- It leads usually to a higher initial effectiveness of superplasticizers [153, 159].
- No significant difference between immediate and delayed addition with high ratios of alkali sulfate/C_3A (~ 2) [159].
- It leads to a longer period of workability but also to strong setting retardation due to less adsorption onto cement particles and longer remaining in aqueous phase [168].
- Polymer consumption reduces, especially for linear polyelectrolyte polymers trapped in OMP. Polymers with side chains extending into aqueous phase are less affected [147, 159].

2.2.3 Lignosulfonate-based plasticizers

Production and structures

Lignosulfonates are by-products from the paper production during sulfite pulping of softwood [169] and hardwood [170]. A waste liquor is extracted that contains decomposition products of lignin and cellulose, sulfonated lignin, sugars and sulfates [171, p. 5]. Lignosulfonates can also be prepared by targeted sulfonation of unsulfonated lignins [169]. Further processing is necessary in order to reduce the sugar content [170] and achieve the required properties of lignosulfonates [169]. Most lignosulfonate-based polymers have either Ca, Na or Mg cations as counter-ions for sulfonic groups [172, p. 148] and contain 1 - 30 % of sugar [171, p. 6]. Lignosulfonates are classified as polydisperse natural polymers [169].

Their molecular weight (1,000 – 100,000 g/mol) depends on the number of their macromolecules. These consist of phenylpropane units that are linked together by different C-C and C-O-C units [172, p. 147]. As functional groups, they contain mainly carboxyl groups, phenolic hydroxyl groups or sulfonic groups [170].

Consumption and dispersion mechanisms

Lignosulfonate molecules initially attach via hydrogen bonds to the surface of unhydrated cement grains (monolayer adsorption) [169, 170]. At later ages, they adsorb onto electrical double-layers on the negatively charged ionized surface of cement particles by Ca^{2+} links (multilayer adsorption) [169]. Lignosulfonates disperse by both, steric hindrance and electrostatic repulsion [170, 173, 174]. The main dispersion mechanism depends e.g. on the pH value of the aqueous solution: if the pH is lower than the pH for iso-electric point determined via zeta potential (pH_{IEP}), steric hindrance dominates. With pH > pH_{IEP}, electrostatic repulsion is the dominant dispersion mechanism [175].

Dispersion efficiency

Lignosulfonates enable an approximate water reduction of 10 % and therefore are classified as plasticizers [176, p. 141]. Modified lignosulfonates can enhance the dispersion that is related e.g. to a reduction of sugar [177] or an optimized increase of the molecular weight [169, 178, 179]. The combination of lignosulfonates with polycondensates has been found to be similar effective as the use of pure polycondensates [176, p. 138]. Beside of chemical modifications, delayed addition of lignosulfonates can improve the workability compared to immediate addition [179, 180].

Impact on early hydration and setting behavior

Lignosulfonates retard both C_3S and C_3A reaction due to their high sugar content [176, p. 105] but also in case of sugar-reduced lignosulfonates [178]. A strong adsorption of the lignosulfonate reduces the retardation [174]. Hardly any differences have been observed between soft- and hardwood lignosulfonates [181] nor between Ca- and Na-lignosulfonates [182]. The retarding effect increases with higher dosage, affecting the C_3S reaction more than the C_3A reaction [179-181]. The formation of CH is delayed and reduced, resulting in overlaying silicate and aluminate reactions [180-182]. Colombo et al. called it "*poisoning of C_3S reaction*" leading to an uncontrolled delay of setting [180]. The smaller retardation of C_3A reaction is related to an enhanced, initial formation of AFt [180, 181]. The secondary aluminate reaction and the along going sulfate depletion is delayed with lignosulfonates [181-183]. The delayed sulfate consumption can favor early AFm formation and stabilization as it has been detected in C_3A-gypsum mixtures with the addition of lignosulfonates [182, 183].

2.2.4 Polycondensate-based superplasticizers

Synthesis

The preparation of naphthalene sulfonate formaldehyde (NSF) starts with the sulfonation of naphthalene by the addition of sulfuric acid (Figure 2-4). The replacement of hydrogen by sulfonate is possible at both α or β positions [132, p. 154]. The condensation of β-naphthalene sulfonic acid takes place with formaldehyde. The carbonyl function of the formaldehyde is protonated and the reactive formaldehyde added to the aromatic ring via electrophilic addition. The polymerization occurs due to a methylol function forming a methylene bridge between two naphthalene molecules each. This polymethylene naphthalene sulfonic acid is neutralized by the addition of NaOH. [132, 172]

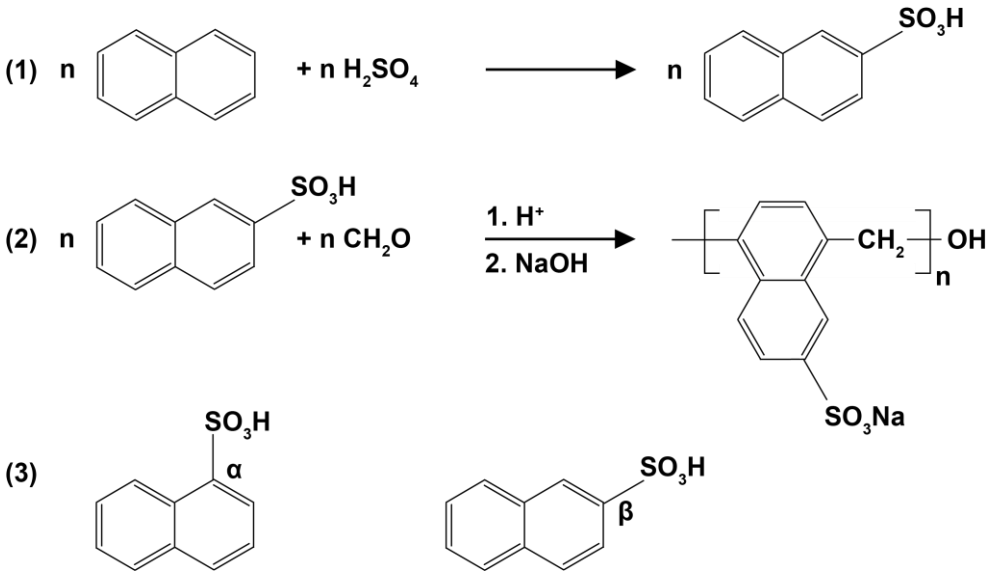

Figure 2-4. Sulfonation (1) and polycondensation (2) processes for the preparation of NSF including α and β positions of the sulfonate group (3); structural formula according to [132, 172, 184]

The synthesis of melamine formaldehyde sulfite (MFS) starts with the reaction of formaldehyde with melamine amino groups to methylolated melamine in alkaline condition (Figure 2-5). One of the methylol groups is sulfonated by sodium hydrogen sulfite ($NaHSO_3$). The polycondensation takes place under acidic conditions and stops once the pH value is > 7. [132]

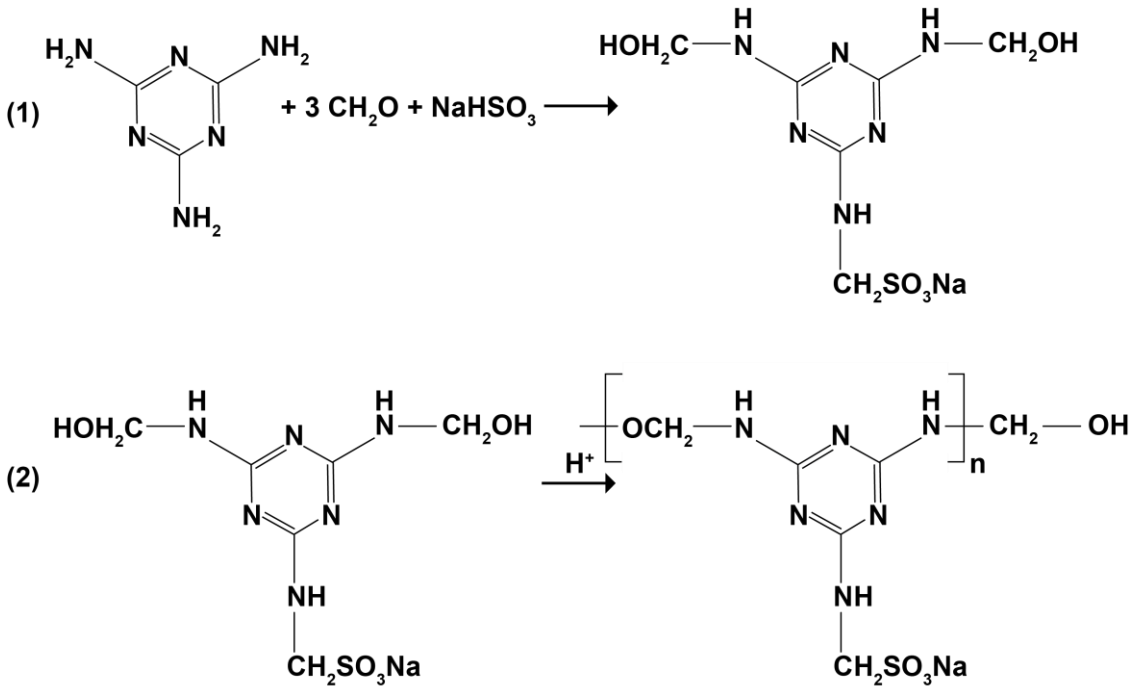

Figure 2-5. Sulfonation (1) and polycondensation (2) processes for the preparation of MFS; structural formula according to [172, p. 150]

Structures

The structure of *NSF* appears as linear molecule leading to a high degree of polydispersity [132, p. 156]. They are mostly used either as Na- or Ca-salt, where the latter contains less residual sulfates due to the precipitation and removal of gypsum in and from solution [172, p. 148]. The molecular weight of NSF ranges from 1,000 to 20,000 g/mol for the highest dispersion [184]. The molecular weight of MFS ranges between 1,200 and 44,000 g/mol, with 7,900 g/mol in average [185]. A common anionic charge density of polycondensate-based superplasticizers is ~ 4,000 µEq/g [152].

Consumption and dispersion mechanisms

NSF and MFS adsorb with their sulfonic groups ($-SO_3^-$) onto positively charged places of the cement grains, following the Langmuir monolayer adsorption model [144, 186, 187]. It alters the zeta potential of cement towards strongly negative values and goes along with electrostatic repulsion as main dispersion mechanism [162, 188]. Slight steric hindrance occurs due to the interaction between the polycondensates themselves.

Dispersion efficiency

Polycondensates adsorb fast onto binder particles and therefore show up a high initial dispersion [189]. Their addition enables a reduction in water demand by approximately 30 % [176, p. 114]. A later addition of NSF or MFS leads to an extended workability period but also to later setting times with larger differences between initial and final setting [168, 172, p. 191]. This behavior is explained by a lower adsorption of polycondensate onto aluminate hydrate phases and an increased dispersion of silicate phases hereby [176, p. 117]. Compared to PCEs, the slump retention of polycondensates decreases faster as the dispersion effect diminishes as soon as the polycondensate is covered by early hydration products [190].

Impact on early hydration and setting behavior

The addition of polycondensate-based superplasticizers hardly affects the hydration of C_3S [191] nor leads to a retarded dissolution of C_3S and C_2S and as consequence a delayed formation of CH [176, p. 117] and CSH [192]. Roncero et al. [192] observed an altered, faster growth rate of AFt which results from accelerated dissolution of C_3A and gypsum going along with the addition of polycondensates. A comparison exhibits that a mixture of NSF and MFS retards the least or accelerates the most, whereas NSF has a more retarding impact than MFS. In fact, MFS retards the cement hydration less than NSF and thus is often used in pre-cast concrete [172, p. 150]. According to Sakai et al., the hydration rate of C_3A remains the same with the addition of NSF [191]. Nonetheless, it is still under discussion whether polycondensate-based superplasticizers do accelerate or retard the aluminate reaction. As polycondensate molecules adsorb primarily on AFt crystals, they can contribute to electrostatic repulsion and avoid flocculation. As consequence of the adsorption of sulfonic groups of NSF and MFS onto AFt, the growth of the typical long AFt needles is delayed and the concrete remains workable for a longer period [143]. This goes along with a 1 h delay of initial and final setting times [168]. Mollah et al. [143] summarized the reasons for retarding effects as follows, based on the research of Gu et al. [193, 194]:

- The diffusion of H_2O and Ca^{2+} ions at the interface between cement grains and pore solution is hindered by the adsorbed superplasticizer molecules.
- The complexation of Ca^{2+} ions with superplasticizer molecules inhibits the nucleation and precipitation of hydrate phases.
- Both growth kinetics and morphology of hydrate phases are altered due to the dispersive effects of superplasticizers.

2.2.5 Polycarboxylate-based superplasticizers

This chapter gives an overview about anionic polycarboxylate-based superplasticizers (PCEs). Cationic and amphoteric polymers are presented in chapter 2.2.6. The information mainly originates from book chapters written by Flatt and Schober [172] and by Gelardi et al. [132] as well as from a review paper of Plank et al. [195].

Structures and synthesis

PCEs often are called "*comb-shaped copolymers*", which refers to their comb-like structure [132, p. 161]. Main components are the backbone that bears carboxylic groups and the side chains consisting of polyethers, combined providing the comb-shape of PCEs. The **backbone** is anionic due to the deprotonation of carboxylic groups and enables the adsorption of the PCEs onto positively charged clinker phases [168]. Typical backbone monomer units, namely (meth)acrylic acid, maleic acid and maleic anhydride, are shown in Figure 2-6. A further representative of backbone groups is the sulfonic group ($-SO_3^-$) [196].

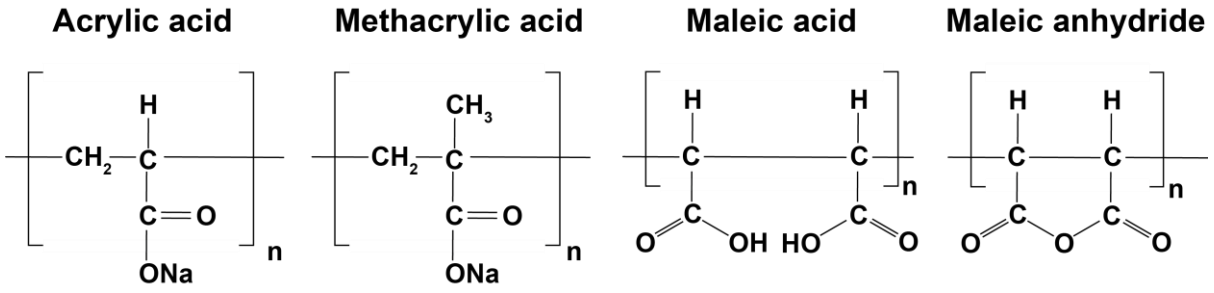

Figure 2-6. Structure of typical backbone monomers: a) acrylic acid, b) methacrylic acid, c) maleic acid and d) maleic anhydride; taken from [132, p. 164]

Common **bonds** between the backbone monomer and the side chain are ester, amide, imide or ether bonds. Whereas the latter three bonds are very stable, ester bonds with (meth)acrylic acid or maleic-based monomers tend to hydrolyze side chains in alkaline media. This leads to more free carboxylic groups and, as consequence, the PCE exhibits a higher anionic charge density and adsorption ability over time [132, p. 164]. **Side chains** consist usually of polyethylene glycol (PEG) with molar masses between 750 and 5,000 g/mol that gives a hydrophilic character to PCEs [132, p. 167]. The amount and length of side chains are the key for steric hindrance. Among other things, the chosen synthesis route depends on the chemical nature of the side chain monomer.

Beside of the five generations given in Table 2-2, further side chain monomers are PTMEG (Jeffamine ®) [197], PAAM (chapter 2.2.6) and XPEG [198]. The latter does crosslink PCE molecules via diesters leading to a stretch out of PCE on the surface of cement and a higher efficiency in theory [195].

As presented in [199], two new macromonomers were introduced in the past few years in China, namely EPEG (2-hydroxy ethyl poly(ethylene glycol)) [200] and GPEG (vinyl ether produced from diethylene glycol vinyl ether and ethylene oxide) [201].

Table 2-2. Generations of PCE superplasticizers including their specific side chain monomers

Generation of PCE	Abbreviation	Side chain monomer	Patent
1st generation	MPEG	ω-Methoxy poly(ethylen glycol) methacrylate ester	[202]
2nd generation	APEG	α-Allyl-ω-methoxy poly(ethylen glycol) / α-Allyl-ω-hydroxy-poly(ethylen glycol) ether	[203]
3rd generation	VPEG	α-Vinyl-ω-hydroxy poly(ethylen glycol) ether	[204]
4th generation	HPEG	α-Methallyl-ω-methoxy poly(ethylen glycol) / α-Methallyl-ω-hydroxy-poly(ethylen glycol) ether	[205]
5th generation	IPEG	Isoprenyl oxy poly(ethylen glycol) ether	[206]

There are two main synthesis routes for PCEs [132, p. 162]. MPEG-based PCEs are synthesized either via esterification of a poly(methacrylic acid) with methoxy poly(ethylene glycol) and the use of both an acid catalyst and vacuum (alternative: azeotropic solvent) for the removal of water. It goes along with long synthesis times and low esterification degrees that are followed by air-entraining of residual MPEGs as disadvantages [207]. An alternative synthesis is the aqueous free radical copolymerization of an ω-methoxy poly(ethylene glycol) methacrylate ester macromonomer with methacrylic acid [208], as shown in Figure 2-7.

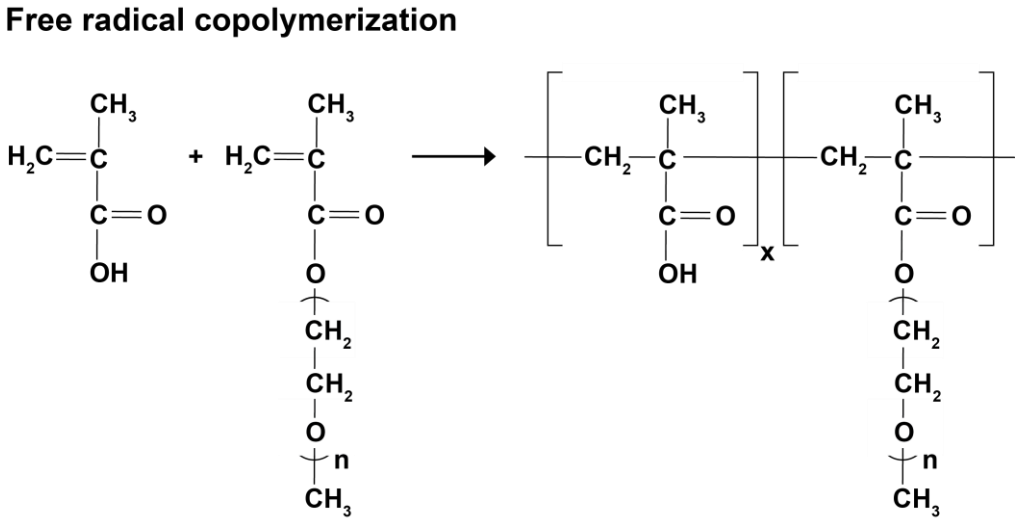

Figure 2-7. Free radical copolymerization of MPEG-based PCE, adapted from [195]

Free radical copolymerization is also the preparation method for APEG- , IPEG- , VPEG- and HPEG-PCEs. Typical APEG-, IPEG-, VPEG- and HPEG-based copolymers are presented in Figure 2-8.

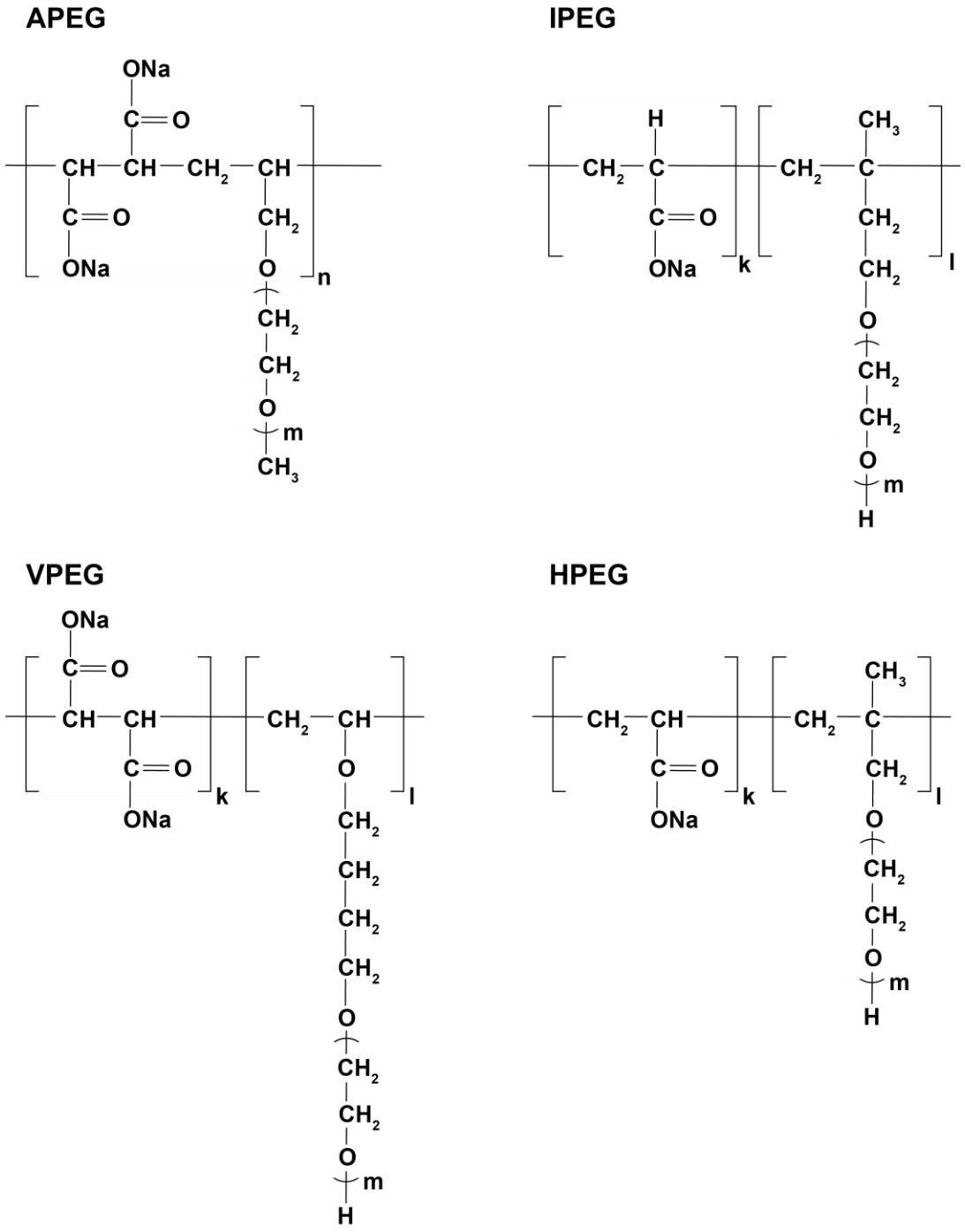

Figure 2-8. APEG-, IPEG-, VPEG- and HPEG-based copolymers, adapted from [195]

The synthesis of PCEs enables e.g. variations in side chain length, backbone length, in the molar ratios of side chain monomer and anchor group monomer. The main advantage of PCEs is their tailormade structure leading to the desired properties.

Flatt and Schober [172, p. 155] as well as Gelardi et al. [132, p. 162] summarized the variety of parameters that affect the performance of PCEs:

- Length of the backbone and of the side chains
- Chemical nature of the backbone (e.g. acrylic, methacrylic or maleic)
- Chemical nature of the side chains (e.g. poly(ethylene glycol) or polypropylene oxide)
- Connection between the backbone and the side chains (e.g. ester, ether or amide)
- Distribution of the side chains along the backbone (gradient or random) [209]
- Charge density

Dispersion and consumption mechanisms

Comb-shaped superplasticizers disperse via both electrostatic repulsion and steric hindrance of the side chains. Among others, Sakai et al. [154], and Sha et al. [151] related this on the one hand to the bonding of anchor groups onto positively charged cement particles and hydration products. Secondly, hydrogen bonds are formed from oxygen atoms of the ether in the side chain with water molecules in the aqueous phase and spread the side chains there, deflocculating the hydrating cement. If PCEs are entrapped in OMP/LDH, less PCEs can adsorb onto cement particles [148], which can be counteracted by long side chains of PCEs [210].

Dispersion efficiency and slump retention

The adsorption of PCEs onto cement particles is decisive for the dispersibility. Beside of cement (paste) characteristics (chapter 2.2.2), the architecture of the PCE has major influence on the dispersion efficiency [211]. Table 2-3 provides a short overview on the structural factors affecting the dispersibility of cement paste [154]. The amount of carboxylates (and other anchor groups) and, as consequence, the backbone charge density determine the adsorption ability of PCEs: the higher the ratio of carboxylates to polyethers, the higher are the adsorption and the dispersibility [157, 212]. The dispersion efficiency increases with lower side chain density / length and higher anionic charge density [213]. Typical ratios of side chain monomer and anchor group monomer range between 2.5 and 3.5 for ready-mix concrete, as well as between 3 and 7 for precast concrete. The side chain length (indicated by the amount of ethylene oxides (n_{EO})) measures 22 to 50 units for ready-mix concrete and 50 to 70 for precast concrete [136].

Table 2-3. Structural factors of PCEs affecting their dispersion behavior [154]

Dispersibility	Structural factor		
	Relative chain length of trunk polymer	Relative graft length	Relative number of grafts
Low dispersibility / short dispersibility retention	long	short	large
High dispersibility	short	long	small
Long dispersibility retention	shorter	long	large

PCEs with high charge density show good dispersion behavior in the beginning due to high adsorption rate and strong steric hindrance with long side chains but poor slump retention, whereas a low charge density leads to a better slump retention after low initial dispersion [151]. Loss in fluidity over time is further proposed to depend on a decreasing ratio of adsorbed PCE to SSA of cement/hydration products (as the SSA of cement increases) [154]. On the other hand, the SO_4^{2-} concentration in the pore solution affects significantly the adsorption equilibrium and more PCE can be adsorbed onto solid particles with decreasing sulfate concentration. Hence, if sufficient amount of (slowly adsorbing) polymer remains in solution, the ratio of adsorption / SSA stays constant with decreasing SO_4^{2-} concentration and the dispersibility retention is extended [154].

Impact on hydration and setting behavior

The adsorption behavior of PCEs has also impact on the hydration kinetics and setting behavior of cementitious systems. A higher dosage of conventional PCEs leads to more pronounced retardation effects [214, 215]. A strong retardation of the dissolution of C_3S has been found on paste level e.g. by Lothenbach et al. [216], leading to a lower degree of C_3S hydration up to 3 d [191] and also to smaller crystal sizes of CH [214]. Among others, Ferrari et al. [217] and Liu et al. [214] explained the delayed silicate reaction with two processes on-going parallelwise: 1) adsorbed molecules on the C_3S surface hinder its dissolution and 2) unadsorbed molecules in solution delay the nucleation of CSH and CH by chelating Ca^{2+} ions [217]. Complexation of Ca^{2+} ions with PCE leads to less free Ca^{2+} ions in liquid phase but a certain, constant amount of Ca^{2+} ions in liquid phase is required for initial setting [215, 218]. As consequence, the complexation of Ca^{2+} ions has been described as main cause for delayed initial and final setting by several authors [163, 168, 215]. Contrary to this, Lothenbach et al. [216] related the retarding effect of PCEs not to the interaction of ions in pore solution with PCE but rather to the steric / electrostatic dispersion and adsorption onto clinker phases.

The addition of PCEs can promote the hydration of C_3A during the first day of hydration [157, 191]. A later sulfate depletion indicates instead a competitive adsorption between sulfate ions and carboxylic groups of the PCEs [157, 161]. The impact of adsorption on retarding effects during early hydration, however, is under discussion. Ferrari et al. [217] related a prolonged dormant period to a lower adsorption rate of PCEs. On contrary, several researchers [213, 219] observed more pronounced retardation effects with higher adsorption ("surface coverage"), which is related to a higher charge density.

Zingg et al. [157] revealed also stronger retardation effects with increased charge density but stated that hindered adsorption has only minor influence on the hydration kinetics. The retardation effect does not depend on the molecular structure of PCEs but on the number of polymer molecules, namely anchoring sites for their adsorption onto surfaces, as well as active functions for Ca^{2+} complexation/chelation by unadsorbed polymers in solution [217]. The molecular weight has little influence on the setting time as stated by Winnefeld et al. [213]. The delayed addition of PCEs enhances even more the retardation effect [168, 219] as well as introducing ester groups (e.g. hydroxyethyl methacrylate (HEMA)) to the side chain of PCEs [220]. Cheung et al. [219] and Tan et al. [220] related this to a lower amount of OMP leading to more polymers in aqueous phase and increasing hereby the retardation effect.

Attempts in order to compensate the delay of silicate reaction are:

- A higher molar ratio of cationic to anionic monomers in zwitterionic PCEs leads to less retardation, which, however, results from lower adsorption [196] and is contrary to previous opinions [214, 217].
- CSH-PCE nanocomposites have been found not only to improve both workability but also to enhance the nucleation / growth of CSH and CH, and hereby the early strength development [126, 221].

The retarding effect is often compared to strength development of cementitious systems. Overall, however, it needs to be put into another perspective, as a significantly lower w/b is possible with PCEs and thus the compressive strength is higher in concrete [222]. Furthermore, the packing density is improved with higher dosage of PCE, which also improves the compressive strength as long as no bleeding occurs [223].

2.2.6 Cationic and amphoteric superplasticizers

Cationic superplasticizers adsorb onto negatively charged silicate clinker phases. Due to the high amount of C_3S and C_2S present in cement, significantly higher dosages of cationic PCE are required for a proper dispersion. The most common cationic monomers are:

- Poly(allylamine hydrochloride) (PAH) [224]
- Diallyl dimethylammonium chloride (DADMAC) [225]
- 2-trimethylammonium ethyl methacrylate chloride (TMAEMC) [226]
- 3-trimethylammonium propyl methacrylamide chloride (MAPTAC) [227]

Amphoteric PCE-based polymers contain both anionic and cationic monomers. This particularity enables the adsorption of amphoteric superplasticizers onto heterogeneously charged binder surfaces [227-229]. Analogous to conventional anionic PCEs, amphoteric superplasticizers consist of backbones and side chains. Acryl acid (AA) [227, 228] or methacrylic acid (MAA) [225, 229-233] are commonly used as anchor groups. APEG [228-230] or MPEG [225, 231-233] monomers are widely chosen as anionic macromonomers. The cationic monomers most studied in amphoteric superplasticizers are DADMAC, TMAEMC and MAPTAC. The main reaction mechanism of amphoteric superplasticizers is steric repulsion [228, 229]. The first amphoteric polymers were patented back in 2000 by Amaya et al. [234]. According to Plank et al. [195] the side chains of **PAAM-PCE** are composed of both anionic PEO groups and cationic polyamidoamine (PAAM) groups. Extremely low w/b can be achieved with PAAM-PCEs [234] while their high prices restrict the application to a small field in concrete technology [195]. For years, researchers focus again on amphoteric superplasticizers [226-231, 233].

Due to the adsorption of cationic monomers onto silicate clinker phases, the adsorption capacity is improved and lower dosages are required compared to anionic PCEs. Polymers with increasing ratios of DADMAC:APEG (and AA:APEG) lead to better dispersion effectiveness as investigations on an AA-APEG-DADMAC polymer revealed [228], also with MAPTAC as cationic monomer, as compared to anionic polymers [227]. With increasing content of the cationic parts, the use of amphoteric PCEs leads to less retarding effects on cement hydration [227]. This can be related to two effects, namely the influence of amphoteric PCEs on diffusion processes on boundary surfaces between clinker and water is less pronounced and further the chemical retardation is reduced due to less carboxylic groups [227]. Chomyn and Plank [235] further found that an amphoteric superplasticizer (with TMAEMC) can enhance the clay tolerance of the PCE compared to conventional anionic PCEs, a problem addressed in the next chapter 2.2.7. Studies towards the interaction of amphoteric superplasticizers with calcined clays are described in detail in chapter 2.2.8.

2.2.7 Interaction of superplasticizers with clay minerals

Clay minerals are undesired companions of clay-bearing aggregates [236] or limestone filler [237], not solely due to a negative impact on the mechanical and durability properties of concrete [238, 239]. Clays in concrete can lead to a loss of superplasticizer dispersion and to a higher water demand.

Regarding the addition of superplasticizers, polycondensates are less sensitive against clay minerals than PCE-based polymers [199, 240, 241]. PCEs adsorb in small amounts with their negatively charged carboxylate groups onto positively charged surfaces of clay particles [167, 242]. In alkaline condition, low amounts of PCE (< 0.6 % by weight of clay) can even increase the viscosity of suspensions with kaolinitic clay as it is assumed that clay particles and PCE molecules induce bridging hydrogen bonds between clay particles. At high dosages (> 3 wt%) steric repulsion forces between the PCE molecules adsorbed on the clay particles dominate the particle interactions [243]. Furthermore, PEG side chains of PCEs intercalate into the interlayers of clay minerals [240, 244] going along with a displacement of water molecules coordinated to the exchangeable cations [242]. Considering the amount of PCE added, the adsorption onto the surface predominates at low dosage, while intercalation effects overrule at higher dosages [167]. This leads to an ineffectiveness of PCE superplasticizers in cementitious systems, even with only small amounts of clay minerals present (≤ 1 % by weight of cement) [24, 167, 240].

Especially montmorillonite is seen critical, as the intercalation effect here is significantly more pronounced than for non-swelling clay minerals [24, 241, 245]. The adsorption of PCE onto the surface of kaolinite and mica is finite [24, 241]. Furthermore, the expansion of kaolinite is limited because of hydrogen bonds between the interlayers, enabling a stable interlayer spacing [245]. Into the montmorillonite layer structure, however, PCEs are strongly incorporated due to its high cation exchange capacity [24, 241] and van der Waals forces that allow easily the uptake of (water) molecules and lead to severe expansions (20 – 30-fold) [245].

Several researchers focused on this problem and suggested the following solutions in order to **enhance the clay tolerance** of superplasticizers:

- Use of PEG-free PCEs in presence of montmorillonite [24].
- Reduction of PCE adsorption on montmorillonite by negatively charged carboxyl terminal groups on PCE backbone that repel from negative charged montmorillonite surfaces [236].
- Modifications of side chains of the PCE towards non-PEO lateral chains (e.g. hydroxyl alkyl methacrylate esters) → adsorption of the polymers onto the clay surface only, avoiding the intercalation into the layers of alumosilicates; compared to conventional PCEs, the adsorption of these tailored PCEs is one tenth only [240, 241].

- Pretreatment of clay-bearing aggregates with cationic monomers which goes along with the disadvantage of fish toxicity [241].
- Addition of sacrificial agents to PCE polymers that intercalate preferably into layers, e.g. of montmorillonite [241].
- Adding a calcium acetate solution to the admixture system - either as pretreatment of aggregates or as co-admixture [242].
- Adding β-cyclodextrin as pendant group to PCE leads to a more pronounced steric hindrance effect [246].
- Higher grafting density of PEO in side chains [247].
- Further so-called << intercalation blockers >> are summarized in [199].

2.2.8 Interaction of superplasticizers with calcined clays

The addition of calcined clays leads to altered pore solution composition [60] and a change in zeta potential. With increasing amount of calcined clay added, the zeta potential shifts towards iso-electrical point (IEP) and blended cement paste tends to agglomerate more [248]. The amount of superplasticizer required for an adequate dispersion and the saturation dosage rises nearly linearly with increasing replacement of clinker by calcined clays [103, 249, 250]. One benefit is that the saturation dosage for PCEs becomes less temperature-sensitive due to the reduction of clinker, which is especially interesting for concrete production at very low or high temperatures [249].

The addition of **lignosulfonates** can lead to false setting due to accelerated C_3A reaction and to significant delays of C_3S dissolution [74, 103]. It results from higher amounts of sulfates in pore solution, increased solubility of gypsum and degradation of lignosulfonates in alkaline medium [181]. This provokes their incorporation into hydrated CA, enhancing the AFt formation [251]. At later ages, lignosulfonates can hinder the conversion of strätlingite and C_3AH_{13} to more stable C_3AH_6, which is also an indicator for the incompatibility with CCBCs [103]. In combination with PCEs, however, a lignosulfonate-based retarder is effective towards both a better performance of PCE and a slump retention of LC³ with up to 30 % calcined clay [118].

At targeted high replacement levels, especially polycondensates and PCEs should be considered as others might exceed dosages recommended by superplasticizer producer and exhibit incompatibilities [103, 250]. Their impact on hydration kinetics of CCBCs is discussed controversially. The addition of polycondensates or PCEs can lead to higher heat of hydration values on the one hand and to extended setting times on the other hand [103, 250]. The influence of **polycondensate-based superplasticizers** on the early hydration of Portland limestone cement paste with metakaolin was observed by Zaribaf and Kurtis [103]. They found that NSF delays the aluminate reaction by 3 hours and has no impact on the silicate reaction.

MFS accelerates the dissolution of C_3A and retards the dissolution of C_3S up to 24 hours, an effect that does not last more than 48 hours though. Further, they related the delayed silicate reaction to Ca^{2+} complexation, which hinders nucleation and precipitation of hydrate phases as soon as the Ca^{2+} ions get in touch with the superplasticizer [103].

PCE-based superplasticizers are found to be the most effective superplasticizers in CCBCs, even at high replacement levels [74, 103, 250, 252, 253]. Zaribaf and Kurtis [103], for instance, stated that the dosage of PCEs, as recommended by the producer, is not exceeded even with 30 wt% metakaolin addition, while those of lignosulfonate- and polycondensate-based plasticizers are exceeded at 10 wt% replacement level already. Nonetheless, they require 2 – 3 times more PCE than neat cement, which relates to the large specific surface area according to Justice and Kurtis [254]. In ternary mixtures with limestone, limestone filler (at least with similar SSA) exhibits a higher saturation dosage and affinity towards PCEs which leads to a lower fluidity capacity [255]. The main adsorption mechanism of CCBCs is steric hindrance going along with long side chains [256]. Schmid et al. [80] described for CCBC mixtures with 20 wt% metamuscovite a significant reduction in yield stress, yet an even enhanced shear-thickening behavior with increasing dosage of an MPEG-based PCE with long side chain. They revealed the w/b as well as type and dosage of superplasticizer as crucial parameters for the dispersion of CCBC mixtures. The addition of PCEs with high anionic charge density enables a strong initial plastification and leads to fast stiffening, whereas less anionic PCEs have a stronger plasticizing effect and cause less consistency retention [248]. Schmid and Plank [257] showed in a comprehensive study, however, that the initial dispersion performance is better for MPEG-based PCE with lower anionic character when possessing a short side chain (n_{EO} = 23), while this effect is reversed with moderate side chain length (n_{EO} = 45). At higher replacement levels (> 20 wt%), the more anionic PCEs perform better in CCBC mixtures. With IPEG-based PCEs, they even found a favored interaction with a calcined common clay (rich in 2:1 phyllosilicates) compared to cement, and with HPEG-based PCEs a superior dispersion performance in CCBCs and pure calcined clay. Investigations by Li et al. [258] confirmed the latter observations for a calcined common clay rich in metakaolin, both as neat calcined clay or as clinker replacement even up to 40 wt%. However, the authors recently also showed differences in the dispersion performance of a HPEG-based PCE depending on the mineralogical and physical characteristics of the calcined common clay used [259]. According to [79, 260], calcined 1:1 phyllosilicates require significantly more superplasticizer than calcined 2:1 phyllosilicates (smectite). However, it is presumed that polyethylene oxide (PEO) side chains intercalate into remaining interlayers of the latter after calcination (chapter 2.1.2), leading to less dispersion efficiency [74]. Ferreiro et al. [79] described an improvement in superplasticizer efficiency when adding the polymer up to 90 seconds and 3 minutes after the water to CCBC with calcined 2:1 and 1:1 phyllosilicates, respectively.

They also described different adsorption behavior of these types of metaphyllosilicates: the adsorption takes place at the edges of calcined 2:1 phyllosilicates (here metasmectite), which hinders the water uptake into their interlayers, whereas the PCEs adsorb onto the amorphous structure of calcined 1:1 phyllosilicates (metakaolin) [79]. For this reason, each calcined clay must be considered separately in order to enhance the dispersion ability. So far, the poor flowability of CCBC mixtures was counteracted by delayed addition of superplasticizer or the use of workability-enhancing particles (e.g. fly ash) [79, 260]. Another option is the use of PCEs with low charge density (< 0.01 mol PEG/mol) containing e.g. a high ionic monomer (2-acrylamido-2-methylpropane sulfonic acid, AMPS) in order to avoid a possible intercalation and to limit interactions with the surface, instead of the layers, of calcined clays [255]. Investigations on a calcined kaolinitic clay with a non-negligible amount of remaining kaolinite did not show any adsorption of the AMPS-PCE onto calcined clay in water but in synthetic cement pore solution (SCPS) [255]. The interaction is related to the presence of multivalent cations that enable the adsorption of PCEs onto negatively charged calcined clay particles (Ca^{2+}-complexation) [144, 196, 255].

In a systematic study, Schmid and Plank [261] demonstrated that individual metaphyllosilicates sorb different amounts of Ca^{2+} ions per their individual BET surface area: metamuscovite ($3.82 \cdot 10^{19}/m^2$) >> metamontmorillonite ($1.25 \cdot 10^{19}/m^2$) > metakaolin ($1.18 \cdot 10^{19}/m^2$) >> metaillite ($0.41 \cdot 10^{19}/m^2$). Further they described the sorption behavior of PCEs after providing additional Ca^{2+} ions for the surface coverage of these metaphyllosilicates in SCPS. Metamuscovite and metamontmorillonite do sorb (including intercalation) more MPEG-based PCE, while the Ca^{2+} adsorption does not significantly change the sorbed amount of HPEG-based PCE. The small difference on the latter is related to the higher initial sorption of Ca^{2+} ions of these two metaphyllosilicates compared to metakaolin. The metakaolin instead can take up two-fold the amount of HPEG-based PCE and shows in general a better sorption behavior with additional Ca^{2+} ions in the solution, regardless of the macromonomer type of PCE. Further, it is assumed that the PCE intercalates into interlayers of metaillite as no saturation point is reached even with Ca^{2+} ion saturation and dosages of up 1 % by weight of solid [261].

In lime suspensions with metakaolin, PCEs with lower anionic charge density do not show any adsorption onto metakaolin particles due to the low pH value found (5.6), but the flowability increases [256]. Navarro-Blasco et al. [256] related the adsorption hindrance to a low amount of carboxylate groups and the backbone charge, that is sterically shielded by long side chains. Further, a similar adsorption affinity of (super)plasticizers was found for calcined marl and cement clinker by Ng and Justnes [74]: a PCE with low effective charge leads to a high, initial dispersion but to a rapid increase in dynamic yield stress over time.

A review paper published by Lei et al. [199] provides a further overview of the interaction of calcined clays with PCE-based superplasticizers, including the poor slump retention as known for CCBCs (chapter 2.1.5). Recent research by Li et al. [124] focused on solutions in order to counteract the rapid slump loss: the addition of Na-gluconate does not succeed to prevent slump loss of CCBC mixtures (replacement level: 30 wt%), whereas the combination of conventional PCEs for precast concrete with Ca-Al-PCE-LDH nanocomposite can even increase the flowability first. Even at replacement levels of 40 wt%, it extends the workability by 60 – 90 minutes as compared to PCEs foreseen for ready-mix concrete. This mechanism works by gradually releasing the PCE, which is located between the inorganic layers of the Ca-Al-LDH, into pore solution and replacing it by sulfate anions [124]. The retarding impact of PCEs on the hydration of CCBCs is the least compared to other types of superplasticizers [103]. Akhlaghi et al. [255] even found that, compared to plain cement, the retardation effect is less pronounced with the addition of calcined clays in the presence of PCEs [255], which is related to accelerated hydration kinetics and shorter setting times by calcined kaolinite-rich clays [103, 250]. Nonetheless, the addition of PCEs can have also negative impact on CCBCs: if the amount of superplasticizer is not well adjusted, it can lead to a loss in fluidity due to bridging effects [255, 262].

Interactions between **amphoteric superplasticizers** and calcined clays were investigated by Schmid et al. [225, 231-233] and most recently by Li et al. [258]. For CCBC with calcined kaolin-rich clay, an MPEG-based PCE with long side chain and MAPTAC as cationic monomer shows a very good dispersion performance with increasing replacement, similar to the outstanding HPEG-based PCE [258]. In other cases, it requires at least four times higher dosages of amphoteric polymers than of conventional anionic PCEs in order to disperse calcined clays adequately [233]. Interestingly, it is also possible that CCBCs require lower amounts of amphoteric superplasticizer than neat cement. With the current knowledge, this is related to the assumption of heterogeneously charged clay surfaces [224, 233]. The dispersion of calcined clays and CCBCs is significantly more effective with DADMAC than with MAPTAC or even TMAEMC as cationic monomers [225, 232]. The time-dependent spread flow remains more constant with increasing amount of cationic monomer [231, 232]. As described for neat cement in chapter 2.2.6, amphoteric superplasticizers have a less retarding or even accelerating effect on the hydration kinetics of CCBCs compared to conventional anionic PCEs [231-233]. Here, the polymer with MAPTAC retards less than that with DADMAC [225].

3 Aims and open questions

The thesis covers two main topics regarding calcined clay blended cements (CCBCs) with the addition of superplasticizers:

I) Rheology and **superplasticizer performance** immediately after water addition

- Which existing rheological models are suitable to describe the rheology of CCBC mixtures?
- What is the role of different physical characteristics of calcined clays and CCBC in terms of modified flowability? How do they influence the demand for superplasticizers?
- Is it possible to predict the flow resistance and interaction with superplasticizers based on the mineralogical composition of a common clay? Regarding this question, what are the differences between kaolinite and representatives of 2:1 phyllosilicates, and how does quartz as component in clays contribute to the flow properties?
- What types of (super)plasticizers perform the best in CCBC mixtures? Which polymer properties within the group of PCE-based superplasticizers lead to a superior, initial dispersion?

II) Time-related flowability and **early hydration behavior**, considering the first 120 minutes and 24 – 48 hours, respectively.

- What are the reasons for rapid slump loss that is often observed with CCBCs?
- Is it possible to prolong the flowability of CCBC mixtures by using specific polymers?
- How does the addition of superplasticizers in CCBC mixtures affect the course of hydration in terms of primary CH formation, dissolution of gypsum, maximum AFt content and primary formation of AFm-Hc?
- To what extent do physical effects of CCBCs overlay the influence of high superplasticizer amounts on the early hydration?

Based on these two topics, suitable mixtures shall be derived as illustrated in Figure 3-1.

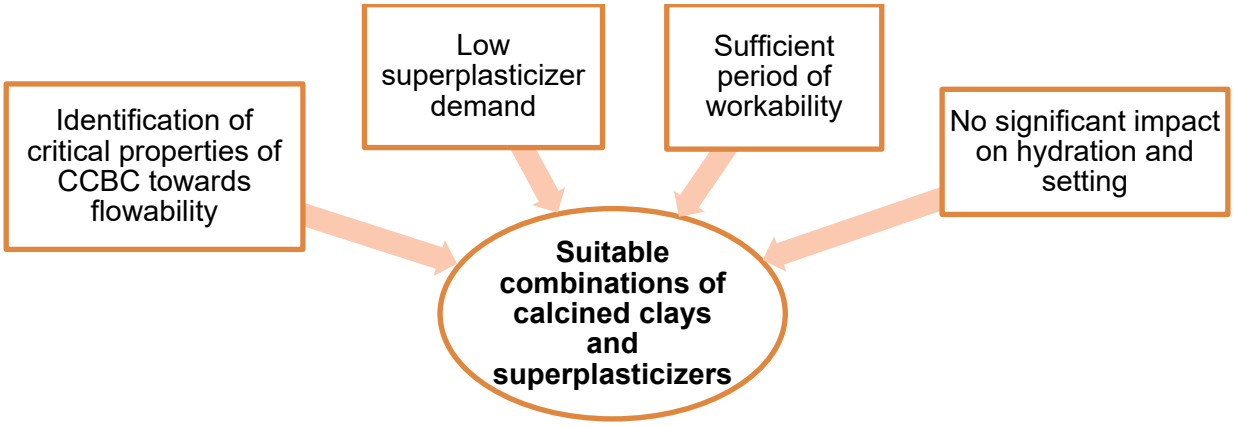

Figure 3-1. Approach to finding suitable mixtures with calcined clays and superplasticizers

4 Overview about materials and methods used

4.1 Materials

An ordinary Portland cement (CEM I 42.5 R, abbreviation: **OPC**) and one Portland limestone cement (CEM II/A-LL 32.5 R, **PLC**), both complying with European standard DIN EN 197-1 [99], are used for the investigations. They originate from the same cement plant and the use of PLC addresses the synergy effect between limestone and calcined clays, as presented in chapter 2.1.4. A previous batch of OPC is named **OPC°** and second batch of the Portland limestone cement is designated as **PLC***.

Three **calcined phyllosilicates** ("metaphyllosilicates") are used to investigate their rheology and interaction with different superplasticizers in cementitious systems: metakaolin (**Mk**), metamuscovite (**Mu**) and metaillite (**Mi**). They are described in detail in the first two journal papers (chapters 7.1 and 7.2).

Quartz is a non-negligible component in common clays [114, 263]. For this reason and to have a comparison of pozzolanic calcined clays with an inert SCM, **quartz powder** (**QP**) is used for selected methods in the first journal paper (chapter 7.1). The particle size distribution shows that the quartz powder is coarse compared to the other binder materials. This relates to the poor grinding ability of quartz on the one hand and that the quartz particles in clays are located in the coarser particle region [2, p. 12].

Beside the metaphyllosilicates, **calcined common clays** are used to compare the findings on metaphyllosilicates with materials representative and valuable for cement industry. In total, five calcined common clays and one calcined kaolinite-rich mine tailing are investigated that differ significantly in their mineralogical composition. The raw material for **TG** (German for "Tongemisch") and **AC** originates from Amaltheen formation (Black Jurassic). The industrial calcination of TG is described in [31]. It is subsequently ground in a roller mill on industrial scale.

Maier et al. [114, 264, 265] provide information on three further materials investigated:

- Kaolin Upper Palatinate (**KUP**) originates from a primary kaolin deposit, formed in Eocene / Miocene by the weathering of granite
- Recycling Kaolin Upper Palatinate (**RKUP**) is a kaolinite-rich mine tailing
- Fireclay Upper Palatinate (**FUP**) are sedimentary, kaolinite-rich clays from Miocene

The raw **MURR** sample originates from Upper Eocene to Upper Miocene sediments from the alpine foreland basin. AC, KUP, RKUP, FUP and MURR are dried to a constant mass at 105 °C and crushed in a jaw crusher to a granule size of ≤ 5 mm.

The pre-crushed material is calcined at 800 °C for 60 minutes in a lab-scale muffle kiln, with batches à 300 g. After calcination, the cooled material is ground for 10 minutes in a vibratory disc mill with agate insert.

Following **superplasticizers** are chosen together with the Chair for Construction Chemistry of Technical University Munich, Germany, within the joint DFG research project:

- Industrial calcium salt of a β-naphthalene sulfonate formaldehyde polycondensate (**NSF**)
- Industrial α-methallyl-ω-methoxy poly(ethylene glycol) ether type PCE **(HPEG**)
- ω-methoxy poly(ethylene glycol) methacrylate ester type PCE with amphoteric character due to diallyl dimethylammonium chloride (DADMAC) as cationic monomer, developed and lab-synthesized by the Chair for Construction Chemistry of Technical University Munich (**amphMPEG**)

Further industrial (super)plasticizers are used within this thesis:

- Isoprenyl oxy poly(ethylene glycol) ether type PCE consisting of IPEG-AA and an IPEG with HEMA in the anchor group (**IPEG1**)
- Isoprenyl oxy poly(ethylene glycol) ether type PCE consisting of IPEG-AA and a vinyloxybutyl polyethylene glycol (VOBPEG)-AA (**IPEG2**)
- Magnesium-lignosulfonate (**Mg-LS**)
- Sodium-lignosulfonate (**Na-LS**)

4.2 Methods

This chapter provides an overview about the methods and instruments used. Further details are provided in the respective publications. The investigations are conducted on clinker-free systems to understand the properties of calcined clays and quartz powder, as well as on blended cements. The cementitious systems are evaluated towards their flowing properties, demand for superplasticizer as well as hydration behavior.

The following methods are used for the clinker-free investigations:

- The morphology and particle shape of metaphyllosilicates, QP and TG are observed via **scanning electronic microscope** EVO LS 15 (Zeiss). Therefore, powder samples are scattered on thin layer of two-component adhesive and gold-coated with a sputter. In high vacuum, an aperture with 20 µm and a secondary electron detector are used with acceleration voltage of 20 kV, spot size of 250 and a working distance at 8.5 mm.
- The zeta potential ζ *[mV]* of all raw and calcined clays as well as of the quartz powder is measured in aqueous phase ($H_2O_{dest.}$ and SCPS according to [225]) by using **electroacoustic spectrometer** DT-310 (Dispersion Technology Instruments).

- The flowability is characterized with **mini slump test** on suspensions of metaphyllosilicates, QP and TG with $H_2O_{dest.}$.
- The rheological behavior of clinker-free suspensions made of metaphyllosilicates, QP and TG with $H_2O_{dest.}$ is measured by using a **rotational viscometer** Viskomat NT (Schleibinger) with the following program: ten minutes at a rotational speed of 120 min^{-1}, each two minutes at 80, 40, 20 min^{-1}. It is analyzed according to Bingham fit, the linear fit between rotational speed and torque resulting in viscosity factor (slope of fit) and yield stress (y-axis intercept of fit) [63, 266].

Based upon the clinker-free investigations, the flowing properties of calcined clay blended cement pastes are investigated as well as the dispersion effectiveness of different superplasticizers. Therefore, the cements are replaced by 20 wt% of metaphyllosilicates, TG or QP and by 30 wt% of calcined common clays (these investigations are limited to PLC*). Higher replacement levels are realistic for calcined common clays [128, 267] or calcined shales [268], whereas those replacement levels are irrelevant for metaphyllosilicates in application. A w/b of 0.50 is chosen to have an as low as possible w/b for strength and durability reasons on the one side and to satisfy the high water demand of calcined clays on the other. Beside of adjusted dosages, the influence of a constant dosage is evaluated towards interactions of PCE superplasticizers with calcined clay blended cements. For both HPEG and amphMPEG, the constant dosage is set at 0.20 %bwob. Further investigations with calcined common clays include constant superplasticizer dosages of 0.05, 0.10 and 0.20 %bwob IPEG1 and IPEG2, as well as 0.05 %bwob HPEG.

The following methods are used to determine the flowing properties and dispersion efficiency of cementitious systems:

- The demand for superplasticizer is evaluated on blended cement paste according to the modified **mini slump test** based on DIN EN 1015-3 [269]. It is an iterative test to achieve a mini slump of 26 cm. For OPC and PLC with Mk, Mu, Mi and TG, the required dosage of NSF, HPEG and amphMPEG is adjusted by the Chair for Construction Chemistry, Technical University Munich. Further mixtures, namely with lignosulfonates or with QP, are tested in the laboratory of the Institute for Construction Materials of the University of the Bundeswehr Munich.
- The slump loss behavior is determined for the mixtures with adjusted superplasticizer dosages by **time-dependent mini slump test**. The test is repeated every 15 minutes until 120 - 135 minutes after water addition.
- The torque, yield stress and viscosity factors as well as flow resistance of blended cement pastes with and without the addition of superplasticizers are evaluated by **rotational viscometer** five minutes after water addition. The equipment and the program are the same

as for clinker-free suspensions. The analysis is based on Bingham fit but as the transformation from the measured values to actual yield stress and viscosity is not possible, the analyzed parameters are named “yield stress factor” and “viscosity factor”, respectively. A further parameter is the flow resistance, as proposed e.g. by Vikan et al. [270]. Therefore, the area under the flow curve is calculated based upon the trapezoidal method between the median torques at 20, 40, 80 and 120 rpm (τ_{20}, τ_{40}, τ_{80}, τ_{120}), see the following equation:

$$FR\left[\frac{Nmm}{min}\right] = 10 * (\tau_{20} + \tau_{40}) + 20 * (\tau_{40} + \tau_{80}) + 20 * (\tau_{80} + \tau_{120})$$

For calcined common clay mixtures, the 15 minutes long measurement starts on the same sample after 5, 30, 50 and 105 minutes to evaluate the time-dependent flow behavior. For the first three measurements, the sample remains and rests in the cylinder. It is removed afterwards and inserted again two minutes before the test at 105 minutes. For pastes with metaphyllosilicates and TG, the torque development is observed at a constant rotational speed of 80 rpm for 120 minutes.

- The influence of calcined clays and the adsorption behavior of superplasticizers is determined via the zeta potential, using the **electroacoustic spectrometer** DT-310 (Dispersion Technology Instruments). The extracted pore solution of reference cement paste is set as ionic background before the actual measurement. The measurement of zeta potential and pH value is carried out for 120 minutes after water addition. The development of zeta potential and pH value shall be correlated with AFt formation and rheometric measurements to provide information on the effectiveness of superplasticizer and the workability period of the investigated mixtures.

The hydration behavior of (blended) cement pastes, without and with superplasticizers, is investigated during the first 36 to 48 hours by:

- Recording the heat flow $\dot{Q}$ *[mW/g$_{cement}$]* via **isothermal calorimeter** TAM Air (TA instruments) at T = 25°C and calculating the heat of hydration *Q [J/g$_{cement}$]*.
- Following the phase development of binder pastes with calcined clays and superplasticizers by **in situ XRD** measurements. The diffractometer Empyrean (PANalytical) has a PIXcel^{1D} detector and Bragg–Brentano^{HD} monochromator. The blended cement paste is transferred into flat metal crucibles and covered by a Kapton film to prevent drying of the fresh paste. The sample holder is connected to a temperature-controlled device (25 °C). Relevant phases and their considered Miller indices are analyzed by HighScore 4.7 (Malvern PANalytical): ettringite (010) and (110) [271], hemicarboaluminate (006) [272], gypsum (020) [273] and portlandite (001) [274]; this method is limited to mixtures without superplasticizers and those with metaphyllosilicates and TG with adjusted dosages.

- Measuring the ultrasonic speed by an **ultrasonic p-wave unit** Vikasonic (Schleibinger). The method is based on the relationship of the sample length and the transit time of ultrasound, which is reduced with ongoing strength development and hence an increased ultrasonic speed is observed. Depending on the sample density and the measured ultrasonic speed, the dynamic modulus of elasticity E_{dyn} *[GPa]* is consulted as criterion for the development of microstructure.

Rheological, electroacoustic, calorimetric and ultrasonic measurements as well as correlations between parameters / significant data points are analyzed with the software Origin 2020 (OriginLab).

4.3 Strategy to address the open questions in publications

For each publication, a chart is developed how the experimental setup addresses the aims and open questions (chapter 3). The first journal paper *"Characteristics of components in calcined clays and their influence on the efficiency of superplasticizers"* (chapter 7.1) investigates the pure materials ("clinker-free systems") and blended cements towards their physical and rheological properties, as well as the initial superplasticizer efficiency in the respective cement mixtures, see Figure 4-1.

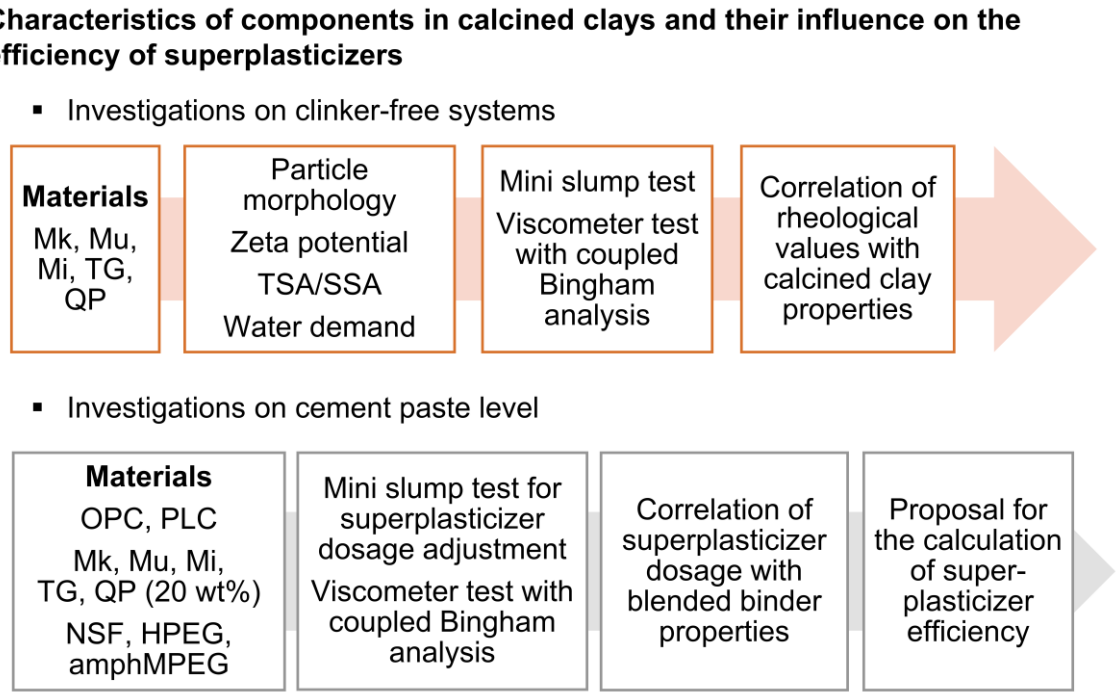

Figure 4-1. Methods and materials used to evaluate the characteristics of calcined clay components towards their influence on flowing properties and superplasticizer efficiency in the first journal paper

The second journal paper treats the *"Rheology, setting and hydration behavior of calcined clay blended cements in interaction with PCE-based superplasticisers"* (chapter 7.2). The same metaphyllsilicates and calcined Amaltheen clay are used as in the first journal paper. The PCEs are added at a constant dosage (0.20 %bwob) in order to distinguish the different calcined clay blended cement (CCBC) mixtures. Beside of rheological measurements, this article provides the combination of isothermal calorimetry, ultrasound and in situ XRD to evaluate the hydration and setting behavior of calcined clay blends (Figure 4-2).

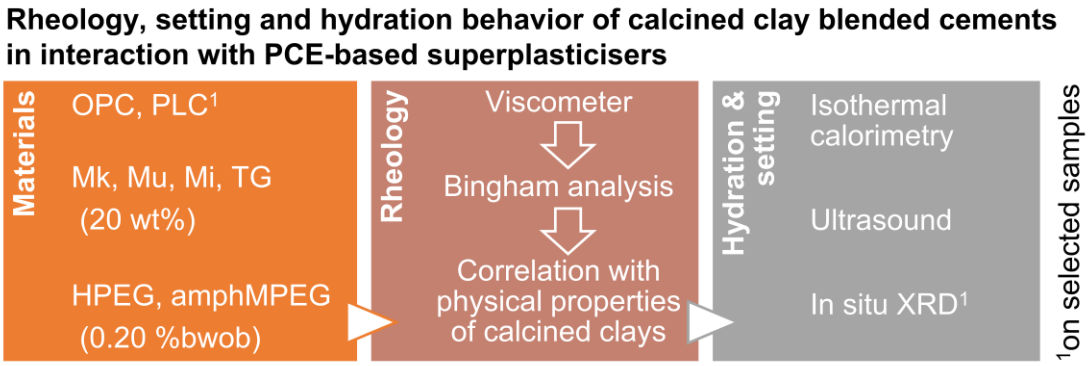

Figure 4-2. Methods and materials used to investigate the rheology and early hydration in the second journal paper

Beside of the influence of pure metaphyllosilicates and TG, the *"Physical and mineralogical properties of calcined common clays and their influence on flow resistance and superplasticizer demand"* have been investigated in the third journal paper (chapter 7.3). The flow properties of CCBC mixtures are determined with rotational viscometer and different rheological models, see Figure 4-3. The efficiency of PCEs in CCBC mixtures with different types of calcined common clays is evaluated. Several physical properties as well as mineralogical phases are identified and to what extent they decrease the flowability or perturb the efficiency of PCEs.

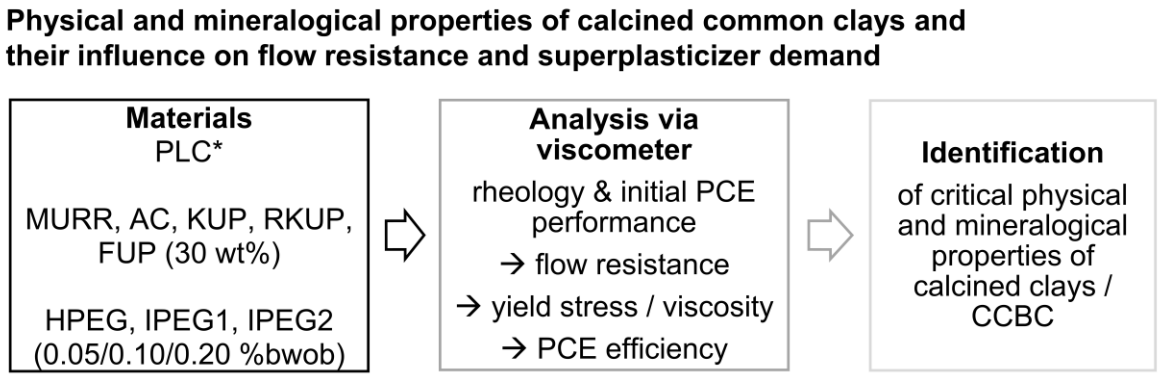

Figure 4-3. Experimental study on the rheology and superplasticizer performance of CCBC mixtures with calcined common clays in the third journal paper

In addition to the zeta potential measurements in the first journal paper, the fourth journal paper includes the zeta potential of metaphyllosilicates in SCPS and of both raw and calcined common clays in $H_2O_{dest.}$ and SCPS. Beside of these measurements, this paper illuminates different aspects on the *"Evaluation of zeta potential of calcined clays and time-dependent flowability of blended cement with customized polycarboxylate-based superplasticizers"* (Figure 4-4 and chapter 7.4). Apart from time-related mini slump tests of PLC blended with metaphyllosilicates, the (subsequent) dispersion of CCBC mixtures with calcined common clays and the addition of HPEG and IPEG1 is determined by rotational viscometer tests and coupled calculation of flow resistance. Thresholds of calcined clay properties are identified that lead to rapid slump loss. Further, zeta potential and calorimetric measurements of PLC, PLC_30AC and PLC_30FUP with different dosages of PCE indicate differences in adsorption of PCE and the impact of different calcined clays and PCEs on (very) early hydration.

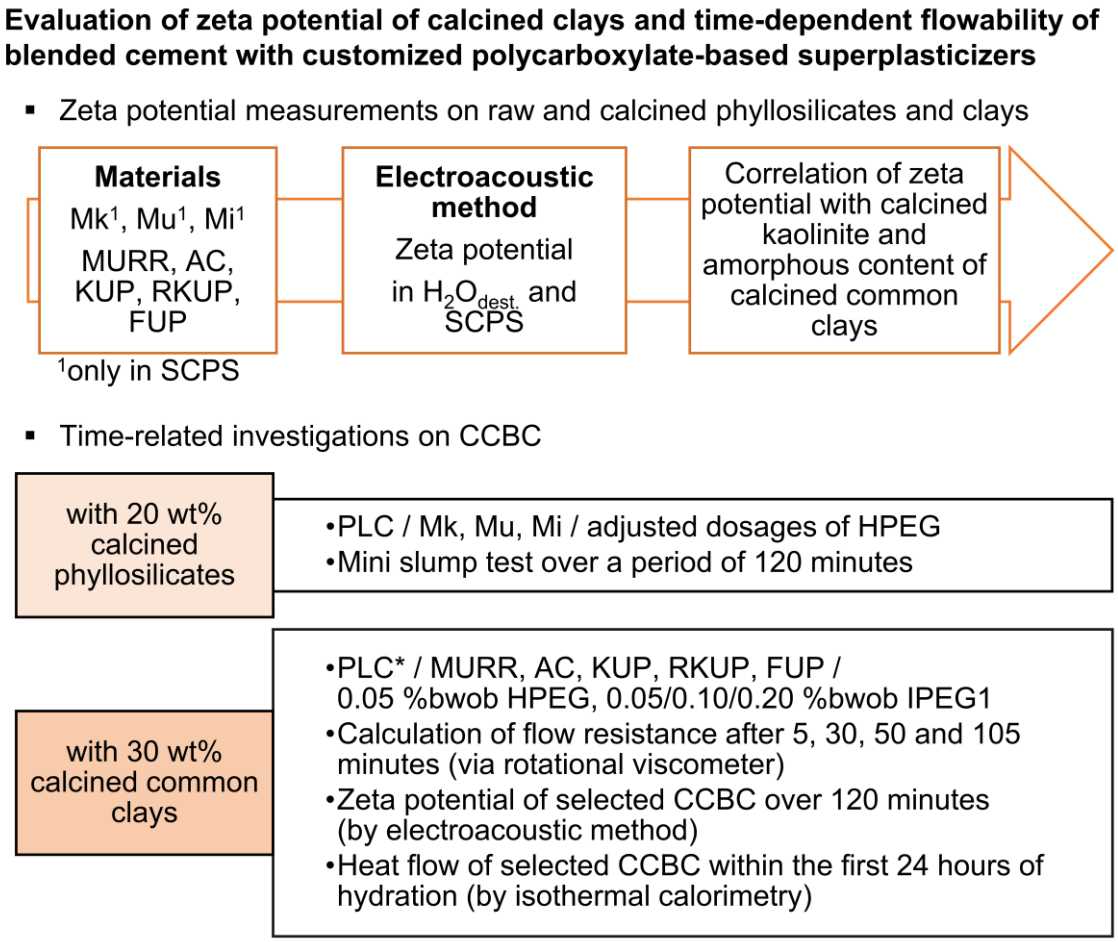

Figure 4-4. Investigations on the zeta potential and time-related flow behavior of CCBC mixtures as published in the fourth journal paper

The first conference paper presents "*Lignosulfonates in cementitious systems blended with calcined clays"* (chapter 7.5). The demand for Mg- and Na-LS is compared between different replacement levels and two calcined clays (Figure 4-5). Further, the rheological and hydration behavior with the addition of lignosulfonates is evaluated.

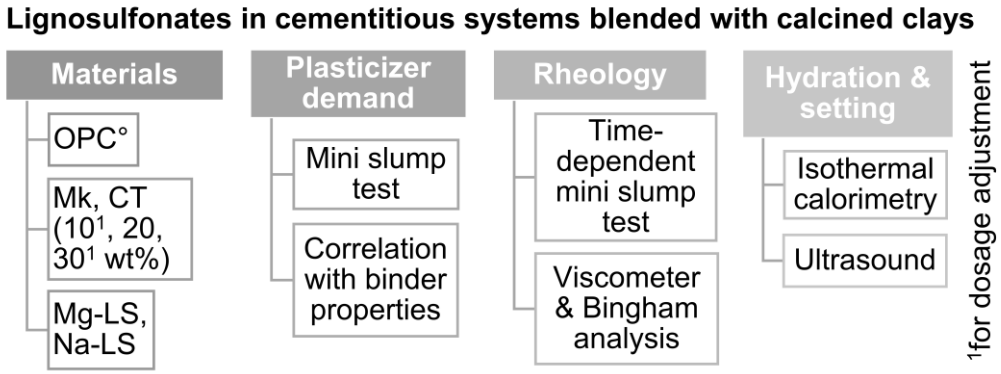

Figure 4-5. Methods and materials used to investigate the demand for lignosulfonates, rheology and early hydration in the first conference contribution

The rheological behavior of calcined clay blended cements, also with the addition of NSF and HPEG, is investigated immediately after water addition, as well as over a period of two hours (Figure 4-6). The results are published in the second conference paper *"An approach to the rheological behavior of cementitious systems blended with calcined clays and superplasticizers"* (chapter 7.6).

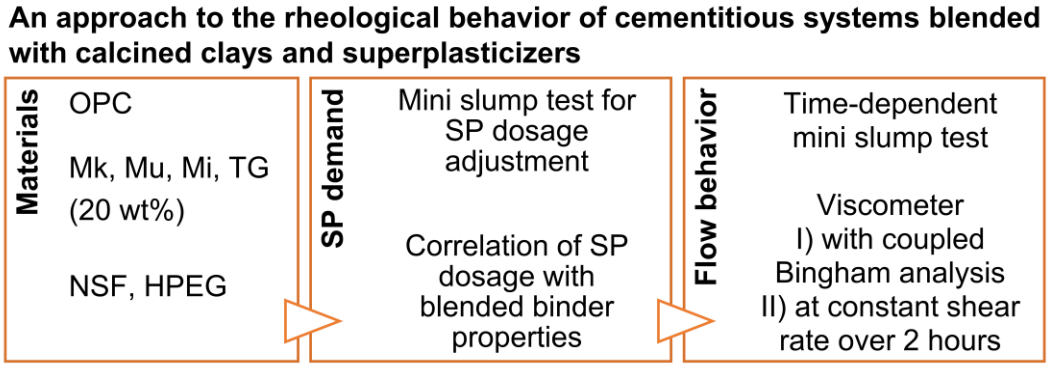

Figure 4-6. Methods and materials used to investigate the demand for NSF and HPEG, initial and time-related rheology in the second conference contribution

Further studies complement the third and fourth journal articles and are published in the third conference contribution *"Feasability study on PCE based superplasticizers in calcined clay blended cements with focus on the type of phyllosilicate"* (chapter 7.7). CCBC mixtures are dispersed with one dosage of IPEG1 and IPEG2 and the flow resistance, as well as the zeta potential, are evaluated over time. Parameters, both from physical as well as mineralogical point of view, that affect rapid slump loss are identified (Figure 4-7).

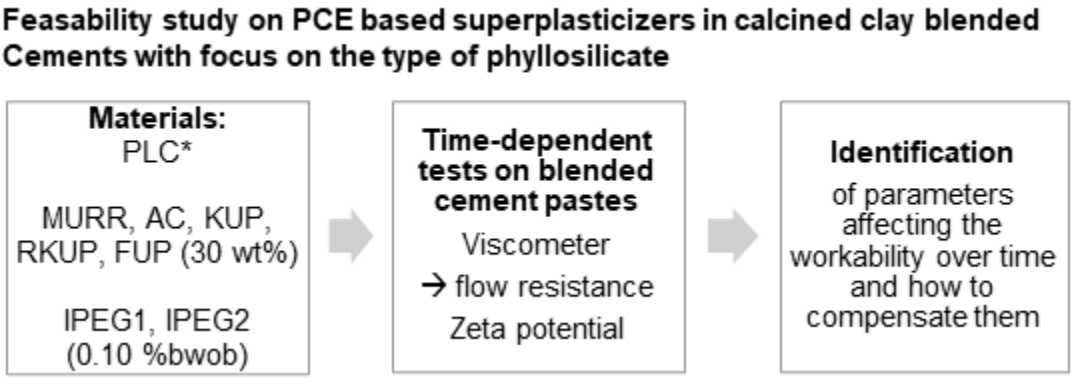

Figure 4-7. Methods and materials used to investigate the time-dependent flow behavior in the third conference contribution

The *"Early hydration behavior of blended cementitious systems containing calcined clays and superplasticizer"* is published in the fourth conference paper in chapter 7.8. It addresses especially the question how adjusted dosages of NSF and HPEG affect the early hydration kinetics of calcined clay blends, observed by isothermal calorimetry and in situ XRD (Figure 4-8).

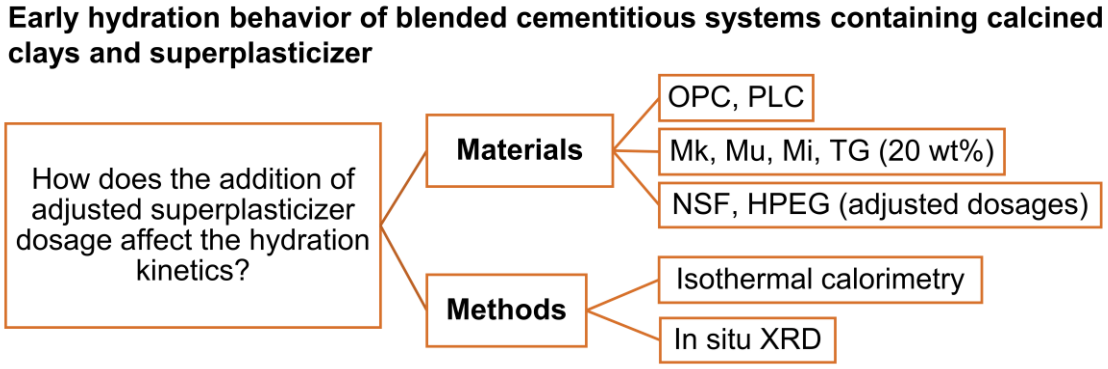

Figure 4-8. Methods and materials used to investigate the early hydration of calcined clay blended cements with superplasticizers in the fourth conference paper

5 Main findings

5.1 Influence of calcined clay characteristics on the rheology and parameters that affect the superplasticizer performance

This chapter first summarizes the main findings regarding the rheological behavior of calcined clay suspensions and CCBC mixtures with different replacement levels, and how it affects the performance of superplasticizers in CCBC mixtures (subchapter 5.1.1).

The following subchapter 5.1.2 discusses the influence of physical and mineralogical parameters of metaphyllosilicates, calcined common clays and CCBCs on the rheological behavior and superplasticizer performance. It considers their particle size, total surface area, zeta potential and water demand as physical parameters and presents them in the context of the various mineralogical compositions of clays.

The chapter concludes with focus on the superplasticizers used and answers the questions, how different superplasticizers, in particular various types of PCEs, interact with CCBC mixtures (subchapter 5.1.3).

5.1.1 Rheological behavior of calcined clay suspensions and cement pastes and the initial efficiency of superplasticizers in CCBC mixtures

The flowability of calcined clay suspensions has been investigated in the first journal paper via mini slump test and rheometer measurements with coupled Bingham analysis. Metaillite (Mi) had the lowest flowability, followed by metakaolin (Mk), metamuscovite (Mu) and the calcined Amaltheen clay (TG). The Mu exhibits a special behavior as it has negative yield stress, which results from very high torque values at high rotational speeds that lead to a low y-intercept with the linear Bingham fit. Furthermore, Mu has a significantly higher viscosity compared to other samples (Mu >> Mi > Mk > TG). The viscosity factors of clinker-free suspensions correlate well with those of CCBC mixtures that contain the respective calcined clay (R^2 = 0.94, 20 wt% replacement level). However, the negative yield stress of clinker-free Mu suspensions does not fit with an extremely high, positive yield stress of OPC/PLC with Mu. As known for plain cement, viscosity and yield stress, respectively flow resistance, decrease with higher w/b for CCBC mixtures. This was found, for instance, for PLC*_30KUP with w/b = 0.40 (Table A-30) and w/b = 0.50 (Table A-34).

The grey area in Figure 5-1 represents the range of all plain cement pastes with w/b = 0.50 (OPC, PLC, PLC*). In terms of viscosity, mixtures with low replacement levels of TG and Mk mixtures as well as with quartz powder (QP), 30 wt% AC and MURR are within or even below this range.

The other mixtures can exceed this viscosity significantly as shown in the first and third journal papers and as in accordance with literature [74, 275]. **Especially the increased viscosity of mixtures with metamuscovite has to be mentioned, as already the addition of 5 wt% exceeds the viscosity factor of mixtures with most of 30 wt% calcined common clays.** In addition, the mixtures with ≥ 10wt % metamuscovite have a high divergence in viscosity between the OPC and PLC cement mixtures, while the influence of cement is minor in other mixtures.

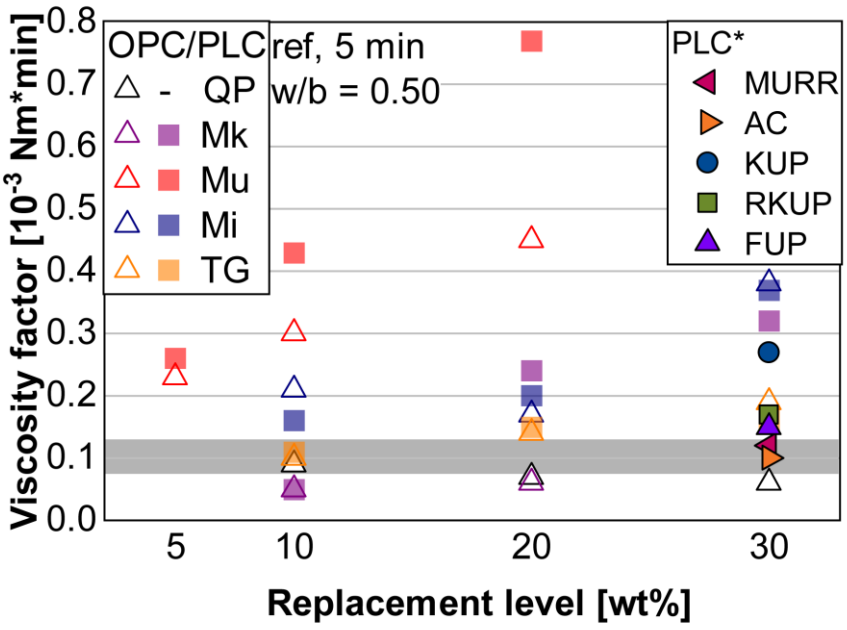

Figure 5-1. Viscosity factors of reference samples at w/b = 0.50 depending on replacement level (grey area indicates range of viscosity factors of plain cement)

Earlier findings in literature [65, 78, 120] have described dilatant flow behavior for metakaolin blended cement paste, a behavior that concludes zero yield stress when using the term “dilatant” correctly. In the present investigations, however, **all reference mixtures show either a linear or non-linear increase in torque with increasing rotational speed and a positive yield stress**. CCBC mixtures show a higher yield stress compared to plain cement, as published by several authors, e.g. [30-32, 91]. Those mixtures that show a non-linear increase in torque have been described as Herschel-Bulkley fluids, following the Power law equation and exhibiting positive yield stress. When considering the median torque values at the respective rotational speeds as data points of interest, the Herschel-Bulkley fits exhibit R^2 values of ≥ 0.99. Herschel-Bulkley fits lead in general to higher yield stress values compared to the Bingham fit, and to a flow index $n > 1$, a trend that has been mathematically described for shear-thickening materials e.g. by Feys et al. [276].

The comparison of the different rheological models is found in Appendix A5: Comparison of linear Bingham fits with modified Bingham and Herschel-Bulkley fits applied to CCBC pastes. Based upon this analysis, either **Bingham or Herschel-Bulkley models are suitable for most CCBC mixtures**, where the modified Bingham model and Herschel-Bulkley model are proposed for non-linear flow curves.

The flow resistance does not take the specific rotational speed-related behavior into account. However, it is a good opportunity to evaluate overall the flowability of the CCBC mixtures and to correlate it with binder properties as shown e.g. by Vikan et al. [270]. Beside of PLC_Mk, the **increase in flow resistance is found to be almost linear with increasing replacement level**, as shown in Figure 5-2. At the same time, it is significantly higher for mixtures with individual metaphyllosilicates than for those with calcined common clays.

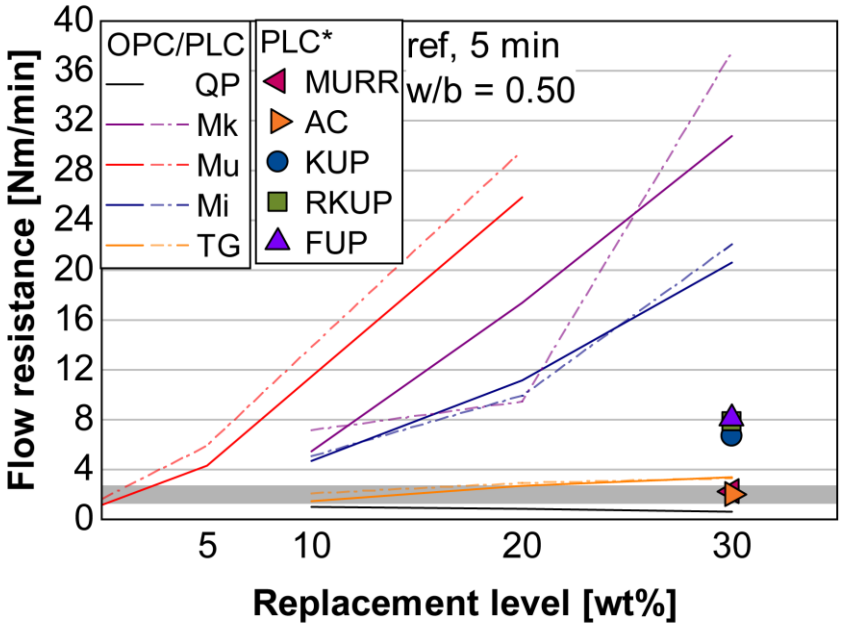

Figure 5-2. Flow resistance of reference samples at w/b = 0.50 depending on replacement level (dashed lines represent PLC samples, dots represent PLC* samples, grey area indicates range of flow resistance of plain cement)

With the amount of superplasticizer added for a comparable mini slump, most of the mixtures identified as Herschel-Bulkley fluids turn into Bingham fluids. The superplasticizers added can reduce the yield stress significantly. Nonetheless, the mixtures with metaphyllosilicates require 3 to 7.5 times more superplasticizer than plain cement, with 20 wt% QP or calcined common clay TG due to their characteristics as described e.g. in the first journal paper and in the subchapter 5.1.2. These findings are also demonstrated by the efficiency of the superplasticizer that considers the relative reduction of yield stress factor, viscosity factor and torque related to the dosage added (Figure 5-3).

For a better comparison between the different CCBCs, further experiments are published with a **constant dosage of PCE** in the second journal paper. The efficiency of 0.20 %bwob PCE is similar for plain cement and CCBC with TG (Figure 5-3). The small difference between these mixtures and the metakaolin mixture shows that a higher efficiency cannot be achieved, as a further reduction of the rheological parameters is impossible. The efficiency decreases with Mk > Mu > Mi. This effect does hold for both PCEs and with both cements used. Again, most of the mixtures with metamuscovite behave in a different manner compared to the other CCBC mixtures. They have negative yield stress factors and a non-linear increase of torque with increasing rotational speed that indicates shear-thickening behavior with both NSF and PCEs. In case of PCEs, Schmid et al. [80] related this phenomenon to the side chain length of PCEs that leads to a higher steric effect. This, however, is contrary to the current findings as HPEG has a significantly shorter side chain length than amphMPEG that leads at least with PLC to Herschel-Bulkley flow behavior. With the observations made with the pure metamuscovite by Neißer-Deiters et al. [16] and related to the high water demand of metamuscovite (mixtures), it rather seems that the superplasticizers used cannot overcome the strong water uptake and as consequence the thixotropy and shear-thickening effect of metamuscovite. This is in agreement with [80], where a higher w/b eliminates the shear-thickening behavior of metamuscovite mixtures. Based on these findings, the efficiency of superplasticizers is lower with calcined 2:1 phyllosilicates than with the calcined 1:1 phyllosilicate metakaolin.

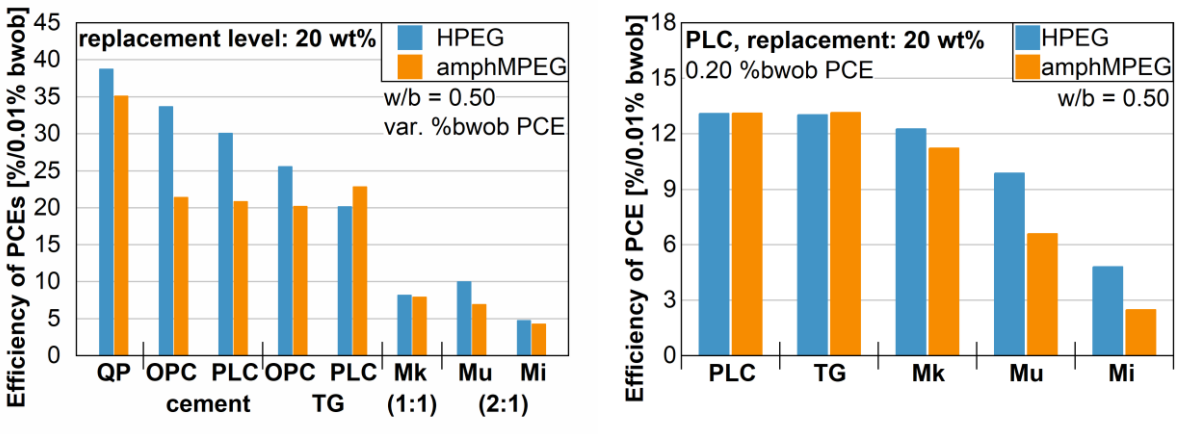

Figure 5-3. Efficiency of superplasticizers (SP) according to the binder system with 20 wt% replacement level at w/b = 0.50; left: with varying PCE dosage for a constant spread, right: with 0.20 %bwob PCE (note the different y-axis)

With the open question why TG exhibits significantly less critical rheological properties and superplasticizer demand, further calcined common clays have been investigated in PLC mixtures. The reference mixtures are divided into Bingham fluids and Herschel-Bulkley fluids, as published in the third journal paper. HPEG, IPEG1 and IPEG2 are added to these mixtures at different constant dosages (0.05, 0.10 and 0.20 %bwob).

While the mixtures classified as Bingham fluids require 0.10 %bwob only to become Newtonian fluids, the Herschel-Bulkley fluids require at least 0.20 %bwob PCE. Overall, the efficiency of PCE decreases with higher dosage / material effort necessary for an adequate dispersion. Figure 5-4 shows that the range of efficiency in mixtures with 30 wt% calcined common clays is between 13 and 32 % at low PCE dosage, which indicates that a) the different PCEs used perform differently and b) the efficiency depends to a large extent on the calcined common clay. The same holds for the constant dosage of 0.20 %bwob used for the dispersion of CCBC with 20 wt% metaphyllosilicates.

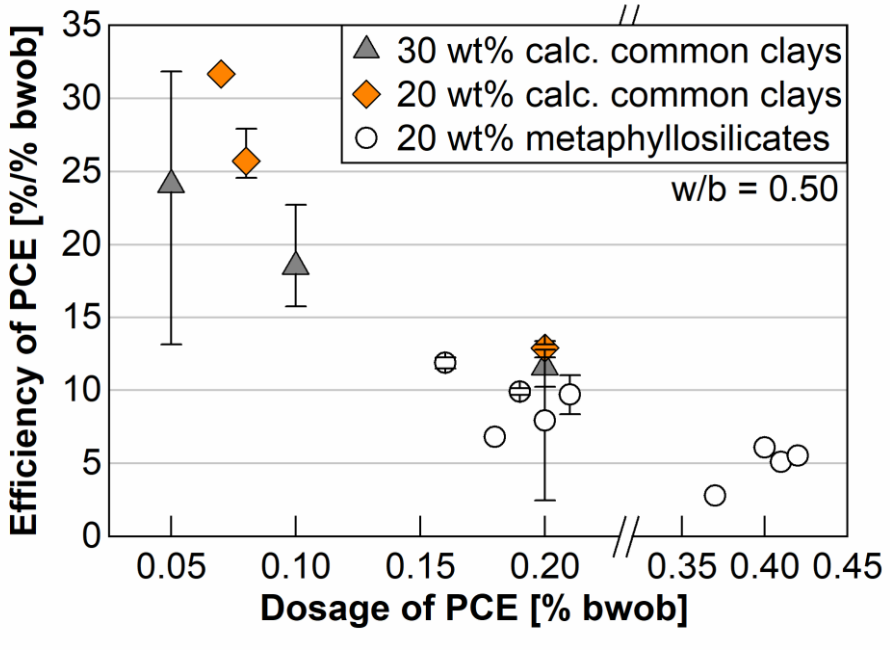

Figure 5-4. Correlation of dosage of PCEs with their efficiency, regardless of type of PCE; mixtures with 20 wt% metaphyllosilicates (n = 23) and calcined common clays (n = 8) are taken from the first and second journal paper, mixtures with 30 wt% calcined common clays (n = 33) from the third journal paper

Figure 5-5 reveals a very good, linear correlation between the efficiency of different PCEs and the reduction in flow resistance (R^2 = 0.945). The data points are provided in Appendix A4: Calculated efficiency of superplasticizers. In detail, the figure considers the CCBC mixtures with varying dosages and an adequate dispersion based on mini slump test from the first journal paper and the CCBC mixtures with 0.20 %bwob PCE from the second journal paper. Furthermore, the CCBC mixtures from the third journal paper are classified according to their achieved flow resistance with PCE in comparison with the flow resistance of plain cement without any PCE. The white symbols stand for mixtures where cement has been replaced by 20 wt% metaphyllosilicates. They confirm that the performance of PCEs is significantly poorer in these CCBC mixtures, with an efficiency mostly below 10 %/0.01% bwob and Red_{FR} ≤ 5 %/0.01% bwob, compared to those with calcined common clays.

In combination with their pozzolanic activity [34, 264, 277], this expresses the better suitability of calcined common clays or shales for their application as SCM, especially at higher replacement levels. However, the results on the initial superplasticizer performance confirm also that the CCBC mixtures require different dosages of superplasticizer to achieve similar flow properties as the original flow properties can vary significantly. The efficiency for an adequate dispersion ranges widely between 10 % and 32 %/0.01%bwob, depending on the calcined common clay added. The range for efficiency (10 - 15 %/0.01%bwob) and Red_{FR} values (4 - 5 %/0.01%bwob) becomes smaller with increasing amount of superplasticizer, indicating a saturation effect.

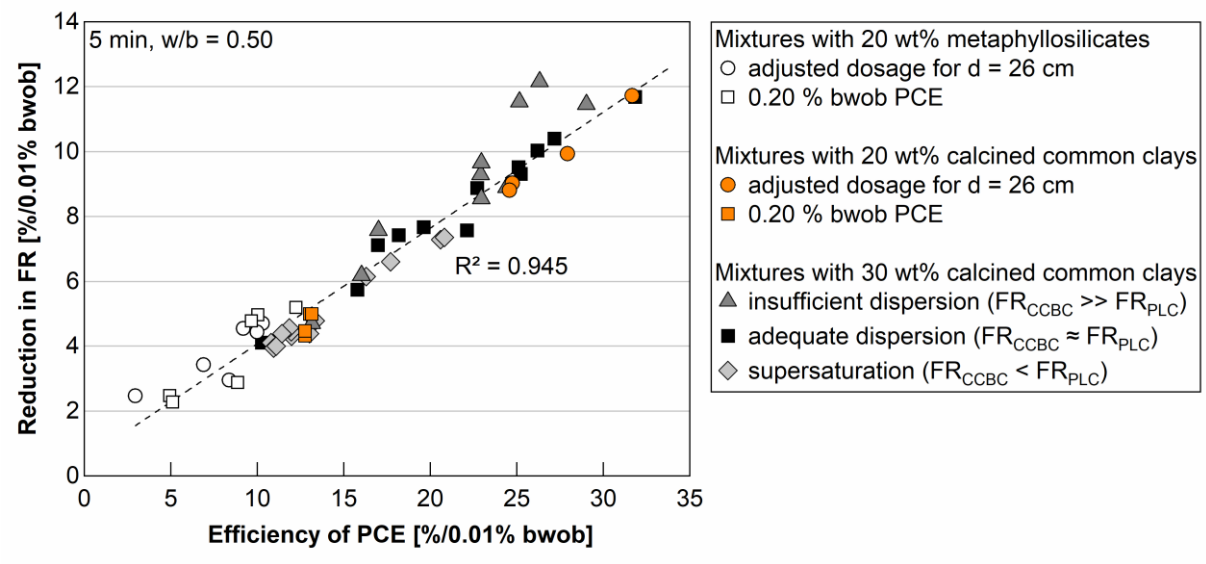

Figure 5-5. Comparison of reduction in flow resistance (FR) and efficiency of PCEs, both related to the superplasticizer dosage used [%/0.01 %bwob] (n = 58)

The investigations show that viscosity, yield stress and flow resistance increase significantly with the addition of calcined clays and strongly depend on the replacement level and type of added material, which is in line with the literature [64, 278]. The yield stress and flow resistance decreases in the following order: OPC/PLC_Mu >> OPC/PLC_Mk > OPC/PLC_Mi >> mixtures with calcined common clays > OPC/PLC > OPC_QP. In terms of rheological models, most of the CCBC mixtures show either Bingham or Herschel-Bulkley fluid behavior. It is concluded that the results derived from metaphyllosilicates are not directly transferable to calcined common clays with complex mineralogical compositions, as the behavior differs significantly even with a comparable quantity of phyllosilicates present in the cementitious system. The observed phenomena will be discussed in the following chapter 5.1.2, that takes the physical parameters as well as the mineralogical composition of (calcined) phyllosilicates and clays into account.

5.1.2 Physical and mineralogical parameters of calcined clays affecting the rheological properties and demand for superplasticizer of cementitious systems

The correlation between chemical and physical properties and the flowability of clinker-free suspensions is discussed in the first journal paper. The discussion on the rheological parameters of CCBC mixtures is limited to the flow resistance, as the trend in yield stress and flow resistance is overall congruent. The used OPC and PLC originate from the same cement plant and have a similar C_3A-to-C_4AF ratio, a factor that affects the adsorption behavior (see chapter 2.2.2). Although limestone filler is known to enhance the workability [279, 280], PLC mixtures require slightly more superplasticizer due to a larger SSA, a finer particle size distribution and 25 % higher content of sulfates that can cause competitive adsorption onto C_3A [161, 281]. The zeta potential of PLC paste has been slightly more negative compared to that of OPC, which results in a lower adsorption of anionic superplasticizers [152].

Figure 5-6 shows that a smaller **particle size** of the calcined clay ($d_{50,CC}$) can, but not necessarily does increase the flow resistance. Even with a comparable particle size distribution of calcined clay and cement, the flow resistance increases with calcined clay. It is observed in the third journal paper, that the flow resistance of mixtures with calcined common clays rises with smaller particle size, resulting in a higher demand for superplasticizer. Therefore, the shape and agglomeration effects are considered in the third journal paper as well.

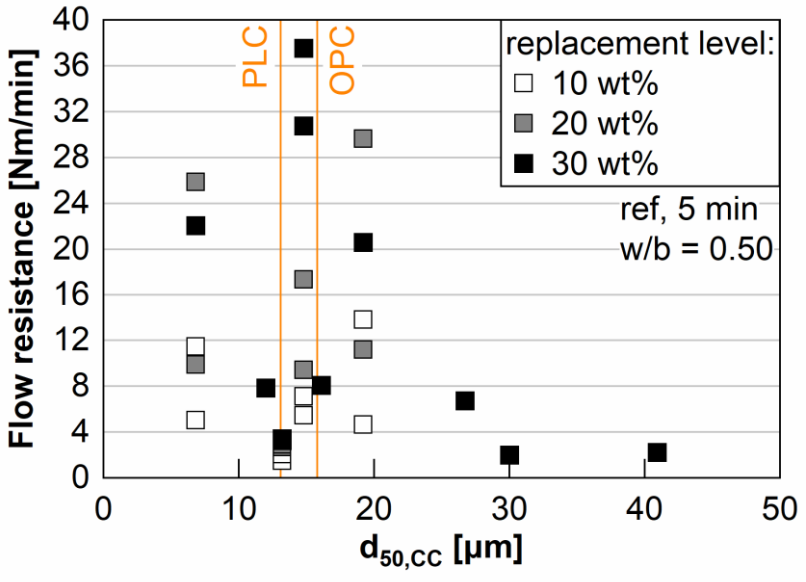

Figure 5-6. Correlation of initial flow resistance with the median particle size of calcined clay ($_{d50,CC}$) with d_{50} values of OPC/PLC marked as orange lines (FR_{OPC} = 1.18 Nm/min, FR_{PLC} = 1.63 Nm/min)

A further reason for the discrepancy in flow resistance between plain cement and CCBC mixtures is the SSA of the materials. The **total surface area** of the binder components (TSA_{binder}), as e.g. proposed by Bentz et al. [282], considers the product of particle density and SSA for both cement and calcined clay and takes the replacement level into account at the same time. Figure 5-7 (left) shows a split trend in flow resistance with increasing TSA: I) linear increase for selected samples with increasing TSA between 20 and 80 m²/cm³ and II) an allometric increase for TSA ≤ 20 m²/cm³, as enlarged in Figure 5-7 (right).

The results show that the TSA is neither a reliable indicator for the prediction of flow resistance, when using it as single parameter, but it correlates overall well with the demand of CCBC mixtures for superplasticizers (Figure 5-10a). A large SSA or TSA leads to an increased demand for superplasticizer due to the increase of original flow resistance. Both, particle size and SSA, as factor of the TSA, depend on the mineralogical composition of raw clay.

Due to their layered structure and increased inner porosity, typical BET SSA values are

- 10 – 20 m²/g for kaolinite [12-14],
- 2 – 14 m²/g for muscovite [8, 16],
- 65 – 100 m²/g for illite [17, p. 64] and
- 61 to even up to 330 m²/g for smectite [18, 19].

With increasing calcination temperature, the SSA decreases significantly for 2:1 phyllosilicates, while it remains rather constant for kaolinite [18, 31, 32]. Quartz, as a non-negligible component in common clays, exhibits usually a lower SSA than cement [283].

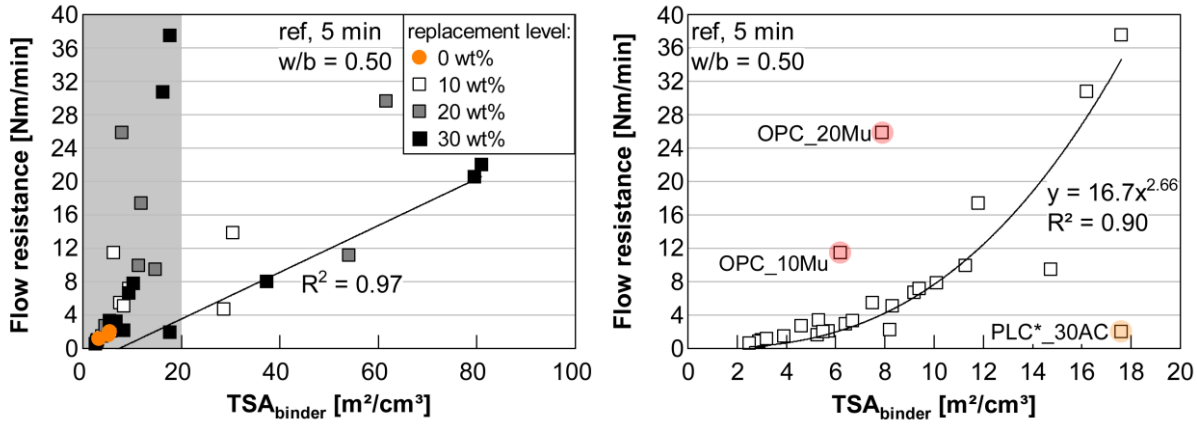

Figure 5-7. Correlation of initial flow resistance the total surface area of the binder (TSA_{binder}); mixtures with TSA_{binder} < 20 m²/cm³ are enlarged on the right (regardless of replacement level; OPC_10/20Mu and PLC*_30AC are excluded for fit)

The calcined common clay AC and pure metakaolin (Mk) have both a similar SSA of 17.2 and 17.8 m²/g, respectively. OPC/PLC_30Mk show a significantly higher flow resistance than PLC*_30AC, which is related to the more **negative zeta potential** of Mk compared to AC. The correlation of zeta potential of metaphyllosilicates and calcined common clays in SCPS with the flow resistance of the respective CCBC mixture (Figure 5-8) shows that a more negative zeta potential value goes along with a higher flow resistance. Metamuscovite mixtures fall once more out of line as the flow resistance is rather high despite of the low zeta potential. The low zeta potential in turn explains beside of the small TSA the low amount of PCEs required for a comparable mini slump value (Figure 5-10b). So far, there has been only few information available on the surface chemistry of phyllosilicates and common clays after thermal activation (dehydroxylation). The first and fourth journal papers give therefore an insight into this complex topic. In distilled water, deprotonation is favored for siloxane groups compared to Al- or Mg-groups, which leads to a stronger, negative zeta potential for metamuscovite than for metakaolin. In alkaline media and with the option to adsorb cations [166, 258, 261], e.g. from SCPS, the zeta potential of metamuscovite turns less negative and exhibits the smallest, negative zeta potential of the metaphases (Figure 5-8).

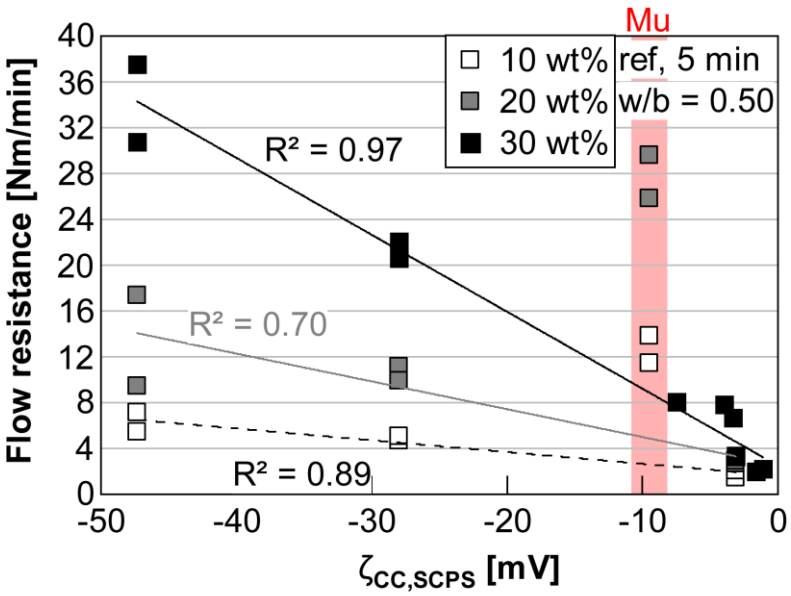

Figure 5-8. Correlation of initial flow resistance of (blended) cement paste with the zeta potential (ζ) of respective calcined clay in SCPS (Mu samples are neglected for R²)

This confirms recent findings of Schmid and Plank [261] who further found that metamuscovite takes up large amounts of Ca^{2+}, leading to high positive zeta potential and good adsorption of PCEs. The study on calcined common clays in the fourth journal paper shows that rather the (calcined) kaolinite content than the total amount of amorphous phase (phyllosilicates) of calcined common clay has an influence on the zeta potential and pH value.

In combination with positively charged sites from aluminate clinker and hydrate phases [152], it increases the flocculation and shear stress, and as consequence the flow resistance or yield stress. Up to now, it is not fully understood, why **the common clays with complex compositions exhibit very small zeta potential values in distilled water and SCPS, although the individual phases themselves have a partially very pronounced negative zeta potential**, see also the zeta potential of quartz and calcite in [166, 284]. Based upon recent publications [258, 285, 286], the adsorption tendency in alkaline environment is assumed to play a key role in combination with the mineralogical composition and SSA.

Figure 5-9 shows a good, linear correlation ($R^2 = 0.80$) of **water demand** of the binder with the initial flow resistance, although the flow resistance does not follow a linear trend for mixtures with water demand < 33 wt%. Especially the high viscosity and the flow resistance of CCBC mixtures with metamuscovite both result from its high water demand that has been observed for untreated (raw) muscovite compared to illite [21] and has been a topic in earlier publications [16, 80, 287]. Among the calcined common clays investigated, KUP with the highest quantity of muscovite in raw clay has one of the highest water demands as well. The higher water demand leads as consequence to a higher demand for NSF (Figure 5-10c) and for lignosulfonates, as published in the first conference paper. In terms of demand for PCEs and their adsorption behavior, however, the zeta potential is the decisive parameter.

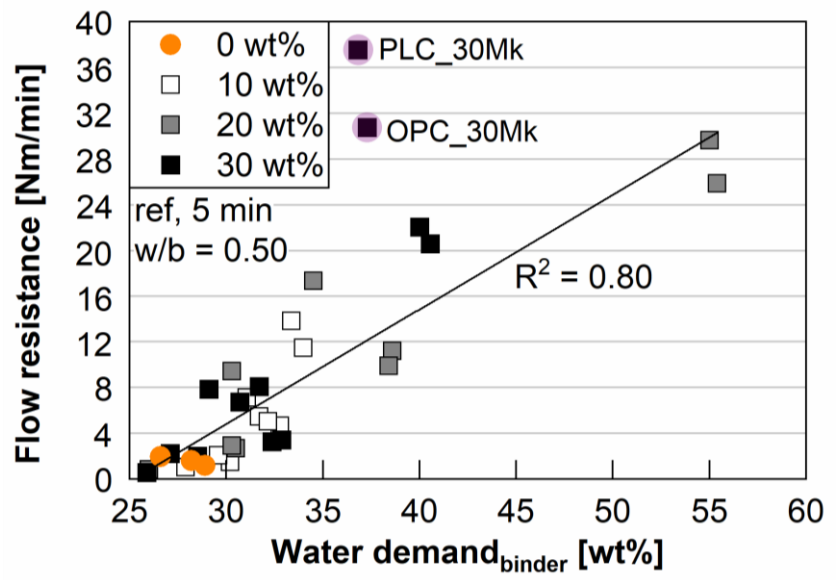

Figure 5-9. Correlation of initial flow resistance of (blended) cement paste with water demand of binder (OPC/PLC_30Mk are neglected for R^2)

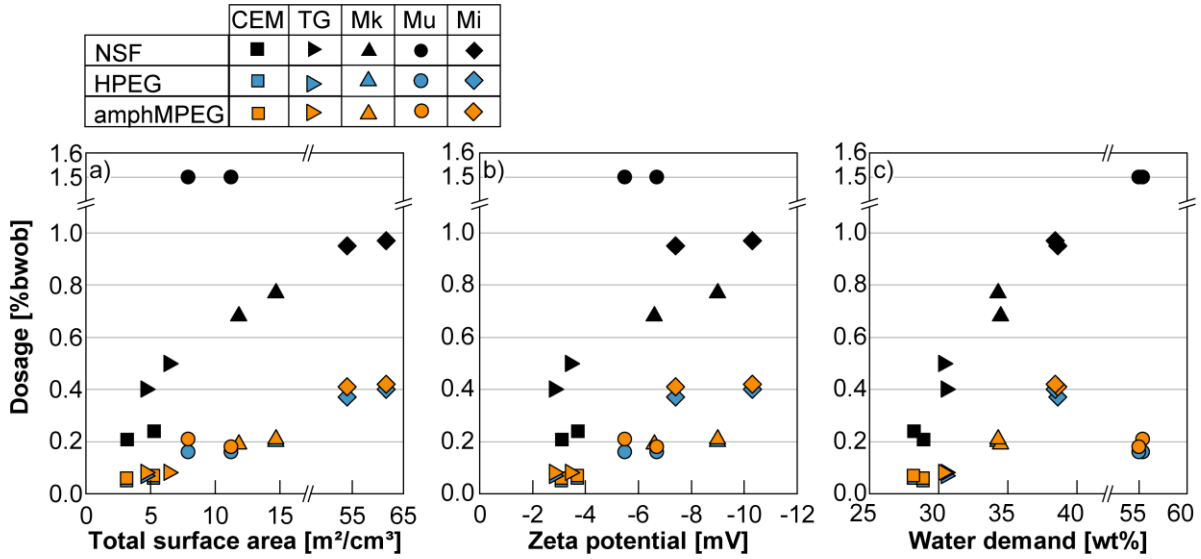

Figure 5-10. Correlations of a) total surface area of blended binder as well as of b) zeta potential and c) water demand of blended cement pastes with the superplasticizer dosages required for a constant spread of 26 ± 0.5 cm

A closer look at the mineralogical composition of common clays in Figure 5-11, however, shows again that it is not as trivial as it may seem to relate the flow resistance and demand for superplasticizer to one single parameter, e.g. the kaolinite content.

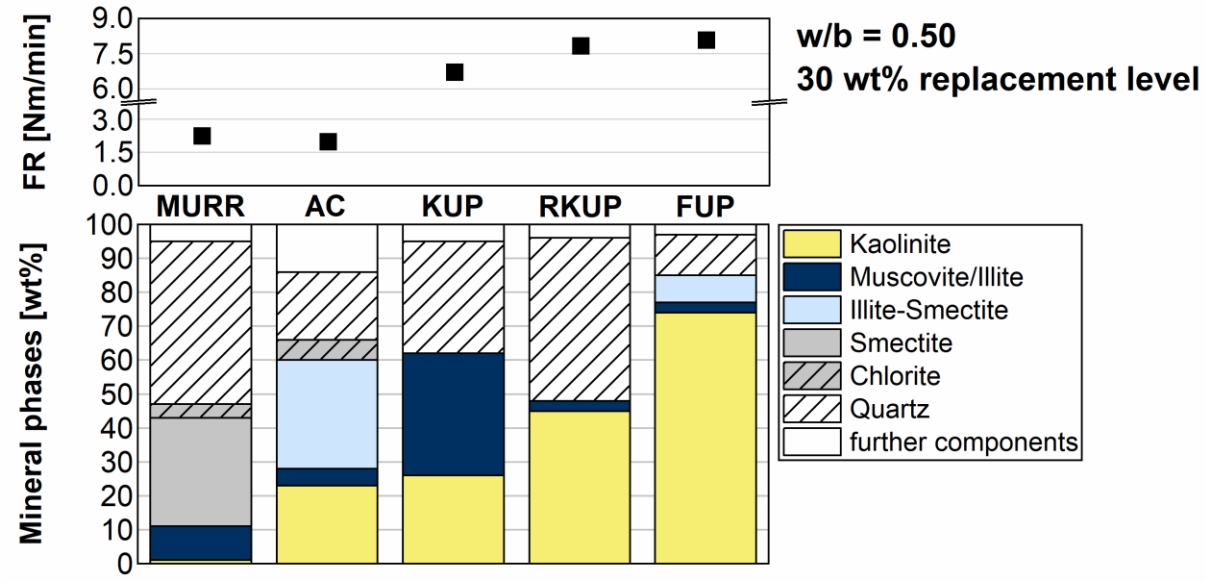

Figure 5-11. Comparison of the mineralogical composition of raw clays with initial flow resistance of blended cement paste at 30 wt% replacement level and w/b = 0.50

The following examples show the complexity of this topic, where **a consideration of several physical and mineralogical properties is crucial**. Details are presented in the third and fourth journal papers.

- AC and KUP have a comparable amount of kaolinite and AC has a significantly higher SSA. Nonetheless the flow resistance of PLC_30KUP is remarkable higher due to a **finer particle size distribution** and the **high water demand** of KUP stemming from its **high muscovite content**. Illite-smectite interstratifications do not increase the flow resistance instead.
- This shows also the comparison of smectitic MURR with kaolinite-rich RKUP as both clays contain a large amount of quartz and PLC_30MURR has a significantly lower flow resistance than PLC_30RKUP. Quartz itself is seen as flow-enhancing, as published in the first journal paper, but it can also enhance the grindability due to deagglomerating effects [288, 289]. This in turn can decrease the flowability again. The particle size distribution of RKUP particles is significantly finer than of MURR, indicating a poorer grindability or higher agglomeration tendency of the latter. This might originate from a lower dehydroxylation degree [277] as 2:1 phyllosilcates require higher temperatures than kaolinite. The low **zeta potential** of MURR results from the negligible amount of kaolinite present, whereas **kaolinite** is the main phase in RKUP beside of quartz. This leads – in combination with the **finer particle size** - to a remarkable higher flow resistance due to increased flocculation.
- The influence of particle size explains the minor difference of PLC_30RKUP and PLC_30FUP. RKUP and FUP are both considered as kaolinite-rich clays, where FUP contains even ~ 30 wt% more kaolinite in raw clay. The increase in flow resistance is less than expected from the higher zeta potential, SSA and water demand of FUP. RKUP however, has a **higher volumetric percentage of fine particles** < 10 µm compared to FUP, which in turn increases the flow resistance in a more pronounced way.

The results show that parameters of mixtures with pure mineral phases are not directly transferable to mixtures with calcined common clays. Nonetheless, the mineral phases present in the respective common clay do influence to a large extent the physical properties of the calcined clays and the binders, as well as the flow properties and demand for superplasticizers as consequence. Table 5-1 summarizes these observed effects of mineral phases, primarily on physical effects and secondary on flow resistance and viscosity. Overall, the results confirm that it is crucial to consider both the physical properties of a (calcined) clay as well as its mineralogical composition. In terms of the phyllosilicates present in raw clay, it is obligatory to distinguish not only between 1:1 and 2:1(:1) phyllosilicates, but also within the group of 2:1 phyllosilicates itself.

In terms of physical parameters, the particle shape (low circularity) and the strongly negative zeta potential are identified as challenging properties beside of commonly addressed parameters, like a large SSA, a high water demand and a fine particle size.

Table 5-1. Overview of mineral phases present in common clays, their main impact on calcined clay properties and as secondary effect on the rheological properties of CCBC mixtures

Mineral phase in raw clay	Impact on …		
	Physical properties of calcined clay and binder	Flow resistance / yield stress	Viscosity
Kaolinite	↑ water demand, ↑ zeta potential	↑↑	↑
Muscovite/ Muscovite/illite	↑↑ water demand	↑↑	↑↑
Illite-smectite/ smectite	↑ water demand, SSA ↓ particle fineness due to agglomeration	↑	↑
Calcite	↓ SSA-to-phyllosilicate ratio due to formation of glass phase (only when present in sufficient quantity; theory based on [290])	↓	-
Quartz	↓ water demand, ↓ SSA	↓	-
	↑ particle fineness due to de-agglomeration	↑	

The transferability from metaphyllosilicates to calcined common clays is limited due to the strongly differing physical properties. This is the reason why the findings in the third journal paper are contrary to earlier findings with pure metaphyllosilicates: the **demand for superplasticizer increases not only with finer particle size, but also with higher amount of kaolinite in raw clay**, which is in agreement with the findings of Ferreiro et al. [79]. This stems in general from the initial flow resistance of the reference mixtures. However, a significant reduction in shear stress (and hence in flow resistance) occurs with the addition of PCE that demonstrates the good interaction of PCEs with calcined kaolinite-rich clays. High amounts of **quartz can increase the efficiency of superplasticizer**.

In terms of 2:1 phyllosilicates, a further differentiation is obligatory:

- Pure illite, as observed in the investigations with metaillite, exhibits a large SSA and strong negative zeta potential, which both are critical for the workability of CCBC mixtures and superplasticizer adsorption. In common clays, however, illite barely occurs as pure phase and rather in illite/smectite interstratifications. Based on the present investigations, a low ratio of illite to smectite is assumed to limit the influence on workability of CCBC mixtures.
- Despite its challenging behavior in other applications, **smectite is an uncritical component after calcination** when it comes to the fresh properties of CCBC mixtures, regardless if present as pure or as illite-smectite interstratification in the raw clay. They do not only lead to a comparable low flow resistance of CCBC mixtures, even at high percentages present in raw clay, but do also interact well with the PCEs investigated.
- **Muscovite** does not only increase the flow resistance significantly but, in addition, **does perturb the effectiveness of superplasticizers** as shown for the mixtures with metamuscovite and the calcined common clay KUP. Among the phases studied, it is identified as the sole challenging phase for conventional superplasticizers with a high sensitivity towards the superplasticizer type and properties.

5.1.3 Influence of type and dosage of superplasticizer on its initial performance in CCBC mixtures

Beside of the properties of calcined clays, it is crucial to investigate the impact of type and dosage of superplasticizer polymers. The first conference paper reveals that it requires up to 5.5 times more lignosulfonate-based plasticizer in order to disperse the investigated CCBCs compared to plain cement. At the chosen w/b and replacement levels, the required dosage exceeds by far the dosage recommended by the supplier and affects the early hydration significantly (chapter 5.2.2). This reveals the **limited suitability of lignosulfonate-based plasticizers** and that the use of other, more efficient superplasticizers is required.

Compared to lignosulfonates, the dispersion of CCBCs is better with β-naphthalene sulfonate formaldehyde polycondensate NSF, which is in agreement with literature [172, p. 148]. Findings by Björnström et al. [188] show that the zeta potential of cement paste turns more negative with naphthalene-based polycondensate than with lignosulfonates, resulting in a better dispersion by higher electrostatic repulsion. This is of special interest as the zeta potential of calcined kaolinite-rich clays is strongly negative in alkaline media and might be beneficial, if dispersion via electrostatic repulsion is aimed. Mixtures with metaillite and metamuscovite demonstrate an increased demand as NSF needs to overcome the large TSA and high water demand of CCBCs with these 2:1 phyllosilicates (Figure 5-12). Especially **in the presence of metamuscovite, a dispersion is impossible with reasonable dosages of NSF**.

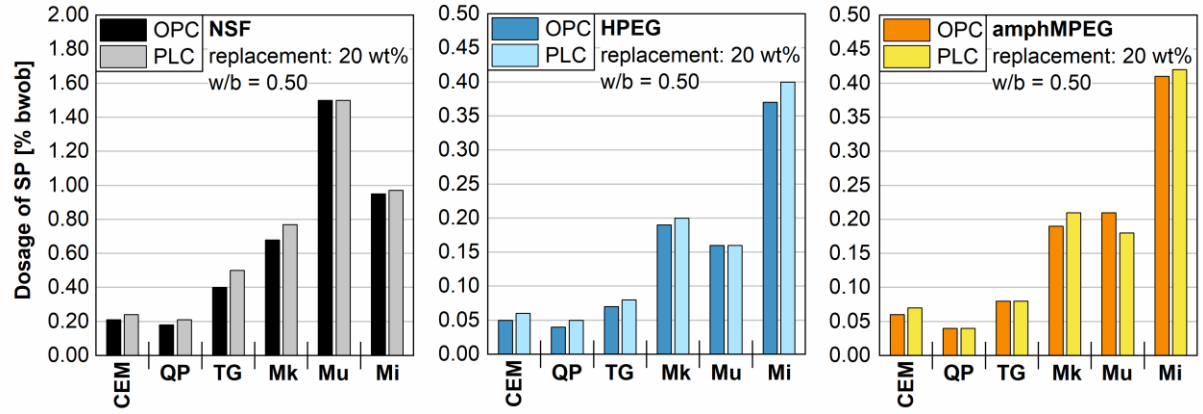

Figure 5-12. Required superplasticizer dosages for cement pastes (except for QP, the information was provided within the joint research project by the Chair of Construction Chemical, Technical University Munich)

Polycarboxylate-ether based superplasticizers (PCEs) show a significantly better dispersion compared to NSF and lignosulfonates. For a similar dispersion, overall lower dosages of HPEG are required than of amphMPEG as found especially for the metamuscovite mixtures (Figure 5-12). Investigations with the same dosage of HPEG and amphMPEG indicate a better adsorption of HPEG as well, as presented in the second journal paper. According to the literature [213, 256], this is mainly related to the higher anionic charge density, at least calculated to their chemical structures, of HPEG compared to amphMPEG, although the latter possesses a cationic monomer (DADMAC). Recent findings by Li et al. [258] revealed an enhanced dispersion due to a cationic monomer (MAPTAC) by its adsorption onto negatively charged sites of calcined clays. Schmid et al. [225, 232] showed furthermore that a low amount of cationic monomer is beneficial and DADMAC, the cationic monomer present in amphMPEG, is more effective than MAPTAC or TMAEMC.

The dispersion efficiency is in the following order: Na-LS < Mg-LS < NSF << amphMPEG < HPEG. A wider range of efficiency is observed here with amphMPEG and HPEG, which reveals a large discrepancy between the addition of calcined common clays and metaphyllosilicates, as presented in the first journal paper. This results from both the differing properties of calcined clays and the rheological properties of CCBC mixtures.

The initial dispersion performance of HPEG is compared with two IPEG-based PCEs (IPEG1, IPEG2) in mixtures with calcined common clays in the third journal paper. HPEG has a similar efficiency (23 – 27 %/0.01%bwob PCE) regardless of the calcined common clay used, while the IPEG-based PCEs are more sensitive when it comes to the individual CCBCs. For the latter, the efficiency ranges between 13 – 26 %/0.01%bwob PCE (IPEG1) and 22 – 32 %/0.01%bwob PCE (IPEG2). This indicates a **less sensitivity of the HPEG-based PCE towards the properties of calcined common clays**.

Beside of their macromonomers and the HEMA in the anchorgroups of IPEG1, the PCEs differ in their molecular weight, side chain length and anionic charge density. There is no trend detectable depending on the molecular weight, as the initial dispersion performance of the IPEG-based PCEs, that have both a low molecular weight, differs in a remarkable way (Figure 5-13a). According to Schmid and Plank [257] an increasing side chain length leads to a better initial dispersion performance if further parameters (type of macromonomer, ratio of anchor group and macromonomer) remain the same. This holds to a certain extent for IPEG1 < IPEG2, while HPEG has a comparable efficiency despite a side chain length of n_{EO} = 66 (Figure 5-13b). A longer side chain can favor the initial dispersion performance but needs to be reconsidered in terms of slump loss prevention [136], which is topic in chapter 5.2.1. Further findings [257] showed that HPEG-based PCEs are the most effective ones, followed by MPEG-based and IPEG-based PCEs. IPEG-based PCEs, however, perform still extraordinarily well in CCBC mixtures [257]. This **positive interaction between IPEG-based PCEs and calcined common clays** is also observed for IPEG2 even though it possesses a rather short side chain length (n_{EO} = 31). Here – in comparison to HPEG - the superplasticizer efficiency increases with higher phyllosilicate content in raw clay as shown in the third journal paper. IPEG1 behaves initially very differently, which is related to the HEMA and its low anionic charge density [136, 220]. Figure 5-13c shows a efficiency range of 22 - 27 %/0.01 %bwob PCE for the majority of CCBC mixtures, where IPEG1 has the lowest anionic charge density and outliers towards lower efficiency (PLC_30RKUP and PLC_30KUP) and IPEG2 the highest anionic charge density and outliers towards higher efficiency (PLC_30AC and PLC_30FUP).

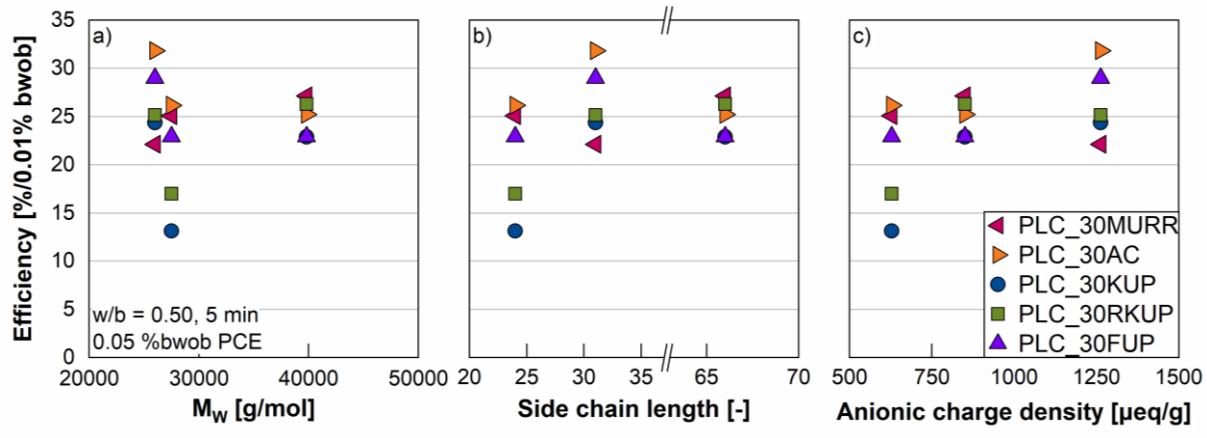

Figure 5-13. Trends in initial superplasticizer efficiency of PCEs in CCBC mixtures according to their molecular weight (M_w), side chain length and anionic charge density

Adding more polymer to the mixtures usually also leads to a higher amount of polymer adsorbed as adsorption isotherms show for instance in [144, 162, 257, 258]. The first three journal papers reveal this for CCBC mixtures as well, where the flow behavior and a saturation dosage are both dominated by the type of calcined clay added. Selected PLC examples demonstrate once more not only the differences between pure metaphyllosilicates (Figure 5-14, left) and calcined common clays (Figure 5-14, right), but also the significant impact of each individual calcined clay. Those with a high demand for superplasticizer have a significant further reduction in flow resistance with increasing dosage, while the impact of a higher dosage is marginal on those CCBC mixtures with low demand. This leads to an assimilated flow resistance for all mixtures (Figure 5-14, right) and to a lower efficiency as shown earlier in Figure 5-4 and the third journal paper.

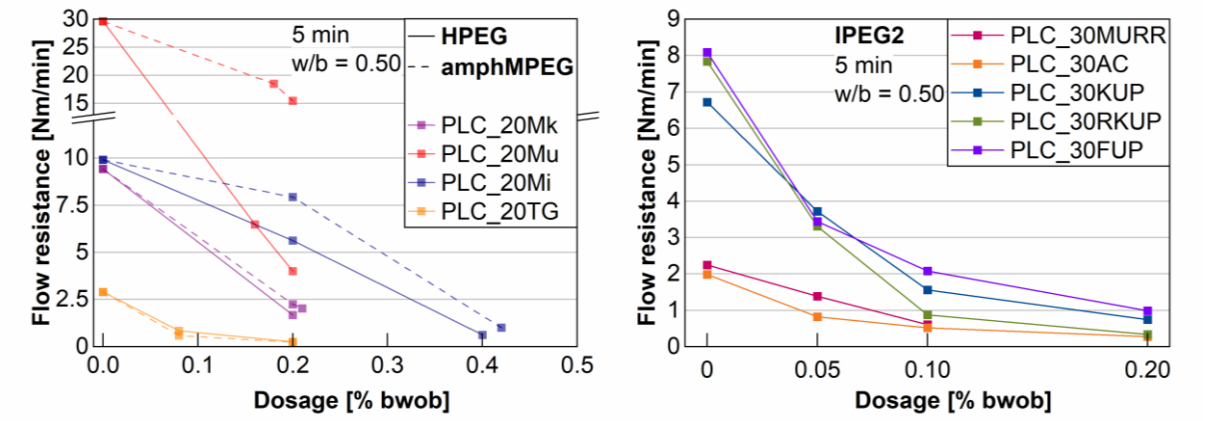

Figure 5-14. Flow resistance of PLC mixtures depending on selected CCBCs and dosage with HPEG and amphMPEG (left) and IPEG2 (right); the lines have no physical meaning but underline the effect of increasing dosage on flow resistance; note the different y-axis

It was found that PCEs work the best in terms of initial dispersion of CCBC mixtures, compared to LS and NSF as known for other cementitious systems [30,32,89]. The further differentiation between several PCEs shows that the initial dispersion performance increases with higher anionic charge density as also known for plain cement [213]. The combination of vinyloxybutyl-poly(ethylene glycol) ether-based (VOBPEG) and IPEG macromonomers in IPEG2, that exhibits the highest anionic charge density, enables an excellent initial dispersion of CCBC mixtures. The HPEG-based PCE shows only a small sensitivity towards the mineralogical composition of calcined clay. Especially muscovite-rich clays can be dispersed better with these two PCEs. All considered macromonomers (HPEG, MPEG, IPEG) lead to proper dispersion, even though the addition of more PCE is necessary for CCBC mixtures. This again is due to the challenging characteristics of calcined clays, such as a large SSA, high water demand and a strongly negative zeta potential. A final judgement is waived due to the different characteristics of each PCE, but overall the findings agree with recent literature [257].

5.2 Time-related flowability and early hydration behavior of CCBC mixtures with superplasticizers on paste level

Beside of the initial rheological behavior and dispersion performance, the behavior over time is of major interest for several applications. The subchapter 5.2.1 presents a brief summary of flow behavior of CCBC mixtures with lignosulfonates, NSF and PCEs within the first two hours after water addition. It discusses which characteristics of calcined clays do influence the slump behavior of CCBC pastes and the mechanism of subsequent dispersion by a PCE with hydroxyethyl methacrylate in its anchor group. The influence of superplasticizers on the early hydration behavior of CCBC pastes is summarized in subchapter 5.2.2.

5.2.1 Facing rapid slump loss in CCBC pastes

With the addition of lignosulfonates, the flowability of CCBC mixtures decreases only slowly or even increases. This is related to the high dosages required but goes along with often unfavored retardation effects as the following chapter 5.2.2 and the first conference contribution reveal.

As reported in literature [118-120], rapid slump loss is observed for CCBC mixtures with conventional polycondensates and PCEs. It occurs especially in the presence of metaphyllosilicates that exhibit a large SSA and high particle fineness, as well as hydration-enhancing alkalis in case of metaillite, as shown in the second conference contribution. The calcined common clay TG introduces alkalis, but also sulfates in form of gypsum and anhydrite. In combination with a smaller SSA, this leads to a slow increase in torque over time. Metamuscovite exhibits a decrease in apparent viscosity over time, which indicates thixotropic behavior. The results demonstrate that mineralogical and physical parameters of metaphyllosilicates and calcined clays dominate the time-related flow behavior. Details on time-related tests are provided in Appendix A7: Time-dependent rheological measurements and Appendix A8: Time-dependent mini slump tests.

In terms of superplasticizer type, the CCBCs show a higher sensitivity towards rapid slump loss with PCEs than with NSF, which is contrary to plain cement [189] and published in the second conference contribution. However, as PCEs are more effective, the aim is to find polymers that enable a workability for at least two hours without the addition of retarder and are applicable for further calcined clays. Therefore, the suitability of an IPEG-based PCE with HEMA in the anchorgroup is evaluated in the fourth journal paper and in the third conference contribution. HEMA decomposes into ethylene glycol and carboxyl groups in alkaline media, which can enable a prolonged dispersion.

Apart from its lower initial performance, IPEG1 can reduce the flow resistance or at least slow down the slump loss compared to most reference CCBC mixtures and those with IPEG2

(Figure 5-15, left). The mixture with KUP, that contains in its raw form significant amounts of muscovite, is not dispersed subsequently with 0.10 %bwob IPEG1. With a smaller dosage, however, a further reduction of flow resistance is observed (Appendix A7: Time-dependent rheological measurements). PLC_30AC, as discussed in the fourth journal paper, requires at least 0.10 %bwob IPEG1 for a subsequent dispersion, although this mixture has a low reference flow resistance. Here, both the **large SSA** of AC **and** the **high phyllosilicate content** of the raw AC **are identified as the critical parameters for rapid slump loss**. PLC_30FUP, that requires the highest amount of PCE, is the only mixture where it is impossible to counteract rapid slump loss even with high dosage and regardless of the type of PCE (Figure 5-15, right). Complementary observations are made by zeta potential measurements in the fourth journal paper and in the third conference contribution. The fast change of zeta potential towards higher, positive values of this CCBC mixture is related to a strong, initial ettringite formation [152] and to the undersulfation, that has been observed also with metakaolin and metaillite, and which is in agreement with [189].

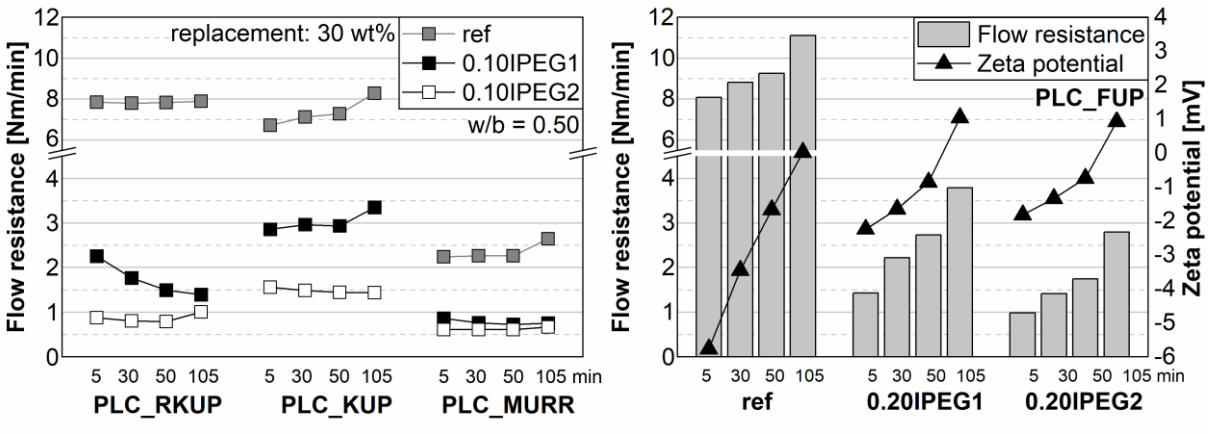

Figure 5-15. Time-related flow resistance of calcined common clays mixtures including reference and with IPEG1 and IPEG2

Compared to the demand for superplasticizer itself, the characteristics causing rapid slump loss need to be differentiated for CCBCs. Critical parameters, derived in the fourth journal paper, are not only the kaolinite but the total phyllosilicate content in raw clay, as well as the SSA of the calcined clay, whereas the water demand rather has a disordered role in this context. Depending on the calcined clay, both the introduction of higher dosages of PCE with hydroxyethyl methacrylate, as well as the optimization of sulfate carrier can prevent rapid slump loss. Further options in order to avoid rapid slump loss have been recently published by Li et al. [124]. They propose the use of PCE-LDH nanocomposites, where the PCE is released gradually from the LDH via exchange with sulfate ions from the pore solution.

5.2.2 Early hydration behavior of CCBCs in the presence of superplasticizers

The early hydration behavior has been observed via isothermal calorimetry and in situ XRD. The reference mixtures are described mainly in the second journal paper and the fourth conference contribution. With Portland limestone cement, the effect of metaphyllosilicates and calcined common clays on the aluminate reaction is more pronounced than with ordinary Portland cement, showing once more the good synergy effect between limestone powder and calcined clays [103-107]. In selected mixtures, both reference and with superplasticizer, sulfate is depleted rapidly. This could be compensated in further investigations with sulfate carrier optimization as proposed e.g. in [291].

The immediate **addition of superplasticizer prolongs the dormant period**, lowers the minimum heat value and retards the primary formation of CH, depending on type and dosage of superplasticizer, as found for CCBCs amongst others by Avet and Scrivener [104]. With the dosage adjusted for an equal dispersion, and as observed for other cementitious systems [292], lignosulfonates have the most retarding effect onto the silicate reaction of CCBC mixtures, followed by polycondensates and PCEs. As a retarded silicate reaction implies a slower strength development, this demonstrates the limited suitability of lignosulfonates for most applications in calcined clay blended concrete. This show also the significant data points, including heat of hydration, as obtained by isothermal calorimetry and provided for all mixtures in Appendix A9: Analysis of isothermal calorimetric measurements. The strong retardation effect of lignosulfonates results from residual sugar but mainly from the high required dosages, as presented in the first conference contribution. Higher dosages are further the reason for a more pronounced retardation by polycondensates than by PCEs, see the fourth conference contribution and as stated e.g. by Zaribaf and Kurtis [103]. The order of **retardation of CH formation by NSF, HPEG and amphMPEG** differs from mixture to mixture. A final judgement on the effective retardation is omitted here, as it is limited for CCBCs to a small range (**≤ 2 hours**) with these superplasticizers.

The influence of superplasticizers on aluminate reaction is of special interest as the calcined clays themselves already show a varying impact on it. The dissolution of gypsum, the along going formation of AFt as well as the formation of AFm-Hc, are summarized as aluminate reaction kinetics. Similar to the silicate reaction, the aluminate reaction is retarded the most with the addition of lignosulfonates. With NSF added, the **time shift in dissolution of gypsum** ranges mostly from – 1.5 to + 3 h compared to mixtures without superplasticizer, similar to HPEG and amphMPEG (see Appendix A10: In situ XRD plots). An accelerated dissolution of gypsum has been also observed by Ahn et al. [253]. They assume that metakaolin takes up sulfate ions from C_3A-sulfate gel phases and more sulfate carrier is dissolved due to the formation of AFt.

Contrary to findings for plain cement by Jansen et al. [293] where a stronger retardation holds for the dissolution of gypsum than for the formation of CH, the impact of the superplasticizers studied on gypsum dissolution is in a similar range as on the formation of CH in CCBCs. For most mixtures, dissolution of gypsum is promoted in mixtures with Portland limestone cement by approximately 3 hours and maximum AFt content is reached up to 8.5 h earlier compared to the respective OPC mixture. This is in agreement with Ramachandran and Chun-Mei [294] that the presence of $CaCO_3$ enhances the formation of AFt. The same holds to a larger extent for the primary formation of AFm-Hc where the differences between the respective OPC and PLC mixtures range from negligible 1.5 hours to significant 12.5 hours. In case of plain cement, OPC with amphMPEG does not show any formation of AFm-Hc within the first 48 hours, while it is already detected after 19.5 hours for PLC with amphMPEG. This confirms findings from the reference mixtures and e.g. from Antoni [295] that AFm phases are formed and AFt is stabilized with limestone present.

The time of maximum AFt content is hardly influenced by superplasticizers. Especially with the addition of PCEs, their **retarding impact on time of maximum AFt content of CCBC mixtures is minor (< 3 hours) when considering the partially high superplasticizer dosages required**. Less reactive mixtures with low demand for superplasticizer even show a more dominant aluminate reaction with superplasticizer added, indicated by a higher heat peak in isothermal calorimetry, and **earlier detection of AFm-Hc** by in situ XRD. This is despite of a slightly later dissolution of gypsum and point of maximum AFt content, which indicates a non-linear ongoing aluminate reaction. Hu and Sun [296] found that PCEs can promote the AFt formation, as they first have an influence on the morphology of AFt due to a hindered crystal growth, leading to an increased surface area of AFt. After sulfate depletion, the interaction between these AFt crystals and unhydrated C_3A is enhanced by the adsorption of PCE onto the surface of both phases, leading to an increased amount of AFt and transformation to AFm-Hc as consequence. Pott et al. [297] observed a higher initial, yet slower AFt formation in plain cement as well as an earlier formation of AFm-Hc with immediate superplasticizer addition. Hence, the observed effect might diminish with delayed superplasticizer addition, that is often practiced in concrete industry. On the other hand, Roncero et al. [192] found an increased rate of AFt formation with subsequent addition of superplasticizer as well, especially with polycondensates. A further theory is that a higher amount of water is available in these mixtures, that enables an unhindered course of hydration as shown by Beuntner [60]. This either results from a low water demand or a subsequent water release as assumed for mixtures with metamuscovite according to the increasing flowability during the first 2 hours observed in the second conference contribution. As consequence, enough water is available then for the formation of water-rich AFt ($C_6A\$H_{32}$ [298]) and AFm-Hc ($C_4A\bar{C}_{0.5}H_{12}$ [298]).

The **incompatibility of NSF and Mu** described in chapter 5.1.3, does also have a significant impact on the hydration of this mixture as observed in the fourth conference contribution. CH is not detected until 12.5 h after water addition (Figure 5-16), although the OPC_20Mu reference shows the shortest dormant period and earliest CH formation of all CCBCs, confirming [299]. The dissolution of gypsum is hindered and, as consequence, the maximum AFt content is reached significantly later, although it occurs closer after gypsum dissolution compared e.g. to reference. Further, no AFm-Hc is observed within the first 48 hours of hydration.

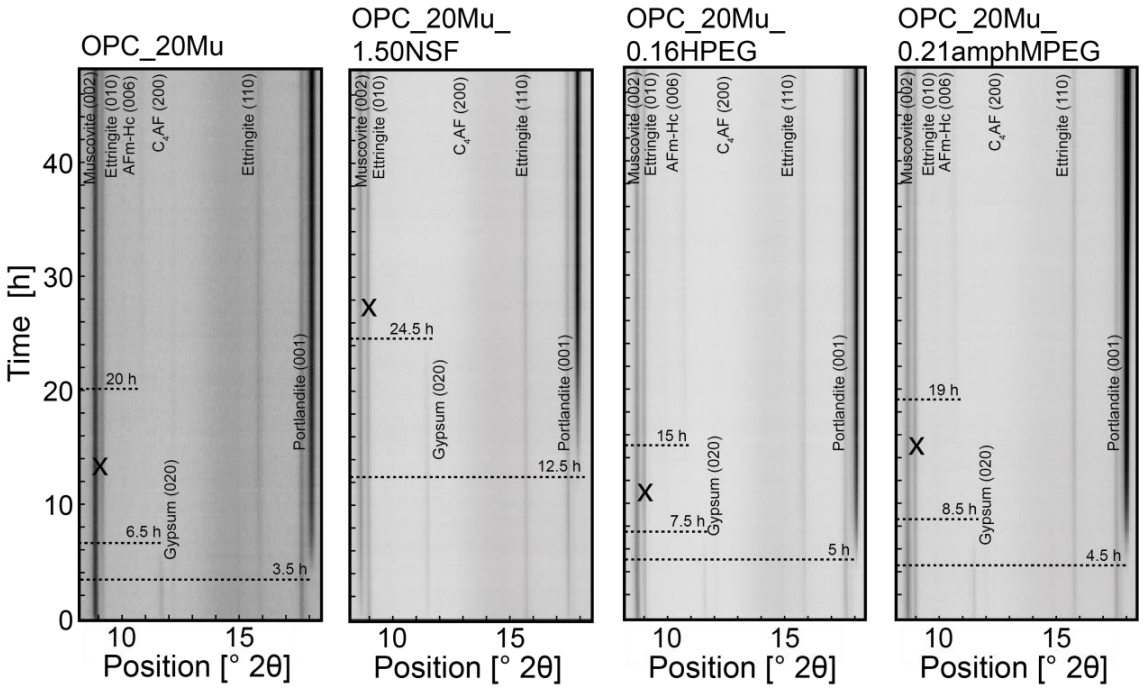

Figure 5-16. In situ X-ray plots from 9.5 to 18.5° 2θ for OPC_20Mu mixtures without superplasticizer and with the addition of NSF, HPEG and amphMPEG (time of maximum AFt is marked as X)

The inhibition of hydrate phase formation is caused by Ca^{2+} complexation and a hindered diffusion of water molecules to Ca^{2+} ions by superplasticizer molecules adsorbed onto cement grains [143], which also explains why a higher dosage leads to more pronounced retardation effects. Overall, it is assumed that Ca^{2+} complexation by superplasticizers is also in CCBCs the main mechanism for retarded reaction kinetics. It lowers the amount of Ca^{2+} ions present in pore solution and hinders hereby the formation of CH, CSH and AFt as found for plain cement e.g. by Uchikawa et al. [300].

Relationship between selected binder properties, superplasticizer dosage and early hydration kinetics

This section addresses the observed effect that calcined clay particles can compensate to a certain extent the retardation effect of high superplasticizer dosages. Investigations with lignosulfonates show that adding the dosage, as required for plain cement, to CCBCs can partially compensate the retardation effect and the setting time according to ASTM C1679-13 [301] is significantly reduced (see the first conference contribution).

The publications in chapters 7.2, 7.4 and 7.8, also do show that a high dosage does not necessarily lead to a strong retardation. Contrary to original assumptions, it is less the solubility of Al and Si ions, than the kaolinite content in raw clay as well as the surface area, that both counteract the retarding effect of superplasticizers. Figure 5-17 correlates the TSA_{binder} to superplasticizer dosage ratio (TSA_{binder}/dosage) with the shift of the time of minimum heat ($t_{Q,min}$) of all investigated mixtures. The difference for the mixtures with and without superplasticizer ($\Delta t_{Q,min}$) diminishes at a higher TSA_{binder}/dosage. It is assumed that a lower TSA reduces the possibility of superplasticizer adsorption and the polymers remain in aqueous phase instead. According to [143, 217], the adsorbed molecules hinder the diffusion of water and Ca^{2+} and cause the retardation hereby, while in addition unadsorbed molecules hinder the nucleation of CSH and CH and the further dissolution of C_3S due to Ca^{2+} complexation. Overall, **the retardation on $t_{Q,min}$ by superplasticizer is < 1 hour for most CCBCs when TSA_{binder}/dosage > 40**. This is remarkable especially for the mixtures with calcined common clays that exhibit a sufficient workability period (chapter 5.2.1) and shows furthermore that a high dosage, if required for the dispersion of binder with challenging properties, not necessarily leads to strong retardation effects.

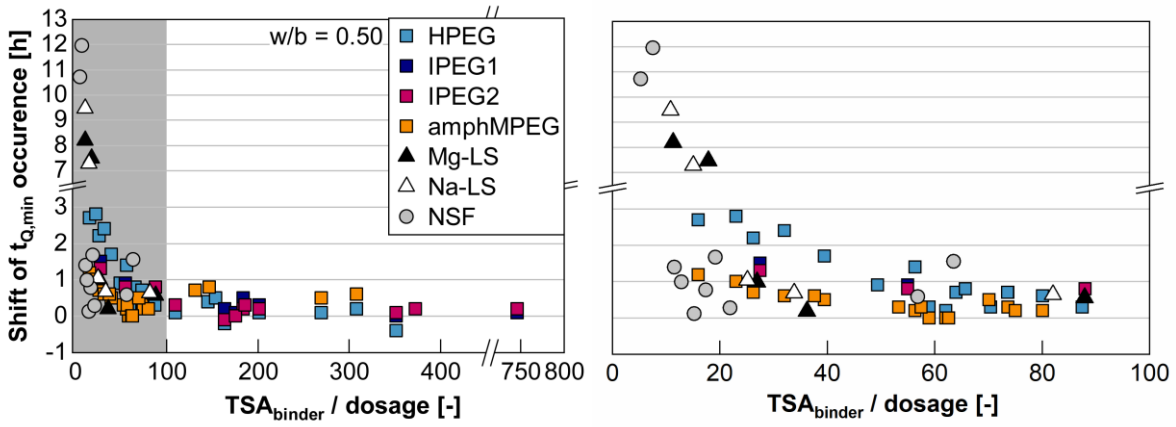

Figure 5-17. Correlation of the TSA_{binder}-dosage ratio with the shifted end of dormant period ($t_{Q,min}$); the right figure shows the grey area at enlarged scale

The retarding impact of superplasticizer dosage diminishes with increasing TSA and increased ettringite formation of the binder system, not only for the dormant period but also for time of maximum heat ($t_{Q,max}$), see the fourth journal paper. The time shift in maximum heat ranges more significantly compared to $t_{Q,min}$, as presented in Figure 5-18 and confirming once more the non-linear retardation effects. The German Committee for Structural Concrete (DAfStb) demands additional measures, e.g. regarding curing, if the workability period of concrete is extended by more than 3 hours [302]. A retardation > 3 h in paste occurs mainly for mixtures with TSA_{binder}/dosage < 40 only. Furthermore and while the shift in $t_{Q,max}$ diminishes with higher TSA_{binder}/dosage, few mixtures even exhibit an earlier maximum peak with PCEs and formation of AFm-Hc than without superplasticizer as mentioned in several publications (chapters 7.2, 7.4 and 7.8).

Overall, those **mixtures that do require less superplasticizer than added, have a stronger retardation that results in a lower heat of hydration** compared to reference after 24 h. For mixtures with increased TSA, often a similar heat of hydration is achieved already after 24 h, indicating once more the compensation in retardation. This has been also demonstrated via ultrasonic measurements in the second journal paper. After 36 - 48 h, only few mixtures have still a significant lower heat of hydration that indicates a slow strength development at the same time and overall, **a TSA/dosage > 40 is assumed to be uncritical** in terms of retardation. Considering that the actual retardation in concrete is less, the retardation caused by superplasticizer addition should not be a problem.

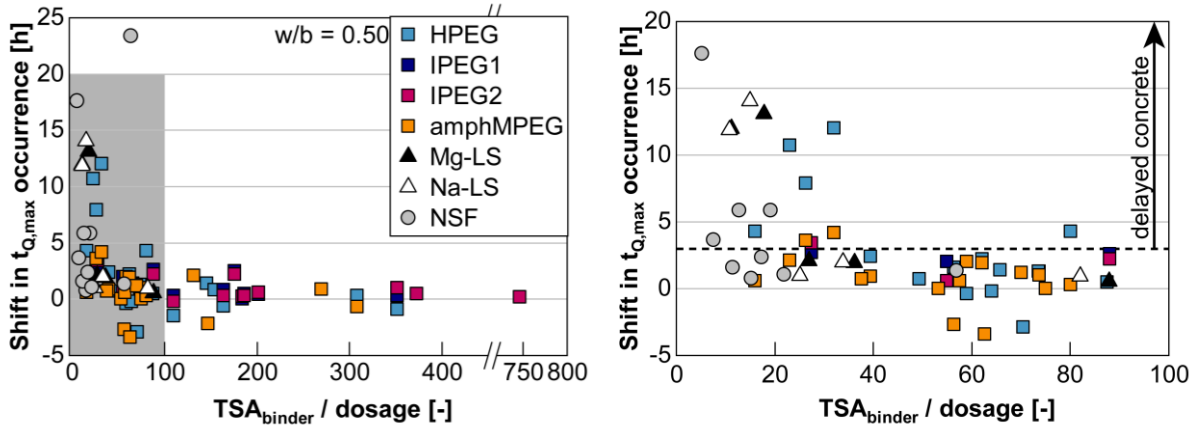

Figure 5-18. Correlation of TSA_{binder}-dosage ratio with the retardation in maximum heat peak ($t_{Q,max}$); the right figure shows the grey area at enlarged scale (note the different y-axis)

Based upon these results and literature review, the following theories are proposed why the SSA of calcined clays, and in consequence the TSA of the binder, as well as the surface charge do favor a limited retardation:

- Due to the increased surface area, the formation of early hydration products is favored despite of the adsorption of superplasticizers onto binder particle surfaces.
- The enhanced and accelerated initial AFt formation, as known for limestone (in case of PLC mixtures) [294] and calcined clays [286], diminishes the retardation effect of superplasticizers on silicate reaction. The strong positive zeta potential of AFt enables the adsorption of superplasticizer onto it, reduces hereby the free amount of superplasticizer in pore solution and enables an unhindered silicate reaction as shown by Plank and Hirsch [152].
- Scherb et al. [286] and Maier et al. [285] do state that calcined clay particles enable the adsorption of Ca^{2+} and subsequently of SO_4^{2-}, which accelerates the aluminate reaction. It was shown that superplasticizers adsorb onto calcined clay particles after Ca^{2+} adsorption, where the ions function as link between negatively charged calcined clays and superplasticizers [66, 258, 261]. This combination of enhanced aluminate reaction and adsorption onto calcined clay particles minimizes the amount of superplasticizer free in aqueous phase and enables an unhindered hydration.

6 Summary and reflection of the thesis

The thesis includes four peer-reviewed, SCI(E)-listed journal articles, as well as four conference contributions. It deals with the questions

I) how calcined clays do affect the rheology of blended cement with focus on their mineralogical and physical characteristics,
II) how their properties do affect the required amount and dispersion performance of superplasticizers as well as
III) to what extent superplasticizers do influence the early hydration of calcined clay blended cements (CCBCs).

The **study of the rheological behavior** was first carried out on pure-phase powder materials, namely quartz and metaphyllosilicates (metakaolin, metaillite and metamuscovite) by using mini slump tests and rotational viscometer. In the further course a transferability to calcined common clays, relevant for application in concrete industry, was systematically attempted for the first time. The mixtures investigated exhibited in parts significantly increased yield stress and viscosity values with the addition of calcined clays. The type of cement played a lesser role, while the water-to-binder ratio, the replacement level and the individual calcined clay did influence the most. Most mixtures could be described by well-known rheological models as Bingham fluid or as shear-thickening Herschel-Bulkley fluids. Among all reference mixtures, solely for the mixture with 30 wt% metakaolin, the Herschel-Bulkley fit was not applicable and Bingham models lead to “negative” viscosity as these mixtures had a non-linear decreasing torque with higher rotational speed. Here, two options are proposed for subsequent investigations: a) verification of this behavior (e.g. by using a parallel-plate rheometer, more data points or different rotational speed ranges) and b) the consideration of further rheological models and physical parameters (e.g. the maximum packing density in a modified Krieger-Dougherty model [70] as proposed by Tregger et al. [68]). As a further parameter, the flow resistance (area under the flow curve) was considered, which was - similar to the yield stress - significantly higher with the addition of metaphyllosilicates than with calcined common clays.

Throughout the study, it has been rather surprising that the calcined Amaltheen clay, that is dominated by 2:1 phyllosilicates, exhibited non-critical physical and rheological properties and showed as consequence a low demand for superplasticizer compared to the pure, calcined 2:1 phyllosilicates. The simulation of superplasticizer efficiency with the individual components showed significant deviations of up to 40 %, which limited the **transferability from phyllosilicates to common clays** as long as physical parameters (like specific surface area, water demand or zeta potential) differ too much from the properties of the actual calcined clay.

The discrepancies between percentage-wise calculated and measured physical properties of calcined clays are compared in Figure 6-1. It is minor for the specific surface area of KUP and RKUP, whereas the deviations are significant for the other calcined common clays. In terms of the water demand, KUP, TG and FUP follow a linear trend (R^2 = 1.00), although the measured water demand is approximately 20 % lower than the calculated values. Overall, the comparison between calculated and measured physical properties leads to poor correlations, which were also related to the different origins and processing techniques of the raw materials. It further limited the prediction of flow resistance of CCBC mixtures, of the demand for superplasticizers and their efficiency. Here, a higher amount of data points with focus on machine learning can increase the chance for an accurate prediction model.

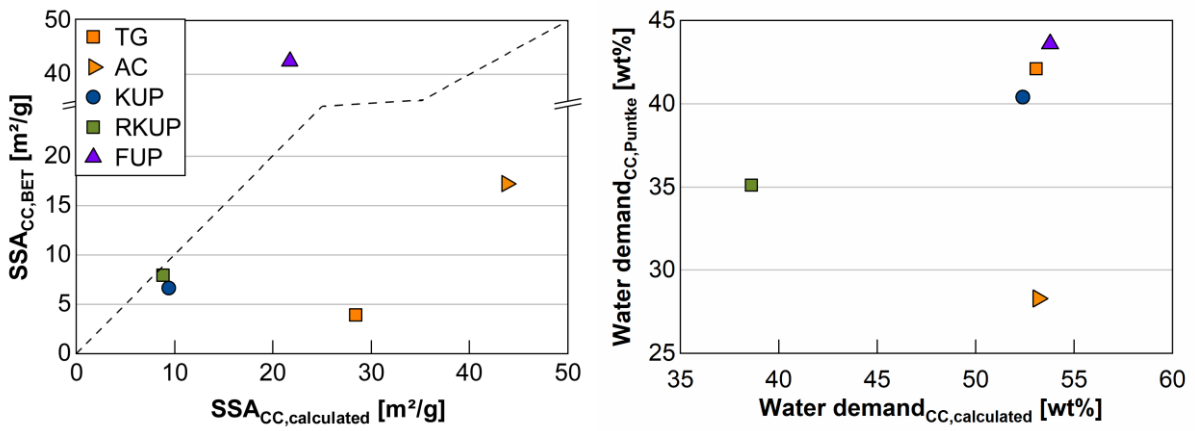

Figure 6-1. Correlation of calculated and measured specific surface area (SSA) (left) and water demand (right) of calcined common clays (CC)

Beuntner et al. [31] compared the properties of an Amaltheen clay at different calcination temperatures, on both industrial and laboratory-scaled production. This Amaltheen clay has been investigated in this thesis as well, both after calcination and milling on industrial and on laboratory scale. The latter product exhibited a lower water demand and coarser particle size but a significantly larger specific surface area. Despite of the small specific surface area of the industrially calcined Amaltheen clay, its addition lead to a significantly higher flow resistance compared to the lab-calcined clay, even with lower replacement level. As the differences between the cement properties were minor, the increased flow resistance resulted from the water demand and the particle size. This brings the thesis to the conclusion that it is crucial to evaluate and control at the same time the flow properties by the processing of clay (calcination and grinding / intergrinding with clinker). Further detailed investigations are required towards the surface chemistry of calcined clays, since comparable low zeta potential values of common clays, both before and after calcination, cannot be explained by the zeta potential of pure phases.

However, it could be shown that the negative zeta potential of calcined clays in alkaline environment, and hereby the flow resistance of CCBC mixtures, increases with increasing kaolinite content in raw clay. Muscovite plays a special role, as it exhibits a pronounced water demand even after calcination and thus increases not only the yield stress and flow resistance, but also the viscosity of cementitious systems. Likewise, illite reduces the flowability. However, illite does usually not exist in highly pure form but rather as illite-smectite interstratifications with different percentages of illite. In contrast to this and to known problems in other applications, smectite does not cause significant difficulties in calcined common clays. Therefore, it requires further tests on mixed-layers / interstratifications with different percentages of each smectite and illite layers. Quartz, if present in nominal amounts in clay, can compensate in parts the challenging properties of the mentioned phyllosilicates and improve the flow characteristics due to small specific surface area and low water demand. On the other hand, it can have a deagglomerating effect during the grinding process and increase hereby the flow resistance due to higher particle fineness. Further research should also assess the role of high calcite amounts in raw clays, as flow-enhancing properties are assumed based on literature and selected results.

The **demand for superplasticizer** is directly linked to the flow resistance of the respective reference CCBC mixture. It increases to different extents depending on the calcined clay added, its water demand, particle fineness and negative zeta potential, the latter mainly resulting from higher kaolinite content. Neglecting the higher dosages required, nonetheless, the performance of superplasticizers does overall not differentiate significantly from plain cement, as lignosulfonates are least and PCEs most efficient in CCBC mixtures. Those PCEs with higher anionic charge density enable a better initial dispersion, regardless of other polymer properties. In further terms of their chemical structure, all conventional macromonomers (HPEG, IPEG, MPEG) exhibit good to excellent dispersion performance. Based on the experiments with metaphyllosilicates and calcined common clays, metamuscovite is the only phase considered as perturbing the performance of superplasticizers and sensitive towards the type of superplasticizer. Apart from the, at least in parts, high demand for superplasticizer, the use of CCBCs can lead to **rapid slump loss**. Compared to plain cement, this effect was observed to be stronger with conventional PCEs than with polycondensates. Depending on the calcined clay, the introduction of additional ester groups (HEMA) into the PCE polymer can lead to a subsequent dispersion of CCBC mixtures. By its decomposition into ethylene glycol and carboxyl groups in alkaline media, a later adsorption can compensate the rapid slump loss. However, decisive parameters for the time-related flowability as well as for the functionality of this special type of polymer need to be considered. These are not only the kaolinite but the total phyllosilicate content in raw clay as well as the specific surface area of the calcined clay, whereas its water demand rather has a disordered role in this context.

In addition, an optimization of sulfate carrier can prevent rapid slump loss, which should be specifically considered in further research regarding the time-related, rheological behavior of CCBC mixtures. The individual consideration of sulfate optimization is an additional observation, revealed while investigating the **early hydration of CCBC mixtures with superplasticizers** via isothermal calorimetry and in situ XRD. In addition, the evaluation of early hydration, setting and along going microstructure development could be extended by using ultrasonic technique. It gave a fundamental insight especially in complex binder systems as CCBC, even at certain consistencies, where the use of common methods, like in situ XRD, is limited due to segregation. The tests on reference mixtures confirmed the influence of calcined clays, already during early hydration, that depends mainly on their particle size and chemo-mineralogical properties. With the addition of superplasticizer, the retardation of early hydration kinetics depends mainly on the characteristics of the calcined clay / CCBC, as well as on the superplasticizer dosage. The present results confirmed that a higher dosage results overall in a stronger retardation, although the absolute retardation was mostly minor for CCBC mixtures – except with lignosulfonates. It was related to a higher ratio of total surface area and superplasticizer dosage that reduced the retardation significantly. CCBC mixtures with superplasticizers had a comparable heat of hydration after 24 h in case of a large total surface area, or after 36 – 48 h with moderate total surface area. The minor retardation was related to the increased surface as the formation of early hydration products is favored despite of the adsorption of superplasticizers onto binder particle surfaces. An enhanced ettringite formation of CCBC enabled an unhindered silicate reaction and (in few cases even earlier) transformation of ettringite to hemicarboaluminate, also in the presence of most superplasticizers. Beside of this and based on recent literature, the adsorption of calcium ions onto calcined clay particles can enable a subsequent adsorption of anionic superplasticizers, removing them from aqueous phase and enabling an unhindered course of hydration.

Based on the present findings, Figure 6-2 provides an overview for the interaction of calcined clays with superplasticizers and what needs to be considered in terms of rheological behavior, demand for superplasticizer, effect on rapid slump loss and early hydration. The thesis could demonstrate the suitability of a great variety of calcined common clays as future SCM also in terms of their rheological behavior in combination with the correct choice of superplasticizer. After an initial characterization in detail, their use can compensate the increasing demand for sustainable binder materials in sufficient quantities and help to reduce the carbon dioxide emissions caused by concrete industry, once calcined clays are widely used. Special focus in future research is required on mixed-layers with different proportions of smectite, the special role of muscovite as non-negligible clay component, as well as a deeper insight into the surface chemistry of thermally treated phyllosilicates and clays.

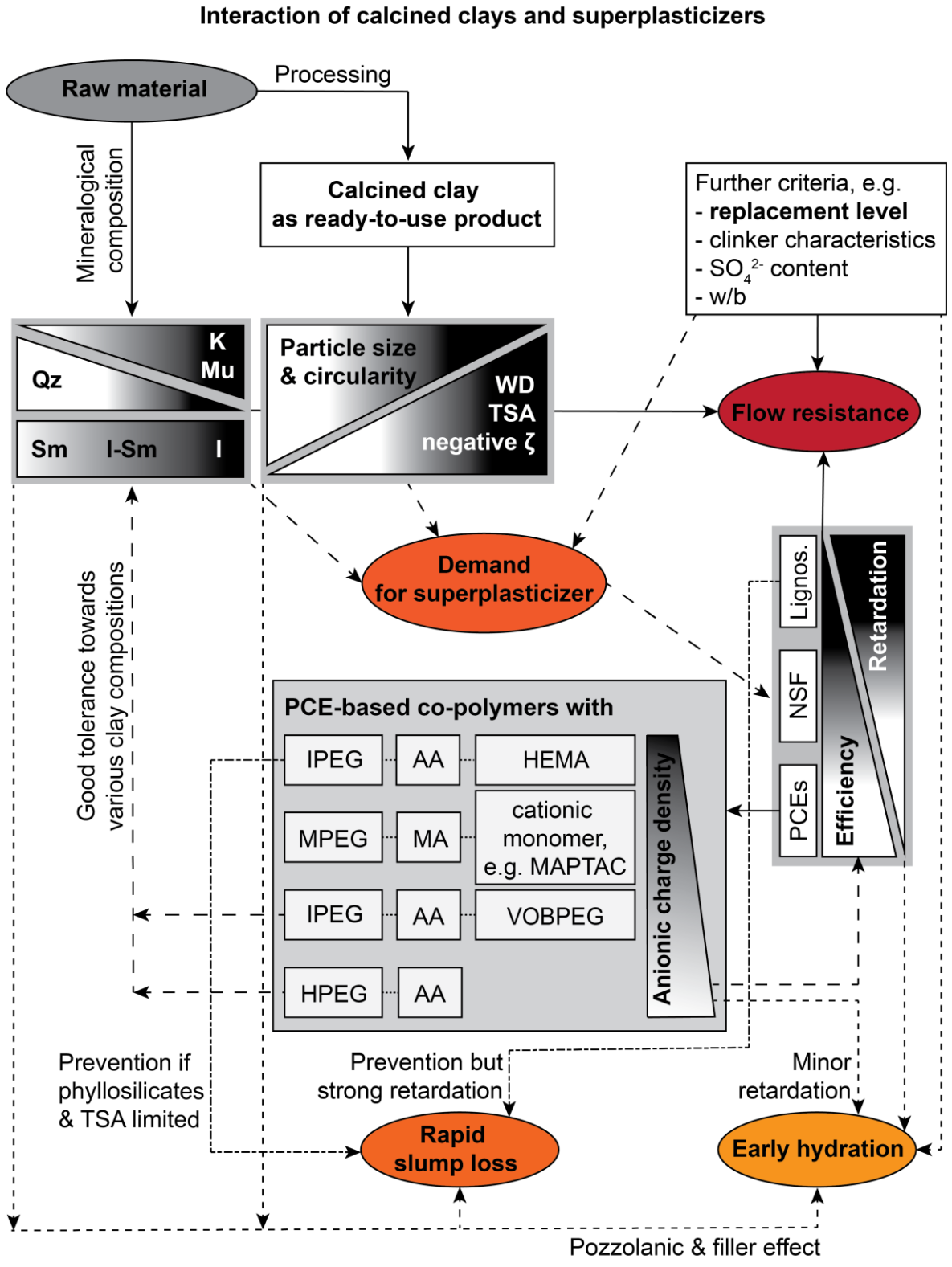

Figure 6-2. Summary of revealed interactions of CCBCs with superplasticizers; depending on the mineralogical composition of raw clay (K = kaolinite, Mu = muscovite, Qz = quartz, Sm = smectite, I-Sm = illite-smectite interstratifications, I = illite) and physical properties of calcined clay (WD = water demand, TSA = total surface area, ζ = zeta potential) as well as the chemical properties of superplasticizers; gradient from dark to white indicates rating from challenging/poor to excellent effect;

7 Publications

7.1 Characteristics of components in calcined clays and their influence on the efficiency of superplasticizers

Peer-reviewed journal paper [Reprint]

"Characteristics of components in calcined clays and their influence on the efficiency of superplasticizers"

Ricarda Sposito, Nancy Beuntner, Karl-Christian Thienel

Cement and Concrete Composites

Volume 110, 103594 (2020)

Cement and Concrete Composites 110 (2020) 103594

Contents lists available at ScienceDirect

Cement and Concrete Composites

journal homepage: http://www.elsevier.com/locate/cemconcomp

Characteristics of components in calcined clays and their influence on the efficiency of superplasticizers

Ricarda Sposito *, Nancy Beuntner, Karl-Christian Thienel

Institute for Construction Materials, Universität der Bundeswehr München, 85577, Neubiberg, Germany

ARTICLE INFO

Keywords:
Calcined clays
Superplasticizers
Rheology
Supplementary cementitious materials

ABSTRACT

Fundamental knowledge towards calcined clays is required to understand their impact on rheology and interaction with superplasticizers in cementitious systems. The rheological behavior is investigated by rotational viscometer and mini slump tests and discussed on clinker-free suspensions considering physical properties of one calcined common clay from Southern Germany and three calcined phyllosilicates (metakaolin, metaillite, metamuscovite). The efficiency of superplasticizers is evaluated for cementitious systems blended with these calcined clays and quartz powder for comparison. Zeta potential, water demand and total surface area are identified as reliable key factors for the demand of superplasticizer - except for metamuscovite. The superplasticizers exhibit better compatibility with quartz-containing calcined common clay than with calcined phyllosilicates. With the methods used, there is no simple correlation between the interaction of the calcined phyllosilicates with superplasticizers and the latter with a calcined clay containing these phyllosilicates.

1. Introduction

The suitability of calcined clays as supplementary cementitious material (SCM) is commonly indicated by its pozzolanic reactivity [1–5] but their addition can lead to reduced workability of concrete [6,7]. The impact on workability starts with the mineralogical composition of the clay as its water demand depends on type of main clay mineral/phyllosilicate [8]. The specific surface area (SSA) [8,9] and water adsorption behavior [10] both go along with a contribution of interlayer space. Kaolinite is an 1:1 phyllosilicate with the chemical formula $Al_2Si_2O_5(OH)_4$ [11]. It exhibits both ordered and disordered structure and low cation exchange capacity which lead to unique properties like low plasticity, SSA and water adsorption compared to other phyllosilicates [8–10,12]. Muscovite ($KAl_2(Si_3AlO_{10})(OH)_2$ [13]) and illite are both non-expandable 2:1 phyllosilicates and structurally belong to the mica group [14]. They both substitute Si^{4+} by Al^{3+} in tetrahedral layers and illite, in addition, substitutes Al^{3+} and Fe^{3+} by Mg^{2+} and Fe^{2+} in octahedral layers [12]. This leads to a lower net negative charge per layer compared to muscovite [15]. Furthermore, illite has an interlayer charge deficit, which is related to a lower content of potassium in interlayers [14,15] and the K^+ can be replaced by H_3O^+ [16]. Illite exhibits a larger SSA (65–100 m^2/g) [9] than muscovite (2–14 m^2/g) [17,18]. On the other hand, muscovite is known for its higher water adsorption in comparison with e.g. illite [14]. The calcination of muscovite can even lead to a slight expansion of interlayers [13] and an increased water absorption capacity [18]. Considering these aspects, it seems that kaolinitic clays are less critical than illitic or muscovite-rich clays. The question is whether the SSA or the water absorption capacity or both parameters are decisive for the rheological behavior and the interaction with superplasticizers. From this point of knowledge, it is not possible yet to assess whether illite or muscovite requires more superplasticizer. By calcination, and depending on the degree of dehydroxylation of phyllosilicates, severe changes can occur in their mineralogical and physical properties, e.g. reduction of SSA [5,8,18–20]. Kaolinite transforms into amorphous metakaolin whereas illite and mica rather keep a crystalline layer structure after dehydroxylation up to higher temperatures [21,22]. The impact of grinding and calcination on the morphology of calcined clays is still under discussion. While Konan et al. [23] observed only slight differences between kaolinite and metakaolin, Cassagnabère et al. [24] stated a significant impact of processing on the particle shape of metakaolin. Claverie et al. [25] even identified spherical metakaolin particles after flash-calcination, similar to those of fly ash. Less superplasticizer is required due to dehydroxylation of phyllosilicates and the associated reduced SSA [26]. One further reason is the reduced intercalation effect of polycarboxylate ether (PCE) superplasticizer known for clay minerals

* Corresponding author..
E-mail addresses: ricarda.sposito@unibw.de (R. Sposito), nancy.beuntner@unibw.de (N. Beuntner), christian.thienel@unibw.de (K.-C. Thienel).

https://doi.org/10.1016/j.cemconcomp.2020.103594
Received 10 December 2019; Received in revised form 4 March 2020; Accepted 13 March 2020
Available online 16 March 2020

[27–29] that cause severe incompatibilities with PCE-based superplasticizers and problems in concrete. Cementitious systems with metakaolin [30,31] or calcined marl [32] are however known for a still higher superplasticizer demand compared to neat cement systems. When it comes to the type of calcined clay, systems with calcined kaolinitic clay require more superplasticizers than those with calcined 2:1 clay according to Ferreiro et al. [33]. They explained this phenomenon by the adsorption of superplasticizers into the amorphous structure of metakaolin, which limits the dispersion effect, whereas polymers can adsorb onto 2:1 clay particles and avoid the intercalation. Schmid et al. [34–36] investigated the interaction of various PCE-based superplasticizers with a calcined common clay from Southern Germany that requires in some cases even less superplasticizer than neat cement paste. The authors' current assumption is that the non-negligible amounts of quartz might be the key parameter in calcined common clays [4,37,38]. Quartz can reduce the yield stress of cement paste or clay/quartz suspensions already at small amounts [39,40]. For this reason, this study considers the properties of calcined clays and one quartz powder for comparison. Within rheological investigations it is examined, if quartz might counteract the challenging rheological properties of calcined phyllosilicates in calcined clay blended cementitious systems. The dispersion effectiveness of one polycondensate and two PCE-based superplasticizers is investigated on different blended cementitious systems to evaluate the demand for superplasticizer depending on type of cement replacement.

2. Materials & methods

2.1. Binder systems

An ordinary Portland cement (*OPC*) CEM I 42.5 R, complying with DIN EN 197–1 [41], is used. Selected data is presented in addition for a Portland limestone cement (*PLC*). In combination with calcined clays, it is comparable with a LC^3 cement [42–45]. The mineralogical composition of the cements is given in Table 1. The cements are partially replaced by five different materials. As representative for common clays, a calcined common clay (*TG*) is chosen that has been described and investigated already in detail [5,46–49]. The raw clay originates geologically from Amaltheen formation (Pliensbachian Lower Jurassic) in Southern Germany. It contains in its natural form different phyllosilicates (25 wt% kaolinite and 45 wt% 2:1 phyllosilicates, including illite and muscovite) and 30 wt% inert components (e.g. quartz, feldspar, calcite, sulfates). One calcined 1:1 phyllosilicate (metakaolin) and two calcined 2:1 phyllosilicates (metaillite and metamuscovite) are investigated. The metakaolin (*Mk*) is a flash-calcined industrial product from the U.S.A. Raw illite sample exhibits 90 wt% of illite as well as traces of quartz, calcite and kaolinite. It has been dry-milled before calcination to reduce initial particle size from $d_{50} = 86$ µm to $d_{50} = 3.7$ µm. Muscovite sample originates from Hebei province, China, and contains 91 wt% of muscovite and 9 wt% of amorphous phase. Illite and muscovite are calcined as powder in a laboratory muffle kiln. The calcination temperatures are derived from thermal analysis to achieve complete dehydroxylation of phyllosilicates and from the amount of soluble aluminum and silicon ions in alkaline solution, for a pozzolanic reactivity as high as possible. It is 770 °C for metaillite (Mi) and 800 °C for metamuscovite (Mu) [50]. Muscovite is a mica and not a clay mineral, but it is a non-negligible component in common clays [18]. For this reason and for a better readability, all calcined materials are designated as "calcined clays" in the following text. The mineralogical composition of the calcined clays is given in Table 2. Quartz powder (QP) is used to evaluate the impact of quartz content in calcined clays on the rheology. Table 3 lists the physical parameters of all binder components, including the "total surface area" (TSA) as product of particle density and SSA according to Bentz et al. [51]. Particle size distribution of the binder components is analyzed by laser granulometry using Horiba LA-960 (Retsch) according to DIN ISO 13320 [52] (Fig. 1).

Parameters for blended binders with OPC and PLC are given in Table 4 and Table 5, respectively. The particle density and TSA are both calculated from the individual parameters of cement and calcined clay or quartz powder according to their mass fraction in binder systems, taken from Table 3. The water demand is determined via standard stiffness according to DIN EN 196–3 [53]. Zeta potential and pH value of the cement pastes (w/b ratio = 0.50) are both measured five times by electroacoustic spectrometer DT-310 (Dispersion Technology Instruments, USA), 15 min after water addition.

2.2. Superplasticizers

Three superplasticizers are selected to investigate their dispersing effectiveness in calcined clay blended cementitious systems. A calcium salt of a β-naphthalene sulfonate formaldehyde polycondensate (*NSF*) with a solid content of 40.0 wt% is used. An industrial α-methallyl-ω-methoxy poly(ethylene glycol) ether type PCE (*HPEG*) with a relatively long side chain ($n_{EO} = 66$) and an anionic charge density of 1751 µeq/g (in H_2O) is investigated. Its solid content is 50.0 wt%. The second PCE based superplasticizer is lab-synthesized within a joint research project by the Department for Construction Chemistry from Technical University Munich (Germany). Its polymer structure has a methacrylic acid monomer, ω-methoxy poly(ethylene glycol) methacrylate ester (MPEG) macromonomer and diallyl dimethylammonium chloride as cationic monomer [57]. Due to the cationic monomer it has an amphoteric character and is hence named *amphMPEG*. It has a significantly longer side chain ($n_{EO} = 113$) and lower anionic charge density (1061 µeq/g in H_2O) compared to HPEG and a solid content of 33.0 wt%.

2.3. Methods

2.3.1. Investigations on single components and clinker-free suspensions

The morphology and particle shapes of binder components are investigated on powder samples, scattered on thin layer of two-

Table 2
Mineralogical composition of calcined clays.

Phase [wt%]	TG	Mk	Mu	Mi
Quartz	16	5	–	–
Mica (high temperature modification of muscovite)	2	1	81	–
Illite	5	–	–	38
Chlorite	<1	–	–	–
Carbonates (calcite)	<1	–	–	5
Feldspars	6	–	–	–
Secondary silicates	6	–	–	–
Hematite	1	–	–	–
Pyrite	1	–	–	–
Sulfates (anhydrite, gypsum)	2	–	–	–
Anatase	–	<1	–	–
Portlandite	–	–	–	<1
Lime	–	–	–	<1
X-ray amorphous	61	93	19	56

Table 1
Mineralogical composition of cements.

Cement	C_3S	C_2S	C_3A	C_4AF	$CaCO_3$	Sulfate carrier	$CaMg(CO_3)_2$	MgO	CaO_{free}
OPC	61.6	18.2	5.8	9.0	0.6	3.2	–	0.9	0.6
PLC	48.9	15.2	5.1	8.1	14.4	4.0	3.0	0.8	0.1

Table 3
Physical parameters of binder components.

Parameter	Standard	OPC	PLC	QP	TG	Mk	Mu	Mi
Particle density [g/cm^3]	[54]	3.17	3.09	2.65	2.63	2.61	2.79	2.72
BET SSA [m^2/g]	[55]	1.0	1.7	0.3	3.9	17.8	11.8	94.6
TSA [m^2/cm^3]	[51]	3.17	5.25	0.80	10.26	46.46	32.92	257.31
Water demand [%]	Puntke method [56]	–	–	18.9/21.8/22.8	42.1/45.8/46.4	56.9/57.8/59.4	79.8/83.2/92.3	67.7/69.7/71.8
d_{10} [μm]	[52]	4.1	2.3	7.2	4.0	3.0	9.3	2.7
d_{50} [μm]		15.8	13.1	61.8	13.2	14.8	19.2	6.8
d_{90} [μm]		46.0	46.0	194.5	37.0	76.2	45.7	61.9
$r_{average}$ [μm]		10.9	20.4	61.7	12.7	15.0	13.0	10.2

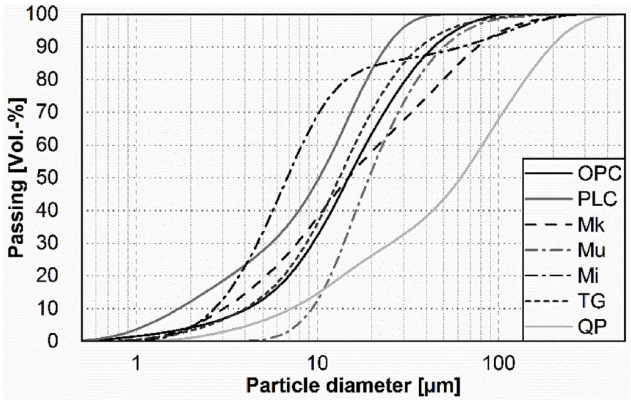

Fig. 1. Particle size distribution of binder components.

component adhesive and gold-coated, by scanning electronic microscope EVO LS 15 (Zeiss, Germany). In high vacuum, an aperture with 20 μm and a secondary electron detector are used with acceleration voltage of 20 kV, spot size of 250 and a working distance at 8.5 mm. The surface charge of binder components is measured and averaged over 3 h on suspensions as zeta potential (ζ) in [mV] via electroacoustic spectrometer DT-310 (Dispersion Technology Instruments, USA). The suspensions with calcined clay or quartz powder (m = 250 g) and distilled water at a w/s ratio = 1.50 are stirred manually for 2 min. The suspension is stirred during measurement continuously by a stirrer (400 rpm) to prevent segregation effects. Mini slump is evaluated for each suspension with a Vicat cone on a slightly wetted glass plate. The diameter of slump is measured four times during two repeats. Rheological measurements are conducted via rotational viscometer Viskomat NT (Schleibinger, Germany) coupled with a water-based circulatory cooling unit (T = 20 °C) on suspensions. Compared to zeta potential and mini slump measurements, the suspensions (m = 350 g) are homogenized in a Hobart mixer at 220 rpm for 120 s due to the higher suspension volume. The high w/s ratio is chosen since torques of metamuscovite suspensions at lower w/s ratios exceed the maximum values for torques measurable by rotational viscometer. The velocity starts at 120 rpm for 10 min and slows down to 80 rpm → 40 rpm → 20 rpm for 2 min each to determine the apparent viscosity and yield stress. Rheological parameters are analyzed according to Bingham equation [58,59] (Equation (1)):

$$T = g + Nh \quad (1)$$

With Torque T ≈ shear stress τ.

Apparent yield stress (y-intercept of flow curve) g ≈ dynamic yield stress τ_0
Velocity N ≈ shear rate $\dot{\gamma}$
Apparent viscosity (slope of flow curve) h ≈ viscosity η

Furthermore, the coefficient of determination (R^2) of the linear fit is used as indicator for mixing stability depending on varying velocity and the median torque at each velocity is determined. The classification regarding the rheological behavior is based on the criteria in Table 6.

The nomenclature for the clinker-free suspensions is *binder*

Table 6
Classification schema for rheological properties.

Apparent yield stress [Nmm]	R^2 [-]	Type of fluid	
g > 0	~1	Bingham fluid [58,59]	
g > 0	≪ 1	Herschel-Bulkey fluid [58]	
g ≤ 0	~1	Newton fluid [58,59]	
g ≤ 0	≪ 1	decreasing flow curve gradient	Shear-thinning (pseudo plastic) fluid [58]
g ≤ 0	≪ 1	increasing flow curve gradient	Shear-thickening (dilatant) fluid [58]

Table 4
Key parameters of blended binders/cement pastes with OPC.

Parameter	OPC	OPC_20QP	OPC_20 TG	OPC_20Mk	OPC_20Mu	OPC_20Mi
Particle density [g/cm^3]	3.17	3.06	3.06	3.06	3.09	3.08
TSA [m^2/cm^3]	3.2	2.9	4.6	11.8	7.9	54.0
Water demand [%]	28.9	26.0	30.5	34.5	55.4	38.6
Zeta potential [mV]	- 3.1	- 1.7	- 2.8	- 6.6	- 5.5	- 7.4
pH [−]	13.0	12.1	12.2	12.2	12.3	12.2

Table 5
Key parameters of blended binders/cement pastes with PLC.

Parameter	PLC	PLC_20QP	PLC_20 TG	PLC_20Mk	PLC_20Mu	PLC_20Mi
Particle density [g/cm^3]	3.09	3.00	3.00	2.99	3.03	3.02
TSA [m^2/cm^3]	5.25	4.26	6.41	14.73	11.27	61.61
Water demand [%]	28.2	25.3	30.3	34.3	55.0	38.4
Zeta potential [mV]	- 3.7	- 2.9	- 3.4	- 9.0	- 6.7	- 10.3
pH [−]	12.6	12.5	12.5	12.3	12.4	12.1

component_H_1.50 where *H* indicates distilled H_2O as fluid and *1.50* the w/s ratio chosen.

2.3.2. Investigations on blended cement pastes

In cementitious systems, the cement is replaced by 20 wt% of quartz powder or calcined clay and the water-to-binder ratio is set constant at 0.50. The required amount of superplasticizer is evaluated via "mini slump test" according to DIN EN 1015–3 [60]. The dosages of active agent in superplasticizers [% by weight of binder, %bwob] are adjusted to get a spread flow of 26 ± 0.5 cm for all cement pastes. The tests (except on QP systems) are conducted by the Department for Construction Chemistry, Technical University Munich (Germany). For the further tests, these adjusted dosages are kept constant using differing amounts of stock solutions, based on distilled water with the respective amount of superplasticizer to eliminate weighing errors. The efficiency of superplasticizers is determined by rotational viscometer on blended cement paste ($m_{binder} = 600$ g) mixed according to DIN EN 196–3 [53]. The measurements start 5 min after water addition and the analysis is carried out analogously to the measurements on clinker-free suspensions. (Blended) cement paste is designated as *type of cement_substitution rate and quartz powder/calcined clay_type of superplasticizer*.

3. Results & discussion

3.1. Particle characteristics and their influence on rheological properties of clinker-free suspensions

QP particles exhibit smooth surfaces and conchoidal marks (Fig. 2a) as also published e.g. by Ref. [61–64]. This results – combined with a coarse particle size distribution (PSD) – in the lowest SSA and water demand (Table 3). Mk exhibits a grainy surface and a structure of stacked layers, similar to the findings of Souri et al. [65]. Contrary to Claverie et al. [25], flash-calcination does not lead to spherical particles of metakaolin (Fig. 2b). Fig. 2c shows a slightly grainy surface of isolated metamuscovite (Mu) platelets with significantly less pronounced layer packages compared to Mk, which corresponds to the lower SSA of Mu

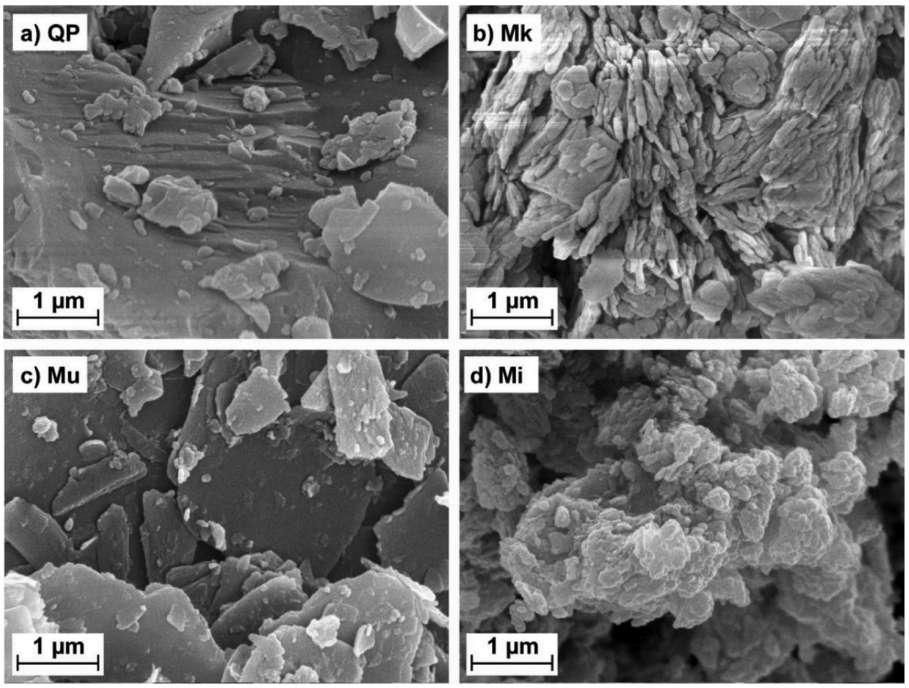

Fig. 2. Particle shapes of pure materials investigated by SEM at 50 k magnification a) QP b) Mk c) Mu d) Mi.

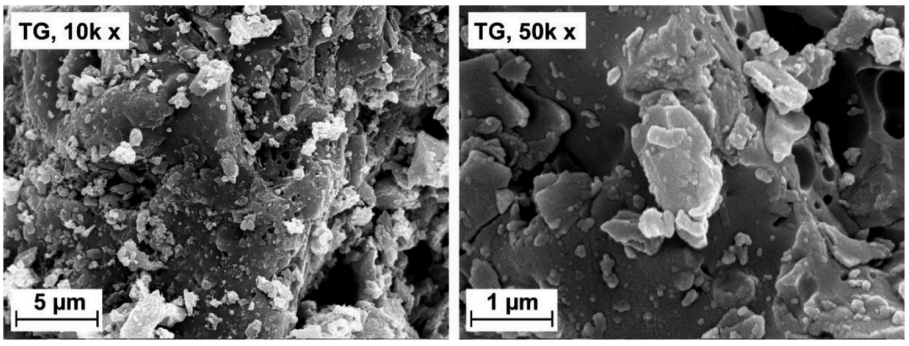

Fig. 3. Particle surface of calcined clay TG at 10 k (left) and 50 k (right) magnification shown by representative spots.

Table 7
Zeta potential (ζ) values of materials suspended in H_2O (w/s ratio = 1.50, duration of measurement = 3 h).

Material	$\zeta_{mean\ value}$ [mV]	ζ_{min} [mV]	ζ_{max} [mV]	Standard deviation σ [mV]
QP	- 16.3	- 17.0	- 15.8	0.2
TG	0.5	- 0.5	2.1	0.6
Mk	- 17.4	- 18.4	- 16.6	0.3
Mu	- 52.0	- 59.1	- 47.7	1.3
Mi	- 21.4	- 22.8	- 20.6	0.5

compared to Mk (Table 3). It reveals that the water demand of the calcined clays cannot be derived from the particle morphology and size analyzed by SEM: although the particle shape is quite smooth and the particles are coarser compared to those of Mk and metaillite (Mi), Mu exhibits the highest water demand of materials investigated (Table 3). Previously, Neißer-Deiters et al. [18] found that the PSD does not correlate with the water demand/water adsorption capacity, which can be confirmed here in a limited way. Compared to the other samples investigated, the SEM image of Mi exhibits diminutive particles agglomerated with larger particles (Fig. 2d). It fits with the PSD of Mi (Fig. 1) and explains – in combination with the mineralogical properties [9,22] - the large SSA of Mi (Table 3). Interestingly, the morphology looks similar to that of kaolinite particles after high energy ball milling [66], which might be due to the fact that the raw material for Mi was dry-milled before calcination. In turn, this takes up the findings of Cassagnabère et al. [24] that grinding has an essential influence on the morphology of calcined clays.

Overviews of calcined common clay (TG) with 10 k and 50 k magnification give an impression of its heterogeneous surface morphology (Fig. 3). It reveals both large areas with smooth surface, similar to that of QP and small, plate-like particles originating from phyllosilicates.

The zeta potential of the calcined clays and quartz powder investigated can be sorted in the following order: Mu ≪ Mi < Mk = QP ≪ TG (Table 7). The calcined phyllosilicates and QP have a constantly negative zeta potential. According to Lowke and Gehlen [67], the zeta potential of ground quartz-H_2O suspension is negative due to the deprotonation of SiO_2, which explains the negative zeta potential of QP. Clay minerals are known for having a negative zeta potential, which alters in case of the addition of Ca^{2+} ions [27,29,68], originating e.g. from clinker phases. Depending on their surface groups at both basal and edge surfaces, phyllosilicates have different tendencies towards protonation: while siloxane groups are difficult to protonate, the protonation of Al- and Mg-groups is favored [69,70]. This leads to anisotropic surface charges of phyllosilicates [71,72]. For example, muscovite

Table 8
Rheological parameters of clinker-free suspensions (w/s ratio = 1.50).

System	Mini slump [cm]	Apparent viscosity [Nmm*min]	Apparent yield stress [Nmm]	R^2 [-]	Median torque at … [rpm]			
					20	40	80	120
QP_H_1.5	–	–	–	–	–	–	–	–
TG_H_1.5	33.1 ± 0.7	0.01	0.21	0.99	0.4	0.6	1.0	1.5
Mk_H_1.5	29.7 ± 1.8	0.02	1.49	1.00	1.9	2.2	3.0	3.8
Mu_H_1.5	31.9 ± 0.8	0.75	- 15.95	0.70	4.9	14.1	35.5	75.6
Mi_H_1.5	15.6 ± 0.2	0.06	11.13	0.97	12.5	13.7	15.9	18.7

Table 9
Classification of linear correlations according to their R^2 values with - - = poor ($R^2 \leq 0.2$), - = minor ($0.2 < R^2 < 0.5$), o = median ($0.5 \leq R^2 < 0.7$), + = good ($0.7 \leq R^2 < 0.9$), + + = very good correlation ($R^2 > 0.9$) (thresholds according to Ref. [77]).

Parameter	Mini slump	Apparent viscosity	Apparent yield stress	Median torque at 120 rpm
Particle density	- - (0.05)	+ (0.72)	- (0.25)	+ (0.85)
SSA	+ + (1.00)	- - (0.07)	- (0.49)	- - (0.01)
TSA	+ + (1.00)	- - (0.06)	- (0.48)	- - (0.01)
Water demand according to Puntke	- - (0.10)	o (0.62)	- - (0.19)	+ (0.75)
d_{50} value	+ (0.72)	- (0.49)	+ (0.89)	- (0.34)
Zeta potential	- - (0.00)	+ (0.83)	- (0.45)	+ + (0.96)

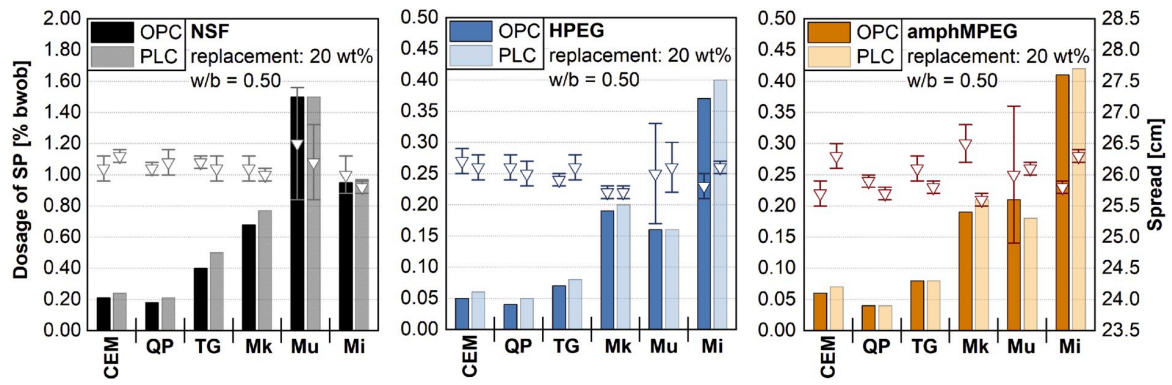

Fig. 4. Required superplasticizer dosages (bars) and median spreads (▾) including standard deviation for cement pastes (information provided by joint research partner, except for QP systems).

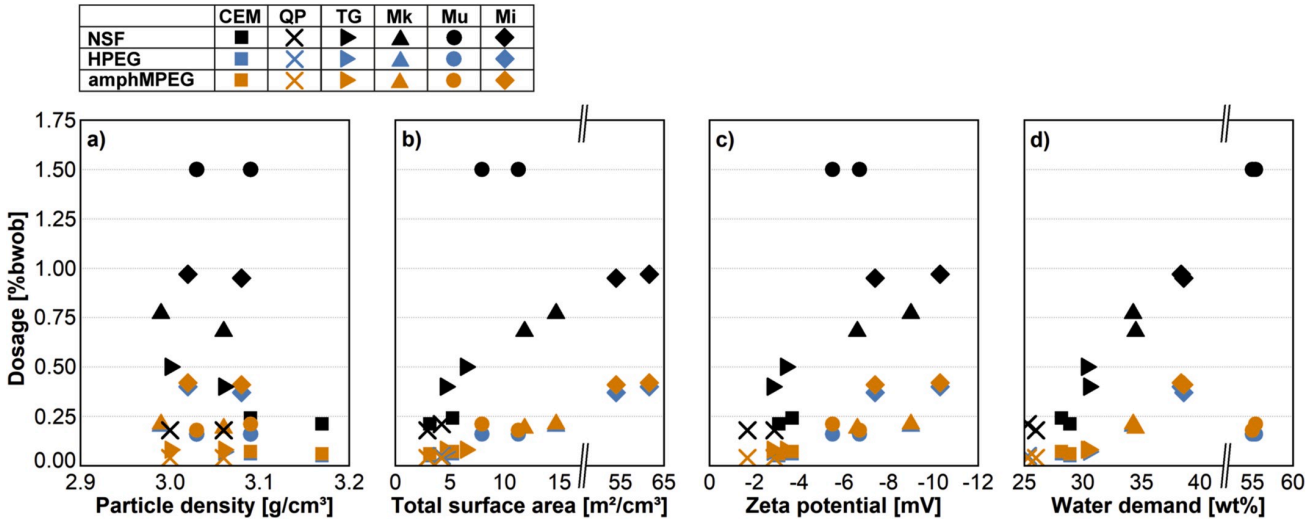

Fig. 5. Correlations between a) particle density, b) total surface area of blended binders, c) zeta potential of blended cement paste and d) water demand of blended binders with the amount of superplasticizer needed for a constant spread of 26 ± 0.5 cm.

exhibits negatively charged basal plane, rather independently of pH value, whereas its edge surface is at least at pH < 8 positively charged. Although there is so far no literature on surface charge of calcined phyllosilicates, this seems to be a reason for their negative zeta potential. TG reveals both a positive (in the beginning of measurement) and slightly negative surface charge (towards the end) over time as also stated by Schmid et al. [34,35]. It remains unclear why the zeta potential of TG is almost neutral since from its mineralogical composition (~68 wt % partly dehydroxylated phyllosilicates, 16 wt% quartz and further components, e.g. feldspar [73]) a negative zeta potential could be expected. With the current knowledge, it is assumed that the particles themselves have both negatively and positively charged edges that are in total almost neutral.

Mini slump tests reveal the following descending order in fluidity: Mi_H_1.5 ≪ Mk_H_1.5 < Mu_H_1.5 < TG_H_1.5. The apparent viscosity of clinker-free suspensions is graded as follows: Mu_H_1.5 ≫ Mi_H_1.5 > Mk_H_1.5 > TG_H_1.5 (Table 8). Both mini slump test and rheometric tests of QP_H_1.5 are not possible due to immediate segregation effects, which indicates excess water. TG_H_1.5 and Mk_H_1.5 have low median torques that go along with low apparent viscosity and yield stress. Mi_H_1.5 exhibits the highest yield stress, which can be explained by the large SSA and water demand of metaillite (Table 3) and by strong bonds of the particles as described by Tregger et al. [74]. Suspensions with TG, Mk and Mi behave like Bingham fluids with positive yield stress and $R^2 \sim 1$ [58,59]. Mu_H_1.5 behaves differently compared to the other calcined materials, as its yield stress is negative at high viscosity. However, this fits with observations of Nosrati et al. [75] where muscovite suspensions had low yield stress at pH > 7. The $R^2 \ll 1$ with increasing flow curve gradient indicates shear-thickening behavior that was previously described for metamuscovite-cement suspensions [76] and it points out the extraordinary behavior of (meta)muscovite as non-negligible component in clays [18].

Linear correlations between physical properties (Tables 3 and 7) and rheological parameters from clinker-free suspensions (Table 8) are evaluated in Table 9, with thresholds according to Ref. [77]. It must be noted, that the results represent four calcined clays of different mineralogy, which might be the reason for a limping judgement and further research is necessary on one material with different processing (calcination, grinding). When one single material is considered, there have been different observations on the correlation between SSA and the particle size distribution (PSD) [18,78]. When looking at different materials, however, there is no correlation between the fineness and the SSA of the particles [51]. This is due to the differences in mineralogy and particle shape, taking into account e.g. of spherical fly ash particles [79,80] versus the particles investigated in this paper (Fig. 2). However, mini slump values of the different materials correlate perfectly with SSA/TSA and well with the d_{50} values of the materials investigated (Table 9). Therefore, the authors assume that the packing density and water film thickness, known from cement paste, both play a key role: a lower SSA leads to a higher water film thickness and as consequence to a higher flowability [81,82]. This is contrary to the observation that the achieved mini slump value does not fit at all with the water demand according to Puntke nor with the zeta potential (Table 9). The authors assume that the chosen w/s ratio of 1.50 has been too high to consider these parameters of the calcined clays for mini slump test, as this method is originally used for mortars [60]. Here, tests with lower w/s ratios might lead to more proper findings. Contrary to the mini slump value, the results derived from rheological measurements do not correlate with SSA/TSA at all (viscosity, torque) or less (yield stress). Tiwari et al. [83] have observed in cementitious systems that the SSA has influence on yield stress, but not on viscosity. Viscosity and torque values fit well with particle density, water demand and zeta potential. The latter correlation

Table 10
Classification of linear correlations according to their R^2 values with - - = poor ($R^2 \leq 0.2$), - = minor ($0.2 < R^2 < 0.5$), o = median ($0.5 \leq R^2 < 0.7$), + = good ($0.7 \leq R^2 < 0.9$), + + = very good correlation ($R^2 > 0.9$) (thresholds according to Ref. [77]).

Parameter	Dosage of NSF	Dosage of HPEG	Dosage of amphMPEG	Dosage of PCE (HPEG; amphMPEG)
Particle density	- - (0.01)	- - (0.03)	- - (0.01)	- - (0.02)
TSA	- - (0.15) Without Mu: + (0.72)	+ + (0.91)	+ (0.88)	+ (0.89)
Zeta potential	- (0.42) Without Mu: + (0.84)	+ (0.73)	+ (0.77)	+ (0.74)
Water demand according to DIN EN 196-3	+ + (0.95)	- - (0.18) Without Mu: + (0.90)	- (0.24) Without Mu: + (0.89)	- - (0.21) Without Mu: + (0.89)

Table 11
Apparent viscosity and yield stress of cementitious systems (w/b ratio of 0.50) with adjusted dosages.

Binder systems	Apparent viscosity [Nmm*min]				Apparent yield stress [Nmm]			
	ref	NSF	HPEG	amph MPEG	ref	NSF	HPEG	amph MPEG
OPC	0.08	0.05	0.05	0.05	6.41	4.64	0.14	1.87
OPC_20QP	0.07	0.05	0.05	0.05	3.53	1.87	0.13	0.70
OPC_20 TG	0.14	0.07	0.09	0.10	17.70			1.05
OPC_20Mk	0.06	0.05	0.07	0.07	169.30			11.78
OPC_5Mu	0.23	–	–	–	23.13	–	–	–
OPC_10Mu	0.30	–	–	–	95.05	–	–	–
OPC_20Mu	0.45	1.76	1.09	1.98	230.90			−30.38
OPC_20Mi	0.17	0.12	0.13	0.13	102.71			−0.04
PLC	0.10	0.03	0.05	0.05	9.45	5.61	1.55	2.78
PLC_20 TG	0.15	0.08	0.09	0.08	19.25	1.12	2.50	0.51

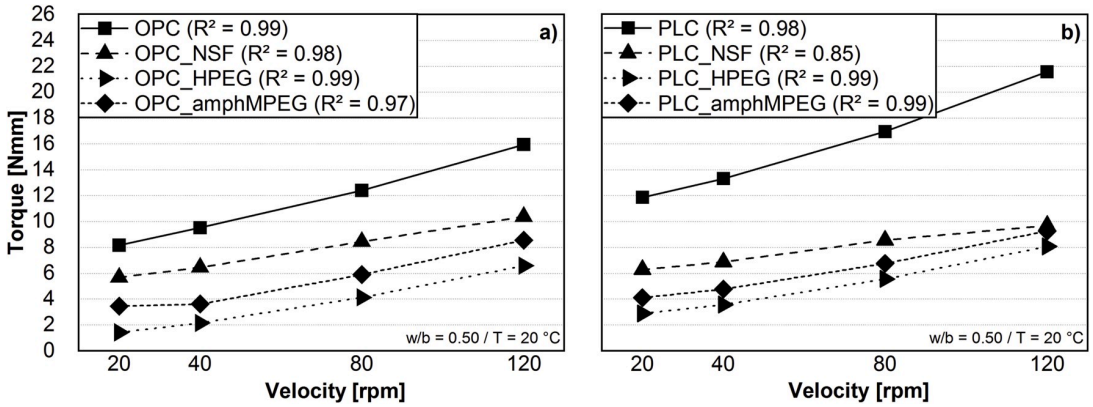

Fig. 6. Median torques of cementitious system a) OPC and b) PLC with various superplasticizers.

is consistent with investigations on pure clay-suspensions where a more negative zeta potential leads to higher flocculation rates [84]. The expected yield stress is difficult to be predicted from the physical properties although d_{50} value and zeta potential correlate well with it (Table 9). Olhero and Ferreira [85] revealed increased yield stress and viscosity with finer particles for silica-based suspensions [83,85].

Hence, there is no physical parameter that correlates consistently with all rheological properties and vice versa (Table 9). Thus, the combination of parameters and testing methods needs to be defined clearly to predict reliably the impact of calcined clays on rheology. In a next step, this knowledge can be transferred to the superplasticizer demand and the rheological properties of blended cementitious systems.

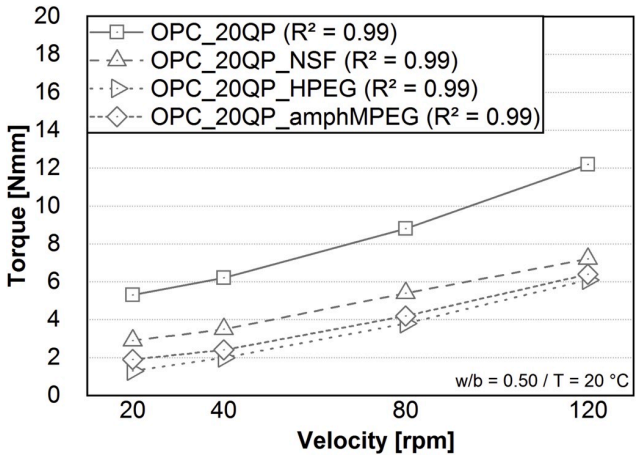

Fig. 7. Median torques of cementitious system OPC_20QP with various superplasticizers.

3.2. Dispersion effectiveness of superplasticizers in calcined clay blended systems

The dispersion effectiveness of superplasticizers is discussed with regard to type of cement, type of superplasticizer and binder constitution. Although limestone filler is known to enhance workability of cementitious systems [86,87], PLC requires continuously more superplasticizer than OPC for identical spread (Fig. 4). This is related to the larger SSA and grinding fineness of PLC (Table 3) but contrary to the lower water demand (Tables 4 and 5). One explanation is the more negative zeta potential of PLC systems (Table 5). A good superplasticizer adsorption behavior is achieved by a positive zeta potential [88]. This means by implication that a more negative zeta potential leads to a lower dispersion by superplasticizers. The results identify PCE polymers being more effective than the polycondensate (NSF) in cementitious systems, which is consistent e.g. with [30,32,89]. Among PCE polymers, the HPEG PCE is slightly more effective than the amphMPEG PCE which is related to the moderate length of side chain and higher anionic charge density of HPEG PCE [90].

Regarding the need for superplasticizer, the binder systems are separated into two groups: those with neat cement, with QP and with TG for one group, those with calcined phyllosilicates for the other. It is not surprising that systems with 20 wt% QP require the lowest superplasticizer dosages as QP exhibits the coarsest PSD, the lowest SSA and water demand, also compared to cement (Table 3). Furthermore, quartz is known to lower viscosity and yield stress [39,40]. Higher amounts of superplasticizer are required for equal dispersion effects when cement is partially replaced by calcined clays, as known from literature [30–32,

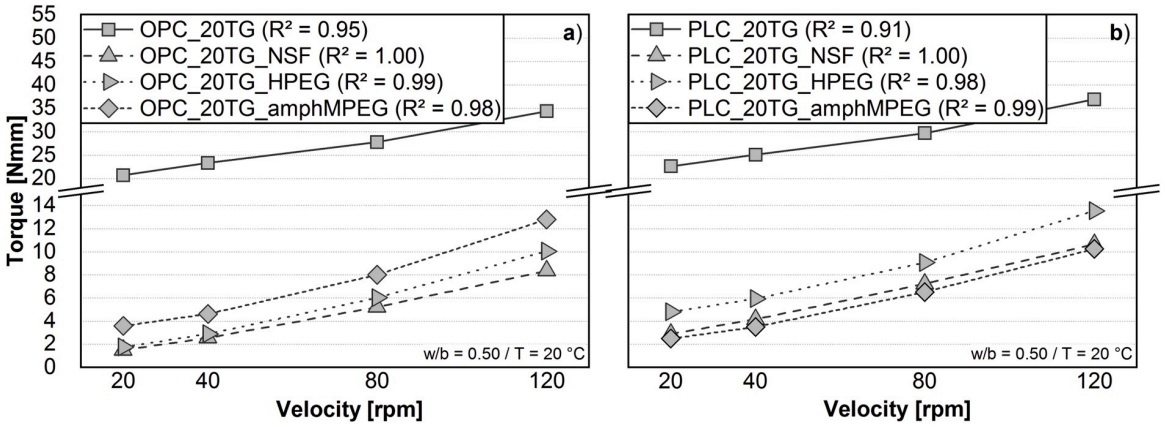

Fig. 8. Median torques of cementitious system a) OPC_20 TG and b) PLC_20 TG with various superplasticizers.

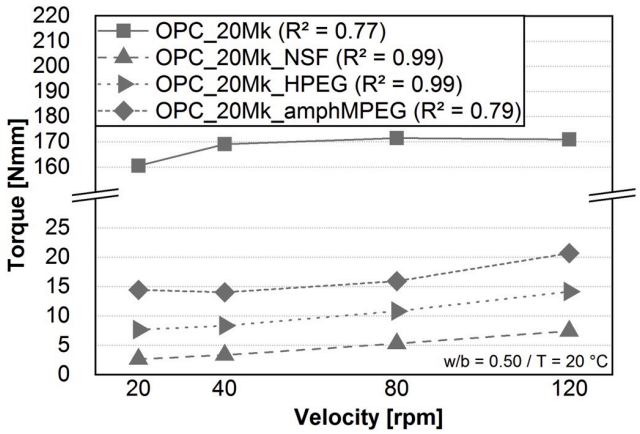

Fig. 9. Median torques of cementitious system OPC_20Mk with various superplasticizers.

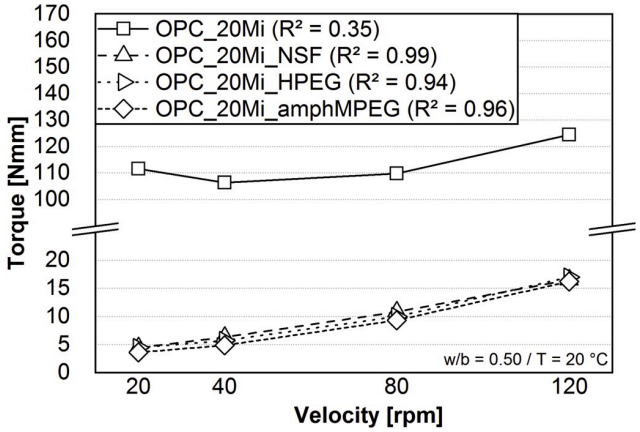

Fig. 10. Median torques of cementitious system OPC_20Mi with various superplasticizers.

91]. With the addition of TG, about twice the amount of NSF is required whereas maximal ~1.4 times higher dosages of HPEG and amphMPEG are needed compared to the neat cement systems. OPC_20 TG and PLC_20 TG are easily to disperse as TG has a similar PSD as the cements, here especially OPC. It exhibits the lowest SSA and water demand of calcined clays investigated (Table 3) and contains a non-negligible

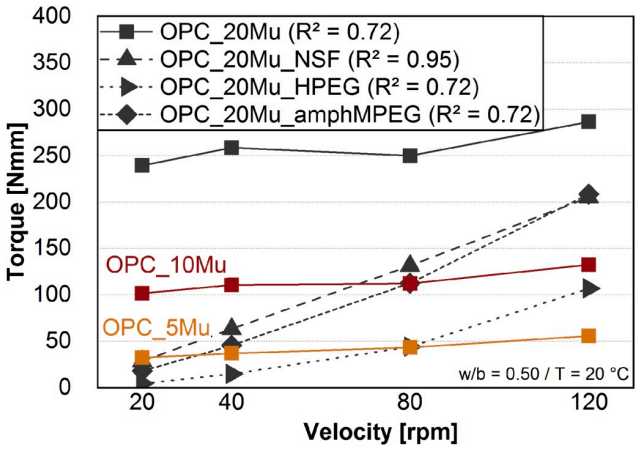

Fig. 11. Median torques of cementitious system OPC_5Mu, OPC_10Mu and OPC_20Mu with various superplasticizers.

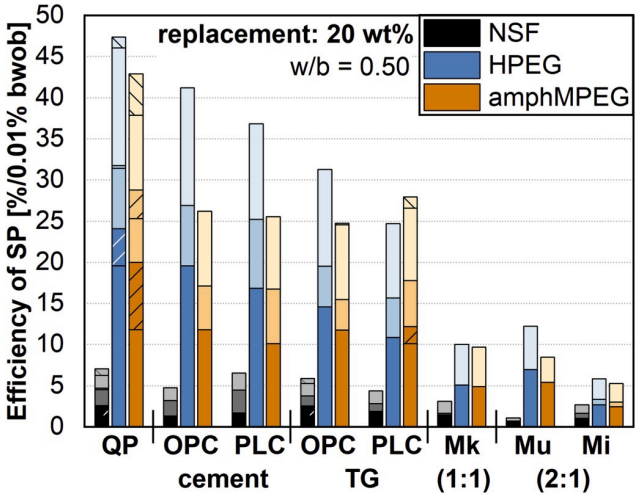

Fig. 12. Efficiency of superplasticizers (SP) [%/0.01% bwob] according to the binder system with 20 wt% substitution rate at w/b ratio = 0.50; opaque, middle, light color indicates reduction of yield stress, viscosity and average shear stress respectively; dashed parts mark higher efficiency compared to neat cement. (For interpretation of the references to color in this figure legend, the reader is referred to the Web version of this article.)

Table 12
TSA and water demand of OPC systems with TG and calcined model clays.

Parameter	OPC with 20 wt% of …		
	TG	25Mk_22.5Mu_22.5Mi_30QP	25Mk_30Mu_15Mi_30QP
TSA [m^2/cm^3]	4.6	17.8	20.0

quantity (16.2 wt%) of quartz. Furthermore, the zeta potential of TG (Table 7) indicates both negatively and positively charged surface sites where the latter are commonly known for a preferred adsorption of anionic superplasticizers [88]. The Amaltheen clay contains ~25 wt% kaolinite and ~40 wt% 2:1 phyllosilicates (predominantly illite and muscovite) in its raw form [5,37]. Considering these phyllosilicates as metaphases after calcination individually, a 3 to 7.5 times higher amount, hence significantly more superplasticizer is required for an adequate dispersion (Fig. 4). Systems with 20 wt% metakaolin need about 3–4 times more superplasticizer, both NSF and PCE, compared to neat cement pastes. The dispersion efficiency of superplasticizer depending on type of calcined phyllosilicate can be sorted as follows:

- NSF: Mk > Mi ≫ Mu
- HPEG: Mu > Mk ≫ Mi
- amphMPEG: Mk = Mu ≫ Mi

With NSF and amphMPEG, the systems with 20 wt% calcined 2:1 phyllosilicates (Mi, Mu) are more challenging regarding the amount of superplasticizer needed than with Mk as calcined 1:1 phyllosilicate which is contrary to Ref. [33]. Especially OPC_20Mu/PLC_20Mu are not dispersed by NSF at all while they reveal a compatibility with both PCE used. There are two possible explanations regarding the incompatibility of Mu and NSF: 1) the effect of the polycondensate is too small to disperse systems with such high water demand [14,18] in a sufficient way or 2) the strongly negative zeta potential of Mu (Table 7) and Mu blended cement pastes (Tables 4 and 5) leads to poor adsorption of anionic polymers. The latter assumption, however, does not fit with the correlation between zeta potential and NSF dosage, shown in Fig. 5. Blends with Mi exhibit a high demand of all superplasticizers, no matter if NSF or PCE. As mentioned in section 3.1, Mi exhibits diminutive particles with rough texture (Fig. 2d) and the highest grinding fineness that results combined with the mineralogical composition [92] in an extremely large SSA, compared to the other binder components investigated (Table 3) [93,94].The enormous demand for superplasticizer might thus result from a preferred adsorption of polymer/water molecules onto Mi surfaces and needs to be investigated further. Nonetheless, it remains still under discussion whether illite or muscovite are more

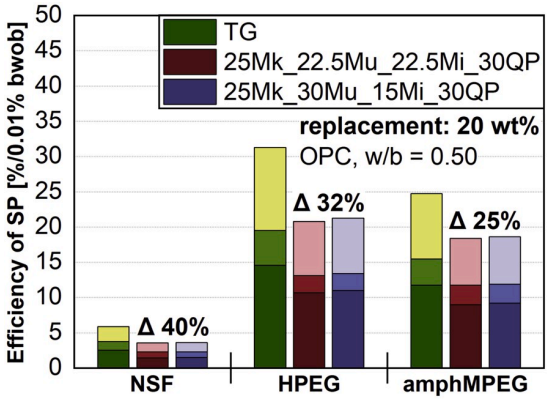

Fig. 13. Comparison of measured efficiency (for TG) and predicted efficiency of model clays calculated from percentage-based efficiency of pure systems with OPC; opaque, middle, light color indicates reduction of yield stress, viscosity and average shear stress respectively.

critical regarding the dispersion effectiveness of superplasticizers and it seems that there is no clear answer, so far. For this reason, it is necessary to take a look at the efficiency towards the rheological behavior in section 3.3.

Analogous to the clinker-free suspensions, it is worth to take a closer look at the physical parameters of the binder systems given in Tables 4 and 5. Therefore, the combined particle density and TSA as well as their zeta potential and water demand are correlated with the adjusted polymer dosages from Fig. 4. While particle density can be a good indicator for apparent viscosity and shear stress of clinker-free suspensions (Table 9), there is only a very poor correlation between particle density and superplasticizer dosage (Fig. 5a and Table 10). Considering the replacement level of 20 wt% in blended cement paste, the only slightly differing particle density of calcined clays seems to have minor impact. Further investigations with volumetric-based replacements and higher levels might point out that the particle density is not a key factor for understanding calcined clay – superplasticizer interaction. The contrary holds for TSA as physical parameter: there are good relationships between the combined TSA and the dosages of NSF and PCE required for similar dispersion while clinker-free suspensions exhibit no relationship between rheological parameters and TSA. It has been discussed already in section 3.1 that SSA, as part of the TSA, is no indicator for viscosity, but it is known as a key parameter for superplasticizer adsorption [93–95].

As mentioned above, the water demand and the zeta potential are no reliable characteristics to derive the rheological behavior of clinker-free suspensions of it. On contrary, an increased water demand and a more negative zeta potential value correlate well with a higher demand for superplasticizers (Fig. 5). The latter relation is again explained by lower adsorption rates of anionic superplasticizers onto negatively charged particles [88,96]. Solely the metamuscovite systems need to be considered separately as the high demand for NSF does not fit with the TSA (Fig. 5b) nor with the zeta potential (Fig. 5c) but well with the water demand (Fig. 5d). This is also congruent with the high water demand of OPC_20Mu and PLC_20Mu as the water adsorbed by calcined clays needs to be compensated by the addition of more superplasticizer. Here it is surprising that OPC_20Mu and PLC_20Mu require relatively low amounts of PCE despite their high water demand.

Although higher amounts of superplasticizer are required for calcined clay blended systems, the dispersion is adequate considering the challenging physical and rheological properties of calcined clays. The superplasticizer dosages correlate well with properties commonly referred to when the superplasticizer demand is discussed. Solely, the system with 20 wt% metamuscovite exhibits an incompatibility with NSF and no plausible correlation between the physical properties and the required amount of different types of superplasticizer. It becomes clear once again that the metamuscovite needs to be considered separately from other calcined phyllosilicates [18,76,97]. With regard to the extremely fine metaillite, a coarser material of the same mineralogy should be examined to differentiate the influence of mineralogy and grinding fineness on the superplasticizer demand more clearly. As shown for the systems with the calcined Amaltheen clay and quartz powder, the necessary amount of superplasticizer can be reduced if a certain amount of quartz is present as it is the case in common clays [98].

3.3. Impact of calcined clays/quartz powder and superplasticizers on the rheology of blended cement paste

The reference PLC and PLC_20 TG both demonstrate higher yield stress and viscosity compared to the corresponding OPC systems (Table 11). With the addition of calcined clays, the apparent viscosity and yield stress are increased, compared to other SCM, which is consistent with publications e.g. from Refs. [32,99]. It was not possible to measure OPC_20Mu due to high initial torques (>500 Nmm). Attempts with lower substitution rates (5 and 10 wt%) reveal drastically

increased apparent viscosity, apparent yield stress and torques of OPC_5Mu and OPC_10Mu with an increasing addition of metamuscovite, which fits with the rheological behavior of Mu in section 3.1. For this reason, the following linear extrapolation is driven for the rheological parameters of OPC_20Mu, although the authors are aware of the deviation between calculated and real values:

- for apparent viscosity: $y = 0.0142\ x + 0.1631$ (with x = substitution rate)
- for apparent yield stress: $y = 13.585\ x - 40.795$

Systems without superplasticizer hence reveal at a w/b ratio of 0.50 the following classifications regarding their yield stress: OPC_20Mu ≫ OPC_20Mk > OPC_20Mi ≫ PLC_20 TG > OPC_20 TG > PLC > OPC > OPC_20QP (Table 11). This correlates – except for Mu – with the yield stress of clinker-free suspensions (Table 8). Corresponding with the results in the previous sections 3.1 and 3.2, the systems with TG exhibit outstanding behavior: the apparent yield stress of OPC_20 TG/PLC_20 TG is closer to that of OPC/PLC than of the systems with calcined phyllosilicates. The relative amount of 2:1 phyllosilicates in TG at a substitution rate of 20 wt% is 8 wt% in binder. Compared to OPC_5Mu and OPC_10Mu however, the OPC_20 TG exhibits significantly lower yield stress and viscosity (Table 11). It demonstrates again that the quartz content in calcined clays is at least one parameter that results in similar flow behavior as for neat cement systems (Cassagnabère et al., 2013). While OPC/OPC_20QP/OPC_20 TG/PLC/PLC_20 TG all exhibit a flow behavior of Bingham fluids with linear shear rates [59], the systems with calcined phyllosilicates are classified as fluids according to the Herschel-Bulkley model with non-linear shear rates [58]. This leads again to the distinction between these two groups as already presented in 3.2. A stronger bond between metakaolin particles [74], a higher binder volume due to mass related clinker replacement [100], a larger SSA [6], the high water demand and flocculating tendency [101] are reasons for an increased yield stress of Mk blended systems and might be extended to other calcined phyllosilicates. The higher density of Mi compared to Mk (Table 3) indicates why OPC_20Mi has lower yield stress than OPC_20Mk despite the higher water demand and SSA of Mi, as it was already shown in clinker-free suspensions (Table 8). The interparticular interactions of binders i.e. van der Waals forces and repulsive double layer forces (indicated by zeta potential) are also commonly known to influence the rheology of cementitious systems [102,103]. While metamuscovite itself, as observed for Mu_H_1.5, exhibits a significantly negative zeta potential (Table 7) and negative yield stress (Table 8), surprisingly contrary effects are observed for metamuscovite blended cement paste. With the chosen substitution rate, the zeta potential of OPC_20Mu (Table 4) is not particularly noticeable among the other blended cement pastes but the yield stress exceeds by far that of other systems (Table 11). So far, zeta potential of calcined clays alone is hardly considered in literature when it comes to the understanding of their rheological behavior while there are several findings on the zeta potential of calcined clay blended systems with superplasticizers [34,35,92]. The addition of superplasticizer reduces marginally the apparent viscosity and significantly the yield stress of all systems (Table 11).

The torque/shear stress of the (blended) cement paste OPC/PLC/OPC_20QP/OPC_20 TG/PLC_20 TG with superplasticizers is <20 Nmm (Fig. 6 to Fig. 8). Most of these systems remain Bingham fluids with apparent yield stress >1 Nmm and $R^2 \sim 1$. Solely OPC_HPEG (Fig. 6a) as well as OPC_20 TG with NSF and HPEG (Fig. 8a) reveal self-flowing properties of Newtonian fluids ($g \approx 0$ and linear relation between shear rate and shear stress, $R^2 \approx 1$) [59] while PLC_NSF exhibits properties of a Herschel-Bulkey fluid ($R^2 = 0.85$) (Fig. 6b).

OPC_20Mk and OPC_20Mi both become Bingham fluids with the addition of PCE (Fig. 9 and Fig. 10). Solely, OPC_20Mk_amphMPEG behaves like a Herschel-Bulkey fluid ($R^2 = 0.79$, apparent yield stress = 11.77 Nmm). OPC_20Mu systems again show up a particular behavior: adding superplasticizers can reduce the viscosity at least to such an extent that rheological measurements become possible at all (Fig. 11). Compared to the viscosity of OPC_5Mu and OPC_10Mu measurements such as the calculated value for OPC_20Mu without superplasticizer, the viscosity of OPC_20Mu with superplasticizer is higher while the yield stress becomes negative (Table 11). Nonetheless, the median torques increase significantly with higher shear rates when superplasticizers added. While the addition of different superplasticizers has only minor impact on the rheology of the other calcined clay or quartz powder blended systems, OPC_20Mu is more sensitive against the type of superplasticizer. The addition of NSF leads to Newtonian fluid behavior ($R^2 \sim 1$) while OPC_20Mu exhibits with the PCE investigated shear-thickening properties ($R^2 \ll 1$) (Fig. 11 and Table 11). The latter findings are consistent with observations that lower w/b ratios and the addition of a MPEG PCE with long side-chain lead to shear-thickening behavior of cementitious systems with metamuscovite [76]. As both PCE polymers have (quite) long side-chains, a higher steric effect might promote shear-thickening behavior according to the assumption of Schmid et al. [76].

3.4. Approach to the calculation of superplasticizer efficiency

The relative reduction of yield stress, viscosity and shear stress compared to each reference system is related to the dosage adjusted for comparable mini slump (Fig. 4). The sum of these three values indicates the efficiency of superplasticizer E [%/0.01 %bwob] (Equation (2)). It should be noted and kept in mind that the calculated values of OPC_20Mu were considered for the efficiency of superplasticizers in metamuscovite systems. Negative values, e.g. in case of increased viscosity, are set as 0% in the sense of "zero efficiency".

$$E = \frac{\left(1 - \frac{g_{sp}}{g_{ref}}\right) + \left(1 - \frac{h_{sp}}{h_{ref}}\right) + \left(1 - \frac{T_{sp}}{T_{ref}}\right)}{d_{sp}} \qquad \text{(Equation 2)}$$

With

$g_{sp}/h_{sp}/T_{sp}$ = yield stress [Nmm]/viscosity [Nmm*min]/average shear stress [Nmm] for binder systems with NSF/HPEG/amphMPEG
$g_{ref}/h_{ref}/T_{ref}$ = yield stress [Nmm]/viscosity [Nmm*min]/average shear stress [Nmm] for binder systems without superplasticizer
d_{sp} = adjusted dosage of NSF/HPEG/amphMPEG [%bwob]

Fig. 12 displays the calculated efficiency, which is separated furthermore in the reduction of yield stress (opaque), viscosity (middle), average shear stress (light). Dashed parts in the column reveal higher efficiency compared to neat cement pastes (OPC and PLC). It points out one more time the significantly higher efficiency of PCE compared to NSF. At the chosen substitution rate, the efficiency of superplasticizers is clearly driven by the type of binder component added. The calculated efficiency is consistently higher in quartz powder blended systems and mostly lower in calcined clay blended systems. Here, the systems with 20 wt% TG are uncritical and the efficiency of superplasticizers comes close to that in neat cement systems. Taking the mineralogy of common clays [98,104] into account, even the impact of a medium content of muscovite (30 wt%) [5,34] in clay is easily compensated by quartz, which lowers the SSA and water demand. Related to the partially extremely high dosages, the efficiency of NSF and both PCE investigated is significantly lower in binder systems with Mk as representative for calcined 1:1 phyllosilicates. The same holds even more with Mu and Mi (calcined 2:1 phyllosilicates) which again relates to the characteristics described in section 3.1. Differences between Mu and Mi systems reveal that NSF has a higher efficiency with Mi, which is in a similar range as for Mk. With the PCE investigated however, the efficiency is higher for Mu. The tendency observed for superplasticizer efficiency hence reveals once again the decisive impact of the pure calcined phyllosilicates in

interaction with different types of polymers as well as the influence of their physical-mineralogical properties on the rheological behavior of blended cement paste.

In a last step, the transferability from pure systems to common clays is evaluated. In order to accomplish this goal, the percentage amount of phyllosilicates and quartz in TG is simulated in two model calcined clays: the content of Mk and QP is set at 25 wt% and 30 wt% respectively. The amount of 2:1 phyllosilicates in TG (45 wt%) is halved for Mu and Mi each in 25Mk_22.5Mu_22.5Mi_30QP and based closer on the mineralogy of TG proposed in Ref. [37] in 25Mk_30Mu_15Mi_30QP. Superplasticizer efficiency of cementitious system with 20 wt% of theses calcined model clays is calculated percentage-based of the efficiency of the pure systems (OPC_20QP/Mk/Mu/Mi) according to their reduction in yield stress (opaque), viscosity (middle) and average shear stress (light) as already presented in Fig. 12. Related to the challenging properties of the calcined 2:1 phyllosilicates investigated, different ratios of Mu and Mi seem to be irrelevant for the superplasticizer efficiency in these systems (Fig. 13). There are significant deviations between the superplasticizer efficiency in OPC_20 TG system and the theoretical values derived for calcined model clay systems (≤40% for NSF and slightly better for PCE). The TSA of OPC systems (Table 4) is calculated on a percentage basis for 25Mk_22.5Mu_22.5Mi_30QP and 25Mk_30Mu_15Mi_30QP. Both TSA are similar but exceed significantly that of OPC_20 TG (Table 12). Furthermore, the particle size distributions of QP and Mi both differ significantly from the PSD of TG (Fig. 1). Despite the significant differences in TSA, the theoretical approach to estimate the efficiency of superplasticizers with model clays is closer to the TG systems than the pure systems: although the TSA is e.g. even larger than for Mk systems (Table 4), the calculated efficiency is better for the calcined model clays. By now, this is explained due to the high amount of coarse QP that compensates the low efficiency in systems with calcined phyllosilicates. It demonstrates the conciseness regarding the individual components and indicates that the efficiency of superplasticizers can be calculated from single component systems with physical properties adjusted to those of common clays.

4. Conclusion

Rheological measurements were conducted on clinker-free suspensions and cementitious systems. In context with the binder systems and superplasticizers investigated, the following aspects are concluded:

- Zeta potential and water demand of calcined clays are good indicators for the rheological behavior of clinker-free suspensions. In cementitious systems, both parameter as well as the total surface area are reliable key factors for the approximation of demand for superplasticizer.
- Systems with metamuscovite need to be treated separately as their demand for superplasticizer does not correlate with the considered factors. As shown for the calcined Amaltheen clay however, the impact of muscovite seems to diminish when it is a part of common clays. The medium muscovite content seems to be uncritical when it comes to the rheological behavior and the compatibility with superplasticizers. This, however, needs to be verified on muscovite-rich clays or mixed-layer mica/smectite.
- As compensation for the challenging phyllosilicates, the amount of quartz plays a decisive role in the workability of calcined clay blended systems. Clays that contain non-negligible amounts of quartz are abundant worldwide. They represent after calcination an appropriate future SCM if a compromise between a proper workability and its pozzolanic reactivity is made.
- As known from literature, the PCE chosen perform significantly better compared to the NSF. NSF exhibits severe incompatibility with metamuscovite systems only. From the point of view of dispersion efficiency, the HPEG is marginally more effective than amphMPEG as it exhibits a shorter side chain length and a higher anionic charge density.
- The influence of cement type is minor and is related with the current knowledge to the physical properties of cement. Further investigations should handle also higher substitution rates as the impact of cement type is expected to be even lower.
- Thus far, the transferability of superplasticizer efficiency from calcined model clays to calcined common clays is limited due to differences in mineralogical composition but especially due to the physical parameters of the single components. To verify the dispersion efficiency of superplasticizers depending on type of phyllosilicate (1:1 vs. 2:1), the metaillite investigated should be compared with a coarser one as its physical properties significantly exceed those of the other calcined phyllosilicates. Further studies should focus on the time-dependent rheological behavior and increased substitution rates for a better evaluation of the dispersion performance.

Acknowledgement

The authors thank Schwenk Zement KG (Germany) for the cements, Liapor GmbH & Co. KG (Germany) for the calcined Amaltheen clay and Bozzetto Group (Italy) for the NSF as well as Jilin Zhongxin Chemical Group Co., Ltd. (China) for the HPEG PCE. The authors like to express their deepest gratitude to Prof. J. Plank and his team from the Department for Construction Chemistry of Technical University Munich (Germany) for the lab-synthesis of the amphMPEG PCE, characterization of superplasticizers and the conduction of mini slump tests within the joint research project. Here, the authors like to thank Deutsche Forschungsgemeinschaft (DFG) for the financial support of the research project “Ecological and energetic optimization of concrete: Interaction of structurally divergent superplasticizers with calcined clays” (PL 472/11–1 and TH 1383/3–1).

Appendix A. Supplementary data

Supplementary data to this article can be found online at https://doi.org/10.1016/j.cemconcomp.2020.103594.

References

[1] A. Tironi, M.A. Trezza, A.N. Scian, E.F. Irassar, Potential use of Argentine kaolinitic clays as pozzolanic material, Appl. Clay Sci. 101 (2014) 468–476.
[2] F. Avet, R. Snellings, A. Alujas Diaz, M. Ben Haha, K. Scrivener, Development of a new rapid, relevant and reliable (R^3) test method to evaluate the pozzolanic reactivity of calcined kaolinitic clays, Cement Concr. Res. 85 (2016) 1–11.
[3] S.E. Schulze, J. Rickert, Suitability of natural calcined clays as supplementary cementitious material, Cement Concr. Compos. 95 (2019) 92–97.
[4] E.F. Irassar, V.L. Bonavetti, C.C. Castellano, M.A. Trezza, V.F. Rahhal, G. Cordoba, R. Lemma, Calcined illite-chlorite shale as supplementary cementing material: thermal treatment, grinding, color and pozzolanic activity, Appl. Clay Sci. 179 (2019) 105143.
[5] N. Beuntner, K.-C. Thienel, Properties of calcined lias delta clay - technological effects, physical characteristics and reactivity in cement, in: K. Scrivener, A. Favier (Eds.), Calcined Clays for Sustainable Concrete - Proceedings of the 1 International Conference on Calcined Clays for Sustainable Concrete, Springer Netherlands, Lausanne, Switzerland, 2015, pp. 43–50.
[6] K. Vance, A. Kumar, G. Sant, N. Neithalath, The rheological properties of ternary binders containing Portland cement, limestone, and metakaolin or fly ash, Cement Concr. Res. 52 (2013) 196–207.
[7] G. Marchetti, J. Pokorny, A. Tironi, M.A. Trezza, V.F. Rahhal, Z. Pavlík, R. Černý, E.F. Irassar, Blended cements with calcined illitic clay: workability and hydration, in: F. Martirena, A. Favier, K. Scrivener (Eds.), Calcined Clays for Sustainable Concrete - Proceedings of the 2nd International Conference on Calcined Clays for Sustainable Concrete, Springer Nature, La Havanna, Cuba, 2018, pp. 311–317.
[8] C. He, B. Osbæck, E. Makovicky, Pozzolanic reactions of six principal clay minerals: activation, reactivity assessments and technological effects, Cement Concr. Res. 25 (8) (1995) 1691–1702.
[9] J.K. Mitchell, K. Soga, Fundamentals of Soil Behavior, third ed., 2005.
[10] C.D. Hatch, J.S. Wiese, C.C. Crane, K.J. Harris, H.G. Kloss, J. Baltrusaitis, Water adsorption on clay minerals as a function of relative humidity: application of BET and freundlich adsorption models, Langmuir 28 (2011) 1790–1803.

[11] B. Velde, D. Righi, A. Meunier, S. Hillier, Origin and Mineralogy of Clays - Clays and the Environment, Springer-Verlag Berlin Heidelberg1995.
[12] K. Jasmund, G. Lagaly, H.M. Köster, E.E. Kohler, M. Müller-Vonmoos, E. A. Niederbudde, K.-H. Schüller, U. Schwertmann, M. Störr, Tonminerale und Tone: Struktur, Eigenschaften, Anwendungen und Einsatz in Industrie und Umwelt, Dr. Dietrich Steinkopff Verlag, Darmstadt, 1993.
[13] F. Jia, J. Su, S. Song, Can natural muscovite be expanded? Colloid. Surface. 471 (2015) 19–25.
[14] W.A. White, E. Pichler, Water-sorption characteristics of clay minerals circular 266, in: I.S.G. Survey (Ed.), Illinois State Geological Survey, Urbana, 1959, p. 20.
[15] M. Brigatti, E. Galán, B. Theng, Structures and mineralogy of clay minerals, in: F. Bergaya, B.K.G. Theng, G. Lagaly (Eds.), Developments in Clay Science, Elsevier, Amsterdam, 2013, pp. 21–81.
[16] F. Nieto, M. Mellini, I. Abad, The role of H_3O^+ in the crystal structure of illite, Clay Clay Miner. 58 (2) (2010) 238–246.
[17] W.R. Caseri, R.A. Shelden, U.W. Suter, Preparation of muscovite with ultrahigh specific surface area by chemical cleavage, Colloid Polym. Sci. 270 (4) (1992) 392–398.
[18] A. Neißer-Deiters, S. Scherb, N. Beuntner, K.-C. Thienel, Influence of the calcination temperature on the properties of a mica mineral as a suitability study for the use as SCM, Appl. Clay Sci. 179 (2019) 105168.
[19] C. He, E. Makovicky, B. Osbæck, Thermal stability and pozzolanic activity of raw and calcined mixed-layer mica/smectite, Appl. Clay Sci. 17 (3–4) (2000) 141–161.
[20] R. Fernandez Lopez, Calcined Clayey Soils as a Potential Replacement for Cement in Developing Countries, Faculté Sciences et Techniques de L'ingénieur, École Polytechnique Fédérale de Lausanne, Lausanne, 2009, p. 154.
[21] R. Fernandez, F. Martirena, K.L. Scrivener, The origin of the pozzolanic activity of calcined clay minerals: a comparison between kaolinite, illite and montmorillonite, Cement Concr. Res. 41 (1) (2011) 113–122.
[22] C. He, E. Makovicky, B. Osbæck, Thermal stability and pozzolanic activity of calcined illite, Appl. Clay Sci. 9 (5) (1995) 337–354.
[23] K.L. Konan, C. Peyratout, A. Smith, J.P. Bonnet, S. Rossignol, S. Oyetola, Comparison of surface properties between kaolin and metakaolin in concentrated lime solutions, J. Colloid Interface Sci. 339 (1) (2009) 103–109.
[24] F. Cassagnabère, P. Diederich, M. Mouret, G. Escadeillas, M. Lachemi, Impact of metakaolin characteristics on the rheological properties of mortar in the fresh state, Cement Concr. Compos. 37 (2013) 95–107.
[25] M. Claverie, F. Martin, J.P. Tardy, M. Cyr, P. De Parseval, O. Grauby, C. Le Roux, Structural and chemical changes in kaolinite caused by flash calcination: formation of spherical particles, Appl. Clay Sci. 114 (2015) 247–255.
[26] VDZ, Calcined clay as a pozzolanic cement constituent, Cement International 14 (1) (2016) 21.
[27] S. Ng, J. Plank, Interaction mechanisms between Na montmorillonite clay and MPEG-based polycarboxylate superplasticizers, Cement Concr. Res. 42 (6) (2012) 847–854.
[28] L. Lei, J. Plank, A concept for a polycarboxylate superplasticizer possessing enhanced clay tolerance, Cement Concr. Res. 42 (10) (2012) 1299–1306.
[29] L. Lei, J. Plank, A study on the impact of different clay minerals on the dispersing force of conventional and modified vinyl ether based polycarboxylate superplasticizers, Cement Concr. Res. 60 (2014) 1–10.
[30] B.H. Zaribaf, K.E. Kurtis, Admixture compatibility in metakaolin–portland-limestone cement blends, Mater. Struct. 51 (2018) 13.
[31] J. Justice, K. Kurtis, Influence of metakaolin surface area on properties of cement-based materials, J. Mater. Civ. Eng. 19 (9) (2007) 762–771.
[32] S. Ng, H. Justnes, Influence of dispersing agents on the rheology and early heat of hydration of blended cements with high loading of calcined marl, Cement Concr. Compos. 60 (2015) 123–134.
[33] S. Ferreiro, D. Herfort, J.S. Damtoft, Effect of raw clay type, fineness, water-to-cement ratio and fly ash addition on workability and strength performance of calcined clay – limestone Portland cements, Cement Concr. Res. 101 (2017) 1–12.
[34] M. Schmid, N. Beuntner, K.-C. Thienel, J. Plank, Colloid-chemical investigation of the interaction between PCE superplasticizers and a calcined mixed layer clay, in: F. Martirena, A. Favier, K. Scrivener (Eds.), Calcined Clays for Sustainable Concrete - Proceedings of the 2 International Conference on Calcined Clays for Sustainable Concrete, Springer, La Havanna, Cuba, 2018, pp. 434–439.
[35] M. Schmid, N. Beuntner, K.-C. Thienel, J. Plank, Amphoteric superplasticizers for cements blended with a calcined clay, in: J. Liu, J. Plank (Eds.), ACI SP 329 - 12 International Conference on Superplasticizers and Other Chemical Admixtures in Concrete, American Concrete Institute, Beijing, China, 2018, pp. 41–54.
[36] M. Schmid, R. Sposito, K.-C. Thienel, J. Plank, Effectiveness of chemically different superplasticizers in calcined clay blended cements, in: A. Parashar, L. Singh, G.D. Rao (Eds.), 3 International Congress on Calcined Clays for Sustainable Concrete, Springer, New Dehli, India, 2019, pp. 189–196.
[37] N. Beuntner, R. Sposito, K.-C. Thienel, Potential of calcined mixed-layer clays as pozzolans in concrete, ACI Mater. J. 116 (4) (2019) 19–29.
[38] E.F. Irassar, A. Tironi, V.L. Bonavetti, M.A. Trezza, C.C. Castellano, V.F. Rahhal, H.A. Donza, A.N. Scian, Thermal treatment and pozzolanic activity of calcined clay and shale, ACI Mater. J. 116 (4) (2019) 133–143.
[39] M. Daukšys, G. Skripkiunas, A. Grinys, Finely ground quartz sand and plasticizing admixtures influence on rheological properties of portland cement paste, Mater. Sci. 16 (4) (2010) 365–372.
[40] J. Kameda, T. Morisaki, Sensitivity of clay suspension rheological properties to pH, temperature, salinity, and smectite-quartz ratio, Geophys. Res. Lett. 44 (19) (2017) 9615–9621.
[41] DIN EN 197-1, Zement - Teil 1: Zusammensetzung, Anforderungen und Konformitätskriterien von Normalzement (Cement - Part 1: Composition, specifications and conformity criteria for common cements), Beuth-Verlag, Berlin, 2011, p. 8.
[42] K. Scrivener, F. Avet, H. Maraghechi, F. Zunino, J. Ston, W. Hanpongpun, A. Favier, Impacting factors and properties of limestone calcined clay cements (LC^3), Green Mater. 7 (1) (2019) 3–14.
[43] F. Avet, L. Sofia, K. Scrivener, Concrete performance of limestone calcined clay cement (LC^3) compared with conventional cements, Adv Civil Eng Mat 8 (3) (2019) 275–286.
[44] K. Scrivener, F. Martirena, S. Bishnoi, S. Maity, Calcined clay limestone cements (LC^3), Cement Concr. Res. 114 (2018) 49–56.
[45] Y. Dhandapani, T. Sakthivel, M. Santhanam, R. Gettu, R.G. Pillai, Mechanical properties and durability performance of concretes with limestone calcined clay cement (LC^3), Cement Concr. Res. 107 (2018) 136–151.
[46] R. Sposito, M. Schmid, N. Beuntner, S. Scherb, J. Plank, K.-C. Thienel, Early hydration behavior of blended cementitious systems containing calcined clays and superplasticizer, in: J. Gemrich (Ed.), 15 International Congress on the Chemistry of Cement, Research Institute of Binding Materials Prague, Prague, Czech Republic, 2019, p. 10.
[47] N. Beuntner, A. Kustermann, K.-C. Thienel, Pozzolanic potential of calcined clay in high-performance concrete, in: M. Serdar, N. Štirmer, J. Provis (Eds.), International Conference on Sustainable Materials, Systems and Structures – SMSS 2019 New Generation of Construction Materials, RILEM Publications S.A.R. L., Rovinj, Croatia, 2019, pp. 470–477.
[48] R. Gmür, K.-C. Thienel, N. Beuntner, Influence of aging conditions upon the properties of calcined clay and its performance as supplementary cementitious material, Cement Concr. Compos. 72 (2016) 114–124.
[49] N. Beuntner, K. Rapp, K.-C. Thienel, Efficiency of calcined clay in cementitious systems, in: T.C. Holland, P.R. Gupta, V.M. Malhotra (Eds.), ACI SP 289 - 12 International Conference on Recent Advances in Concrete Technology and Sustainability Issues, Sheridan Books, Prag, 2012, pp. 413–424.
[50] S. Scherb, N. Beuntner, K.-C. Thienel, Reaction kinetics of the basic clays present in natural mixed clays, in: F. Martirena, A. Favier, K. Scrivener (Eds.), Calcined Clays for Sustainable Concrete - Proceedings of the 2 International Conference on Calcined Clays for Sustainable Concrete, Springer Nature, La Havanna, Cuba, 2018, pp. 427–433.
[51] D.P. Bentz, C.F. Ferraris, M.A. Galler, A.S. Hansen, J.M. Guynn, Influence of particle size distributions on yield stress and viscosity of cement–fly ash pastes, Cement Concr. Res. 42 (2) (2012) 404–409.
[52] ISO 13320, Particle Size Analysis - Laser Diffraction Methods, 2009, p. 51.
[53] DIN EN 196-3, Prüfverfahren für Zement - Teil 3: Bestimmung der Erstarrungszeiten und der Raumbeständigkeit (Methods of testing cement - Part 3: Determination of setting times and soundness), Beuth-Verlag, Berlin, Germany, 2009, p. 17.
[54] DIN EN ISO 17892-3, Geotechnical Investigation and Testing - Laboratory Testing of Soil - Part 3: Determination of Particle Density, Beuth-Verlag, 2015, p. 21.
[55] DIN ISO 9277, Determination of the Specific Surface Area of Solids by Gas Adsorption - BET Method, Beuth-Verlag, Berlin, 2003, p. 19.
[56] M. Hunger, H.J.H. Brouwers, Flow analysis of water–powder mixtures: application to specific surface area and shape factor, Cement Concr. Compos. 31 (1) (2009) 39–59.
[57] M. Schmid, R. Sposito, K.-C. Thienel, J. Plank, Novel zwitterionic PCE superplasticizers for calcined clays and their application in calcined clay blended cements, in: J. Gemrich (Ed.), 15 International Congress on the Chemistry of Cement, Research Institute of Binding Materials Prague, Prague, Czech Republic, 2019, p. 8.
[58] V.A. Hackley, C.F. Ferraris, Guide to Rheological Nomenclature - Measurements in Ceramic Particulate Systems, National Institute of Standards and Technology (NIST), Gaithersburg, Maryland, USA, 2001. III, 29.
[59] H.A. Barnes, K. Walters, The yield stress myth? Rheol. Acta 24 (4) (1985) 323–326.
[60] DIN EN 1015-3, Prüfverfahren für Mörtel für Mauerwerk-Teil 3: Bestimmung der Konsistenz von Frischmörtel (mit Ausbreittisch) (Methods of test for mortar for masonry - Part 3: Determination of consistence of fresh mortar (by flow table)), Beuth-Verlag, Berlin, 2007, p. 12.
[61] A.K. Warrier, H. Pednekar, B.S. Mahesh, R. Mohan, S. Gazi, Sediment grain size and surface textural observations of quartz grains in late quaternary lacustrine sediments from Schirmacher Oasis, East Antarctica: paleoenvironmental significance, Pol. Sci. 10 (1) (2016) 89–100.
[62] A.M. Ali, E. Padmanabhan, Quartz surface morphology of Tertiary rocks from North East Sarawak, Malaysia: implications for paleo-depositional environment and reservoir rock quality predictions, Petrol. Explor. Dev. 41 (6) (2014) 761–770.
[63] G. Li, K.H.R. Moelle, A SEM study of conchoidal structures on fracture surfaces of sandstones, Tectonophysics 216 (3) (1992) 255–272.
[64] N.N. Gindy, Environmental implications of electron microscope study of quartz grains' surface textures on khors sediments, Lake Nasser, Egypt, The Egyptian Journal of Aquatic Research 41 (1) (2015) 41–47.
[65] A. Souri, H. Kazemi-Kamyab, R. Snellings, R. Naghizadeh, F. Golestani-Fard, K. Scrivener, Pozzolanic activity of mechanochemically and thermally activated kaolins in cement, Cement Concr. Res. 77 (2015) 47–59.
[66] N. Vdović, I. Jurina, S.D. Škapin, I. Sondi, The surface properties of clay minerals modified by intensive dry milling — revisited, Appl. Clay Sci. 48 (4) (2010) 575–580.

[67] D. Lowke, C. Gehlen, The zeta potential of cement and additions in cementitious suspensions with high solid fraction, Cement Concr. Res. 95 (2017) 195–204.
[68] L. Zhang, Q. Lu, Z. Xu, Q. Liu, H. Zeng, Effect of polycarboxylate ether comb-type polymer on viscosity and interfacial properties of kaolinite clay suspensions, J. Colloid Interface Sci. 378 (1) (2012) 222–231.
[69] C. Tournassat, E. Ferrage, C. Poinsignon, L. Charlet, The titration of clay minerals: II. Structure-based model and implications for clay reactivity, J. Colloid Interface Sci. 273 (1) (2004) 234–246.
[70] M.J. Avena, M.M. Mariscal, C.P. De Pauli, Proton binding at clay surfaces in water, Appl. Clay Sci. 24 (1) (2003) 3–9.
[71] X. Yin, L. Yan, J. Liu, Z. Xu, J.D. Miller, Anisotropic surface charging of chlorite surfaces, Clay Clay Miner. 61 (2) (2013) 152–164.
[72] L. Yan, A.H. Englert, J.H. Masliyah, Z. Xu, Determination of anisotropic surface characteristics of different phyllosilicates by direct force measurements, Langmuir 27 (21) (2011) 12996–13007.
[73] W.N. Houston, The Surface Chemistry and Geochemistry of Feldspar Weathering, McMaster University, Hamilton, Ontario, 1972, p. 126.
[74] N.A. Tregger, M.E. Pakula, S.P. Shah, Influence of clays on the rheology of cement pastes, Cement Concr. Res. 40 (3) (2010) 384–391.
[75] A. Nosrati, J. Addai-Mensah, W. Skinner, Muscovite clay mineral particle interactions in aqueous media, Powder Technol. 219 (2012) 228–238.
[76] M. Schmid, R. Sposito, K.-C. Thienel, J. Plank, The shear-thickening effect of meta muscovite as SCM and its influence on the rheological properties of ecologically optimized cementitious systems, in: V. Mechtcherine (Ed.), 2 International RILEM Conference on Rheology and Processing of Construction Materials (RheoCon2), Springer, Dresden, Germany, 2019.
[77] G. Kundt, H. Krentz, Ä. Glass, Epidemiologie und Medizinische Biometrie, Shaker Verlag, Aachen, 2011.
[78] I. Dubois, S. Holgersson, S. Allard, M. Malmström, Correlation between particle size and surface area for chlorite and K-feldspar, in: P. Birkle, I.S. Torres Alvarado (Eds.), 13 International Conference on Water-Rock Interaction, CRC Press, Guanajuato, Mexico, 2010, pp. 717–720.
[79] S. Ng, H. Justnes, Influence of plasticizers on the rheology and early heat of hydration of blended cements with high content of fly ash, Cement Concr. Compos. 65 (2016) 41–54.
[80] C.F. Ferraris, K.H. Obla, R. Hill, The influence of mineral admixtures on the rheology of cement paste and concrete, Cement Concr. Res. 31 (2) (2001) 245–255.
[81] G. Marchetti, V.F. Rahhal, E.F. Irassar, Influence of packing density and water film thickness on early-age properties of cement pastes with limestone filler and metakaolin, Mater. Struct. 50 (2) (2017) 11, 111.
[82] H.H.C. Wong, A.K.H. Kwan, Rheology of cement paste: role of excess water to solid surface area ratio, J. Mater. Civ. Eng. 20 (2) (2008) 189–197.
[83] A.K. Tiwari, M.M. Panseriya, P.C. Mathur, S. Chowdhury, Effect of supplementary cementitious materials on the rheology of blended cements, in: V.M. Malhotra, P. R. Gupta, T.C. Holland (Eds.), ACI SP 303 - 13th International Conference on Recent Advances in Concrete Technology and Sustainability Issues, ACI, Ottawa, 2015, pp. 205–216.
[84] M. Chorom, P. Rengasamy, Dispersion and zeta potential of pure clays as related to net particle charge under varying pH, electrolyte concentration and cation type, Eur. J. Soil Sci. 46 (4) (1995) 657–665.
[85] S.M. Olhero, J.M.F. Ferreira, Influence of particle size distribution on rheology and particle packing of silica-based suspensions, Powder Technol. 139 (1) (2004) 69–75.
[86] V. Shah, A. Parashar, G. Mishra, S. Medepalli, S. Krishnan, S. Bishnoi, Influence of cement replacement by limestone calcined clay pozzolan on the engineering properties of mortar and concrete, Adv. Cement Res. (2018) 1–11.
[87] B. González-Fonteboa, D. Carro-López, J. de Brito, F. Martínez-Abella, S. Seara-Paz, S. Gutiérrez-Mainar, Comparison of ground bottom ash and limestone as additions in blended cements, Mater. Struct. 50 (1) (2017) 84.
[88] J. Plank, C. Hirsch, Impact of zeta potential of early cement hydration phases on superplasticizer adsorption, Cement Concr. Res. 37 (4) (2007) 537–542.
[89] O. Burgos-Montes, M. Palacios, P. Rivilla, F. Puertas, Compatibility between superplasticizer admixtures and cements with mineral additions, Construct. Build. Mater. 31 (Supplement C) (2012) 300–309.
[90] F. Winnefeld, S. Becker, J. Pakusch, T. Götz, Effects of the molecular architecture of comb-shaped superplasticizers on their performance in cementitious systems, Cement Concr. Compos. 29 (4) (2007) 251–262.
[91] B.H. Zaribaf, B. Uzal, K. Kurtis, Compatibility of superplasticizers with limestone-metakaolin blended cementitious system, in: K. Scrivener, A. Favier (Eds.), Calcined Clays for Sustainable Concrete - Proceedings of the 1st International Conference on Calcined Clays for Sustainable Concrete, Springer Netherlands, Lausanne, Switzerland, 2015, pp. 427–434.
[92] J. Herrmann, J. Rickert, Interactions between cements with calcined clay and superplasticizers, in: V.M. Malhotra, P.R. Gupta, T.C. Holland (Eds.), ACI SP 302 - 11 International Conference on Superplasticizers and Other Chemical Admixtures in Concrete, American Concrete Institute, Ottawa, Canada, 2015, pp. 299–314.
[93] E. Sakai, K. Yamada, A. Ohta, Molecular structure and dispersion-adsorption mechanisms of comb-type superplasticizers used in Japan, J. Adv. Concr. Technol. 1 (1) (2003) 16–25.
[94] K. Yamada, Basics of analytical methods used for the investigation of interaction mechanism between cements and superplasticizers, Cement Concr. Res. 41 (7) (2011) 793–798.
[95] R. Sposito, I. Dürr, K.-C. Thienel, Lignosulfonates in cementitious systems blended with calcined clays, in: V. Falikman, R. Realfonzo, P. Hájek, P. Riva (Eds.), ACI SP 326 - 2nd International Workshop on Durability and Sustainability of Concrete Structures, Sheridan Books, Moscow, Russia, 2018, pp. 10.1–10.10.
[96] K. Yoshioka, E.-i. Tazawa, K. Kawai, T. Enohata, Adsorption characteristics of superplasticizers on cement component minerals, Cement Concr. Res. 32 (10) (2002) 1507–1513.
[97] R. Sposito, M. Schmid, J. Plank, K.-C. Thienel, An Approach to the Rheological Behavior of Cementitious Systems Blended with Calcined Clays and Superplasticizers, 11 International Conference on Cementitious Materials and Alternative Binders for Sustainable Concrete, Toulouse, 2020. submitted for publication.
[98] M. Maier, N. Beuntner, K.-C. Thienel, An approach for the evaluation of local raw material potential for calcined clay as SCM, based on geological and mineralogical data: examples from German clay deposits, in: B. Shashank (Ed.), Calcined Clays for Sustainable Concrete - Proceedings of the 3 International Conference on Calcined Clays for Sustainable Concrete, Springer Singapore, Delhi, India, 2020.
[99] R. Siddique, M.I. Khan, Supplementary Cementing Materials, Springer, Berlin Heidelberg, 2011.
[100] E.F. Irassar, V. Rahhal, C. Pedrajas, R. Talero, Rheology of Portland Cement Pastes with Calcined Clays Additions, CTSI Clean Technologies and Sustainable Industries Organization, Washington, DC, 2014, pp. 308–311. Cleantech 2014.
[101] E. Moulin, P. Blanc, D. Sorrentino, Influence of key cement chemical parameters on the properties of metakaolin blended cements, Cement Concr. Compos. 23 (6) (2001) 463–469.
[102] D. Lowke, Interparticle forces and rheology of cement based suspensions, in: Z. Bittnar, P.J.M. Bartos, J. Němeček, V. Šmilauer, J. Zeman (Eds.), 3 International Symposium on Nanotechnology in Construction (NICOM3), Springer Berlin Heidelberg, Prague, Czech Republic, 2009, pp. 295–301.
[103] M. Haist, Zur Rheologie und den physikalischen Wechselwirkungen bei Zementsuspensionen, Fakultät für Bauingenieur-, Geo- und Umweltwissenschaften, Universität Karlsruhe (TH), Karlsruhe, 2010, p. 205.
[104] C.A. Alexiades, M.L. Jackson, Quantitative clay mineralogical analysis of soils and sediments, in: S.W. Bailey (Ed.), Clays and Clay Minerals - Proceedings of the 14th National Conference, Pergamon, Berkeley, California, 1966, pp. 35–52.

7.2 Rheology, setting and hydration of calcined clay blended cements in interaction with PCE-based superplasticisers

Peer-reviewed journal paper [Reprint]

"Rheology, setting and hydration of calcined clay blended cements in interaction with PCE-based superplasticisers"

Ricarda Sposito, Nancy Beuntner, Karl-Christian Thienel

Magazine of Concrete Research

Volume 73, Issue 15, pp. 785 – 797 (August 2021)

Cite this article
Sposito R, Beuntner N and Thienel KC
Rheology, setting and hydration of calcined clay blended cements in interaction with PCE-based superplasticisers.
Magazine of Concrete Research,
https://doi.org/10.1680/jmacr.19.00488

Research Article
Paper 1900488
Received 04/10/2019; Revised 14/12/2019; Accepted 16/12/2019

Keywords: admixtures/cement/cementitious materials/rheological/rheological properties

Magazine of Concrete Research

ice Publishing

Rheology, setting and hydration of calcined clay blended cements in interaction with PCE-based superplasticisers

Ricarda Sposito
Research Assistant, Institute for Construction Materials, University of the Bundeswehr Munich, Neubiberg, Germany (corresponding author: ricarda.sposito@unibw.de) (Orcid:0000-0002-7213-1814)

Nancy Beuntner
Laboratory Head of Institute, Institute for Construction Materials, University of the Bundeswehr Munich, Neubiberg, Germany (Orcid:0000-0002-3724-8240)

Karl-Christian Thienel
Full-time Professor and Head of Institute, Institute for Construction Materials, University of the Bundeswehr Munich, Neubiberg, Germany (Orcid:0000-0002-4087-6205)

Calcined clays represent a promising supplementary cementitious material (SCM) to face the growing demand for binders and to compensate for the decreasing availability of established SCMs worldwide. A fundamental knowledge about the interaction of cementitious systems with polycarboxylate ether (PCE)-based superplasticisers is required for their optimised use as clinker substitute. As clays contain different phyllosilicates, this study focuses on the behaviour of calcined phyllosilicates (metakaolin, metamuscovite, metaillite) and one calcined naturally occurring clay. The impact on the rheology, hydration and setting behaviour of blended cement pastes with two PCE-based superplasticisers is investigated using rotational viscometry, isothermal calorimetry and ultrasound, respectively. The investigations reveal a good dispersion effectiveness of both PCE-based superplasticisers even with challenging calcined phyllosilicates. The demand for superplasticiser can be derived largely from the physical properties of calcined materials, except for metamuscovite. The calcined naturally occurring clay is easily dispersed due to its high quartz content. The physical properties are also key parameters for the hydration and setting: the high specific surface area and pozzolanic properties of calcined phyllosilicates can compensate for retardation effects whereas there can be a significant retardation due to superplasticiser overdosage. Calcined clays with quartz may represent a promising future clinker substitute for the concrete industry in view of hitherto uncritical superplasticiser dosages.

Notation

g	apparent yield stress (Nmm)
h	apparent viscosity (Nmm.min)
m_{binder}	mass of binder component (g)
N	velocity (rpm)
n_{EO}	ethylene oxide units in superplasticiser side chain
$Q_{\max}$	maximum heat of hydration (mW/g)
$Q_{\min}$	minimum heat of hydration (mW/g)
R^2	stability index for viscosimetric measurements
T	torque (Nmm)
$t_{Q,\max}$	time of maximum heat of hydration (h)
$t_{Q,\min}$	time of minimum heat of hydration (h)
$t_{US,\max}$	time of maximum ultrasonic acceleration (h)
$t_{US,\min}$	time of minimum ultrasonic acceleration (h)
$US_{\max}$	maximum ultrasonic acceleration (m/s²)
$US_{\min}$	minimum ultrasonic acceleration (m/s²)
γ	shear rate
η	viscosity
τ	shear stress
τ_0	dynamic shear stress

Introduction

Calcined clays represent an attractive supplementary cementitious material (SCM) in the face of an increasing demand for binder components. Their influence on workability starts with the mineralogical composition of the raw clays, as their water demand depends on the type of clay mineral (He *et al.*, 1995). The dehydroxylation by calcination goes hand in hand with a decrease in specific surface area (SSA) (Beuntner and Thienel, 2015; He *et al.*, 1995; He *et al.*, 2000; Neißer-Deiters *et al.*, 2019). Due to the still-larger SSA compared to other SCMs and cements, calcined clay blended systems require the use of a superplasticiser (Beuntner *et al.*, 2019). Recent findings by Neißer-Deiters *et al.* (2019) even revealed an increasing water absorption capacity of muscovite by calcination, which can require additional measures for a proper workability of calcined muscovite-containing clays. Metakaolin (Mk)-blended cement paste exhibits both thixotropic and dilatant flow behaviour (Curcio and DeAngelis, 1998). Besides the SSA, the surface charge of clays before and after calcination should be considered as the main parameter for the adsorption of superplasticisers. Schmid *et al.* (2018a, 2018b, 2018c) assume heterogeneous surface charges of calcined Amaltheen clay (TG), leading to good adsorption behaviour of superplasticisers, whereas systems with Mk (Zaribaf *et al.*, 2015; Zaribaf and Kurtis, 2018) or calcined marl (Ng and Justnes, 2015a) are known for a higher superplasticiser demand compared to plain cement systems. Systems with calcined kaolinitic clay require more superplasticisers than those with calcined 2 : 1 clay, according to Ferreiro *et al.* (2017).

Magazine of Concrete Research

Apart from their significant impact on workability, calcined clays have a pozzolanic contribution on clinker reaction kinetics during early hydration and can promote the aluminate clinker reaction (Beuntner, 2019; Danner *et al.*, 2012; Scherb *et al.*, 2018). A fundamental understanding regarding the reaction kinetics of calcined clays in combination with superplasticisers in practical cementitious systems is urgently needed. Therefore, different phyllosilicates have to be investigated in combination with promising superplasticisers. Polycondensate- and polycarboxylate ether (PCE)-based superplasticisers can both retard (Prince *et al.*, 2002) and accelerate (Roncero *et al.*, 2002; Sakai *et al.*, 2006) the aluminate clinker reaction, while the silicate clinker reaction is usually retarded (Cheung *et al.*, 2011; Jansen *et al.*, 2012; Lothenbach and Winnefeld, 2007). According to Mollah *et al.* (2000) and several other authors (Cheung *et al.*, 2011; Jansen *et al.*, 2012; Marchon, 2016), the reasons for this are: (*a*) complexation of calcium ions, (*b*) hindered dissolution of clinker phases, (*c*) modified nucleation during hydration due to the adsorption of PCE on cement grains and hydrate phases and (*d*) disequilibrium of aluminate, silicate and sulfate carrier.

Calcined clays require huge amounts of lignosulfonates that exceed recommended dosage limits and lead to strong retardation effects (Sposito *et al.*, 2018). Polycondensates retard the aluminate clinker reaction and formation of ettringite while PCE-based superplasticisers exhibit the least influence on the hydration kinetics of calcined clay blended systems (Ng and Justnes, 2015a; Zaribaf and Kurtis, 2018).

For a better understanding of calcined clay–superplasticiser interactions, it is worth looking at other pozzolans. Fly ash enhances the fluidity of cement paste due to its round particle shape, and with superplasticiser the hydration kinetics are retarded by both the fly ash and superplasticiser (Ng and Justnes, 2016). The accelerating effect of silica fume can be diminished by the preferred adsorption of retarding PCE molecules on the surface of silica fume particles (Meng *et al.*, 2016). On the other hand, the preferred adsorption of PCE on silica fume leads to less adsorption on clinker grains, which enables their unhindered hydration (Meng *et al.*, 2016). Hence, the influence of the cementitious system on the reaction kinetics depends largely on the amount of silica fume and superplasticiser (Meng *et al.*, 2016; Meng *et al.*, 2019).

Besides the dosage of superplasticiser (Marchon, 2016; Meng *et al.*, 2019; Winnefeld, 2012) and the binder constitutions, the molecular structure and the chemical composition of PCE-based superplasticisers both influence the reaction kinetics of cementitious systems. According to Winnefeld *et al.* (2007), a more pronounced retardation relates to an increased charge density. Furthermore, the mechanisms of retardation seem to differ between methacrylate-based and acrylate-based PCE superplasticisers: while the former hinders the dissolution of tricalcium silicate (by adsorption), the latter rather prevents the nucleation of calcium silicate hydrate (C–S–H) (Regnaud *et al.*, 2011).

Taking this knowledge into account, a fundamental understanding of the interaction of calcined clays with superplasticisers in practical cementitious systems is urgently needed. The first part of this paper deals with the modification of rheological behaviour of cement pastes due to the addition of different calcined clays and with the effectiveness of PCE-based superplasticisers in calcined clay blended systems. The second part discusses the influence of calcined clays in interaction with PCE on hydration and setting behaviour, and proposes how to combine established methods in order to better predict the hydration and setting of calcined clay blended systems.

Research significance

This study focuses on the use of calcined clays with their challenging physical properties as clinker replacement in the face of the demand for suitable superplasticisers in the modern concrete industry. As usually higher amounts of superplasticisers are required for an equal dispersion, the addition of superplasticisers can have a significant impact on hydration and setting behaviour. This paper presents the interaction of different clay components with PCE-based superplasticisers regarding both the rheology and hydration/setting behaviour. For the latter, it proposes an analysis for the altered reaction mechanisms of calcined clay blended systems.

Experimental programme

Materials and binder systems

An ordinary Portland cement (OPC) and a Portland limestone cement (PLC) (for selected data) were used in the experimental programme. The mineralogical composition of the cements is given in Table 1. Both cements were substituted by 20 wt% of calcined clays at a water/binder (w/b) ratio of 0·50. TG from southern Germany was chosen – this has been described in detail elsewhere, for example in Beuntner *et al.* (2019). TG

Table 1. Mineralogical composition of OPC and PLC

	Component: %								
Cement	Tricalcium silicate	Dicalcium silicate	Tricalcium aluminate	Tetracalcium aluminoferrite	Calcium carbonate	Sulfate carrier	Dolomite	Magnesium oxide	Free calcium oxide
OPC	61·6	18·2	5·8	9·0	0·6	3·2	—	0·9	0·6
PLC	48·9	15·2	5·1	8·1	14·4	4·0	3·0	0·8	0·1

Table 2. Physical parameters of binder components and ion-solubility of calcined clays

Parameter	OPC	PLC	Mk	Mu	Mi	TG
Particle density: g/cm^3	3·17	3·09	2·61	2·79	2·72	2·63
Brunauer–Emmett–Teller SSA: m^2/g	1·0	1·7	17·8	11·8	94·6	3·9
Water demand of cementitious systems: %	28·9	28·2	34·5/34·3	55·4/55·0	38·6/38·4	30·5/30·3
Water demand (Puntke): %	—	—	56·9	79·8	67·7	42·1
			57·8	83·2	69·7	45·8
			59·4	92·3	71·8	46·4
d_{10}: μm	4·1	2·3	3·0	9·3	2·7	4·0
d_{50}: μm	15·8	13·1	14·8	19·2	6·8	13·2
d_{90}: μm	46·0	46·0	76·2	45·7	61·9	37·0
Silicon ion solubility: wt%	—	—	15·6	4·0	0·5	1·8
Aluminium ion solubility: wt%	—	—	14·2	1·5	0·3	1·1

contains in its natural form different phyllosilicates (25 wt% kaolinite and 45 wt% 2 : 1 clay minerals, e.g. illite and muscovite) and 30 wt% inert components (e.g. quartz, feldspar, calcite, sulfates). An industrially used Mk, metaillite (Mi) and metamuscovite (Mu) were investigated as calcined phyllosilicates. The Mi and Mu were calcined as powders in a laboratory muffle kiln at 770 and 800°C, respectively. Raw illite had been dry-milled before calcination to reduce the particle size at delivery from $d_{50} = 86$ μm to $d_{50} = 3{\cdot}7$ μm. Muscovite is not a clay, but for simplicity all calcined materials are designated as 'calcined clays', as they also are in the following text. Table 2 lists the physical parameters of all binder components and solubility of ions of calcined clays analysed on elution according to DIN EN ISO 11885 (DIN, 2009b). Water demand is determined on binder systems according to DIN EN 196-3 (DIN, 2009a) and for calcined clays according to Puntke (Hunger and Brouwers, 2009).

Two superplasticisers were selected to investigate their effectiveness in calcined clay blended cementitious systems by using 0·20% active agent by weight of binder (%bwob). An α-methallyl-ω-methoxy poly(ethylene glycol) ether type PCE (HPEG) with a side chain length of $n_{EO} = 66$ and anionic charge density of 1751 μeq/g was investigated. Its solid content is 50·0 wt%. A second PCE-based superplasticiser was synthesised in the Department for Construction Chemistry of the Technical University Munich, Germany. It is an amphoteric polymer (amphMPEG) with a methacrylic acid monomer, ω-methoxy poly(ethylene glycol) methacrylate ester (MPEG) macromonomer and a diallyl dimethylammonium chloride as cationic monomer. It has a longer side chain ($n_{EO} = 113$) and lower anionic charge density (1061 μeq/g) compared to HPEG, and its solid content is 33·0 wt%. The solid content was considered as an active agent while the residual superplasticiser was considered as 'water' for the w/b ratio. Hence, the systems always contained the same amount of active agent and water. Stock solutions containing 1 l with superplasticiser and water were prepared to reduce weighing errors.

The samples were designated in the following order: (*i*) type of cement; (*ii*) substitution rate; (*iii*) type of calcined clay; (*iv*) dosage of superplasticiser; and (*v*) type of superplasticiser.

Methods

Rheological measurements were conducted on blended cement paste ($m_{binder} = 600$ g) according to DIN EN 196-3 (DIN, 2009a) using a rotational viscometer, the Viskomat NT (Schleibinger, Germany). This was coupled with a water-based circulatory cooling unit set at 20°C. The velocity started at 120 rpm for 10 min and successively slowed down to 80, 40 and then 20 rpm for 2 min each. Rheological parameters were analysed according to the Bingham equation (Barnes and Walters, 1985; Hackley and Ferraris, 2001) (Equation 1).

$$T = g + Nh \quad (1)$$

where torque (T) ≈ shear stress (τ); apparent yield stress (y-intercept of flow curve) (g) ≈ dynamic yield stress (τ_0); velocity (N) ≈ shear rate (γ); and apparent viscosity (slope of flow curve) (h) ≈ viscosity (η).

The classification regarding the rheological behaviour was based on the criteria in Table 3.

Table 3. Classification schema for rheological properties of suspensions

Apparent yield stress, g: Nmm	R^2	Type of fluid	
$g > 0$	∼1	Bingham fluid (Barnes and Walters, 1985; Hackley and Ferraris, 2001)	
	≪1	Herschel–Bulkey fluid (Hackley and Ferraris, 2001)	
$g \leq 0$	∼1	Newton fluid (Barnes and Walters, 1985; Hackley and Ferraris, 2001)	
	≪1	Decreasing flow curve gradient	Shear-thinning (pseudoplastic) fluid (Hackley and Ferraris, 2001)
		Increasing flow curve gradient	Shear-thickening (dilatant) fluid (Hackley and Ferraris, 2001)

Magazine of Concrete Research

The hydration kinetics were determined for 36 h by isothermal calorimetry with TAM Air (TA Instruments, Delaware/USA) at 25°C. Each binder was homogenised for 30 s before the paste was mixed for 60 s by hand. The samples were transferred into plastic ampoules for calorimetric measurements. The resulting heat flow was calculated per 1 g of cement. The cumulative heat of hydration (HH; in J/g) was calculated by integrating the heat flow over time and multiplying it by 3·6 to adjust the units. It was set at 0 J/g at the end of the rest period (when the heat flow began to rise again).

The early setting behaviour and hardening of binder systems were measured indirectly for 36 h via the development of ultrasound speed (m/s) by an ultrasonic p-wave unit, Vikasonic (Schleibinger, Buchbach/Germany). According to several authors, this is a reliable and suitable method for systems with different consistencies (Lootens and Bentz, 2016; Trtnik *et al.*, 2009). Segregation effects can be counteracted by adding quartz to cement paste (von Daake, 2016; von Daake and Stephan, 2015). Thus, binder systems with 40 vol% of quartz powder and 60 vol% of pure and blended cement paste were mixed when superplasticisers were used. Reference systems without superplasticisers were measured on cement pastes only. The equipment was stored in a climate chamber (20°C/65% relative humidity) during measurement. For the correlation of ultrasonic speed development with isothermal calorimetry, the original curve of ultrasonic speed was analysed based on von Daake (2016) as follows.

(*a*) The data points were reduced to a total amount of 1000.
(*b*) The reduced curve was smoothed by a Savitzky–Golay filter (10 points, 2nd degree polynomial).
(*c*) The smoothed curve was derived by time (1st order), which results in the acceleration of ultrasound (divided by 3600 to adjust the units).
(*d*) The acceleration of ultrasound (m/s^2) was smoothed by a Savitzky–Golay filter (100 points, 2nd degree polynomial).

In order to prove the correlation between heat flow and setting behaviour, selected in situ XRD measurements were conducted. The sample preparation was analogous to the isothermal calorimetry. The blended cement paste was transferred into flat metal crucibles and covered by a Kapton film to prevent drying of the fresh paste. The hydration behaviour was observed by X-ray diffraction (XRD), using, Empyrean (PANalytical, Almelo/Netherlands), with PIXcel^{1D} detector and Bragg–Brentano^{HD} monochromator. The XRD sample holder was connected to a temperature-controlled device (25°C). The time-dependent appearance and disappearance of phases were determined by qualitative peak analysis of representative main reflexes with the following Miller indices: ettringite ((010) and (110)) (Goetz-Neunhoeffer and Neubauer, 2005), hemicarboaluminate (006) (Runcevski *et al.*, 2012), gypsum (020) (Schofield *et al.*, 2000), anhydrite (020) (Kirfel and Will, 1980) and portlandite (001) (Busing and Levy, 1957), using the software Highscore Plus 4·7 (PANalytical, Almelo/Netherlands).

Results

Rheological behaviour

The reference systems with 20 wt% Mu could not be measured using the rotational viscometer. To address this, the amount of Mu was reduced to 10 wt% and 5 wt%. With these results included, the yield stress of reference systems has the following order: OPC/PLC_20Mu≫OPC_20Mk/PLC_20Mi>OPC_20Mi/PLC_20Mk≫OPC/PLC_20TG>OPC/PLC. The apparent viscosity is similar for OPC and OPC_20Mk as well as for OPC_20Mi and OPC_20TG, respectively. PLC systems exhibit higher apparent viscosity compared to OPC systems where PLC_20Mk has the highest and PLC the lowest value.

Independent of HPEG and amphMPEG, apparent viscosity is reduced for OPC/PLC and OPC/PLC_20TG, it stays similar to reference for OPC_20Mk whereas it is reduced for PLC_20Mk and is even slightly increased in OPC/PLC_20Mi systems. All systems, OPC/PLC_20Mu especially, reveal a (slightly) higher

Table 4. Apparent viscosity and yield stress of cementitious systems with and without 0·20%bwob PCE

	Apparent viscosity, *h*: Nmm.min			Apparent yield stress, *g*: Nmm		
Binder systems	Ref	HPEG	amphMPEG	Ref	HPEG	amphMPEG
OPC	0·08	0·03	0·05	6·41	–0·55	1·87
OPC_20Mk	0·06	0·05	0·07	169·30	6·97	11·77
OPC_20Mu	—	0·83	1·98	—	–23·28	–30·38
OPC_20Mi	0·17	0·20	0·22	102·71	21·78	42·20
OPC_20TG	0·14	0·06	0·06	17·70	–0·94	–0·92
PLC	0·10	0·03	0·03	9·47	–0·57	–0·52
PLC_20Mk	0·24	0·05	0·06	77·50	13·82	17·20
PLC_20Mu	—	1·00	1·67	—	–23·70	43·44
PLC_20Mi	0·20	0·23	0·28	86·35	41·36	61·22
PLC_20TG	0·15	0·05	0·05	19·26	–0·92	–0·82

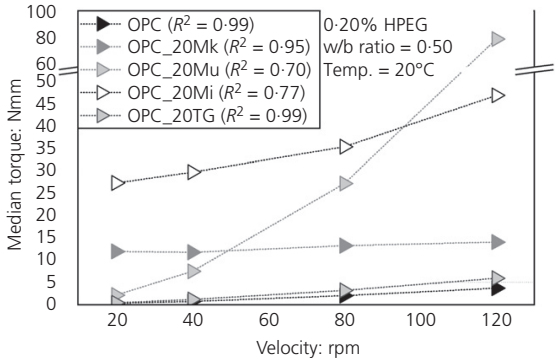

Figure 1. Median torques of OPC_x_0·20HPEG systems

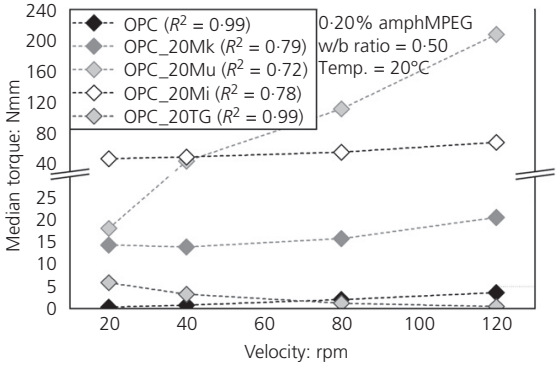

Figure 2. Median torques of OPC_x_0·20amphMPEG systems

viscosity with amphMPEG compared to HPEG, indicating the better adsorption behaviour of the latter.

Yield stress, one of the main parameters for concrete workability (Colombo *et al.*, 2017), is significantly reduced with the addition of PCE. Again, OPC/PLC_20Mu systems stand out for its extraordinary behaviour due to highly negative yield stress (Table 4). As the negative values are physically implausible, they are assumed to be zero and suggest self-flowing properties (Barnes and Walters, 1985). PLC_20Mu_0·20amphMPEG still exhibits a high yield stress due to a less effective dispersion of amphMPEG compared to HPEG. The yield stress of OPC/PLC and OPC/PLC_20TG is slightly negative or close to zero, which indicates the behaviour of a Newton fluid as R^2 values are ∼1 (Figures 1 and 2). The biggest reduction of yield stress due to the addition of the superplasticisers is shown by OPC/PLC_20Mk followed by OPC/PLC_20Mi systems, which still maintain the highest yield stress of all systems. While OPC/PLC_20Mk_0·20HPEG systems represent Bingham fluids, OPC/PLC_20Mk_0·20amphMPEG and OPC/PLC_20Mi systems are classified as Herschel–Bulkey fluids as

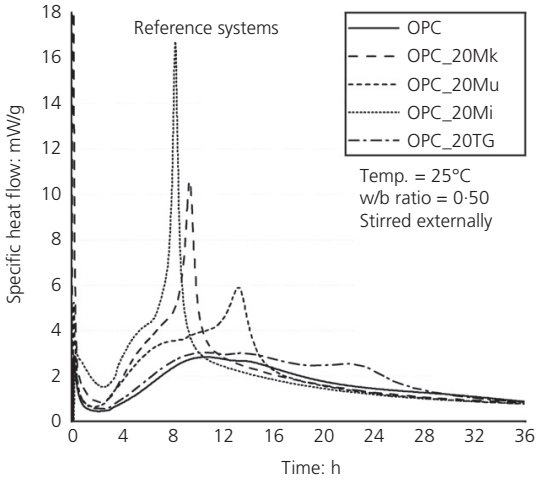

Figure 3. Heat flow of OPC_x systems without superplasticiser

there is a non-linear ratio of revolutions to mean torque values (Figures 1 and 2). Again, OPC/PLC_20Mu systems behave differently: they have low yield stress values at low velocity that increase significantly with higher velocity, which is more pronounced with amphMPEG (Figure 2). Considering the negative yield stress, the low R^2 values and the curve shapes, OPC_20Mu systems are classified as shear-thickening fluids (Table 3).

Development of heat flow and heat of hydration

Figure 3 exemplarily demonstrates the impact of 20 wt% of calcined clays on the reaction kinetics of OPC. The end of rest period, $t_{Q,\min}$, indicated as an inflection point after the decrease of heat flow, is in the range of 1·8–2·5 h for the reference systems without superplasticiser (Table 5). The heat flows of OPC_20Mi and OPC_20Mk result after 8/9 h only in the highest $Q_{\max}$ values (Table 5), indicating the aluminate clinker reaction according to Hesse *et al.* (2011). OPC_20Mu reveals a broader shoulder and a lower aluminate peak but still a remarkable pozzolanic contribution of Mu. OPC and OPC_20TG have a similar heat flow curve for the first 15 h. Subsequently, OPC_20TG exhibits a broad peak with its maximum at 22 h, which can again be associated with the pozzolanic activity of TG.

The heat flow curves for binder systems with 0·20%bwob of HPEG (Figure 4) and amphMPEG (Figure 5) reveal that the rest period of binder systems investigated is delayed with the addition of PCE. Adding more PCE than required – as assumed for OPC/PLC and OPC/PLC_20TG from rheological measurements – can prolong the rest period significantly by up to 2·8 h. This is accompanied by a subsequent increase in heat flow, whereas the effect is less distinct for OPC_20Mu systems and

Magazine of Concrete Research

Rheology, setting and hydration of calcined clay blended cements in interaction with PCE-based superplasticisers
Sposito, Beuntner and Thienel

Table 5. Significant Q values (mW/g) during heat flow measurements at time t (h)

System	Q_{min}	$t_{Q,min}$	$Q_{max,1}$	$t_{Q,max,1}$	$Q_{max,2}$	$t_{Q,max,2}$
OPC	0·4	2·1	2·8	10·5	2·7	13·7
OPC_0·20HPEG	0·2	4·8	—	—	3·0	18·0
OPC_0·20amphMPEG	0·3	3·3	—	—	3·1	14·3
PLC	0·5	2·0	2·7	8·2	3·4	15·8
PLC_0·20HPEG	0·2	4·2	—	—	2·8	18·0
PLC_0·20amphMPEG	0·3	2·7	—	—	3·9	13·9
OPC_20Mk	0·9	2·5	—	—	10·6	9·4
OPC_20Mk_0·20HPEG	0·7	2·7	—	—	8·1	8·9
OPC_20Mk_0·20amphMPEG	0·7	2·5	—	—	9·5	11·3
OPC_20Mu	0·6	1·8	—	—	5·9	13·2
OPC_20Mu_0·20HPEG	0·3	3·5	—	—	7·8	15·6
OPC_20Mu_0·20amphMPEG	0·5	2·4	—	—	7·4	14·1
OPC_20Mi	1·5	2·5	—	—	16·7	8·2
OPC_20Mi_0·20HPEG	1·3	2·7	—	—	15·4	9·1
OPC_20Mi_0·20amphMPEG	1·2	3·0	—	—	14·1	9·6
OPC_20TG	0·5	2·2	3·0	10·5	3·0	20·8
OPC_20TG_0·20HPEG	0·2	5·0	3·1	18·6	3·0	24·2
OPC_20TG_0·20amphMPEG	0·4	3·2	3·1	15·7	3·3	21·0
PLC_20TG	0·6	2·1	2·6	8·0	5·4	14·5
PLC_20TG_0·20HPEG	0·3	4·5	3·3	18·2	2·5	22·0
PLC_20TG_0·20amphMPEG	0·4	2·7	—	—	5·6	14·1

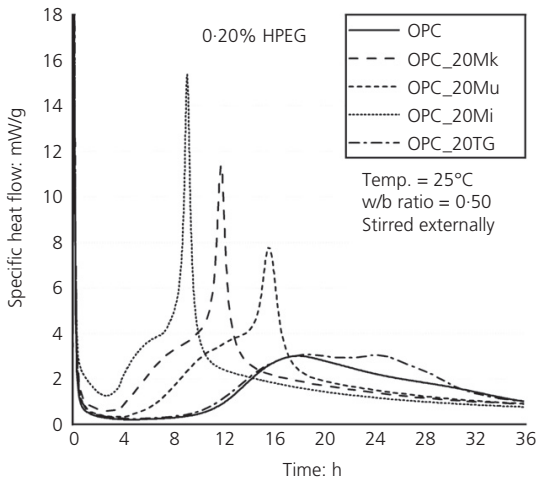

Figure 4. Heat flow of OPC_x systems with 0·20%bwob HPEG

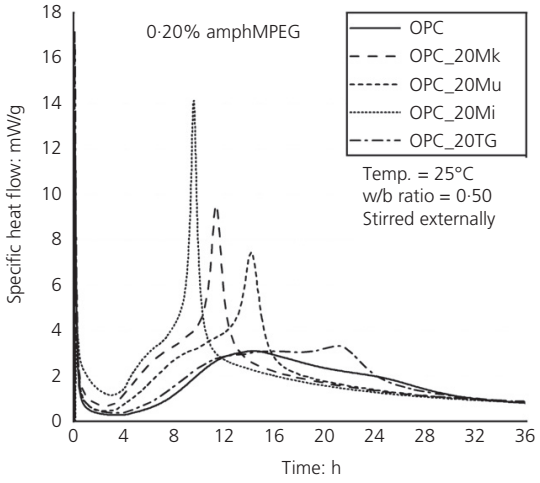

Figure 5. Heat flow of OPC_x systems with 0·20%bwob amphMPEG

marginal for OPC_20Mk and OPC_20Mi systems. For all dispersed systems, Q_{min} values are slightly lower than for the reference systems (Table 5). The retarding impact is here more pronounced with the addition of HPEG compared to amphMPEG.

The same holds, except for OPC_20Mk and PLC systems, even to a larger extent for the retarding effect of Q_{max} occurrence (Table 5). Using 0·20%bwob of PCE, the main peak $Q_{max,1}$ of OPC disappears and $Q_{max,2}$ occurs up to 4·3 h later. Peak $Q_{max,1}$ of OPC_20TG still arises with similar values but partially up to 8 h later while $Q_{max,2}$ occurs as much as 10·7 h later (Table 5). Regarding the main peak of systems with calcined phyllosilicates, the impact of 0·20%bwob PCE seems, once again, to be minor: OPC_20Mu systems reveal a retardation of ≤2·4 h but higher Q_{max} values. OPC_20Mk and OPC_20Mi systems have lower Q_{max} values with the addition of PCE but less retardation (≤1·9 h).

Table 6 lists HH values. The values at 3 h are low due to the reset at the end of the rest period of each system and hence will not be further considered in the discussion. After 6 h, the HH of systems with superplasticiser is significantly lower

Table 6. Development of heat of hydration within the first 36 h of hydration

	Heat of hydration for selected time: J/g				
System	3 h	6 h	12 h	24 h	36 h
OPC	1	12	65	155	208
OPC_0·20HPEG	<1	<1	10	115	185
OPC_0·20amphMPEG	<1	4	40	152	219
PLC	2	16	74	169	206
PLC_0·20HPEG	<1	2	22	121	159
PLC_0·20amphMPEG	<1	8	58	150	187
OPC_20Mk	2	27	133	214	258
OPC_20Mk_0·20HPEG	<1	15	90	168	251
OPC_20Mk_0·20amphMPEG	1	18	115	206	252
OPC_20Mu	3	34	106	212	253
OPC_20Mu_0·20HPEG	<1	4	51	187	237
OPC_20Mu_0·20amphMPEG	1	12	75	199	244
OPC_20Mi	3	37	147	220	261
OPC_20Mi_0·20HPEG	2	29	135	207	248
OPC_20Mi_0·20amphMPEG	<1	12	127	206	250
OPC_20TG	2	14	80	199	243
OPC_20TG_0·20HPEG	<1	1	12	127	209
OPC_20TG_0·20amphMPEG	<1	5	47	176	229
PLC_20TG	2	17	77	184	223
PLC_20TG_0·20HPEG	<1	2	23	129	172
PLC_20TG_0·20amphMPEG	<1	9	60	163	204

Table 7. Time (h) of minima and maxima of ultrasonic speed acceleration

System	$t_{US,min,1}$	$t_{US,max,1}$	$t_{US,min,2}$	$t_{US,max,2}$
OPC	3·8	—	—	13·6
OPC_0·20HPEG	4·6	—	—	16·9
OPC_0·20amphMPEG	3·3	—	—	14·0
PLC	3·8	6·4	11·8	18·6
PLC_0·20HPEG	4·5	14·2	—	17·7
PLC_0·20amphMPEG	3·7	14·9	—	—
OPC_20Mk	3·8	5·7	6·5	14·2
OPC_20Mk_0·20HPEG	4·0	5·6	7·9	11·0
OPC_20Mk_0·20amphMPEG	3·8	5·3	7·4	10·7
OPC_20Mu	3·0	7·0	10·8	13·0
OPC_20Mu_0·20HPEG	—	7·4	11·9	14·3
OPC_20Mu_0·20amphMPEG	3·0	7·2	12·1	14·3
OPC_20Mi	3·7	5·5	6·2	9·4
OPC_20Mi_0·20HPEG	3·7	5·4	6·5	10·0
OPC_20Mi_0·20amphMPEG	4·2	5·3	—	9·05
OPC_20TG	3·9	—	—	13·5
OPC_20TG_0·20HPEG	3·5	17·7	23·6	25·9
OPC_20TG_0·20amphMPEG	3·4	11·1	14·2	19·8
PLC_20TG	3·6	5·7	7·8	16·2
PLC_20TG_0·20HPEG	3·8	4·2	4·6	17·0
PLC_20TG_0·20amphMPEG	2·9	5·6	9·5	16·0

compared to that of the reference systems as the increase of their heat flow curves is less pronounced and occurs later (Table 6). After 12 h, the HH of OPC, OPC_20Mu and OPC_20TG systems with superplasticisers reaches ≤60% of reference values of HH only, whereas the HH of OPC_20Mk and OPC_20Mi systems are partially less retarded and thus closer to the reference values (≤92%). The type of PCE is more decisive for PLC and PLC_20TG systems: the retardation is significantly lower with amphMPEG compared with HPEG. HH values after 24 h and 36 h indicate that systems with PCE almost achieve or even exceed a similar level to the reference systems whereas HPEG systems still lag somewhat behind – except of OPC_20Mk and OPC_20Mi systems. All HH values are higher for amphMPEG systems than for HPEG systems, indicating the smaller impact of amphMPEG on the reaction kinetics. OPC/PLC and OPC/PLC_20TG are

significantly retarded, which is related to an overdose of superplasticiser as shown for the rheological behaviour.

Setting behaviour according to ultrasound acceleration

The derived ultrasonic speed, namely its acceleration, shows up minimum and maximum values, designated as $t_{US,\min}$ and $t_{US,\max}$ respectively, as given in Table 7. With the addition of PCE, slight retardation effects of $t_{US,\min,1}$ are observed. In OPC/PLC and OPC/PLC_20TG, the retarding effect on $t_{US,\max}$ is pronounced whereas the influence of PCE on the systems with calcined phyllosilicates is minor. For the system with calcined clays, it is notable that two maximum peaks occur for the system with calcined clays, which is discussed along with isothermal calorimetry and in situ XRD in Section 'Analysis of the microstructure development with the help of ultrasound method'.

Discussion

Interaction of calcined clays and PCE-based superplasticisers with regard to the rheology of cement paste

The differences between HPEG and amphMPEG regarding their dispersing effectiveness are minor. However, HPEG can reduce viscosity and yield stress better than amphMPEG. This might be due to its higher anionic charge density and shorter side chain length, which better interact with calcined clay blended systems (Navarro-Blasco *et al.*, 2014).

Contrary to the literature (Curcio and DeAngelis, 1998; Moulin *et al.*, 2001; Vance *et al.*, 2013), Mk-blended systems reveal no dilatant behaviour, which might be due to the relatively low replacement level of 20 wt%. By contrast, OPC_20Mu systems are classified as shear-thickening fluid (Table 3), which is consistent with the findings of Schmid *et al.* (2019). Viscosity is slightly increased for OPC/PLC_20Mi systems with the addition of PCE, which runs contrary to other systems with fine particles – for example silica fume (Meng *et al.*, 2019) – but might be within the range of measurement error. In general, both PCE-based superplasticisers perform better with the calcined 1 : 1 phyllosilicate than with the calcined 2 : 1 phyllosilicates used. This is contrary to Ferreiro *et al.* (2017), who assume that the higher dispersion effectiveness results from the mineralogical structure of the phyllosilicates after dehydroxylation: superplasticisers seem to be isolated in the highly disordered structure of Mk and are not completely available for dispersion. Compared to 1 : 1 phyllosilicates, calcined 2 : 1 phyllosilicates retain their multilayered structure after calcination and superplasticisers are adsorbed on particle edges that prevent intercalation effects in the remaining pseudo-laminar structure (Ferreiro *et al.*, 2017; Ng and Justnes, 2015b).

Taking a closer look at the physical properties of the binder systems with PCE added, there is a considerable exponential increase in viscosity and in yield stress depending on water demand (Figure 6). The correlation fits better for the apparent viscosity than for yield stress. As OPC/PLC_20Mu systems exhibit the highest water demand but negative yield stress, those values are not considered in the curve fitting but confirm to a large extent the high water uptake of Mu (Neißer-Deiters *et al.*, 2019) and its rheological behaviour (Schmid *et al.*, 2019). When it comes to the OPC/PLC_20Mi systems, one additional parameter to consider is the grinding fineness, resulting in the large SSA of Mi, shown in Table 2, which both affect significantly the demand for superplasticiser (Plank *et al.*, 2009) and the rheological behaviour. Figure 7 reveals for both apparent viscosity and yield stress a certain correlation with total surface area (TSA) (product of particle density and SSA taken on a percentage basis from the binder materials in

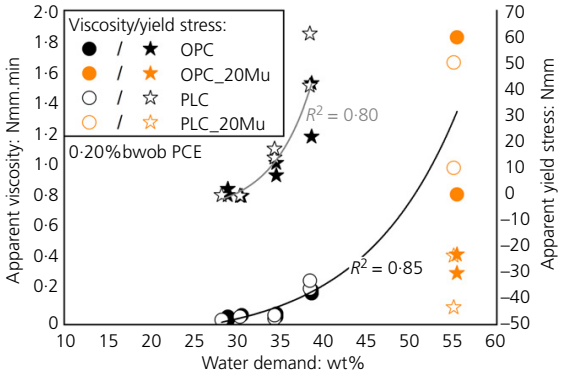

Figure 6. Correlation of water demand with rheological parameters of systems with 0·20% superplasticiser

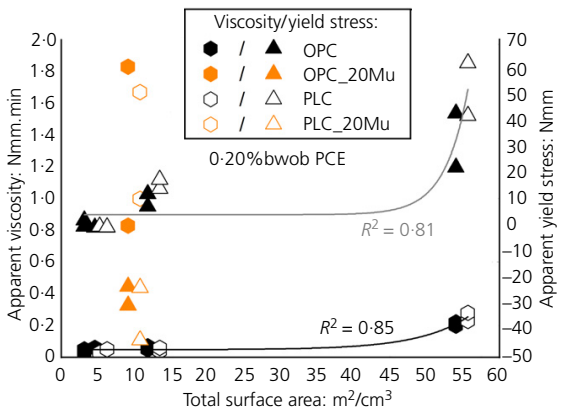

Figure 7. Correlation of TSA with rheological parameters of systems with 0·20% superplasticiser

Magazine of Concrete Research

Table 2), as previously mentioned by Bentz *et al.* (2012). Again, Mu systems fall out of line as the rheological values obtained do not fit with the relatively low TSA of 9·12 and 10·78 m^2/cm^3 for OPC_20Mu and PLC_20Mu, respectively. Nonetheless, it is incorrect to assume that the PCE-based superplasticisers investigated are incompatible with Mu as there is definitely a reduction in shear stress. As already mentioned, muscovite is not a clay but, as a phyllosilicate, is a non-negligible component in naturally occurring clays considered as future SCMs (Beuntner *et al.*, 2019; Maier *et al.*, 2019; Schulze and Rickert, 2019). It is important for concrete technology whether there is a critical muscovite content in clays that perturbs the workability of calcined clay blended systems. TG contains in its raw form ~25 wt% kaolinite and 45 wt% 2 : 1 phyllosilicates (mica, illite) (Beuntner *et al.*, 2019), and the particles are finer than those of OPC, Mk or Mu (Table 2). Nonetheless, the rheological behaviour is comparable to that of OPC/PLC systems with the addition of superplasticiser due to the low SSA and water demand of TG (Table 2). One plausible reason is the non-negligible amount of quartz (~18 wt%) (Beuntner *et al.*, 2019), which is responsible for the reduced yield stress of cement paste (Daukšys *et al.*, 2010). These observations highlight the need to investigate all constituents of clays and not only systems with individual calcined clays.

Regarding the observed effects, both PCE-based superplasticisers can disperse most of the investigated systems sufficiently where the efficiency seems to be slightly superior for HPEG compared to amphMPEG. With the dosage chosen, OPC/PLC_20Mi and OPC/PLC_20Mu still reveal a high viscosity and shear stress but a significant reduction of both parameters with the addition of PCE. The rheological behaviour of OPC/PLC_20TG is remarkable compared to neat cement pastes and systems with calcined phyllosilicates, and, as a possible key parameter, its quartz content is worth being part of further research.

Impact of calcined clays with PCE on the early hydration kinetics

The physical properties of calcined clays dominate the heat flow during the first hours of hydration. The aluminate reaction, indicated by the maximum peak Q_{max} according to Hesse *et al.* (2011), is significantly accelerated for systems with calcined phyllosilicates, as also described by Scherb *et al.* (2018). In the case of Mi systems, this is related to the high grinding fineness and large SSA (Lapeyre *et al.*, 2019). The high Q_{max} of OPC_20Mk originates from high solubility of aluminium and silicon ions (Table 2) such as from overlaying effects of silicate and aluminate reaction (Antoni *et al.*, 2012; Beuntner, 2019).

With the addition of PCE, the rest period of binder systems investigated is delayed, as described, for example, by Avet and Scrivener (2018). The retarding impact is here more pronounced with the addition of HPEG compared to amphMPEG, which might be due to its higher charge density (Winnefeld *et al.*, 2007). The rise of heat flow after the rest period is due to the dissolution of C_3S and the concurrent formation of portlandite and C-S-H (Bellmann *et al.*, 2010; Bergold *et al.*, 2013; Hesse *et al.*, 2011) as well as due to the perpetual formation of ettringite for systems with calcined clays (Scherb *et al.*, 2018). Delays of $Q_{max,1}$ and $Q_{max,2}$ of differing severity such as higher Q_{max} values indicate non-linear shifts and merging effects in reaction kinetics as known from the literature (Jansen *et al.*, 2012; Ng and Justnes, 2016; Zhang *et al.*, 2015).

As described for the rheological properties, the investigations with isothermal calorimetry reveal that the physical characteristics of the calcined clays investigated also seem to have a major influence on the reaction kinetics. Especially for systems with Mk and Mi, there seems to be a compensation between the retarding effect known from PCE by the filler and the pozzolanic effect of Mk and Mi, respectively, as previously published for silica fume (Meng *et al.*, 2019). Considering the type of PCE, amphMPEG seems to have less retardation effect than HPEG and, when PCE dosages are adjusted to meet the demands of each system, the retardation should be less as well.

Analysis of the microstructure development with the help of ultrasound method

For OPC and OPC_20TG systems, the acceleration of ultrasound is nearly congruent with their heat flow curves as shown for OPC_0·20amphMPEG in Figure 8. The time of minimum acceleration $t_{US,min,1}$ is in a similar range to the end of rest period $t_{Q,min}$ and reveals again the mostly retarding effect of PCE. Systems with calcined phyllosilicates exhibit a split course, indicating two separate processes, as shown exemplarily for OPC_20Mu_0·20amphMPEG in Figure 9. Complementary in situ XRD measurements show that primary portlandite

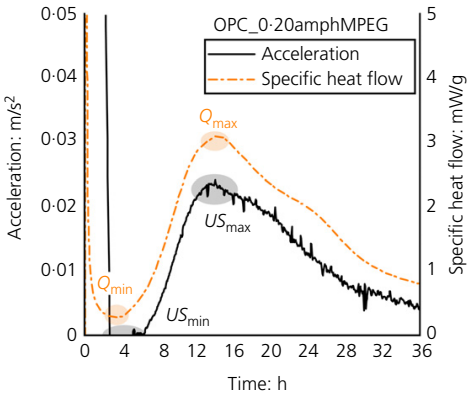

Figure 8. Analysis of reaction kinetics of OPC_0·20amphMPEG

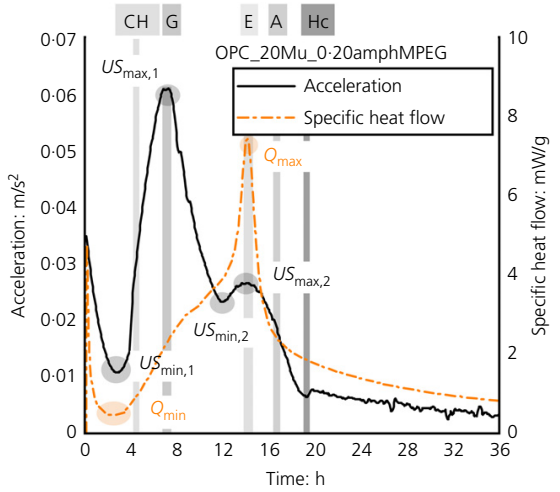

Figure 9. Analysis of reaction kinetics of OPC_20Mu_0·20amphMPEG (A, anhydrite; CH, portlandite; E, ettringite; G, gypsum; Hc, hemicarboaluminate)

formation can be related to half of the acceleration phase observed by ultrasound. In isothermal calorimetry, this usually determines the initial set (Wadsö *et al.*, 2016). The first maximum ultrasound acceleration $US_{max,1}$ correlates with the dissolution of gypsum. This complies with findings of Scherb *et al.* (2018) who assume that a continuous ettringite formation during this period causes the broad shoulder of heat flow for calcined phyllosilicate blended systems. Robeyst and De Belie (2009) and Robeyst *et al.* (2011) combine a semi-adiabatic calorimeter with ultrasonic p-wave measurements and conclude a correlation between the maximum of ultrasound acceleration and final set such as a similar course of ultrasonic acceleration and heat flow. According to Kjellsen *et al.* (1991), the formation of C–S–H needles furthermore leads to a denser microstructure and thus should result in an accelerated ultrasound. The second minimum in acceleration curve, $t_{US,min,2}$, is congruent with the beginning of the main peak in isothermal calorimetry and occurs earlier for highly reactive systems with Mk and Mi. The occurrence of the (second) maximum of acceleration, $t_{US,max,2}$, and heat flow curves, $t_{Q,max,2}$, correlates well (Figure 10) and indicates both the reactivity of calcined clays (Mi > Mk > Mu > TG) such as their interaction with superplasticisers. Both maxima, Q_{max} and $US_{max,2}$, fit well with the dissolution of anhydrite and maximum ettringite content, hence the secondary aluminate reaction as reported by Hesse *et al.* (2011) and Scherb *et al.* (2018). The first detection of hemicarboaluminate coincides again with the deceleration and the decline of heat flow after the second maxima. Combining isothermal calorimetry with ultrasonic method and in situ XRD can hence give a fundamental insight into the setting behaviour of complex systems.

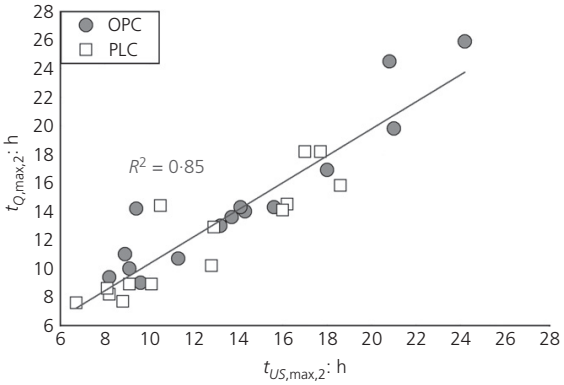

Figure 10. Correlation of $t_{US,max,2}$ and $t_{Q,max,2}$ for OPC (R^2 = 0·87) and PLC (R^2 = 0·80) systems

Conclusions and outlook

Based on the results and analysis previously described, the following conclusions can be drawn and possible future research outlined.

- PCE-based superplasticisers efficiently reduced the yield and shear stress of the binder systems investigated. Polymers with a shorter side chain and higher anionic charge density tended to be more effective.
- Rheological properties depend to a large extent on the physical properties of the binder components.
- Mu behaves completely differently from other phyllosilicates. As a non-negligible component in naturally occurring clays, it requires extra attention. Further investigations will focus on a critical content of muscovite regarding the workability of calcined clay blended systems.
- TG is easily dispersed compared to pure calcined phyllosilicates. Additional experiments should reveal to what extent quartz is a key parameter in compensating for the critical behaviour of phyllosilicates.
- A lower anionic charge density leads to less pronounced retardation effects in hydration kinetics.
- Depending on the type of calcined clay, the retardation effects can be partially compensated for by the pozzolanic properties of calcined phyllosilicates.
- The combination of isothermal calorimetry and ultrasonic measurements with in situ XRD provides a detailed insight into the setting behaviour and development of calcined clay blended systems during early hydration.

Acknowledgements

The authors would like to thank Schwenk Zement KG (Germany) for the cements, Liapor GmbH & Co. KG (Germany) for providing the TG and Jilin Zhongxin Chemical Group Co., Ltd. (China) for the supply of the HPEG PCE.

The authors wish to express their deepest gratitude to Deutsche Forschungsgemeinschaft (DFG) for the financial support of the research project 'Ecological and energetic optimisation of concrete: Interaction of structurally divergent superplasticisers with calcined clays' (PL 472/11-1 and TH 1383/3-1). They express their deepest gratitude to Prof. J. Plank and M. Schmid from the Department for Construction Chemistry of the Technical University Munich (Germany) for synthesising and providing the PCE-based polymer with amphoteric character (amphMPEG) within the joint DFG research project.

REFERENCES

Antoni M, Rossen J, Martirena F and Scrivener K (2012) Cement substitution by a combination of metakaolin and limestone. *Cement and Concrete Research* **42(12)**: 1579–1589.

Avet F and Scrivener K (2018) Investigation of the calcined kaolinite content on the hydration of limestone calcined clay cement (LC3). *Cement and Concrete Research* **107**: 124–135.

Barnes HA and Walters K (1985) The yield stress myth? *Rheologica Acta* **24(4)**: 323–326.

Bellmann F, Damidot D, Möser B and Skibsted J (2010) Improved evidence for the existence of an intermediate phase during hydration of tricalcium silicate. *Cement and Concrete Research* **40(6)**: 875–884.

Bentz DP, Ferraris CF, Galler MA, Hansen AS and Guynn JM (2012) Influence of particle size distributions on yield stress and viscosity of cement–fly ash pastes. *Cement and Concrete Research* **42(2)**: 404–409.

Bergold ST, Goetz-Neunhoeffer F and Neubauer J (2013) Quantitative analysis of C–S–H in hydrating alite pastes by in situ XRD. *Cement and Concrete Research* **53**: 119–126.

Beuntner N (2019) *Zur Eignung und Wirkungsweise Calcinierter Tone als Reaktive Bindemittelkomponente in Zement*. Beuth, Berlin, Germany (in German).

Beuntner N and Thienel KC (2015) Properties of calcined Lias delta clay – technological effects, physical characteristics and reactivity in cement. In *Calcined Clays for Sustainable Concrete – Proceedings of the 1st International Conference on Calcined Clays for Sustainable Concrete, Lausanne, Switzerland* (Scrivener K and Favier A (eds)). Springer, Berlin, Germany, pp. 43–50.

Beuntner N, Sposito R and Thienel KC (2019) Potential of calcined mixed-layer clays as pozzolans in concrete. *ACI Materials Journal* **116(4)**: 19–29.

Busing WR and Levy HA (1957) Neutron diffraction study of calcium hydroxide. *The Journal of Chemical Physics* **26(3)**: 563–568.

Cheung J, Jeknavorian A, Roberts L and Silva D (2011) Impact of admixtures on the hydration kinetics of Portland cement. *Cement and Concrete Research* **41(12)**: 1289–1309.

Colombo A, Geiker MR, Justnes H, Lauten RA and De Weerdt K (2017) On the effect of calcium lignosulfonate on the rheology and setting time of cement paste. *Cement and Concrete Research* **100**: 435–444.

Curcio F and DeAngelis BA (1998) Dilatant behavior of superplasticized cement pastes containing metakaolin. *Cement and Concrete Research* **28(5)**: 629–634.

Danner T, Ostnor T and Justnes H (2012) Calcined marl as a pozzolan for sustainable development of the cement and concrete industry. In *12th International Conference on Recent Advances in Concrete Technology and Sustainability Issues, Prague, Czech Republic* (Holland TC, Gupta PR and Malhotra VM (eds)). Sheridan Books, Chelsea, MI, USA.

Daukšys M, Skripkiunas G and Grinys A (2010) Finely ground quartz sand and plasticizing admixtures influence on rheological properties of portland cement paste. *Materials Science* **16(4)**: 365–372.

DIN (Deutsches Institut für Normung) (2009a) DIN EN 196-3: Methods of testing cement – part 3: determination of setting times and soundness. DIN, Berlin, Germany.

DIN (2009b) DIN EN ISO 11885:200: Water quality – determination of selected elements by inductively coupled plasma optical emission spectrometry (ICP-OES). DIN, Berlin, Germany.

Ferreiro S, Herfort D and Damtoft JS (2017) Effect of raw clay type, fineness, water-to-cement ratio and fly ash addition on workability and strength performance of calcined clay – limestone portland cements. *Cement and Concrete Research* **101**: 1–12.

Goetz-Neunhoeffer F and Neubauer J (2005) Refined ettringite ($Ca_6Al_2(SO_4)_3(OH)_{12}{\cdot}26H_2O$) structure for quantitative X-ray diffraction analysis. *Powder Diffraction* **21(1)**: 4–11.

Hackley VA and Ferraris CF (2001) *Guide to Rheological Nomenclature – Measurements in Ceramic Particulate Systems*. National Institute of Standards and Technology (NIST), Gaithersburg, MD, USA.

He C, Osbæck B and Makovicky E (1995) Pozzolanic reactions of six principal clay minerals: activation, reactivity assessments and technological effects. *Cement and Concrete Research* **25(8)**: 1691–1702.

He C, Makovicky E and Osbæck B (2000) Thermal stability and pozzolanic activity of raw and calcined mixed-layer mica/smectite. *Applied Clay Science* **17(3-4)**: 141–161.

Hesse C, Goetz-Neunhoeffer F and Neubauer J (2011) A new approach in quantitative in situ XRD of cement pastes: correlation of heat flow curves with early hydration reactions. *Cement and Concrete Research* **41(1)**: 123–128.

Hunger M and Brouwers HJH (2009) Flow analysis of water–powder mixtures: application to specific surface area and shape factor. *Cement and Concrete Composites* **31(1)**: 39–59.

Jansen D, Neubauer J, Goetz-Neunhoeffer F, Haerzschel R and Hergeth WD (2012) Change in reaction kinetics of a Portland cement caused by a superplasticizer – calculation of heat flow curves from XRD data. *Cement and Concrete Research* **42(2)**: 327–332.

Kirfel A and Will G (1980) Charge density in anhydrite, $CaSO_4$, from X-ray and neutron diffraction measurements. *Acta Crystallographica Section B* **36(12)**: 2881–2890.

Kjellsen KO, Detwiler RJ and Gjørv OE (1991) Development of microstructures in plain cement pastes hydrated at different temperatures. *Cement and Concrete Research* **21(1)**: 179–189.

Lapeyre J, Ma H and Kumar A (2019) Effect of particle size distribution of metakaolin on hydration kinetics of tricalcium silicate. *Journal of the American Ceramic Society* **102(10)**: 5976–5988.

Lootens D and Bentz DP (2016) On the relation of setting and early-age strength development to porosity and hydration in cement-based materials. *Cement and Concrete Composites* **68**: 9–14.

Lothenbach B and Winnefeld F (2007) Influence of superplasticizers on the hydration of portland cement. In *Proceedings of the 12th International Congress on the Chemistry of Cement, Montreal, Canada* (Beaudoin JJ, Maker JM and Raki L (eds)). Cement Association of Canada, Ottowa, ON, Canada, pp. 9–12.

Maier M, Beuntner N and Thienel KC (2019) An approach for the evaluation of local raw material potential for calcined clay as SCM, based on geological and mineralogical data: examples from German clay deposits. In *Calcined Clays for Sustainable Concrete – Proceedings of the 3rd International Conference on Calcined Clays for Sustainable Concrete, Delhi, India* (Parashar A,

Singh L and Rao DG (eds)). Springer Netherlands, Berlin, Germany.

Marchon D (2016) *Controlling Cement Hydration through the Molecular Structure of Comb Copolymer Superplasticizers*. Doctoral thesis, ETH Zürich, Zurich, Switzerland.

Meng W, Lunkad P, Kumar A and Khayat K (2016) Influence of silica fume and polycarboxylate ether dispersant on hydration mechanisms of cement. *The Journal of Physical Chemistry C* **120(47)**: 26814–26823.

Meng W, Kumar A and Khayat K (2019) Effect of silica fume and slump-retaining polycarboxylate-based dispersant on the development of properties of portland cement paste. *Cement and Concrete Composites* **99**: 181–190.

Mollah MYA, Adams WJ, Schennach R and Cocke DL (2000) A review of cement–superplasticizer interactions and their models. *Advances in Cement Research* **12(4)**: 153–161.

Moulin E, Blanc P and Sorrentino D (2001) Influence of key cement chemical parameters on the properties of metakaolin blended cements. *Cement and Concrete Composites* **23(6)**: 463–469.

Navarro-Blasco I, Pérez-Nicolás M, Fernández JM *et al.* (2014) Assessment of the interaction of polycarboxylate superplasticizers in hydrated lime pastes modified with nanosilica or metakaolin as pozzolanic reactives. *Construction and Building Materials* **73**: 1–12.

Neißer-Deiters A, Scherb S, Beuntner N and Thienel KC (2019) Influence of the calcination temperature on the properties of a mica mineral as a suitability study for the use as SCM. *Applied Clay Science* **179**: 105168.

Ng S and Justnes H (2015a) Influence of dispersing agents on the rheology and early heat of hydration of blended cements with high loading of calcined marl. *Cement and Concrete Composites* **60**: 123–134.

Ng S and Justnes H (2015b) *Rheology of Blended Cements with Superplasticizers*. Concrete Innovation Centre, Trondheim, Norway.

Ng S and Justnes H (2016) Influence of plasticizers on the rheology and early heat of hydration of blended cements with high content of fly ash. *Cement and Concrete Composites* **65**: 41–54.

Plank J, Schroefl C, Gruber M, Lesti M and Sieber R (2009) Effectiveness of polycarboxylate superplasticizers in ultra-high strength concrete: the importance of PCE compatibility with silica fume. *Journal of Advanced Concrete Technology* **7(5)**: 5–12.

Prince W, Edwards-Lajnef M and Aïtcin PC (2002) Interaction between ettringite and a polynaphthalene sulfonate superplasticizer in a cementitious paste. *Cement and Concrete Research* **32(1)**: 79–85.

Regnaud L, Rossino C, Alfani R and Vichot A (2011) Effect of comb type superplasticizers on hydration kinetics of industrial portland cements. In *Proceedings of the 13th International Congress on the Chemistry of Cement, Madrid, Spain* (Palomo Á, Zaragoza A and AgüÍ JCL (eds)). Instituto de Ciencias de la Construcción, Madrid, Spain, pp. 389–408.

Robeyst N and De Belie N (2009) Monitoring the setting of concrete by measuring the change in ultrasonic p-wave energy. In *NDTCE'09: Non-Destructive Testing in Civil Engineering, Nantes, France* (Abraham O and Dérobert X (eds)). Laboratoire Central des Ponts et Chaussées, Paris, France, pp. 649–654.

Robeyst N, De Schutter G, Grosse C and De Belie N (2011) Monitoring the effect of admixtures on early-age concrete behaviour by ultrasonic, calorimetric, strength and rheometer measurements. *Magazine of Concrete Research* **63(10)**: 707–721.

Roncero J, Valls S and Gettu R (2002) Study of the influence of superplasticizers on the hydration of cement paste using nuclear magnetic resonance and X-ray diffraction techniques. *Cement and Concrete Research* **32(1)**: 103–108.

Runcevski T, Dinnebier RE, Magdysyuk OV and Pöllmann H (2012) Crystal structures of calcium hemicarboaluminate and carbonated calcium hemicarboaluminate from synchrotron powder diffraction data. *Acta Crystallographica Section B* **68**: 493–500.

Sakai E, Kasuga T, Sugiyama T, Asaga K and Daimon M (2006) Influence of superplasticizers on the hydration of cement and the pore structure of hardened cement. *Cement and Concrete Research* **36(11)**: 2049–2053.

Scherb S, Beuntner N, Köberl M and Thienel KC (2018) The early hydration of cement with the addition of calcined clay – from single phyllosilicate to clay mixture. In *Ibausil – 20: Internationale Baustofftagung, Weimar, Germany* (Fischer HB and Volke A (eds)). F.A. Finger-Institut für Baustoffkunde, Weimar, Germany, pp. 658–666.

Schmid M, Beuntner N, Thienel KC and Plank J (2018a) Amphoteric superplasticizers for cements blended with a calcined clay. In *12th International Conference on Superplasticizers and Other Chemical Admixtures in Concrete, Beijing, China* (Liu J and Plank J (eds)). American Concrete Institute, Farmington Hills, MI, USA, pp. 41–54.

Schmid M, Beuntner N, Thienel KC and Plank J (2018b) Colloid-chemical investigation of the interaction between PCE superplasticizers and a calcined mixed layer clay. In *Calcined Clays for Sustainable Concrete – Proceedings of the 2nd International Conference on Calcined Clays for Sustainable Concrete, La Havanna, Cuba* (Martirena F, Favier A and Scrivener K (eds)). Springer, Berlin, Germany, pp. 434–439.

Schmid M, Sposito R, Thienel KC and Plank J (2018c) Novel zwitterionic superplasticizers for cements blended with calcined clays. *Ibausil – 20: Internationale Baustofftagung, Weimar, Germany* (Fischer HB and Volke A (eds)). F.A. Finger-Institut für Baustoffkunde, Weimar, Germany, pp. 842–849.

Schmid M, Sposito R, Thienel KC and Plank J (2019) The shear-thickening effect of meta muscovite as SCM and its influence on the rheological properties of ecologically optimized cementitious systems. In *2nd International RILEM Conference on Rheology and Processing of Construction Materials, Dresden, Germany* (Mechtcherine V (ed.)). RILEM, Paris, France.

Schofield PF, Wilson CC, Knight KS and Stretton IC (2000) Temperature related structural variation of the hydrous components in gypsum. *Crystalline Materials* **215(12)**: 707.

Schulze SE and Rickert J (2019) Suitability of natural calcined clays as supplementary cementitious material. *Cement and Concrete Composites* **95**: 92–97.

Sposito R, Dürr I and Thienel KC (2018) Lignosulfonates in cementitious systems blended with calcined clays. In *2nd International Workshop on Durability and Sustainability of Concrete Structures, Moscow, Russia* (Falikman V, Realfonzo R, Hájek P and Riva P (eds)). Sheridan Books, Chelsea, MI, USA, pp. 10.11–10.10.

Trtnik G, Valič M, Kavčič F and Turk G (2009) Comparison between two ultrasonic methods in their ability to monitor the setting process of cement pastes. *Cement and Concrete Research* **39(10)**: 876–882.

Vance K, Kumar A, Sant G and Neithalath N (2013) The rheological properties of ternary binders containing Portland cement, limestone, and metakaolin or fly ash. *Cement and Concrete Research* **52**: 196–207.

von Daake HF (2016) *Möglichkeiten zur Optimierung der Wirkungsweise bauchemischer Zusatzmittel durch Mechanismen der kontrollierten Wirkstofffreisetzung*. Doctoral thesis, Technische Universität Berlin, Germany (in German).

von Daake HF and Stephan D (2015) Kombination von ultraschall und kalorimetrie zur untersuchung der frühen zementhydratation unter einfluss bauchemischer zusatzmittel. In *Ibausil – 19: Internationale Baustofftagung, Weimar, Germany* (Fischer HB, Boden C and

Neugebauer M (eds)). F.A. Finger – Institut für Baustoffkunde, Weimar, Germany, pp. 727–734 (in German).

Wadsö L, Berodier E, Bizzozero J *et al.* (2016) Calorimetry. In: *A Practical Guide to Microstructural Analysis of Cementitious Materials*. CRC Press, Boca Raton, FL, USA, pp. 37–74.

Winnefeld F (2012) Interaction of superplasticizers with calcium sulfoaluminate cements. In *10th International Conference on Superplasticizers and Other Chemical Admixtures, Prague, Czech Republic*. American Concrete Institute, Farmington Hills, MI, USA, pp. 21–36.

Winnefeld F, Becker S, Pakusch J and Götz T (2007) Effects of the molecular architecture of comb-shaped superplasticizers on their performance in cementitious systems. *Cement and Concrete Composites* **29(4)**: 251–262.

Zaribaf BH and Kurtis KE (2018) Admixture compatibility in metakaolin–portland-limestone cement blends. *Materials and Structures* **51**: 13.

Zaribaf BH, Uzal B and Kurtis K (2015) Compatibility of superplasticizers with limestone-metakaolin blended cementitious system. In *Calcined Clays for Sustainable Concrete – Proceedings of the 1st International Conference on Calcined Clays for Sustainable Concrete, Lausanne, Switzerland* (Scrivener K and Favier A (eds)). Springer, Berlin, Germany, pp. 427–434.

Zhang YR, Kong XM, Lu ZB, Lu ZC and Hou SS (2015) Effects of the charge characteristics of polycarboxylate superplasticizers on the adsorption and the retardation in cement pastes. *Cement and Concrete Research* **67**: 184–196.

How can you contribute?

To discuss this paper, please submit up to 500 words to the editor at journals@ice.org.uk. Your contribution will be forwarded to the author(s) for a reply and, if considered appropriate by the editorial board, it will be published as a discussion in a future issue of the journal.

7.3 Physical and mineralogical properties of calcined common clays and their impact on flow resistance and superplasticizer demand

Peer-reviewed journal paper [Reprint]

"Physical and mineralogical properties of calcined common clays and their impact on flow resistance and superplasticizer demand"

Ricarda Sposito, Matthias Maier, Nancy Beuntner, Karl-Christian Thienel

Cement and Concrete Research

Volume 154, 106743 (2022)

Cement and Concrete Research 154 (2022) 106743

Contents lists available at ScienceDirect

Cement and Concrete Research

journal homepage: www.elsevier.com/locate/cemconres

Physical and mineralogical properties of calcined common clays as SCM and their impact on flow resistance and demand for superplasticizer

Ricarda Sposito *, Matthias Maier, Nancy Beuntner, Karl-Christian Thienel

Institute for Construction Materials, University of the Bundeswehr München, Werner-Heisenberg-Weg 39, 85579 Neubiberg, Germany

ARTICLE INFO

Keywords:
Calcined clays
Flow resistance
Kaolinite content
PCE
Superplasticizer

ABSTRACT

Physical properties of calcined clays differ significantly and depend to a large extent on the mineralogy of the raw clays. In this study, four common clays and one kaolinite-rich mine tailing are calcined at 800 °C. Their impact on flow properties of blended cement paste is measured via rotational viscometer and analyzed by (modified) Bingham and Herschel-Bulkley model, combined with the calculation of flow resistance. The demand for superplasticizers rises significantly due to the special characteristics of calcined clays, namely particle size, a high water demand and negative zeta potential. Muscovite present in raw clay is critical as it increases the water demand, yield stress and viscosity. In general, the addition of three industrial polycarboxylate-based superplasticizers (PCEs) reveals good dispersion. Calcined kaolinite-rich clays require more PCE compared to calcined clays rich in 2:1 phyllosilicates. The studied PCEs interact well with all types of metaphyllosilicates besides metamuscovite.

1. Introduction

Considering the desperate need for supplementary cementitious materials (SCM), the calcination of common clays or shales (with impurities like quartz) becomes of interest, as they are available in many regions of the world. The pozzolanic activity of calcined common clays origins, besides their kaolinite content, to a lesser extent from 2:1 phyllosilicates, like illite or smectite, present in raw clay [1–9].

The addition of calcined clays, however, alters the rheological properties of cementitious systems significantly, indicated by higher yield stress, viscosity, cohesion and adhesion values [10]. Calcined clays can increase the degree of shear-thickening due to flocculation and high water adsorption [11–13]. Approaches to characterize the rheological behavior of calcined clay blended cement pastes by Bingham and Herschel-Bulkley models [14] have been published e.g. in [10,15–18]. Tregger et al. [19] also considered the volume fraction by using the compressive rheology method and modified Bingham equation according to Papanastasiou [20]. For flocculating mixtures, they proposed a Krieger & Dougherty model, that was originally used to describe non-flocculating suspensions [21]. It was modified by Soua et al. [22] and took not only the viscosity and volume fraction into account, but also the maximum packing density of the flocs as well as the shear and yield stress of the suspension [19]. The advantage of this modified model is the consideration of entrapped water into but also its release from the flocs. Blachier et al. [23] doubted the use of Krieger & Dougherty model as it does not consider non-spherical shaped particles, a morphology that does also apply for calcined clays [15]. They rather proposed an evaluation of the hydrodynamic volume of particles instead of their real solid volume as it considers the aqueous phase entrapped in the particles [23]. Irassar et al. [24] compared the shear stress of different calcined clay additions and cements at varying shear rates. Ng and Justnes [25] described the rheological behavior of cement blended with calcined marl by using the area under the flow curve, designated as flow resistance.

Going along with the altered rheological behavior, the addition of calcined clays as SCM, especially at high replacement levels, requires more superplasticizer compared to neat cement [15,26,27]. Sonebi et al. [28] simulated the influence of viscosity modifying agents and superplasticizers on metakaolin-based cement suspensions by using another modified Bingham model proposed by Khayat & Yahia [29]. When it comes to the mineralogical composition of clays, the influence of the individual phases, especially of 1:1 and 2:1 phyllosilicates, on the required amount of superplasticizer is still under discussion. Beigh et al. [30] revealed more challenging rheological properties for a calcined clay that is rather coarse but contains residual kaolinite due to non-complete dehydroxylation, in comparison to a finer calcined clay

* Corresponding author.
E-mail address: ricarda.sposito@unibw.de (R. Sposito).

https://doi.org/10.1016/j.cemconres.2022.106743
Received 22 March 2021; Received in revised form 5 January 2022; Accepted 4 February 2022

where the kaolinite has been fully transformed to amorphous phase (metakaolinite). They related the observed effects on rheological properties to intercalation of polyethylene glycol side chains of conventional PCE into kaolinite structure [30]. Intercalation is well known for swelling clay minerals, e.g. smectite [31], whereas for instance Lei & Plank found that adsorption of PCEs onto kaolinite and muscovite only appears on their surface [32]. Akhlaghi et al. [33] further found that no intercalation of AMPS-PCE takes place into a calcined kaolinite-rich clay (metakaolin content after calcination: 42 wt%), that contained significant amounts of residual kaolinite, 16 wt% of quartz and < 2 wt% other mineral phases. It is yet unclear, however, what happens to those clay minerals that are sensitive towards intercalation, when their dehydroxylation is completed. Ferreiro et al. [11] described that kaolinite-rich clays require more superplasticizer than smectitic clays as superplasticizer polymers can be entrapped into the amorphous structure of metakaolin caused by dehydroxylation, while 2:1 phyllosilicates keep their layered structure and superplasticizers adsorb only at their edges. In contrast, a better superplasticizer performance is identified for cements blended with metakaolin compared to metaillite and metamuscovite, as well as a low superplasticizer demand for calcined common clay and quartz powder in [15]. From this point of knowledge, the assumption of the authors was that the impurities (e.g. quartz) in common clays are beneficial in terms of a lower water demand and specific surface area (SSA) [15]. Beside these parameters, the surface charge of cementitious materials is identified as indicator for rheological behavior and the superplasticizer demand [5,15]. Recent publications revealed a decreasing positive zeta potential of blended cement with increasing kaolinite content [34,35]. This leads to the assumption that the mineralogical composition of the raw clays plays a key role when it comes to the rheological behavior and the demand for superplasticizer. The results, however, do also show that it is difficult to transfer the findings from pure materials to heterogeneous clays as physical parameters vary significantly [15,34]. Li et al. [26] demonstrated the possibility of Ca^{2+} adsorption onto a calcined kaolinite-rich clay that in turn favors the superplasticizer adsorption. This was confirmed by Schmid and Plank where additional Ca^{2+} improves the adsorption of PCE onto metakaolin, whereas this effect is minor for metamuscovite, metamontmorillonite and non-existent for the metaillite investigated [36].

As already known from neat cement, PCE-based superplasticizers show the best efficiency with calcined clay blended systems as well [15,26,27,37]. For this reason, the present study shows the interaction of tailor-made superplasticizers with Portland limestone cement blended with calcined common clays, that vary in types and amounts of phyllosilicates as well as their physical parameters. In addition, the authors describe different approaches to analyze rheological measurements and evaluate the dispersion performance of PCEs in calcined clay blended systems.

2. Materials & methods

2.1. Materials

2.1.1. Cement

A Portland limestone cement (PLC) complying with DIN EN 197-1 [38] is used. Its mineralogical composition and physical parameters are given in Table 1 and Table 3, respectively. Previous investigations revealed that the PLC used requires slightly higher superplasticizer dosages compared to ordinary Portland cement from the same cement plant [15,39]. On the other hand, the use of PLC can reduce further the amount of clinker, promote the aluminate reaction and diminish the influence of carbonates present in clays.

2.1.2. Calcined clays

Four common clays and one clay-rich mine tailing, all originating from Southern Germany, are investigated after calcination for 60 min in a laboratory muffle kiln. A detailed characterization of the raw materials and towards the pozzolanic activity of the calcined clays was previously published by Maier et al. [8]. Their designation and a short description of the geological origin is given hereafter, as well as a mineralogical composition in Table 2:

- MURR: Upper Eocene to Upper Miocene sediments of the alpine foreland basin
- AC: Marine sediments of a continental shelf from early Jurassic
- KUP: Primary kaolin deposit formed between Eocene and Miocene
- RKUP: Kaolinite-rich mine tailing
- FUP: Sedimentary kaolinite-rich clays deposited in the Miocene

The raw materials are dried at 105 °C until mass constant and pre-crushed in a jaw crusher. The approximate particle size before calcination is ≤5 mm. The temperature is set constant at 800 °C to ensure a high pozzolanic reactivity of the phyllosilicates. Previous investigations by thermal analysis revealed lower temperatures for the main dehydroxylation peak of all investigated clays [40]. Furthermore, this temperature is in the range of the optimum calcination temperature of illites and smectites regarding pozzolanic reactivity [41–44]. It is still significantly below the formation temperature of new crystalline phases like spinel or mullite [45]. After calcination process, the calcined clays are ground for 10 min in a vibrating disk mill with agate insert.

All calcined common clays exhibit pozzolanic reactivity after calcination, verified by the evolved heat after 72 h according to R^3 test [46] and the amount of Al and Si ions solved in alkaline solution (Table 3). The particles of the calcined clays have been analyzed by both static light scattering (SLS) diffractometry according to the Mie theory (ISO 13320:2020 [47]) and by digital image analysis (DIA), (ISO 13322-2:2006 [48]), using a Bettersizer S3 Plus (3P Instruments). The calcined clay samples were dispersed in demineralized water at 1600

Table 2
Mineralogical composition of raw clays [35,40].

Phase [wt%]	MURR	AC	KUP	RKUP	FUP
Quartz	48	20	33	48	12
Kaolinite	1	23	26	45	74
Illite/muscovite	10	5	36[a]	3	3
Illite-smectite	–	32	–	–	8
Smectite	32	–	–	–	–
Chlorite	4	6	–	–	–
Calcite	1	7	–	–	–
Dolomite	< 1	1	–	–	–
Feldspar	5	4	–	–	–
Rutile	–	< 1	1	–	1
Anatase	–	2	–	< 1	1
Pyrite	–	1	–	–	–
Hematite	–	–	–	< 1	–
Goethite	–	–	4	3	–

[a] Identified as muscovite in [8].

Table 1
Mineralogical composition of cement (information provided by the supplier).

Mineralogical composition of PLC [wt%]									
C_3S	C_2S	C_3A	C_4AF	$CaCO_3$	Sulfate carrier	$CaMg(CO_3)_2$	MgO	$Ca(OH)_2$	CaO_{free}
48.7	14.4	5.4	6.9	15.6	2.9	2.3	0.9	1.2	0.2

Table 3
Physical parameters of cement and calcined clays used (n.d. = not determined, SCPS = synthetic cement pore solution).

Parameter	Standard/method/instrument	PLC	MURR	AC	KUP	RKUP	FUP
SSA [m^2/g]	[49] SA-9601 MP, Horiba Instruments Inc.	1.8	5.3	17.2	6.6	7.9	42.4
Blaine surface area [cm^2/g]	[50]	4341	n.d.	n.d.	n.d.	n.d.	n.d.
Particle density [g/cm^3]	[51] Pycnomatic-ATC, Thermo Scientific	3.07	2.72	2.67	2.70	2.63	2.63
d_{10} [µm]	Static laser light diffraction by Bettersizer S2 Plus, 3P Instruments	2.3[a]	4.6	3.6	6.4	2.2	2.8
d_{50} [µm]		13.1[a]	40.9	30.0	26.7	12.0	16.1
d_{90} [µm]		46.0[a]	150.4	161.9	86.9	81.0	56.3
Optimum water demand [wt%]	DIN EN 196-3 [52]	26.6	n.d.	n.d.	n.d.	n.d.	n.d.
Water demand [wt%]	Puntke method [53]	n.d.	32.8	28.3	40.4	35.1	43.6
Zeta potential [mV] in SCPS (w/s = 1.50) [35]	Electroacoustic method by DT-310, Dispersion Technology Instruments [15]	n.d.	−1.1	−1.6	−3.3	−4.0	−7.5
Evolved heat after 72 h [$J/g_{calcined\ clay}$]	R^3 test by isothermal calorimeter TamAir, TA Instruments [46]	n.d.	166.2	290.7	251.3	454.3	666.4
Al_{sol} [mmol/L]	Elution of calcined clay in 10 wt% NaOH solution with coupled ICP-OES	n.d.	0.4	1.7	2.3	4.0	8.5
Si_{sol} [mmol/L]	[54]	n.d.	1.2	2.7	3.3	5.0	11.4

[a] Particle size distribution of PLC was measured by laser particle size analyzer LA-950, Horiba.

revolutions per minute (rpm). In order to prevent agglomeration effects, ultrasound treatment took place at 50 W for 3 min. Each calcined clay sample was measured three times. The $d_{10}/d_{50}/d_{90}$ values derived from SLS are given in Table 3, together with further significant parameters of the calcined clays. For BET measurements according to DIN ISO 9277 [49], the calcined clay samples were degassed at $T = 150$ °C for 30 min. The differential distribution of particle diameters and the circularity, which addresses the 3D form of particles, are given in Fig. 1.

2.1.3. Superplasticizers

The influence of three industrial PCE-based superplasticizers is investigated in PLC and in calcined clay blended cements. An α-methallyl-ω-methoxy poly(ethylene glycol) ether type PCE with acrylic acid (AA) as anchor group is used. This polymer (abbreviation: HPEG) already exhibited good compatibilities with calcined clay blended systems [15,16,37,39]. The authors assume that the dispersion effectiveness is related to the moderate side chain length and a high anionic charge density. Furthermore, two isoprenyl oxy poly(ethylene glycol) ether type PCEs (IPEG1 and IPEG2) are used, whose anchor groups are made up of AA as well. IPEG1 consists of two AA-IPEG polymers: one has an additional ester group (hydroxyethyl methacrylate) that decomposes to ethylene glycol and carboxyl groups in alkaline media, enabling subsequent dispersion. This shall prevent rapid slump loss, which often occurs with calcined clay blended cements [16,30,55–58]. IPEG2 is a copolymer that consists of AA-IPEG and AA-vinyloxybutyl polyethylene glycol (VOBPEG). The latter has been investigated for instance as stabilizer in C-S-H suspensions in order to enhance an accelerated hydration [59]. This polymer shall promote early strength development, which is desired e.g. for precast concrete. Further, calcined clays are known to reduce the early strength of cementitious systems [6,60], a problem that might be compensated when adding VOBPEG. Information on the molecular weight, anionic charge density and side chain length of the PCE-based superplasticizers are summarized in Table 4. The side chains of IPEG1 and IPEG2 are considered to be 'short' compared to the one of HPEG (Δn_{EO} = 42/35), where IPEG1 exhibits the shortest side chain length. The chemical structures of the HPEG PCE and the two IPEG PCEs are provided in Fig. 2.

2.1.4. Characteristics of binder mixtures and nomenclature

In blended binder mixtures, the PLC is replaced by 30 wt% of calcined clays. Due to only minor differences in their particle densities, the replacement by calcined clay is mass-related instead of volume-based. Nonetheless, the authors are aware of the differences between neat cement and blended mixtures. The PLC and the respective calcined clay are homogenized by hand, before the blend is further mixed in a Hobart mixer. A water-to-binder ratio (w/b) = 0.50 is chosen in order to compare the following results with earlier investigations, e.g. [15,37]. At w/b = 0.50, small dosages of PCE-based superplasticizers were sufficient to properly disperse mixtures blended with one calcined common

Table 4
Molecular weight, anionic charge density and side chain length of PCE-based superplasticizers.

Parameter	HPEG	IPEG1	IPEG2
Molecular weight [g/mol]	39,800	~ 27,500	~ 26,000
Side chain length [-]	moderate	short	short
Anionic charge density in H_2O dest. [µeq/g]	850	628	1390

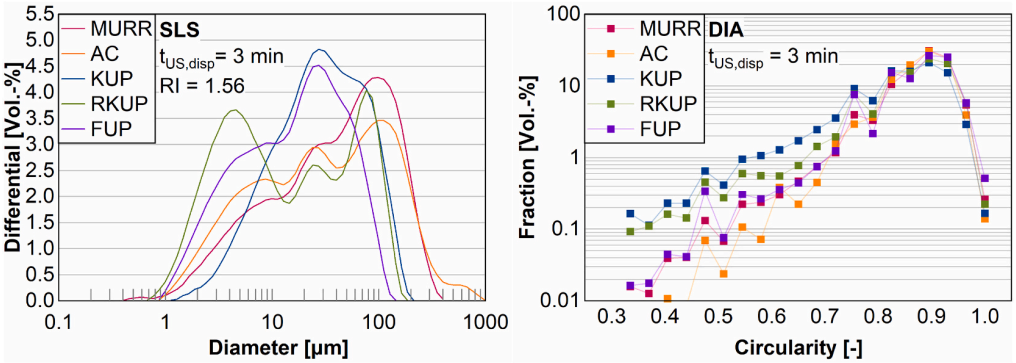

Fig. 1. Particle size analysis of calcined common clays by static light scattering (SLS) with refraction index (RI) = 1.56 (left) and circularity of calcined common clays derived from digital image analysis (DIA) after dispersion for 3 min in ultrasound at 50 W (right).

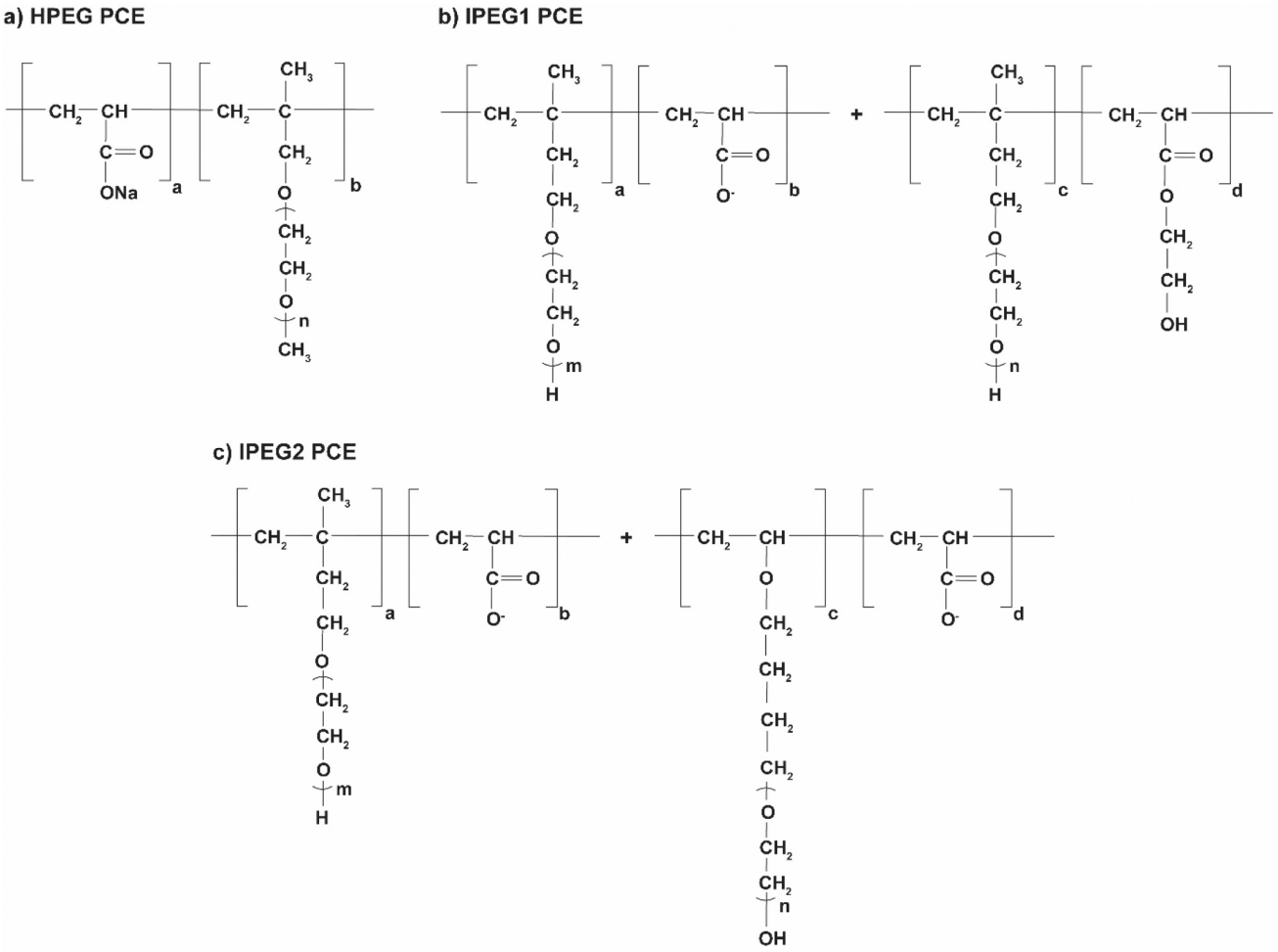

Fig. 2. Structural formulae of a) HPEG PCE, b) IPEG1 PCE and c) IPEG2 PCE.

clay [15,16,39]. In addition, a w/b = 0.40 is chosen for selected mixtures. The dosages of active agent in PCE-based superplasticizers are set at 0.05, 0.10 and 0.20% by weight of binder (%bwob). The liquid component of PCEs is subtracted from the amount of water. Solutions of two liters, based on distilled water with the required amount of PCEs, are used to eliminate weighing errors. Blended cement paste is designated as PLC_*type of calcined clay*_*dosage and type of PCE*.

Among other things, this paper correlates physical parameters of binder mixtures with their rheological properties. The total surface area (TSA) according to Bentz et al. [61] has been identified as reliable parameter to understand the rheological properties of calcined clay blended cements. It is the product of SSA and particle density, respecting both the cement and each calcined clay at the mass related ratio of 70:30. The same ratio-based calculation holds for the water demand. The authors are aware that the methods differ between the water demand to achieve standard stiffness of cement and the water demand of calcined clays that is derived from Puntke method [53]. Nonetheless, this combination revealed plausible correlations in a previous publication of the authors [62]. Table 5 shows the calculated values of particle density, TSA and water demand.

Table 5
Combined physical parameters of binder mixtures (replacement level = 30 wt %).

Parameter	PLC	PLC_ MURR	PLC_ AC	PLC_ KUP	PLC_ RKUP	PLC_ FUP
Particle density [g/cm^3]	3.07	2.96	2.95	2.96	2.94	2.94
Total surface area [m^2/cm^3]	5.5	8.2	17.6	9.2	10.1	37.3
Water demand [wt%]	26.6	28.5	27.1	30.7	29.1	31.7

2.2. Methods

2.2.1. Measurements with rotational viscometer

Rheological measurements are conducted with a rotational viscometer Viskomat NT (Schleibinger, Germany) that is coupled with a water-cooling unit (T = 20 °C) in order to eliminate the fluctuations in temperature. The pastes include a mass of binder = 600 g and the respective amount of water-PCE solution. They are homogenized according to mixing regime of DIN EN 196-3 [52] in a Hobart mixer. The measurements start 5 min after water addition. The rotational speed starts at 120 min^{-1} for 10 min (including pre-shearing of the sample) and slows down to 80 min^{-1} → 40 min^{-1} → 20 min^{-1} for 2 min each and torque [Nmm] is recorded. Due to the limited amount of each lab-calcined clay, in combination with the high variety of PCE dosages and demand for material per each measurement ($m_{calcined\ clay}$ = 180 g), single measurements are conducted. However, in case of strong fluctuations/invalid data, the measurement is repeated to obtain valid data (cf. SD-Fig. 1 in supplementary data).

2.2.2. Analysis of rheological parameters

The raw data is analyzed using the software Origin 2020 (OriginLab).

For each step of rotational speed, data points are only collected once an equilibrium is obtained and averaged as 'median torque' (see SD-Fig. 2 in the supplementary data). At the stage with the highest rotational speed, which also acts as pre-shear, the discrepancy between initial torque and torque at equilibrium is greatest. For this reason and although it takes 8 min longer, it is not guaranteed that the same amount of data points is collected as for the other steps. However, the frequency of data recording (10 s^{-1}) generally enables sufficient points to be obtained per step and measurement.

This paper uses two methods to describe the relation between rotational speed and torque. On the first hand, rheological parameters are analyzed following the Bingham model [14,63] as it previously revealed good correlations with calcined clay blends [37]. It considers the linear fit of the flow curve between 120 min^{-1} and 20 min^{-1}.The y-intercept represents the yield stress factor "g" [Nmm] (≈ dynamic yield stress τ_0) and the slope equals the viscosity factor "h" [Nmm*min] (≈ plastic viscosity μ). However, as the classic Bingham model does not consider whether the investigated material is shear-thinning or shear-thickening, the analysis by modified Bingham model [64] and Herschel-Bulkley fit [14] is provided in SD-Table 1 in the supplementary data.

Further, the flow resistance (FR) is derived from the obtained data points as this approach revealed good correlations between physical and chemical cement characteristics in earlier investigations by Vikan et al. [65,66]. In the present paper, the FR is calculated as the area under the flow curve for rotational speeds between 120 min^{-1} and 20 min^{-1} and the median torque, using the trapezoidal method in 3 sections (120–80, 80–40 and 40–20 min^{-1}), see also ref. [35]. The authors are aware that mixtures with different viscosity and yield stress values can result in a similar flow resistance.

2.2.3. Analysis of initial dispersion performance of PCE

The authors previously presented an approach to calculate the efficiency (E) of superplasticizer, e.g. in calcined clay blended systems [15]. It takes the reduced yield stress factor (g_{sp}), viscosity factor (h_{sp}) and median torque (T_{sp}) into account and relates them to reference values ($g_{ref}/h_{ref}/T_{ref}$). This reduction is divided by the dosage of superplasticizer added (d_{sp} [0.01%bwob]), see Eq. (1). This approach can be helpful on the one hand if the dosage is adapted to another parameter, e.g. initial slump, and on the other hand to observe saturation effects when using various dosages for one mixture. Efficiency is set at 0%/0.01% bwob in case of increased values compared to reference without superplasticizer.

$$E\left[\frac{\%}{0.01\%bwob}\right] = \frac{\left(1-\frac{g_{sp}}{g_{ref}}\right)+\left(1-\frac{h_{sp}}{h_{ref}}\right)+\left(1-\frac{T_{sp}}{T_{ref}}\right)}{d_{sp}} \quad (1)$$

Efficiency of superplasticizers is compared with the reduction in flow resistance ($Red_{FR} = FR_{sp}/FR_{ref} * 100\%$). Red_{FR} shall represent another indicator that is easily derived in order to predict the (initial) dispersion performance of superplasticizers.

3. Results & discussion

3.1. Rheological properties of calcined clay blended cement pastes

3.1.1. Basic rheological parameters of calcined clay blended cement pastes

As shown in Table 6, calcined clays blended binders exhibit an (at least slightly) increased viscosity and higher yield stress, which has been often observed in literature [55,67,68]. As consequence, the addition of calcined clays increases the flow resistance in a remarkable way, with up to four times the flow resistance compared to PLC reference. The increased flow resistance results from high torque values, especially at higher rotational speed. The impact of calcined common clays can be divided into 2 groups: (I) PLC_MURR and PLC_AC behave similar to PLC reference, while (IIa) PLC_KUP shows a significant increase in viscosity, yield stress and flow resistance. The effect on yield stress and flow resistance is even more pronounced for (IIb) PLC_RKUP and PLC_FUP. Beside of an increased viscosity at w/b = 0.40, the yield stress factor is four times higher for both PLC and PLC_KUP compared to w/b = 0.50. At lower w/b, the flow resistance is increased by 200–250%. Nonetheless, PLC has still a lower yield stress and flow resistance at a lower w/b than the calcined clay blended cements from group II at w/b = 0.50. In previous studies, cement paste with 20 wt% calcined common clay showed Bingham fluid behavior, while the rheological behavior with calcined pure phyllosilicates rather has been described with the Herschel-Bulkley model due to non-linear increase of torque with increasing rotational speed [15]. The present results do reveal Bingham behavior for group I) with R^2 values close to 1 for the Bingham fit. Group II) shows non-linear flow behavior and a flow index >2 based on Herschel-Bulkley fit, which indicates a more pronounced shear-thickening behavior (see SD-Figs. 5 to 7 and SD-Table 1 of the supplementary data, respectively).

PLC_KUP samples have a high viscosity factor compared to their yield stress factor, also with the addition of PCE (Fig. 3). A strong increase of torque at high rotational speed - due to a high viscosity of the paste - leads to comparable low yield stress. It is usually related to shear-thickening behavior. On the one hand, high viscosity is an aimed effect e.g. to avoid segregation effects of self-compacting concrete but leads to poor flowability on the other side [67]. This has been also observed in pure metamuscovite mixtures [12], which explains the rheological behavior of PLC_KUP as the raw KUP contains non-negligible amounts of muscovite (Table 2). The range for viscosity and yield stress factors of PLC_MURR and PLC_AC mixtures is rather narrow in presence and absence of PCEs. This is related to the relatively low reference values shown in Table 6. With high dosages of PCEs, few mixtures even exhibit a 'negative' yield stress factor analyzed with linear Bingham fit, shown in Fig. 3 and Table 8. This effect does not apply when using the modified

Table 6
Rheological values of binder pastes (references) after 5 min; replacement level = 30 wt%, w/b = 0.50 if not noted otherwise.

Mixtures	Viscosity factor [Nmm*min]	Yield stress factor [Nmm]	Flow resistance [Nmm/min]	Median torque [Nmm] at a rotational speed of …			
				20 min^{-1}	40 min^{-1}	80 min^{-1}	120 min^{-1}
PLC[a]	0.11 ± 0.01	12.2 ± 0.7	1987 ± 69	14.6 ± 0.6	16.7 ± 0.7	20.6 ± 0.8	25.8 ± 0.9
PLC_MURR	0.12	14.1	2240	17.2	19.1	22.8	29.3
PLC_AC[a]	0.10 ± 0.00	13.8 ± 0.6	2067 ± 68	16.1 ± 0.7	17.8 ± 0.7	21.3 ± 0.9	25.9 ± 0.6
PLC_KUP	0.26	49.4	6723	56.5	60.2	67.4	82.8
PLC_RKUP	0.16	66.9	7841	71.2	74.2	78.5	88.2
PLC_FUP	0.14	71.4	8090	75.6	77.2	80.7	89.6
PLC (w/b = 0.40)	0.26	42.0	5923	47.9	52.7	60.0	73.2
PLC_KUP (w/b = 0.40)	0.68	197.0	24,076	217.2	222.1	240.6	280.8

[a] Relative error ≤ 7.4% for PLC and ≤ 4.3% for PLC_AC.

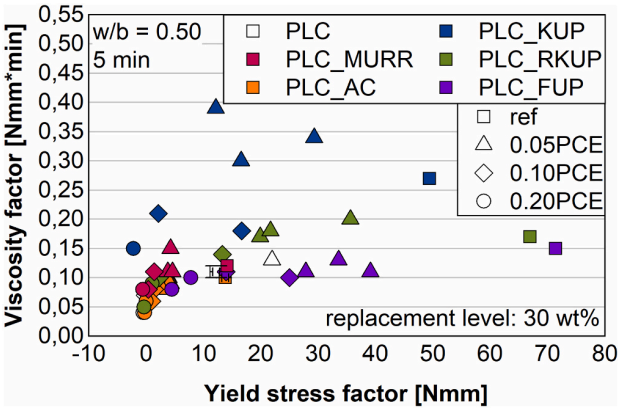

Fig. 3. Comparison of yield stress with viscosity for binder pastes without (squared dots) and with the addition of 0.05, 0.10 and 0.20%bwob PCE (n = 49).

Bingham or Herschel-Bulkley model, where the respective mixtures exhibit very small yield stress values (see SD-Table 1 in supplementary data). A yield stress close to zero, however, indicates strong bleeding and segregation effects [69], which is often a result of excessive superplasticizer dosage to the respective mixture. Therefore, the mixtures with negative yield stress factor are considered as unstable. This topic is further addressed in Section 3.2.1.

PLC, PLC_AC and especially PLC_FUP mixtures have a low viscosity-to-yield stress ratio. The low viscosity factor of PLC_FUP mixtures results from high torque also at low rotational speeds and a rather small difference in median torque at the chosen rotational speeds. At the same time, the torque level of binder paste is significantly increased with the addition of FUP, which leads to high yield stress. The results show significantly differing rheological behavior with the addition of different calcined clays. In a next step, material properties are identified that affect the flow resistance of calcined clay blended cement paste.

3.1.2. Physical and mineralogical parameters affecting the flow resistance of calcined clay blended cement paste

The particle size distribution (PSD) or grinding fineness of powder materials is known to affect the rheological behavior. Fig. 4a shows that the flow resistance of pastes blended with calcined clays decreases significantly with coarser PSD. This holds especially for mixtures with AC and MURR that both exhibit significant higher d_{50} and d_{90} values compared to the other calcined clays. Although the calcined clays have been calcined and ground according to the same procedure, their PSD differ significantly (Fig. 1 left). All samples exhibit a maximum (or shoulder) at a particle size of 25–35 µm. The kaolinite-rich clays have a higher fraction in the smaller particle region, indicated either by a peak around 4.5 µm or a pronounced shoulder up to 10 µm, respectively. The high quartz content favors here the measurability of the particle size distribution of RKUP, while the particles tend to agglomerate in FUP at the application-oriented low impact during dispersion in ultrasound bath (3 min at 50 W). While FUP has a sharp decline after the maximum, quartz-rich clays have a further maximum (shoulder) at 100–130 µm. Quartz is known to be arranged in the coarser particle region of clays due to its hardness and, as consequence, poor grindability [70,p. 12]. According to Irassar et al. [3], however, the presence of quartz in clays/shales can enhance the grindability due to de-agglomerating properties. Beside of the quartz, the high volume fraction of coarse particles (> 70 µm) of MURR, AC and KUP is related to the 2:1 phyllosilicates present in these clays. With the current knowledge, it is related to a lower dehydroxylation degree that increases the agglomeration of smectite/muscovite/illite crystals, represented as rather coarse particles. This phenomenon is also shown by recent scanning electron microscope images of calcined common clays [71] and is a possible reason why quartz-rich clays have a) a rather fine PSD (RKUP, KUP) and b) like MURR a high d_{90} value (Table 3). Further, RKUP and FUP exhibit the finest PSD due to their high kaolinite content. A finer PSD results often in an increased activity of pozzolanic SCMs [72] but surely needs to be reconsidered when it comes to the rheological properties [34]. The circularity, given in Fig. 1 (right), addresses the 3D form of a particle, where 1 equals a sphere. For all calcined common clays, most of the particles possess a circularity between 0.86 and 0.93. Especially KUP, however, exhibits an increased volume of particles with circularities < 0.8. Few fractions even have circularities of <0.5 or 0.3, which can decrease the flowability due to higher friction (Fig. 1, right).

The PSD itself does not directly correlate with the SSA of (calcined) clays, due to the dominating inner porosity of the clay minerals [73,74] and strong agglomeration of clay particles. Therefore, it is crucial to analyze further parameters.

The flow resistance increases for calcined clay blended cements with TSA values >10 m^2/cm^3 (Fig. 4b). At the same time, an increase from ~10 m^2/cm^3 (PLC_RKUP) to 37.3 m^2/cm^3 (PLC_FUP) does not lead to a remarkable increase in flow resistance as one might expect from this significant difference in TSA. The same holds for their viscosity and yield stress factors. As shown in Table 6, PLC_AC has a similar viscosity, yield stress and flow resistance as PLC and PLC_MURR although PLC_AC has a significantly higher TSA (17.6 m^2/cm^3). The authors assume that the latter results from the high amount of phyllosilicates present in raw AC. Especially smectite is known for a very large SSA with values of 323–505 m^2/g [75,76], whereas illite and kaolinite exhibit SSA values of

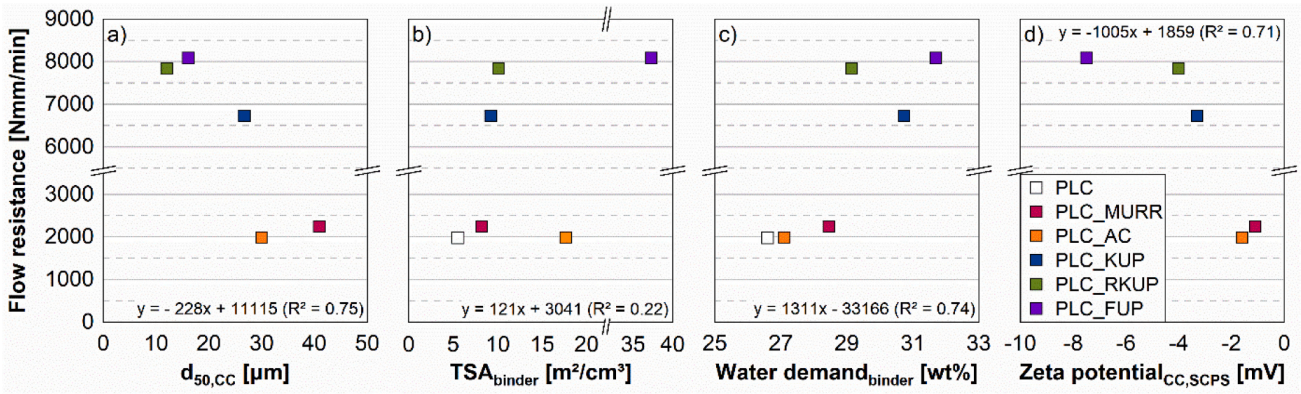

Fig. 4. Correlation of initial flow resistance of calcined clay blended pastes with a) d_{50} value of calcined clay (CC), b) total surface area (TSA), c) water demand of binder, and d) zeta potential of respective calcined clay in synthetic cement pore solution (SCPS); equations and R^2 values correspond to linear fits of the data points; replacement level = 30 wt%, w/b = 0.50.

65–100 m^2/g [77] and 15 [78] – 207 m^2/g [75], respectively. The SSA of 2:1 phyllosilicates decreases by calcination but it is still larger than the SSA of cement [13,76,79]. Compared to FUP, however, the SSA of AC is rather low. Danner et al. [80] described the formation of a glass phase during calcination at $T = 800$ °C, if enough calcite is present in smectitic or illitic clays. As AC contains 7 wt% calcite and 37 wt% 2:1 phyllosilicates (Table 2), the formation of a glassy surface of the particles might occur during the calcination of AC. This is indicated by a high amorphous content of calcined AC (49 wt%) and could in turn lead to a comparable low SSA and water demand despite of the high amount of phyllosilicates in AC.

FUP does neither contain any calcite nor a remarkable amount of 2:1 phyllosilicates. PLC_FUP exhibits the highest water demand of all binder mixtures, where the water demand of FUP is related to its large SSA (Table 3) stemming from strongly disordered kaolinite. Maier et al. [8] recently found good correlations between the degree of kaolinite disorder of raw clay and the SSA of the respective calcined clay. PLC_AC exhibits a low water demand in comparison to its TSA, which confirms that there is not necessarily a correlation between the SSA and water demand of particles [6,81]. Reference binder mixtures with a water demand <29 wt% have a low flow resistance, while the flow resistance increases significantly with higher water demand (Fig. 4c). The range of water demand appears to be small from 26.6 to 31.7 wt% (Table 5), but nonetheless there is an influence of water demand on the flow resistance of blended cements as also stated by refs. [82,83].

The sharp increase in flow resistance as correlated with d_{50} value of calcined clay, combined TSA and water demand, is also observed with the negative zeta potential of calcined clays in SCPS (Fig. 4d). Calcined clays with zeta potential values more negative than – 2 mV tend to increase the flow resistance significantly. Flow resistance increases as the overall negatively charged calcined clay particles agglomerate with positively charged aluminate clinker phases and early hydration products [84,85] or do adsorb cations released from clinker phases [7,86]. Here, a more negative zeta potential of calcined clay enhances the effect of Ca^{2+} to function as a kind of adhesive between the calcined clay particles and therefore leads to higher flow resistance. As previously stated, the zeta potential of calcined clays decreases with higher amount of kaolinite present in clay [35].

As consequence, the flow resistance of blended paste increases with increasing kaolinite content present in raw clay, although the correlation is not linear at all (Fig. 5). The same holds for the yield stress factor (Table 6). $MURR_{raw}$ and $RKUP_{raw}$, for instance, contain a similar amount of phyllosilicates in total. However, $MURR_{raw}$ consists mainly of 2:1 phyllosilicates (muscovite/illite and smectite), while $RKUP_{raw}$ possesses a high amount of kaolinite, which leads to a significant higher flow resistance and yield stress in PLC_RKUP. AC_{raw} contains in total 66 wt% of phyllosilicates, similar to KUP_{raw} (62 wt%). When taking a look at Fig. 5, the main difference are illite-smectite interstratifications present in AC_{raw}, whereas mainly muscovite is present in KUP_{raw} beside of kaolinite and quartz. As already mentioned, the range of flow resistance is relatively close for PLC_KUP, PLC_RKUP and PLC_FUP. The high amount of muscovite in KUP_{raw} might not only be the reason for higher viscosity (Table 6 and Fig. 3) and shear-thickening behavior as revealed for metamuscovite [12] but also for the high flow resistance and yield stress in PLC_KUP. The high water demand of KUP (Table 3), leading to high flow resistance, yield stress and viscosity, agrees with findings of Neißer-Deiters et al. [13] who revealed an increased water uptake of a muscovite-rich mica mineral after calcination. High amounts of quartz that are present in KUP and RKUP (Table 2) cannot compensate the influence of muscovite/illite or kaolinite, although quartz itself is known for workability enhancing properties [87]. However, it might be the reason for a rather low SSA of these two calcined clays but also the reason for the high grinding fineness when considering quartz as deagglomeration aid [3]. RKUP has a kaolinite content between KUP and FUP, with quartz as its second main component. Contrary to previous assumptions of the authors [15], quartz can obviously not necessarily reduce the impact on flow resistance. In case of PLC_RKUP, the larger fraction of RKUP particles with small particle size (< 10 μm) and low circularity (Fig. 1) does rather contribute to a higher flow resistance, which lies in a similar range as for PLC_FUP, where FUP contains only small amounts of quartz. Nonetheless, further components might favor a lower flow resistance due to beneficial particle morphology, as for instance the smooth surface of quartz [88] or possible formed glass phases leading to a significant reduction of SSA [80].

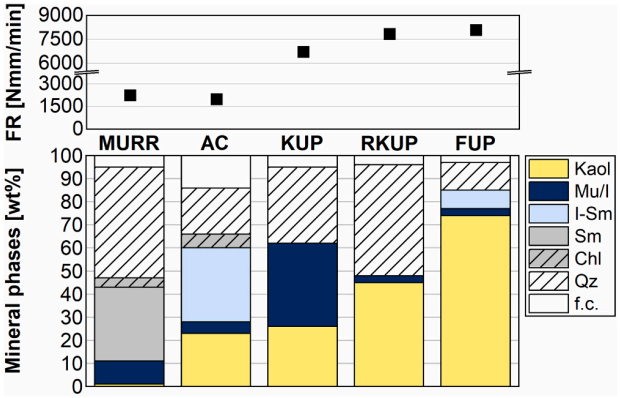

Fig. 5. Comparison of the mineralogical composition of raw clays (Kaol = kaolinite, Mu/I = muscovite/illite, I-Sm = illite-smectite, Sm = smectite, Chl = chlorite, Qz = quartz, f.c = further components) with initial flow resistance of calcined clay blended cements (replacement level = 30 wt%, w/b = 0.50).

Based upon the results obtained on paste level (w/b = 0.50) and with the investigated calcined common clays, the following parameters are identified as critical towards rheological behavior:

- d_{50} value of calcined clays <30 μm
- TSA of binder >10 m^2/cm^3
- water demand of binder >29 wt%
- zeta potential of calcined clays in SCPS < −2 mV

These thresholds relate to a huge extent on the mineralogy of clays, where high amounts of phyllosilicates lead to an increased SSA also after calcination, while quartz impurities can compensate the large SSA to a certain degree. Kaolinite is identified as main component leading to a strong negative zeta potential and thus to a higher flow resistance. High amounts of muscovite do result in a high flow resistance and increased viscosity. Furthermore, it is worth to mention that smectitic phases do not cause flowability problems if they are present in calcined common clays. In ceramics, they are an unfavored component as smectite particles attach to each other or to other particles, leading to increased flocculation [89]. As next step, the initial dispersion performance of three PCEs in calcined clay blended cements is evaluated with focus on the superplasticizer properties and the mineralogical composition of (calcined) clays.

3.2. Parameters affecting the initial dispersion performance of PCE in calcined clay blended cement paste

3.2.1. Superplasticizer properties and dosage

Taking a look at the properties of the three PCEs, their initial efficiency does not correlate with the molecular weight of superplasticizers and the influence of a longer side chain length seems to be minor when adding 0.05 %bwob of PCE (Fig. 6a and b). Plank et al. [26,27] found a longer side chain length to be more effective but that it is rather the type of macromonomer, which is decisive for dispersion performance. The former trend is observed in few mixtures (PLC_KUP and PLC_RKUP), but a final conclusion is omitted here as the *co*-polymers vary in their macromonomers (Fig. 2). The efficiency rather increases with higher

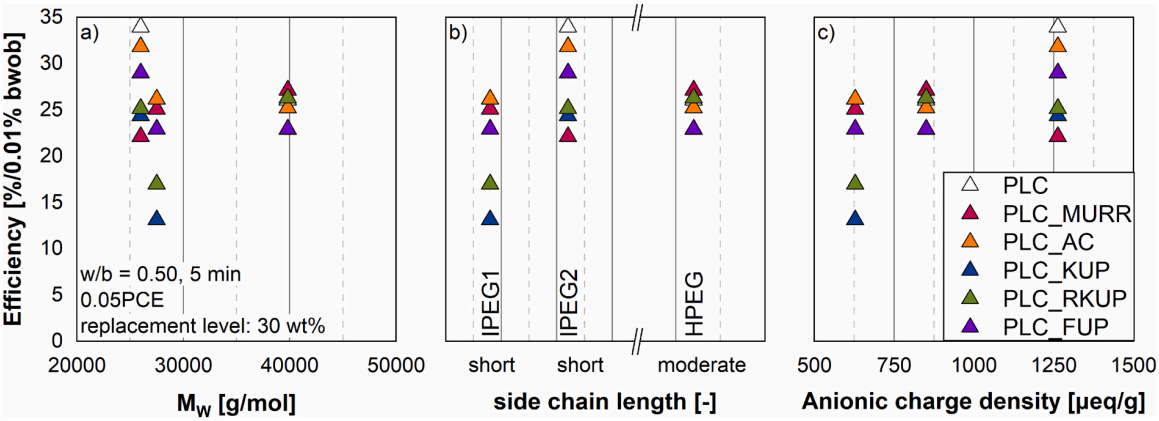

Fig. 6. Efficiency of 0.05%bwob superplasticizer depending on a) molecular weight (M_w), b) side chain length and c) anionic charge density.

anionic charge density (Fig. 6c), which is in good agreement with literature [27,90,91]. The results show that PCEs with IPEG and HPEG macromonomers are suitable for the dispersion of calcined clay blended systems, as previously observed in [26,27]. So far, there is hardly any literature on superplasticizers with vinyloxybutyl polyethylene glycol, the other macromonomer present in IPEG2 beside of the name-giving IPEG macromonomer. Furthermore, the molar ratio of the macromonomers and the anchor groups is under seal, but a higher ratio is assumed for IPEG2 according to the high anionic charge density. Except for few mixtures, the initial efficiency of the three PCEs is in a similar range (~ 23–27%/0.01%bwob).

If aiming for a comparable viscosity factor as for PLC reference (0.12 Nmm*min), low dosages of PCE are sufficient, except for PLC_KUP and PLC_RKUP. The viscosity factor is increased for few mixtures with the addition of 0.05%bwob PCE. This effect is especially observed for PLC_KUP and PLC_RKUP and considered as the reason for a rather low superplasticizer efficiency. However, it decreases with the addition of higher dosages of IPEG1 and IPEG2 (Table 7), which is in agreement with findings from literature [92]. In general, the addition of superplasticizer reduces the viscosity to a less extent than the yield stress, which has been also observed by Lorentz et al. [34].

Table 8 shows that the yield stress factors of PLC_MURR and PLC_AC are at a low level (<5 Nmm) with 0.05 and 0.10%bwob PCE. Mixtures of PLC, PLC_MURR and PLC_AC with 0.20%bwob PCE are not considered as they revealed negative yield stress factors according to the linear Bingham fit, indicating segregation. This holds for PLC_KUP and PLC_RKUP only with 0.20%bwob IPEG2. These mixtures require more than 0.10%bwob IPEG1 and between 0.05 and 0.10%bwob IPEG2 in order to achieve a yield stress in the range of PLC_ref (11.6 Nmm, see Table 6 and Table 8). PLC_FUP demands for more than 0.10%bwob PCE to reach similar values.

Comparable to the yield stress, the flow resistance is significantly reduced with 0.05%bwob PCE for all mixtures, except for PLC_0.05IPEG1 (Fig. 7). PLC_0.05IPEG1 exhibits a higher yield stress and flow resistance compared to the reference immediately after water addition, while a subsequent Red_{FR} was observed [35]. The authors stumble over this result as the plain PLC should be the least challenging material when it comes to dispersion. Overall, IPEG1 achieves a significantly lower Red_{FR} compared to HPEG and IPEG2 due to low initial adsorption of IPEG1. For instance, 0.20%bwob IPEG1 achieve a comparable Red_{FR} as 0.10%bwob IPEG2, that demonstrates once more the strong, immediate dispersion by IPEG2. The dispersion is overall improved with more IPEG PCE added but the further Red_{FR} with increasing superplasticizer dosage is comparable low for PLC_FUP and PLC_AC due to the high performance with 0.05%bwob IPEG PCE already (Fig. 7). Taking a look at the absolute values of flow resistance, as provided in Table 9, a further reduction does hardly take place neither with 0.20%bwob IPEG1 nor IPEG2 for PLC, PLC_MURR and PLC_AC. These mixtures exhibit comparable uncritical flow properties without superplasticizer and a certain saturation effect is achieved with this dosage of PCE. At the same time, PLC_KUP and PLC_RKUP need higher dosages for a further reduction in both yield stress and flow resistance, which is possible with the chosen superplasticizers. PLC_KUP exhibits only a small Red_{FR} with 0.05%bwob PCE. It achieves a significant higher Red_{FR} with a higher amount of PCE added, which complements the findings on yield stress factor. As consequence, IPEG1 is still the least efficient in PLC_KUP, whereas IPEG2 behaves similar as in the other calcined clay blended systems. PLC_FUP, that is the most critical mixture, demands for 0.20%bwob IPEG PCE to achieve a flow resistance similar to PLC reference (~ 2000 Nmm/min). Overall, all mixtures show a good percentage of Red_{FR}. The absolute values in yield stress and flow resistance, however, depend strongly on the initial flow properties and hence on the properties of the calcined clays added.

3.2.2. *Compatibility of PCE-based superplasticizers with calcined common clays*

HPEG reveals the most stable Red_{FR}/efficiency regardless of the calcined clay blended system, see Fig. 7 and Fig. 8. Compared to other

Table 7
Viscosity factors of binder paste with 0.05HPEG and varying dosage of IPEG1/2 (replacement level = 30 wt%; w/b = 0.50); n.d. = not determined, seg. = segregating/unstable mixture.

Mixtures	Viscosity factor [Nmm*min] with the addition of …						
	0.05 HPEG	0.05 IPEG1	0.10 IPEG1	0.20 IPEG1	0.05 IPEG2	0.10 IPEG2	0.20 IPEG2
PLC	0.10	0.13	0.09	seg.	0.08	seg.	seg.
PLC_MURR	0.11	0.11	0.11	seg.	0.15	0.08	n.d.
PLC_AC	0.09	0.09	0.08	seg.	0.08	0.06	seg.
PLC_KUP	0.30	0.34	0.18	n.	0.39	0.21	seg.
PLC_RKUP	0.17	0.20	0.14	0.09	0.18	0.10	seg.
PLC_FUP	0.13	0.11	0.10	0.10	0.11	0.11	0.08

Table 8
Yield stress factors of binder paste with increasing dosage of IPEG1 and IPEG2 (replacement level = 30 wt%, w/b = 0.50); analyzed via linear Bingham fit; n.d. = not determined, seg. = segregating/unstable mixture.

Mixtures	Yield stress factors [Nmm] with the addition of …						
	0.05 HPEG	0.05 IPEG1	0.10 IPEG1	0.20 IPEG1	0.05 IPEG2	0.10 IPEG2	0.20 IPEG2
PLC	4.0	22.0	1.6	seg.	2.8	seg.	seg.
PLC_MURR	3.7	4.6	1.4	seg.	4.3	0.4	n.d.
PLC_AC	4.3	4.1	1.5	seg.	2.8	1.0	seg.
PLC_KUP	16.6	29.3	16.7	n.d.	12.2	2.1	seg.
PLC_RKUP	19.9	35.6	13.3	1.0	21.7	2.3	seg.
PLC_FUP	33.6	39.1	25.0	7.8	27.8	13.9	4.5

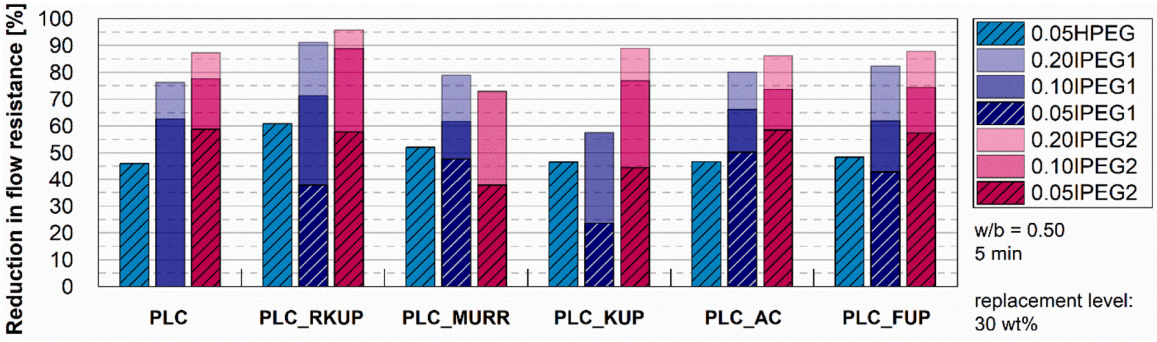

Fig. 7. Initial reduction in flow resistance of binder pastes with varying superplasticizer dosage.

Table 9
Flow resistance of binder pastes with PCE after 5 min; replacement level = 30 wt%, w/b = 0.50 if not noted otherwise; n.d. = not determined, mixtures with FR < 500 Nmm/min are considered as seg. = segregating/unstable mixture.

Mixtures	Flow resistance [Nmm/min] with the addition of …						
	0.05 HPEG	0.05 IPEG1	0.10 IPEG1	0.20 IPEG1	0.05 IPEG2	0.10 IPEG2	0.20 IPEG2
PLC	1069	2875	738	seg.	815	seg.	seg.
PLC_MURR	1076	1174	859	seg.	1390	608	n.d.
PLC_AC	1062	990	673	seg.	826	524	seg.
PLC_KUP	3597	5140	2859	n.d.	3732	1559	742
PLC_RKUP	3071	4870	2256	693	3312	877	seg.
PLC_FUP	4182	4623	3084	1431	3452	2077	987
PLC[a]	3153	4895	n.d.	n.d.	3321	n.d.	n.d.
PLC_KUP[a]	21,607	19,665	n.d.	n.d.	23,624	n.d.	**n.**

[a] w/b = 0.40

calcined clay blends, PLC_AC and PLC_FUP interact the least with HPEG. Thanks to a remarkable decrease in viscosity, the performance of 0.05% bwob IPEG1 and IPEG2 is among the best in these mixtures, despite of the initial low dispersion of IPEG1. IPEG2 shows an outstanding performance for PLC_AC and PLC_FUP, although AC_{raw} and FUP_{raw} both possess the highest amounts of phyllosilicates present in raw clay (Table 2) as well as the largest SSA (Table 3). Kaolinite and illite-smectite interstratifications, both present in AC_{raw} and FUP_{raw}, seem not to interfere the interaction with PCEs, once they are transformed to metaphases (metakaolinite, metaillite-smectite) by calcination of the clays. So far, it is unclear whether calcined clays do take up anionic charged superplasticizers. However, as cations released from clinker phases can adsorb onto negatively charged calcined clay sites, as shown e.g. by [7,18,26], these turn into less negatively or even positively charged surface sites [35,93] and can enhance the PCE adsorption. The very early formation of first ettringite nuclei, enhanced by the presence of limestone [94] and calcined clays [7,95], can also favor the adsorption of PCEs onto positively charged aluminate hydrates. Here, a large SSA could increase this effect as more nucleation sites are provided. The efficiency of 0.05%bwob IPEG1 and IPEG2 is rather low for PLC_KUP and PLC_RKUP due to an increase in viscosity. This confirms, in case of PLC_KUP, on the one hand the low superplasticizer efficiency in muscovite-rich mixtures [15]. On the other hand, as shown for PLC_RKUP, it is contrary to the assumptions that a) quartz can enhance the superplasticizer efficiency and b) kaolinite-rich clays are less critical than those rich in 2:1 phyllosilicates [15] as this holds only for HPEG, but for neither of the two IPEG-based PCEs. The good compatibility of HPEG, especially with quartz-rich calcined clays, is related to the adsorption of Ca^{2+} onto quartz [96]. This enables the adsorption of anionic charged superplasticizers onto originally negatively charged particles by the charge reversal of the latter [97,98]. Further the dispersion performance of all PCEs, in particular of the IPEG-based ones, is related to the adsorption of Ca^{2+} onto calcined clays as previously stated e.g., by [7,18,26].

This is also the reason, why IPEG1 and IPEG2 both interact well with mixtures that exhibit a large surface area. The good interaction of IPEG2 with challenging calcined clay blends is also demonstrated by the increasing trend in performance with higher amounts in kaolinite but also with the total amount of phyllosilicates present in raw clay (Fig. 8). A possible explanation is that heterogeneously [99] but in total

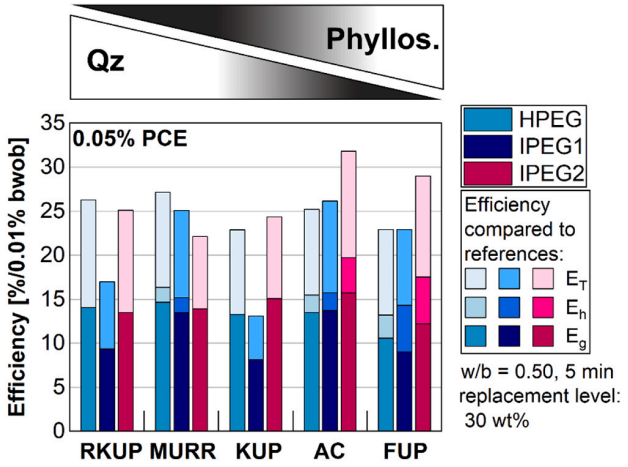

Fig. 8. Initial superplasticizer efficiency in calcined clay blended cement paste, sorted according to descending quartz (Qz) and increasing phyllosilicate (Phyllos.) content present in respective raw clay with 0.05%bwob PCE regardless of final flowing properties; E_T = efficiency on median torque; E_g = efficiency on viscosity; E_h = efficiency on yield stress;

negatively charged sites of calcined clays [35] favor the adsorption of IPEG2 not only onto positively charged clinker surfaces but also onto calcined clay particles. This phenomenon has been previously observed, for instance, for silica fume by Schröfl et al. [100] where a combination of macromonomers (APEG for silica fume and MPEG for clinker phases) enhanced the dispersion by selective adsorption. They [100] related it to the steric positioning of -COO^- groups that suits better for Ca^{2+} located at specific surfaces on the silica fume, while MPEG interacts preferably with hydrating clinker phases. For the IPEG2 in this present study, the "*substrate-selective adsorption*" [100] might be modified as follows: if IPEG2 is added to PLC only, it performs the best with an achieved efficiency of 34%/0.01%bwob. If calcined clays are added, IPEG2, that consists of AA-IPEG and AA-VOBPEG copolymers, seems to adsorb (preferably) onto them. This holds also for the kaolinite-rich clays and results in high Red_{FR} (Fig. 7) and efficiency (Fig. 8).

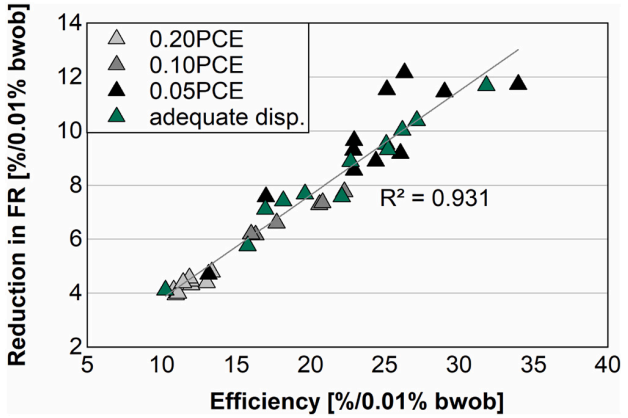

Fig. 9. Comparison of reduction in flow resistance and efficiency [%/0.01% bwob] of PCE, both related to superplasticizer dosage [%/0.01%bwob] (n = 40); green triangles represent mixtures investigated within this study that have achieved similar flowing properties as PLC_ref. (For interpretation of the references to color in this figure legend, the reader is referred to the web version of this article.)

3.3. Classification of the superplasticizer performance in calcined clay blended systems

In a final step, the efficiency and the reduction in flow resistance (Red_{FR}) both enable a further evaluation of the superplasticizer performance at different dosages, also from an economical point of view. Fig. 9 demonstrates a very good, linear correlation between the efficiency and Red_{FR} (R^2 = 0.931). The range of efficiency and Red_{FR} values becomes smaller with increasing amount of superplasticizer, indicating a certain saturation effect. However, the results on the initial superplasticizer performance confirm that the calcined clay blends require different dosages of superplasticizer in order to achieve similar flowing properties as the original flow properties can vary significantly.

A final evaluation compares the rheological properties of calcined clay blends after the addition of PCE with those of PLC_ref. In Table 10, a superplasticizer-dosage combination is considered as suitable (✓) if the following thresholds taken from PLC_ref are obtained: viscosity factor ≈ 0.12 Nmm·min, yield stress factor ≈ 11.6 Nmm and flow resistance ≈ 1975 Nmm/min (Table 6). If the obtained values are strongly above these thresholds, especially for yield stress factor and flow resistance, the mixture is considered as insufficiently dispersed (x). The addition of too much superplasticizer (o) is indicated in case of significantly lower values (yield stress factor close to 0 Nmm or even negative; flow resistance <1000 Nmm/min). The calcined clay blends of group I) (MURR and AC) do need only 0.05%bwob PCE for proper dispersion and show saturation effects already at the next higher dosage. The mixtures of group II) require at least 0.10%bwob, in case of PLC_FUP rather 0.20% bwob PCE in order to obtain similar yield stress factors and flow resistance values as PLC_ref. Solely with IPEG2, a dosage of 0.20%bwob leads to saturation of all mixtures.

A decreasing particle size, as well as a high kaolinite content present in raw clay that in turn leads to high negative zeta potential are identified as the main parameters affecting the flow resistance and as consequence the demand for superplasticizer (Fig. 10). The findings regarding a higher superplasticizer demand for kaolinite-rich clays are in good agreement with those of Ferreiro et al. [11]. The comparable small particle size can also result from the kaolinite phase in combination with quartz, which functions as de-agglomerating during grinding process according to Irassar et al. [3]. The presence of quartz itself does not induce a good flowability of blended cement paste, but it can improve not only the grindability but also the properties of calcined clays in terms of a lower SSA, water demand and as consequence the flowability. Contrary to previous results with HPEG [15], an increasing amount of 2:1 phyllosilicates does not necessarily lead to a decreased efficiency of superplasticizer. As already reported for PLC_AC, but also for PLC_MURR, where both clays are rich in illite-smectite and smectite, the superplasticizer efficiency is excellent but depends on the type of polymer added. As KUP exhibits a low SSA, this shows – in combination with the findings of PLC_FUP and PLC_AC - that the interpretation of SSA can lead to wrong assumptions in terms of both the rheological behavior and the interaction with superplasticizers. It is rather the high amount of muscovite that a) leads to an increased water demand (Table 3) and b) is the reason for the least compatibility with PCEs, confirming earlier findings [13,15,16,37,44]. Special viscosity-reducing superplasticizers might be required, if adding calcined muscovite-rich clays and aiming for low viscosity. Similar to viscosity-modifying agents, the use of calcined muscovite-rich clays rather can be considered in applications where a high viscosity is required, e.g. in self-compacting concrete as stated for metakaolin by Cyr and Mouret [67].

4. Conclusions

The rheological properties of Portland limestone cement have been compared with those of mixtures blended with four calcined common clays and one calcined clay-rich mine tailing. The results reveal a significant range in altered flowing properties, depending on the physical

Table 10
Overview of combinations that achieve similar flowability as PLC_ref (✓), have an insufficient dispersion (x) or contain too much superplasticizer or even tend to segregate (o); replacement level = 30 wt%, w/b = 0.50 (n.d. = not determined).

Mixtures	Similar flowing properties as for PLC_ref achieved with …						
	0.05 HPEG	0.05 IPEG1	0.10 IPEG1	0.20 IPEG1	0.05 IPEG2	0.10 IPEG2	0.20 IPEG2
PLC_MURR	✓	✓	o	o	✓	o	n.d.
PLC_AC	✓	✓	o	o	✓	o	o
PLC_KUP	x	x	✓	n.d.	x	✓	o
PLC_RKUP	x	x	✓	o	x	o	o
PLC_FUP	x	x	x	✓	x	✓	o

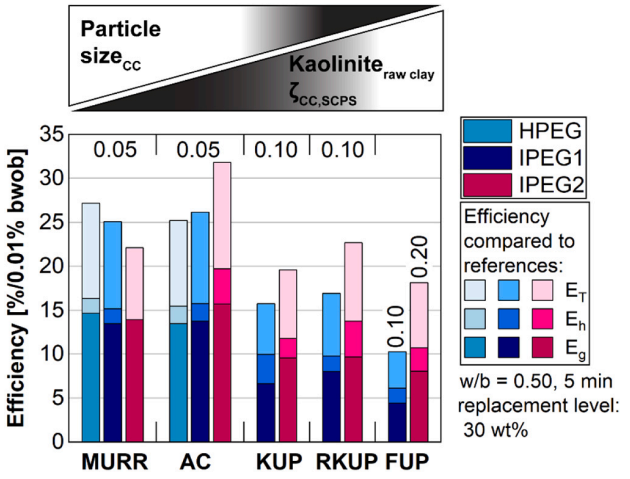

Fig. 10. Tendency of superplasticizer efficiency in calcined clay blended cement pastes, decreasing with finer particle size, higher kaolinite content in raw clay and and more negative zeta potential of calcined clays in SCPS; with dosages required for similar flowing properties as for PLC_ref; respective dosages are provided above the bars and stem from Table 10.

and mineralogical properties of binder and calcined clay added respectively. A water demand of binder higher than 29 wt% is identified as critical parameter, as well as a fine particle size and strong negative zeta potential of calcined clays (<−2 mV). The physical parameters depend to a large extent on the mineralogical composition of the clay, as it not only influences the grindability but also the SSA, water demand and surface charge of the calcined clay. Both, the zeta potential and the SSA increases with more kaolinite in raw clay, where especially highly disordered kaolinite in raw clay contributes to a larger SSA and to a lesser extent to a higher water demand of the calcined clay. Muscovite is identified as further critical phase as it increases the water demand and the viscosity in a remarkable way. Smectite is an uncritical component after calcination, despite its troublemaking behavior in other contexts, like ceramics or in clay-bearing aggregates (freeze-thaw-resistance of concrete and loss in PCE efficiency). Quartz as impurity in clay can lower the SSA and water demand and is beneficial not only in terms of flowing behavior. The same holds for a glass phase possibly formed during calcination in the presence of calcite and smectite. This theory, however, is mainly based upon literature and needs to be verified in further investigations.

The studied, industrial PCE-based superplasticizers can decrease the viscosity and flow resistance sufficiently. The performance increases with the anionic charge density of PCEs, as known for plain cement. HPEG-based PCE is insensitive towards the calcined clay added and interacts slightly better with calcined quartz-rich clays, while IPEG-based PCEs perform even better in the presence of phyllosilicates. Especially in combination with a vinyloxybutyl polyethylene glycol-based polymer, that is known to enhance early strength development, these PCEs are a promising solution to compensate known drawbacks of calcined clays. Based upon the original flowing properties, the need for superplasticizer increases with a higher particle fineness, as well as a higher kaolinite content and more negative zeta potential. While kaolinite and smectite do not interfere with the superplasticizers, muscovite has to be considered again as critical phase as the superplasticizer performance weakens in its presence. The adsorption of calcium ions onto calcined clays and an along-going charge reversal, as well as the initial ettringite formation that is promoted in the presence of limestone as also of calcined clays, can favor the adsorption of anionic superplasticizers. For this reason, the authors recommend a delayed superplasticizer addition, that is common in concrete industry. Overall, however, calcined common clays with moderate kaolinite content are considered as attractive SCMs as they not only show pozzolanic properties but also require less superplasticizer as calcined kaolinite-rich clays for a proper workability. In a next step, the time-dependent flowability needs to be evaluated to find practicable solutions for concrete industry.

CRediT authorship contribution statement

Ricarda Sposito: Conceptualization, Methodology, Investigation, Validation, Data curation, Writing – original draft. **Matthias Maier:** Methodology, Data curation, Writing – review & editing. **Nancy Beuntner:** Conceptualization, Writing – review & editing. **Karl-Christian Thienel:** Supervision, Writing – review & editing.

Declaration of competing interest

The authors declare that they have no known competing financial interests or personal relationships that could have appeared to influence the work reported in this paper.

Acknowledgement

The authors like to thank Prof. J. Plank and his team from the Chair for Construction Chemistry of Technical University Munich (Germany) for measuring the charge density of the PCEs. They also thank Strobel Quarzsand GmbH, Goerg & Schneider GmbH, Dr. Andreas Murr, Mr. Peter Jell (Degelhof clay pit), and Liapor GmbH & Co. KG for providing the raw clays and Schwenk Zement KG for the cement. Furthermore they thank BASF Construction Solutions GmbH (Germany) as well as Jilin Zhongxin Chemical Group Co., Ltd. (China) for the PCE samples.

Appendix A. Supplementary data

Supplementary data to this article can be found online at https://doi.org/10.1016/j.cemconres.2022.106743.

References

[1] T. Danner, H. Justnes, G. Norden, T. Østnor, Feasibility of calcined marl as an alternative pozzolanic material, in: K. Scrivener, A. Favier (Eds.), Calcined Clays for Sustainable Concrete, Springer, Netherlands, 2015, pp. 67–73.
[2] T. Østnor, H. Justnes, T. Danner, Reactivity and microstructure of calcined marl as supplementary cementitious material, in: K. Scrivener, A. Favier (Eds.), Calcined Clays for Sustainable Concrete, Springer, Netherlands, 2015, pp. 237–244.
[3] E.F. Irassar, V.L. Bonavetti, C.C. Castellano, M.A. Trezza, V.F. Rahhal, G. Cordoba, R. Lemma, Calcined illite-chlorite shale as supplementary cementing material: thermal treatment, grinding, color and pozzolanic activity, Appl. Clay Sci. 179 (2019), 105143.
[4] E.F. Irassar, A. Tironi, V.L. Bonavetti, M.A. Trezza, C.C. Castellano, V.F. Rahhal, H.A. Donza, A.N. Scian, Thermal treatment and pozzolanic activity of calcined clay and shale, ACI Mater. J. 116 (2019) 133–143.
[5] G. Marchetti, V. Rahhal, Z. Pavlík, M. Pavlíková, E.F. Irassar, Assessment of packing, flowability, hydration kinetics, and strength of blended cements with illitic calcined shale, Constr. Build. Mater. 254 (2020), 119042.
[6] N. Beuntner, R. Sposito, K.-C. Thienel, Potential of calcined mixed-layer clays as pozzolans in concrete, ACI Mater. J. 116 (2019) 19–29.
[7] S. Scherb, M. Maier, N. Beuntner, K.-C. Thienel, J. Neubauer, Reaction kinetics during early hydration of calcined phyllosilicates in clinker-free model systems, Cem. Concr. Res. 143 (2021), 106382.
[8] M. Maier, N. Beuntner, K.-C. Thienel, Mineralogical characterization and reactivity test of common clays suitable as supplementary cementitious material, Appl. Clay Sci. 202 (2021), 105990.
[9] G. Cardinaud, E. Rozière, O. Martinage, A. Loukili, L. Barnes-Davin, M. Paris, D. Deneele, Calcined clay – limestone cements: hydration processes with high and low-grade kaolinite clays, Constr. Build. Mater. 277 (2021), 122271.
[10] T.R. Muzenda, P. Hou, S. Kawashima, T. Sui, X. Cheng, The role of limestone and calcined clay on the rheological properties of LC3, Cem. Concr. Compos. 107 (2020), 103516.
[11] S. Ferreiro, D. Herfort, J.S. Damtoft, Effect of raw clay type, fineness, water-to-cement ratio and fly ash addition on workability and strength performance of calcined clay – limestone Portland cements, Cem. Concr. Res. 101 (2017) 1–12.
[12] M. Schmid, R. Sposito, K.-C. Thienel, J. Plank, The shear-thickening effect of meta muscovite as SCM and its influence on the rheological properties of ecologically optimized cementitious systems, in: V. Mechtcherine (Ed.), 2nd International RILEM Conference on Rheology and Processing of Construction Materials (RheoCon2), Springer, Dresden, Germany, 2019.
[13] A. Neißer-Deiters, S. Scherb, N. Beuntner, K.-C. Thienel, Influence of the calcination temperature on the properties of a mica mineral as a suitability study for the use as SCM, Appl. Clay Sci. 179 (2019).
[14] V.A. Hackley, C.F. Ferraris, in: Guide to Rheological Nomenclature - Measurements in Ceramic Particulate Systems 29, National Institute of Standards and Technology (NIST), Gaithersburg, Maryland, USA, 2001, p. III.
[15] R. Sposito, N. Beuntner, K.-C. Thienel, Characteristics of components in calcined clays and their influence on the efficiency of superplasticizers, Cem. Concr. Compos. 110 (2020), 103594.
[16] R. Sposito, M. Schmid, J. Plank, K.-C. Thienel, An approach to the rheological behavior of cementitious systems blended with calcined clays and superplasticizers, in: A. Tagnit-Hamou (Ed.), ACI SP 349 11th International Conference on Cementitious Materials and Alternative Binders for Sustainable Concrete, American Concrete Institute, online, 2021, pp. 659–685.
[17] K. Vance, A. Kumar, G. Sant, N. Neithalath, The rheological properties of ternary binders containing Portland cement, limestone, and metakaolin or fly ash, Cem. Concr. Res. 52 (2013) 196–207.
[18] P. Pardo, P.V. Christensen, K. Keiding, D. Herfort, J. Skibsted, Surface properties of calcined clays and their dispersion in blended Portland cement pastes, in: 13th International Congress on the Chemistry of CementMadrid, Spain, 2011, p. 51.
[19] N.A. Tregger, M.E. Pakula, S.P. Shah, Influence of clays on the rheology of cement pastes, Cem. Concr. Res. 40 (2010) 384–391.
[20] T.C. Papanastasiou, Flows of materials with yield, J. Rheol. 31 (1987) 385–404.
[21] I.M. Krieger, T.J. Dougherty, A mechanism for non-newtonian flow in suspensions of rigid spheres, Transactions of the Society of Rheology 3 (1959) 137–152.
[22] Z. Soua, O. Larue, E. Vorobiev, J.-L. Lanoisellé, Estimation of floc size in highly concentrated calcium carbonate suspension obtained by filtration with dispersant, Colloids Surf. A Physicochem. Eng. Asp. 274 (2006) 1–10.
[23] C. Blachier, A. Jacquet, M. Mosquet, L. Michot, C. Baravian, Impact of clay mineral particle morphology on the rheological properties of dispersions: a combined X-ray scattering, transmission electronic microscopy and flow rheology study, Appl. Clay Sci. 87 (2014) 87–96.
[24] E.F. Irassar, V. Rahhal, C. Pedrajas, R. Talero, Rheology of portland cement pastes with calcined clays additions, in: Cleantech 2014, CTSI Clean Technologies and Sustainable Industries Organization, Washington, DC, 2014, pp. 308–311.
[25] S. Ng, H. Justnes, Influence of dispersing agents on the rheology and early heat of hydration of blended cements with high loading of calcined marl, Cem. Concr. Compos. 60 (2015) 123–134.
[26] R. Li, L. Lei, T. Sui, J. Plank, Effectiveness of PCE superplasticizers in calcined clay blended cements, Cem. Concr. Res. 141 (2021), 106334.
[27] M. Schmid, J. Plank, Dispersing performance of different kinds of polycarboxylate (PCE) superplasticizers in cement blended with a calcined clay, Constr. Build. Mater. 258 (2020), 119576.
[28] M. Sonebi, M. Lachemi, K.M.A. Hossain, Optimisation of rheological parameters and mechanical properties of superplasticised cement grouts containing metakaolin and viscosity modifying admixture, Constr. Build. Mater. 38 (2013) 126–138.
[29] K.H. Khayat, A. Yahia, Effect of welan gum-high-range water reducer combinations on rheology of cement grout, ACI Mater. J. 94 (1997) 365–372.
[30] M. Beigh, V.N. Nerella, C. Schroefl, V. Mechtcherine, Studying the rheological behavior of limestone calcined clay cement (LC3) mixtures in the context of extrusion- based 3D-printing, in: A. Parashar, L. Singh, D.G. Rao (Eds.), 3rd International Conference on Calcined Clays for Sustainable ConcreteNew Delhi, India, 2019.
[31] P. Borralleras, I. Segura, M.A.G. Aranda, A. Aguado, Influence of the polymer structure of polycarboxylate-based superplasticizers on the intercalation behaviour in montmorillonite clays, Constr. Build. Mater. 220 (2019) 285–296.
[32] L. Lei, J. Plank, A study on the impact of different clay minerals on the dispersing force of conventional and modified vinyl ether based polycarboxylate superplasticizers, Cem. Concr. Res. 60 (2014) 1–10.
[33] O. Akhlaghi, T. Aytas, B. Tatli, D. Sezer, A. Hodaei, A. Favier, K. Scrivener, Y. Z. Menceloglu, O. Akbulut, Modified poly(carboxylate ether)-based superplasticizer for enhanced flowability of calcined clay-limestone-gypsum blended Portland cement, Cem. Concr. Res. 101 (2017) 114–122.
[34] B. Lorentz, H. Zhu, D. Mapa, K.A. Riding, A. Zayed, Effect of clay mineralogy, particle size, and chemical admixtures on the rheological properties of CCIL and CCI/II systems, in: S. Bishnoi (Ed.), Calcined Clays for Sustainable Concrete - Proceedings of the 3rd International Conference on Calcined Clays for Sustainable Concrete, Springer, Singapore, 2020, pp. 211–218.
[35] R. Sposito, M. Maier, N. Beuntner, K.-C. Thienel, Evaluation of zeta potential of calcined clays and time-dependent flowability of blended cement with customized polycarboxylate-based superplasticizers, Constr. Build. Mater. 308 (2021), 125061.
[36] M. Schmid, J. Plank, Interaction of individual meta clays with polycarboxylate (PCE) superplasticizers in cement investigated via dispersion, zeta potential and sorption measurements, Appl. Clay Sci. 207 (2021), 106092.
[37] R. Sposito, N. Beuntner, K.-C. Thienel, Rheology, setting and hydration of calcined clay blended cements in interaction with PCE-based superplasticisers, Mag. Concr. Res. 73 (2021) 785–797.
[38] DIN EN 197-1, Cement - Part 1: Composition, specifications and conformity criteria for common cements, in: Zement - Teil 1: Zusammensetzung, Anforderungen und Konformitätskriterien von Normalzement, Beuth-Verlag, Berlin, 2011, p. 8.
[39] R. Sposito, M. Schmid, N. Beuntner, S. Scherb, J. Plank, K.-C. Thienel, Early hydration behavior of blended cementitious systems containing calcined clays and superplasticizer, in: J. Gemrich (Ed.), 15th International Congress on the Chemistry of Cement, Research Institute of Binding Materials Prague, Prague, Czech Republic, 2019, p. 10.
[40] M. Maier, N. Beuntner, K.-C. Thienel, An approach for the evaluation of local raw material potential for calcined clay as SCM, based on geological and mineralogical data: Examples from German clay deposits, in: S. Bishnoi (Ed.), Calcined Clays for Sustainable Concrete - Proceedings of the 3rd International Conference on Calcined Clays for Sustainable Concrete, Springer, Singapore, 2020, pp. 37–47.
[41] A. Alujas, R.S. Almenares, S. Betancourt, C. Leyva, Pozzolanic reactivity of low grade kaolinitic clays: influence of mineralogical composition, in: K. Scrivener, A. Favier (Eds.), Calcined Clays for Sustainable Concrete, Springer, Netherlands, 2015, pp. 339–345.
[42] S. Hollanders, R. Adriaens, J. Skibsted, Ö. Cizer, J. Elsen, Pozzolanic reactivity of pure calcined clays, Appl. Clay Sci. 132–133 (2016) 552–560.
[43] T. Danner, G. Norden, H. Justnes, Characterisation of calcined raw clays suitable as supplementary cementitious materials, Appl. Clay Sci. 162 (2018) 391–402.
[44] S. Scherb, N. Beuntner, K.-C. Thienel, Reaction kinetics of the basic clays present in natural mixed clays, in: F. Martirena, A. Favier, K. Scrivener (Eds.), Calcined Clays for Sustainable Concrete - Proceedings of the 2nd International Conference on Calcined Clays for Sustainable Concrete, Springer, Dordrecht, Netherlands, 2018, pp. 427–433.
[45] S. Lee, Y.J. Kim, H.-S. Moon, Phase transformation sequence from kaolinite to mullite investigated by an energy-filtering transmission electron microscope, J. Am. Ceram. Soc. 82 (1999) 2841–2848.
[46] ASTM C1489 - 20, in: Standard Test Methods for Measuring the Reactivity of Supplementary Cementitious Materials by Isothermal Calorimetry and Bound Water Measurements, ASTM International, West Conshohocken, PA, 2020, p. 5.
[47] ISO 13320, in: Particle Size Analysis - Laser Diffraction Methods, 2020, p. 59.
[48] ISO 13322-2, in: Particle Size Analysis - Image Analysis Methods - Part 2: Dynamic Image Analysis Methods, 2006, p. 24.
[49] DIN ISO 9277, in: Determination of the Specific Surface Area of Solids by Gas Adsorption - BET Method, Beuth-Verlag, Berlin, 2003, p. 19.
[50] DIN EN 196-6, Methods of testing cement - Part 6: Determination of fineness, in: Prüfverfahren für Zement - Teil 6: Bestimmung der Mahlfeinheit, Beuth Verlag, Belrin, Germay, 2019, p. 21.
[51] DIN EN ISO 17892-3, in: Geotechnical Investigation and Testing - Laboratory Testing of Soil - Part 3: Determination of Particle Density, Beuth-Verlag, Berlin, Germany, 2015, p. 21.

[52] DIN EN 196-3, Methods of Testing Cement - Part 3: Determination of Setting Times and Soundness, in: Prüfverfahren für Zement - Teil 3: Bestimmung der Erstarrungszeiten und der Raumbeständigkeit, Beuth-Verlag, Berlin, Germany, 2009, p. 17.
[53] M. Hunger, H.J.H. Brouwers, Flow analysis of water–powder mixtures: application to specific surface area and shape factor, Cem. Concr. Compos. 31 (2009) 39–59.
[54] A. Buchwald, C. Kaps, M. Hohmann, Alkali-activated binders and pozzolan cement binders – compete binder reaction or two sides of the same story? in: H. Justnes (Ed.), 11th International Conference on the Chemistry of CementDurban, South Africa, 2003, pp. 1238–1246.
[55] N. Nair, K. Mohammed Haneefa, M. Santhanam, R. Gettu, A study on fresh properties of limestone calcined clay blended cementitious systems, Constr. Build. Mater. 254 (2020), 119326.
[56] Y. Chen, C. Romero Rodriguez, Z. Li, B. Chen, O. Çopuroğlu, E. Schlangen, Effect of different grade levels of calcined clays on fresh and hardened properties of ternary-blended cementitious materials for 3D printing, Cem. Concr. Compos. 114 (2020), 103708.
[57] E. Moulin, P. Blanc, D. Sorrentino, Influence of key cement chemical parameters on the properties of metakaolin blended cements, Cem. Concr. Compos. 23 (2001) 463–469.
[58] F. Cassagnabère, P. Diederich, M. Mouret, G. Escadeillas, M. Lachemi, Impact of metakaolin characteristics on the rheological properties of mortar in the fresh state, Cem. Concr. Compos. 37 (2013) 95–107.
[59] L. Nicoleau, T. Gädt, L. Chitu, G. Maier, O. Paris, Oriented aggregation of calcium silicate hydrate platelets by the use of comb-like copolymers, Soft Matter 9 (2013) 4864–4874.
[60] C. Ouellet-Plamondon, S. Scherb, M. Köberl, K.-C. Thienel, Acceleration of cement blended with calcined clays, Constr. Build. Mater. 245 (2020), 118439.
[61] D.P. Bentz, C.F. Ferraris, M.A. Galler, A.S. Hansen, J.M. Guynn, Influence of particle size distributions on yield stress and viscosity of cement–fly ash pastes, Cem. Concr. Res. 42 (2012) 404–409.
[62] R. Sposito, I. Dürr, K.-C. Thienel, Lignosulfonates in cementitious systems blended with calcined clays, in: V. Falikman, R. Realfonzo, P. Hájek, P. Riva (Eds.), ACI SP 326 - 2nd International Workshop on Durability and Sustainability of Concrete Structures, American Concrete Institute, Moscow, Russia, 2018, pp. 10.11-10.10.
[63] H.A. Barnes, K. Walters, The yield stress myth? Rheol. Acta 24 (1985) 323–326.
[64] A. Yahia, K.H. Khayat, Analytical models for estimating yield stress of high-performance pseudoplastic grout, Cem. Concr. Res. 31 (2001) 731–738.
[65] H. Vikan, H. Justnes, F. Winnefeld, R. Figi, Correlating cement characteristics with rheology of paste, Cem. Concr. Res. 37 (2007) 1502–1511.
[66] H. Vikan, H. Justnes, R. Figi, Influence of cement and plasticizer type on the rheology and reactivity of cementitious binders, in: V.M. Malhotra (Ed.), ACI SP 239 - 8th CanMET/ACI Intl Conference on Superplasticizers and Other Chemical Admixtures in Concrete, Sheridan Books, Sorrento, Italy, 2006, pp. 455–470.
[67] M. Cyr, M. Mouret, Rheological characterization of superplasticized cement pastes containing mineral admixtures: consequences on self-compacting concrete design, in: V.M. Malhotra (Ed.), ACI SP 217 - 7th CANMET/ACI International Conference on Superplasticizers and Other Chemical Admixtures in Concrete, American Concrete Institute, Berlin, Germany, 2003.
[68] D. Małaszkiewicz, M. Osipiuk, Effect of mineral additions on rheology and fresh properties of cement pastes and mortars, in: V. Mechtcherine, K. Khayat, E. Secrieru (Eds.), Rheology and Processing of Construction Materials, Springer International Publishing, Cham, 2020, pp. 116–124.
[69] A.W. Saak, H.M. Jennings, S.P. Shah, New methodology for designing self-compacting concrete, ACI Mater. J. 98 (2001) 429–439.
[70] K. Jasmund, G. Lagaly, H.M. Köster, E.E. Kohler, M. Müller-Vonmoos, E. A. Niederbudde, K.-H. Schüller, U. Schwertmann, M. Störr, Tonminerale und Tone: Struktur, Eigenschaften, Anwendungen und Einsatz in Industrie und Umwelt, Dr. Dietrich Steinkopff Verlag, Darmstadt, 1993.
[71] M. Maier, R. Sposito, N. Beuntner, K.-C. Thienel, Particle characteristics of calcined clays and limestone and their impact on the early hydration and sulfate demand of blended cement, Cem. Concr. Res. 154 (2022), 106736.
[72] T. Danner, H. Justnes, The influence of production parameters on pozzolanic reactivity of calcined clays, Nordic Concr. Res. 59 (2018) 1–12.
[73] F. Zunino, K.L. Scrivener, Improving the behaviour of calcined clay as supplementary cementitious materials by a combination of controlled grinding and particle selection, in: S. Bishnoi (Ed.), Calcined Clays for Sustainable Concrete, Springer, Singapore, Singapore, 2020, pp. 157–162.
[74] E.F. Aglietti, J.M. Porto Lopez, E. Pereira, Mechanochemical effects in kaolinite grinding. I. Textural and physicochemical aspects, Int. J. Miner. Process. 16 (1986) 125–133.
[75] G.J. Ross, Relationships of specific surface area and clay content to shrink-swell potential of soils having different clay mineralogical compositions, Can. J. Soil Sci. 58 (1978) 159–166.
[76] C. He, B. Osbæck, E. Makovicky, Pozzolanic reactions of six principal clay minerals: activation, reactivity assessments and technological effects, Cem. Concr. Res. 25 (1995) 1691–1702.
[77] J.K. Mitchell, K. Soga, Fundamentals of Soil Behavior, 3 ed., Wiley, 2005.
[78] C. He, E. Makovicky, B. Osbæck, Thermal stability and pozzolanic activity of calcined kaolin, Appl. Clay Sci. 9 (1994) 165–187.
[79] N. Beuntner, K.-C. Thienel, Properties of calcined lias delta clay - technological effects, physical characteristics and reactivity in cement, in: K. Scrivener, A. Favier (Eds.), Calcined Clays for Sustainable Concrete - Proceedings of the 1st International Conference on Calcined Clays for Sustainable Concrete, Springer, Dordrecht, Netherlands, 2015, pp. 43–50.
[80] T. Danner, G. Norden, H. Justnes, The effect of calcite in the raw clay on the pozzolanic activity of calcined illite and smectite, in: S. Bishnoi (Ed.), Calcined Clays for Sustainable Concrete - Proceedings of the 3rd International Conference on Calcined Clays for Sustainable Concrete, Springer, Singapore, 2020, pp. 131–138.
[81] R. Gmür, K.-C. Thienel, N. Beuntner, Influence of aging conditions upon the properties of calcined clay and its performance as supplementary cementitious material, Cem. Concr. Compos. 72 (2016) 114–124.
[82] P.C.R.A. Abrão, F.A. Cardoso, V.M. John, Efficiency of Portland-pozzolana cements: water demand, chemical reactivity and environmental impact, Constr. Build. Mater. 247 (2020), 118546.
[83] B.B. Sabir, S. Wild, J. Bai, Metakaolin and calcined clays as pozzolans for concrete: a review, Cem. Concr. Compos. 23 (2001) 441–454.
[84] J. Plank, C. Hirsch, Impact of zeta potential of early cement hydration phases on superplasticizer adsorption, Cem. Concr. Res. 37 (2007) 537–542.
[85] K. Yoshioka, E.-I. Tazawa, K. Kawai, T. Enohata, Adsorption characteristics of superplasticizers on cement component minerals, Cem. Concr. Res. 32 (2002) 1507–1513.
[86] M. Maier, S. Scherb, A. Neißer-Deiters, N. Beuntner, K.-C. Thienel, Hydration of cubic tricalcium aluminate in the presence of calcined clays, J. Am. Ceram. Soc. 104 (2021) 3619–3631.
[87] M. Daukšys, G. Skripkiunas, A. Grinys, Finely ground quartz sand and plasticizing admixtures influence on rheological properties of Portland cement paste, Mater. Sci. (Medziagotyra) 16 (2010) 365–372.
[88] N.N. Gindy, Environmental implications of electron microscope study of quartz grains' surface textures on khors sediments, Lake Nasser, Egypt, The Egyptian Journal of Aquatic Research 41 (2015) 41–47.
[89] W.B. Jepson, Kaolins: their properties and uses, Philosophical Transactions of the Royal Society of London. Series A, Mathematical and Physical Sciences 311 (1984) 411–432.
[90] R. Flatt, I. Schober, Superplasticizers and the rheology of concrete, in: N. Roussel (Ed.), Understanding the Rheology of Concrete, Woodhead Publishing, 2012, pp. 144–208.
[91] F. Winnefeld, S. Becker, J. Pakusch, T. Götz, Effects of the molecular architecture of comb-shaped superplasticizers on their performance in cementitious systems, Cem. Concr. Compos. 29 (2007) 251–262.
[92] C.F. Ferraris, K.H. Obla, R. Hill, The influence of mineral admixtures on the rheology of cement paste and concrete, Cem. Concr. Res. 31 (2001) 245–255.
[93] A. Habbaba, J. Plank, Surface chemistry of ground granulated blast furnace slag in cement pore solution and its impact on the effectiveness of polycarboxylate superplasticizers, J. Am. Ceram. Soc. 95 (2012) 768–775.
[94] V.S. Ramachandran, Z. Chun-Mei, Thermal analysis of the 3CaO · Al2O3-CaSO4 · 2H2O-CaCO3-H2O system, Thermochim Acta 106 (1986) 273–282.
[95] M. Palou, E. Kuzielová, M. Žemlička, R. Novotný, J. Másilko, The effect of metakaolin upon the formation of ettringite in metakaolin–lime–gypsum ternary systems, J. Therm. Anal. Calorim. 133 (2018) 77–86.
[96] D. Lowke, C. Gehlen, The zeta potential of cement and additions in cementitious suspensions with high solid fraction, Cem. Concr. Res. 95 (2017) 195–204.
[97] M.Y.A. Mollah, W.J. Adams, R. Schennach, D.L. Cocke, A review of cement–superplasticizer interactions and their models, Adv. Cem. Res. 12 (2000) 153–161.
[98] Y. Zhang, X. Kong, Correlations of the dispersing capability of NSF and PCE types of superplasticizer and their impacts on cement hydration with the adsorption in fresh cement pastes, Cem. Concr. Res. 69 (2015) 1–9.
[99] M. Schmid, N. Beuntner, K.-C. Thienel, J. Plank, Amphoteric superplasticizers for cements blended with a calcined clay, in: J. Liu, Z. Wang, T.C. Holland, J. Huang, J. Plank (Eds.), ACI SP 329–12th International Conference on Superplasticizers and Other Chemical Admixtures in Concrete, American Concrete Institute, Beijing, China, 2018, pp. 41–54.
[100] C. Schröfl, M. Gruber, J. Plank, Preferential adsorption of polycarboxylate superplasticizers on cement and silica fume in ultra-high performance concrete (UHPC), Cement Concrete Res 42 (2012) 1401–1408.

7.4 Evaluation of zeta potential of calcined clays and time-dependent flowability of blended cement with customized polycarboxylate-based superplasticizers

Peer-reviewed journal paper [Reprint]

"Evaluation of zeta potential of calcined clays and time-dependent flowability of blended cement with customized polycarboxylate-based superplasticizers"

Ricarda Sposito, Matthias Maier, Nancy Beuntner, Karl-Christian Thienel

Construction and Building Materials

Volume 308, 125061 (2021)

Construction and Building Materials 308 (2021) 125061

Contents lists available at ScienceDirect

Construction and Building Materials

journal homepage: www.elsevier.com/locate/conbuildmat

Evaluation of zeta potential of calcined clays and time-dependent flowability of blended cements with customized polycarboxylate-based superplasticizers

Ricarda Sposito *, Matthias Maier, Nancy Beuntner, Karl-Christian Thienel

Institute for Construction Materials, University of the Bundeswehr Munich, Werner-Heisenberg-Weg 39, Neubiberg, 85579, Germany

A B S T R A C T

Workability of cementitious systems is often limited when blending them with calcined clays. The first part of the study compares for the first time results of zeta potential measurements on both, raw/calcined clays in water and synthetic cement pore solution as well as on a Portland limestone cement replaced by 30 wt% of calcined clay. This helps to identify critical parameters that reduce the workability, also over time. The second part evaluates the time-related flow behavior via mini slump test and rotational viscometer and, by using isothermal calorimetry, early hydration kinetics of different calcined common clays with two polycarboxylate-based (PCE) superplasticizers. The results reveal a high negative zeta potential resulting from high kaolinite content. A large specific surface area enhances flocculation and nucleation, while an increasing amount of phyllosilicates and soluble aluminum ions accelerate ettringite formation also with the addition of PCE. Tailor-made PCE, however, can compensate rapid loss in flowability and enable a sufficient workability period without affecting early strength development significantly for most calcined clay blended systems.

1. Introduction

Cements blended with calcined kaolinitic clays and limestone came into focus of concrete technology worldwide during the past decade. They yield outstanding synergetic performance towards hydration, mechanical and durability properties in search of promising supplementary cementitious materials (SCM) for the future [1–7]. On the other hand, the desired addition of calcined kaolinitic clays goes along with certain obstacles as kaolinite-rich clays are not abundant available in the topsoil, especially in the northern hemisphere [8] and find applications in other industries as well [9]. For this reason, several researchers started to investigate further types of clays towards their suitability as SCM [10–14]. These clays are often dominated by 2:1 clay minerals and usually referred to as common clays [15].

Due to their physico-chemical properties, like a high negative zeta potential, specific surface area and water adsorption tendency, calcined clays lead to increased flocculation rates and decrease the workability of cementitious systems [16–18]. Depending on the replacement level and type of calcined clay added, high amounts of superplasticizer can be necessary for a proper dispersion of calcined clay blended systems. To the best knowledge of the authors, it is still under discussion which type of phyllosilicate as elementary component in clays is more critical when it comes to the dispersion efficiency of superplasticizers. Ferreiro et al. [19] have revealed that systems with calcined kaolinitic clay require more superplasticizer than those with calcined smectitic clay, as superplasticizers can intercalate into the amorphous structure of metakaolin and reduce their efficiency hereby. Investigations on pure, calcined phyllosilicates (so called metaphyllosilicates), however, exhibited the tendency that calcined 2:1 phyllosilicates (metaillite, metamuscovite) are more critical than calcined 1:1 phyllosilicate (metakaolin) when it comes to the efficiency of superplasticizers [16,17,20]. Recent results show that it depends on the type of PCE polymer as well, which perform well with which type of calcined clay [21]. Rapid slump loss is a known and often unfavored parameter of calcined clay blended cements, also with the addition of common polycondensate- and PCE-based superplasticizers [20,22–24]. The addition of lignosulfonate-based plasticizers can prevent rapid slump loss but might lead to strong retardation as consequence of high dosages needed [25]. From this point of view, the use of tailor-made PCE is required to enable a proper workability over time without significantly affecting the hydration process. Li and Plank [26] suggest the use of layered double hydroxide nanocomposites that entrap PCE in the beginning and release is stepwise for an extended dispersion. Tan et al. [27] propose in another context the use of PCE with additional hydroxyethyl methacrylate, an

* Corresponding author.
E-mail addresses: ricarda.sposito@unibw.de (R. Sposito), matthias.maier@unibw.de (M. Maier), nancy.beuntner@unibw.de (N. Beuntner), christian.thienel@unibw.de (K.-C. Thienel).

https://doi.org/10.1016/j.conbuildmat.2021.125061
Received 8 January 2021; Received in revised form 17 September 2021; Accepted 25 September 2021
Available online 5 October 2021

ester group that decomposes into glycol and carboxyl groups in alkaline media. These carboxyl groups can adsorb subsequently onto cement particles and prolong the workability period.

The zeta potential is seen as a remote effect of the surface charge of particles [28] and is usually a good indicator for the adsorption behavior of superplasticizers onto them [29,30]. So far, it is rather unclear to what extent the zeta potential of clays alters with their calcination and the along-going dehydroxylation of phyllosilicates. In their raw form, phyllosilicates exhibit an overall negative zeta potential that depends, among other things, on the pH value of the aqueous phase [28,31–36]. With a higher pH value, the zeta potential of clay minerals turns more negative [28,31,32,36]. Their zeta potential can turn positive in synthetic cement pore solution (SCPS) or with the addition of Ca^{2+} ions [32] due to the adsorption of the latter onto negatively charged surfaces.

Recent findings of the authors demonstrated that the zeta potential of individual metaphyllosilicates in distilled water remains strongly negative, whereas a calcined common clay has a small negative zeta potential close to 0 mV, all in all correlating well with the rheological properties of calcined clay-water suspensions [17]. From this point of view, the present study shall evaluate the zeta potential of application-relevant common clays with a wide range of mineralogical compositions, before and after calcination.

Beside of their impact on rheology, calcined clays are known for their influence on the hydration behavior of cementitious systems. During early hydration, preferred ettringite and earlier AFm-Hc formation takes place controlled by chemical-mineralogically controlled processes of calcined clays [37–39]. Beside of the calcination and grinding processing, the pozzolanic reactivity depends mainly on the amount and type of phyllosilicates present in clay [39,40]. With the addition of polycondensate- or PCE-based superplasticizers, the sulfate depletion and aluminate reaction can be even more promoted although the reason is still unclear [41–43]. The addition of superplasticizers to calcined clay blended cements usually leads to retardation effects, especially on silicate (alite) reaction [16,41,42,44]. This has been also known from other cementitious systems [45–48]. Depending on the characteristics of calcined clay, they can compensate the retarding effects of superplasticizers, e.g. via additional nucleation sites, and lead to altered setting behavior [16].

Based upon this knowledge, this paper is divided into two parts of research. It evaluates the zeta potential of raw and calcined common clays in distilled water and highly alkaline SCPS, as well as the zeta potential of calcined clay blended cement over time. The time-dependent rheological behavior of the latter is discussed in combination with the early hydration kinetics and the findings from zeta potential development of calcined clay blended cement paste. It aims to identify especially the influence of the zeta potential of calcined clays in combination with the mineralogy of clays onto the efficacy of tailor-made PCE during first 120 min after water addition, as well as effects of PCE on the first 24 h of hydration.

2. Materials & methods

2.1. Binder components

A Portland limestone cement (PLC), CEM II/A-LL 32.5 R complying with DIN EN 197–1 [49], is replaced by 20 wt% of metaphyllosilicates in a first step: an industrial metakaolin (Mk), lab-scale calcined metamuscovite (Mu) and metaillite (Mi). These three materials and their processing as well as the PLC have been described extensively by the authors in [17]. For further tests, PLC is partially replaced by 30 wt% of four calcined common clays and a clay-rich mine tailing (Recycling Kaolin Upper Palatinate, short: RKUP [12]), respectively. A higher replacement level is possible due to further components in common clays and aimed for a clinker reduction as high as possible. The calcined common clays are designated according to its provider (MURR) or to their geological / geographical origin: Amaltheen clay (AC), Kaolin Upper Palatinate (KUP), Fireclay Upper Palatinate (FUP). A detailed description on the origin and the mineralogy of the raw AC, KUP, FUP and RKUP is published in [12,40]. The five latter materials are calcined at 800 °C in a lab muffle kiln and ground after cooling in a vibratory disc mill RS 200 (Retsch, Germany) at 700 min^{-1} for 10 min. Table 1 summarizes the physical parameters of all solid materials used within this investigation program. The particle sizes of the calcined common clays have been measured by static laser diffraction, see details in [21]. Table 2 shows the mineralogical composition of raw MURR, AC, KUP, FUP and RKUP analyzed by Q-XRD. Table 3 provides the amorphous content and the calcined kaolinite content, as well as the amount of soluble silicon and aluminum ions of calcined clays, measured via ICP-OES after 20 h eluting in 10 wt% NaOH solution [50] as indicator for the pozzolanic activity of each calcined common clay. The amorphous content is determined on powder samples of calcined clays via X-ray diffraction by using a PANalytical Empyrean with Bragg-Brentano^{HD} and PIXcel^{1D} linear detector. The quantification of amorphous phase is performed with external standard method according to [51] with zincite as standard material. The calcined kaolinite content is calculated based upon kaolinite content from raw clay (Table 2) and a proposal of Avet and Scrivener [1] that has been described extensively by Maier et al. [40].

2.2. Superplasticizers

Two industrial superplasticizers are selected to investigate their time dependent effectiveness in calcined clay blended systems. Their structural formulae are provided in Fig. 1. An α-methallyl-ω-methoxy poly (ethylene glycol) ether type PCE (HPEG) with a moderate side chain length ($n_{EO} = 66$) is investigated. Its anionic charge density is 850 µeq/g in distilled water and its solid content is 50.0 wt%. The HPEG PCE showed promising results in dispersing challenging calcined clay blended systems in previous investigations [16,17,20,21,55]. In the further course of investigations, it is used as reference with a constant dosage of 0.05 %bwob (% active agent by weight of binder). At w/b = 0.50, this dosage enables a proper initial dispersion of neat cement paste and cement with calcined common clay TG.

An isoprenyl oxy poly(ethylene glycol) ether type PCE (IPEG1) with acrylic acid as anchor group and short side chain ($n_{EO} < 25$) is used. Its anionic charge density is 628 µeq/g in distilled water and its solid content is 29.0 wt%. It consists of two AA-IPEG polymers, where one anchor group has an additional ester group (hydroxyethyl methacrylate). This type of PCE improves the slump retention over time [27] and

Table 1
Physical parameters of PLC, metaphyllosilicates and calcined common clays.

Material	Particle density [g/cm³] [52]	BET [m²/g] [53]	Water demand [wt %] [54]	Particle size distribution d_{10} [µm]	d_{50} [µm]	d_{90} [µm]
PLC [17]	3.09	1.7	–	2.3	13.1	46.0
Mk [17]	2.61	17.8	56.9 / 57.8 / 59.4	3.0	14.8	76.2
Mu [17]	2.79	11.8	79.8 / 83.2 / 92.3	9.3	19.2	45.7
Mi [17]	2.72	94.6	67.7 / 69.7 / 71.8	2.7	6.8	61.9
MURR	2.72	5.3	32.8 / 34.0 / 34.2	4.6	40.9	150.4
AC	2.67	17.2	28.3 / 30.8 / 32.7	3.6	30.0	161.9
KUP	2.70	6.6	40.4 / 47.4 / 51.2	6.4	26.7	86.9
RKUP	2.63	7.9	35.1 / 38.9 / 39.4	2.2	12.0	81.0
FUP	2.63	42.4	43.6 / 44.5 / 46.6	2.8	16.1	56.3

Table 2
Mineralogical composition of raw MURR, AC, KUP, FUP and RKUP (before calcination); the mineralogy of AC, KUP, FUP and RKUP is taken from [12]

Phase [wt%]	$MURR_{raw}$	AC_{raw}	KUP_{raw}	$RKUP_{raw}$	FUP_{raw}
Quartz	48	20	33	48	12
Kaolinite	1	23	26	45	74
Muscovite/illite	10	5	36*	3	3
Illite-smectite	–	32	–	–	8
Smectite	32	–	–	–	–
Chlorite	4	6	–	–	–
Calcite	1	7	–	–	–
Dolomite	< 1	1	–	–	–
Feldspar	5	4	–	–	–
Rutile	–	< 1	1	–	1
Anatase	–	2	–	< 1	1
Pyrite	–	1	–	–	–
Hematite	–	–	–	< 1	–
Goethite	–		4	3	–

* identified as muscovite in[40]

Table 3
Amorphous content, calcined kaolinite content and ion solubility of calcined common clays.

Parameter	MURR	AC	KUP	RKUP	FUP
Amorphous phase [wt%]	27	49	37	39	84
Calcined kaolinite content [wt%]	1	22	23	41	69
$Si_{soluble}$ [mmol/L]	1.2	2.7	3.3	5.0	11.4
$Al_{soluble}$ [mmol/L]	0.4	1.7	2.3	4.0	8.5
Si/Al [-]	2.88	1.64	1.45	1.25	1.34

shall counteract the rapid loss in workability known for calcined clay blended systems by decomposition of hydroxyethyl methacrylate into carboxyl and glycol groups in alkaline media. The dosage steps for IPEG1 are set at 0.05, 0.10 and 0.20 %bwob, where the dosage represents the solid content in PCE and the liquid part is subtracted from the mixing water. The PCE are added immediately with the water: water-PCE solutions (à 2 L) are prepared with the respective amount of superplasticizer in distilled water.

2.3. Methods and nomenclature

Zeta potential (ZP) of raw and calcined common clays is measured in distilled water. In addition, the ZP of metaphyllosilicates and common clays is measured in synthetic cement pore solution (SCPS). The measurements shall reveal changes in ZP by calcination and differences between ZP in distilled water and SCPS. The SCPS contains 0.4 g/l Ca^{2+}, 7.1 g/l K^{+}, 2.2 g/l Na^{+} and 8.3 g/l SO_4^{2-} [56]. The powder material (m = 250 g) is added to 375 g distilled water / SCPS (liquid-to-solid ratio = 1.50) and stirred manually for 2 min. The ZP of each powder material is measured 7 times via electroacoustic spectrometer DT-310 (Dispersion Technology Instruments, USA), while being continuously stirred at 400 rpm to prevent segregation effects.

Time-dependent mini slump tests are conducted on cements with 20 wt% metaphyllosilicates and with the addition of adjusted HPEG dosage over a period of 120 min. The required amount of HPEG has been evaluated for each system via mini slump test according to DIN EN 1015–3 [57] by the Chair for Construction Chemistry, Technical University Munich (Germany). The exact procedure and the respective dosages are given in [17]. The homogenized binder (m = 400 g) is added to the respective amount of water-PCE solution and mixed in a Hobart mixer (including 60 s stirring, 60 s rest, 120 s stirring). The first test takes place 5 min after water addition and is repeated after another 10 min in intervals of 15 min. Between each measurement, the cement paste is covered with a damp cloth to prevent drying-up and mixed for another 60 s by hand before conducting the next mini slump test. For the evaluation of flowability, a slump flow of 26 cm is calculated as 100 % of flowability. A Vicat cone is used as equipment for mini slump test, where the bottom diameter (8 cm) represents 0 % of flowability. The time-dependent mini slump test provides a first evaluation of (rapid) slump loss and enables, in combination with further methods, a proper understanding of workability on cement paste level.

The rotational viscometer, the coupled cooling unit (T = 20 °C) and the mixing procedure for rheological measurements are described in [17]. Time-dependent rheological measurements are conducted at four times: 5, 30, 50 and 105 min after water addition. For the first 3 measurements, the paste remains in the viscometer. After the third measurement, it is filled into a cup and covered with a damp cloth, analogously to the sample for mini slump test. Two minutes before the last measurement begins, the sample is stirred up manually and filled back into the viscometer. Each measurement records the torque (T_v) at rotational speeds (v) of 120 revolutions per minute (min^{-1}) for 10 min, followed by 80 rpm, 40 rpm and 20 min^{-1} for 2 min each. For each rotational speed, the median torque [Nmm] is calculated from data points once an equilibrium state is obtained. Based on proposals of Vikan et al. [58,59], the flow resistance [Nmm·min^{-1}] is calculated as the area under the flow curve from 20 to 120 rpm following the trapezoidal method with 3 intervals (v_1 = 120, v_2 = 80 min^{-1}, v_3 = 40 min^{-1} and v_4 = 20 min^{-1}), based on Equation (1).

$$FR\left[Nmm \bullet \min^{-1}\right] = \frac{1}{2}\sum_{n=1}^{4}\left[\left(f(v_n) + f(v_{n+1})\right) \bullet (v_{n+1} - v_n)\right] \quad (1)$$

The insert of the median torques [Nmm] at 20, 40, 80 and 120 min^{-1}, as well as of the rotational speeds themselves [min^{-1}] leads to the following, simplified term in Equation (2):

$$FR\ \left[Nmm \cdot \min^{-1}\right] = 10\ T_{20} + 30\ T_{40} + 40\ T_{80} + 20\ T_{120} \quad (2)$$

The flow resistance, used as parameter for initial flowability, has

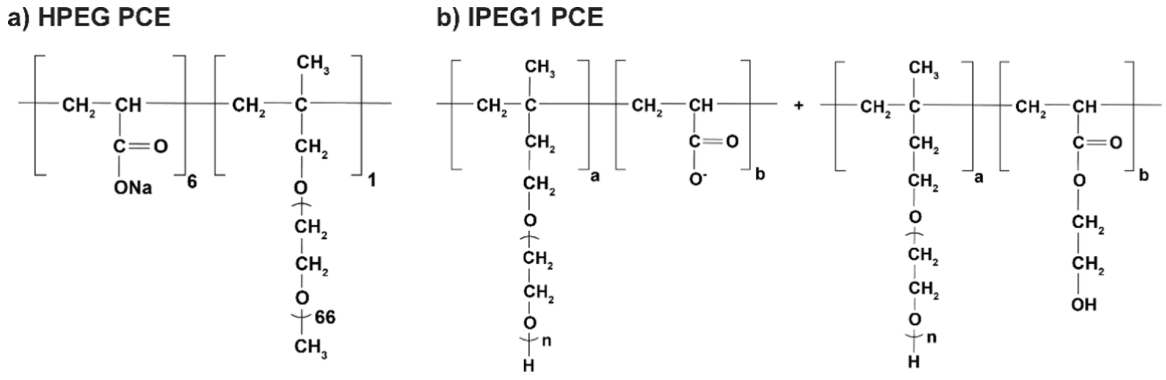

Fig. 1. Structural formulae of HPEG and IPEG1.

previously shown good correlations with physical and mineralogical parameters of calcined clays [21]. It is of special interest for systems with negative, physically impossible yield stress, which has been detected by linear Bingham fit for superfluidized as well as shear-thickening/shear-thinning systems beforehand [16,17]. Supplementary data further provides the rheological analysis based on Bingham model modified by Yahia and Khayat [60], as well as with Herschel-Bulkley fit [61].

The zeta potential (ZP) and pH value is measured for selected blended cement paste over a total time of 2 h. The pore solution of PLC is set as ionic background. Therefore, 100 g of cement are mixed with distilled water (w/c = 0.50) for 5 min by hand. The cement paste is poured into a Büchner funnel with a prewetted filter paper and the pore solution of the cement paste is extracted by vacuum process. Based on this extracted pore solution, the background is determined three times by the electroacoustic spectrometer described beforehand. Beside of the ionic background, the spectrometer considers initial particle density and mean particle size of the binder components. For the actual measurement, the binder (m = 360 g) and the respective amount of distilled water / water-PCE solution for w/b = 0.50 are mixed for 5 min by hand. The paste is constantly stirred at 300 rpm to avoid segregation during the entire measurement. The ZP is summarized for intervals of 5–21 min, 30–46 min, 50–66 min and 105–121 min, which represent the times of the rheological measurements. During the course of very early hydration, the ionic background as well as the particle characteristics change. Changes in ZP indicate the adsorption of (super)plasticizers onto binder components on the one hand and the formation of hydration phases on the other. When the ZP becomes less negative or even positive, steric hinderance is assumed to be the main dispersion mechanism of a superplasticizer polymer, like it is known for PCE [62]. An absolute differentiation between adsorption-related and hydration-related change of ZP is hence impossible, but the trend in ZP is used for comparison in combination with rheological measurements and calorimetric studies.

The first 24 h of hydration kinetics are observed by using isothermal calorimeter TAM Air (TA Instruments, Delaware/USA). The binder (m = 5 g) is homogenized for 30 s before mixing the paste for 60 s by hand. Each sample is transferred into a plastic ampoule and immediately afterwards into the calorimeter. For each system, the measurement is conducted at least twice to secure reproducibility. The resulting heat flow is averaged and related to 1 g of cement. The heat flow curves indicate, according to Bullard et al. [63], four stages of clinker reaction in cements: I) initial reaction, II) period of slow reaction, III) acceleration period and IV) deceleration period. Within this paper, the focus is especially on the question how the addition of superplasticizer in varying amounts affects stages II and III of calcined clay blended cements. Cumulative heat of hydration is calculated by integration of heat flow over time and the multiplication by 3.6 to adjust the units. It is set at 0 J/g at the end of rest period. Cement paste samples are designated as *PLC_30type of calcined clay_dosage and type of PCE*, e.g. PLC_30AC_0.10IPEG1.

3. Results and discussion

3.1. Zeta potential of used materials in water and SCPS

The zeta potential (ZP) of metaphyllosilicates in distilled water has been discussed in comparison with quartz powder and TG by the authors [17]. When measuring the ZP in SCPS, the ZP becomes more negative for the metaphyllosilicates. This is in compliance with literature, that an increasing pH value leads to a more negative ZP [36] as edge surfaces turn to be negatively charged [33,34]. In addition, the order of ZP changes for metaphyllosilicates: it is the least negative for metamuscovite (Mu) < metaillite (Mi) and the most negative for metakaolin (Mk), see Table 4. One possible reason, again derived from findings on clay minerals [36], is the tendency of the metaphyllosilicates to adsorb H^+ ions: the lower the amount of H^+ in solution, the lower is the negative ZP. With increasing water demand (Table 1), which is especially known for metamuscovite [64], the absolute value of negative ZP becomes smaller. However, this does not apply for common clays that contain further components beside of clay minerals.

Before calcination, the ZP of common clays ranges between – 0.2 mV and – 10.2 mV (Table 4). KUP exhibits a low ZP at pH = 4.4, which is related to its high content in muscovite (Table 2) and positively charged edge surfaces of muscovite at pH < 8 [65]. This is also the reason for a lower ZP of MURR. For RKUP, the high amount of quartz seems to compensate the strong negative ZP of kaolinite although the ZP of quartz is also negative in H_2O due to deprotonation of SiO_2 [66]. AC and FUP exhibit the highest, negative ZP values due to the high amount of phyllosilicates / kaolinite. It is impossible to compare the absolute values of ZP before and after calcination due to differences in pH value. However, by calcination, the sorting of ZP in H_2O changes to MURR < AC < KUP < RKUP < FUP according to their (calcined) kaolinite content (Table 2 and Table 3). The pH decreases for suspensions with kaolinite-rich clays and increases for suspensions with clays rich in 2:1 phyllosilicates, which fits with the pH values of Mk-H_2O and Mu-H_2O/Mi-H_2O, respectively. However, in comparison with metaphyllosilicates, the ZP values are less negative in SCPS and for MURR even partially positive (Table 4). This indicates the adsorption of cations (Ca^{2+}, Na^+ and K^+) from SCPS onto the calcined clay surface, which has also been observed for clay minerals [31,32]. The amorphous content of calcined clay does not indicate the trend of zeta potential (R^2 = 0.728), see Fig. 2a. As observed in distilled water, the absolute values increase with higher calcined kaolinite content (R^2 = 0.923), see Fig. 2b. The present results show more likely that both the pH value and the mineralogical composition, as known for clay minerals [32,33,36] and further materials [66], significantly affect the ZP of calcined clays and as consequence their possibility to adsorb superplasticizers.

3.2. Zeta potential and pH value of calcined clay blended cement paste

Zeta potential (ZP) measurements are limited to PLC as plain cement sample, PLC_30AC with AC representing a calcined clay with medium

Table 4
Zeta potential ζ [mV] of metaphyllosilicates and raw / calcined common clays in distilled water and SCPS (l/s = 1.50) including the pH values of each suspension.

Material	Zeta potential [mV] at l/s = 1.50 …				
	In H_2O dest.		In SCPS after calcination		
	Before calcination	After calcination	$\zeta_{ø}$	ζ_{min}	ζ_{max}
Mk	–	− 17.4 [17] (pH = 4.5)	− 47.3 (pH = 11.1)	– 46.4	– 48.0
Mu	–	− 52.0 [17] (pH = 8.3)	− 9.5 (pH = 12.3)	− 8.3	– 10.3
Mi	–	− 21.4 [17] (pH = 9.7)	− 28.0 (pH = 10.9)	– 27.5	– 28.5
MURR	− 5.1 (pH = 6.8)	− 1.4 (pH = 10.9)	− 1.1 (pH = 12.2)	− 1.6	+ 0.4
AC	− 9.5 (pH = 6.3)	− 2.7 (pH = 9.2)	− 1.6 (pH = 12.0)	− 2.0	− 1.2
KUP	− 0.2 (pH = 4.4)	− 5.4 (pH = 5.1)	− 3.3 (pH = 11.8)	− 3.6	− 2.7
RKUP	− 5.6 (pH = 7.1)	− 7.5 (pH = 4.5)	− 4.0 (pH = 12.0)	− 4.5	− 3.3
FUP	− 10.2 (pH = 5.8)	− 8.8 (pH = 5.1)	− 7.5 (pH = 10.8)	− 7.9	− 7.3

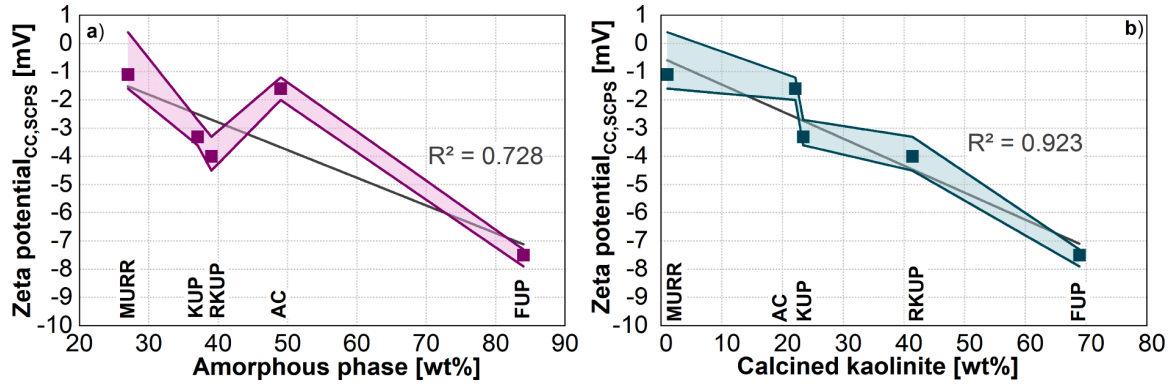

Fig. 2. Zeta potential of calcined clays (CC) in SCPS in correlation with a) the amorphous content and b) the calcined kaolinite content [wt%]

kaolinite, yet high phyllosilicate content, and PLC_30FUP with kaolinite-rich FUP. PLC_30FUP exhibits the highest negative ZP which relates to the strong negative ZP of calcined clays (Table 4), followed by PLC_30AC and PLC (Fig. 3). It is known that a less negative or even positive zeta potential favors the adsorption of anionic superplasticizers [29,67].

With the addition of PCE, the initial ZP changes towards less negative values indicating an immediate adsorption and a dispersion effect via steric hindrance. In case of PLC, the change in ZP is more pronounced for 0.05HPEG compared to 0.05IPEG1, which results from a longer side chain and a possible higher initial adsorption of HPEG (cf. section 2.2). The stepwise alteration of ZP by adsorption is shown for 0.05, 0.10 and 0.20 %bwob IPEG1 in PLC and PLC_30AC. PLC_30AC shows the most significant change between reference and 0.20IPEG1, where the zeta potential even turns slightly positive. Schmid and Plank [68] recently showed that PCE can adsorb onto metaphyllosilicate particles, enhanced by the prior adsorption of Ca^{2+} of SCPS / clinker onto negatively charged particles. Li et al. [26,69] further found that calcined clays adsorb in SCPS even higher amounts of PCE than in ordinary Portland cement. This can also explain why the absolute gap in zeta potential between reference systems and systems with PCE is higher for calcined clay blended cements compared to PLC. A final judgement, which type of calcined clay adsorbs more PCE, however, is omitted here due to the limited data. Future investigations focus further on the ion and superplasticizer adsorption behavior of calcined common clays.

Over time, the ZP of PLC changes only slightly, while the negative ZP of PLC_30AC diminishes linearly towards a less negative value (Fig. 4). Indicated by the most pronounced slope, PLC_30FUP yields the most extreme change from the most negative ZP to 0 mV after 105 min. This rapid change indicates a fast initial ettringite formation, when considering the specific surface area and the amount of soluble ions of the

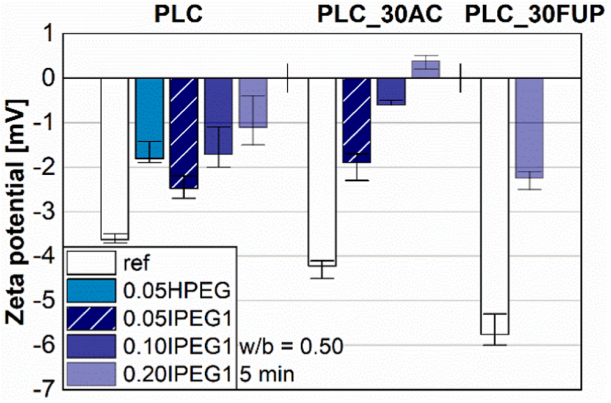

Fig. 3. Zeta potential [mV] of PLC, PLC_30AC and PLC_30FUP without and with varying amounts of PCE (w/b = 0.50, 5 min after water addition).

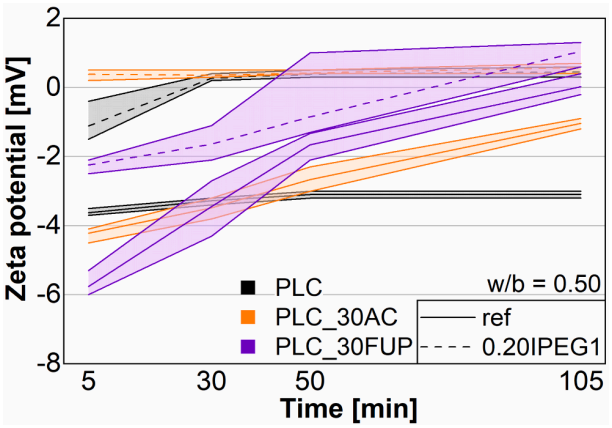

Fig. 4. Zeta potential [mV] of PLC, PLC_30AC and PLC_30FUP without and with 0.20 %bwob IPEG1 over time.

calcined clays (Table 1 and Table 3, respectively). With the addition of 0.20IPEG1 as well, PLC_30FUP shows the most significant change of ZP over time, which can explain both ettringite formation on the one hand and retarded adsorption of IPEG1 on the other hand as ZP of cement turns less negative with the adsorption of steric hindering PCE [47]. However, in combination with the flow resistance results (Fig. 6f), it is assumed that the significant change rather stems from strong, initial ettringite formation as a subsequent dispersion is not evident for this system. ZP of PLC_30AC remains rather constant and indicates a stronger retardation effect onto the latter system. The same holds for PLC, except of the jump in ZP from – 1.1 to + 0.3 mV after 30 min, due to later adsorption of IPEG1, which enables a subsequent reduction in flow resistance (shown in Fig. 6a). Further data points with lower amounts of PCE reveal a similar trend in ZP (Table 5).

Table 6 provides the corresponding pH values obtained during the time-related zeta potential measurements. It is commonly known that the zeta potential strongly depends on the pH value of the suspension, as shown e.g. in refs. [36,70,71]. Similar to the investigations in SCPS (Table 4), the pH value decreases with higher amounts of calcined kaolinite present in the cement blend. The initial measurements (after 5 min) further demonstrate that the addition of usually acidic PCE (pH ≈ 4 [72]) decreases the pH value of the cement pastes. This effect remains constant over time for PLC and PLC_AC, regardless of the PCE dosage. PLC_30FUP in contrast reveals a rapid increase in pH over the first 105 min, which indicates, along-going with strong changes in zeta potential, faster ongoing hydration kinetics. Time-dependent changes in flowability will be discussed in the following sections 3.3 and 3.4, as well as effects on early hydration in section 3.5.

Table 5
Median, minimum and maximum zeta potential ($\zeta_{ø}$, ζ_{min}, ζ_{max}) of PLC and PLC_30AC with 0.05HPEG and 0.05/0.10IPEG1 over time.

	Time [min]	PLC			PLC_30AC	
		0.05HPEG	0.05IPEG1	0.10IPEG1	0.05IPEG1	0.10IPEG1
$\zeta_{ø}$	5	− 1.8	− 2.5	− 1.7	− 1.9	− 0.6
[mV]	30	− 1.7	− 0.9	0.1	− 1.8	− 0.6
	50	− 1.4	− 0.2	0.2	− 1.8	− 0.5
	105	− 1.0	0.3	0.3	− 1.2	0.1
ζ_{min}	5	− 1.9	− 2.7	− 2.0	− 2.3	− 0.6
[mV]	30	− 1.8	− 1.5	− 0.6	− 2.0	− 0.6
	50	− 1.5	− 1.0	− 0.3	− 2.1	− 0.6
	105	− 1.0	− 0.8	0.2	− 1.4	− 0.4
ζ_{max}	5	− 1.4	− 2.2	− 1.1	− 1.7	− 0.5
[mV]	30	− 1.6	1.1	0.6	− 1.6	− 0.5
	50	− 1.2	1.0	0.5	− 1.5	− 0.4
	105	− 1.0	0.9	0.5	− 0.9	0.4

Table 6
pH values [-] of PLC, PLC_30AC and PLC_30FUP without and with varying amounts of PCE after 5, 30, 50 and 105 min.

System	PCE	pH [-] after …			
		5 min	30 min	50 min	105 min
PLC	ref	12.6	12.6	12.6	12.6
	0.05HPEG	12.3	12.5	12.5	12.6
	0.05IPEG1	12.7	12.7	12.7	12.7
	0.10IPEG1	12.4	12.5	12.5	12.6
	0.20IPEG1	12.4	12.4	12.4	12.5
PLC_30AC	ref	12.2	12.2	12.1	12.1
	0.05IPEG1	12.0	12.0	12.0	12.1
	0.10IPEG1	12.2	12.2	12.3	12.3
	0.20IPEG1	11.7	11.8	11.8	11.9
PLC_30FUP	ref	11.9	12.1	12.2	12.4
	0.20IPEG1	11.8	12.1	12.2	12.4

3.3. Time dependent flowability of cement paste with metaphyllosilicates

The following results reveal how the mostly negative zeta potential of calcined clays affects the initial and time dependent effectiveness of modern PCE superplasticizers. Fig. 5 presents the flowability with dosages of HPEG adjusted for an initial slump of 26 cm (flowability = 100 %). PLC and the systems blended with metaphyllosilicate have a rapid decline in flowability and do not flow at all after 120 min. Especially PLC_20Mi has a fast decrease in flowability within the first 60 min, declining less rapidly afterwards. Mi and Mk show rapid loss in flowability also in combination with ordinary Portland cement with either naphthalene sulfonated based superplasticizer or HPEG [20]. Up to now, the authors explain this with the high fineness and large SSA, especially of Mi, as well as due to a high water uptake of the materials. The question arises whether calcined common clays do have a slower decline in flowability or – in reverse – which parameters do favor a rapid loss in flowability. Is it possible to face this problem with a suitable PCE superplasticizer?

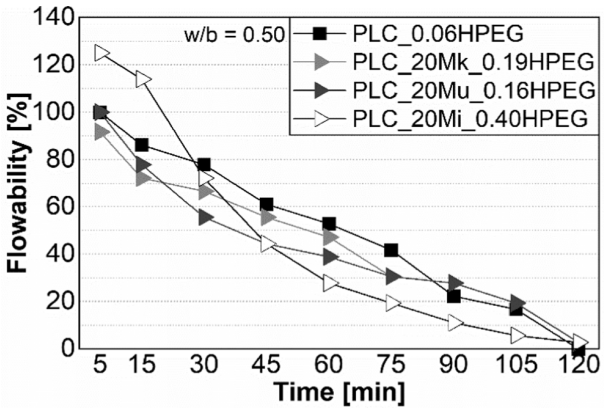

Fig. 5. Time dependent flowability for PLC systems with 20 wt% replacement by Mk, Mu, Mi and TG and the addition of adjusted dosage of HPEG.

3.4. Time dependent flow resistance of calcined clay blended cement pastes

Taking a look at Table 7, the area under the flow curve, expressed as initial flow resistance (FR) [Nmm min^{-1}], is similar for PLC, PLC_30MURR and PLC_30AC. While the FR remains constant or even decreases for PLC and PLC_30MURR, respectively, it increases during the first 50 min slightly more rapidly for PLC_30AC. After 120 min, these systems have a similar FR again. PLC_30KUP, PLC_30RKUP and PLC_30FUP have a significantly higher initial FR that increases significantly over time for PLC_30KUP and PLC_30FUP, while it remains constant for PLC_30RKUP. When comparing the physical properties of these calcined clays in Table 1, this is due to the lower water demand of RKUP leading to a lower water adsorption onto these particles and therefore a longer workability. The initial FR (5 min after water addition) is discussed in detail in [21] and results from the kaolinite content of raw clay (Table 2), a large SSA and water demand of calcined clays (Table 1) and a strong negative zeta potential in alkaline milieu (Table 4). As assumed for mini slump test results, a significant increase in FR over time does also stem from a large SSA and water uptake by calcined clays [23,64]. As consequence, it is urgently necessary to find solutions how to prolong the workability of calcined clay blended systems.

For each system and time interval, the reduction in FR is calculated by relating the FR with PCE to the FR without PCE, multiplied by 100 %. The addition of 0.05HPEG leads to higher initial reduction in FR (45.9 – 60.8 %) compared to 0.05IPEG1 (23.5 – 50.2 %). It indicates a better initial adsorption of HPEG, which is related to its higher anionic charge density [30,73]. A further reduction in FR, compared to reference without PCE at the respective time, takes place for most of the systems (Fig. 6) with both 0.05HPEG and 0.05IPEG1, except for PLC_30FUP (Fig. 6f). IPEG1 can reduce the FR at later times more significantly compared to HPEG, which is in good agreement with the observations of Tan et al. [27]. In consequence, the calcined clay blended cements

Table 7
Time dependent flow resistance for (blended) cement paste without superplasticizer (w/b = 0.50).

System	Flow resistance without PCE [Nmm min^{-1}] after …			
	5 min	30 min	50 min	105 min
PLC	1987	1859	1869	2414
PLC_30MURR	2240	2260	2264	2642
PLC_30AC	2067	2074	2124	2543
PLC_30KUP	6723	7120	7288	8287
PLC_30RKUP	7841	7805	7840	7900
PLC_30FUP	8090	8825	9258	11,108

(except of PLC_30RKUP) have a similar reduction in FR of 43.2 – 62.6 % and 40.9 – 61.5 % after 105 min with 0.05HPEG or 0.05IPEG1, respectively. With higher dosages, the initial reduction in FR ranges between 57.5 and 71.2 % by 0.10IPEG1 and between 76.2 and 91.2 % by 0.20IPEG1, where the PLC_30RKUP shows the highest, initial reduction (Fig. 6e). Over time, 0.10IPEG1 increases further the percentage reduction in FR for all systems except of PLC_30AC and PLC_30FUP. With 0.20IPEG1, it is possible to increase it for PLC_30AC after 105 min (Fig. 6c) whereas for PLC_30FUP, the reduction in FR decreases rapidly also at this high dosage of IPEG (Fig. 6f). As consequence, the reduction in FR exhibits a wider range of 50.9 – 82.3 % (0.10IPEG1) as well as 65.8 – 94.3 % (0.20IPEG1) after 105 min.

Table 8 compares the ability of a further reduction in FR by using varying amounts of IPEG1 with both mineralogical and physical parameters of the clays. Systems with a replacement of 30 wt% by kaolinite-rich calcined clay (FUP) go along with no further reduction in FR when using the chosen dosages up to 0.20 %bwob. However, the table demonstrates that even systems with low-kaolinite clays (23 wt%) can cause slight difficulties in maintaining their workability over time and the retarded fluidification comes to pass only at higher dosages, while calcined clays with a comparable amount of kaolinite or even higher do not have these problems. Hence, this parameter cannot be the sole reason for a rapid loss in workability from the mineralogical point of view. Rather it is related to the total content of phyllosilicates, including kaolinite, illite, smectite, illite–smectite mixed-layer, muscovite and chlorite, in clays. While IPEG1 is able to further reduce the flow resistance compared to reference systems for clays with a content in phyllosilicates < 62 wt%, it starts to struggle with 66 wt%. Vice versa this means, by using the example of RKUP (Table 2), that even clays with 45 wt% of kaolinite do not cause severe problems, when using a proper PCE, if the other phases in clay, e.g. high amounts of quartz, favor a good workability over time. Further it is in this context worth to consider the pH value of cement paste / pore solution, which becomes smaller with AC and even more pronounced with kaolinite-rich FUP (Table 6), as the decomposition of hydroxyethyl methacrylate in IPEG1 into carboxyl groups (that subsequently adsorb onto positively charged surfaces) and glycol groups is mainly driven by strongly alkaline media.

Regarding the physical parameters, that are closely connected to the mineralogical composition, the water demand according to Puntke [54] does not represent an indicator if a further reduction in FR is possible with IPEG1. The SSA – determined by BET method - of a calcined common clay can give a hint on it: calcined clays with low SSA (here < 7.9 m^2/g) are not as challenging as calcined clays with a higher SSA, where not even 0.20IPEG1 can maintain or further increase the reduction in FR (Table 8). In summary this means, that both inner and outer parameters need to be considered when aiming for a proper, long

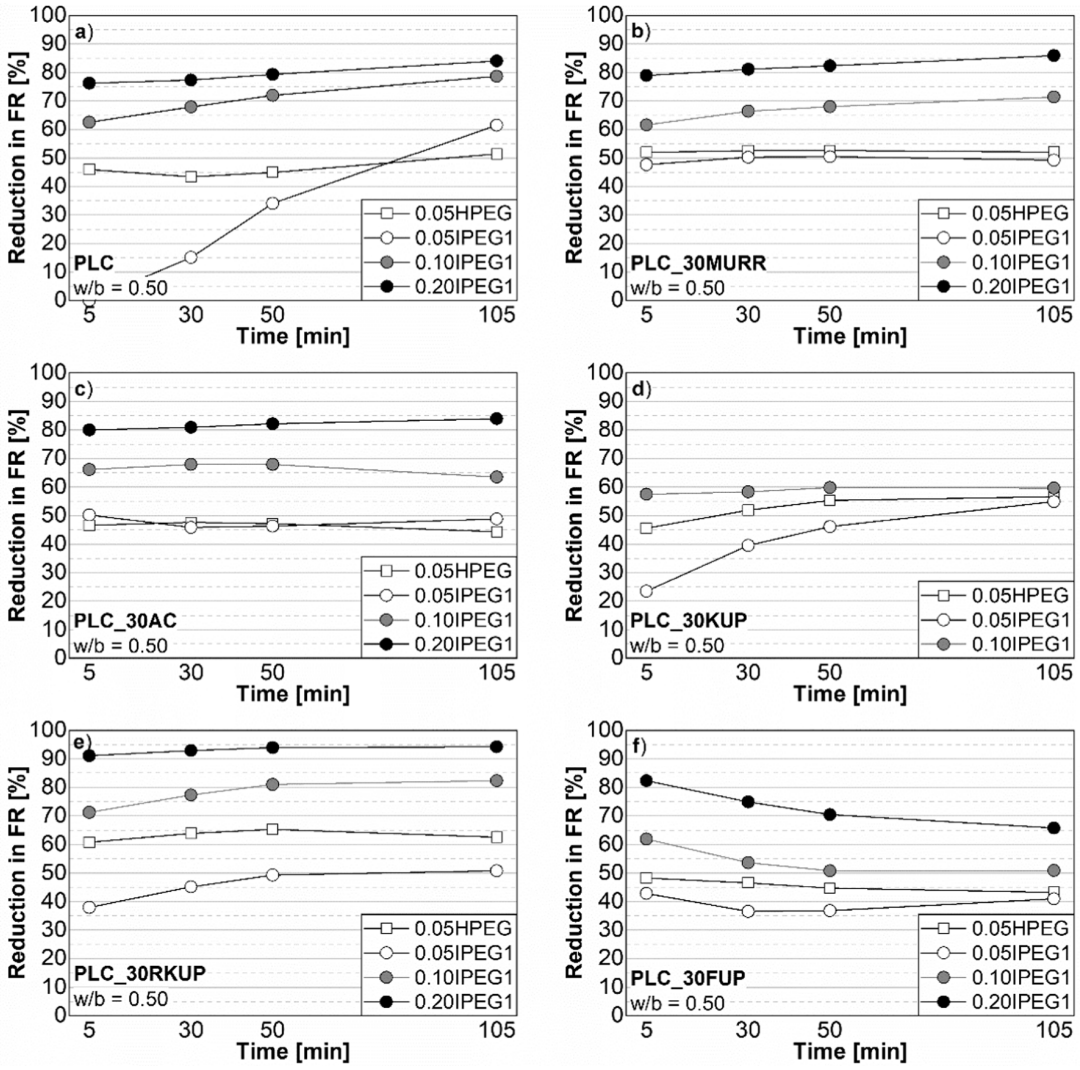

Fig. 6. Time dependent reduction in flow resistance (FR) for a) PLC, b) PLC_30MURR, c) PLC_30AC, d) PLC_30KUP, e) PLC_30RKUP and f) PLC_30FUP systems.

Table 8
Time dependent reduction in flow resistance (FR) compared to references without PCE depending on kaolinite / phyllosilicate content in raw clay, on water demand and BET SSA of calcined clays as well as on the dosage of IPEG1 (x = constant further reduction; ● = partial further reduction; ○ = no further reduction).

Kaolinite in raw clay [wt%]	Further reduction in FR over time with … %bwob IPEG1			Phyllosilicates in raw clay [wt%]	Further reduction in FR over time with … %bwob IPEG1		
	0.05	0.10	0.20		0.05	0.10	0.20
1	x	x	x	47 / 48	x	x	x
23	○	●	x				
26	x	x	–	62	x	x	–
45	x	x	x	66	○	●	x
74	○	○	○	85	○	○	○

Water demand [wt%]	Further reduction in FR over time with … %bwob IPEG1			BET SSA [m^2/g]	Further reduction in FR over time ... %bwob IPEG1		
	0.05	0.10	0.20		0.05	0.10	0.20
28.3	○	●	x	< 7.9	x	x	x
32.8 – 40.4	x	x	x	17.2	○	●	x
43.6	○	○	○	42.4	○	○	○

workability of complex calcined clay blends: how much phyllosilicates does the raw clay contain and, in a next step, what about the zeta potential, the water demand and the specific surface area of the calcined clay? Although the outer parameters, e.g. water-to-binder ratio and replacement level, remain mostly constant within this study, they should not be left unmentioned as they are crucial for the necessary amount of superplasticizer [55,74].

Furthermore, flow resistance and respective ZP of (blended) cement paste show overall a moderate correlation 5 min after water addition, while it is excellent (R^2 = 0.993) e.g. within PLC_30AC system with varying amounts of PCE (Fig. 7). The more negative the ZP is, the higher is in general the initial flow resistance. This is explained by I) heterogeneous ZP of reference systems and its components, leading to higher flocculation rates [24] and by II) lower immediate superplasticizer adsorption, depending on type and dosage of PCE. After 105 min, the ZP of several systems decreases or even turns positive without significant changes in FR, related to a combination of subsequent superplasticizer adsorption (which leads to a further reduction in FR) and initial ettringite formation, a positively charged hydrate phase [30]. According to Jakob et al. [75], ettringite formation has the main influence on time-dependent rheology during very early hydration. For the systems with 30 wt% FUP, however, both the ZP and FR change drastically, indicating a strong initial ettringite formation that a) dominates the development of ZP and b) increases the FR.

The results show that with the right combination of calcined clay and dosage of PCE with hydroxyethyl methacrylate can extend the workability over the two hours observed. Critical parameters, that have been identified, are a high content in phyllosilicates as well as a large SSA – both affecting not only the interaction with superplasticizers [21] but also their reactivity, contributing as filler effect during very early age [76,77].

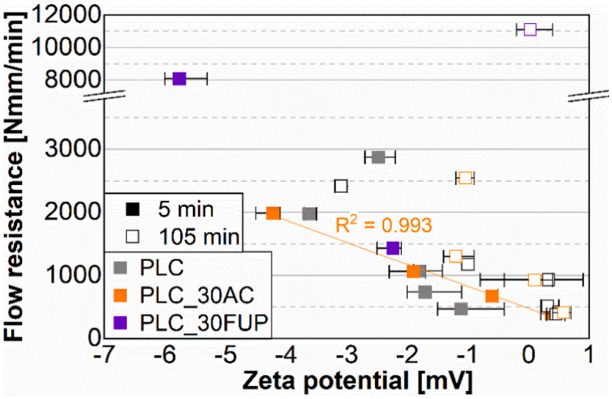

Fig. 7. Correlation of zeta potential and flow resistance of PLC, PLC_30AC and PLC_30FUP without and with the addition of varying amount of PCE, 5 and 105 min after water addition (w/b = 0.50, T = 20 °C).

3.5. Early hydration kinetics of a Portland limestone cement with calcined common clays and superplasticizers

The final section of this paper presents the effects of superplasticizer on the further course of very early hydration. The replacement of cement by 30 wt% AC or FUP slightly prolongs rest period $t_{Q,min}$ but results in higher heat values Q_{min} at this time, see Fig. 8 and Fig. 9. The acceleration period is significantly shortened and the maximum heat, designated as $Q_{max,2}$ as for plain cements usually two maxima do occur and this peak refers to the "sulfate depletion peak", is more pronounced for PLC_30AC and PLC_30FUP compared to PLC. These results are related to the filler effect [78] and contribution of AC and FUP already during very early hydration and are in good agreement with [37,79]. Scherb et al. [37] describe a continuous ettringite formation ongoing in parallel with silicate reaction in calcined clay blended systems during acceleration period. The significant differences between PLC_30AC and PLC_30FUP are due to their differences in specific surface area and amount of soluble Al and Si ions (Table 1) as previously stated by Maier et al. [40]. Furthermore, as shown in Fig. 8c, the sharp peak of PLC_30FUP indicates rapid sulfate depletion, which could be addressed with further sulfate addition as described by Zunino and Scrivener [78].

The rest period is prolonged with the addition of PCE (Fig. 9). It is noticeable that the effect regardless of type and dosage of PCE on PLC_30FUP is minor, while it is most significant for PLC. With the addition of 0.05HPEG, acceleration period exhibits partially higher values and $Q_{max,2}$ occurs earlier, particularly for PLC_30AC (Fig. 8b). An accelerated dissolution of gypsum / aluminate reaction going along with HPEG has been observed also for other calcined clay blended systems [41] and is well known for PCE in plain systems [80,81]. The addition of IPEG1, on contrary, prolongs rest and acceleration period significantly for PLC and PLC_30AC and lowers the heat flow during acceleration period. This effect leads to higher $Q_{max,2}$ values with increasing dosage of IPEG1 in PLC systems, while there is rather only a shift in time for PLC_30AC. These merging effects have been observed by several authors [44,82,83] and are explained by a non-linear retardation (faster ongoing reactions after initial retardation [82]). On contrary, PLC_30FUP systems hardly show any shifts in time (neither $t_{Q,min}$ nor $t_{Qmax,2}$) but $Q_{max,2}$ values decrease from 10.4 mW/g_{cement} (ref) to 8.3 mW/g_{cement} with 0.20IPEG1. The minor shift of significant reactions during the first 24 h of heat flow fits well with the rapid increase in flow resistance and

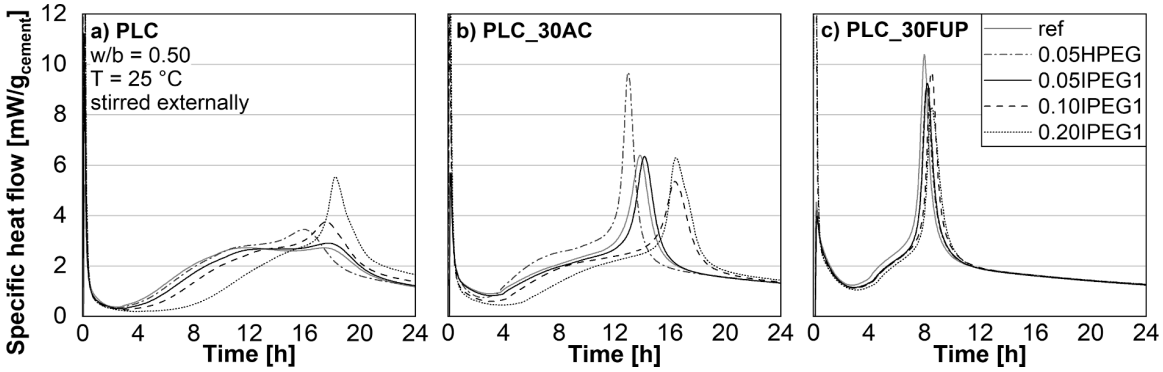

Fig. 8. Specific heat flow curves of a) PLC, b) PLC_30AC and c) PLC_30FUP systems.

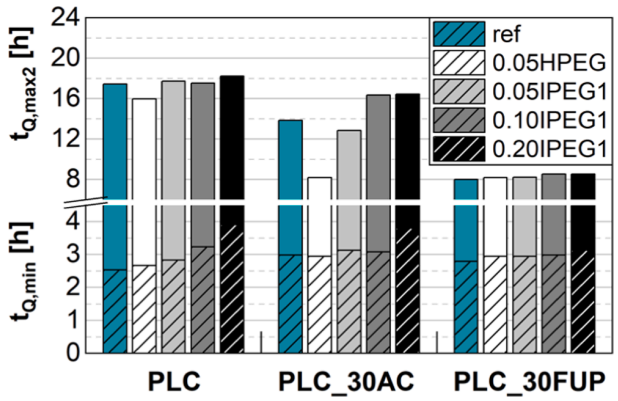

Fig. 9. Significant times during heat flow: $t_{Q,min}$ as end of rest period and $t_{Q,max2}$ where the maximum heat occurs.

the strong changes in zeta potential despite the addition of 0.20IPEG1 (Fig. 7). This is in good agreement with findings of Meng et al. [84] who revealed good correlations of yield stress after 70 min and occurrence of maximum heat for cementitious systems with silica fume and PCE.

The heat of hydration after 24 h ranges between 137 and 152 J/g_{cement} for PLC and is slightly higher for PLC_30AC and PLC_30FUP with 151–166 J/g_{cement} and 155–165 J/g_{cement}, respectively. Hence, at least 90 % of reference heat are reached at this time, despite the use of superplasticizer. The present results show that moderate to highly reactive calcined clays do compensate retardation effects induced by high amounts of PCE, which are often required for proper workability. PCE polymers with specific properties that enable a sufficiently long workability period do not necessarily affect the setting times and early strength development.

4. Conclusion

This study compares for the first time differences in zeta potential of raw and calcined common clays with a wide range of mineralogical compositions. Further, the time dependent flow resistance of calcined clay blended cement pastes was studied by rheological experiments. The dispersion capability over time was evaluated for a HPEG-based and an IPEG-based PCE, where the latter possesses additional hydroxyethyl methacrylate in its anchor group, which offers a solution for longer workability for most of the calcined common clays investigated. In addition, their zeta potential and hydration kinetics were observed for the first two and 24 h of hydration, respectively. Based on these results, the following new remarks were found:

- The zeta potential of clays changes by their calcination and tends to smaller negative values. Common clays have here, compared to pure phyllosilicates, a significantly less negative zeta potential. Future studies should follow, that evaluate the changes in surface charge characteristics of phyllosilicates during their dehydroxylation process as well as the reasons for significant differences between phyllosilicates and common clays regarding their zeta potential.
- Compared to zeta potential of calcined clays in distilled water, their zeta potential turns less negative, partially even positive in synthetic cement pore solution (SCPS), which is explained by a higher pH and the adsorption of cations from the SCPS onto calcined clays. With increasing kaolinite content in raw clay, the pH decreases and the zeta potential increases towards more negative values in both raw and calcined clays.
- The trend in zeta potential is also transferable to calcined clay blended cements, where the impact of calcined clays with small zeta potential is minor on flow resistance and superplasticizer demand. This is of special interest for concrete industry, as common clays are abundant worldwide and can be used in large amounts to reduce the clinker content in concrete. Pronounced changes in zeta potential of calcined clay blended cement paste towards positive values lead to the conclusion that a rapidly increasing flow resistance is caused not only by the physical interaction of the particles in blended paste, but also by a strong initial ettringite formation in the presence of highly reactive calcined clays during very early age. In future investigations, this can be verified by using X-ray diffractometry on stopped cement paste samples.
- The total amount of phyllosilicates in clay needs to be considered as well in terms of workability, as a high content can interfere with a proper dispersion of PCE over time. Further, a larger specific surface area of calcined clay is revealed as critical parameter in terms of time-related flow behavior, while the influence of kaolinite content and water demand is minor in this case.
- Calorimetric measurements reveal only minor retardation effects caused by superplasticizers for these systems. Plain Portland limestone cement, on contrary, shows a more pronounced, non-linear retardation. After 24 h of hydration, main reactions are complete for the systems investigated and heat of hydration is $\geq$ 90 % related to reference, despite of the use of superplasticizer. In combination with a sufficient workability period, this enables the practical use of calcined common clays even with higher dosages of superplasticizer that are often required for proper workability.

Declaration of Competing Interest

The authors declare that they have no known competing financial interests or personal relationships that could have appeared to influence the work reported in this paper.

Acknowledgement

The authors thank Schwenk Zement KG (Germany) for the Portland limestone cement, Jilin Zhongxin Chemical Group Co., Ltd. (China) for the HPEG PCE and BASF Construction Solutions GmbH (Germany) for the IPEG-based superplasticizer. They also thank Strobel Quarzsand GmbH, Goerg & Schneider GmbH, Dr. Andreas Murr, Mr. Peter Jell (Degelhof clay pit), and Liapor GmbH & Co. KG for providing the raw common clays. The authors like to express their deepest gratitude to Prof. J. Plank and his team from the Chair for Construction Company of Technical University Munich (Germany) for the characterization of the superplasticizers and the conduction of mini slump tests within a joint research project. Here, the authors like to thank Deutsche Forschungsgemeinschaft (DFG) for the financial support of the research project “Ecological and energetic optimization of concrete: Interaction of structurally divergent superplasticizers with calcined clays” (grant number TH 1383/3-1).

References

[1] F. Avet, K. Scrivener, Investigation of the calcined kaolinite content on the hydration of Limestone Calcined Clay Cement (LC3), Cement Concrete Res 107 (2018) 124–135.
[2] G. Mishra, A.C. Emmanuel, S. Bishnoi, Influence of temperature on hydration and microstructure properties of limestone-calcined clay blended cement, Mater Struct 52 (5) (2019), https://doi.org/10.1617/s11527-019-1390-5.
[3] F. Zunino, K. Scrivener, Limestone Calcined Clay Cements (LC3): Effect of Raw Material Properties on Hydration and Strength, in: M. Serdar, N. Štirmer, J. Provis (Eds.), International Conference on Sustainable Materials, Systems and Structures – SMSS 2019 New Generation of Construction Materials, RILEM Publications S.A.R.L, Rovinj, Croatia, 2019, pp. 457–461.
[4] Z. Shi, S. Ferreiro, B. Lothenbach, M.R. Geiker, W. Kunther, J. Kaufmann, D. Herfort, J. Skibsted, Sulfate resistance of calcined clay – Limestone – Portland cements, Cement Concrete Res 116 (2019) 238–251.
[5] Y. Dhandapani, T. Sakthivel, M. Santhanam, R. Gettu, R.G. Pillai, Mechanical properties and durability performance of concretes with Limestone Calcined Clay Cement (LC3), Cement Concrete Res 107 (2018) 136–151.
[6] Y. Dhandapani, M. Santhanam, Assessment of pore structure evolution in the limestone calcined clay cementitious system and its implications for performance, Cement and Concrete Composites 84 (2017) 36–47.
[7] Y. Dhandapani, M. Santhanam, Investigation on the microstructure-related characteristics to elucidate performance of composite cement with limestone-calcined clay combination, Cement Concrete Res 129 (2020), 105959.
[8] A. Ito, R. Wagai, Global distribution of clay-size minerals on land surface for biogeochemical and climatological studies, Scientific Data 4 (1) (2017), 170103.
[9] H.H. Murray, Industrial Applications of Kaolin, Clays and Clay Minerals 10 (1) (1961) 291–298.
[10] T. Danner, Reactivity of Calcined Clays, Department of Natural Sciences and Engineering, NTNU, Trondheim, Faculty of Natural Science and Technology, 2013, p. 229.
[11] N. Beuntner, R. Sposito, K.-C. Thienel, Potential of Calcined Mixed-Layer Clays as Pozzolans in Concrete, ACI Materials Journal 116 (4) (2019) 19–29.
[12] M. Maier, N. Beuntner, K.-C. Thienel, An approach for the evaluation of local raw material potential for calcined clay as SCM, based on geological and mineralogical data: Examples from German clay deposits, in: S. Bishnoi (Ed.), Calcined Clays for Sustainable Concrete - Proceedings of the 3rd International Conference on Calcined Clays for Sustainable Concrete, 2020, pp. 37–47.
[13] E.F. Irassar, V.L. Bonavetti, C.C. Castellano, M.A. Trezza, V.F. Rahhal, G. Cordoba, R. Lemma, Calcined illite-chlorite shale as supplementary cementing material: Thermal treatment, grinding, color and pozzolanic activity, Applied Clay Science 179 (2019), 105143.
[14] A. Trümer, H.-M. Ludwig, M. Schellhorn, R. Diedel, Effect of a calcined Westerwald bentonite as supplementary cementitious material on the long-term performance of concrete, Applied Clay Science 168 (2019) 36–42.
[15] H.H. Murray, Applied Clay Mineralogy, Volume 2: Occurrences, Processing and Applications of Kaolins, Elsevier, 2007.
[16] R. Sposito, N. Beuntner, K.-C. Thienel, Rheology, setting and hydration of calcined clay blended cements in interaction with PCE-based superplasticisers, Mag Concrete Res 73 (15) (2021) 785–797.
[17] R. Sposito, N. Beuntner, K.-C. Thienel, Characteristics of components in calcined clays and their influence on the efficiency of superplasticizers, Cement and Concrete Composites 110 (2020), 103594.
[18] P. Hou, T.R. Muzenda, Q. Li, H. Chen, S. Kawashima, T. Sui, H. Yong, N. Xie, X. Cheng, Mechanisms dominating thixotropy in limestone calcined clay cement (LC3), Cement Concrete Res 140 (2021), 106316.
[19] S. Ferreiro, D. Herfort, J.S. Damtoft, Effect of raw clay type, fineness, water-to-cement ratio and fly ash addition on workability and strength performance of calcined clay – Limestone Portland cements, Cement Concrete Res 101 (2017) 1–12.
[20] R. Sposito, M. Schmid, J. Plank, K.-C. Thienel, An approach to the rheological behavior of cementitious systems blended with calcined clays and superplasticizers, in: A. Tagnit-Hamou (Ed.), ACI SP 349 11th International Conference on Cementitious Materials and Alternative Binders for Sustainable Concrete, American Concrete Institute, online, 2021, pp. 659–685.
[21] R. Sposito, M. Maier, N. Beuntner, K.-C. Thienel, Physical and mineralogical properties of calcined common clays as SCM and their impact on flow resistance and demand for superplasticizer, under revision in Cement and Concrete Research.
[22] N. Nair, K. Mohammed Haneefa, M. Santhanam, R. Gettu, A study on fresh properties of limestone calcined clay blended cementitious systems, Constr Build Mater 254 (2020), 119326.
[23] Y. Chen, C. Romero Rodriguez, Z. Li, B. Chen, O. Çopuroğlu, E. Schlangen, Effect of different grade levels of calcined clays on fresh and hardened properties of ternary-blended cementitious materials for 3D printing, Cement and Concrete Composites 114 (2020), 103708.
[24] E. Moulin, P. Blanc, D. Sorrentino, Influence of key cement chemical parameters on the properties of metakaolin blended cements, Cement and Concrete Composites 23 (6) (2001) 463–469.
[25] R. Sposito, I. Dürr, K.-C. Thienel, Lignosulfonates in cementitious systems blended with calcined clays, in: V. Falikman, R. Realfonzo, P. Hájek, P. Riva (Eds.), ACI SP 326 – 2nd International Workshop on Durability and Sustainability of Concrete Structures, American Concrete Institute, Moscow, Russia, 2018, pp. 10.1-10.10.
[26] R. Li, L. Lei, T. Sui, J. Plank, Approaches to achieve fluidity retention in low-carbon calcined clay blended cements, Journal of Cleaner Production 311 (2021), 127770.
[27] H. Tan, X. Li, S. Jian, B. Ma, M. Liu, Effect of the ester group in side chain of polycarboxylate superplasticizer on the cement hydration process, ZKG int. 69 (7–8) (2016) 60–67.
[28] M. CHOROM, P. RENGASAMY, Dispersion and zeta potential of pure clays as related to net particle charge under varying pH, electrolyte concentration and cation type, European Journal of Soil Science 46 (4) (1995) 657–665.
[29] D. Lowke, C. Gehlen, Effect of Pore Solution Composition on Zeta Potential and Superplasticizer Adsorption, in: V.M. Malhotra, P.R. Gupta, T.C. Holland (Eds.), ACI SP 302 - Eleventh International Conference on Superplasticizers and other Chemical Admixtures in Concrete, American Concrete Institute, Ottawa, Canada, 2015, pp. 253–264.
[30] J. Plank, C. Hirsch, Impact of zeta potential of early cement hydration phases on superplasticizer adsorption, Cement Concrete Res 37 (4) (2007) 537–542.
[31] S. Ng, J. Plank, Interaction mechanisms between Na montmorillonite clay and MPEG-based polycarboxylate superplasticizers, Cement Concrete Res 42 (6) (2012) 847–854.
[32] L. Lei, J. Plank, A study on the impact of different clay minerals on the dispersing force of conventional and modified vinyl ether based polycarboxylate superplasticizers, Cement Concrete Res 60 (2014) 1–10.
[33] L. Zhang, Q. Lu, Z. Xu, Q. Liu, H. Zeng, Effect of polycarboxylate ether comb-type polymer on viscosity and interfacial properties of kaolinite clay suspensions, J Colloid Interf Sci 378 (1) (2012) 222–231.
[34] M.J. Avena, M.M. Mariscal, C.P. De Pauli, Proton binding at clay surfaces in water, Applied Clay Science 24 (1) (2003) 3–9.
[35] X. Yin, L. Yan, J. Liu, Z. Xu, J.D. Miller, Anisotropic Surface Charging of Chlorite Surfaces, Clays and Clay Minerals 61 (2) (2013) 152–164.
[36] Y. Yukselen-Aksoy, A. Kaya, A study of factors affecting on the zeta potential of kaolinite and quartz powder, Environmental Earth Sciences 62 (4) (2011) 697–705.
[37] S. Scherb, N. Beuntner, M. Köberl, K.-C. Thienel, The early hydration of cement with the addition of calcined clay - From single phyllosilicate to clay mixture, in: H.-B. Fischer, A. Volke (Eds.) 20. Internationale Baustofftagung ibausil, F.A. Finger-Institut für Baustoffkunde, Prof. Dr.-Ing. H.-M. Ludwig, Weimar, Germany, 2018, pp. 658-666.
[38] M. Maier, S. Scherb, A. Neißer-Deiters, N. Beuntner, K.-C. Thienel, Hydration of cubic tricalcium aluminate in the presence of calcined clays, J Am Ceram Soc 104 (7) (2021) 3619–3631.
[39] S. Scherb, M. Maier, N. Beuntner, K.-C. Thienel, J. Neubauer, Reaction kinetics during early hydration of calcined phyllosilicates in clinker-free model systems, Cement Concrete Res 143 (2021), 106382.
[40] M. Maier, N. Beuntner, K.-C. Thienel, Mineralogical characterization and reactivity test of common clays suitable as supplementary cementitious material, Applied Clay Science 202 (2021), 105990.
[41] R. Sposito, M. Schmid, N. Beuntner, S. Scherb, J. Plank, K.-C. Thienel, Early hydration behavior of blended cementitious systems containing calcined clays and superplasticizer, in: J. Gemrich (Ed.), 15th International Congress on the Chemistry of Cement, Prague, Czech Republic, Research Institute of Binding Materials Prague, 2019, p. 10.
[42] B.H. Zaribaf, K.E. Kurtis, Admixture compatibility in metakaolin–portland-limestone cement blends, Mater Struct 51 (2018) 13.
[43] T.-H. Ahn, K.-B. Shim, J.-S. Ryou, The relationship between various super-plasticizers and hydration of mortar incorporating metakaolin, Journal of Ceramic Processing Research 16 (2) (2015) 181–187.
[44] S. Ng, H. Justnes, Influence of plasticizers on the rheology and early heat of hydration of blended cements with high content of fly ash, Cement and Concrete Composites 65 (2016) 41–54.
[45] U. Pott, C. Jakob, D. Jansen, J. Neubauer, D. Stephan, Investigation of the incompatibilities of cement and superplasticizers and their influence on the rheological behavior, Materials 13 (977) (2020) 21.
[46] M. Palacios, F. Puertas, P. Bowen, Y.F. Houst, Effect of PCs superplasticizers on the rheological properties and hydration process of slag-blended cement pastes, J Mater Sci 44 (10) (2009) 2714–2723.

[47] F. Winnefeld, S. Becker, J. Pakusch, T. Götz, Effects of the molecular architecture of comb-shaped superplasticizers on their performance in cementitious systems, Cement and Concrete Composites 29 (4) (2007) 251–262.
[48] B. Lothenbach, F. Winnefeld, R. Figi, The influence of superplasticizers on the hydration of Portland cement, 12th International Congress on the Chemistry of Cement, Montreal, Canada, 2007.
[49] D.I.N. En, 197–1, Zement - Teil 1: Zusammensetzung, Anforderungen und Konformitätskriterien von Normalzement (Cement - Part 1: Composition, specifications and conformity criteria for common cements), Beuth-Verlag, Berlin, 2011, p. 8.
[50] A. Buchwald, C. Kaps, M. Hohmann, Alkali-Activated Binders and Pozzolan Cement Binders – Compete Binder Reaction or two Sides of the same Story? in: H. Justnes (Ed.), 11th International Conference on the Chemistry of Cement Durban, South Africa, 2003, pp. 1238–1246.
[51] B.H. O'Connor, M.D. Raven, Application of the Rietveld refinement procedure in assaying powdered mixtures, Powder Diffr 3 (1) (1988) 2–6.
[52] DIN En ISO, 17892–3, Geotechnical investigation and testing - Laboratory testing of soil - Part 3: Determination of particle density, Beuth-Verlag, Berlin, Germany, 2015, p. 21.
[53] D.I.N. Iso, 9277, Determination of the specific surface area of solids by gas adsorption - BET method, Beuth-Verlag, Berlin, 2003, p. 19.
[54] W. Puntke, Wasseranspruch von feinen Kornhaufwerken, Beton 52 (5) (2002) 242–248.
[55] M. Schmid, J. Plank, Dispersing Performance of Different Kinds of Polycarboxylate (PCE) Superplasticizers in Cement Blended With a Calcined Clay, Constr Build Mater 258 (2020), 119576.
[56] M. Schmid, R. Sposito, K.-C. Thienel, J. Plank, Novel zwitterionic PCE superplasticizers for calcined clays and their application in calcined clay blended cements, in: J. Gemrich (Ed.), 15th International Congress on the Chemistry of Cement, Prague, Czech Republic, Research Institute of Binding Materials Prague, 2019, p. 8.
[57] DIN EN 1015-3, Prüfverfahren für Mörtel für Mauerwerk-Teil 3: Bestimmung der Konsistenz von Frischmörtel (mit Ausbreittisch) (Methods of test for mortar for masonry - Part 3: Determination of consistence of fresh mortar (by flow table)), Beuth-Verlag, Berlin, 2007, p. 12.
[58] H. Vikan, H. Justnes, F. Winnefeld, R. Figi, Correlating cement characteristics with rheology of paste, Cement Concrete Res 37 (11) (2007) 1502–1511.
[59] H. Vikan, H. Justnes, R. Figi, Influence of Cement and Plasticizer Type on the Rheology and Reactivity of Cementitious Binders, in: V.M. Malhotra (Ed.), ACI SP 239–8th CanMET/ACI Intl Conference on Superplasticizers and other Chemical Admixtures in Concrete, Sheridan Books, Sorrento, Italy, 2006, pp. 455–470.
[60] A. Yahia, K.H. Khayat, Analytical models for estimating yield stress of high-performance pseudoplastic grout, Cement Concrete Res 31 (5) (2001) 731–738.
[61] V.A. Hackley, C.F. Ferraris, Guide to Rheological Nomenclature - Measurements in Ceramic Particulate Systems, National Institute of Standards and Technology (NIST), Gaithersburg, Maryland, USA, 2001, pp. III, 29.
[62] J. Plank, B. Sachsenhauser, Impact of Molecular Structure on Zeta Potential and Adsorbed Conformation of α-Allyl-ω-Methoxypolyethylene Glycol - Maleic Anhydride Superplasticizers, Journal of Advanced Concrete Technology 4 (2) (2006) 233–239.
[63] J.W. Bullard, H.M. Jennings, R.A. Livingston, A. Nonat, G.W. Scherer, J. S. Schweitzer, K.L. Scrivener, J.J. Thomas, Mechanisms of cement hydration, Cement Concrete Res 41 (12) (2011) 1208–1223.
[64] A. Neißer-Deiters, S. Scherb, N. Beuntner, K.-C. Thienel, Influence of the calcination temperature on the properties of a mica mineral as a suitability study for the use as SCM, Applied Clay Science 179 (2019) 105168, https://doi.org/10.1016/j.clay.2019.105168.
[65] L. Yan, A.H. Englert, J.H. Masliyah, Z. Xu, Determination of Anisotropic Surface Characteristics of Different Phyllosilicates by Direct Force Measurements, Langmuir 27 (21) (2011) 12996–13007.
[66] D. Lowke, C. Gehlen, The zeta potential of cement and additions in cementitious suspensions with high solid fraction, Cement Concrete Res 95 (2017) 195–204.
[67] K. Yoshioka, E.-I. Tazawa, K. Kawai, T. Enohata, Adsorption characteristics of superplasticizers on cement component minerals, Cement Concrete Res 32 (10) (2002) 1507–1513.
[68] M. Schmid, J. Plank, Interaction of individual meta clays with polycarboxylate (PCE) superplasticizers in cement investigated via dispersion, zeta potential and sorption measurements, Applied Clay Science 207 (2021), 106092.
[69] R. Li, L. Lei, T. Sui, J. Plank, Effectiveness of PCE superplasticizers in calcined clay blended cements, Cement Concrete Res 141 (2021), 106334.
[70] L.M. Vane, G.M. Zang, Effect of aqueous phase properties on clay particle zeta potential and electro-osmotic permeability: Implications for electro-kinetic soil remediation processes, J Hazard Mater 55 (1) (1997) 1–22.
[71] S.A. Hussain, Ş. Demirci, G. Özbayoğlu, Zeta Potential Measurements on Three Clays from Turkey and Effects of Clays on Coal Flotation, J Colloid Interf Sci 184 (2) (1996) 535–541.
[72] C. Chomyn, J. Plank, Impact of different synthesis methods on the dispersing effectiveness of isoprenol ether-based zwitterionic and anionic polycarboxylate (PCE) superplasticizers, Cement Concrete Res 119 (2019) 113–125.
[73] I. Navarro-Blasco, M. Pérez-Nicolás, J.M. Fernández, A. Duran, R. Sirera, J. I. Alvarez, Assessment of the interaction of polycarboxylate superplasticizers in hydrated lime pastes modified with nanosilica or metakaolin as pozzolanic reactives, Constr Build Mater 73 (2014) 1–12.
[74] S. Chandra, J. Björnström, Influence of cement and superplasticizers type and dosage on the fluidity of cement mortars—Part I, Cement Concrete Res 32 (10) (2002) 1605–1611.
[75] C. Jakob, D. Jansen, N. Ukrainczyk, E. Koenders, U. Pott, D. Stephan, J. Neubauer, Relating Ettringite Formation and Rheological Changes during the Initial Cement Hydration: A Comparative Study Applying XRD Analysis, Rheological Measurements and Modeling, Materials 12 (2019) 2957.
[76] F. Zunino, K. Scrivener, Studying The Influence of the Filler Effect of SCMs on the Sulfate Requirement of Blended Cements, in: A. Tagnit-Hamou (Ed.), ACI SP 349 11th International Conference on Cementitious Materials and Alternative Binders for Sustainable Concrete, American Concrete Institute, online, 2021, pp. 117–124.
[77] M. Maier, R. Sposito, N. Beuntner, K.-C. Thienel, Particle characteristics of calcined clays and limestone and their impact on the early hydration and sulfate demand of blended cement, Cement Concrete Res (Submitted).
[78] F. Zunino, K. Scrivener, Factors influencing the sulfate balance in pure phase C_3S/C_3A systems, Cement Concrete Res 133 (2020), 106085.
[79] J. Tang, S. Wei, W. Li, S. Ma, P. Ji, X. Shen, Synergistic effect of metakaolin and limestone on the hydration properties of Portland cement, Constr Build Mater 223 (2019) 177–184.
[80] E. Sakai, T. Kasuga, T. Sugiyama, K. Asaga, M. Daimon, Influence of superplasticizers on the hydration of cement and the pore structure of hardened cement, Cement Concrete Res 36 (11) (2006) 2049–2053.
[81] A. Zingg, F. Winnefeld, L. Holzer, J. Pakusch, S. Becker, R. Figi, L. Gauckler, Interaction of polycarboxylate-based superplasticizers with cements containing different C3A amounts, Cement and Concrete Composites 31 (3) (2009) 153–162.
[82] D. Jansen, J. Neubauer, F. Goetz-Neunhoeffer, R. Haerzschel, W.-D. Hergeth, Change in reaction kinetics of a Portland cement caused by a superplasticizer — Calculation of heat flow curves from XRD data, Cement Concrete Res 42 (2) (2012) 327–332.
[83] Y.-R. Zhang, X.-M. Kong, Z.-B. Lu, Z.-C. Lu, S.-S. Hou, Effects of the charge characteristics of polycarboxylate superplasticizers on the adsorption and the retardation in cement pastes, Cement Concrete Res 67 (2015) 184–196.
[84] W. Meng, A. Kumar, K.H. Khayat, Effect of Silica Fume and Slump-Retaining Polycarboxylate-based Dispersant on the Development of Properties of Portland Cement Paste, Cement and Concrete Composites 99 (2019) 181–190.

7.5 Lignosulfonates in cementitious systems blended with calcined clays

Conference paper [Reprint]

"Lignosulfonates in cementitious systems blended with calcined clays"

Ricarda Sposito, Isabel Dürr, Karl-Christian Thienel

ACI SP 326 – 2nd International Workshop on Durability and Sustainability of Concrete Structures

Moscow, Russia, 6th – 7th June 2018, pp. 10.1 – 10.10

SP-326—10

Lignosulfonates in Cementitious Systems Blended with Calcined Clays

Ricarda Sposito, Isabel Dürr, and Karl-Christian Thienel

Synopsis: Calcined clays play an important role when it comes to efficient supplementary cementitious materials (SCM) required in future. The substitution of clinker by calcined clays requires the application of water reducing agents to ensure a good workability of concrete due to high specific surface area and water demand of calcined clays. The interaction of two calcined clays with two lignosulfonate-based plasticizers was investigated in cement paste with respect to their dispersing and setting behavior. A good correlation was obtained between higher substitution rates and higher required plasticizer dosages when the same dispersing effects are aimed at as for ordinary Portland cement. These high dosages result in significant retardation effects in hydration behavior. When same dosages are used for all investigated systems and workability effects are disregarded, the retardation impact on cementitious systems with aluminum-rich calcined clays is less than for pure cement paste. If dosages are optimized regarding workability and setting behavior, lignosulfonates are a suitable plasticizer for cementitious systems with calcined clays.

Keywords: calcined clays, calorimetry, hydration kinetics, lignosulfonates, plasticizer, setting behavior

10.1

Sposito et al.

Biography: **Ricarda Sposito** is research associate at the Institute for Construction Materials, University of the Bundeswehr Munich, Germany. She received her BSc in civil engineering from University of Applied Sciences Munich and her MSc in civil engineering from Technical University Munich. Her research interests include concrete technology, calcined clays and their interaction with (super) plasticizers.

Isabel Dürr is officer in the German air force. She received her BSc and MSc in civil engineering from University of the Bundeswehr Munich, Germany. Her master's thesis was about the influence of lignosulfonates on the hydration kinetics, setting behavior and rheology of cement pastes blended with calcined clays.

ACI member **Karl-Christian Thienel** is professor and head of the Institute for Construction Materials, University of the Bundeswehr Munich, Germany. He received his diploma and Dr. degree in civil engineering from TU Braunschweig. He was Alexander-von-Humboldt "Feodor–Lynen" stipendiary at ACBM, Northwestern University, Evanston, IL, and head of R&D at Liapor GmbH & Co. KG. He is chairman of CEN/TC 177 and member of CEN/TC 154 SC5. His research interests include calcined clays, lightweight concrete and aggregate.

INTRODUCTION

The demand for ecologically optimized concrete is increasing significantly due to economic growth and high CO_2 emissions by cement industry, causing around 5 % of total anthropogenic CO_2 emissions worldwide [1]. Globally insufficient supply of long-time established supplementary cementitious materials (SCM) and an increasing demand for binders make sustainable innovations essential for the future [2]. Calcined clays come more and more into focus as a promising alternative because of worldwide deposits of suitable clays and significantly lower CO_2 emissions during the calcination process compared to clinker production [3]. One side effect of calcined clays is their high water demand and higher specific surface area as compared to cements, depending on the mineralogical composition of the individual clay.

Therefore (super) plasticizers are often used for investigations of mortars and concretes containing calcined clays to ensure workability but without respecting their influence in detail. Lignosulfonates (LS) are commonly used plasticizers since the 1930s. It is known that they influence reaction kinetics and setting behavior of cementitious systems, while affecting hydration kinetics of clinker phases, especially of C_3A [4-9]. Additionally, the more LS is used in cementitious system, the more pronounced is the impact on C_3S hydration [5, 8]. The initial dissolution of C_3S is retarded [9] and formation of calcium hydroxide is both delayed and decreased [8]. Due to competitive behavior of gypsum and LS for interaction with C_3A, first ettringite formation was delayed in a pure C_3A-gypsum system [9], while in systems with ordinary Portland cement it was even accelerated but the second C_3A hydration / ettringite formation was retarded [8]. The interaction of LS with clinker phases and the competitive behavior with sulfates as setting controlling agents result in an altered setting behavior. Time of addition, dosage and type of LS can also affect setting and rheological behavior of cementitious systems [9, 10].

The main objective of this study was gaining a fundamental understanding of the interaction between calcined clays and lignosulfonate-based plasticizers in cementitious systems. Especially differences in physical and chemical properties of calcined clays and of lignosulfonates should be investigated in detail.

EXPERIMENTAL INVESTIGATION

Materials

An ordinary Portland cement (OPC) CEM I 42.5 R, complying with the European standard DIN EN 197-1 [11], was used as cement and partly substituted by 20 w% of calcined clays. Two different calcined clays were investigated. The first calcined clay is an industrially-used metakaolin (Mk) from the USA. The other clay is an Amaltheen mixed-layer clay originating from southern Germany [12, 13]. It contains in its natural form different phyllosilicates (25 w% kaolinite and 45 w% 2:1 clay minerals, e.g. illite and muscovite) and 30 w% inert components (e.g. quartz, feldspar, calcite, sulfates). Preliminary investigations revealed that pozzolanic activity of this calcined mixed-layer clay (CT) is highest when calcination temperatures ranges between 700 and 800 °C (1292 and 1472 °F) [12]. The calcination procedure is described in detail in [12, 13]. After calcination at 750 °C (1382 °F) for 30 minutes, the CT was ground in an industrial roller mill. Table 1 gives the chemical characterization of the test materials. Table 2 contains the physical parameters of all binders. Water demand was determined according to DIN EN 196-3 [14] for cement and according to Puntke [15] for calcined clays.

Borregaard LignoTech, Norway provided as plasticizers two softwood-based, purified lignosulfonates in powder form: one magnesium-lignosulfonate (Mg-LS) and one sodium-lignosulfonate (Na-LS). The producer provided information about the chemical properties of both LS (see Table 3).

Methods

The flowability of cement paste was determined by "mini slump test" according to DIN EN 1015-3 [16]. In a first step, w/b ratio was set for neat cement paste without any calcined clay or lignosulfonate to achieve a spread flow of 18 ± 0.5 cm (7.1 ± 0.2 in.). To compare the dispersion effects of lignosulfonates but also the influence of

calcined clays, the dosages of Mg-LS and Na-LS were adjusted to get a spread flow of 26 ± 0.5 cm (10.2 ± 0.2 in.) for cement pastes without and with 20 w% calcined clay as SCM. Slump loss behavior was determined over a time of 135 minutes for the mix designs with w/b ratio and plasticizer dosages determined beforehand. The "mini slump test" was repeated at 15-minutes intervals with the same material which was placed back in a cup and covered by a moist cloth after each test to prevent drying-up of the (blended) cement paste.
For investigating the hydration kinetics, the specific heat flow was measured at constant temperature of 25 °C (77 °F) by using an isothermal calorimeter TAM Air (TA Instruments, Delaware/USA). The pastes were mixed by hand for approximately 90 seconds outside of the calorimeter in a temperature controlled room at 25 °C (77 °F) to prevent an external, thermal influence on hydration kinetics. Specific heat flow was calculated over time and related to the mass content of cement in hardened cement paste. Setting time was determined according to ASTM C1679-13[17] as the moment when half the maximum of the main hydration peak is reached.
Furthermore, early setting behavior and hardening of mortar was measured by an ultrasonic unit Vikasonic (Schleibinger, Buchbach/Germany) with integrated datalogger. Since measurements on cement paste with LS were not reliable, mortars with 40 vol% of quartz powder and 60 vol% of cement paste were mixed. Compared to measurements with Vicat apparatus according to DIN EN 196-3 [14] deviation error is in general reduced from 34 % on average to only 18 % when ultrasound method is applied. In order to eliminate external influences, the equipment was stored in climate chamber (20 °C, 68 °F/65 % r.h.) during measurements. Young's modulus was calculated based on the density of mortar and continuously recorded speed of ultrasound and used for the subsequent discussion as an indicator for setting progress.

EXPERIMENTAL RESULTS AND DISCUSSION

Determination of w/b ratio and dosage of plasticizer

The w/b ratio for the required spread flow was set at 0.45 for the reference cement paste made with OPC only. The evaluated dosages of solid LS powder [% by weight of binder, % bwob] which were necessary to reach a spread flow of 26 ± 0.5 cm (10.2 ± 0.2 in.) at w/b ratio of 0.45 are given in Table 4. The dispersing effects of Mg-LS and Na-LS are similar for OPC only (0.15/0.16 % bwob) and OPC_20CT (0.45/0.47 % bwob) but differ significantly for OPC_20Mk (0.69 % bwob Mg-LS < 0.82 % bwob Na-LS). The higher demand of LS in systems blended with calcined clays, especially with Mk, results from the high specific surface area (SSA) of calcined clay particles. The combined SSA of the binder originates from the individual SSA of cement and of calcined clay according to their percentage of weight in binder systems. To prove a certain linearity between combined SSA and required dosage, the dosages of LS were adjusted for additional substitution rates (10 w% and 30 w%) as shown in Fig. 1 and Fig. 2. It is obvious that the required dosage increases with higher substitution rates and the linearity is given within one OPC-calcined clay system but is not valid for combined SSA. A further reason for these high LS dosages can be the substitution by mass instead of volume. As the densities of CT and Mk are lower than the density of cement, the total binder volume increases as more OPC is replaced by calcined clay. As the particle densities of CT and Mk are similar, thus this cannot be the reason for partially significantly differing dosages. Considering the water demand of the (blended) binder material, the required dosage vs. combined water demand is shown in Fig. 3. Beside good correlations within one binder system (OPC_CT and OPC_Mk), it is remarkable that systems depending on plasticizer show especially for Na-LS ($R^2 = 0.9837$) also good correlations (for Mg-LS: $R^2 = 0.8862$). In general, type and substitution rate of binder has a main influence on the dispersing effect of LS.

Slump loss behavior over time

With the acquired dosages taken from the preceding tests, the dispersion behavior of cement pastes with both LS was evaluated over a period of 135 minutes (see Fig. 4). Pastes with OPC only (OPC_Mg-LS, OPC_Na-LS) and OPC_20CT_Na-LS exhibit a rapid decrease of spread flow, especially during the first 45 minutes. Spread flow of OPC_20CT_Mg-LS is nearly constant within the first hour and decreases only slightly until the end of measurements at 135 minutes (here the trend is in parallel with OPC_20CT_Na-LS but on a higher level due to reduced slump loss during the first hour). In the beginning, cement pastes with metakaolin and LS have the same dispersing behavior as OPC_20CT_Mg-LS but between 45 and 120 minutes spread flow increases compared to initial spread flow. It seems that LS is adsorbed and interacts in another, still unknown manner on Mk compared to cement and also to CT which can be explained by the high SSA of Mk. There might be a depot effect for Mk which leads to a delayed release and dispersing impact of LS on the blended cement paste. Another possible reason is the high dosage used for systems with Mk which can result in an adsorption plateau as described for cementitious systems by Colombo et al. [18]. An accompanying effect of a high LS dosage is a retarding effect as seen in isothermal calorimetry and ultrasound measurements (see Fig. 7 and Fig. 10).

Hydration kinetics

Compared to OPC system without LS, OPC_LS systems with 0.14 % bwob Mg-LS or 0.15 % bwob Na-LS have prolonged induction periods but simultaneous acceleration periods resulting in a retardation of approximately

3 hours for the main silicious peaks which occur after 12 hours for OPC and after 15 hours for both OPC_LS systems (see Fig. 5). The intensity of the silicate peaks is similar for all the systems ranging from 2.37 mW/g_{cement} for OPC_Na-LS to 2.47 mw/g_{cement} for OPC. For OPC_LS systems, the sulfate depletion peak which indicates the aluminate reaction and the formation of ettringite is less retarded than the main peak and slightly increased compared to OPC. A third peak, indicating the formation of mono phases according to Hesse [19], is not detectable for OPC but indicated for both OPC_LS. OPC_Mg-LS and OPC_Na-LS exhibit similar heat flow curves during the observed 48 hours, hence there is no significant influence of lignosulfonate type (Mg/Na) at comparable dosages.
For OPC_20CT systems, the induction period is also extended due to LS which inhibits the silicate reaction (see Fig. 6), as already stated e.g. by [9]. The aluminate reaction, which is represented by the main peak in the heat flow curve of OPC_20CT, is significantly more affected. This reaction is influenced to a huge extend by aluminum-rich SCM like calcined clays as previously published e.g. in [20]. For OPC_20CT, this peak appears after about 20 hours, hence two hours after the aluminate peak of OPC. The induction period is slightly shorter for OPC_20CT_LS systems as compared to OPC_LS but the retardation of the aluminate reaction is more pronounced (~ 2.5 hours) for comparable dosages (0.14 % bwob Mg-LS / 0.15 % bwob Na-LS). By applying the dosages generated from mini slump test (0.45 % bwob Mg-LS / 0.47 % bwob Na-LS), the induction periods are extremely extended which results in a total retardation of approximately 12 hours. This effect leads to an overlay of the silicate and aluminate reactions at about 32 hours.
Induction period is shortened when metakaolin is part of the binder in cementitious systems. Both, silicate and aluminate reactions are more promoted for cementitious systems blended with metakaolin due to its high content of soluble Al_2O_3 and its mineralogical structure [20]. This is indicated in isothermal calorimetry by a significantly higher heat flow maximum (6.60 mW/g_{cement}) at earlier hydration time (13 h) for OPC_20Mk. Fig. 7 reveals a significant influence of LS when added to OPC_20Mk systems: the more LS is used, the more the induction period is prolonged and the more silicate and aluminate reactions are retarded and become less incisive. As already described for OPC_20CT, higher dosages of lignosulfonates (e.g. 0.82 % bwob Na-LS) result in an overlapping of silicate and aluminate reactions for OPC_20Mk as well. Compared to OPC_20CT, this effect occurs even with higher dosages 5 – 6 hours earlier for OPC_20Mk_LS at about 26 / 27 hours. As the dosage of Mg-LS is less than the one of Na-LS it is not surprising that the aluminate peak of OPC_20Mk_Mg-LS is still higher and less retarded than the peak of OPC_20Mk_Na-LS.
Overall, the influence of LS is stronger in cementitious systems with calcined clays than in pure cement systems. As the dosage is related to the weight of binder (% bwob) and considering a replacement of OPC by 20 w% calcined clay, more LS should be available for the remaining cement particles in the system unless there is an intercalation effect of LS in calcined clay particles.
Setting times calculated according to ASTM C1679-13 [17] are given in Table 5 for the reference systems and those with 0.14 % bwob Mg-LS / 0.15 % bwob Na-LS. Compared to OPC only, setting time of OPC_20CT occurs later while OPC_20Mk yields an accelerated setting behavior. When LS is used in cementitious system (OPC_LS), setting time is retarded for up to 2.3 hours. In blended systems however, it is difficult to calculate the setting time from the heat flow curve due to overlay effects. Nonetheless, retardation effect is minimized when same dosages are used as for OPC only. Especially for OPC_20Mk_LS, the setting time occurs to be only marginally later (≤ 1 hour) than without LS. This observed effect leads to similar setting time for OPC_20CT_LS as well as for OPC_LS and even retardation can be eliminated partially.

Setting behavior and microstructure of blended cementitious systems
Fig. 8 to Fig. 10 both show the development of Young's modulus of (blended) cementitious systems. All curves were smoothed by a Savitzky-Golay filter and with a third order polynomial to reduce external oscillation effects caused during measurement.
The development of Young's modulus with time exhibits for OPC only an inflexion point after about 7 hours of hydration leading to a continuous increase up to 21.2 GPa after 48 hours. The initialization of increase fits well with onset of initial setting (after 7.4 hours) according to ASTM 1679-13 measured from isothermal calorimetry. OPC_Mg-LS has similar behavior during the first seven hours, followed by a linear increase of Young's modulus to 17.5 GPa at 22 hours. Afterwards the curve rises less significantly up to 24.6 GPa after 48 hours and is 16 % higher than for OPC only. Between the first three and nine hours of hydration, Young's modulus is marginally higher for OPC_Na-LS than for OPC and OPC_Mg-LS but still in same range considering measurement accuracy. Until 18 hours, OPC_Na-LS behaves in a similar way to OPC_Mg-LS. After 23 hours of hydration, Young's modulus of OPC_Na-LS is higher than of OPC_Mg-LS and reaches 26.9 GPa at 48 hours. The higher values of Young's modulus for systems with LS correlate well with the second and third peaks of the heat flow curves indicating an additional formation of ettringite and a transformation of ettringite into mono phases. In general, the influence of small dosages of LS (0.14 % bwob Mg-LS / 0.15 % bwob Na-LS) seems negligible on setting time when the initialization of the increase is considered as commencement of initial setting.

Young's modulus for OPC_20CT is constant during the first 6.5 hours of hydration, indicating a commencement of setting at this time, and the value increased continuously to 18.5 GPa after 48 hours. For OPC_20CT, it is about 13 % less than for OPC which can be explained by the pozzolanic reaction of CT [20]. Young's modulus develops similarly for both OPC_20CT_LS systems which is ascribed to similar dosages of both LS. However, OPC_20CT_Na-LS is less retarded than OPC_20CT_Mg-LS which is compensated after about 42 hours. After 48 hours, the values for Young's modulus of both OPC_20CT_LS are identical (17.2 GPa) and about 7 % less than OPC_20CT without LS. Ultrasound measurements prove a strong retardation effect induced by higher dosages of LS. A significant increase of Young's modulus does not start until 20 hours of hydration, the time when induction period ends in isothermal calorimetry (see Fig. 6). It seems that determination of setting according to ASTM 1679-13 is suitable only to a limited extent when it comes to systems with LS. At the same time it is difficult to determine setting time of OPC_20CT_LS by ultrasonic measurement.
The modulus of elasticity of OPC_20Mk increases exponentially during the first 13 hours of hydration to 10 GPa which indicates early setting. Subsequently the development of Young's modulus slows down and results with 20 GPa on a level between OPC and OPC_20CT system after 48 hours. The prolonged induction period of OPC_20Mk_Mg-LS measured by isothermal calorimetry (Fig. 7) is also observed during ultrasonic measurement and indicated by stagnation of Young's modulus until 16 hours. The main increase of the stiffness values takes place between 16 and 28 hours which correlates also well with the main peak of heat flow curve. Until 48 hours, OPC_20Mk_Mg-LS reaches a value of 15 GPa, hence 25 % less than OPC_20Mk. The increase of Young's modulus is slower due to longer induction period for OPC_20Mk_Mg-LS than for OPC_20Mk only but the development is similar when a stiffness value of 10 GPa is reached. Contrary to calorimetric investigations and even if more Na-LS is necessary to disperse OPC_20Mk, the retardation effect of OPC_20Mk_Na-LS is less compared to OPC_20Mk_Mg-LS. Its Young's modulus starts to increase immediately, even though slowly until 16 hours – the end of induction period according to heat flow curve (see Fig. 7). Again, the main increase is measured until a value of 10 GPa is reached (at 25 hours) but further development of the modulus of elasticity is steeper compared to OPC_20Mk and OPC_20Mk_Mg-LS. After 48 hours, this development results in a value between the other two OPC_20Mk systems (18.4 GPa) but indicating that it might exceed the Young's modulus of OPC_20Mk. As already observed by isothermal calorimetry, hydration kinetics and setting behavior of systems with Mk are less retarded than systems with CT even if higher dosages of LS are used.

SUMMARY AND CONCLUSIONS

The dispersion behavior of lignosulfonate-based plasticizers in cement paste blended with two types of calcined clays and their influence on reaction mechanisms of cementitious systems was investigated. Based on the experiments the following conclusions can be drawn:

1. Higher dosages of LS are required for systems with calcined clays. The adsorption and intercalation behavior of LS on and in calcined clay particles should be investigated. It is necessary to get a fundamental understanding about why high dosages of LS are required for systems with calcined clays since specific surface area and water demand were confirmed to be not the only reasons for required high dosages.
2. A longer workability can be guaranteed by using LS in cement-calcined clays systems due to higher dosages, a possible depot effect and the retarding impact of LS.
3. Retarding effects concerning especially silicate reaction but also aluminate reaction depend mainly on dosage of LS. However, in cement-calcined clays systems retardation can be less significant than in pure cement systems. It is desirable to investigate the hydration kinetics by in-situ x-ray diffraction. This method helps to identify the formation of hydration products during early hydration and complements findings from isothermal calorimetry.
4. Delayed setting needs to be considered in the context of standardization work. If setting times are in the range required by standards, LS are a sustainable option for concretes with alternative SCM like calcined clays.

ACKNOWLEDGMENTS

The authors like to thank Borregaard LignoTech, Norway, for providing the lignosulfonates and Liapor GmbH & Co. KG for the supply of calcined mixed-layer clay CT.

REFERENCES

[1] WBCSD, IEA. "Cement Technology Roadmap 2009: carbon emissions reductions up to 2050," World Business Council for Sustainable Development and International Energy Agency, 2009.
[2] Schwarzkopp, F., et al., "The Demand for Primary and Secondary Raw Materials in the Mineral and Building Materials Industry in Germany up to 2035," Bundesverband Baustoffe - Steine und Erden e. V. (German Building Materials Association), Berlin, 2016

[3] Worrell, E., et al., "Carbon Dioxide Emissions from the Global Cement Industry," Annual Review of Energy and the Environment, V. 26, No. 1, 2001, pp. 303-329.
[4] Danner, T., Justnes, H., Geiker, M. and Lauten, R.A., "Early hydration of C3A–gypsum pastes with Ca-and Na-lignosulfonate." Cement and Concrete Research, V. 79, 2016, pp. 333-343.
[5] Danner, T.A., Justnes, H., Geiker, M.R. and Lauten, R.A., "Effect of Lignosulfonate Plasticizers on the Hydration of C3A." 14th International Congress on the Chemistry of Cement, Beijing, China. 2015.
[6] Ramachandran, V.S., "Interaction of calcium lignosulfonate with tricalcium silicate, hydrated tricalcium silicate, and calcium hydroxide," Cement and Concrete Research, V. 2, No. 2, 1972, pp. 179-194.
[7] Ramachandran, V.S., and Feldman, R.F., "Effect of calcium lignosulfonate on tricalcium aluminate and its hydration products," Matériaux et Construction, V. 5, No. 2, 1972, pp. 67-76.
[8] Danner, T., Justnes, H., Geiker, M. and Lauten, R.A., "Phase changes during the early hydration of Portland cement with Ca-lignosulfonates," Cement and Concrete Research, V. 69, 2015, pp. 50-60.
[9] Justnes, H. and S. Ng, "Lignosulfonate as Plasticizer for Cement: the Effect of Type, Dosage, Time of Addition and Clinker Mineralogy," in The 7th International Conference of Asian Concrete Federation "Sustainable Concrete for now and the Future," Hanoi, Vietnam, 2016.
[10] Colombo, A., "The interaction between calcium lignosulfonate and cement," NTNU, Trondheim, Norway, 2017.
[11] IN EN 197-1, "Zement - Teil 1: Zusammensetzung, Anforderungen und Konformitätskriterien von Normalzement (Cement – Part 1: Composition, specifications and conformity criteria for common cements)," Beuth-Verlag, Berlin, 2011.
[12] Beuntner, N. and K.-C. Thienel, "Properties of Calcined Lias Delta Clay - Technological Effects, Physical Characteristics and Reactivity in Cement," in 1st International Conference Calcined Clays for Sustainable Concrete, K. Scrivener and A. Favier, Editors, Springer Netherlands, Lausanne, 2015, pp. 43-50.
[13] Gmür, R., K.-C. Thienel, and N. Beuntner, "Influence of aging conditions upon the properties of calcined clay and its performance as supplementary cementitious material," Cement and Concrete Composites,.V. 72, 2016, pp. 114-124.
[14] DIN EN 196-3, "Prüfverfahren für Zement - Teil 3: Bestimmung der Erstarrungszeiten und der Raumbeständigkeit," 2009.
[15] Puntke, W., "Wasseranspruch von feinen Kornhaufwerken (Water demand of fine loose particles)," Beton, V. 52, No. 5, 2002, pp. 242-248.
[16] DIN EN 1015-3, "Prüfverfahren für Mörtel für Mauerwerk-Teil 3: Bestimmung der Konsistenz von Frischmörtel (mit Ausbreittisch)", 2007.
[17] ASTM C1679-13, "Standard Practice for Measuring Hydration Kinetics of Hydraulic Cementitious Mixtures Using Isothermal Calorimetry," *ASTM International*, West Conshohocken, PA, 2013.
[18] Colombo, A., et al., "On the mechanisms of consumption of calcium lignosulfonate by cement paste," *Cement and Concrete Research*, V. 98, 2017, pp. 1-9.
[19] Hesse, C., "Der Reaktionsverlauf der frühen Hydratation von Portlandzement in Relation zur Temperatur, in Naturwissenschaftlichen Fakultät," Friedrich-Alexander-Universität Erlangen-Nürnberg, 2009.
[20] Beuntner, N., "Zur Eignung und Wirkungsweise calcinierter Tone als reaktive Bindemittelkomponente in Zement, in Fakultät für Bauingenieurwesen und Umweltwissenschaften," Universität der Bundeswehr München, Neubiberg, 2017.

TABLES AND FIGURES

Table 1- Chemical analysis of test materials (– = not measured items; * information provided by producer)

Oxides / Parameters	OPC*	Mk	CT
SiO_2, w%	20.1	54.6	45.4
Al_2O_3, w%	5.4	40.1	20.5
CaO, w%	60.7	< 0.1	5.0
Fe_2O_3, w%	2.9	1.8	6.9
MgO, w%	1.8	0.2	2.3
SO_3, w%	3.4	< 0.1	1.7
TiO_2, w%	0.3	1.4	0.0
Na_2O, w%	-	0.3	0.5
K_2O, w%	-	0.3	3.5
Na_2O_{equ}	0.65	0.50	2.47
LOI, w%	1.80	1.03	0.02
Soluble Al-ions in alkaline solution after 20 h, w%	-	14.25	0.76
Soluble Si-ions in alkaline solution after 20 h, w%	-	15.65	1.39

Table 2- Physical parameters of test materials

Parameters	OPC	Mk	CT
Particle density, g/cm³ (lb/in³)	3.14 (0.113)	2.61 (0.094)	2.63 (0.095)
BET SSA, m²/g (in²/lb)	1.2 (843,690)	17.8 (12,514,742)	3.9 (2,741,993)
Water demand, w%	28.0	64.5/64.8/66.2	42.1/45.8/46.4
d_{10}, µm (in.)	3.5 ($0.13*10^{-3}$)	3.0 ($0.12*10^{-3}$)	4.0 ($0.16*10^{-3}$)
d_{50}, µm (in.)	16.0 ($0.63*10^{-3}$)	14.8 ($0.58*10^{-3}$)	13.2 ($0.52*10^{-3}$)
d_{90}, µm (in.)	55.0 ($2.16*10^{-3}$)	76.2 ($3.00*10^{-3}$)	37.0 ($1.46*10^{-3}$)

Table 3- Molar masses (M_w, M_n) and chemical composition of Na-LS and Mg-LS**

	M_w	M_n	SO_4^{2-}	Ca^{2+}	Mg^{2+}	Na^+	COOH	Total sugar
	g/mol (lb/mol)		w% on dry mass					
Mg-LS	23,400 (51.6)	4,500 (9.9)	1.1	< 0.1	2.5	< 0.1	6.0	3.5
Na-LS	35,600 (78.5)	2,400 (5.3)	2.2	0.3	< 0.1	8.5	8.4	1.3°

** information provided by Borregaard LignoTech, Norway
° reduced sugars (total sugar content was not analyzed due to very low sugar content)

Table 4- Dosages in % by weight of binder (% bwob) of lignosulfonates for a spread flow of 26 ± 0.5 cm (10.2 ± 0.2 in.)

Binder systems	Mg-LS, % bwob	Na-LS, % bwob
100 w% cement (OPC)	0.14	0.15
80 w% cement, 20 w% CT (OPC_20CT)	0.45	0.47
80 w% cement, 20 w% Mk (OPC_20Mk)	0.69	0.82

Table 5- Setting times of (blended) cementitious systems measured by isothermal calorimetry and analyzed according to ASTM C1679-13 [17]

Binder systems	Setting time [h]				
	(1) Without LS	(2) 0.14%bwob Mg-LS	retardation Δ [(2) – (1)]	(3) 0.15%bwob Na-LS	retardation Δ [(3) – (1)]
OPC	7.4	9.6	2.2	9.7	2.3
OPC_20CT	8.3	9.1	0.8	9.3	1.0
OPC_20Mk	6.1	6.9	0.8	7.0	0.9

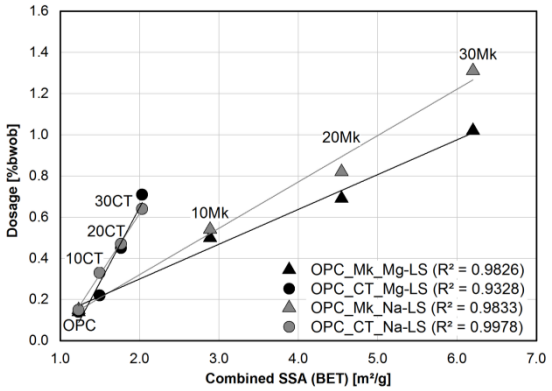

Fig. 1 - Required dosage of LS depending on combined specific surface area (SSA) of the (blended) binder and on varying substitution rate of calcined clays (0 w% to 30 w%)

Sposito et al.

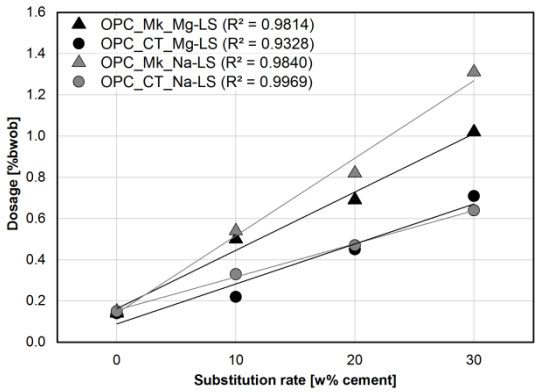

Fig. 2 - Required dosage of LS depending on substitution rate of calcined clays (0 w% to 30 w%)

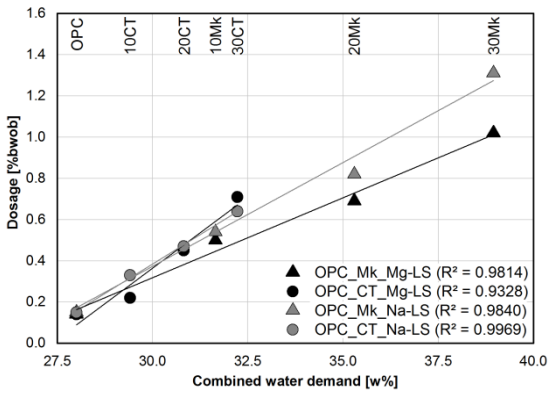

Fig. 3 - Required dosage of LS depending on combined water demand of the (blended) binder and on varying substitution rate of calcined clays (0 w% to 30 w%)

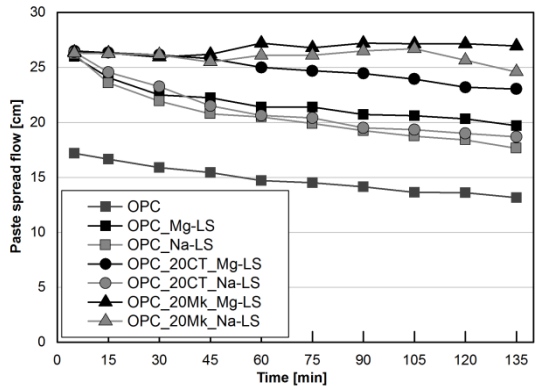

Fig. 4 – Time dependent slump loss behavior for blended cement pastes with LS

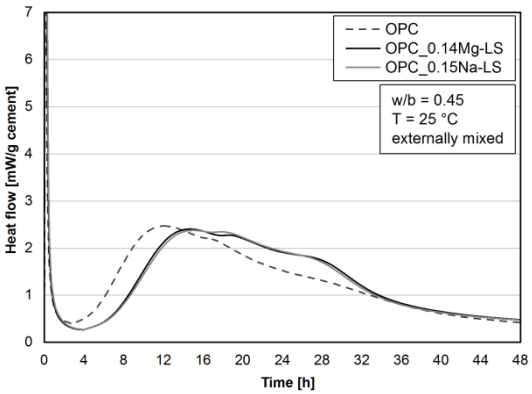

Fig. 5 – Heat flow of neat cement paste with and without LS

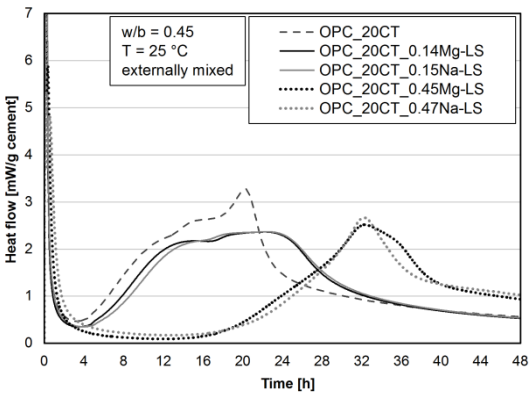

Fig. 6 – Heat flow of cement paste blended with calcined mixed-layer clay at different LS and dosages

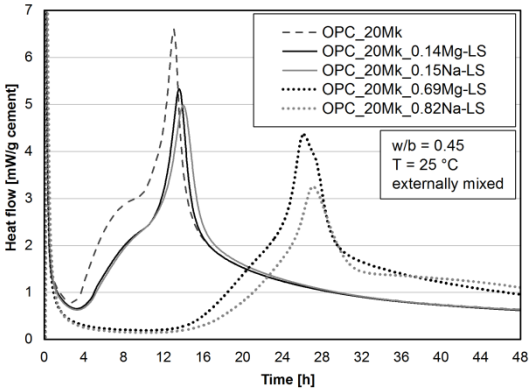

Fig. 7 – Heat flow of cement paste blended with metakaolin at different LS and dosages

Sposito et al.

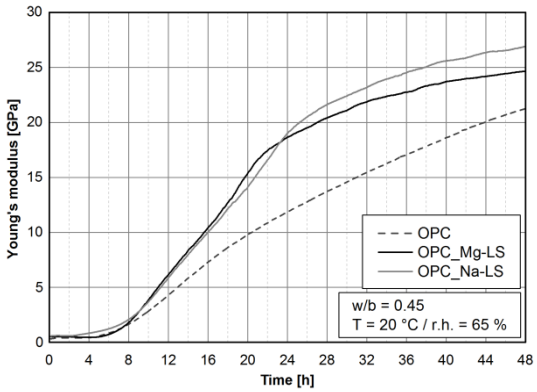

Fig. 8 – Development of Young's modulus for neat OPC mortar with quartz powder and different LS

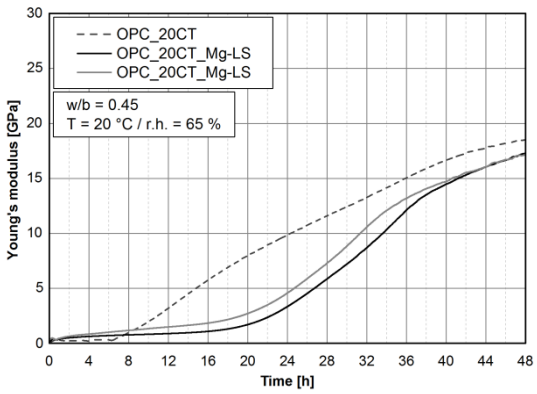

Fig. 9 – Development of Young's modulus for mortar blended with calcined mixed-layer clay and different LS

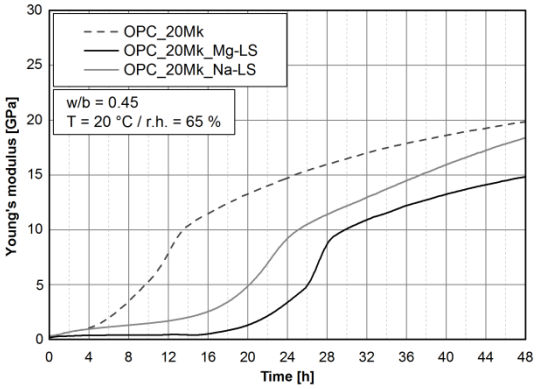

Fig. 10 – Development of Young's modulus for mortar blended with metakaolin and different LS

7.6 An approach to the rheological behavior of cementitious systems blended with calcined clays and superplasticizers

Conference paper [Reprint]

"An approach to the rheological behavior of cementitious systems blended with calcined clays and superplasticizers"

Ricarda Sposito, Marlene Schmid, Johann Plank, Karl-Christian Thienel

ACI SP 349: 11th International Conference on Cementitious Materials and Alternative Binders for Sustainable Concrete

held online, 7th – 10th June 2021, pp. 659 - 685

SP-349: 11th ACI/RILEM International Conference on Cementitious Materials and Alternative Binders for Sustainable Concrete

An Approach to the Rheological Behavior of Cementitious Systems Blended with Calcined Clays and Superplasticizers

Ricarda Sposito, Marlene Schmid, Johann Plank and Karl-Christian Thienel

Synopsis: Calcined clays represent a promising future supplementary cementitious material (SCM) because of the worldwide availability of suitable clays and low material-related CO_2 emissions during calcination. The application of superplasticizers is inevitable for a secured workability of cementitious systems with calcined clays due to their specific chemophysical properties. For their prospective use as SCM, a sound knowledge is elementary about the interaction of calcined clays with superplasticizers depending on clay and polymer structure. An ordinary Portland cement is replaced by 20 wt% of calcined clays. Four different calcined materials are used: one calcined clay mixture, industrial metakaolin, a metaillite and a metamuscovite. One polycondensate and one polycarboxylate-based polymer, both industrial products, are chosen as superplasticizers. The required dosages are adjusted by the same slump flow, so a similar dispersing behavior for all systems is given immediately after water addition. Over a period of two hours after water addition, the rheological behavior is evaluated via mini slump test and by rotational viscometer. The impact of different velocities during measurements with the viscometer provides further information related to the viscosity of these systems.

Keywords: calcined clays, superplasticizers, rheology, viscosity, workability

Biography: **Ricarda Sposito** is research associate at the Institute for Construction Materials, Bundeswehr University Munich, Germany. She received her B.Sc. in civil engineering from University of Applied Sciences Munich and her M.Sc. in civil engineering from Technical University of Munich (TUM), Germany. Her research interests include concrete technology, calcined clays and their interaction with superplasticizers.

Marlene Schmid is Ph.D. student at the Chair of Construction Chemistry at Technical University of Munich (TUM), Germany. She studied chemistry at TUM and received her B.Sc. and M.Sc. from there. Her research focuses on the synthesis and performance of novel superplasticizers for cements containing calcined clays as supplementary cementitious material.

Johann Plank is full professor at the Institute of Construction Chemistry of Technical University of Munich (TUM), Germany. He studied chemistry, acquired a Ph.D. degree at Regensburg University and then worked at SKW Trostberg AG in construction chemicals. Since 2001, he holds the Chair of Construction Chemistry at TUM. His research interests include cement chemistry, concrete admixtures, organic-inorganic composite and nano materials, colloid chemistry, concrete, dry-mix mortars, photo catalysis, oil well cementing and energy-saving materials.

ACI member **Karl-Christian Thienel** is professor and head of the Institute for Construction Materials, Bundeswehr University Munich, Germany. He received his diploma and Dr. degree in civil engineering from TU Braunschweig, Germany. He was Alexander-von-Humboldt “Feodor–Lynen” stipendiary at ACBM, Northwestern University, Evanston, IL, and head of R&D at Liapor GmbH & Co. KG. He is chairman of CEN/TC 177 and CEN/TC 154 SC5. His research interests include calcined clays, lightweight concrete and lightweight aggregate.

SP-349: 11th ACI/RILEM International Conference on Cementitious Materials and Alternative Binders for Sustainable Concrete

INTRODUCTION

Calcined clays as potential supplementary cementitious material (SCM) come strongly into focus of research [1-3]. Especially calcined clay mixtures with different phyllosilicates and further minerals are interesting as future SCM as they are available worldwide in sufficient quantities. The suitability of calcined clays as SCM is usually evaluated by their pozzolanic reactivity, e.g. in [2, 4-6]. For a look at the suitability in its entirety, the impact of calcined clays on the workability of cementitious systems needs to be considered as well. The influence on workability starts with the mineralogical composition of the raw clay. He et al. described already in 1995 that the water demand depends on type of clay mineral: montmorillonite > mica > non-expandable clays [7]. The specific surface area (SSA) [7, 8] and the water adsorption behavior [9] decrease due to a smaller contribution of interlayer surface area in the following order: montmorillonite > illite > kaolinite.

The calcination has further influence on the properties of calcined clays. The degree of dehydroxylation is often a parameter for the optimum calcination temperature of clays, which leads to significant changes in mineralogical and physical properties. Again, the type of clay mineral has main impact on mineralogical changes. Kaolinite, the best known 1:1 phyllosilicate, transforms to structural disordered (amorphous) metakaolin by dehydroxylation [10]. Illite and mica, both 2:1 phyllosilicates, keep a crystalline structure also after complete dehydroxylation [10, 11]. The dehydroxylation goes along with a decrease of SSA which is according to He et al. [11] due to the agglomeration of the particles and – at even higher temperatures – due to first sintering effects.

Less superplasticizer is needed with increasing calcination temperature due to the reduced SSA [12]. One reason is the reduced intercalation effect of polycarboxylate ether (PCE) superplasticizer into clay minerals [13-15] by the dehydroxylation of clay mineral interlayers. Furthermore, the surface charge of clays before and after calcination should be considered as main parameter for the adsorption of superplasticizers. Schmid et al. assume heterogeneous surface charges of calcined

clay mixtures due to their different components leading to good overall adsorption behavior of superplasticizers [16].

Current research focuses on three different types of clay mixtures: kaolinite-rich, kaolinite-poor and illitic clay mixtures [5, 6, 17-22]. However, in clay mixtures a complete dehydroxylation of all phyllosilicates is unrealistic [23, 24] as each phyllosilicate has a different ideal temperature for dehydroxylation, e.g. ~ 550 °C for kaolinite [25] and ~ 930 °C for illite [11]. The calcination temperature needs to be evaluated by the best possible degree of dehydroxylation, a high solubility of reactive aluminum and silicon ions but also by considering the increasing energy demand and costs of calcination at higher temperatures.

Cement paste blended with metakaolin exhibits both thixotropic and dilatant flow behavior where the dilatant behavior predominates with increased content of metakaolin and leads to a higher viscosity [26]. According to Vance et al. [27] a higher SSA but also the agglomeration potential, which leads to an increased water demand, of metakaolin are reasons for a reduced workability of blended mortar which is characterized by higher yield stress and plastic viscosity. Calcined muscovite (a common phyllosilicate in clay mixtures) leads to a shear-thickening behavior of cementitious systems which is more pronounced with increasing amount of superplasticizer and reduced at higher water/binder ratios due to less binder in suspension [28]. The addition of illitic calcined clay results also in a decreased workability due to loss of packing and increased SSA compared to pure cement systems [19].

Cementitious systems blended with metakaolin [29, 30] or calcined marl [31] are known for their higher superplasticizer demand compared to plain cement systems. Schmid et al. [16, 32, 33] investigated for the first time the interaction of various PCE-based superplasticizers with a calcined clay mixture. Anionic PCE polymers can adsorb on this calcined clay mixture due to its heterogeneous surface charge [32]. The investigations revealed an increasing amount of water needed for initial consistency (spread of 18 cm), however for an equal dispersion to a spread of

26 cm the dosage of amphoteric superplasticizers (polymers holding both anionic and cationic functionalities) is equal [16] or even lower [33] for systems with 20 wt% calcined clay mixture than for neat cement paste. When it comes to the type of calcined clay, systems with calcined kaolinitic clay require more superplasticizers than those with calcined 2:1 clay (montmorillonite) [34]. Ferreiro et al. explain this phenomenon by the adsorption behavior of superplasticizers into the amorphous structure of metakaolin, which prevents the superplasticizer from dispersing, whereas polymers can adsorb onto 2:1 clay particles and avoid the intercalation into their pseudo-laminar structure [34].

EXPERIMENTAL PROGRAM

Materials and nomenclature

An ordinary Portland cement (*C*) CEM I 42.5 R, complying with the European standard DIN EN 197-1 [35], is used. Its main mineralogical components are 61.6 wt% C_3S, 18.2 wt% C_2S, 5.8 wt% C_3A, 9.0 wt% C_4AF and 3.2 wt% sulfate carrier. An Amaltheen clay mixture (*TG*) originating from southern Germany is chosen. Its processing is described in detail in [21, 36]. It contains in its natural form different phyllosilicates (25 wt% kaolinite and 45 wt% 2:1 clay minerals, e.g. illite and muscovite) and 30 wt% inert components (e.g. quartz, feldspar, calcite, sulfates). For a better understanding of the individual impact of its components on the rheological behavior of cementitious systems, three calcined phyllosilicates are investigated: an industrially-used metakaolin (*Mk*), metaillite (*Mi*) and metamuscovite (*Mu*). The latter are calcined as powder in a laboratory muffle kiln at 770 °C (1418 °F) (Mi) and at 800 °C (1472 °F) (Mu). Muscovite is not a clay but for simplification all calcined materials are designated as “calcined clays” in the following text. Table 1 gives the chemical analysis of the calcined clays. Table 2 contains the physical parameters of all binder components. Water demand is determined according to DIN EN 196-3 [37] for cement and for blended systems with 20 wt% of calcined clays.

Two industrial superplasticizers are selected to investigate their dispersing effectiveness in calcined clay blended cementitious systems. As representative for polycondensates, the calcium salt of a *β*-naphthalene sulfonate formaldehyde polycondensate (*NSF*) with a solid content of 40.0 wt% is used. An *α*-methallyl-*ω*-methoxy poly(ethylene glycol) ether type PCE (*HPEG*) with a relatively long side chain (n_{EO} = 66) and high anionic charge density is investigated as representative for polycarboxylate-based superplasticizers of the newest generation. Its solid content is 50.0 wt%. The structural formulae of the superplasticizers are shown in Figure 1. Cement paste samples are designated as *C_substitution rate and type of calcined clay_dosage and type of superplasticizer.*

Methods

The flowability of cement paste is determined by "mini slump test" according to DIN EN 1015-3 [38] at a constant water-to-binder ratio of 0.50. The dosages of active agent in superplasticizers [% by weight of binder, %bwob] are adjusted to get a spread flow of 26 ± 0.5 cm (10.2 ± 0.2 in.) for cement pastes without and with 20 wt% calcined clay as SCM. This procedure permits a comparison of the dispersion effects of the two superplasticizers but also the influence of calcined clays.

Slump loss behavior is determined over a time of 120 minutes for the mix designs determined beforehand. For the time-dependent test, the homogenized binder (m_{binder} = 400 g (0.882 lb)) is added to differing amounts of stock solutions (based on distilled water with a constant w/b ratio of 0.50 including the necessary amount of superplasticizer). After stirring the blended paste manually for 60 seconds, a rest of 60 seconds and further stirring for another 120 seconds, the paste is filled into a Vicat cone (bottom diameter = 8 cm (3.15 in.)) on a slightly wetted glass plate. The cone is lifted and when the blended paste stops flowing, the spread is measured twice perpendicular to each other and averaged. This test takes place for the first time five minutes after water addition and is repeated after another ten minutes in intervals of 15 minutes. Between the measurements, the blended paste is stored in a covered vessel to prevent its drying-up and is mixed for another 60

seconds before repeating the slump test. For the evaluation of flowability, a slump flow of 26 cm (10.2 in.) is set as 100 % of flowability and the bottom diameter of Vicat cone as 0 % of flowability. For viscosity measurements, blended cement paste with $m_{binder} = 600$ g (1.323 lb) is mixed according to DIN EN 196-3 [37]. The time dependent torque, yield stress and viscosity of blended cement paste are measured with rotational viscometer Viskomat NT (Schleibinger, Germany) with a water-based circulatory cooling unit set at a temperature of 20 °C (68 °F) to prevent external temperature influences. The measurements start five minutes after water addition. For the torque development over time, a constant velocity of 80 revolutions per minute (rpm) is set.

To determine the relative viscosity and yield stress, another measurement with different velocities is conducted. The velocity starts at 120 rpm for ten minutes and slows down to 80 rpm → 40 rpm → 20 rpm for two minutes each. Rheological parameters are analyzed according to Bingham equation [39, 40]:

$$\mathbf{T = g + Nh}$$

With T torque ≈ shear stress τ

Relative yield stress (y-intercept of flow curve) g ≈ dynamic yield stress τ_0

Velocity N ≈ shear rate $\dot{\gamma}$

Relative viscosity (slope of flow curve) h ≈ viscosity η.

EXPERIMENTAL RESULTS AND DISCUSSION

Dispersing effectiveness of superplasticizers depending on binder system

Mini slump tests reveal that increased superplasticizer dosages are required for same dispersion effects when cement is replaced by calcined clays (Figure 2). The results show up that the PCE polymer (HPEG) is more effective than the polycondensate (NSF) in blended cementitious systems as already described in [29, 41, 42]. The dispersing with NSF requires at least twice as much polymer in systems with calcined clays compared to pure cement system (0.21 %bwob NSF). The

most critical systems are C_20Mi with 0.95 %bwob NSF and C_20Mu with even 1.50 %bwob NSF required for a spread flow of 26 cm (10.2 in.). When HPEG PCE is used as superplasticizer, again C_20Mi has high demand of the polymer (0.37 %bwob). C_20Mu reveals a significantly better compatibility and requires 0.16 %bwob HPEG only. This dosage is even less than for the system C_20Mk (0.19 %bwob). Nonetheless, the dispersion of C_20Mu by NSF and by HPEG is subject to strong fluctuations leading to a broader span of spread when using the same amount of superplasticizer (results of three repeatings are shown in Figure 2). Furthermore, the applicability of mini slump test for systems with metamuscovite should be reconsidered as they reveal thixotropic behavior as already described by Schmid et al. in [28]. C_20TG needs only marginally higher dosage of HPEG (Δ 0.02 %bwob) compared to reference. Although the clay mixture contains ~ 11 wt% illite and 30 wt% muscovite in its raw form [32], the binder system with calcined clay mixture is easily to disperse which might be due to high quartz content (16.2 wt%) present in TG. According to Kameda & Morisaki [43], an increased quartz content can lead to lower viscosity and yield stress of clay-quartz suspensions. TG exhibits furthermore the lowest specific surface area (SSA) and water demand of calcined clays investigated (Table 2).

For a better understanding of the dosage of superplasticizer required for an adequate dispersion, it is necessary to take also a closer look on the physical parameters of the investigated binder systems. According to Sakai et al. [44] and Yamada [45], the SSA of cement particles is an indicator – although not the only one – for the demand of superplasticizer. As already mentioned, another important parameter for workability is the water demand of binders [46]. The total surface area (TSA), determined as product of density and SSA by Bentz et al. [47], and the combined water demand of the binder are shown in Figure 3. The values are calculated from the individual parameters of cement and of calcined clay according to their mass fraction in binder systems (100 wt% cement or 80 wt% cement and 20 wt% calcined clay).

There is a certain correlation between the TSA and the dosages determined with HPEG. This can explain especially the low dosage of HPEG needed for C_20Mu (0.16 %bwob) with TSA_{Mu} = 7.9 m²/cm³ and the high dosage of HPEG required for C_20Mi (0.37 %bwob) as Mi has a TSA of 54 m²/cm³. The high TSA of Mi again results on the one hand from its mineralogical composition, as also described by Herrmann and Rickert [48] but also from high grinding fineness (Table 2) which is subject of further research. For systems with NSF, there also seems to exist a certain correlation even though C_20Mu requires the highest dosage of NSF (1.50 %bwob) despite its relatively low combined TSA. On the other hand, it is not surprising that C_20Mu requires this amount of NSF respecting its high combined water demand (34.2 wt%) as water adsorbed by calcined clays needs to be compensated by the addition of more superplasticizer. All in all, a good correlation can be observed between combined water demand of different binder systems and required dosages of NSF and HPEG as already described for lignosulfonates in calcined clay blended systems [49]. The type of polymer is especially decisive in case of C_Mu systems as they are incompatible with NSF polycondensate but show very good performance in combination with HPEG PCE despite the high water demand of Mu.

Time dependent flow behavior of cementitious systems with calcined clays

The systems with calcined phyllosilicates C_Mk, C_Mu and C_Mi exhibit no flowability at all as long as no superplasticizer is added. Hence, there are no mini slump tests on reference systems over time. The flowability of blended cement paste can be an adequate indicator for the workability of concretes. When NSF polycondensate is used, flowability of C_0.21NSF declines during the first 45 minutes after water addition and stays constant until 120 minutes (Figure 4) whereas C_0.05HPEG has a slow and constant decrease of flowability during the whole 120 minutes (Figure 5). The systems with calcined phyllosilicates behave differently with superplasticizers: C_20Mk and C_20Mi loose significantly their flowability during the first 120 minutes. The effect is less pronounced for C_20Mk_0.68NSF (Figure 4) than for C_20Mk_0.19HPEG (Figure 5) and similar

for both C_20Mi systems. C_20Mi reveals 10 % (with 0.95 %bwob NSF) and 20 % (with 0.37 %bwob HPEG) remaining flowability after only 75 minutes. The fast stiffening process of C_20Mi can again be due to the high fineness of Mi (d_{50} = 6.8 µm ($0.27*10^{-3}$ in.)) and its high SSA and a resulting filler/nucleation effect for first hydrate products, as known e.g. for limestone but also for calcined clays [50, 51]. Flowability of C_20Mu slightly increases with the addition of 1.50 %bwob NSF (Figure 4). This holds also for the blended paste made with 0.16 %bwob HPEG (Figure 5). C_20TG exhibits with both the addition of NSF (Figure 4) and HPEG (Figure 5) only a slow decrease of flowability and a similar flow behavior as pure cement system.

The findings of time dependent mini slump tests are consistent with rheological measurements over time. Viscosity of C_20Mk increases linearly with the addition of NSF and HPEG. In the beginning, the torque is lower and increases slower for C_20Mk_0.68NSF (Figure 6) than for C_20Mk_0.19HPEG (Figure 7) and stays < 20 Nmm (0.18 lbf*in.) until minute 120. C_20TG_0.40NSF has the same torque as C_20Mk_0.68NSF for the first 45 minutes and remains lower afterwards for the rest of the measurement. C_20TG_0.07HPEG shows up a similar viscosity behavior as C_20TG_0.40NSF. C_20Mi yields constant torque for 45 minutes with 0.95 %bwob NSF (Figure 6) and for 35 minutes with 0.37 %bwob HPEG (Figure 7). After this period, C_20Mi_0.95NSF exhibits a linear increase of torque resulting in the highest torque of all NSF systems after 90 minutes (Figure 6). C_20Mi_0.37HPEG shows up an asymptotic increase of torque, which is also the highest of all HPEG systems after ~ 80 minutes. These moments fit well with loss of flowability measured by time dependent mini slump tests (Figure 4 and Figure 5). C_20Mu systems reveal opposite torque behavior: high torques are observed at the beginning of the measurements, both with NSF and HPEG, which decrease rapidly during the first 15 minutes and keep asymptotically decreasing until the end of the measurements (Figure 6 and Figure 7). This agrees with the gain in flowability of C_20Mu_1.50NSF (Figure 4) and C_20Mu_0.16HPEG

(Figure 5) and thixotropic behavior, that had been already observed for metamuscovite in [28], over time [52].

The flowability of systems with calcined clays tends to decrease faster with the addition of HPEG compared to NSF while the opposite is observed and known from literature for pure cement systems [53, 54]. Until now, there is no reasonable explanation on this phenomenon and the findings need to be expanded with further superplasticizers. However, the results fit well with observations on hydration kinetics where NSF has a more pronounced retarding effect compared to HPEG [55]. Physical parameters of the calcined clays seem to dominate the flow behavior and should be considered not only when it comes to the demand of superplasticizer but also regarding to the required workability periods for placing concrete.

Influence of calcined clays and superplasticizers on the viscosity of blended cement pastes

The systems without superplasticizer reveal at w/b ratio of 0.50 the following classification regarding their yield stresses: C_20Mu ≫ C_20Mk > C_20Mi ≫ C_20TG > C [56]. The use of calcined clays increase yield stress whereby the influence of Mu is significant and the impact of TG the least. Reference system C and C_20TG exhibit flow behavior of Bingham fluids with linear shear rates [40] and C_20Mk and C_20Mi are classified as fluids according to the Herschel-Bulkley model with non-linear shear rates. Due to high initial torque (> 500 Nmm) (4.43 lbf*in.), it is not even possible to measure the system C_20Mu. According to Moulin et al. [46], the high water demand of metakaolin is one reason for an increased yield stress. Further possible reasons could be a higher volume of binder at same mass due to the lower density compared to cement [57], its higher specific surface area [27] and an increased tendency to flocculation of metakaolin particles which might lead to thixotropic behavior [46]. These findings can be transferred to the systems with the other calcined clays investigated. The higher density of Mi compared to Mk (Table 2) might be the reason why C_20Mi has lower yield stress than C_20Mk despite the higher water demand and SSA of Mi. The interparticular interactions of binders i.e. van der Waals forces and repulsive

double layer forces (indicated by zeta potential) are also commonly known to influence the rheology of cementitious systems [58, 59]. So far, zeta potential of calcined clays was hardly considered when it comes to the understanding of their rheological behavior while there are several findings on the zeta potential of calcined clay blended systems with superplasticizers [16, 32, 48].

The addition of superplasticizer reduced the shear stress significantly and in both cases, with NSF (Figure 8) as well as with HPEG (Figure 9), torques of blended cement pastes are < 20 Nmm (0.18 lbf*in.) apart from C_20Mu systems. This is not surprising since all systems investigated here have been adjusted to similar dispersion by mini slump test (Figure 2). Pure cement system C_0.05HPEG shows rheological characteristics of a Newtonian fluid with relative yield stress close to 0 and linear relation between shear rate and shear stress ($R^2 \sim 1$). C_0.21NSF remains a Bingham fluid as its relative yield stress was > 1 and R^2 value is also ~ 1 (Table 3). C_20Mk and C_20Mi become both with the addition of NSF and HPEG also Bingham fluids. C_20TG reveals slightly negative yield stress with the addition of superplasticizers (Table 3) which means that C_20TG has self-flowing properties when fluidized by superplasticizers and is classified as Newtonian fluid [40]. Again, C_20Mu systems show up a particular behavior: Adding superplasticizers can reduce the viscosity at least to such an extent that rheological measurements become possible at all. Nonetheless, the median torques increase significantly to up to 205 Nmm (1.81 lbf*in.) at 120 rpm with 1.50 %bwob NSF (Figure 8) and less pronounced (107 Nmm, 0.95 lbf*in.) with 0.16 %bwob HPEG (Figure 9). This agrees with the time dependent rheological measurements of C_20Mu systems in Figure 6 and Figure 7 on the one hand and fluctuating slump values with same superplasticizer dosages on the other hand (Figure 2). While the addition of different superplasticizers has no significant impact on the rheology of the other calcined clay blended systems, C_20Mu is more sensitive against the type of superplasticizer. Both C_20Mu systems with NSF and HPEG exhibit negative yield stresses (Table 3). C_20Mu_1.50NSF exhibits Newtonian fluid behavior ($R^2 \sim 1$) while C_20Mu_0.16HPEG reveals shear-thickening properties ($R^2 \ll 1$).

The latter findings are consistent with observations that lower w/b ratios and the addition of a MPEG PCE with long side-chain (Figure 1) lead to shear-thickening behavior of cementitious systems with metamuscovite [28]. As the investigated HPEG polymer has also a quite long side-chain, the assumption of the authors [28] that the more pronounced steric effect promotes shear-thickening behavior of metamuscovite systems can be demonstrated again.

SUMMARY AND CONCLUSIONS

- Cementitious systems blended with calcined clays require more superplasticizer than pure cement systems to achieve the same workability. Investigations could prove higher effectiveness of HPEG PCE compared to polycondensate NSF. Especially cementitious systems with metamuscovite seem to be incompatible with NSF while dispersion is good with HPEG PCE.
- Systems with metaillite demand for high amounts of superplasticizers due to high grinding fineness and specific surface area. Further measurements on the same calcined phyllosilicate yet with different physical parameters will be executed to investigate this influence on dispersion. The calcined clay mixture reveals the lowest demand for superplasticizer due to its physical properties similar to cement and heterogeneous surface charge making it even more attractive for concrete technology.
- Slump loss of blended systems is slightly accelerated for HPEG PCE compared to NSF. This is contrary to observations with pure cement systems that usually exhibit longer workability frames with PCE than with polycondensates. These findings need to be examined with further polymers.
- Additionally interparticular interactions need to be considered in further investigations to understand the rheology of cementitious systems with calcined clays. Systems with calcined phyllosilicates tend to exhibit thixotropic / shear-thickening behavior. These effects are not

observed for the calcined clay mixture investigated which might be due to its high quartz content.

ACKNOWLEDGMENTS

The authors like to thank Schwenk Zement KG (Germany) for providing the cements and Liapor GmbH & Co. KG (Germany) for the supply of calcined clay mixture. They also thank Bozzetto Group (Italy) and Jilin Zhongxin Chemical Group Co., Ltd. (China) for providing the superplasticizers. Furthermore, the authors wish to express their deepest gratitude to Deutsche Forschungsgemeinschaft (DFG) for the financial support of the research project “Ecological and energetic optimization of concrete: Interaction of structurally divergent superplasticizers with calcined clays” (PL 472/11-1 and TH 1383/3-1).

REFERENCES

1. Beuntner, N., „Zur Eignung und Wirkungsweise calcinierter Tone als reaktive Bindemittelkomponente in Zement,“ Fakultät für Bauingenieurwesen und Umweltwissenschaften, Universität der Bundeswehr München, Neubiberg, 2017, 207 pp.
2. Tironi, A., Trezza, M.A., Scian, A.N., and Irassar, E.F., „Potential use of Argentine kaolinitic clays as pozzolanic material“, *Applied Clay Science*, V. 101, 2014, pp. 468-476.
3. Antoni, M., „Investigation of cement substitution by blends of calcined clays and limestone,“ Faculté des Sciences et Techniques de L'ingénieur, École Polytechnique Fédérale de Lausanne, Lausanne, 2013, 254 pp.
4. Avet, F., Snellings, R., Alujas Diaz, A., Ben Haha, M., and Scrivener, K., „Development of a new rapid, relevant and reliable (R3) test method to evaluate the pozzolanic reactivity of calcined kaolinitic clays“, *Cement and Concrete Research*, V. 85, 2016, pp. 1-11.
5. Schulze, S.E., and Rickert, J., „Suitability of natural calcined clays as supplementary cementitious material“, *Cement and Concrete Composites*, V. 95, 2019, pp. 92-97.

6. Lemma, R., Castellano, C.C., Bonavetti, V., Trezza, M.A., Rahhal, V.F., and Irassar, E.F., „Thermal Transformation of Illitic-Chlorite Clay and Its Pozzolanic Activity“, in *Calcined Clays for Sustainable Concrete - Proceedings of the 2nd International Conference on Calcined Clays for Sustainable Concrete*, Martirena, F., Favier, A., and Scrivener, K., Editors. Springer Nature, La Havanna, Cuba, 2018, pp. 266-272.
7. He, C., Øsbæck, B., and Makovicky, E., „Pozzolanic reactions of six principal clay minerals: Activation, reactivity assessments and technological effects“, *Cement and Concrete Research*, V. 25, No. 8, 1995, pp. 1691-1702.
8. Mitchell, J.K., and Soga, K., Fundamentals of Soil Behavior. 3 ed., 2005, 592 pp.
9. Hatch, C.D., Wiese, J.S., Crane, C.C., Harris, K.J., Kloss, H.G., and Baltrusaitis, J., „Water Adsorption on Clay Minerals As a Function of Relative Humidity: Application of BET and Freundlich Adsorption Models“, *Langmuir*, V. 28, 2011, pp. 1790-1803.
10. Fernandez, R., Martirena, F., and Scrivener, K.L., „The origin of the pozzolanic activity of calcined clay minerals: a comparison between kaolinite, illite and montmorillonite“, *Cement and Concrete Research*, V. 41, No. 1, 2011, pp. 113-122.
11. He, C., Makovicky, E., and Øsbæck, B., „Thermal stability and pozzolanic activity of calcined illite“, *Applied Clay Science*, V. 9, No. 5, 1995, pp. 337-354.
12. VDZ, „Calcined clay as a pozzolanic cement constituent“, *Cement International*, V. 14, No. 1, 2016, pp. 21.
13. Ng, S., and Plank, J., „Effect of Side Chain Length of Methacrylate Ester (MPEG) – Based PCE Superplasticizers on Their Interactions with Na-montmorillonite Clay“, in *18. Internationale Baustofftagung ibausil*, F. A. Finger - Institut für Baustoffkunde der Bauhaus-Universität Weimar, Weimar, 2012, 8 pp.
14. Ng, S., and Plank, J., „Study on the Interaction of Na-montmorillonite Clay with Polycarboxylates“, in *ACI SP 288 - 10th International Conference on Superplasticizers and*

other Chemical Admixtures, Malhotra, V.M., Editor, American Concrete Institute, Prague, Czech Republic, 2012, 407-421 pp.

15. Ng, S., and Plank, J., „Interaction mechanisms between Na montmorillonite clay and MPEG-based polycarboxylate superplasticizers“, *Cement and Concrete Research*, V. 42, No. 6, 2012, pp. 847-854.
16. Schmid, M., Beuntner, N., Thienel, K.-C., and Plank, J., „Amphoteric superplasticizers for Cements Blended with a Calcined Clay“, in *ACI SP 329 - 12th International Conference on Superplasticizers and Other Chemical Admixtures in Concrete*, Liu, J., and Plank, J., Editors, American Concrete Institute, Beijing, China, 2018, 41-54 pp.
17. Lemma, R., Irassar, E.F., and Rahhal, V., „Calcined Illitic Clays as Portland Cement Replacements“, in *Calcined Clays for Sustainable Concrete - Proceedings of the 1st International Conference on Calcined Clays for Sustainable Concrete*, Scrivener, K., and Favier, A., Editors. Springer Netherlands, Dordrecht, 2015, pp. 269-276.
18. Cordoba, G., Rossetti, A., Falcone, D., and Irassar, E.F., „Sulfate and Alkali-Silica Performance of Blended Cements Containing Illitic Calcined Clays“, in *Calcined Clays for Sustainable Concrete - Proceedings of the 2nd International Conference on Calcined Clays for Sustainable Concrete*, Martirena, F., Favier, A., and Scrivener, K., Editors. Springer Nature, La Havanna, Cuba, 2018, pp. 117-123.
19. Marchetti, G., Pokorny, J., Tironi, A., Trezza, M.A., Rahhal, V.F., Pavlík, Z., Černý, R., and Irassar, E.F., „Blended Cements with Calcined Illitic Clay: Workability and Hydration“, in *Calcined Clays for Sustainable Concrete - Proceedings of the 2nd International Conference on Calcined Clays for Sustainable Concrete*, Martirena, F., Favier, A., and Scrivener, K., Editors. Springer Nature, La Havanna, Cuba, 2018, pp. 311-317.
20. Tironi, A., Trezza, M.A., Scian, A.N., and Irassar, E.F., „Assessment of pozzolanic activity of different calcined clays“, *Cement and Concrete Composites*, V. 37, 2013, pp. 319-327.

21. Beuntner, N., and Thienel, K.-C., „Properties of Calcined Lias Delta Clay - Technological Effects, Physical Characteristics and Reactivity in Cement“, in *Calcined Clays for Sustainable Concrete - Proceedings of the 1st International Conference on Calcined Clays for Sustainable Concrete*, Scrivener, K., and Favier, A., Editors. Springer Netherlands, Lausanne, 2015, pp. 43-50.

22. Alujas, A., Fernández, R., Quintana, R., Scrivener, K.L., and Martirena, F., „Pozzolanic reactivity of low grade kaolinitic clays: influence of calcination temperature and impact of calcination products on OPC hydration“, *Applied Clay Science*, V. 108, 2015, pp. 94-101.

23. Beuntner, N., „Leistungsfähigkeit großtechnisch calcinierter Tone und deren Wirksamkeit in zementären Systemen“, in *Innovationen in Beton - 1. DAfStb-Jahrestagung mit 54. Forschungskolloquium*, Breitenbücher, R., and Mark, P., Editors, Deutscher Ausschuss für Stahlbeton, Bochum, 2013, 239-244 pp.

24. Scherb, S., Beuntner, N., and Thienel, K.-C., „Reaction kinetics of the basic clays present in natural mixed clays“, in *Calcined Clays for Sustainable Concrete - Proceedings of the 2nd International Conference on Calcined Clays for Sustainable Concrete*, Martirena, F., Favier, A., and Scrivener, K., Editors. Springer Nature, La Havanna, Cuba, 2018, pp. 427-433.

25. He, C., Makovicky, E., and Osbæck, B., „Thermal stability and pozzolanic activity of calcined kaolin“, *Applied Clay Science*, V. 9, No. 3, 1994, pp. 165-187.

26. Curcio, F., and DeAngelis, B.A., „Dilatant behavior of superplasticized cement pastes containing metakaolin“, *Cement and Concrete Research*, V. 28, No. 5, 1998, pp. 629-634.

27. Vance, K., Kumar, A., Sant, G., and Neithalath, N., „The rheological properties of ternary binders containing Portland cement, limestone, and metakaolin or fly ash“, *Cement and Concrete Research*, V. 52, 2013, pp. 196-207.

28. Schmid, M., Sposito, R., Thienel, K.-C., and Plank, J., „The shear-thickening effect of meta muscovite as SCM and its influence on the rheological properties of ecologically optimized

cementitious systems“, in *2nd International RILEM Conference on Rheology and Processing of Construction Materials (RheoCon2)*, Mechtcherine, V., Editor, Dresden, 2019 pp.

29. Zaribaf, B.H., and Kurtis, K.E., „Admixture compatibility in metakaolin–portland-limestone cement blends“, *Materials and Structures*, V. 51, No. 1, 2018, pp. 13.
30. Zaribaf, B.H., Uzal, B., and Kurtis, K., „Compatibility of superplasticizers with limestone-metakaolin blended cementitious system“, in *Calcined Clays for Sustainable Concrete - Proceedings of the 1st International Conference on Calcined Clays for Sustainable Concrete*, Scrivener, K., and Favier, A., Editors. Springer, 2015, pp. 427-434.
31. Ng, S., and Justnes, H., „Influence of dispersing agents on the rheology and early heat of hydration of blended cements with high loading of calcined marl“, *Cement and Concrete Composites*, V. 60, 2015, pp. 123-134.
32. Schmid, M., Beuntner, N., Thienel, K.-C., and Plank, J., „Colloid-chemical investigation of the interaction between PCE superplasticizers and a calcined mixed layer clay“, in *Calcined Clays for Sustainable Concrete - Proceedings of the 2nd International Conference on Calcined Clays for Sustainable Concrete*, Martirena, F., Favier, A., and Scrivener, K., Editors. Springer, La Havanna, Cuba, 2018, pp. 434-439.
33. Schmid, M., Sposito, R., Thienel, K.-C., and Plank, J., „Novel Zwitterionic Superplasticizers for Cements Blended with Calcined Clays“, in *20. Internationale Baustofftagung ibausil*, Fischer, H.-B., and Volke, A., Editors. F.A. Finger-Institut für Baustoffkunde der Bauhaus-Universität Weimar, Weimar, 2018, pp. 842-849.
34. Ferreiro, S., Herfort, D., and Damtoft, J.S., „Effect of raw clay type, fineness, water-to-cement ratio and fly ash addition on workability and strength performance of calcined clay – Limestone Portland cements“, *Cement and Concrete Research*, V. 101, 2017, pp. 1-12.

35. DIN EN 197-1, „Zement - Teil 1: Zusammensetzung, Anforderungen und Konformitätskriterien von Normalzement (Cement - Part 1: Composition, specifications and conformity criteria for common cements)“, 2011, 8 pp.

36. Gmür, R., Thienel, K.-C., and Beuntner, N., „Influence of aging conditions upon the properties of calcined clay and its performance as supplementary cementitious material“, *Cement and Concrete Composites*, V. 72, 2016, pp. 114-124.

37. DIN EN 196-3, „Prüfverfahren für Zement - Teil 3: Bestimmung der Erstarrungszeiten und der Raumbeständigkeit (Methods of testing cement - Part 3: Determination of setting times and soundness)“, 2009 pp.

38. DIN EN 1015-3, „Prüfverfahren für Mörtel für Mauerwerk-Teil 3: Bestimmung der Konsistenz von Frischmörtel (mit Ausbreittisch) (Methods of test for mortar for masonry - Part 3: Determination of consistence of fresh mortar (by flow table))“, 2007 pp.

39. Hackley, V.A., and Ferraris, C.F., „Guide to Rheological Nomenclature - Measurements in Ceramic Particulate Systems“, 2001, III, 29 pp.

40. Barnes, H.A., and Walters, K., „The yield stress myth?“, *Rheologica Acta*, V. 24, No. 4, 1985, pp. 323-326.

41. Ng, S., and Justnes, H., „Rheology of blended cements with superplasticizers“, Concrete Innovation Centre (COIN), Trondheim, 2015, 55 pp.

42. Burgos-Montes, O., Palacios, M., Rivilla, P., and Puertas, F., „Compatibility between superplasticizer admixtures and cements with mineral additions“, *Construction and Building Materials*, V. 31, No. Supplement C, 2012, pp. 300-309.

43. Kameda, J., and Morisaki, T., „Sensitivity of Clay Suspension Rheological Properties to pH, Temperature, Salinity, and Smectite-Quartz Ratio“, *Geophysical Research Letters*, V. 44, No. 19, 2017, pp. 9615-9621.

44. Sakai, E., Yamada, K., and Ohta, A., „Molecular Structure and Dispersion-Adsorption Mechanisms of Comb-Type Superplasticizers Used in Japan“, *Journal of Advanced Concrete Technology*, V. 1, No. 1, 2003, pp. 16-25.

45. Yamada, K., „Basics of analytical methods used for the investigation of interaction mechanism between cements and superplasticizers“, *Cement and Concrete Research*, V. 41, No. 7, 2011, pp. 793-798.

46. Moulin, E., Blanc, P., and Sorrentino, D., „Influence of key cement chemical parameters on the properties of metakaolin blended cements“, *Cement and Concrete Composites*, V. 23, 2001, pp. 463-469.

47. Bentz, D.P., Ferraris, C.F., Galler, M.A., Hansen, A.S., and Guynn, J.M., „Influence of particle size distributions on yield stress and viscosity of cement–fly ash pastes“, *Cement and Concrete Research*, V. 42, No. 2, 2012, pp. 404-409.

48. Herrmann, J., and Rickert, J., „Interactions between cements with calcined clay and superplasticizers“, in *ACI SP 302 - 11th International Conference on Superplasticizers and Other Chemical Admixtures in Concrete*, Malhotra, V.M., Gupta, P.R., and Holland, T.C., Editors. American Concrete Institute, Ottawa, Canada, 2015, pp. 299-314.

49. Sposito, R., Dürr, I., and Thienel, K.-C., „Lignosulfonates in cementitious systems blended with calcined clays“, in *ACI SP 326 - 2nd International Workshop on Durability and Sustainability of Concrete Structures*, Falikman, V., et al., Editors, Sheridan Books, Moscow, Russia, 2018, 10.1-10.10 pp.

50. Oey, T., Kumar, A., Bullard, J.W., Neithalath, N., and Sant, G., „The Filler Effect: The Influence of Filler Content and Surface Area on Cementitious Reaction Rates“, *Journal of the American Ceramic Society*, V. 96, No. 6, 2013, pp. 1978-1990.

51. Wild, S., Khatib, J.M., and Jones, A., „Relative strength, pozzolanic activity and cement hydration in superplasticised metakaolin concrete“, *Cement and Concrete Research*, V. 26, No. 10, 1996, pp. 1537-1544.

52. Rubio-Hernández, F.J., Velázquez-Navarro, J.F., and Galindo-Rosales, F.J., „Rheological characterization of a time dependent fresh cement paste“, *Mechanics of Time-Dependent Materials*, V. 13, No. 2, 2009, pp. 199-206.

53. Chandra, S., and Björnström, J., „Influence of superplasticizer type and dosage on the slump loss of Portland cement mortars—Part II“, *Cement and Concrete Research*, V. 32, No. 10, 2002, pp. 1613-1619.

54. Collepardi, M., and Valente, M., „Recent Developments in Superplasticizers“, in *ACI SP 239 - 8th International Conference on Superplasticizers and other Chemical Admixtures in Concrete*, Malhotra, V.M., Editor. Sheridan Books, Sorrento, Italy, 2006, pp. 1-14.

55. Sposito, R., Schmid, M., Beuntner, N., Scherb, S., Plank, J., and Thienel, K.-C., „Early hydration behavior of blended cementitious systems containing calcined clays and superplasticizer“, in *15th International Congress on the Chemistry of Cement*, Peřka, L., and Gemrich, J., Editors, Prague, Czech Republic, 2019, 10 pp.

56. Sposito, R., Beuntner, N., Thienel, K.-C., Schmid, M., and Plank, J., „Calcinierte Tone als innovativer Zementersatzstoff und ihre Wechselwirkungen mit Fließmitteln in Zementleim“, in *4. Grazer Betonkolloquium*, Tue, Nguyen V., Editor. Tue, Nguyen Viet, Graz, 2018, pp. 185-192.

57. Irassar, E.F., Rahhal, V., Pedrajas, C., and Talero, R., „Rheology of portland cement pastes with calcined clays additions“, in *Cleantech 2014*. CTSI Clean Technologies and Sustainable Industries Organization, Washington, DC, 2014, pp. 308-311.

58. Lowke, D., „Interparticle Forces and Rheology of Cement Based Suspensions“, in *3rd International Symposium on Nanotechnology in Construction (NICOM3)*, Bittnar, Z., et al., Editors. Springer Berlin Heidelberg, Prague, Czech Republic, 2009, pp. 295-301.

59. Haist, M., „Zur Rheologie und den physikalischen Wechselwirkungen bei Zementsuspensionen,“ Fakultät für Bauingenieur-, Geo- und Umweltwissenschaften, Universität Karlsruhe (TH), Karlsruhe, 2010, 205 pp.

TABLES AND FIGURES

Table 1- Chemical analysis of calcined clays

Oxides / Parameters	Mk	Mu	Mi	TG
SiO_2, wt%	54.6	47.5	49.5	53.2
Al_2O_3, wt%	40.1	32.8	21.3	22.2
CaO, wt%	< 0.1	0.2	6.9	6.5
Fe_2O_3, wt%	1.8	5.1	6.6	8.0
MgO, wt%	0.2	0.1	2.9	2.7
SO_3, wt%	0.1	0.1	0.1	2.0
TiO_2, wt%	1.4	0.8	0.7	1.0
Na_2O, wt%	0.3	0.6	0.3	0.4
K_2O, wt%	0.3	12.1	6.3	3.3
Na_2O_{equ}	0.50	8.56	4.44	2.57
Soluble Al-ions in alkaline solution after 20 h, wt%	14.25	0.26	1.55	1.09
Soluble Si-ions in alkaline solution after 20 h, wt%	15.65	0.51	4.02	1.80

Table 2- Physical parameters of test materials

Parameters	C	Mk	Mu	Mi	TG
Particle density, g/cm³ (lb/in³)	3.17 (0.113)	2.61 (0.094)	2.79 (0.101)	2.72 (0.098)	2.63 (0.095)
BET SSA, m²/g (in²/lb)	1.0 (703,070)	17.8 (12,514,742)	11.8 (8,296,221)	94.6 (66,510,000)	3.9 (2,750,000)
Water demand, wt%	28.9	34.5	55.4	38.6	30.5
d_{10}, µm (in.)	4.1 ($0.16*10^{-3}$)	3.0 ($0.12*10^{-3}$)	9.3 ($0.37*10^{-3}$)	2.7 ($0.11*10^{-3}$)	4.0 ($0.16*10^{-3}$)
d_{50}, µm (in.)	15.8 ($0.62*10^{-3}$)	14.8 ($0.58*10^{-3}$)	19.2 ($0.76*10^{-3}$)	6.8 ($0.27*10^{-3}$)	13.2 ($0.52*10^{-3}$)
d_{90}, µm (in.)	46.0 ($1.81*10^{-3}$)	76.2 ($3.00*10^{-3}$)	45.7 ($1.80*10^{-3}$)	61.9 ($2.44*10^{-3}$)	37.0 ($1.46*10^{-3}$)

Table 3-Viscosity parameters of blended cement pastes with superplasticizers: relative viscosity, relative yield stress and R^2

Systems	Relative viscosity, Nmm*min (lbf*in.*min)	Relative yield stress, Nmm (lbf*in.)	R^2 [-]
C_0.21NSF	0.05 ($0.42*10^{-3}$)	4.64 ($41.10*10^{-3}$)	0.98
C_0.05HPEG	0.05 ($0.47*10^{-3}$)	0.14 ($1.28*10^{-3}$)	0.99
C_20Mk_0.68NSF	0.05 ($0.43*10^{-3}$)	1.52 ($13.45*10^{-3}$)	0.99
C_20Mk_0.19HPEG	0.07 ($0.60*10^{-3}$)	5.88 ($52.04*10^{-3}$)	0.99
C_20Mu_1.50NSF	1.76 ($15.60*10^{-3}$)	-7.76 ($-68.68*10^{-3}$)	0.95
C_20Mu_0.16HPEG	1.09 ($9.68*10^{-3}$)	-26.52 ($-234.73*10^{-3}$)	0.72
C_20Mi_0.95NSF	0.12 ($1.10*10^{-3}$)	1.54 ($13.66*10^{-3}$)	0.99
C_20Mi_0.37HPEG	0.13 ($1.18*10^{-3}$)	0.82 ($7.28*10^{-3}$)	0.94
C_20TG_0.40NSF	0.07 ($0.62*10^{-3}$)	-0.13 ($-1.15*10^{-3}$)	1.00
C_20TG_0.07HPEG	0.09 ($0.76*10^{-3}$)	-0.34 ($-3.01*10^{-3}$)	0.99

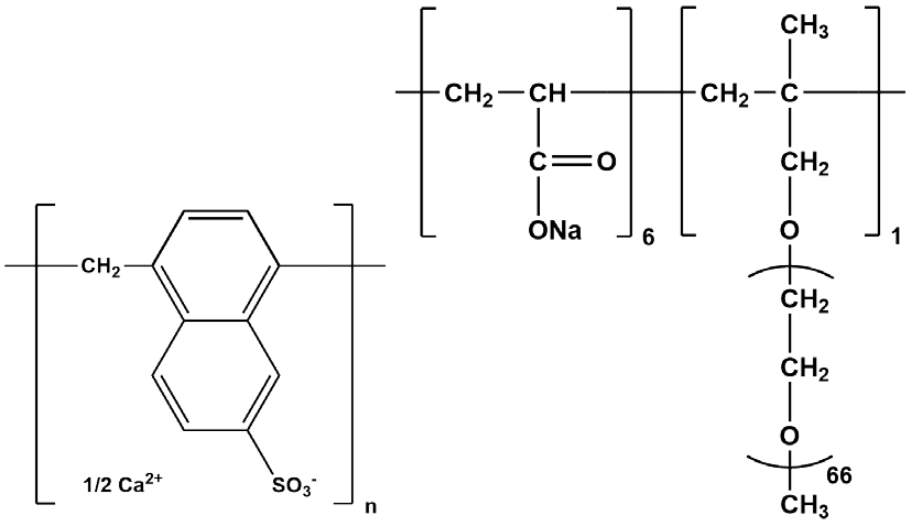

Figure 1-Structural formulae of investigated polycondensate polymer NSF (left) and polycarboxylate-based polymer HPEG (right)

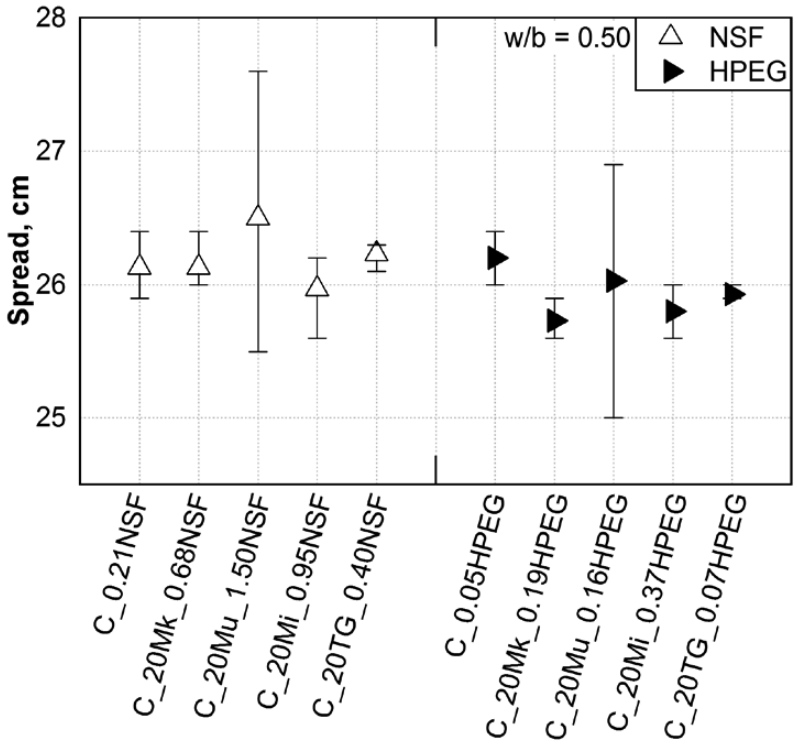

Figure 2-Spread of blended systems with adjusted dosage of superplasticizer (1 cm = 0.39 in.)

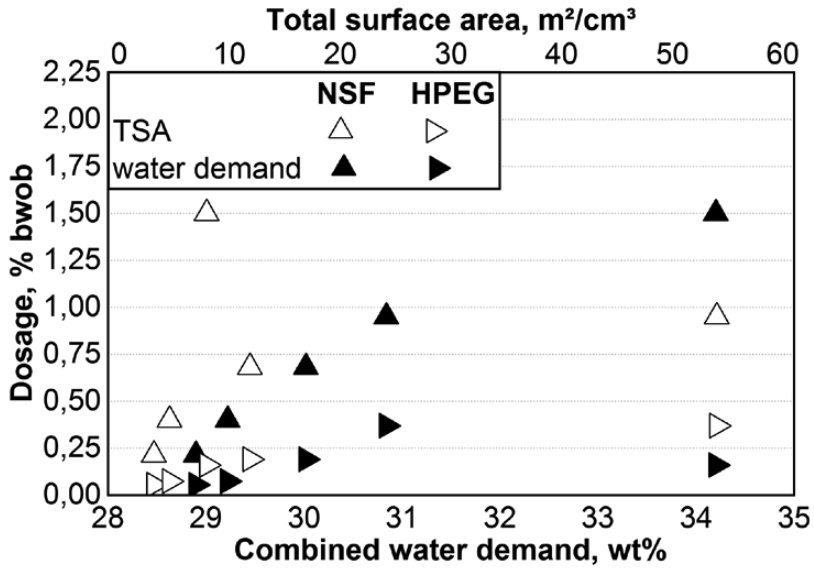

Figure 3-Correlation between required superplasticizer dosages and physical parameters of binders

(1 m²/cm³ = 176.39 ft²/in³ ;1 m²/g = 305.15 ft²/oz)

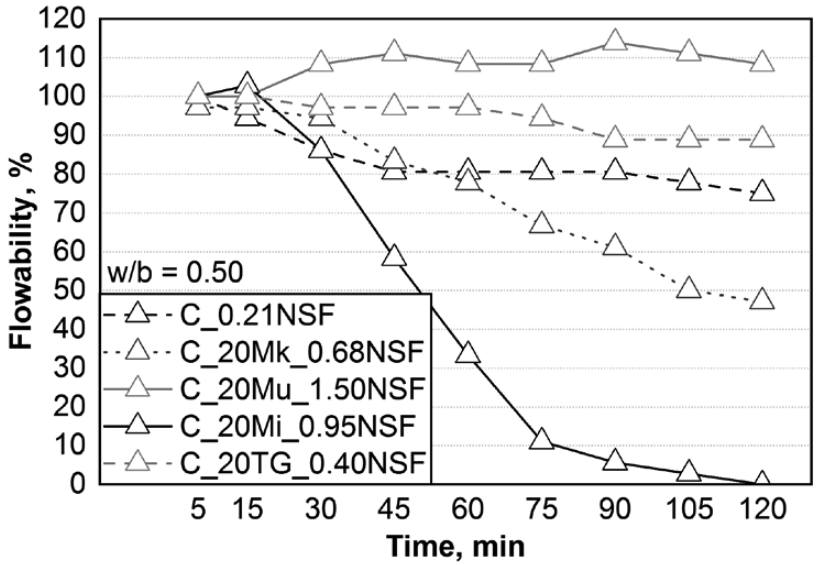

Figure 4-Time dependent flowability of blended cement paste with NSF superplasticizer

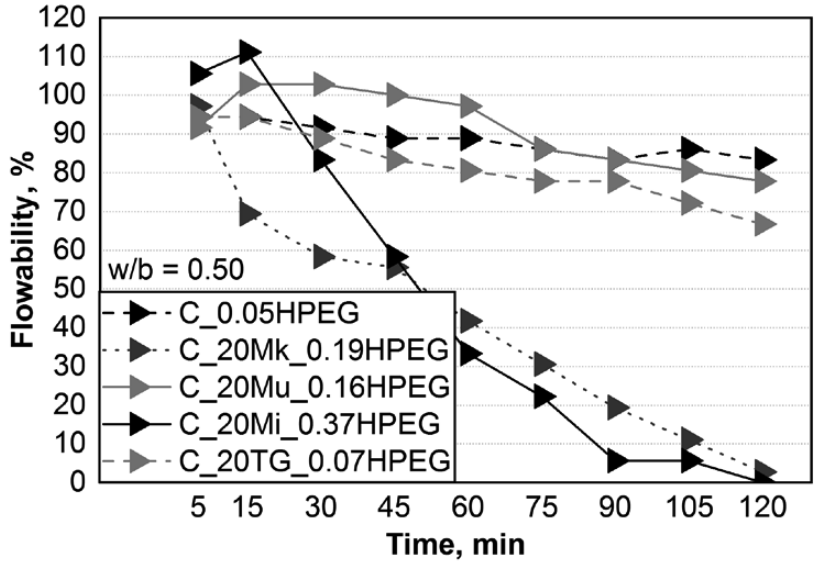

Figure 5- Time dependent flowability of blended cement paste with HPEG superplasticizer

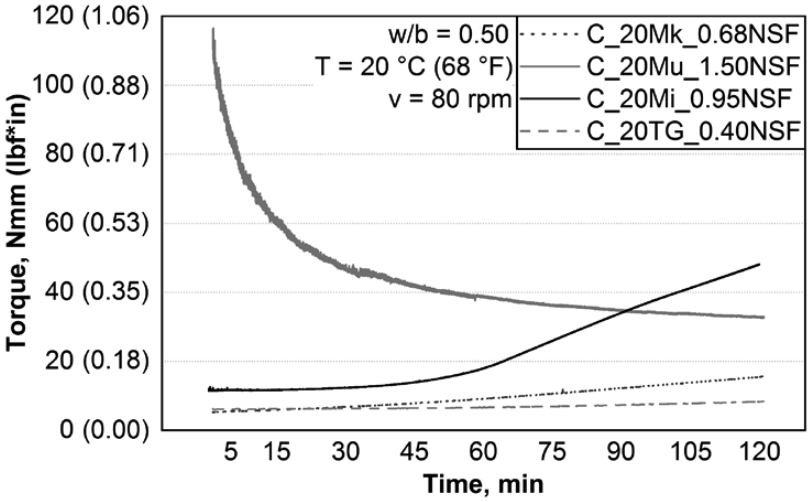

Figure 6- Time dependent torque for blended cement paste with NSF superplasticizer

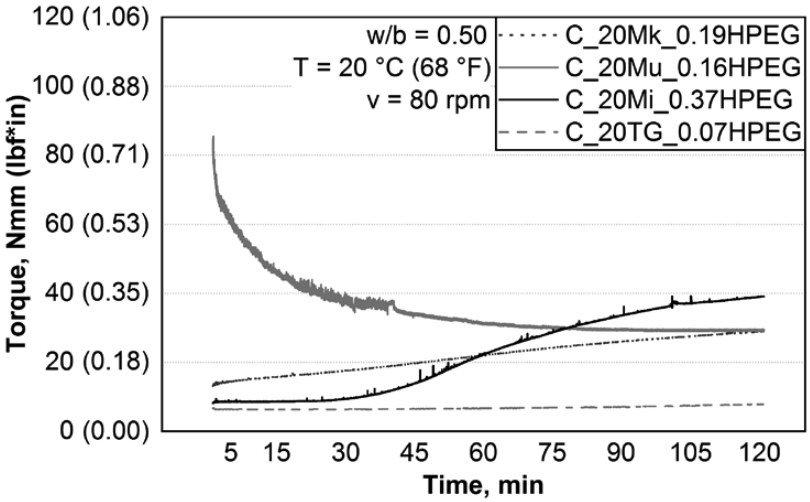

Figure 7- Time dependent torque for blended cement paste with HPEG superplasticizer

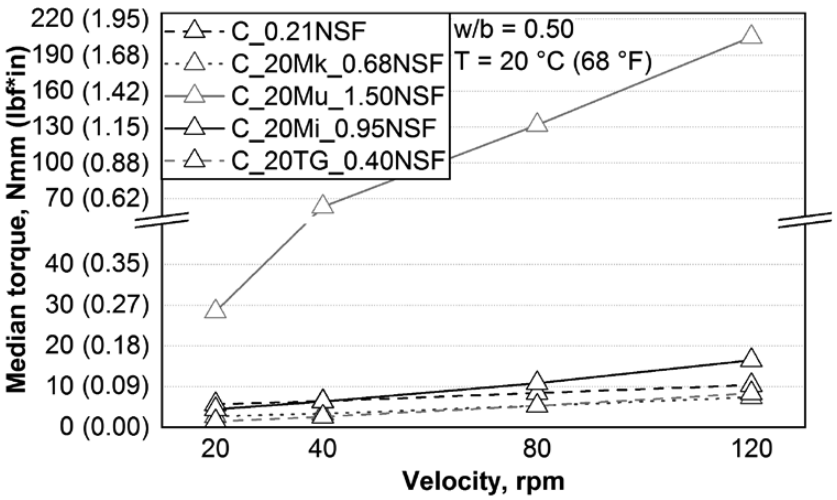

Figure 8-Median torques of blended cement paste with NSF superplasticizer at different velocities

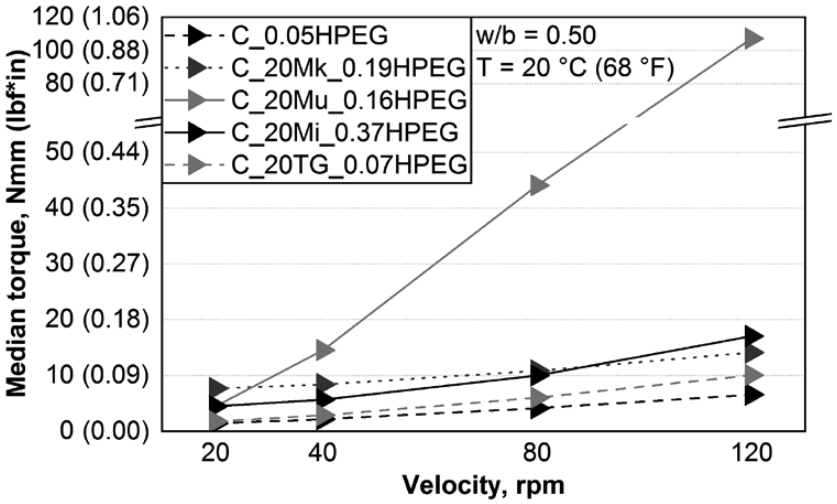

Figure 9- Median torques of blended cement paste with HPEG superplasticizer at different velocities

7.7 Feasability study on PCE based superplasticizers in calcined clay blended cements with focus on the type of phyllosilicate

Conference paper [Reprint]

"Feasability study on PCE based superplasticizers in calcined clay blended cements with focus on the type of phyllosilicate"

Ricarda Sposito, Matthias Maier, Nancy Beuntner, Karl-Christian Thienel

ACI SP 354: 13th International Conference on Superplasticizers and Other Chemical Admixtures in Concrete (formerly CANMET)

Milan, Italy, 6th – 8th June 2022, pp. 233 - 246

SP-354: Superplasticizers and Other Chemical Admixtures in Concrete—Conference Proceedings

Feasibility study on PCE based superplasticizers in calcined clay blended cements with focus on the type of phyllosilicate

Ricarda Sposito, Matthias Maier, Nancy Beuntner and Karl-Christian Thienel

Synopsis: The use of calcined clays as clinker replacement requires the addition of effective superplasticizers. Phyllosilicates in clays are known for their contribution on the pozzolanic reactivity after calcination. Previous investigations on single components of clays identified metaphases of phyllosilicates as the challenging minerals, whereas quartz can promote a proper workability and effectiveness of superplasticizers. It is still under discussion which type of calcined phyllosilicate (1:1 or 2:1), namely metakaolin or metamuscovite / metaillite is more challenging regarding their interaction with superplasticizers. A comparison of these single phyllosilicates among each other and with calcined clays relevant for cement industry is limited due to physical properties differing too significantly.

The study focuses on the question whether calcined clays with 1:1 or 2:1 phyllosilicates interact better with polycarboxylate ether based superplasticizers (PCEs) in cementitious systems under the consideration of their physical properties. Five calcined common clays originating from German clay pits are used. The clays differ significantly in their mineralogical composition before calcination, especially regarding their amount of kaolinite, muscovite and quartz. A Portland limestone cement is replaced by 30 % by weight of calcined clay. Two PCEs are used that exhibited good compatibilities with calcined clays in investigations beforehand. Measurements with a rotational viscometer determine the flow resistance each 5, 30, 50 and 105 minutes after water addition. In combination with the adsorption behavior analyzed via zeta potential measurements, the results give a fundamental knowledge about the efficiency of superplasticizer depending on type of calcined clay.

Keywords: calcined clays, flow resistance, hydration kinetics, superplasticizers, workability

Ricarda Sposito is doctoral candidate at the Institute for Construction Materials, Universität der Bundeswehr München, Germany. She received her B.Eng. in civil engineering from University of Applied Sciences Munich and her M.Sc. in civil engineering from Technical University of Munich (TUM), Germany. Her research interests include concrete technology, calcined clays and their interaction with superplasticizers.

Matthias Maier is doctoral candidate at the Institute for Construction Materials, Universität der Bundeswehr München, Germany. He received his B.Sc. and M.Sc. in Earth Science from University of Innsbruck. His research interests include mineralogy of clay minerals and cementitious materials.

Nancy Beuntner is researcher and laboratory scientific head at the Institute for Construction Materials, Universität der Bundeswehr München, Germany, where she received her Dr. degree. After her diploma in civil engineering, with special focus on building materials at Bauhaus University Weimar, Germany, she had worked in the cement industry for 6 years. Her research interests include supplementary cementitious materials and the development of modern concrete.

ACI member **Karl-Christian Thienel** is professor and head of the Institute for Construction Materials, Universität der Bundeswehr München, Germany. He received his diploma and Dr. degree in civil engineering from TU Braunschweig, Germany. He was Alexander-von-Humboldt “Feodor–Lynen” stipendiary at ACBM, Northwestern University, Evanston, IL, and head of R&D at Liapor GmbH & Co. KG. He is chairman of CEN/TC 177 and CEN/TC 154 SC5. His research interests include calcined clays, lightweight concrete and lightweight aggregate.

SP-354: Superplasticizers and Other Chemical Admixtures in Concrete—Conference Proceedings

INTRODUCTION

The cement research community focusses on calcined clays for several years now due to an increasing demand for supplementary cementitious materials (SCM) and a reduced availability of well-established SCM. Metakaolin, especially in combination with limestone, represents the mostly investigated calcined clay, as it is an important constituent of LC³ binders [1]. Further soil materials, e.g. illitic clays, are abundant worldwide and do show pozzolanic properties after calcination as well [2-4]. The addition of calcined clays affects significantly rheological properties of cementitious systems, by increasing the yield stress, viscosity and thixotropy. Muzenda et al. [5] observed a 15 times higher static yield stress in calcined clay limestone blended cements compared to ordinary Portland cement. The main contribution was related to the calcined clay. In the presence of 30 wt% calcined clay, plastic viscosity and dynamic yield stress increased by up to 700 % and 800 %, respectively. The thixotropy was eight times higher than for the reference system due to high water adsorption at 2 minutes of resting time. Shear-thickening behavior was observed by Schmid et al. [6] and, as consequence for their modified rheological behavior, calcined blended cements require the use of suitable superplasticizers. Cement paste blended with 20 wt% metamuscovite showed higher apparent viscosity with increasing rotational speed at w/b = 0.50 and in the presence of 0.30/0.35 % of MPEG-based PCE. At w/b = 0.65, the blended cement paste showed shear-thinning behavior even without or < 0.10 % of this PCE, due to sufficiently available water to disperse the particles. Ng and Justnes [7] used the flow resistance, which represents the area under the descending flow curve, to describe the rheological behavior of cement paste with calcined marl. The flow resistance increased by 150 % with 20 wt% calcined marl compared to plain cement, which was related to the high water adsorption of calcined marl. In the presence of 0.2 % PCE, the flow resistance was more than halved although the PCE performance was weaker than in neat cement. The authors attributed this to the intercalation of (long) poly(ethylene oxide) side chains of PCE into remaining interlayers of smectite, which was present in marl.

It is still under discussion, to what extent the mineralogical composition of clays does affect the demand for superplasticizer. Beigh et al. [8] revealed more challenging rheological properties for a coarse calcined clay with residual kaolinite in comparison to a finer calcined kaolinitic clay that has been fully dehydroxylated. The authors related the observed effects to intercalation of conventional PCEs into kaolinite structure. Intercalation is well known for swelling clay minerals like montmorillonite [9]. In comparison, Lei and Plank [10] found that PCEs adsorb only onto the surface of kaolin and muscovite. It is unclear what happens to clay minerals, that are sensitive towards intercalation, when their dehydroxylation is completed. Further, neither the adsorption mechanism of superplasticizers onto calcined clays nor the interaction with different clay components are fully understood so far. Schmid and Plank [11] recently investigated the adsorption behavior of PCEs onto different calcined phyllosilicates. The authors found that metakaolin sorbs larger amounts of PCEs than calcined 2:1 phyllosilicates do, when its surface is fully covered with Ca^{2+}. This phenomenon was related to the more negative surface charge of metakaolin, which requires more Ca^{2+} for charge reversal and PCE sorption, as consequence. Lorentz et al. [12] revealed a decreasing positive zeta potential of blended cement with increasing kaolin content. Complementing to these findings, the authors [13] found that a higher kaolinite content in clay leads to a more negative zeta potential value of calcined clays in synthetic cement pore solution. Ferreiro et al. [14] stated that kaolinite-rich clays require more superplasticizer than smectitic clays. The authors explained it by the entrapping of the superplasticizer polymer into the amorphous structure of metakaolin, while superplasticizers adsorb only at the edges of calcined 2:1 phyllosilicates. A higher superplasticizer efficiency was identified for cements blended with metakaolin compared to metaillite and metamuscovite [15]. Calcined common clays with further components (e.g. quartz) often have a lower water demand and require less superplasticizer in concrete than, for instance, metakaolin. In addition to the water demand, further parameters, such as particle size, specific surface area and surface charge of cementitious materials, were identified as indicators for rheological behavior and superplasticizer demand [15-17]. This leads to the assumption that the mineralogical composition of clays plays a key role towards the rheological behavior and the demand for superplasticizer. The results, however, did also show that it is impossible to transfer the findings from pure materials to common clays as physical parameters vary significantly [12, 15]. Rapid slump loss and strong increase in shear stress are both often observed when calcined clays are used [18, 19]. For 3D printing, this phenomenon, which is related to enhanced particle flocculation and water adsorption, is beneficial as it enables a good buildability. For conventional ready-mix concrete, however, it can cause significant problems if the period of workability is limited. Li et al. [20] found that the addition of Na-gluconate does not compensate rapid slump loss at a replacement level of 30 % by weight (wt%). The authors proposed instead the combination of conventional PCEs with Ca-Al-PCE-LDH nanocomposite, which can even increase the flowability in the first time and extends the workability by 60 to 90 minutes even at a replacement level of 40 wt%. The PCE, which is located between the inorganic layers of the Ca-Al-LDH, is gradually released into pore solution and replaced by sulfate ions [20]. This study presents the interaction of five calcined clay blended Portland limestone cements

with two IPEG-based PCEs, where one of them contains hydroxyethyl methacrylate (HEMA) in its anchor group. The initial flow resistance is compared with the physical parameters of the binder / calcined clays and with the mineralogical composition of the raw clay, respectively. The reduction in flow resistance is observed over a period of two hours, including selected zeta potential tests of calcined clay blended cements to discuss the adsorption behavior.

RESEARCH SIGNIFICANCE

Calcined clays represent a promising future SCM that possesses challenging properties at the same time. The mineralogical composition of clays depends on their geological origin and differs significantly from region to region. As a result of their specific physical and mineralogical properties, the addition of calcined clays leads to modified flowing properties of cementitious systems. For this reason, four common clays and one kaolinite-rich mine tailing have been investigated after calcination towards their interaction with two IPEG-based PCEs. The study offers a better understanding of how to handle complex calcined clay blended systems, an option on how to avoid rapid slump retention and proposes polymers that are suitable for a proper dispersion.

EXPERIMENTAL PROGRAM

Materials and nomenclature

Four calcined common clays (designated as: AC, FUP, KUP, MURR) and one kaolinite-rich mine tailing (RKUP) were chosen to replace a Portland limestone cement (PLC) by 30 wt%. The mineralogical composition of PLC is given in Table 1. The raw clays differed significantly in their mineralogy (Table 2) and were characterized intensively before and after calcination by Maier et al. [4]. They were thermally treated in charges of 300 g in a lab-scale muffle kiln for 60 minutes at 800 °C. At the chosen temperature, a complete dehydroxylation of the phyllosilicates, that are present in these clays, is usually achieved [21-25] and no new crystalline phases form yet [26, 27]. Table 3 provides the physical parameters of all powder materials: particle density was determined via Helium pycnometer Pycnomatic ATC (ThermoFisher Scientific) [28] and BET specific surface area via N_2 adsorption with SA-9601 MP (Horiba Instruments Inc.) [29]. The water demand of PLC was evaluated according to DIN EN 196-3 to achieve standard stiffness [30]. The water demand of calcined clays was determined by Puntke method [31]. The particle size distribution of calcined clays was analyzed via static laser light diffraction by Bettersizer S3 Plus (3P Instruments). Here, the diameter at 10, 50 and 90 % passing (d_{10}, d_{50}, d_{90}) are provided. The zeta potential of calcined clays in synthetic cement pore solution (SCPS) was investigated at a SCPS-to-calcined clay ratio of 1.50. The detailed experimental setup is described in [13]. The ion composition of SCPS was 0.4 g/l Ca^{2+}, 7.1 g/l K^+, 2.2 g/l Na^+, 8.3 g/l SO_4^{2-} [32]. The solubility of Si and Al ions was evaluated by eluting the calcined clays in 400 ml of 10 wt% NaOH solution for 20 h according to Surana and Joshi [33]. The amount of soluble Si and Al ions was measured in filtered, acidified solution (pH = 1) via inductively coupled plasma optical emission spectrometry, using Varian ICP-OES 720 ES.

Table 1. Mineralogical composition of PLC

C_3S	C_2S	C_3A	C_4AF	$CaCO_3$	Sulfate carrier	$CaMg(CO_3)_2$	MgO	CaO_{free}	$Ca(OH)_2$	Quartz
wt%										
48.7	14.4	5.4	6.9	15.6	4.2	2.3	0.8	0.2	1.2	0.4

Table 2. Mineralogical composition of raw clays

Phase, wt%	$MURR_{raw}$	AC_{raw}	KUP_{raw}	$RKUP_{raw}$	FUP_{raw}
Quartz	48.1	20.0	33.2	47.7	12.6
Kaolinite	1.0	22.6	25.7	45.0	70.6
Muscovite/Illite	9.6	4.7	36.1	3.1	12.9
Illite-Smectite	-	31.8	-	-	-
Smectite	31.5	-	-	-	-
Chlorite	3.7	5.6	-	-	-
Calcite	0.9	7.4	-	-	-
Dolomite	0.2	1.1	-	-	-
Feldspar	5.1	3.8	-	-	1.2
Rutile/Anatase	-	2.2	0.7	0.4	2.7
Pyrite	-	0.9	-	-	-
Hematite	-	-	-	0.4	-
Goethite	-	-	4.3	3.3	-

Table 3. Physical parameters of Portland limestone cement (PLC) and calcined clays and Al-/Si-solubility of calcined clays

Parameter	PLC	MURR	AC	KUP	RKUP	FUP
Particle density, g/cm³	3.07	2.72	2.67	2.70	2.63	2.63
BET surface area, m²/g	1.8	5.3	17.2	6.6	7.9	42.4
Water demand, wt%	26.6	32.8	28.3	40.4	35.1	43.6
$d_{10,}$ µm	-	4.6	3.6	6.4	2.2	2.8
$d_{50,}$ µm	-	40.9	30.0	26.7	12.0	16.1
$d_{90,}$ µm	-	150.4	161.9	86.9	81.0	56.3
Zeta potential, mV	-	- 1.3	- 1.6	- 3.3	- 4.0	- 7.5
Si, mmol/l	-	1.17	2.74	3.28	4.98	11.39
Al, mmol/l	-	0.41	1.67	2.26	4.00	8.52
Si/Al ratio, -	-	2.88	1.64	1.45	1.25	1.34

Two industrial PCEs were used at a dosage of 0.10 % by weight of binder (%bwob) to investigate their effectiveness in calcined clay blended cement paste. Selected tests were conducted with 0.20 %bwob PCE. The dosage represented the amount of active agent in the respective PCE. Both superplasticizers were isoprenyl oxy poly(ethylene glycol) ether (IPEG) type PCEs and had acrylic acid (AA) as anchor groups. Details on their properties are given in Table 4. IPEG1 consisted of two IPEG-AA polymers, where one anchor group had an additional ester group, hydroxyethyl methacrylate (HEMA), that should enable a prolonged workability by alkali-related charge release (Figure 1). IPEG2 had an IPEG-AA, as well as a vinyloxybutyl polyethylene glycol (VOBPEG)-AA polymer (Figure 2). The proportions of the different polymers were under disclosure.

Table 4. Properties of PCE-based superplasticizers (anionic charge density has been measured by the Chair for Construction Chemistry of TU Munich; further parameters are provided by the supplier)

PCE	Solid content, wt%	$M_{N,}$ g/mol	$M_{W,}$ g/mol	PDI [-]	Anionic charge density in H_2O dest., [µeq/g]	n_{EO} [-]
IPEG1	28.7	~ 19,500	~ 27,500	1.4	628	24
IPEG2	38.6	~ 19,000	~ 26,000	1.4	1,390	31

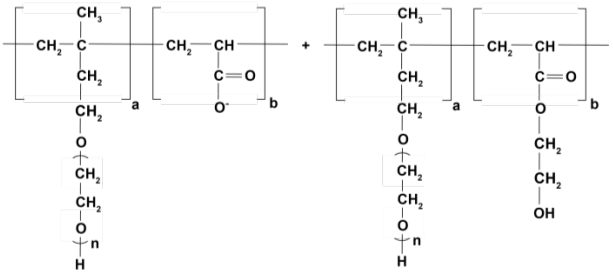

Figure 1. Chemical structure of IPEG1

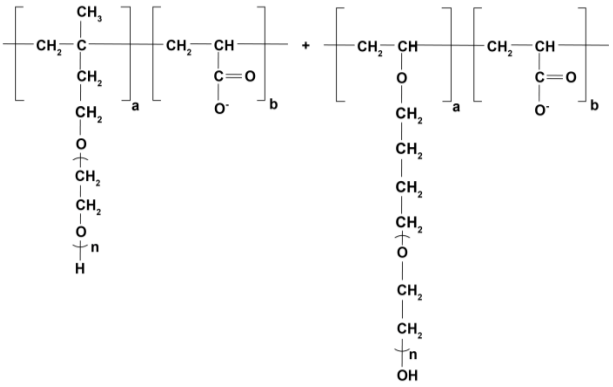

Figure 2. Chemical structure of IPEG2

Methods

For rheological measurements, cement paste (m_{binder} = 600 g, water-to-binder ratio (w/b) = 0.5) was mixed according to DIN EN 196-3 [30]. A rotational viscometer Viskomat NT (Schleibinger, Germany) was used in combination with a coupled cooling unit, that ensured a constant temperature of T = 20 °C. Time-dependent rheological measurements were conducted for four times: 5, 30, 50 and 105 minutes after water addition. For the first three measurements, the cement paste remained in the viscometer. Afterwards, the cement paste was filled into a cup and covered with a damp cloth to prevent drying up. Two minutes before the last measurement began, the sample was stirred up manually and filled back into the rotational viscometer. Each measurement recorded the torque at a rotational speed of 120 revolutions per minute (rpm) for 10 minutes, followed by 80 rpm, 40 rpm and 20 rpm for 2 minutes each. The flow resistance was calculated as the area under the flow curve by using the trapezoidal method as proposed by Vikan et al. [34, 35].

For calcined clay blended cement paste, the zeta potential and pH values were both continuously observed over a period of 120 minutes. The pore solution of PLC was set as ionic background. Therefore, m = 100 g of cement were mixed with distilled water at w/b = 0.50 for 5 minutes by hand. The cement paste was poured into a Büchner funnel with a prewetted filter paper. The pore solution was extracted of the cement paste by vacuum process. Based on this extracted pore solution, the background was determined three times by electroacoustic spectrometer DT-310 (Dispersion Technology Instruments, USA). Beside of the ionic background, the spectrometer considers the particle density and mean particle size of the binder components. For the actual measurement, the binder (m = 360 g) and the respective amount of distilled water / water-PCE solution for w/b = 0.50 were mixed for 3 minutes by hand and the measurement started at 5 minutes after water addition. The paste was constantly stirred at 300 rpm to avoid segregation. The zeta potential was summarized for the intervals of 5-21, 30-46, 50-66 and 105-121 minutes, respectively, and compared with the flow resistance at these time intervals. Changes in zeta potential indicated the adsorption of PCE onto binder components on the one hand and the formation of very early hydrate phases on the other hand.

EXPERIMENTAL RESULTS AND DISCUSSION

Influence of physical and mineralogical parameters of clays on the initial dispersion by IPEG-PCE based superplasticizers

Table 5 shows the initial flow resistance of systems without superplasticizer and with 0.10 %bwob of IPEG1 and IPEG2, respectively. The addition of IPEG1 and IPEG2 reveals significant differences between these PCEs, where IPEG2 shows a better initial dispersion behavior than IPEG1 (Figure 3). This is related to the higher anionic charge density of IPEG2 compared to IPEG1 (Table 4), which generally leads to a better adsorption onto binder particles [36, 37]. This effect was also observed for calcined clay blended systems e.g., in [15, 38, 39]. However, IPEG1 does also reduce the flow resistance by at least 58 %, when using 0.10 %bwob. The ranges for IPEG1 and IPEG2 are between 58 – 71 % and 73 – 89 %, respectively, and depend to a large extent on the individual binder system. The highest reduction in flow resistance is achieved for PLC_RKUP system that exhibits a high flow resistance without superplasticizer, but an excellent reduction with the addition of both PCEs. This brings up the question to what extent physical and mineralogical properties of calcined clays influence the efficiency of superplasticizers?

Table 5. Initial flow resistance of used systems

System	Initial flow resistance, Nmm/min					
	PLC	PLC_AC	PLC_FUP	PLC_RKUP	PLC_KUP	PLC_MURR
Reference	1975	1987	8090	7841	6723	2240
0.10IPEG1	738	673	3084	2256	2859	859
0.10IPEG2	443	524	608	877	1559	608

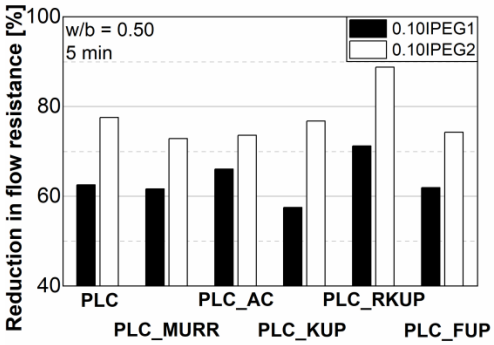

Figure 3. Reduction in initial flow resistance with addition of PCE (5 minutes after water addition)

In previous publications, good correlations were identified between total surface area (TSA), water demand and zeta potential values of blended cements with their demand for superplasticizer [15, 38]. The results at hand show that the TSA is not a reliable indicator for the prediction of flow resistance as there is a significant increase in flow resistance but also a higher efficiency of PCEs for TSA > 10 m²/cm³ (Figure 4a). As observed in [15], some binder systems fall out of line. Here, PLC_AC systems show a low flow resistance despite a high TSA (17.6 m²/cm³). For the same calcined Amaltheen clay, a BET specific surface area of 4 - 5 m^2/g was observed when calcined at 750 °C [15, 40]. This is related to the structural breakdown of 2:1 phyllosilicates, that leads to a significant decrease in BET specific surface area, which remains constant over a larger range for kaolinite after dehydroxylation [41]. Beuntner and Thienel [42] found a BET of 20 m^2/g for calcination temperatures at 600 °C and a decrease to 5 m^2/g when surpassing the dehydroxylation temperature according to thermogravimetric measurements. It is hence possible that the BET of AC (17.2 m^2/g) is related to a still intact crystalline structure despite a complete dehydroxylation. This leads to a high TSA, but nonetheless to a lower flow resistance than for most of the other calcined clay blended cements. A water demand of the reference systems that is lower than 29 wt% causes a low flow resistance, while the latter increases significantly with higher water demand (Figure 4b). With the addition of 0.10 %bwob PCE, the reduction in flow resistance is less significant for the systems with low water demand. This is related to a sufficient quantity of water in these mixtures, that are able to flow and do require less superplasticizer at a w/b = 0.50. Systems with higher water demand and TSA, however, need more PCE to decrease their flow resistance significantly. The gaps of flow resistance, as observed for both, combined TSA and water demand, do also fit with the d_{50} value as well as with zeta potential value of calcined clay in SCPS. The flow resistance of systems without PCEs correlates very well with the average particle diameter as the flow resistance decreases significantly with coarser particles (d_{50} value > 30 µm) (Figure 4c). Calcined clays with zeta potential values more negative than - 2 mV tend to increase the flow resistance significantly (Figure 4d). The flow resistance (flocculation) increases as the negatively charged calcined clay particles adsorb onto positively charged aluminate hydrates [36, 37] or do adsorb cations released from clinker phases. Here, a more negative zeta potential value of calcined clay enhances the effect of Ca^{2+} ions to function as a kind of adhesive between the calcined clay particles and therefore leads to a higher flow resistance. If cations released from clinker phases can adsorb onto negatively charged calcined clay sites as shown in [43], these turn into less negatively or even positively charged surface sites [13, 44] and may be available for subsequent PCE adsorption. Schmid and Plank [11] showed that metaphyllosilicates adsorb different amounts of Ca^{2+} per m² BET specific surface area (metamuscovite >> metamontmorillonite > metakaolin >> metaillite). However, only metakaolin revealed a higher amount of sorbed PCE when a saturation by Ca^{2+} was obtained. With the addition of 0.10 %bwob PCE, the tendency of flow resistance with respect to water demand and zeta potential values remains the same as for reference systems. However, the differences between the binder systems diminish significantly. Attempts to correlate the reduction in flow resistance [%] by adding IPEG PCE with the above-mentioned physical parameters did not yield proper linear nor other correlations.

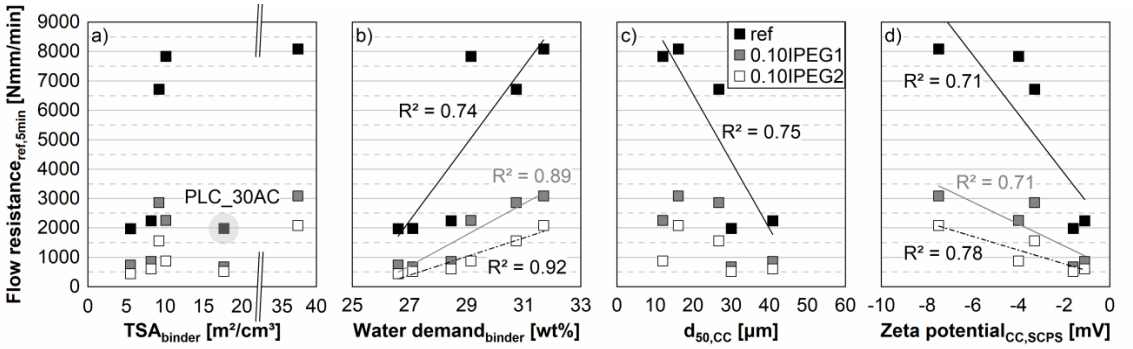

Figure 4. Correlations between a) TSA, b) water demand of blended binder, c) average particle sizes of calcined clays and d) zeta potential of calcined clays in SCPS and flow resistance after 5 minutes

All investigated calcined clays have been ground according to the same procedure but nevertheless they differ significantly in their particle size distribution. The grindability depends to a large extent on the mineralogy of the clays. Quartz in clays / shales, for instance, can lead to bimodal or even trimodal distributions [3] and is enriched in the coarser particle section [45]. Contrary to the previous assumption of the authors [15, 38], the amount of quartz in clay does not indicate the effect on flow resistance (Figure 5a). The amount and type of phyllosilicates in the clay is much more decisive. Here similar observations are made as for the physical parameters: for a kaolinite content > 25 wt% in raw clay, the flow resistance without superplasticizer increases significantly and hereby the superplasticizer efficiency when PCEs are used (Figure 5b). The authors recently revealed that calcined kaolinite-rich clays possess a higher fraction of particles with d = 4.5 µm up to 10 µm [17]. On the contrary, clays rich in 2:1 phyllosilicates (> 37 wt%) lead to lower flow resistance of calcined clay blended systems (Figure 5c). Hence, it is crucial to state that the "lower efficiency" of PCEs for binders with calcined 2:1 phyllosilicates-dominated clays stems from a lower demand for superplasticizers itself. It should also be mentioned that the raw clays of those systems with high flow resistance (PLC_RKUP, PLC_FUP, PLC_KUP) contain mainly illite or muscovite, while those rich in illite-smectite interstratifications (PLC_MURR and PLC_AC) go along with a lower flow resistance. To a certain extent, it confirms earlier results where both calcined illite and muscovite caused severe changes in rheological behavior, indicated by higher torque and viscosity values [6, 15, 18, 38]. It further agrees with findings of Ferreiro et al. [14], where calcined illite-smectite clays required lower superplasticizer dosages than calcined kaolinite clays. Another side effect might be the presence of calcite beside of illite-smectite and smectite in raw AC (Table 2). According to Danner et al. [46], a glass phase is formed during the calcination of calcite-containing clays, which significantly improves their pozzolanic activity. This possibly formed glass phase might be also the reason for the comparable low specific surface area of AC despite its high content in phyllosilicates. As consequence, this can favor a low flow resistance, as known e.g., for spherical shaped, glassy fly ashes. Overall, these results show how important it is to consider not solely the kaolinite content but the whole, often very complex mineralogical composition of clays.

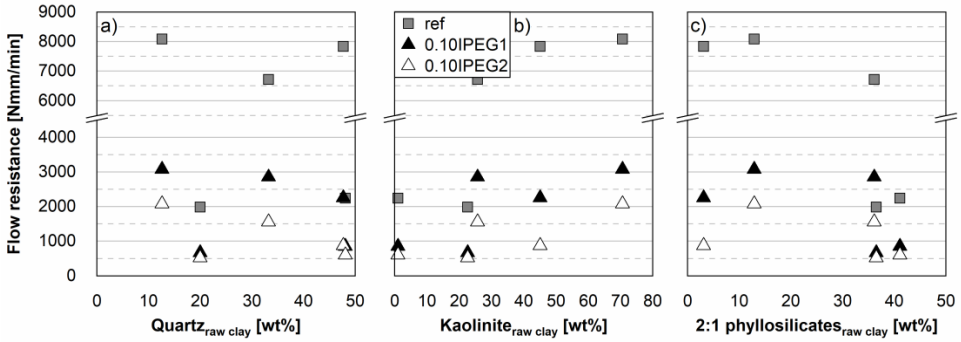

Figure 5. Correlations of content in a) quartz, b) kaolinite and c) 2:1 phyllosilicate in raw clays with initial flow resistance

Time dependent flow resistance and zeta potential of calcined clay blended cement paste

For PLC, the addition of IPEG PCE leads to a significant decrease in flow resistance over two hours. With IPEG1, the flow resistance is further lowered due to the decomposition of HEMA into carboxyl and glycol groups. This charge release in alkaline environment has been observed already by Tan et al. [47]. The increase in flow resistance is only marginal with IPEG2. Especially after 105 minutes, the flow resistance of PLC is still low enough to ensure a proper workability. The negative zeta potential value is reduced, which indicates an initial adsorption onto PLC that increases with more IPEG-based PCE added. Within the first 30 minutes after water addition, the zeta potential values change more significantly with IPEG PCE. This indicates either a further adsorption of PCE or an enhanced initial formation of ettringite, which is known for its positive zeta potential [37]. After 30 minutes, the zeta potential values remain stable for dosages of 0.10 and 0.20 %bwob, which explains the constant flow resistance with IPEG PCE and indicates the end of initial ettringite formation. While the flow resistance of PLC_ref increases significantly between 50 and 105 minutes, its zeta potential value does hardly change during this period. It is possible that an equilibrium of negatively and positively charged surfaces of clinker and hydrate phases offsets significant changes in zeta potential.

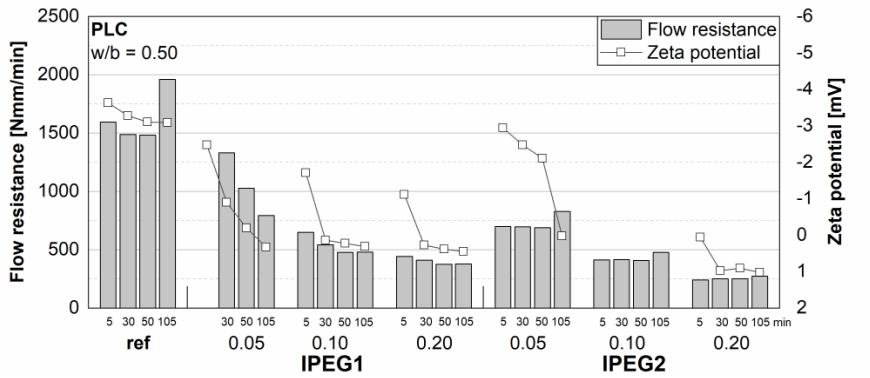

Figure 6. Time dependent zeta potential and flow resistance for PLC systems including reference and varying dosages of IPEG1/2 (note that the zeta potential of PLC_0.10IPEG2 was not determined)

Depending on the type of calcined clay added, the flow resistance can sharply increase during the first two hours observed (Figure 7 to Figure 9). For PLC_AC and PLC_FUP, the references without PCE show significant changes in both flow resistance and zeta potential values. The time-dependent changes compared to PLC (Figure 6) are related to an enhanced ettringite formation by the addition of calcined clays, which was observed during very early hydration [48-50]. The addition of IPEG PCEs does in parts counteract the changes in both flow resistance and zeta potential values. As also observed for PLC, the zeta potential diminishes from strong negative values to positive zeta potential values or at least smaller negative values, 5 minutes after water addition. The positive zeta potential value of PLC_AC with 0.20 %bwob IPEG PCE indicates an immediate saturation of binder surface by anionic PCE. These findings agree with those of Pardo et al. [43] who revealed similar interactions of calcined clays with superplasticizers. The addition of IPEG1 to PLC_AC indicates a slightly better initial adsorption, but a less pronounced subsequent dispersion in comparison to PLC system. As neither flow resistance nor zeta potential hardly change over time, IPEG1 hinders at least a continuous, small increase in flow resistance as observed with IPEG2 (Figure 7). The fluctuation of zeta potential values around 0 mV with 0.20 %bwob IPEG2 demonstrates ongoing complex adsorption mechanisms, not only between clinker and calcined clay particles as well as hydrate phases, but also with the superplasticizer.

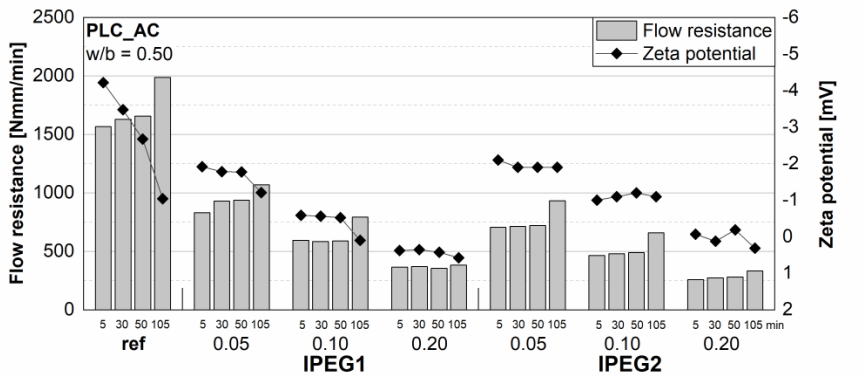

Figure 7. Time dependent zeta potential and flow resistance for PLC_AC systems including reference and 0.20 %bwob IPEG1/2

PLC_FUP requires 0.20 %bwob PCE to achieve a proper workability as previous investigations of the authors showed [17]. The flow resistance increases with PCEs as strongly as without PCE, even with the addition of 0.20 %bwob IPEG1 (Figure 8). Hence, a subsequent dispersion by the adsorption of additional carboxyl groups, that stem from the decomposition of HEMA in IPEG1, is not possible for this system. One possible reason is the strong negative zeta potential value of FUP in alkaline environment (- 7.5 mV) that results from a high kaolinite content in raw clay (Table 2) [13]. Further, the ettringite formation is enhanced during very early hydration due to the extraordinary high specific surface area of FUP and additional nucleation sites as consequence [51]. Although ettringite exhibits a positive zeta potential value and enables usually a good adsorption of anionic superplasticizers [37], this effect seems to diminish for PLC_FUP. Furthermore, FUP exhibits the highest water demand of all calcined clays used (Table 3) and the authors cannot exclude the entrapping of PCE into FUP leading to rapid loss in superplasticizer efficiency, as assumed e.g. by Beigh et al. [8]. Beside of the parameters described, a further reason might be a lower pH value in PLC_FUP (pH = 11.9 after 5 minutes in reference) compared to PLC (pH = 12.6) and PLC_AC (pH = 12.2) systems [13]. This could hinder the originally alkali-related decomposition of HEMA and therefore a subsequent dispersion by IPEG1. This lower pH value was already observed for calcined clays with increasing kaolinite content in SCPS, which was related to a higher adsorption of OH^- ions [13].

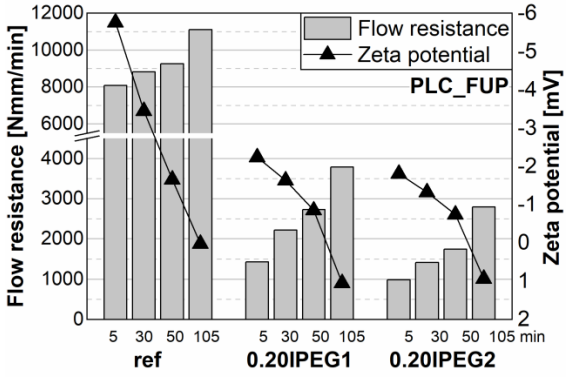

Figure 8. Time dependent zeta potential and flow resistance for PLC_FUP systems including reference and 0.20 %bwob IPEG1/2; note different scale factor for flow resistance compared to Figure 6 and Figure 7

PLC_RKUP, PLC_KUP and PLC_MURR do also show a proper reduction in flow resistance with the addition of 0.10 %bwob IPEG PCE during the first two hours (Figure 9). The influence of different PCE dosages was recently published by the authors in [17]. Therefore, they omit the differences between 0.10 and 0.20 %bwob for these blended cements here. With IPEG1, the flow resistance of PLC_RKUP decreases even slightly further over time, which results in a similar flow resistance with IPEG1 and IPEG2 after 105 minutes. Despite the high metakaolinite content, the RKUP-SCPS solution showed a pH value of 12, which is related to the high quartz content. Preliminary investigations [52] showed that quartz-SCPS and metakaolin-SCPS solutions have an initial pH value of 13.0 and 11.0, respectively, at a liquid-to-solid ratio of 1.0.

Hence, it is assumed that also the pH value of PLC_RKUP is high enough to ensure a subsequent decomposition of HEMA and the dispersion by additional carboxyl groups. In PLC_KUP, the subsequent dispersion by 0.10 %bwob IPEG1 is not achieved, but the increase in flow resistance is slowed down compared to the reference. In general, the system with the calcined muscovite-rich clay KUP is more sensitive towards the type of PCE and shows a lower reduction in flow resistance compared to the other calcined clays. PLC_MURR has a low flow resistance even without the addition of PCE, and dosages beyond 0.05 wt% indicated saturation effects [17]. Hence, the initial flow resistance is slightly higher with IPEG1 compared to IPEG2, but both values are in a similar range. Regardless of the reference flow resistance, the flow resistance of most of the calcined clay blended cements remains stable or decreases even more with IPEG1 over time. IPEG2, instead, has a better initial dispersion performance and the flow resistance increases only slightly in its presence. This knowledge is crucial for the practical application of calcined clays as SCM to ensure an often desired, sufficiently long workability.

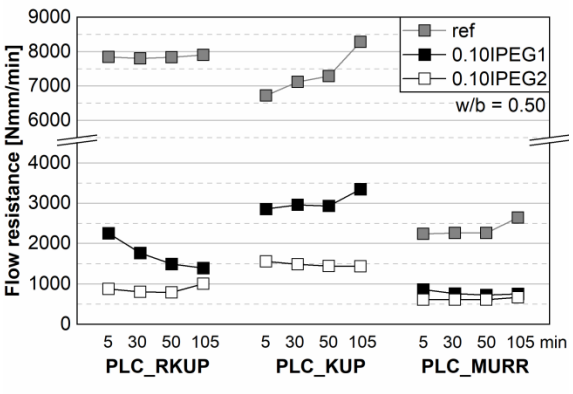

Figure 9. Time dependent flow resistance for PLC_RKUP, PLC_KUP and PLC_MURR without and with 0.10% IPEG PCE; note different scale factor for flow resistance compared to Figure 6 to Figure 8

CONCLUSION

- Thresholds for total surface area and water demand of binder are identified to estimate the influence of calcined clays on flow resistance of blended cement paste. The same holds for the particle size distribution and zeta potential of calcined clays, as well as the complex mineralogical composition of common clays. The quartz content is found not to be a reliable indicator. Moreover, the content in kaolinite and 2:1 phyllosilicates is decisive for the rheological behavior of calcined clay blended cements. Calcined kaolinite-rich clays require more superplasticizer as they cause a high flow resistance. At the same time, they show a good interaction with IPEG-based PCEs. Muscovite perturbs not only the flowability, but also the effectiveness of superplasticizers, while smectite does not cause any trouble in terms of the rheological properties. However, this requires verification not solely by investigating further paste, but also mortar and concrete samples.
- The PCE with higher anionic charge density (IPEG2) shows a better initial adsorption, which confirms common knowledge from literature. The PCE with HEMA (IPEG1) enables a subsequent dispersion if the blended cement paste provides a sufficiently high alkaline environment for the decomposition of HEMA into carboxyl and glycol groups. The addition of calcined kaolinite-rich clays might lower the pH value to such an extent that they reduce or even hinder the subsequent charge release. However, further investigations are required in order to evaluate the adsorption behavior of PCEs onto calcined clays individually, as e.g. by TOC method.
- Strong time-dependent changes in flow resistance and zeta potential values suggest an enhanced flocculation rate and initial ettringite formation with the addition of calcined clays. Both IPEG-based PCEs slow down the increase in flow resistance or lead even to a further decrease in flow resistance. Smaller changes in zeta potential are related to a slower ongoing clinker reaction with the addition of PCEs.
- The current findings confirm that a properly chosen superplasticizer can enable a sufficiently long water retention, which is often a problem in calcined clay blended systems. Nonetheless, each calcined clay requires an individual solution as the mineralogical and physical properties vary significantly.

ACKNOWLEDGMENTS

The authors like to thank Prof. J. Plank and his team from the Chair for Construction Chemistry of Technical University Munich (Germany) for measuring the anionic charge density of the superplasticizers. They also thank Strobel Quarzsand GmbH, Goerg & Schneider GmbH, Dr. Andreas Murr, Mr. Peter Jell (Degelhof clay pit), and Liapor GmbH & Co. KG for providing the clays, as well as Schwenk Zement KG for the cement and BASF Construction Solutions GmbH, all from Germany, for the superplasticizer samples.

REFERENCES

1. Antoni, M., et al., *Cement substitution by a combination of metakaolin and limestone.* Cement and Concrete Research, 2012. **42**(12): p. 1579-1589.
2. Danner, T., et al., *Feasibility of Calcined Marl as an Alternative Pozzolanic Material*, in *Calcined Clays for Sustainable Concrete*, K. Scrivener and A. Favier, Editors. 2015, Springer Netherlands. p. 67-73.
3. Irassar, E.F., et al., *Calcined illite-chlorite shale as supplementary cementing material: Thermal treatment, grinding, color and pozzolanic activity.* Applied Clay Science, 2019. **179**: p. 105143.
4. Maier, M., N. Beuntner, and K.-C. Thienel, *Mineralogical characterization and reactivity test of common clays suitable as supplementary cementitious material.* Applied Clay Science, 2021. **202**: p. 105990.
5. Muzenda, T.R., et al., *The role of limestone and calcined clay on the rheological properties of LC3.* Cement and Concrete Composites, 2020. **107**: p. 103516.
6. Schmid, M., et al., *The shear-thickening effect of meta muscovite as SCM and its influence on the rheological properties of ecologically optimized cementitious systems*, in *2nd International RILEM Conference on Rheology and Processing of Construction Materials (RheoCon2)*, V. Mechtcherine, Editor. 2019, Springer: Dresden, Germany.
7. Ng, S. and H. Justnes, *Influence of dispersing agents on the rheology and early heat of hydration of blended cements with high loading of calcined marl.* Cement and Concrete Composites, 2015. **60**: p. 123-134.
8. Beigh, M., et al., *Studying the rheological behavior of limestone calcined clay cement (LC³) mixtures in the context of extrusion- based 3D-printing*, in *Calcined Clays for Sustainable Concrete - Proceedings of the 3rd International Conference on Calcined Clays for Sustainable Concrete*, S. Bishnoi, Editor. 2020, Springer: Singapore. p. 229-235.
9. Tan, H., et al., *Mechanism of intercalation of polycarboxylate superplasticizer into montmorillonite.* Applied Clay Science, 2016. **129**: p. 40-46.
10. Lei, L. and J. Plank, *A study on the impact of different clay minerals on the dispersing force of conventional and modified vinyl ether based polycarboxylate superplasticizers.* Cement and Concrete Research, 2014. **60**: p. 1-10.
11. Schmid, M. and J. Plank, *Interaction of individual meta clays with polycarboxylate (PCE) superplasticizers in cement investigated via dispersion, zeta potential and sorption measurements.* Applied Clay Science, 2021. **207**: p. 106092.
12. Lorentz, B., et al., *Effect of Clay Mineralogy, Particle Size, and Chemical Admixtures on the Rheological Properties of CCIL and CCI/II Systems*, in *Calcined Clays for Sustainable Concrete - Proceedings of the 3rd International Conference on Calcined Clays for Sustainable Concrete*, S. Bishnoi, Editor. 2020, Springer: Singapore. p. 211-218.
13. Sposito, R., et al., *Evaluation of zeta potential of calcined clays and time-dependent flowability of blended cement with customized polycarboxylate-based superplasticizers.* Construction and Building Materials, 2021. **308**: p. 125061.
14. Ferreiro, S., D. Herfort, and J.S. Damtoft, *Effect of raw clay type, fineness, water-to-cement ratio and fly ash addition on workability and strength performance of calcined clay – Limestone Portland cements.* Cement and Concrete Research, 2017. **101**: p. 1-12.
15. Sposito, R., N. Beuntner, and K.-C. Thienel, *Characteristics of components in calcined clays and their influence on the efficiency of superplasticizers.* Cement and Concrete Composites, 2020. **110**(103594).
16. Marchetti, G., et al., *Assessment of packing, flowability, hydration kinetics, and strength of blended cements with illitic calcined shale.* Construction and Building Materials, 2020. **254**: p. 119042.
17. Sposito, R., et al., *Physical and mineralogical properties of calcined common clays as SCM and their impact on flow resistance and demand for superplasticizer.* Cement and Concrete Research, 2022. **154**(106743).
18. Sposito, R., et al., *An approach to the rheological behavior of cementitious systems blended with calcined clays and superplasticizers*, in *ACI SP 349 11th International Conference on Cementitious*

Materials and Alternative Binders for Sustainable Concrete, A. Tagnit-Hamou, Editor. 2021, American Concrete Institute: online. p. 659-685.

19. Chen, Y., et al., *Effect of different grade levels of calcined clays on fresh and hardened properties of ternary-blended cementitious materials for 3D printing.* Cement and Concrete Composites, 2020. **114**: p. 103708.
20. Li, R., et al., *Approaches to achieve fluidity retention in low-carbon calcined clay blended cements.* Journal of Cleaner Production, 2021. **311**: p. 127770.
21. Garg, N. and J. Skibsted, *Pozzolanic reactivity of a calcined interstratified illite/smectite (70/30) clay.* Cement and Concrete Research, 2016. **79**: p. 101-111.
22. Neißer-Deiters, A., et al., *Influence of the calcination temperature on the properties of a mica mineral as a suitability study for the use as SCM.* Applied Clay Science, 2019. **179**(105168).
23. Danner, T., G. Norden, and H. Justnes, *Characterisation of calcined raw clays suitable as supplementary cementitious materials.* Applied Clay Science, 2018. **162**: p. 391-402.
24. Alujas, A., et al., *Pozzolanic reactivity of low grade kaolinitic clays: influence of calcination temperature and impact of calcination products on OPC hydration.* Applied Clay Science, 2015. **108**: p. 94-101.
25. Hollanders, S., et al., *Pozzolanic reactivity of pure calcined clays.* Applied Clay Science, 2016. **132–133**: p. 552-560.
26. Lee, S., Y.J. Kim, and H.-S. Moon, *Phase Transformation Sequence from Kaolinite to Mullite Investigated by an Energy-Filtering Transmission Electron Microscope.* Journal of the American Ceramic Society, 1999. **82**(10): p. 2841-2848.
27. Buchwald, A., et al., *The suitability of thermally activated illite/smectite clay as raw material for geopolymer binders.* Applied Clay Science, 2009. **46**(3): p. 300-304.
28. DIN EN ISO 17892-3, *Geotechnical investigation and testing - Laboratory testing of soil - Part 3: Determination of particle density*. 2015, Beuth-Verlag: Berlin, Germany. p. 21.
29. DIN ISO 9277, *Determination of the specific surface area of solids by gas adsorption - BET method*. 2003, Beuth-Verlag: Berlin. p. 19.
30. DIN EN 196-3, *Prüfverfahren für Zement - Teil 3: Bestimmung der Erstarrungszeiten und der Raumbeständigkeit (Methods of testing cement - Part 3: Determination of setting times and soundness)*. 2009, Beuth-Verlag: Berlin, Germany. p. 17.
31. Hunger, M. and H.J.H. Brouwers, *Flow analysis of water–powder mixtures: Application to specific surface area and shape factor.* Cement and Concrete Composites, 2009. **31**(1): p. 39-59.
32. Schmid, M., et al., *Novel zwitterionic PCE superplasticizers for calcined clays and their application in calcined clay blended cements*, in *15th International Congress on the Chemistry of Cement*, J. Gemrich, Editor. 2019, Research Institute of Binding Materials Prague: Prague, Czech Republic. p. 8.
33. Surana, M.S. and S.N. Joshi, *Spectrophotometric method for estimating the reactivity of pozzolanic materials.* Advances in Cement Research, 1998. **1**(4): p. 238-242.
34. Vikan, H., et al., *Correlating cement characteristics with rheology of paste.* Cement and Concrete Research, 2007. **37**(11): p. 1502-1511.
35. Vikan, H., H. Justnes, and R. Figi, *Influence of Cement and Plasticizer Type on the Rheology and Reactivity of Cementitious Binders*, in *ACI SP 239 - 8th CanMET/ACI Intl Conference on Superplasticizers and other Chemical Admixtures in Concrete*, V.M. Malhotra, Editor. 2006, Sheridan Books: Sorrento, Italy. p. 455-470.
36. Yoshioka, K., et al., *Adsorption characteristics of superplasticizers on cement component minerals.* Cement and Concrete Research, 2002. **32**(10): p. 1507-1513.
37. Plank, J. and C. Hirsch, *Impact of zeta potential of early cement hydration phases on superplasticizer adsorption.* Cement and Concrete Research, 2007. **37**(4): p. 537-542.
38. Sposito, R., N. Beuntner, and K.-C. Thienel, *Rheology, setting and hydration of calcined clay blended cements in interaction with PCE-based superplasticisers.* Magazine of Concrete Research, 2019. **73**(15): p. 785-797.
39. Navarro-Blasco, I., et al., *Assessment of the interaction of polycarboxylate superplasticizers in hydrated lime pastes modified with nanosilica or metakaolin as pozzolanic reactives.* Construction and Building Materials, 2014. **73**: p. 1-12.
40. Beuntner, N., R. Sposito, and K.-C. Thienel, *Potential of Calcined Mixed-Layer Clays as Pozzolans in Concrete.* ACI Materials Journal, 2019. **116**(4): p. 19-29.
41. He, C., B. Osbæck, and E. Makovicky, *Pozzolanic reactions of six principal clay minerals: activation, reactivity assessments and technological effects.* Cement and Concrete Research, 1995. **25**(8): p. 1691-1702.

42. Beuntner, N. and K.-C. Thienel, *Properties of Calcined Lias Delta Clay - Technological Effects, Physical Characteristics and Reactivity in Cement*, in *Calcined Clays for Sustainable Concrete - Proceedings of the 1st International Conference on Calcined Clays for Sustainable Concrete*, K. Scrivener and A. Favier, Editors. 2015, Springer: Dordrecht, Netherlands. p. 43-50.
43. Pardo, P., et al. *Surface properties of calcined clays and their dispersion in blended Portland cement pastes*. in *13th International Congress on the Chemistry of Cement*. 2011. Madrid, Spain.
44. Habbaba, A. and J. Plank, *Surface Chemistry of Ground Granulated Blast Furnace Slag in Cement Pore Solution and Its Impact on the Effectiveness of Polycarboxylate Superplasticizers.* Journal of the American Ceramic Society, 2012. **95**(2): p. 768-775.
45. Zunino, F. and K.L. Scrivener, *Improving the Behaviour of Calcined Clay as Supplementary Cementitious Materials by a Combination of Controlled Grinding and Particle Selection*, in *Calcined Clays for Sustainable Concrete*, S. Bishnoi, Editor. 2020, Springer Singapore: Singapore. p. 157-162.
46. Danner, T., G. Norden, and H. Justnes, *The Effect of Calcite in the Raw Clay on the Pozzolanic Activity of Calcined Illite and Smectite*, in *Calcined Clays for Sustainable Concrete - Proceedings of the 3rd International Conference on Calcined Clays for Sustainable Concrete*, S. Bishnoi, Editor. 2020, Springer: Singapore. p. 131-138.
47. Tan, H., et al., *Effect of the ester group in side chain of polycarboxylate superplasticizer on the cement hydration process.* ZKG International, 2016. **69**(7-8): p. 60-67.
48. Scherb, S., et al., *The early hydration of cement with the addition of calcined clay - From single phyllosilicate to clay mixture*, in *20. Internationale Baustofftagung ibausil*, H.-B. Fischer and A. Volke, Editors. 2018, F.A. Finger-Institut für Baustoffkunde, Prof. Dr.-Ing. H.-M. Ludwig: Weimar, Germany. p. 658-666.
49. Scherb, S., et al., *Reaction kinetics during early hydration of calcined phyllosilicates in clinker-free model systems.* Cement and Concrete Research, 2021. **143**: p. 106382.
50. Beuntner, N. and K.-C. Thienel, *Pozzolanic efficiency of calcined clays in blended cements with focus on the early hydration.* Advances in Cement Research, Ahead of print: p. 1-32.
51. Maier, M., et al., *Hydration of cubic tricalcium aluminate in the presence of calcined clays.* Journal of the American Ceramic Society, 2021. **104**(7): p. 3619-3631.
52. Sasse, T., *Evaluierung des Zetapotentials von Zementersatzstoffen in Abhängigkeit ausgewählter Messparameter*, in *Fakultät für Bauingenieurwesen und Umweltwissenschaften, Institut für Werkstoffe des Bauwesens*. 2019, Universität der Bundeswehr München: Neubiberg. p. 66.

7.8 Early hydration behavior of blended cementitious systems containing calcined clays and superplasticizer

Conference paper [Reprint]

"Early hydration behavior of blended cementitious systems containing calcined clays and superplasticizer"

Ricarda Sposito, Marlene Schmid, Nancy Beuntner, Sebastian Scherb, Johann Plank, Karl-Christian Thienel

15th International Congress on the Chemistry of Cement

Prague, Czech Republic, 16th – 20th September 2019, ID 57, 10 p.

Early hydration behavior of blended cementitious systems containing calcined clays and superplasticizer

Ricarda Sposito[1,a], Marlene Schmid[2,b], Nancy Beuntner[1,c], Sebastian Scherb[1,d], Johann Plank[2,e], Karl-Christian Thienel[1,f]

[1]*Institute for Construction Materials, University of the Bundeswehr Munich, Neubiberg, Germany*
[2]*Chair of Construction Chemistry, Technical University Munich, Garching, Germany*

[a]ricarda.sposito@unibw.de
[b]marlene.schmid@bauchemie.ch.tum.de
[c]nancy.beuntner@unibw.de
[d]sebastian.scherb@unibw.de
[e]sekretariat@bauchemie.ch.tum.de
[f]christian.thienel@unibw.de

ABSTRACT

Calcined clays represent a promising material because of worldwide deposits of suitable clays and low CO2 emissions during calcination process for facing the increasing demand for sustainable supplementary cementitious materials (SCM). One side effect of calcined clays is their high water demand as compared to cements. The application of superplasticizers is inevitable to ensure the workability of concretes with calcined clays as SCM. Early hydration kinetics, namely silicate and aluminate reaction of clinker phases, can be significantly modified by superplasticizers. Until now, their compatibility was barely investigated although it depends mainly on type of superplasticizer and on mineralogy of calcined clays. Main objective of this study is to evaluate the influence of selected superplasticizers on reaction kinetics of blended cementitious systems containing different types of calcined clay by investigating their hydration behavior.

Four calcined clays are investigated: one calcined mixed layer clay which contains in its natural form approximately 25 w% kaolinite and 45 w% 2:1 clay minerals. The interaction with superplasticizers and those individual phyllosilicates is investigated on an industrially-used flash-calcined metakaolin, a calcined illitic clay and a calcined muscovite. Two different types of superplasticizers are used. One ordinary Portland cement and one Portland limestone cement are used as cement components.

The hydration kinetics of blended cement pastes is measured by isothermal calorimetry in combination with in-situ X-ray diffraction during first 48 hours of hydration at a temperature of 25 °C. The findings are completed by investigations with scanning electron microscopy at different timings during early hydration.

15th International Congress on the Chemistry of Cement
Prague, Czech Republic, September 16-20, 2019

1. INTRODUCTION

Calcined clays as potential supplementary cementitious material (SCM) come strongly into focus of research (Antoni 2013, Beuntner 2017, Tironi et al. 2014). Especially calcined mixed layer clays with different phyllosilicates and further minerals are interesting as future SCM as they are available in sufficient quantities worldwide. Calcined clays have a pozzolanic impact on clinker reaction kinetics already during early hydration (Beuntner 2017, Danner et al. 2012, Scherb et al. 2018). Beside further CO_2 savings (Cancio Díaz et al. 2017), the addition of limestone is known to have good synergy effects with calcined clays in cementitious systems (Antoni et al. 2015, Martirena Hernández & Scrivener 2015, Tironi et al. 2017, Vance et al. 2013). The mineralogy of clay has according to Hermann & Rickert (2015) a significant impact on the specific surface area and hence on the required dosages of superplasticizers. Calcined clays exhibit a high specific surface area and water demand and require the use of superplasticizers in concrete (Thienel & Beuntner 2018).

There is a wide range of observations when it comes to the influence of superplasticizers on the hydration kinetics of ordinary Portland cement. According to Prince et al. (2002), polynaphthalene sulfonate superplasticizers retard the hydration of C_3A while Roncero et al. (2002) found out that both polycondensates and PCE polymers accelerate the reaction of C_3A, the formation of ettringite and the dissolution of gypsum. Sakai et al. (2006) also observed an accelerated reaction of C_3A but a lower rate of hydration due to the addition of different types of superplasticizers. These findings were also made by Lothenbach et al. (2007) investigating a PCE with OPC: the dissolution of C_3S was strongly retarded during the first 30 h of hydration by adding PCE. Investigations on the interaction of calcined clays and lignosulfonates revealed that dosages required for equal dispersion effects exceed dosage limits and lead to strong retardation effects (Sposito et al. 2018). Polycondensates retard the aluminate clinker reaction and formation of ettringite (Zaribaf & Kurtis 2018), but also accelerate pozzolanic reaction of metakaolin compared to PCE (Ahn et al. 2015). According to Ng & Justnes (2015) and Zaribaf & Kurtis (2018), PCE exhibit the highest dispersion effectiveness and the least influence on hydration kinetics. Taking this knowledge into account, the impact of diverse superplasticizers on the hydration behavior of cementitious systems blended with different types of cements and calcined clays is investigated.

2. MATERIALS AND METHODS

2.1 Materials

2.1.1 Cements

One ordinary Portland cement (OPC) CEM I 42.5 R and one Portland limestone cement (PLC) CEM II/A-LL 32.5 R, complying with (DIN EN 197-1 2011), are used. Their mineral phase contents are given in Table 1 and the physical parameters are listed in Table 3.

Table 1. Mineralogical analysis of cements (information provided by producer)

Cement	Mineral phase [wt%]						
	C_3S	C_2S	C_3A	C_4AF	CaO_{free}	Sulfates	Calcite
OPC	61.6	18.2	5.8	9.0	0.6	3.2	0.6
PLC	48.9	15.2	5.1	8.1	0.1	4.0	14.4

2.1.2 Calcined clays

Three calcined phyllosilicates and one calcined mixed layer clay are investigated. The metakaolin (Mk) is an industrially used product, flash-calcined at 550 °C with 93 wt% amorphous content, 5 wt% quartz and traces of anatase and mica. Metaillite (Mi) and metamuscovite (Mu) are calcined for 60 min in a lab muffle kiln at 770 °C (Mi) and 800 °C (Mu). The temperatures were chosen according to dehydroxylation temperature obtained by DTG and by highest solubility of Al- and Si-ions in alkaline solution. Mi possesses 56.4 wt% amorphous content, 4.9 wt% calcite, 38.2 wt% illite and traces of portlandite and lime. Mu has 19.2 wt% amorphous phases and 80.8 wt% muscovite (high-temperature modification). The origin, the calcination procedure and the grinding process of the mixed layer clay (TG) are described in (Beuntner & Thienel 2017, Gmür et al. 2016). Its mineralogical composition is given in Table 2, the

solubility of Al and Si ions of calcined clays and the physical parameters of all binders are displayed in Table 3.

Table 2. Mineralogical composition of calcined mixed layer clay (TG)

	Phase [wt%]										
	Quartz	Muscovite	Calcite	Illite	Chlorite	Feldspar	Secondary Silicates	Hematite	Ores	Sulfates	Amorphous
TG	16.2	2.2	0.6	4.6	0.4	6.0	6.3	0.6	1.1	1.6	60.8

Table 3. Physical parameters of cements (OPC, PLC), metakaolin (Mk), metamuscovite (Mu), metaillite (Mi) and calcined mixed layer clay (TG)

Parameter	Method	OPC	PLC	Mk	Mu	Mi	TG
Particle density [g/cm³]	He-pycnometer	3.17	3.09	2.61	2.79	2.72	2.63
Specific surface area [m²/g]	(DIN ISO 9277 2003)	1.0	1.7	17.8	11.8	94.6	3.9
Water demand [wt%]	(DIN EN 196-3 2009)	28.9	28.2	34.5	55.4	38.6	30.5
d_{10} [µm]	(ISO 13320 2009)	4.1	2.3	3.0	9.3	2.7	4.0
d_{50} [µm]		15.8	13.1	14.8	19.2	6.8	13.2
d_{90} [µm]		46.0	46.0	76.2	45.7	61.9	37.0
Si-ions solubility [wt%]	Inductively coupled plasma optical emission spectrometry (ICP-OES)	-	-	15.65	0.51	4.02	1.80
Al-ions solubility [wt%]		-	-	14.25	0.26	1.55	1.09
Si/Al ratio [-]		-	-	1.10	1.93	2.59	1.65

2.1.3 Superplasticizers

Two industrial superplasticizers are selected to investigate their influence on the hydration behavior on calcined clay blended cementitious systems. As representative for polycondensates, the calcium salt of a β-naphthalene sulfonate formaldehyde polycondensate (abbreviation: *NSF*) with a solid content of 40.0 wt% is used. As polycarboxylate-based superplasticizer, an α-methallyl-ω-methoxy poly(ethylene glycol) ether (HPEG) type PCE with a long side chain and a high anionic charge density (abbreviation: *HPEG*) is investigated. Its solid content is 50.0 wt%.

The dosages of superplasticizers (Table 4) are adjusted for each binder system in cement paste for a constant spread of 26 cm ± 0.5 cm by a modified mini slump test according to (DIN EN 1015-3 2007).

All dosages represent the active agent as % by weight of binder (%bwob) and are constantly used for all methods.

Table 4. Dosages of superplasticizers [%bwob]

Superplasticizer	OPC with					PLC with				
	-	20Mk	20Mu	20Mi	20TG	-	20Mk	20Mu	20Mi	20TG
NSF	0.21	0.68	1.50	0.95	0.40	0.24	0.77	1.50	0.97	0.50
HPEG	0.05	0.19	0.16	0.37	0.07	0.06	0.20	0.16	0.40	0.08

2.2 Methods

The cements are constantly substituted by 20 wt% of calcined clays at a water-to-binder (w/b) ratio of 0.50. The samples are designated as *cement_substitution rate and type of calcined clay_dosage and type of superplasticizer.* The hydration kinetics are determined by isothermal calorimetry with TAM Air (TA Instruments, Delaware/USA) and by in-situ X-ray diffraction (XRD) at 25 °C. The blended binder is homogenized for 30 seconds before the blended cement pastes are mixed for 60 seconds by hand for all methods. The samples are transferred into plastic ampoules for calorimetric measurements. The resulting heat flow is calculated to 1 g of cement [mW/g_{cement}]. For in-situ XRD, the blended cement pastes are transferred into flat metal crucibles and covered by a Kapton film to prevent drying up of the fresh paste. The hydration behavior is observed by an X-ray diffractometer Empyrean (PANalytical, Almelo/Netherlands) with PIXcel^{1D} detector and Bragg-Brentano^{HD} monochromator. Each measurement is in a range from 6 to 40 °2Θ and takes 15 min. The XRD sample holder is connected to a temperature-controlled device. The development of crystalline phases is illustrated by using isolines view of software Highscore Plus 4.7 (PANalytical, Almelo/Netherlands). The time-dependent appearance and disappearance of phases is determined by qualitative peak analysis of ettringite (hkl phase 110) (Goetz-Neunhoeffer & Neubauer 2005), AFm-Hc (006) (Runcevski et al. 2012), gypsum (020) (Schofield et al. 2000) and portlandite (001) (Busing & Levy 1957). The ettringite (110) is chosen as there are overlaying effects of ettringite (010) and the high temperature modification of muscovite (002) (Catti et al. 1989) in the systems with metamuscovite and superplasticizers.

3. RESULTS AND DISCUSSION

3.1 Influence of superplasticizers on reaction kinetics during the first 48 hours of hydration

A small peak after the maximum indicates the aluminate reaction (dissolution of C_3A and strong precipitation of ettringite according to Hesse et al. (2011)) for OPC (Figure 1) while PLC exhibits a dominant peak due to aluminate reaction (Figure 2). The addition of calcined clays has a significant influence on the reaction kinetics. OPC/PLC_20Mi yield the highest peak intensities after only 8.2 h. The acceleration is attributed to the fineness and high specific surface area of Mi (see Table 3). The high main peaks of OPC/PLC_20Mk result from the high solubility of Al and Si ions of Mk (Table 3). The high main peak intensities for Mk and Mi systems both may result from overlaying silicate and aluminate reactions as described by Beuntner (2017) for Mk. Systems with Mu exhibit accelerated silicate reactions compared to systems with cement only despite the low solubility of ions and the comparably coarse granulometry of Mu (Table 3). OPC/PLC_20Mu show up broader shoulders and lower aluminate peak intensities compared to Mi and Mk systems, indicating still a significant pozzolanic contribution of Mu to hydration kinetics. In a less distinctive manner, the addition of 20 wt% TG to OPC does also slightly accelerate the reaction kinetics until the aluminate shoulder is reached due to its fineness compared to OPC. This effect does not apply to PLC systems as PLC and TG have a more similar fineness (Table 3). While there is no significant peak detectable in the declining heat flow curve of OPC, OPC_20TG exhibits a broad shoulder at 23 h, which can be associated with the pozzolanic contribution of TG to aluminate reaction. The heat flow curves for PLC_20Mu, PLC_20TG and PLC are congruent during the first 10 h and differ later on in the appearance and intensity of the aluminate peak. Hence, a good synergy effect of PLC and 20 wt% TG can be confirmed. Scherb et al. (2018) attribute furthermore the decline of the main peak of systems with calcined clays and limestone to the formation of AFm hemicarboaluminate (AFm-Hc) phase.

15th International Congress on the Chemistry of Cement
Prague, Czech Republic, September 16-20, 2019

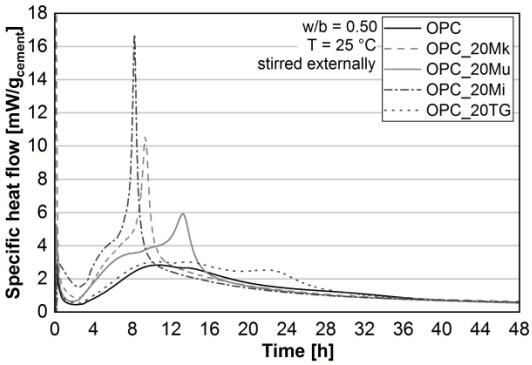

Figure 1. Heat flow of OPC systems without superplasticizers

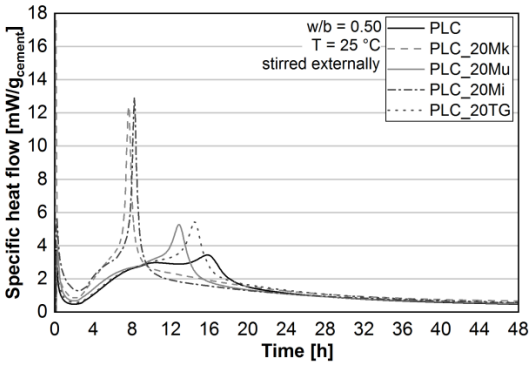

Figure 2. Heat flow of PLC systems without superplasticizers

Adding the polycondensate (NSF) has a retarding effect on the aluminate reaction by 1 h (OPC_0.21NSF/PLC_0.24NSF) which confirms findings of Prince et al. (2002). For systems with Mk, Mi or TG, the rest periods are prolonged by up to 1.7 h. Despite the high dosages of NSF in OPC_20Mi_0.95NSF and OPC_20Mk_0.68NSF and considering both the retarded end of rest period and occurrence of the aluminate peaks, the systems exhibit similar heat flow curves as OPC_20Mi/20Mk (Figure 3). The higher intensity of the main peak of OPC_20Mk_0.68NSF can be explained by overlapping chemo-mineralogical reactions and a boost of pozzolanic reactivity by polycondensates as already observed by Ahn et al. (2015). PLC_20Mi_0.97NSF shows up a general retardation of 1.5 h but a slightly higher intensity of the aluminate peak (Figure 4). Despite a lower dosage compared to PLC_20Mi_0.97NSF, PLC_20Mk_0.77NSF is more affected by NSF: the rest period is slightly more extended and the main peak is significantly less intense and occurs even 3.6 h later than without superplasticizer. Ten repeats of measurement were necessary for OPC/PLC_20Mu_1.50NSF due to bleeding during measurement. The averaging of the individual measurements shows a strong retardation of both the silicate and aluminate reaction. Although the systems with TG need the second lowest dosages of NSF, the superplasticizer has a certain influence on the reaction kinetics. Both systems are retarded by approximately 1 h compared to cement systems with NSF. Between 12 and 20 h, OPC_20TG_0.40NSF exhibits a constant level of heat flow, which is elevated afterwards by further pozzolanic contribution of TG. As the maximum peak is higher for OPC_20TG_0.40NSF (Figure 3) and occurs slightly earlier compared to OPC_20TG (Figure 1) without superplasticizer, NSF might provide a little boost to pozzolanic reactivity at least in systems with ordinary Portland cement. The findings of Ahn et al. (2015) on the interaction of metakaolin and polycondensates hence are also applicable to the investigated calcined mixed layer clay with OPC. Similar findings hold less pronounced also for PLC_20TG_0.50NSF (Figure 4) compared to PLC_20TG (Figure 2).

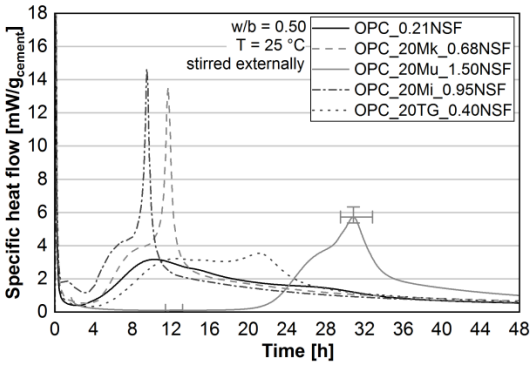

Figure 3. Heat flow of OPC_x_NSF systems

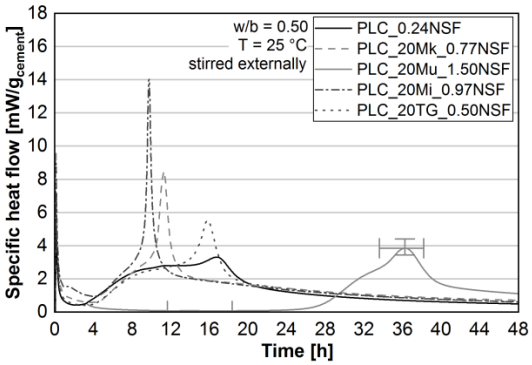

Figure 4. Heat flow of PLC_x_NSF systems

Using HPEG superplasticizer leads to a slightly prolonged rest period for OPC_0.05HPEG (Figure 5) and PLC_0.06HPEG (Figure 6). For pure cement systems, the retarding effect of HPEG on aluminate

15th International Congress on the Chemistry of Cement
Prague, Czech Republic, September 16-20, 2019

reaction is also less than the impact of NSF confirming earlier findings (Ng & Justnes 2015, Zaribaf & Kurtis 2018). The rest periods are shorter for all systems with calcined clays when HPEG is used instead of NSF. OPC_20Mk_0.19HPEG and OPC_20Mi_0.37HPEG exhibit lower main peak intensities at similar times compared to systems with NSF. This effect goes along with broader shoulders on the left side of the peaks, which indicate earlier ongoing hydration processes (Figure 5). Although PLC_20Mi_0.40HPEG has the highest dosage of HPEG, the retardation of the main peak compared to PLC_20Mi is negligible whereas PLC_20Mk_0.20HPEG exhibits a retardation of 1.3 h compared to PLC_20Mk with half the amount of HPEG used. OPC_20Mu shows up only a slight retardation of main peak whereas the HPEG PCE even has an immense acceleration effect on reaction kinetics in PLC_20Mu_0.16HPEG, both resulting in significantly higher intensities compared to OPC/PLC_20Mu. At low dosages (0.16 %bwob) of HPEG, they exhibit better compatibilities than with 1.50 %bwob NSF. Systems with TG and HPEG reveal similar heat flow curves as systems with OPC only and especially with PLC only: the curves of OPC_0.05HPEG and OPC_20TG_0.07HPEG are congruent during the first 14 h until the aluminate part of the pozzolanic reaction of TG commences. Compared to the systems without superplasticizer and with NSF, the curves of the PLC_20TG_0.08HPEG and the PLC_0.06HPEG system almost coincide and differ only in the intensity of their main peaks.

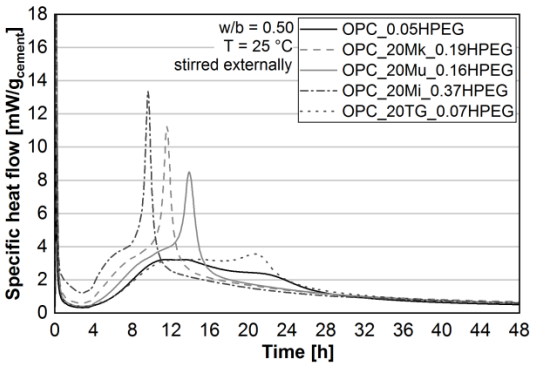

Figure 5. Heat flow of OPC_x_HPEG systems

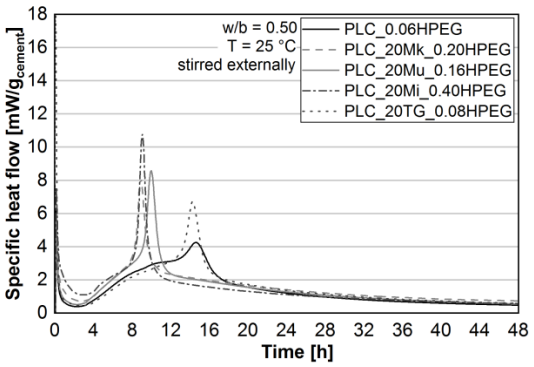

Figure 6. Heat flow of PLC_x_HPEG systems

3.2 Influence of superplasticizers on formation of hydrate phases using the example of OPC and OPC-metamuscovite systems

Results from in situ XRD are limited to OPC and OPC_20Mu systems as the latter are influenced the most by superplasticizers. All systems show up an immediate formation of ettringite. It goes along with dissolution of gypsum, which is completed earlier for OPC_0.21NSF and later for OPC_0.05HPEG compared to OPC (Figure 7). The latter finding fits with results from Jansen et al. (2012) where a PCE retarded the dissolution of gypsum. While there is no formation of AFm-Hc during the first 48 h of hydration in the OPC system, both superplasticizers precipitate the formation of AFm-Hc, which is detectable after 28 h (OPC_0.21NSF) and 36.5 h (OPC_0.05HPEG). The formation of portlandite (CH) starts between 4.5 and 5 h for all OPC systems. The main part of CH formation is completed after 10 h (OPC_0.21NSF) and 11.5 h (OPC) while it persists until 16.5 h for OPC_0.05HPEG. These results fit well with the maxima in the heat flow curves from calorimetric measurements.

Gypsum is dissolved in OPC_20Mu earlier than in OPC as observed beforehand by Scherb et al. (2018). The dissolution of gypsum is accelerated further in OPC_20Mu_0.16HPEG (Figure 8) which explains the high intensity of its main peak in the heat flow curve in Figure 5. In OPC_20Mu_1.50NSF it takes 24.5 h to dissolve the gypsum completely. Formation of AFm-Hc starts after 20 h (OPC_20Mu) and 15 h (OPC_20Mu_0.16HPEG), while there is no AFm-Hc detectable in OPC_20Mu_1.50NSF during the first 48 h. Portlandite (CH) is detectable after 3.25 h (OPC_20Mu) and 4.75 h (OPC_20Mu_0.16HPEG) and the main reaction takes place until 13.5 and 12.5 h respectively. In OPC_20Mu_1.50NSF, the (main) formation of CH is strongly retarded. It does not start before a time of 12.5 h (Figure 8) and continues until 26.5 h. These observations confirm the results of isothermal calorimetry where the rest period of OPC_20Mu_1.50NSF does not end before a time of 12.5 h (Figure 3). Not least due to its extremely high amount, NSF retards both aluminate and silicate reaction in the cement-Mu system. HPEG promotes the aluminate reaction and slightly retards the silicate reaction. Winnefeld (2012) reports both a stronger retardation with increasing amount of superplasticizer and a stronger retardation of PCE than

15th International Congress on the Chemistry of Cement
Prague, Czech Republic, September 16-20, 2019

of naphthalene sulfonate superplasticizers if the same amount is used. As less HPEG is needed for the same dispersion effects, it concludes that the retardation is less as well.

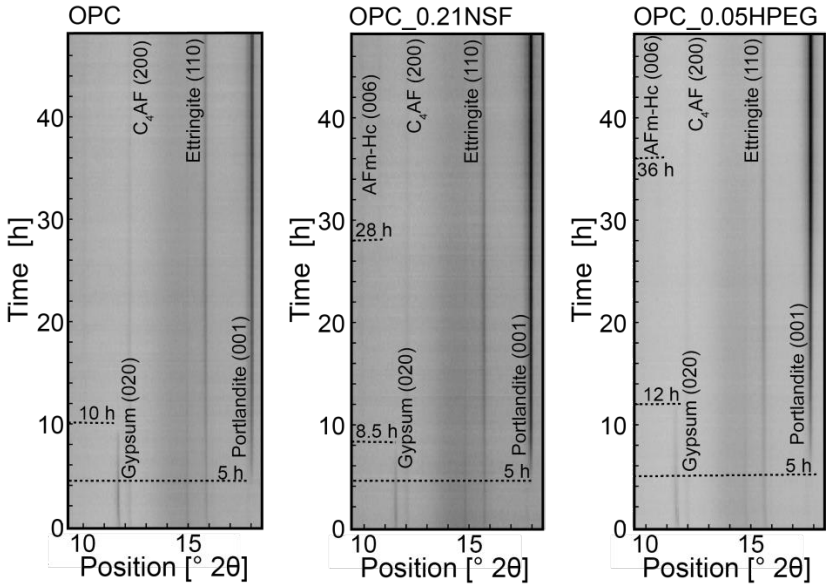

Figure 7. In situ X-ray plots from 9.5 to 18.5 °2Θ for OPC systems

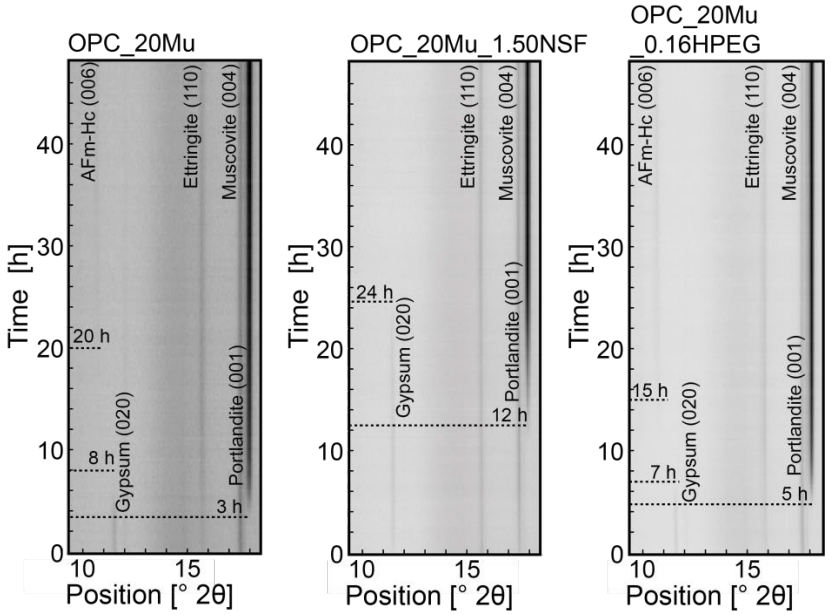

Figure 8. In situ X-ray plots from 9.5 to 18.5 °2Θ for OPC_20Mu systems

4. CONCLUSION

The previous investigation program highlights the effect of superplasticizers on the hydration kinetics of cementitious systems containing calcined clays. The main influences are on the dissolution of gypsum as sulfate carrier as well as on the beginning of formation of portlandite and AFm-Hc. Investigated binder systems require in general higher dosages of polycondensate than of PCE, which lead partially to stronger retardation effects. Selected systems exhibit incompatibilities with NSF indicated by late formation of portlandite or dissolution of gypsum whereas the investigated HPEG PCE exhibits a

superior compatibility with calcined clay blended cementitious systems and has only minor or partially even boosting impact on the pozzolanic reaction kinetics, e.g. on the formation of AFm-Hc. Nonetheless also the addition of NSF can slightly accelerate hydration kinetics confirming earlier findings from literature. Commonly known synergy effects between Portland limestone cement and calcined clays hold also for systems dispersed with superplasticizers.

Calcined mixed layer clays are particularly promising due to their mineralogical composition as they are capable to interact even with low dosages of superplasticizers thus resulting in good dispersing effects and exhibiting a similar hydration behavior as pure cement systems. In general, the influence of the amount of superplasticizer on the retardation of hydration increases non-linearly with increasing dosage and is compensated by the addition of calcined clays. In further studies, the demand for superplasticizers and the compensation of retarding effects by calcined clays should be considered in detail as there are - beside the mineralogy of calcined clays - several more parameters (e.g. grinding fineness) which affect the hydration kinetics.

5. ACKNOWLEDGEMENT

The authors like to thank Schwenk Zement KG for sponsoring the cements and Liapor GmbH & Co. KG for providing the calcined mixed layer clay. They also thank Bozzetto Group and Jilin Zhongxin Chemical Group Co., Ltd. for the supply of the superplasticizers. Furthermore, the authors wish to express their deepest gratitude to Deutsche Forschungsgemeinschaft for the financial support of the research project “Ecological and energetic optimization of concrete: Interaction of structurally divergent superplasticizers with calcined clays” (PL 472/11-1 and TH 1383/3-1).

6. REFERENCES

Ahn, T-H, Shim, K-B, & Ryou, J-S (2015). „*The relationship between various superplasticizers and hydration of mortar incorporating metakaolin*,“ Journal of Ceramic Processing Research, Vol. 16, No. 2, pp. 181-187.

Antoni, M (2013). „*Investigation of cement substitution by blends of calcined clays and limestone*,“ Faculté des Sciences et Techniques de L'ingénieur, École Polytechnique Fédérale de Lausanne, Lausanne, 254 pp.

Antoni, M, Baquerizo, L, & Matschei, T (2015). „*Investigation of ternary mixes made of clinker limestone and slag or metakaolin: Importance of reactive alumina and silica content*,“ in *Calcined Clays for Sustainable Concrete*, Scrivener, K., and Favier, A., Editors. Springer Netherlands, pp. 545-553.

Beuntner, N (2017). „*Zur Eignung und Wirkungsweise calcinierter Tone als reaktive Bindemittelkomponente in Zement*,“ Fakultät für Bauingenieurwesen und Umwelt-wissenschaften, Universität der Bundeswehr München, Neubiberg, 207 pp.

Beuntner, N, & Thienel, K-C (2017). „*Performance and properties of concrete made with calcined clays*,“ in *ACI SP 320 - 10th ACI/RILEM International Conference on Cementitious Materials and Alternative Binders for Sustainabe Concrete*, Tagnit-Hamou, A., Editor. Sheridan Books, Montreal, Canada, pp. 7.1-7.12.

Busing, WR, & Levy, HA (1957). „*Neutron Diffraction Study of Calcium Hydroxide*,“ The Journal of Chemical Physics, Vol. 26, No. 3, pp. 563-568.

Cancio Díaz, Y, Sánchez Berriel, S, Heierli, U, Favier, AR, Sánchez Machado, IR, Scrivener, KL, Martirena Hernández, JF, & Habert, G (2017). „*Limestone calcined clay cement as a low-carbon solution to meet expanding cement demand in emerging economies*,“ Development Engineering, Vol. 2, pp. 82-91.

Catti, M, Ferraris, G, & G., I (1989). „*Thermal strain analysis in the crystal structure of muscovite at 700 °C*,“ European Journal of Mineralogy, Vol. 1, No. 5, pp. 625-632.

Danner, T, Ostnor, T, & Justnes, H (2012). „*Calcined marl as a pozzolan for sustainable development of the cement and concrete industry*," in ACI SP 289 - 12th International Conference on Recent Advances in Concrete Technology and Sustainability Issues. Prague, pp. 357-368.

DIN EN 196-3 (2009). „*Prüfverfahren für Zement - Teil 3: Bestimmung der Erstarrungszeiten und der Raumbeständigkeit (Methods of testing cement - Part 3: Determination of setting times and soundness)*".

DIN EN 197-1 (2011). „*Zement - Teil 1: Zusammensetzung, Anforderungen und Konformitätskriterien von Normalzement (Cement - Part 1: Composition, specifications and conformity criteria for common cements)*".

DIN EN 1015-3 (2007). „*Prüfverfahren für Mörtel für Mauerwerk-Teil 3: Bestimmung der Konsistenz von Frischmörtel (mit Ausbreittisch) (Methods of test for mortar for masonry - Part 3: Determination of consistence of fresh mortar (by flow table))*".

DIN ISO 9277 (2003). „*Bestimmung der spezifischen Oberfläche von Feststoffen durch Gasadsorption nach dem BET-Verfahren (Determination of the specific surface area of solids by gas adsorption - BET method)*".

Gmür, R, Thienel, K-C, & Beuntner, N (2016). „*Influence of aging conditions upon the properties of calcined clay and its performance as supplementary cementitious material*," Cement and Concrete Composites, Vol. 72, pp. 114-124.

Goetz-Neunhoeffer, F, & Neubauer, J (2005). „*Refined ettringite (Ca6Al2(SO4)3(OH)12·26H2O) structure for quantitative X-ray diffraction analysis*," Powder Diffraction, Vol. 21, No. 1, pp. 4-11.

Herrmann, J, & Rickert, J (2015). „*Interactions between cements with calcined clay and superplasticizers*," in 11th Int. Conference on Superplasticizers and Other Chemical Admixtures in Concrete. Ottawa, Canada, pp. 299-314.

Hesse, C, Goetz-Neunhoeffer, F, & Neubauer, J (2011). „*A new approach in quantitative in-situ XRD of cement pastes: Correlation of heat flow curves with early hydration reactions*," Cement and Concrete Research, Vol. 41, No. 1, pp. 123-128.

ISO 13320 (2009). „*Particle size analysis - Laser diffraction methods*".

Jansen, D, Neubauer, J, Goetz-Neunhoeffer, F, Haerzschel, R, & Hergeth, WD (2012). „*Change in reaction kinetics of a Portland cement caused by a superplasticizer — Calculation of heat flow curves from XRD data*," Cement and Concrete Research, Vol. 42, No. 2, pp. 327-332.

Lothenbach, B, Winnefeld, F, & Figi, R (2007). „*The influence of superplasticizers on the hydration of Portland cement*," in *12th International Congress on the Chemistry of Cement*, Montreal, Canada pp.

Martirena Hernández, F, & Scrivener, K (2015). „*Development and introduction of a low clinker, low carbon, ternary blend cement in Cuba*," in *Calcined Clays for Sustainable Concrete*, Scrivener, K., and Favier, A., Editors. Springer, Dordrecht, pp. 323-329.

Ng, S, & Justnes, H (2015). „*Influence of dispersing agents on the rheology and early heat of hydration of blended cements with high loading of calcined marl*," Cement and Concrete Composites, Vol. 60, pp. 123-134.

Prince, W, Edwards-Lajnef, M, & Aïtcin, PC (2002). „*Interaction between ettringite and a polynaphthalene sulfonate superplasticizer in a cementitious paste*," Cement and Concrete Research, Vol. 32, No. 1, pp. 79-85.

Roncero, J, Valls, S, & Gettu, R (2002). „*Study of the influence of superplasticizers on the hydration of cement paste using nuclear magnetic resonance and X-ray diffraction techniques*," Cement and Concrete Research, Vol. 32, No. 1, pp. 103-108.

Runcevski, T, Dinnebier, RE, Magdysyuk, OV, & Pollmann, H (2012). „*Crystal structures of calcium hemicarboaluminate and carbonated calcium hemicarboaluminate from synchrotron powder diffraction data*," Acta Crystallographica Section B, Vol. 68, No. 5, pp. 493-500.

Sakai, E, Kasuga, T, Sugiyama, T, Asaga, K, & Daimon, M (2006). „*Influence of superplasticizers on the hydration of cement and the pore structure of hardened cement*," Cement and Concrete Research, Vol. 36, No. 11, pp. 2049-2053.

Scherb, S, Beuntner, N, Köberl, M, & Thienel, K-C (2018). „*The early hydration of cement with the addition of calcined clay - from single phyllosilicate to clay mixture*," in 20th International Conference on Building Materials. Weimar, Germany, pp. 658-666.

Schofield, PF, Wilson, CC, Knight, KS, & Stretton, IC (2000). „*Temperature related structural variation of the hydrous components in gypsum*," Zeitschrift für Kristallographie - Crystalline Materials, Vol. 215, No. 12, pp. 707.

Sposito, R, Dürr, I, & Thienel, K-C (2018). „*Lignosulfonates in cementitious systems blended with calcined clays*," in *SP-326 Durability and Sustainability of Concrete Structures - 2nd Workshop Proceedings*, Falikman, V., et al., Editors. Sheridan Books, Moscow, Russia, pp. 10.1-10.10.

Thienel, K-C, & Beuntner, N (2018). „*Calcinierte Tone und ihr Potenzial für die moderne Betontechnologie*," in 14. Symposium Baustoffe und Bauwerkserhaltung KIT - Betone der Zukunft - Herausforderungen und Chancen. Karlsruhe, pp. 37-48.

Tironi, A, Scian, AN, & Irassar, EF (2017). „*Blended cements with limestone filler and kaolinitic calcined clay: filler and pozzolanic effects*," Journal of Materials in Civil Engineering, Vol. 29, No. 9, pp. 8.

Tironi, A, Trezza, MA, Scian, AN, & Irassar, EF (2014). „*Potential use of Argentine kaolinitic clays as pozzolanic material*," Applied Clay Science, Vol. 101, pp. 468-476.

Vance, K, Aguayo, M, Oey, T, Sant, G, & Neithalath, N (2013). „*Hydration and strength development in ternary portland cement blends containing limestone and fly ash or metakaolin*," Cement and Concrete Composites, Vol. 39, pp. 93-103.

Winnefeld, F (2012). „*Interaction of superplasticizers with calcium sulfoaluminate cements*," in 10th International Conference on Superplasticizers and Other Chemical Admixtures in Concrete. Prague, pp. 17.

Zaribaf, BH, & Kurtis, KE (2018). „*Admixture compatibility in metakaolin–portland-limestone cement blends*," Materials and Structures, Vol. 51, No. 1, pp. 13.

8 References

1. Scripture, E.W., *Cement mix (US patent 2,169,980)*. 1939: USA. p. 3.
2. Jasmund, K., G. Lagaly, H.M. Köster, E.E. Kohler, M. Müller-Vonmoos, E.A. Niederbudde, K.-H. Schüller, U. Schwertmann, and M. Störr, *Tonminerale und Tone: Struktur, Eigenschaften, Anwendungen und Einsatz in Industrie und Umwelt*. 1993, Darmstadt: Dr. Dietrich Steinkopff Verlag. XIV, 490.
3. Ito, A. and R. Wagai, *Global distribution of clay-size minerals on land surface for biogeochemical and climatological studies.* Scientific Data, 2017. **4**(1): p. 170103.
4. Velde, B., D. Righi, A. Meunier, and S. Hillier, *Origin and Mineralogy of Clays - Clays and the Environment*. 1995: Springer-Verlag Berlin Heidelberg. XV.
5. Gridi-Bennadji, F., B. Beneu, J.P. Laval, and P. Blanchart, *Structural transformations of Muscovite at high temperature by X-ray and neutron diffraction.* Applied Clay Science, 2008. **38**(3–4): p. 259-267.
6. Aparicio, P., X. Arroyo, J. Cuadros, R. Ferrell, S. Fiore, J. Forsman, F. Huertas, P. Komadel, J. Madejová, A. Meunier, F. Nieto, A. Plançon, and J. Srodon, *Interstratified Clay Minerals: Origin, Characterization and Geochemical Significance*. AIPEA Educational Series. Vol. 1. 2013, Bari: Digilabs.
7. Zhang, Y., Q. Liu, J. Xiang, S. Zhang, and R.L. Frost, *Insight into morphology and structure of different particle sized kaolinites with same origin.* Journal of Colloid and Interface Science, 2014. **426**: p. 99-106.
8. Caseri, W.R., R.A. Shelden, and U.W. Suter, *Preparation of muscovite with ultrahigh specific surface area by chemical cleavage.* Colloid and Polymer Science, 1992. **270**(4): p. 392-398.
9. Au, P.-I., S.-Y. Siow, L. Avadiar, E.-M. Lee, and Y.-K. Leong, *Muscovite mica and koalin slurries: Yield stress–volume fraction and deflocculation point zeta potential comparison.* Powder Technology, 2014. **262**: p. 124-130.
10. Huggett, J.M., *SEDIMENTARY ROCKS | Clays and Their Diagenesis*, in *Encyclopedia of Geology*, R.C. Selley, L.R.M. Cocks, and I.R. Plimer, Editors. 2005, Elsevier: Oxford. p. 62-70.
11. Keller, W.D., R.C. Reynolds, and A. Inoue, *Morphology of Clay Minerals in the Smectite-to-Illite Conversion Series by Scanning Electron Microscopy.* Clays and Clay Minerals, 1986. **34**(2): p. 187-197.
12. He, C., E. Makovicky, and B. Osbæck, *Thermal stability and pozzolanic activity of calcined kaolin.* Applied Clay Science, 1994. **9**(3): p. 165-187.
13. Sánchez-Soto, P.J., M. del Carmen Jiménez de Haro, L.A. Pérez-Maqueda, I. Varona, and J.L. Pérez-Rodríguez, *Effects of dry grinding on the structural changes of kaolinite powders.* Journal of the American Ceramic Society, 2000. **83**(7): p. 1649-1657.
14. Soro, N.S., *Influence des ions fer sur les transformations thermiques de la kaolinite*. 2003, Université de Limoges: Limoges. p. 158.
15. Schuttlefield, J.D., D. Cox, and V.H. Grassian, *An investigation of water uptake on clays minerals using ATR-FTIR spectroscopy coupled with quartz crystal microbalance measurements.* Journal of Geophysical Research: Atmospheres, 2007. **112**(D21303): p. 14.
16. Neißer-Deiters, A., S. Scherb, N. Beuntner, and K.-C. Thienel, *Influence of the calcination temperature on the properties of a mica mineral as a suitability study for the use as SCM.* Applied Clay Science, 2019. **179**(105168).
17. Mitchell, J.K. and K. Soga, *Fundamentals of Soil Behavior*. 3 ed. 2005: Wiley. 592.
18. He, C., B. Osbæck, and E. Makovicky, *Pozzolanic reactions of six principal clay minerals: activation, reactivity assessments and technological effects.* Cement and Concrete Research, 1995. **25**(8): p. 1691-1702.
19. Macht, F., K. Eusterhues, G.J. Pronk, and K.U. Totsche, *Specific surface area of clay minerals: Comparison between atomic force microscopy measurements and bulk-gas (N2) and -liquid (EGME) adsorption methods.* Applied Clay Science, 2011. **53**(1): p. 20-26.

20. Hatch, C.D., J.S. Wiese, C.C. Crane, K.J. Harris, H.G. Kloss, and J. Baltrusaitis, *Water Adsorption on Clay Minerals As a Function of Relative Humidity: Application of BET and Freundlich Adsorption Models.* Langmuir, 2011. **28**: p. 1790-1803.
21. White, W.A. and E. Pichler, *Water-Sorption Characteristics of Clay Minerals Circular 266*, I.S.G. Survey, Editor. 1959, Illinois State Geological Survey: Urbana. p. 20.
22. Hussain, S.A., Ş. Demirci, and G. Özbayoğlu, *Zeta Potential Measurements on Three Clays from Turkey and Effects of Clays on Coal Flotation.* Journal of Colloid and Interface Science, 1996. **184**(2): p. 535-541.
23. Chorom, M. and P. Rengasamy, *Dispersion and zeta potential of pure clays as related to net particle charge under varying pH, electrolyte concentration and cation type.* European Journal of Soil Science, 1995. **46**(4): p. 657-665.
24. Lei, L. and J. Plank, *A study on the impact of different clay minerals on the dispersing force of conventional and modified vinyl ether based polycarboxylate superplasticizers.* Cement and Concrete Research, 2014. **60**: p. 1-10.
25. Sposito, G., N.T. Skipper, R. Sutton, S.-H. Park, A.K. Soper, and J.A. Greathouse, *Surface geochemistry of the clay minerals.* Proceedings of the National Academy of Sciences, 1999. **96**(7): p. 3358-3364.
26. Bridson, D., T.W. Davies, and D.P. Harrison, *Properties of flash-calcined kaolinite.* Clay and Clay Minerals, 1985. **33**(3): p. 258-260.
27. Salvador, S., *Pozzolanic properties of flash-calcined kaolinite: A comparative study with soak-calcined products.* Cement and Concrete Research, 1995. **25**(1): p. 102-112.
28. Teklay, A., C. Yin, and L. Rosendahl, *Flash calcination of kaolinite rich clay and impact of process conditions on the quality of the calcines: A way to reduce CO_2 footprint from cement industry.* Applied Energy, 2015. **162**: p. 1218-1224.
29. San Nicolas, R., M. Cyr, and G. Escadeillas, *Characteristics and applications of flash metakaolins.* Applied Clay Science, 2013. **83–84**: p. 253-262.
30. Beuntner, N., R. Sposito, and K.-C. Thienel, *Potential of Calcined Mixed-Layer Clays as Pozzolans in Concrete.* ACI Materials Journal, 2019. **116**(4): p. 19-29.
31. Beuntner, N. and K.-C. Thienel, *Properties of Calcined Lias Delta Clay - Technological Effects, Physical Characteristics and Reactivity in Cement*, in *Calcined Clays for Sustainable Concrete - Proceedings of the 1st International Conference on Calcined Clays for Sustainable Concrete*, K. Scrivener and A. Favier, Editors. 2015, Springer: Dordrecht, Netherlands. p. 43-50.
32. Danner, T., *Reactivity of Calcined Clays*, in *Faculty of Natural Science and Technology, Department of Natural Sciences and Engineering*. 2013, NTNU: Trondheim. p. 229.
33. Almenares, R.S., L.M. Vizcaíno, S. Damas, A. Mathieu, A. Alujas, and F. Martirena, *Industrial calcination of kaolinitic clays to make reactive pozzolans.* Case Studies in Construction Materials, 2017. **6**: p. 225-232.
34. Alujas, A., R. Fernández, R. Quintana, K.L. Scrivener, and F. Martirena, *Pozzolanic reactivity of low grade kaolinitic clays: influence of calcination temperature and impact of calcination products on OPC hydration.* Applied Clay Science, 2015. **108**: p. 94-101.
35. Irassar, E.F., A. Tironi, V.L. Bonavetti, M.A. Trezza, C.C. Castellano, V.F. Rahhal, H.A. Donza, and A.N. Scian, *Thermal Treatment and Pozzolanic Activity of Calcined Clay and Shale.* ACI Materials Journal, 2019. **116**(4): p. 133-143.
36. Fernandez, R., F. Martirena, and K.L. Scrivener, *The origin of the pozzolanic activity of calcined clay minerals: a comparison between kaolinite, illite and montmorillonite.* Cement and Concrete Research, 2011. **41**(1): p. 113-122.
37. Garg, N. and J. Skibsted, *Pozzolanic reactivity of a calcined interstratified illite/smectite (70/30) clay.* Cement and Concrete Research, 2016. **79**: p. 101-111.
38. Skibsted, J. and R. Snellings, *Reactivity of supplementary cementitious materials (SCMs) in cement blends.* Cement and Concrete Research, 2019. **124**: p. 105799.
39. Bich, C., J. Ambroise, and J. Péra, *Influence of degree of dehydroxylation on the pozzolanic activity of metakaolin.* Applied Clay Science, 2009. **44**(3–4): p. 194-200.
40. Hollanders, S., R. Adriaens, J. Skibsted, Ö. Cizer, and J. Elsen, *Pozzolanic reactivity of pure calcined clays.* Applied Clay Science, 2016. **132–133**: p. 552-560.

41. Bellotto, M., A. Gualtieri, G. Artioli, and S.M. Clark, *Kinetic study of the kaolinite-mullite reaction sequence. Part I: Kaolinite dehydroxylation.* Physics and Chemistry of Minerals, 1995. **22**(4): p. 207-217.
42. Tironi, A., M.A. Trezza, A.N. Scian, and E.F. Irassar, *Thermal analysis to assess pozzolanic activity of calcined kaolinitic clays.* Journal of Thermal Analysis and Calorimetry, 2014. **117**(2): p. 547-556.
43. Lamberov, A.A., E.Y. Sitnikova, and A.S. Abdulganeeva, *Kinetic features of phase transformation of kaolinite into metakaolinite for kaolin clays from different deposits.* Russian Journal of Applied Chemistry, 2021. **85**(6): p. 892-897.
44. Guggenheim, S., Y.-H. Chang, and A.F. Koster van Groos, *Muscovite dehydroxylation: High temperature studies.* American Mineralogist, 1987. **72**: p. 537-550.
45. Grim, R.E., W.F. Bradley, and G. Brown, *X-ray Identification and Crystal Structures of Clay Minerals*, in *Crystal Structures of Clay Minerals and their X-Ray Identification*, G.W. Brindley and W.F. Bradley, Editors. 1951, Mineralogical Society: London. p. 138-172.
46. Mackenzie, R.C. and A.A. Milne, *The effect of grinding on micas. I. Muscovite.* Mineralogical Magazine and Journal of the Mineralogical Society, 1953. **30**(222): p. 178-185.
47. Jia, F., J. Su, and S. Song, *Can Natural Muscovite be Expanded?* Colloids and Surfaces A: Physicochemical and Engineering Aspects, 2015. **471**: p. 19-25.
48. Udagawa, S., K. Urabe, and H. Hasu, *The crystal structure of muscovite dehydroxylate.* Journal of the European Ceramic Society, Petrologists and Economic Geologists, 1974. **69**(11): p. 381-389.
49. Mackenzie, K.J.D., I.W.M. Brown, C.M. Cardile, and R.H. Meinhold, *The thermal reactions of muscovite studied by high-resolution solid-state 29-Si and 27-AI NMR.* Journal of Materials Science, 1987. **22**(7): p. 2645-2654.
50. Trümer, A. and H.-M. Ludwig, *Assessment of Calcined Clays According to the Main Criterions of Concrete Durability*, in *Calcined Clays for Sustainable Concrete - Proceedings of the 2nd International Conference on Calcined Clays for Sustainable Concrete*, F. Martirena, A. Favier, and K. Scrivener, Editors. 2018, Springer: Dordrecht, Netherlands. p. 475-481.
51. He, C., E. Makovicky, and B. Osbæck, *Thermal stability and pozzolanic activity of calcined illite.* Applied Clay Science, 1995. **9**(5): p. 337-354.
52. Buchwald, A., M. Hohmann, K. Posern, and E. Brendler, *The suitability of thermally activated illite/smectite clay as raw material for geopolymer binders.* Applied Clay Science, 2009. **46**(3): p. 300-304.
53. Jiang, T., G. Li, G. Qiu, X. Fan, and Z. Huang, *Thermal activation and alkali dissolution of silicon from illite.* Applied Clay Science, 2008. **40**(1–4): p. 81-89.
54. Garg, N. and J. Skibsted, *Thermal Activation of a Pure Montmorillonite Clay and Its Reactivity in Cementitious Systems.* The Journal of Physical Chemistry C, 2014. **118**(21): p. 11464-11477.
55. He, C., E. Makovicky, and B. Osbæck, *Thermal treatment and pozzolanic activity of Na- and Ca-montmorillonite.* Applied Clay Science, 1996. **10**(5): p. 351-368.
56. Lothenbach, B., K. Scrivener, and R.D. Hooton, *Supplementary cementitious materials.* Cement and Concrete Research, 2011. **41**(12): p. 1244-1256.
57. Ambroise, J., S. Maximilien, and J. Pera, *Properties of Metakaolin blended cements.* Advanced Cement Based Materials, 1994. **1**(4): p. 161-168.
58. Wang, A., K. Kovler, J.L. Provis, A. Buchwald, M. Cyr, C. Patapy, S. Kamali-Bernard, L. Courard, and K. Sideris, *Metakaolin*, in *Properties of Fresh and Hardened Concrete Containing Supplementary Cementitious Materials*, N. De Belie, M. Soutsos, and E. Gruyaert, Editors. 2018, Springer International Publishing: Cham, Germany. p. 153-179.
59. Antoni, M., J. Rossen, F. Martirena, and K. Scrivener, *Cement substitution by a combination of metakaolin and limestone.* Cement and Concrete Research, 2012. **42**(12): p. 1579-1589.

60. Beuntner, N., *Zur Eignung und Wirkungsweise calcinierter Tone als reaktive Bindemittelkomponente in Zement (On the suitability and mode of action of calcined clays as reactive binder components in cement)*, in *Fakultät für Bauingenieurwesen und Umweltwissenschaften*. 2017, Universität der Bundeswehr München: Neubiberg. p. 207.
61. Lothenbach, B. and F. Winnefeld, *Thermodynamic modelling of the hydration of Portland cement.* Cement and Concrete Research, 2006. **36**(2): p. 209-226.
62. Bonavetti, V.L., V.F. Rahhal, and E.F. Irassar, *Studies on the carboaluminate formation in limestone filler-blended cements.* Cement and Concrete Research, 2001. **31**(6): p. 853-859.
63. Hackley, V.A. and C.F. Ferraris, *Guide to Rheological Nomenclature - Measurements in Ceramic Particulate Systems*. 2001, National Institute of Standards and Technology (NIST): Gaithersburg, Maryland, USA. p. III, 29.
64. Muzenda, T.R., P. Hou, S. Kawashima, T. Sui, and X. Cheng, *The role of limestone and calcined clay on the rheological properties of LC3.* Cement and Concrete Composites, 2020. **107**: p. 103516.
65. Vance, K., A. Kumar, G. Sant, and N. Neithalath, *The rheological properties of ternary binders containing Portland cement, limestone, and metakaolin or fly ash.* Cement and Concrete Research, 2013. **52**: p. 196-207.
66. Pardo, P., P.V. Christensen, K. Keiding, D. Herfort, and J. Skibsted. *Surface properties of calcined clays and their dispersion in blended Portland cement pastes*. in *13th International Congress on the Chemistry of Cement*. 2011. Madrid, Spain.
67. Lorentz, B., H. Zhu, D. Mapa, K.A. Riding, and A. Zayed, *Effect of Clay Mineralogy, Particle Size, and Chemical Admixtures on the Rheological Properties of CCIL and CCI/II Systems*, in *Calcined Clays for Sustainable Concrete - Proceedings of the 3rd International Conference on Calcined Clays for Sustainable Concrete*, S. Bishnoi, Editor. 2020, Springer: Singapore. p. 211-218.
68. Tregger, N.A., M.E. Pakula, and S.P. Shah, *Influence of clays on the rheology of cement pastes.* Cement and Concrete Research, 2010. **40**(3): p. 384-391.
69. Papanastasiou, T.C., *Flows of Materials with Yield.* Journal of Rheology, 1987. **31**(5): p. 385-404.
70. Soua, Z., O. Larue, E. Vorobiev, and J.-L. Lanoisellé, *Estimation of floc size in highly concentrated calcium carbonate suspension obtained by filtration with dispersant.* Colloids and Surfaces A: Physicochemical and Engineering Aspects, 2006. **274**(1): p. 1-10.
71. Krieger, I.M. and T.J. Dougherty, *A Mechanism for Non-Newtonian Flow in Suspensions of Rigid Spheres.* Transactions of the Society of Rheology, 1959. **3**(1): p. 137-152.
72. Blachier, C., A. Jacquet, M. Mosquet, L. Michot, and C. Baravian, *Impact of clay mineral particle morphology on the rheological properties of dispersions: A combined X-ray scattering, transmission electronic microscopy and flow rheology study.* Applied Clay Science, 2014. **87**: p. 87-96.
73. Irassar, E.F., V. Rahhal, C. Pedrajas, and R. Talero, *Rheology of portland cement pastes with calcined clays additions*, in *Cleantech 2014*. 2014, CTSI Clean Technologies and Sustainable Industries Organization: Washington, DC. p. 308-311.
74. Ng, S. and H. Justnes, *Influence of dispersing agents on the rheology and early heat of hydration of blended cements with high loading of calcined marl.* Cement and Concrete Composites, 2015. **60**: p. 123-134.
75. Marchetti, G., V.F. Rahhal, and E.F. Irassar, *Influence of packing density and water film thickness on early-age properties of cement pastes with limestone filler and metakaolin.* Materials and Structures, 2017. **50**(111): p. 11.
76. Sfikas, I.P., E.G. Badogiannis, and K.G. Trezos, *Rheology and mechanical characteristics of self-compacting concrete mixtures containing metakaolin.* Construction and Building Materials, 2014. **64**: p. 121-129.
77. Marchetti, G., J. Pokorny, A. Tironi, M.A. Trezza, V.F. Rahhal, Z. Pavlík, R. Černý, and E.F. Irassar, *Blended Cements with Calcined Illitic Clay: Workability and Hydration*, in

Calcined Clays for Sustainable Concrete - Proceedings of the 2nd International Conference on Calcined Clays for Sustainable Concrete, F. Martirena, A. Favier, and K. Scrivener, Editors. 2018, Springer: Dordrecht, Netherlands. p. 310-317.

78. Curcio, F. and B.A. DeAngelis, *Dilatant behavior of superplasticized cement pastes containing metakaolin.* Cement and Concrete Research, 1998. **28**(5): p. 629-634.
79. Ferreiro, S., D. Herfort, and J.S. Damtoft, *Effect of raw clay type, fineness, water-to-cement ratio and fly ash addition on workability and strength performance of calcined clay – Limestone Portland cements.* Cement and Concrete Research, 2017. **101**: p. 1-12.
80. Schmid, M., R. Sposito, K.-C. Thienel, and J. Plank, *The shear-thickening effect of meta muscovite as SCM and its influence on the rheological properties of ecologically optimized cementitious systems*, in *2nd International RILEM Conference on Rheology and Processing of Construction Materials (RheoCon2)*, V. Mechtcherine, Editor. 2019, Springer: Dresden, Germany.
81. Beuntner, N. and K.-C. Thienel, *Performance and properties of concrete made with calcined clays*, in *ACI SP 320 - 10th ACI/RILEM International Conference on Cementitious Materials and Alternative Binders for Sustainabe Concrete*, A. Tagnit-Hamou, Editor. 2017, Sheridan Books: Montreal, Canada. p. 7.1-7.12.
82. Duan, P., Z. Shui, W. Chen, and C. Shen, *Efficiency of mineral admixtures in concrete: Microstructure, compressive strength and stability of hydrate phases.* Applied Clay Science, 2013. **83–84**: p. 115-121.
83. Tironi, A., M.A. Trezza, A.N. Scian, and E.F. Irassar, *Incorporation of Calcined Clays in Mortars: Porous Structure and Compressive Strength.* Procedia Materials Science, 2012. **1**: p. 366-373.
84. Tironi, A., M.A. Trezza, A.N. Scian, and E.F. Irassar, *Kaolinitic calcined clays: Factors affecting its performance as pozzolans.* Construction and Building Materials, 2012. **28**(1): p. 276-281.
85. Beuntner, N., A. Kustermann, and K.-C. Thienel, *Pozzolanic potential of calcined clay in high-performance concrete*, in *International Conference on Sustainable Materials, Systems and Structures – SMSS 2019 New Generation of Construction Materials*, M. Serdar, N. Štirmer, and J. Provis, Editors. 2019, RILEM Publications S.A.R.L.: Rovinj, Croatia. p. 470-477.
86. Zhao, D. and R. Khoshnazar, *Microstructure of cement paste incorporating high volume of low-grade metakaolin.* Cement and Concrete Composites, 2020. **106**: p. 103453.
87. Tironi, A., R. Sposito, G.P. Cordoba, S.V. Zito, V. Rahhal, K.-C. Thienel, and E.F. Irassar, *Influence of different calcined clays to the water transport performance of concretes.* Magazine of Concrete Research, Ahead of print(2100031): p. 1-13.
88. Tironi, A., C.C. Castellano, V.L. Bonavetti, M.A. Trezza, A.N. Scian, and E.F. Irassar, *Kaolinitic calcined clays – Portland cement system: Hydration and properties.* Construction and Building Materials, 2014. **64**: p. 215-221.
89. Cordoba, G., S.V. Zito, R. Sposito, V.F. Rahhal, A. Tironi, K.-C. Thienel, and E.F. Irassar, *Concretes with calcined clay and calcined shale: workability, mechanical and transport properties.* Journal of Materials in Civil Engineering, 2020. **32**(8): p. 040202241-11.
90. Irassar, E.F., G. Cordoba, S.V. Zito, A. Rossetti, V.F. Rahhal, and F. Dario, *Durability of blended cements containing illitic calcined clays*, in *15th International Congress on the Chemistry of Cement*, J. Gemrich, Editor. 2019, Research Institute of Binding Materials Prague: Prague, Czech Republic. p. 11.
91. Vu, D.D., P. Stroeven, and V.B. Bui, *Strength and durability aspects of calcined kaolin-blended Portland cement mortar and concrete.* Cement and Concrete Composites, 2001. **23**(6): p. 471-478.
92. Soroka, I. and N. Stern, *Calcareous fillers and the compressive strength of portland cement.* Cement and Concrete Research, 1976. **6**(3): p. 367-376.
93. Cyr, M., P. Lawrence, and E. Ringot, *Efficiency of mineral admixtures in mortars: Quantification of the physical and chemical effects of fine admixtures in relation with compressive strength.* Cement and Concrete Research, 2006. **36**(2): p. 264-277.

94. Irassar, E.F., *Sulfate attack on cementitious materials containing limestone filler — A review.* Cement and Concrete Research, 2009. **39**(3): p. 241-254.
95. Craeye, B., G. De Schutter, B. Desmet, J. Vantomme, G. Heirman, L. Vandewalle, Ö. Cizer, S. Aggoun, and E.H. Kadri, *Effect of mineral filler type on autogenous shrinkage of self-compacting concrete.* Cement and Concrete Research, 2010. **40**(6): p. 908-913.
96. Wang, D., C. Shi, N. Farzadnia, Z. Shi, H. Jia, and Z. Ou, *A review on use of limestone powder in cement-based materials: Mechanism, hydration and microstructures.* Construction and Building Materials, 2018. **181**: p. 659-672.
97. De Weerdt, K., M. Ben Haha, G. Le Saout, K.O. Kjellsen, H. Justnes, and B. Lothenbach, *Hydration mechanisms of ternary Portland cements containing limestone powder and fly ash.* Cement and Concrete Research, 2011. **41**(3): p. 279-291.
98. Menéndez, G., V. Bonavetti, and E.F. Irassar, *Strength development of ternary blended cement with limestone filler and blast-furnace slag.* Cement and Concrete Composites, 2003. **25**(1): p. 61-67.
99. DIN EN 197-1, *Zement - Teil 1: Zusammensetzung, Anforderungen und Konformitätskriterien von Normalzement (Cement - Part 1: Composition, specifications and conformity criteria for common cements)*. 2011, Beuth-Verlag: Berlin, Germany. p. 8.
100. ASTM C595 / C595M-19, *Standard Specification of Blended Hydraulic Cements*. 2019, ASTM International: West Conshohocken, PA. p. 8.
101. Pérez, A., A. Favier, K. Scrivener, and F. Martirena, *Influence Grinding Procedure, Limestone Content and PSD of Components on Properties of Clinker-Calcined Clay-Limestone Cements Produced by Intergrinding*, in *Calcined Clays for Sustainable Concrete - Proceedings of the 2nd International Conference on Calcined Clays for Sustainable Concrete*, F. Martirena, A. Favier, and K. Scrivener, Editors. 2018, Springer: Dordrecht, Netherlands. p. 358-365.
102. Antoni, M., L. Baquerizo, and T. Matschei, *Investigation of ternary mixes made of clinker limestone and slag or metakaolin: Importance of reactive alumina and silica content*, in *Calcined Clays for Sustainable Concrete - Proceedings of the 1st International Conference on Calcined Clays for Sustainable Concrete*, K. Scrivener and A. Favier, Editors. 2015, Springer: Dordrecht, Netherlands. p. 545-553.
103. Zaribaf, B.H. and K.E. Kurtis, *Admixture compatibility in metakaolin–portland-limestone cement blends.* Materials and Structures, 2018. **51**: p. 13.
104. Avet, F. and K. Scrivener, *Investigation of the calcined kaolinite content on the hydration of Limestone Calcined Clay Cement (LC³).* Cement and Concrete Research, 2018. **107**: p. 124-135.
105. Avet, F., E. Boehm-Courjault, and K. Scrivener, *Investigation of C-A-S-H composition, morphology and density in Limestone Calcined Clay Cement (LC³).* Cement and Concrete Research, 2019. **115**: p. 70-79.
106. Vance, K., M. Aguayo, T. Oey, G. Sant, and N. Neithalath, *Hydration and strength development in ternary portland cement blends containing limestone and fly ash or metakaolin.* Cement and Concrete Composites, 2013. **39**: p. 93-103.
107. Puerta-Falla, G., M. Balonis, G. Le Saout, N. Neithalath, and G. Sant, *The Influence of Metakaolin on Limestone Reactivity in Cementitious Materials*, in *Calcined Clays for Sustainable Concrete - Proceedings of the 1st International Conference on Calcined Clays for Sustainable Concrete*, K. Scrivener and A. Favier, Editors. 2015, Springer: Dordrecht, Netherlands. p. 11-19.
108. Mishra, G., A.C. Emmanuel, and S. Bishnoi, *Influence of temperature on hydration and microstructure properties of limestone-calcined clay blended cement.* Materials and Structures, 2019. **52**(91): p. 13.
109. Dhandapani, Y. and M. Santhanam, *Assessment of pore structure evolution in the limestone calcined clay cementitious system and its implications for performance.* Cement and Concrete Composites, 2017. **84**: p. 36-47.
110. Dhandapani, Y., T. Sakthivel, M. Santhanam, R. Gettu, and R.G. Pillai, *Mechanical properties and durability performance of concretes with Limestone Calcined Clay Cement (LC³).* Cement and Concrete Research, 2018. **107**: p. 136-151.

111. Shi, Z., S. Ferreiro, B. Lothenbach, M.R. Geiker, W. Kunther, J. Kaufmann, D. Herfort, and J. Skibsted, *Sulfate resistance of calcined clay – Limestone – Portland cements.* Cement and Concrete Research, 2019. **116**: p. 238-251.
112. Tironi, A., A.N. Scian, and E.F. Irassar, *Blended cements with limestone filler and kaolinitic calcined clay: filler and pozzolanic effects.* Journal of Materials in Civil Engineering, 2017. **29**(9): p. 8.
113. Matschei, T., B. Lothenbach, and F.P. Glasser, *The role of calcium carbonate in cement hydration.* Cement and Concrete Research, 2007. **37**(4): p. 551-558.
114. Maier, M., N. Beuntner, and K.-C. Thienel, *An approach for the evaluation of local raw material potential for calcined clay as SCM, based on geological and mineralogical data: Examples from German clay deposits*, in *Calcined Clays for Sustainable Concrete - Proceedings of the 3rd International Conference on Calcined Clays for Sustainable Concrete*, S. Bishnoi, Editor. 2020, Springer: Singapore. p. 37-47.
115. Dietel, J., L.N. Warr, M. Bertmer, A. Steudel, G.H. Grathoff, and K. Emmerich, *The importance of specific surface area in the geopolymerization of heated illitic clay.* Applied Clay Science, 2017. **139**: p. 99-107.
116. Walker, R. and S. Pavía, *Physical properties and reactivity of pozzolans, and their influence on the properties of lime–pozzolan pastes.* Materials and Structures, 2010. **44**(6): p. 1139-1150.
117. DIN ISO 9277, *Determination of the specific surface area of solids by gas adsorption - BET method*. 2003, Beuth-Verlag: Berlin. p. 19.
118. Nair, N., K. Mohammed Haneefa, M. Santhanam, and R. Gettu, *A study on fresh properties of limestone calcined clay blended cementitious systems.* Construction and Building Materials, 2020. **254**: p. 119326.
119. Chen, Y., C. Romero Rodriguez, Z. Li, B. Chen, O. Çopuroğlu, and E. Schlangen, *Effect of different grade levels of calcined clays on fresh and hardened properties of ternary-blended cementitious materials for 3D printing.* Cement and Concrete Composites, 2020. **114**: p. 103708.
120. Moulin, E., P. Blanc, and D. Sorrentino, *Influence of key cement chemical parameters on the properties of metakaolin blended cements.* Cement and Concrete Composites, 2001. **23**(6): p. 463-469.
121. Cassagnabère, F., P. Diederich, M. Mouret, G. Escadeillas, and M. Lachemi, *Impact of metakaolin characteristics on the rheological properties of mortar in the fresh state.* Cement and Concrete Composites, 2013. **37**: p. 95-107.
122. Beigh, M., V.N. Nerella, C. Schroefl, and V. Mechtcherine, *Studying the rheological behavior of limestone calcined clay cement (LC³) mixtures in the context of extrusion-based 3D-printing*, in *Calcined Clays for Sustainable Concrete - Proceedings of the 3rd International Conference on Calcined Clays for Sustainable Concrete*, S. Bishnoi, Editor. 2020, Springer: Singapore. p. 229-235.
123. Hou, P., T.R. Muzenda, Q. Li, H. Chen, S. Kawashima, T. Sui, H. Yong, N. Xie, and X. Cheng, *Mechanisms dominating thixotropy in limestone calcined clay cement (LC3).* Cement and Concrete Research, 2021. **140**: p. 106316.
124. Li, R., L. Lei, T. Sui, and J. Plank, *Approaches to achieve fluidity retention in low-carbon calcined clay blended cements.* Journal of Cleaner Production, 2021. **311**: p. 127770.
125. Ouellet-Plamondon, C., S. Scherb, M. Köberl, and K.-C. Thienel, *Acceleration of cement blended with calcined clays.* Construction and Building Materials, 2020. **245**: p. 118439.
126. Kanchanason, V. and J. Plank, *Effect of calcium silicate hydrate – polycarboxylate ether (C-S-H–PCE) nanocomposite as accelerating admixture on early strength enhancement of slag and calcined clay blended cements.* Cement and Concrete Research, 2019. **119**: p. 44-50.
127. Gettu, R., M. Santhanam, R.G. Pillai, Y. Dhandapani, T. Sakthivel, S. Rengaraju, S. Rathnarajan, F.M. Suma, A.S. Basavaraja, S. Prakasan, and N.V.G. Nair, *Summary of 4-Years of Research at IIT Madras on Concrete with Limestone Calcined Clay Cement (LC3)*, in *International Conference on Sustainable Materials, Systems and Structures –*

SMSS 2019 New Generation of Construction Materials, M. Serdar, N. Štirmer, and J. Provis, Editors. 2019, RILEM Publications S.A.R.L.: Rovinj, Croatia. p. 449-456.
128. Thienel, K.-C. and N. Beuntner, *Effects of calcined clay as low carbon cementing materials on the properties of concrete*, in *Concrete in the Low Carbon Era*, M.R. Jones, et al., Editors. 2012, University of Dundee – Concrete Technology Unit: Dundee, UK. p. 504-518.
129. Deutsche Bauchemie e.V., *Jahresbericht 2017/2018*. 2018: Frankfurt/Main. p. 80.
130. Schröter, N. and P. Fischer, *Entwicklung und Trends bei Betonzusatzmitteln.* Beton, 2010. **6**.
131. Mark, J.G., *Concrete and Hydraulic Cement*. 1938: USA.
132. Gelardi, G., S. Mantellato, D. Marchon, M. Palacios, A.B. Eberhardt, and R.J. Flatt, *Chemistry of chemical admixtures*, in *Science and Technology of Concrete Admixtures*, P.-C. Aïtcin and R.J. Flatt, Editors. 2016, Woodhead Publishing. p. 149-218.
133. Hattori, K.-I. and Y. Tanino, *Separation and molecular weight determination of the fraction from the paper chromatography of the condensates of sodium b-naphthalene sulfonate and formaldehyde.* The Journal of the Society of Chemical Industry, Japan, 1963. **66**(1): p. 55-58.
134. Aignesberger, A. and J. Plank, *Säuregruppen enthaltende thermostabile, hydrophile Kondensationsprodukte von Aldehyden und Ketonen (DE3144673A1)*. 1983, SKW Trostberg AG: Germany.
135. Zou, N. and J. Plank, *Intercalation of Sulfanilic Acid-Phenol-Formaldehyde Polycondensate into Hydrocalumite Type Layered Double Hydroxide.* Zeitschrift für anorganische und allgemeine Chemie, 2012. **638**(14): p. 2292-2296.
136. Jeknavorian, A.A., *Polycarboxylate Ether High-Range Water-Reducing Admixtures.* Concrete International, 2019. **41**(10): p. 49-55.
137. Plank, J. and H. Bian, *Method to assess the quality of casein used as superplasticizer in self-levelling compounds.* Cement and Concrete Research, 2010. **40**(5): p. 710-715.
138. Mosquet, M., Y. Chevalier, S. Brunel, J.P. Guicquero, and P. Le Perchec, *Polyoxyethylene di-phosphonates as efficient dispersing polymers for aqueous suspensions.* Journal of Applied Polymer Science, 1997. **65**(12): p. 2545-2555.
139. Mosquet, M., P. Maitrasse, and J.P. Guicquero, *Ethoxylated di-phosphonate: An extreme molecule for extreme applications*, in *ACI SP 217 - 7th CANMET/ACI International Conference on Superplasticizers and Other Chemical Admixtures in Concrete*, V.M. Malhothra, Editor. 2003, American Concrete Institute: Berlin, Germany. p. 161-175.
140. Stecher, J. and J. Plank, *Phosphated Comb Polymers - A New Generation of Highly Effective Superplasticizers*, in *8th International RILEM Symposium on Self-Compacting Concrete - SCC 2016*, K.H. Khayat, Editor. 2016, RILEM Publications SARL: Washington, D.C., USA. p. 61-71.
141. Stecher, J. and J. Plank, *Novel concrete superplasticizers based on phosphate esters.* Cement and Concrete Research, 2019. **119**: p. 36-43.
142. Houst, Y.F., P. Bowen, F. Perche, A. Kauppi, P. Borget, L. Galmiche, J.-F. Le Meins, F. Lafuma, R.J. Flatt, I. Schober, P.F.G. Banfill, D.S. Swift, B.O. Myrvold, B.G. Petersen, and K. Reknes, *Design and function of novel superplasticizers for more durable high performance concrete (superplast project).* Cement and Concrete Research, 2008. **38**(10): p. 1197-1209.
143. Mollah, M.Y.A., W.J. Adams, R. Schennach, and D.L. Cocke, *A review of cement–superplasticizer interactions and their models.* Advances in Cement Research, 2000. **12**(4): p. 153-161.
144. Zhang, Y. and X. Kong, *Correlations of the dispersing capability of NSF and PCE types of superplasticizer and their impacts on cement hydration with the adsorption in fresh cement pastes.* Cement and Concrete Research, 2015. **69**: p. 1-9.
145. Hirsch, C., D. Vlad, J.-Y. Yang, P. Chatziagorastou, and J. Plank, *Adsorption von Fliessmitteln an Mineralphasen der frühen Zementhydratation.* GDCh-Monographie Band, 2003. **27**: p. 187-194.

146. Hirsch, C., *Untersuchungen zur Wechselwirkung zwischen polymeren Fliessmitteln und Zementen bzw. Mineralphasen der frühen Zementhydration*, in *Faculty of Chemistry*. 2005, Technical University Munich: Munich. p. 272.
147. Flatt, R.J. and Y.F. Houst, *A simplified view on chemical effects perturbing the action of superplasticizers.* Cement and Concrete Research, 2001. **31**(8): p. 1169-1176.
148. Plank, J., D. Zhimin, H. Keller, F. v. Hössle, and W. Seidl, *Fundamental mechanisms for polycarboxylate intercalation into C_3A hydrate phases and the role of sulfate present in cement.* Cement and Concrete Research, 2010. **40**(1): p. 45-57.
149. Plank, J. and B. Sachsenhauser, *Impact of Molecular Structure on Zeta Potential and Adsorbed Conformation of α-Allyl-ω-Methoxypolyethylene Glycol - Maleic Anhydride Superplasticizers.* Journal of Advanced Concrete Technology, 2006. **4**(2): p. 233-239.
150. Kubens, S., *Interaction of cement and admixtures and its influence on rheological properties*, in *F.A. Finger-Institut für Baustoffkunde*. 2010, Bauhaus-Universität Weimar: Weimar. p. 192.
151. Sha, S., M. Wang, C. Shi, and Y. Xiao, *Influence of the structures of polycarboxylate superplasticizer on its performance in cement-based materials-A review.* Construction and Building Materials, 2020. **233**: p. 117257.
152. Plank, J. and C. Hirsch, *Impact of zeta potential of early cement hydration phases on superplasticizer adsorption.* Cement and Concrete Research, 2007. **37**(4): p. 537-542.
153. Hanehara, S. and K. Yamada, *Rheology and early age properties of cement systems.* Cement and Concrete Research, 2008. **38**(2): p. 175-195.
154. Sakai, E., K. Yamada, and A. Ohta, *Molecular Structure and Dispersion-Adsorption Mechanisms of Comb-Type Superplasticizers Used in Japan.* Journal of Advanced Concrete Technology, 2003. **1**(1): p. 16-25.
155. Nakano, T., K. Ichitsubo, D. Kurokawa, and M. Ichikawa, *The effect of cooling rate on the fluidity of mortar made from kiln clinker.* Cement and Concrete Research, 2008. **38**(5): p. 643-648.
156. Plank, J. and C. Hirsch, *Superplasticizer Adsorption on Synthetic Ettringite*, in *ACI SP 239 - 7th CanMET/ACI Intl Conference on Superplasticizers and other Chemical Admixtures in Concrete*, V.M. Malhotra, Editor. 2003, American Concrete Institute: Berlin, Germany. p. 283-298.
157. Zingg, A., F. Winnefeld, L. Holzer, J. Pakusch, S. Becker, R. Figi, and L. Gauckler, *Interaction of polycarboxylate-based superplasticizers with cements containing different C_3A amounts.* Cement and Concrete Composites, 2009. **31**(3): p. 153-162.
158. Dietermann, M. and I. Hauschild, *Einfluss von Zementparametern auf das Zusammenwirken von Zement und Fließmittel*, in *16. Internationale Baustofftagung ibausil*, H.-B. Fischer, Editor. 2006, F. A. Finger-Institut für Baustoffkunde (Prof. J. Stark): Weimar, Germany. p. 1-631 - 1-638.
159. Habbaba, A., Z. Dai, and J. Plank, *Formation of organo-mineral phases at early addition of superplasticizers: The role of alkali sulfates and C_3A content.* Cement and Concrete Research, 2014. **59**: p. 112-117.
160. Yamada, K., S. Hanehara, and M. Matsuhisa, *Fluidizing mechanism of cement paste added with polycarboxylate type superplasticizer analyzed from the point of adsorption behavior (in Japanese).* Proceedings of the Japanese Concrete Institute, 1998. **20**(2): p. 73-78.
161. Yamada, K., S. Ogawa, and S. Hanehara, *Controlling of the adsorption and dispersing force of polycarboxylate-type superplasticizer by sulfate ion concentration in aqueous phase.* Cement and Concrete Research, 2001. **31**(3): p. 375-383.
162. Yoshioka, K., E.-i. Tazawa, K. Kawai, and T. Enohata, *Adsorption characteristics of superplasticizers on cement component minerals.* Cement and Concrete Research, 2002. **32**(10): p. 1507-1513.
163. Hanehara, S. and K. Yamada, *Interaction between cement and chemical admixture from the point of cement hydration, absorption behaviour of admixture, and paste rheology.* Cement and Concrete Research, 1999. **29**(8): p. 1159-1165.

164. Pointeau, I., P. Reiller, N. Macé, C. Landesman, and N. Coreau, *Measurement and modeling of the surface potential evolution of hydrated cement pastes as a function of degradation.* Journal of Colloid and Interface Science, 2006. **300**(1): p. 33-44.
165. Nachbaur, L., P.-C. Nkinamubanzi, A. Nonat, and J.-C. Mutin, *Electrokinetic Properties which Control the Coagulation of Silicate Cement Suspensions during Early Age Hydration.* Journal of Colloid and Interface Science, 1998. **202**(2): p. 261-268.
166. Lowke, D. and C. Gehlen, *The zeta potential of cement and additions in cementitious suspensions with high solid fraction.* Cement and Concrete Research, 2017. **95**: p. 195-204.
167. Ng, S. and J. Plank, *Interaction mechanisms between Na montmorillonite clay and MPEG-based polycarboxylate superplasticizers.* Cement and Concrete Research, 2012. **42**(6): p. 847-854.
168. Uchikawa, H., D. Sawaki, and S. Hanehara, *Influence of kind and added timing of organic admixture on the composition, structure and property of fresh cement paste.* Cement and Concrete Research, 1995. **25**(2): p. 353-364.
169. Zhor, J., *Effect of Functional Groups on the Performance of Lignosulfonates in Cement-Water Systems*, in *ACI SP 239 - 8th CanMET/ACI Intl Conference on Superplasticizers and other Chemical Admixtures in Concrete*, V.M. Malhotra, Editor. 2006, Sheridan Books: Sorrento, Italy. p. 507-524.
170. Colombo, A., M. Geiker, H. Justnes, R.A. Lauten, and K. De Weerdt, *On the mechanisms of consumption of calcium lignosulfonate by cement paste.* Cement and Concrete Research, 2017. **98**: p. 1-9.
171. Rixom, R. and N. Mailvaganam, *Chemical Admixtures for Concrete*. 3 ed. 1999, London: E & FN Spon. XVIII, 438.
172. Flatt, R. and I. Schober, *Superplasticizers and the rheology of concrete*, in *Understanding the Rheology of Concrete*, N. Roussel, Editor. 2012, Woodhead Publishing. p. 144-208.
173. Sebök, T. and O. Stráeněl, *Relationships between the properties of ligninsulphonates and parameters of modified samples with cement binders.: Part II. Study of relationships between molar parameters of ligninsulphonates and characteristics of the samples tested.* Cement and Concrete Research, 1999. **29**(4): p. 591-594.
174. Myrvold, B.O., *Adsorption of Lignosulphonates on Cement and the Hydration Products of Cements*, in *ACI SP 239 - 8th CanMET/ACI Intl Conference on Superplasticizers and other Chemical Admixtures in Concrete*, V.M. Malhotra, Editor. 2006, Sheridan Books: Sorrento, Italy. p. 285-296.
175. Li, R., D. Yang, W. Guo, and X. Qiu, *The adsorption and dispersing mechanisms of sodium lignosulfonate on Al_2O_3 particles in aqueous solution.* Holzforschung (Wood Research and Technology), 2013. **67**(4): p. 387-394.
176. Ramachandran, V.S., J. Bensted, M.M. Collepardi, W.L. Dolch, R.F. Feldman, R.C. Joshi, R.P. Lohtia, N.P. Mailvaganam, V.M. Malhotra, Y. Ohama, V.S. Ramachandran, V.B. Ratinov, and T.I. Rozenberg, *Concrete Admixtures Handbook. Properties, Science, and Technology*. 2nd ed. 1996, Park Ridge, New Jersey, U.S.A.: Noyes Publications. 1153.
177. Rixom, M.R. and J. Waddicor, *Role of Lignosulfonates as Superplasticizers*, in *ACI SP 68 - Developments in the Use of Superplasticizers*. 1981, American Concret Institute: Detroit. p. 359-380.
178. Reknes, K. and J. Gustafsson, *Effect of Modifications of Lignosulfonate on Adsorption on Cement and Fresh Concrete Properties*, in *ACI SP 195 - 6th CANMET/ACI Conference on Superplasticizers and Other Chemical Admixtures in Concrete*, V.M. Malhotra, Editor. 2000, American Concrete Institute: Nice, France. p. 127-141.
179. Justnes, H. and S. Ng, *Lignosulfonate as plasticizer for cement: the effect of type, dosage, time of addition and clinker mineralogy*, in *The 7th International Conference of Asian Concrete Federation "Sustainable concrete for now and the future"*. 2016: Hanoi, Vietnam. p. 8.

180. Colombo, A., M.R. Geiker, H. Justnes, R.A. Lauten, and K. De Weerdt, *On the effect of calcium lignosulfonate on the rheology and setting time of cement paste.* Cement and Concrete Research, 2017. **100**: p. 435-444.
181. Danner, T., H. Justnes, M. Geiker, and R.A. Lauten, *Phase changes during the early hydration of Portland cement with Ca-lignosulfonates.* Cement and Concrete Research, 2015. **69**: p. 50-60.
182. Danner, T., H. Justnes, M.R. Geiker, and R.A. Lauten, *Effect of Lignosulfonate Plasticizers on the Hydration of C_3A*, in *14th International Congress on the Chemistry of Cement*. 2015: Beijing, China.
183. Danner, T., H. Justnes, M. Geiker, and R.A. Lauten, *Early hydration of C_3A–gypsum pastes with Ca- and Na-lignosulfonate.* Cement and Concrete Research, 2016. **79**: p. 333-343.
184. Pieh, S., *Polymere Dispergiermittel I. Molmasse und Dispergierwirkung der Melamin- und Naphthalin-Sulfonsäure-Formaldehyd-Polykondensate.* Die Angewandte Makromolekulare Chemie, 1987. **154**(1): p. 145-159.
185. Cunningham, J.C., B.L. Dury, and T. Gregory, *Adsorption characteristics of sulphonated melamine formaldehyde condensates by high performance size exclusion chromatography.* Cement and Concrete Research, 1989. **19**(6): p. 919-928.
186. Qian, Y. and G. De Schutter, *Different Effects of NSF and PCE Superplasticizer on Adsorption, Dynamic Yield Stress and Thixotropy of Cement Pastes.* Materials, 2018. **11**(5): p. 695.
187. Daimon, M. and D.M. Roy, *Rheological properties of cement mixes: II. Zeta potential and preliminary viscosity studies.* Cement and Concrete Research, 1979. **9**(1): p. 103-109.
188. Björnström, J. and S. Chandra, *Effect of superplasticizers on the rheological properties of cements.* Materials and Structures, 2003. **36**(10): p. 685-692.
189. Chandra, S. and J. Björnström, *Influence of superplasticizer type and dosage on the slump loss of Portland cement mortars—Part II.* Cement and Concrete Research, 2002. **32**(10): p. 1613-1619.
190. Aiad, I., S. Abd El-Aleem, and H. El-Didamony, *Effect of delaying addition of some concrete admixtures on the rheological properties of cement pastes.* Cement and Concrete Research, 2002. **32**(11): p. 1839-1843.
191. Sakai, E., T. Kasuga, T. Sugiyama, K. Asaga, and M. Daimon, *Influence of superplasticizers on the hydration of cement and the pore structure of hardened cement.* Cement and Concrete Research, 2006. **36**(11): p. 2049-2053.
192. Roncero, J., S. Valls, and R. Gettu, *Study of the influence of superplasticizers on the hydration of cement paste using nuclear magnetic resonance and X-ray diffraction techniques.* Cement and Concrete Research, 2002. **32**(1): p. 103-108.
193. Gu, P., P. Xie, and J.J. Beaudoin, *Microstructural characterization of the transition zone in cement systems by means of A.C. impedance spectroscopy.* Cement and Concrete Research, 1993. **23**(3): p. 581-591.
194. Gu, P., P. Xie, J.J. Beaudoin, and C. Jolicoeur, *Investigation of the retarding effect of superplasticizers on cement hydration by impedance spectroscopy and other methods.* Cement and Concrete Research, 1994. **24**(3): p. 433-442.
195. Plank, J., E. Sakai, C.W. Miao, C. Yu, and J.X. Hong, *Chemical admixtures — Chemistry, applications and their impact on concrete microstructure and durability.* Cement and Concrete Research, 2015. **78, Part A**: p. 81-99.
196. Zhang, Y.-R., X.-M. Kong, Z.-B. Lu, Z.-C. Lu, and S.-S. Hou, *Effects of the charge characteristics of polycarboxylate superplasticizers on the adsorption and the retardation in cement pastes.* Cement and Concrete Research, 2015. **67**: p. 184-196.
197. Arfaei, A., D.C. Darwin, E. Gartner, B.-W. Chun, H. Koyata, and L.L. Kuo, *Cement admixture product having improved rheological properties and process of forming same (US5633298A)*. 1997, W. R. Grace & Co.-Conn.: USA.
198. Tahara, H., H. Ito, Y. Mori, and M. Mizushima, *Cement additive, method for producing the same, and cement composition (US5476885A)*. 1995.

199. Lei, L., M. Palacios, J. Plank, and A.A. Jeknavorian, *Interaction between polycarboxylate superplasticizers and non-calcined clays and calcined clays: A review.* Cement and Concrete Research, 2022. **154**: p. 106717.
200. Liu, G., X. Qin, X. Wei, Z. Wang, and J. Ren, *Study on the monomer reactivity ratio and performance of EPEG-AA (ethylene-glycol monovinyl polyethylene glycol–acrylic acid) copolymerization system.* Journal of Macromolecular Science, Part A, 2020. **57**(9): p. 646-653.
201. Dong, J., Q. Luo, C. Hu, J. Ji, H. Liu, and L. Zhai, *Polyether macromonomer, polycarboxylate water-reducer and its methods for making and using same from it (CN108102085A)*. 2018: China.
202. Tsubakimoto, T., M. Hosoido, H. Tawara, and T. Hirata, *Cement dispersant (JPS5874552A)*, N. Shokubai, Editor. 1983: Japan.
203. Akimoto, S.-I., S. Honda, and T. Yasukohchi, *Additives for cement (EP0291073B1)*. 1992, NOF Corp: Japan.
204. Albrecht, G., J. Weichmann, J. Penkner, and A. Kern, *Copolymers based on oxyalkyleneglycol alkenyl ethers and derivatives of unsaturated dicarboxylic acids (EP0736553B1)*. 2001: Germany.
205. Hamada, D., F. Yamato, T. Mizunuma, and H. Ichikawa, *Additive mixture for cement-based concrete or mortar contains a copolymer of polyalkoxylated unsaturated acid and a mixture of alkoxylated carboxylic acid with a corresponding ester and/or an alkoxylated alcohol (DE10048139A1)*. 2001, Kao Corp: Japan.
206. Yamamoto, M., T. Uno, Y. Onda, H. Tanaka, A. Yamashita, T. Hirata, and N. Hirano, *Copolymer for cement admixtures and its production process and use (US6727315B2)*. 2004: Japan.
207. Guicquero, J.P., P. Maitrasse, M.A. Mosquet, and A. Sers, *A water soluble or water dispersible dispersing agent (FR2776285A1)*. 1999: France.
208. Plank, J., K. Pöllmann, N. Zouaoui, P.R. Andres, and C. Schaefer, *Synthesis and performance of methacrylic ester based polycarboxylate superplasticizers possessing hydroxy terminated poly(ethylene glycol) side chains.* Cement and Concrete Research, 2008. **38**(10): p. 1210-1216.
209. Pourchet, S., S. Liautaud, D. Rinaldi, and I. Pochard, *Effect of the repartition of the PEG side chains on the adsorption and dispersion behaviors of PCP in presence of sulfate.* Cement and Concrete Research, 2012. **42**(2): p. 431-439.
210. Plank, J., Z. Dai, N. Zouaoui, and D. Vlad, *Intercalation of Polycarboxylate Superplasticizers into C_3A Hydrate Phases*, in *ACI SP 239 - 8th CanMET/ACI Intl Conference on Superplasticizers and Other Chemical Admixtures in Concrete*, V.M. Malhothra, Editor. 2006, American Concrete Institute: Sorrento, Italy. p. 201-214.
211. Giraudeau, C., J.-B. D'Espinose De Lacaillerie, Z. Souguir, A. Nonat, and R.J. Flatt, *Surface and Intercalation Chemistry of Polycarboxylate Copolymers in Cementitious Systems.* Journal of the American Ceramic Society, 2009. **92**(11): p. 2471-2488.
212. Alonso, M.M., M. Palacios, F. Puertas, A.G. de la Torre, and M.A.G. Aranda, *Effect of polycarboxylate admixture structure on cement paste rheology.* Materiales de Construcción, 2007. **57**(286): p. 17.
213. Winnefeld, F., S. Becker, J. Pakusch, and T. Götz, *Effects of the molecular architecture of comb-shaped superplasticizers on their performance in cementitious systems.* Cement and Concrete Composites, 2007. **29**(4): p. 251-262.
214. Liu, M., J. Chen, Y. Gao, G. Zheng, and J. Lei, *Effects of the Adsorption Characteristics of PCE on C_3S Hydration*, in *ACI SP 329 - 12th International Conference on Superplasticizers and Other Chemical Admixtures in Concrete*, J. Liu, et al., Editors. 2018, American Concrete Institute: Beijing, China. p. 213-224.
215. Puertas, F., H. Santos, M. Palacios, and S. Martínez-Ramírez, *Polycarboxylate superplasticiser admixtures: effect on hydration, microstructure and rheological behaviour in cement pastes.* Advances in Cement Research, 2005. **17**(2): p. 77-89.
216. Lothenbach, B., F. Winnefeld, and R. Figi, *The influence of superplasticizers on the hydration of Portland cement*, in *12th International Congress on the Chemistry of Cement*. 2007: Montreal, Canada. p. W1-05.2.

217. Ferrari, G., V. Russo, M. Dragoni, G. Artioli, M.C. Dalconi, M. Secco, L. Tamborrino, and L. Valentini, *The Influence of C_3A on the Dissolution Kinetics of Alite/Gypsum Mixtures in the Presence of PCEs*, in *ACI SP 302 - 11th International Conference on Superplasticizers and Other Chemical Admixtures*, V.M. Malhotra, P.R. Gupta, and T.C. Holland, Editors. 2015, American Concrete Institute: Ottawa, Canada. p. 227-242.
218. Uchikawa, H., S. Uchida, K. Ogawa, and S. Hanehara, *Influence of $CaSO_4 \cdot 2H_2O$, $CaSO_4 \cdot 12H_2O$ and $CaSO_4$ on the initial hydration of clinker having different burning degree.* Cement and Concrete Research, 1984. **14**(5): p. 645-656.
219. Cheung, J., A. Jeknavorian, L. Roberts, and D. Silva, *Impact of admixtures on the hydration kinetics of Portland cement.* Cement and Concrete Research, 2011. **41**(12): p. 1289-1309.
220. Tan, H., X. Li, S. Jian, B. Ma, and M. Liu, *Effect of the ester group in side chain of polycarboxylate superplasticizer on the cement hydration process.* ZKG International, 2016. **69**(7-8): p. 60-67.
221. Kanchanason, V. and J. Plank, *Effectiveness of a calcium silicate hydrate – Polycarboxylate ether (C-S-H–PCE) nanocomposite on early strength development of fly ash cement.* Construction and Building Materials, 2018. **169**: p. 20-27.
222. Abdalla, L.B., K. Ghafor, and A. Mohammed, *Testing and modeling the young age compressive strength for high workability concrete modified with PCE polymers.* Results in Materials, 2019. **1**: p. 100004.
223. Zhang, Z., Q. Feng, W. Zhu, X. Lin, K. Chen, W. Yin, and C. Lu, *Influence of Sand-Cement Ratio and Polycarboxylate Superplasticizer on the Basic Properties of Mortar Based on Water Film Thickness.* Materials, 2021. **14**(17): p. 4850.
224. Schmid, M., N. Beuntner, K.-C. Thienel, and J. Plank, *Colloid-chemical investigation of the interaction between PCE superplasticizers and a calcined mixed layer clay*, in *Calcined Clays for Sustainable Concrete - Proceedings of the 2nd International Conference on Calcined Clays for Sustainable Concrete*, F. Martirena, A. Favier, and K. Scrivener, Editors. 2018, Springer: Dordrecht, Netherlands. p. 434-439.
225. Schmid, M., R. Sposito, K.-C. Thienel, and J. Plank, *Novel zwitterionic PCE superplasticizers for calcined clays and their application in calcined clay blended cements*, in *15th International Congress on the Chemistry of Cement*, J. Gemrich, Editor. 2019, Research Institute of Binding Materials Prague: Prague, Czech Republic. p. 8.
226. Miao, C., Q. Ran, J. Liu, Y. Mao, Y. Shang, and J. Sha, *New Generation Amphoteric Comb-like Copolymer Superplasticizer and Its Properties.* Polymers and Polymer Composites, 2011. **19**(1): p. 1-8.
227. Jiang, L., X. Kong, Z. Lu, and S. Hou, *Preparation of amphoteric polycarboxylate superplasticizers and their performances in cementitious system.* Journal of Applied Polymer Science, 2015. **132**(4): p. 8.
228. Cao, Q., S. Lv, and D. Li, *Study on Dispersion Properties of an Amphoteric Polycarboxylate Superplasticizer on Cement Pastes.* Advanced Materials Research, 2012. **502**: p. 208-211.
229. Sun, N., J.J. Qin, W.J. Guo, J. Zhang, M.S. Pei, Y.F. Wang, and S.N. Wang, *Synthesis and Properties of an Amphoteric Superplasticizer Compatible with Sulphoaluminate Cement.* Advanced Materials Research, 2011. **306-307**: p. 1688-1692.
230. Guo, W., N. Sun, J. Qin, J. Zhang, M. Pei, Y. Wang, and S. Wang, *Synthesis and properties of an amphoteric polycarboxylic acid-based superplasticizer used in sulfoaluminate cement.* Journal of Applied Polymer Science, 2012. **125**(1): p. 283-290.
231. Schmid, M., R. Sposito, K.-C. Thienel, and J. Plank, *Effectiveness of Chemically Different Superplasticizers in Calcined Clay Blended Cements*, in *Calcined Clays for Sustainable Concrete - Proceedings of the 3rd International Conference on Calcined Clays for Sustainable Concrete*, S. Bishnoi, Editor. 2019, Springer: Singapore. p. 201-209.
232. Schmid, M., R. Sposito, K.-C. Thienel, and J. Plank, *Novel Zwitterionic Superplasticizers for Cements Blended with Calcined Clays*, in *20. Internationale*

Baustofftagung ibausil, H.-B. Fischer and A. Volke, Editors. 2018, F.A. Finger-Institut für Baustoffkunde der Bauhaus-Universität Weimar: Weimar, Germany. p. 842-849.
233. Schmid, M., N. Beuntner, K.-C. Thienel, and J. Plank, *Amphoteric superplasticizers for Cements Blended with a Calcined Clay*, in *ACI SP 329 - 12th International Conference on Superplasticizers and Other Chemical Admixtures in Concrete*, J. Liu, et al., Editors. 2018, American Concrete Institute: Beijing, China. p. 41-54.
234. Amaya, T., A. Ikeda, J. Imamura, A. Kobayashi, K. Saito, W.M. Danzinger, and T. Tomoyose, *Cement dispersant and concrete composition containing the dispersant (JP3336456B2)*. 2002: Japan.
235. Chomyn, C. and J. Plank, *Impact of different synthesis methods on the dispersing effectiveness of isoprenol ether-based zwitterionic and anionic polycarboxylate (PCE) superplasticizers.* Cement and Concrete Research, 2019. **119**: p. 113-125.
236. Chen, G., J. Lei, Y. Du, X. Du, and X. Chen, *A polycarboxylate as a superplasticizer for montmorillonite clay in cement: Adsorption and tolerance studies.* Arabian Journal of Chemistry, 2017. **11**(6): p. 747-755.
237. Courard, L., F. Michel, and J. Pierard, *Influence of clay in limestone fillers for self-compacting cement based composites.* Construction and Building Materials, 2011. **25**(3): p. 1356-1361.
238. Nehdi, M.L., *Clay in cement-based materials: Critical overview of state-of-the-art.* Construction and Building Materials, 2014. **51**: p. 372-382.
239. Tan, H., B. Gu, B. Ma, X. Li, C. Lin, and X. Li, *Mechanism of intercalation of polycarboxylate superplasticizer into montmorillonite.* Applied Clay Science, 2016. **129**: p. 40-46.
240. Lei, L. and J. Plank, *A concept for a polycarboxylate superplasticizer possessing enhanced clay tolerance.* Cement and Concrete Research, 2012. **42**(10): p. 1299-1306.
241. Plank, J., *Einfluss von Tonmineralien auf die Wirkung von PCE-Fließmitteln.* Beton, 2016: p. 288 - 290.
242. Ait-Akbour, R., C. Taviot-Guého, F. Leroux, P. Boustingorry, and F. Leising, *Interaction of Montmorillonite with Poly(ethylene Glycol) and Poly(methacrylic Acid) Polymers. Consequences on the Influence of Clays on Superplasticizer Efficiency*, in *ACI SP 302 - 11th International Conference on Superplasticizers and Other Chemical Admixtures in Concrete*, V.M. Malhotra, P.R. Gupta, and T.C. Holland, Editors. 2015, American Concrete Institute: Ottawa, Canada. p. 463-476.
243. Zhang, L., Q. Lu, Z. Xu, Q. Liu, and H. Zeng, *Effect of polycarboxylate ether comb-type polymer on viscosity and interfacial properties of kaolinite clay suspensions.* Journal of Colloid and Interface Science, 2012. **378**(1): p. 222-231.
244. Lei, L. and J. Plank, *Synthesis and Properties of a Vinyl Ether-Based Polycarboxylate Superplasticizer for Concrete Possessing Clay Tolerance.* Industrial & Engineering Chemistry Research, 2014. **53**(3): p. 1048-1055.
245. Liu, X., Z.M. Wang, H. Wu, and H.Q. Li, *Effects of Clay on Flow Properties of Polycarboxylate Superplasticizer and its Control Measure.* Advanced Materials Research, 2013. **690-693**: p. 682-685.
246. Xu, H., S. Sun, Q. Yu, and J. Wei, *Effect of β-cyclodextrin pendant on the dispersion robustness of polycarboxylate superplasticizer toward kaolin.* Polymer Composites, 2018. **39**(3): p. 755-761.
247. Tan, H., X. Li, M. Liu, B. Ma, B. Gu, and X. Li, *Tolerance of cement for clay minerals: effect of side-chain density in polyethylene oxide (PEO) superplasticizer additives.* Clay and Clay Minerals, 2016. **64**(6): p. 732-742.
248. Herrmann, J. and J. Rickert, *Interactions between cements with calcined clay and superplasticizers*, in *ACI SP 302 - 11th International Conference on Superplasticizers and Other Chemical Admixtures in Concrete*, V.M. Malhotra, P.R. Gupta, and T.C. Holland, Editors. 2015, American Concrete Institute: Ottawa, Canada. p. 299-314.
249. Herrmann, J. and J. Rickert, *Influences of temperature on interactions between superplasticizers and cements with fly ash or calcined clay*, in *15th International Congress on the Chemistry of Cement*, J. Gemrich, Editor. 2019, Research Institute of Binding Materials Prague: Prague, Czech Republic. p. 10.

250. Zaribaf, B.H., B. Uzal, and K. Kurtis, *Compatibility of superplasticizers with limestone-metakaolin blended cementitious system*, in *Calcined Clays for Sustainable Concrete - Proceedings of the 1st International Conference on Calcined Clays for Sustainable Concrete*, K. Scrivener and A. Favier, Editors. 2015, Springer: Dordrecht, Netherlands. p. 427-434.
251. Stöber, S. and H. Pöllmann, *Crystalchemistry of Organic Sulfonates Used as Cement Additives.* Materials Science Forum, 1998. **278-281**: p. 904-908.
252. Ng, S. and H. Justnes, *Study on the Rheology of Fly Ash Versus Calcined Marl Blended Cements with Polycarboxylate-Based Superplasticizers*, in *ACI SP 302 - 11th International Conference on Superplasticizers and Other Chemical Admixtures*, V.M. Malhotra, P.R. Gupta, and T.C. Holland, Editors. 2015, American Concrete Institute: Ottawa, Canada. p. 387-400.
253. Ahn, T.-H., K.-B. Shim, and J.-S. Ryou, *The relationship between various super-plasticizers and hydration of mortar incorporating metakaolin.* Journal of Ceramic Processing Research, 2015. **16**(2): p. 181-187.
254. Justice, J. and K. Kurtis, *Influence of Metakaolin Surface Area on Properties of Cement-Based Materials.* Journal of Materials in Civil Engineering, 2007. **19**(9): p. 762-771.
255. Akhlaghi, O., T. Aytas, B. Tatli, D. Sezer, A. Hodaei, A. Favier, K. Scrivener, Y.Z. Menceloglu, and O. Akbulut, *Modified poly(carboxylate ether)-based superplasticizer for enhanced flowability of calcined clay-limestone-gypsum blended Portland cement.* Cement and Concrete Research, 2017. **101**(Supplement C): p. 114-122.
256. Navarro-Blasco, I., M. Pérez-Nicolás, J.M. Fernández, A. Duran, R. Sirera, and J.I. Alvarez, *Assessment of the interaction of polycarboxylate superplasticizers in hydrated lime pastes modified with nanosilica or metakaolin as pozzolanic reactives.* Construction and Building Materials, 2014. **73**: p. 1-12.
257. Schmid, M. and J. Plank, *Dispersing Performance of Different Kinds of Polycarboxylate (PCE) Superplasticizers in Cement Blended With a Calcined Clay.* Construction and Building Materials, 2020. **258**: p. 119576.
258. Li, R., L. Lei, T. Sui, and J. Plank, *Effectiveness of PCE superplasticizers in calcined clay blended cements.* Cement and Concrete Research, 2021. **141**: p. 106334.
259. Li, R., M. Schmid, T. Sui, and J. Plank, *Influence of Calcined Clays on Workability of Low Carbon Composite Cements*, in *CIGOS 2021, 6th International Conference on Geotechnics, Civil Engineering and Structures - Emerging Technologies and Applications for Green Infrastructure*, C. Ha-Minh, et al., Editors. 2022, Springer Singapore: Singapore. p. 677-685.
260. Ferreiro, S., D. Herfort, and J.S. Damtoft, *Influence of Clay Type on Performance of Calcined Clay – Limestone Portland Cements*, in *Calcined Clays for Sustainable Concrete - Proceedings of the 2nd International Conference on Calcined Clays for Sustainable Concrete*, F. Martirena, A. Favier, and K. Scrivener, Editors. 2018, Springer: Dordrecht, Netherlands. p. 176-182.
261. Schmid, M. and J. Plank, *Interaction of individual meta clays with polycarboxylate (PCE) superplasticizers in cement investigated via dispersion, zeta potential and sorption measurements.* Applied Clay Science, 2021. **207**: p. 106092.
262. Bhosale, P.S. and J.C. Berg, *Poly(acrylic acid) as a rheology modifier for dense alumina dispersions in high ionic strength environments.* Colloids and Surfaces A: Physicochemical and Engineering Aspects, 2010. **362**(1): p. 71-76.
263. Danner, T., G. Norden, and H. Justnes, *Characterisation of calcined raw clays suitable as supplementary cementitious materials.* Applied Clay Science, 2018. **162**: p. 391-402.
264. Maier, M., N. Beuntner, and K.-C. Thienel, *Mineralogical characterization and reactivity test of common clays suitable as supplementary cementitious material.* Applied Clay Science, 2021. **202**: p. 105990.
265. Maier, M., B. Forster, N. Beuntner, and K.-C. Thienel, *Potential of calcined recycling kaolin from silica sand processing as supplementary cementitious material*, in *Calcined Clays for Sustainable Concrete - Proceedings of the 3rd International Conference on*

Calcined Clays for Sustainable Concrete, S. Bishnoi, Editor. 2020, Springer: Singapore. p. 75-83.
266. Barnes, H.A. and K. Walters, *The yield stress myth?* Rheologica Acta, 1985. **24**(4): p. 323-326.
267. Thienel, K.-C., N. Beuntner, and J. Schrenk, *Ökologisch und technisch verbesserte Betone durch den Einsatz alternativer Zusatzstoffe*, in *Tagung der GDCh-Fachgruppe Bauchemie*, B. Middendorf, A. Wetzel, and J. Arend, Editors. 2014, GDCh-Fachgruppe Bauchemie: Kassel, Germany. p. 1.
268. Marchetti, G., V. Rahhal, Z. Pavlík, M. Pavlíková, and E.F. Irassar, *Assessment of packing, flowability, hydration kinetics, and strength of blended cements with illitic calcined shale.* Construction and Building Materials, 2020. **254**: p. 119042.
269. DIN EN 1015-3, *Prüfverfahren für Mörtel für Mauerwerk-Teil 3: Bestimmung der Konsistenz von Frischmörtel (mit Ausbreittisch) (Methods of test for mortar for masonry - Part 3: Determination of consistence of fresh mortar (by flow table))*. 2007, Beuth-Verlag: Berlin. p. 12.
270. Vikan, H., H. Justnes, F. Winnefeld, and R. Figi, *Correlating cement characteristics with rheology of paste.* Cement and Concrete Research, 2007. **37**(11): p. 1502-1511.
271. Goetz-Neunhoeffer, F. and J. Neubauer, *Refined ettringite ($Ca_6Al_2(SO_4)_3(OH)_{12}\cdot 26H_2O$) structure for quantitative X-ray diffraction analysis.* Powder Diffraction, 2005. **21**(1): p. 4-11.
272. Runcevski, T., R.E. Dinnebier, O.V. Magdysyuk, and H. Pöllmann, *Crystal structures of calcium hemicarboaluminate and carbonated calcium hemicarboaluminate from synchrotron powder diffraction data.* Acta Crystallographica Section B, 2012. **68**(5): p. 493-500.
273. Schofield, P.F., C.C. Wilson, K.S. Knight, and I.C. Stretton, *Temperature related structural variation of the hydrous components in gypsum.* Zeitschrift für Kristallographie - Crystalline Materials, 2000. **215**(12): p. 707.
274. Busing, W.R. and H.A. Levy, *Neutron Diffraction Study of Calcium Hydroxide.* The Journal of Chemical Physics, 1957. **26**(3): p. 563-568.
275. Siddique, R. and M.I. Khan, *Supplementary Cementing Materials*. Engineering Materials. 2011, Berlin Heidelberg: Springer. 287.
276. Feys, D., R. Verhoeven, and G. De Schutter, *Evaluation of Time Independent Rheological Models Applicable to Fresh Self-Compacting Concrete.* Applied Rheology, 2007. **17**(5): p. 56244-1-56244-10.
277. Irassar, E.F., V.L. Bonavetti, C.C. Castellano, M.A. Trezza, V.F. Rahhal, G. Cordoba, and R. Lemma, *Calcined illite-chlorite shale as supplementary cementing material: Thermal treatment, grinding, color and pozzolanic activity.* Applied Clay Science, 2019. **179**: p. 105143.
278. Aramburo, C., C. Pedrajas, V. Rahhal, M. González, and R. Talero, *Calcined clays for low carbon cement: Rheological behaviour in fresh Portland cement pastes.* Materials Letters, 2019. **239**: p. 24-28.
279. Shah, V., A. Parashar, G. Mishra, S. Medepalli, S. Krishnan, and S. Bishnoi, *Influence of cement replacement by limestone calcined clay pozzolan on the engineering properties of mortar and concrete.* Advances in Cement Research, 2018: p. 1-11.
280. González-Fonteboa, B., D. Carro-López, J. de Brito, F. Martínez-Abella, S. Seara-Paz, and S. Gutiérrez-Mainar, *Comparison of ground bottom ash and limestone as additions in blended cements.* Materials and Structures, 2017. **50**(1): p. 84.
281. Han, S. and J. Plank, *Mechanistic study on the effect of sulfate ions on polycarboxylate superplasticisers in cement.* Advances in Cement Research, 2013. **25**(4): p. 200-207.
282. Bentz, D.P., C.F. Ferraris, M.A. Galler, A.S. Hansen, and J.M. Guynn, *Influence of particle size distributions on yield stress and viscosity of cement–fly ash pastes.* Cement and Concrete Research, 2012. **42**(2): p. 404-409.
283. Tavares, L.R.C., J.F.T. Junior, L.M. Costa, A.C. da Silva Bezerra, P.R. Cetlin, and M.T.P. Aguilar, *Influence of quartz powder and silica fume on the performance of Portland cement.* Scientific Reports, 2020. **10**(1): p. 21461.

284. Al Mahrouqi, D., J. Vinogradov, and M.D. Jackson, *Zeta potential of artificial and natural calcite in aqueous solution.* Advances in Colloid and Interface Science, 2017. **240**: p. 60-76.
285. Maier, M., S. Scherb, A. Neißer-Deiters, N. Beuntner, and K.-C. Thienel, *Hydration of cubic tricalcium aluminate in the presence of calcined clays.* Journal of the American Ceramic Society, 2021. **104**(7): p. 3619-3631.
286. Scherb, S., M. Maier, N. Beuntner, K.-C. Thienel, and J. Neubauer, *Reaction kinetics during early hydration of calcined phyllosilicates in clinker-free model systems.* Cement and Concrete Research, 2021. **143**: p. 106382.
287. Scherb, S., N. Beuntner, and K.-C. Thienel, *Reaction kinetics of the basic clays present in natural mixed clays*, in *Proceedings of the 2nd International Conference on Calcined Clays for Sustainable Concrete*, F. Martirena, A. Favier, and K. Scrivener, Editors. 2018, Springer: Dordrecht, Netherlands. p. 427-433.
288. Makó, É., R.L. Frost, J. Kristóf, and E. Horváth, *The Effect of Quartz Content on the Mechanochemical Activation of Kaolinite.* Journal of Colloid and Interface Science, 2001. **244**(2): p. 359-364.
289. Hamzaoui, R., F. Muslim, S. Guessasma, A. Bennabi, and J. Guillin, *Structural and thermal behavior of proclay kaolinite using high energy ball milling process.* Powder Technology, 2015. **271**(0): p. 228-237.
290. Danner, T., G. Norden, and H. Justnes, *The Effect of Calcite in the Raw Clay on the Pozzolanic Activity of Calcined Illite and Smectite*, in *Calcined Clays for Sustainable Concrete - Proceedings of the 3rd International Conference on Calcined Clays for Sustainable Concrete*, S. Bishnoi, Editor. 2020, Springer: Singapore. p. 131-138.
291. Zunino, F. and K. Scrivener, *Factors influencing the sulfate balance in pure phase C_3S/C_3A systems.* Cement and Concrete Research, 2020. **133**: p. 106085.
292. Ng, S. and H. Justnes, *Influence of plasticizers on the rheology and early heat of hydration of blended cements with high content of fly ash.* Cement and Concrete Composites, 2016. **65**: p. 41-54.
293. Jansen, D., J. Neubauer, F. Goetz-Neunhoeffer, R. Haerzschel, and W.D. Hergeth, *Change in reaction kinetics of a Portland cement caused by a superplasticizer — Calculation of heat flow curves from XRD data.* Cement and Concrete Research, 2012. **42**(2): p. 327-332.
294. Ramachandran, V.S. and Z. Chun-Mei, *Thermal analysis of the $3CaO \cdot Al_2O_3$-$CaSO_4 \cdot 2H_2O$-$CaCO_3$-H_2O system.* Thermochimica Acta, 1986. **106**: p. 273-282.
295. Antoni, M., *Investigation of cement substitution by blends of calcined clays and limestone*, in *Faculté des Sciences et Techniques de L'ingénieur*. 2013, École Polytechnique Fédérale de Lausanne: Lausanne. p. 254.
296. Hu, K. and Z. Sun, *Influence of Polycarboxylate Superplasticizers with Different Functional Units on the Early Hydration of C_3A-Gypsum.* Materials, 2019. **12**(7): p. 1132.
297. Pott, U., C. Jakob, D. Jansen, J. Neubauer, and D. Stephan, *Investigation of the incompatibilities of cement and superplasticizers and their influence on the rheological behavior.* Materials, 2020. **13**(977): p. 21.
298. Matschei, T., B. Lothenbach, and F.P. Glasser, *The AFm phase in Portland cement.* Cement and Concrete Research, 2007. **37**(2): p. 118-130.
299. Scherb, S., N. Beuntner, M. Köberl, and K.-C. Thienel, *The early hydration of cement with the addition of calcined clay - From single phyllosilicate to clay mixture*, in *20. Internationale Baustofftagung ibausil*, H.-B. Fischer and A. Volke, Editors. 2018, F.A. Finger-Institut für Baustoffkunde, Prof. Dr.-Ing. H.-M. Ludwig: Weimar, Germany. p. 658-666.
300. Uchikawa, H., S. Hanehara, T. Shirasaka, and D. Sawaki, *Effect of admixture on hydration of cement, adsorptive behavior of admixture and fluidity and setting of fresh cement paste.* Cement and Concrete Research, 1992. **22**(6): p. 1115-1129.
301. ASTM C1679-17, *Standard Practice for Measuring Hydration Kinetics of Hydraulic Cementitious Mixtures Using Isothermal Calorimetry*. 2018, ASTM International: West Conshohocken, PA. p. 15.

302. Deutscher Ausschuss für Stahlbeton, *Richtlinie für Beton mit verlängerter Verarbeitbarkeitszeit (Verzögerter Beton) (DAfStb guideline for concrete with prolonged workability period (delayed concrete))*. 2006, Deutscher Ausschuss für Stahlbeton. p. 8.

9 Appendix

9.1 Appendix A1: Supplementary data for clinkerfree investigations and materials

Preliminary investigations[1] showed the zeta potential of quartz powder (QP), calcined Amaltheen clay (TG) and metakaolin (Mk) depending on the water-to-solid ratio (w/s) (Figure A-1, left) and pH value (Figure A-1, right).

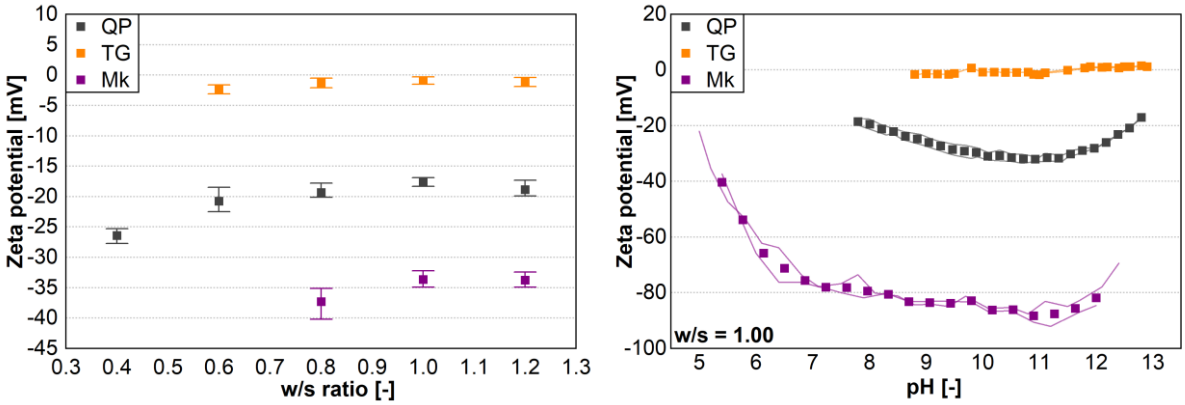

Figure A-1. Zeta potential of pure materials in distilled water depending on w/s ratio (left) and pH value (right)

Figure A-2 and Figure A-3 show the single and averaged zeta potential measurements of meta-phyllosilicates as well as of raw and calcined common clays in distilled water and over a period of three hours. Table A-1 shows the single data points and standard deviation of the zeta potential of meta-phyllosilicates and calcined common clays as measured in SCPS. Figure A-4 shows the torque curves of metaphyllosilicates dispersed in distilled water at w/s = 1.0 (left) and w/s = 1.5 (right).

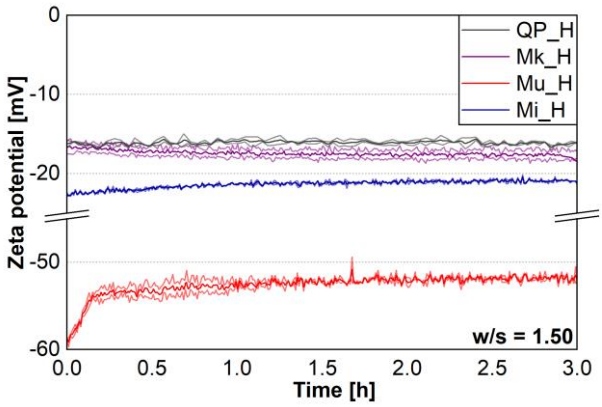

[1] Sasse, T., *Evaluierung des Zetapotentials von Zementersatzstoffen in Abhängigkeit ausgewählter Messparameter*, in *Fakultät für Bauingenieurwesen und Umweltwissenschaften, Institut für Werkstoffe des Bauwesens*. 2019, Universität der Bundeswehr München: Neubiberg. p. 66

Figure A-2. Time dependent zeta potential of quartz powder and metaphyllosilicates in distilled water at w/s = 1.50

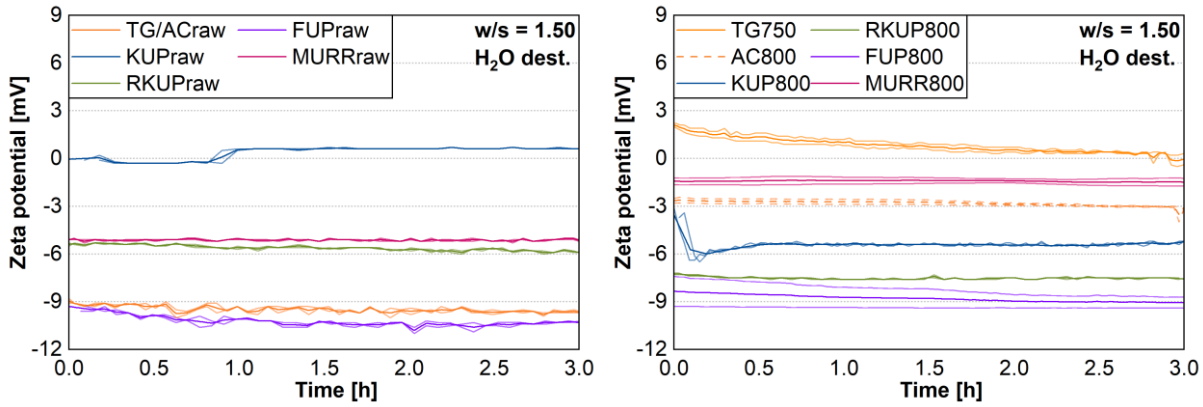

Figure A-3. Zeta potential of raw clays (left) and calcined common clays (right) in distilled water at w/s = 1.50

Table A-1. Zeta potential of metaphyllosilicates and calcined common clays in SCPS (w/s = 1.50)

Mixture	#1 [mV]	#2 [mV]	#3 [mV]	#4 [mV]	#5 [mV]	#6 [mV]	#7 [mV]	σ [mV]
Mk_SCPS	- 48.0	- 47.7	- 46.4	- 47.3	- 46.8	- 47.7	- 48.0	0.56
Mu_SCPS	- 8.3	- 9.8	- 10.3	- 8.7	- 9.5	- 10.0	- 9.4	0.66
Mi_SCPS	- 28.5	- 27.5	- 27.9	- 28.3	- 27.7	- 28.0	- 28.3	0.33
AC800_SCPS	- 1.2	- 1.5	- 1.4	- 1.9	- 1.4	- 2.0	- 1.8	0.28
KUP800_SCPS	- 2.8	- 2.7	- 3.5	- 3.2	- 3.6	- 3.4	- 3.6	0.35
RKUP800_SCPS	- 3.3	- 3.5	- 3.6	- 4.4	- 4.5	- 4.3	- 4.2	0.45
FUP800_SCPS	- 7.3	- 7.3	- 7.5	- 7.3	- 7.9	- 7.6	- 7.4	0.21
MURR800_SCPS	0.4	- 1.1	- 1.2	- 1.6	- 1.4	- 1.4	- 1.3	0.62

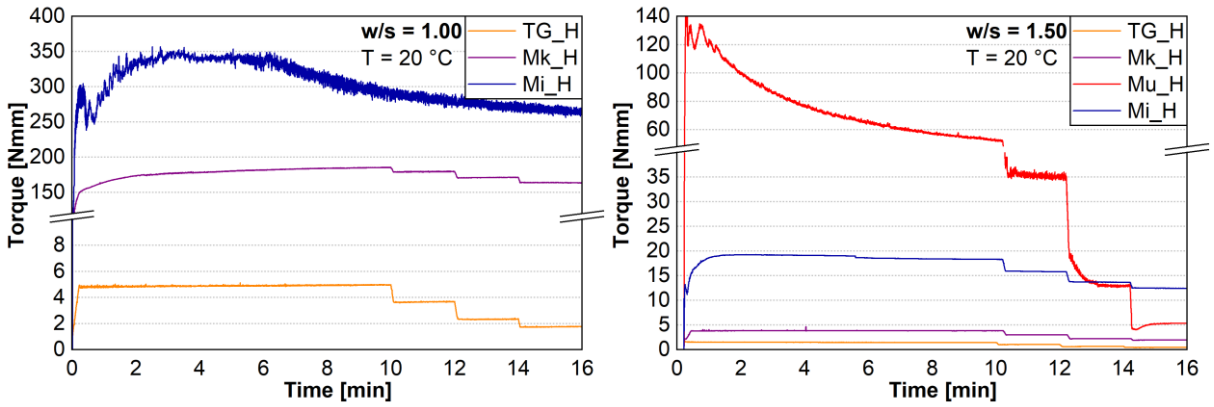

Figure A-4. Torque curves of TG/Mk/Mi_H suspensions at w/s = 1.00 (left) and of TG/Mk/Mu/Mi_H suspensions at w/s = 1.50 (right)

The influence of different ultrasound power (50W vs. 200 W) on dispersing two calcined common clays and as consequence on their particle size distribution (PSD) as measured by static laser scattering (SLS) is shown in Figure A-5. The difference in PSD of quartz-rich RKUP, although the coarse fraction (~ 100 µm) reduces with higher power. The PSD of FUP, which has a significantly higher kaolinite content in raw clay, changes significantly: with 200W, the fraction at ~ 25 µm reduces and the fraction at ~ 5 µm increases.

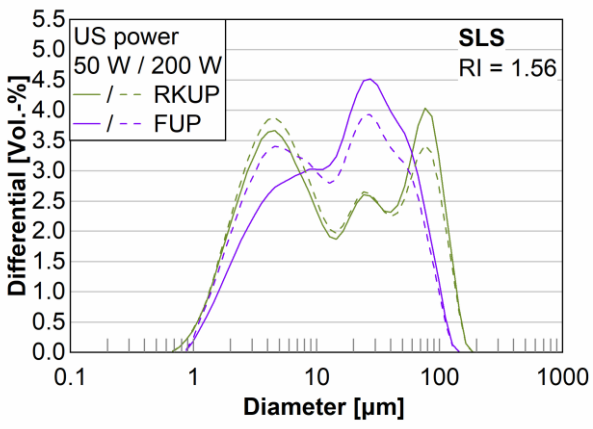

Figure A-5. Influence of ultrasound (US) power dispersion on the particle size analysis of calcined common clays, using the calcined kaolinite-rich clays RKUP and FUP as example

9.2 Appendix A2: Electroacoustic measurements of cementitious systems

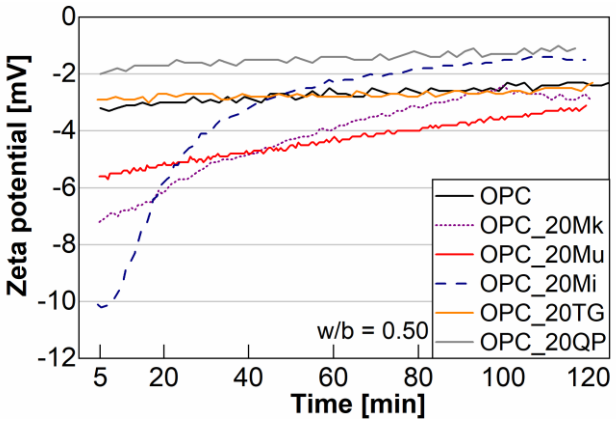

Figure A-6. Time-related zeta potential of OPC mixtures with 20 wt% Mk, Mu, Mi, TG and QP (w/b = 0.50)

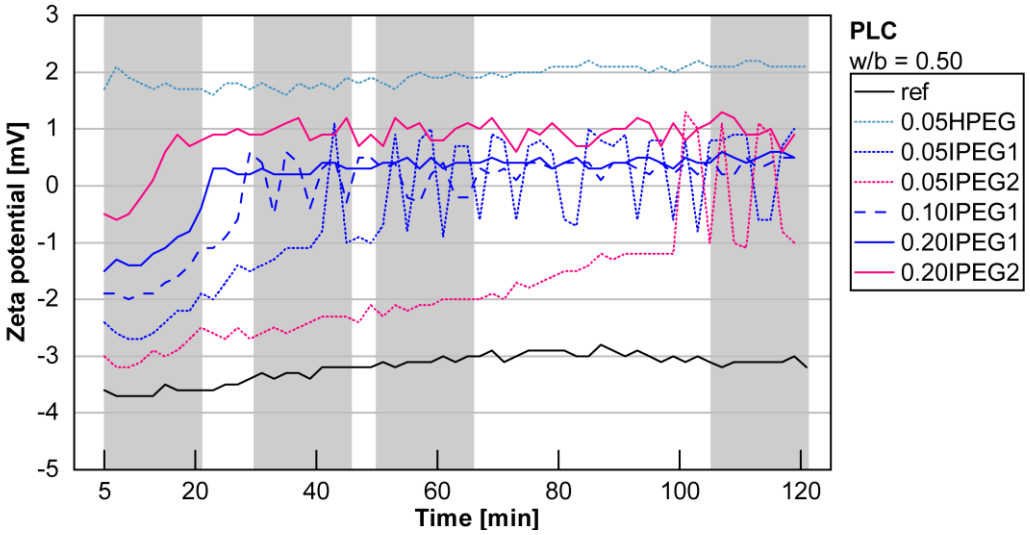

Figure A-7. Time-related zeta potential of PLC* mixtures with various amounts and types of PCE (w/b = 0.50)

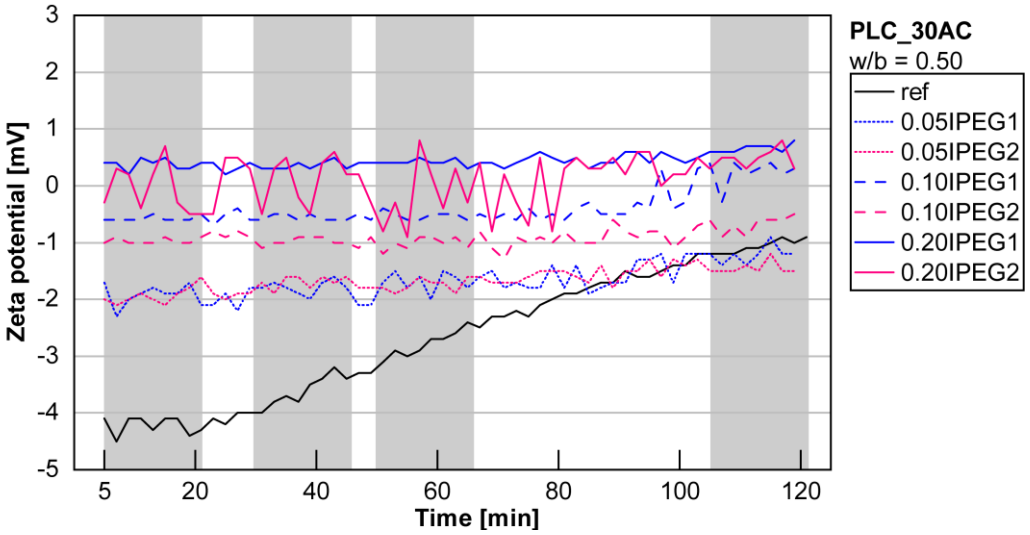

Figure A-8. Time-related zeta potential of PLC*_30AC mixtures with various amounts and types of PCE (w/b = 0.50)

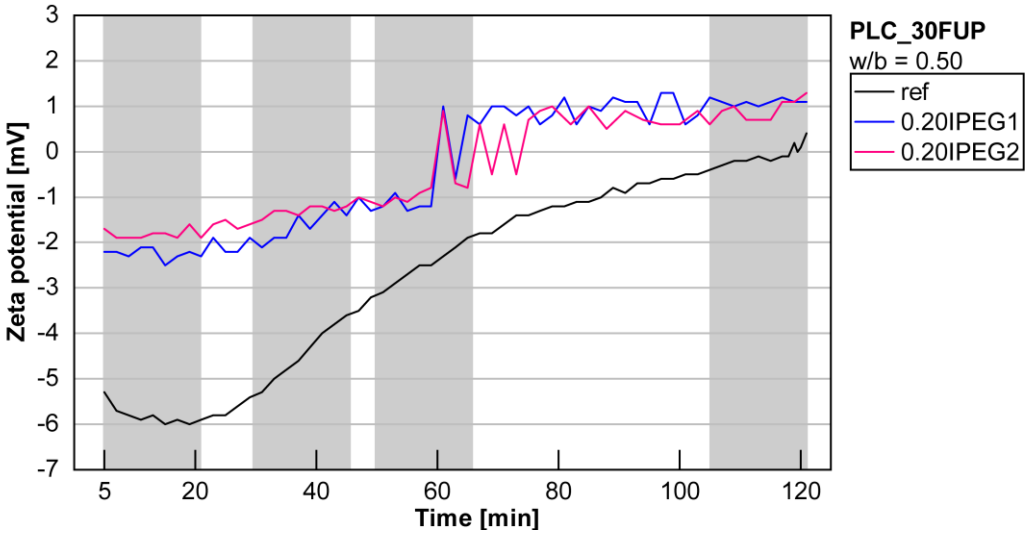

Figure A-9. Time-related zeta potential of PLC*_30FUP mixtures with various amounts and types of PCE (w/b = 0.50)

9.3 Appendix A3: Rheological analysis of CCBC pastes by linear Bingham model and flow resistance

This section of appendix includes the rheological parameters of CCBC mixtures with metaphyllosilicates and the calcined common clay TG. Results for mixtures with the other calcined common clays are provided in Appendix A7: Time-dependent rheological measurements.

The following abbreviations are used in the tables of this section:

Abbreviation	Definition
FR	Flow resistance [Nmm/min]
g	Yield stress factor [Nmm]
h	Viscosity factor [Nmm·min]
T	Torque [Nmm]
x	Replacement level [wt%] and type of metaphyllosilicate/calcined common clay
y	Dosage [%bwob] and type of superplasticizer

Table A-2. Rheological parameters of OPC°_x_yLS mixtures (w/b = 0.45)

Mixture		h [Nmm·min]	g [Nmm]	R² [-]	Median T [Nmm] at … [rpm]				FR [Nmm/min]
x	y				20	40	80	120	
-	-	0.11	17.0	0.95	19.3	21.6	26.2	30.7	2504
-	0.14Mg-	0.07	7.6	0.87	9.0	10.4	13.2	16.0	1249
-	0.15Na-	0.06	9.4	0.80	10.9	12.0	14.4	16.7	1378
20CT	-	0.19	39.5	0.97	43.9	47.2	54.9	62.6	5299
20CT	0.45Mg-	0.18	0.4	0.99	4.1	7.7	15.1	22.5	1328
20CT	0.47Na-	0.17	3.2	0.99	6.7	10.1	17.1	24.0	1536
20Mk	-	0.20	115.9	0.65	120.3	124.2	131.9	139.7	12999
20Mk	0.69Mg-	0.25	- 3.6	0.93	1.4	6.3	16.2	26.1	1375
20Mk	0.82Na-	0.22	- 2.1	1.00	2.4	6.9	15.9	24.9	1364

Table A-3. Rheological parameters of OPC_x reference mixtures (w/b = 0.50)

Mixture x	h [Nmm·min]	g [Nmm]	R² [-]	Median T [Nmm] at … [rpm]				FR [Nmm/min]
				20	40	80	120	
-	0.08	6.4	0.99	8.2	9.5	12.4	15.9	1182
10QP	0.09	4.5	0.99	6.5	7.8	10.9	15.0	1037
20QP	0.07	3.5	0.99	5.3	6.2	8.8	12.2	839
30QP	0.06	2.0	1.00	3.3	4.1	6.4	8.9	592
10TG	0.10	8.1	0.98	10.4	12.1	15.5	20.4	1495
20TG	0.14	17.7	0.95	20.7	23.3	27.8	34.4	2708
30TG	0.19	21.3	0.86	26.0	29.1	34.5	44.8	3410
10Mk	0.05	50.7	0.95	51.6	53.1	55.0	57.3	5455
20Mk	0.06	169.3	0.77	169.8	172.0	174.5	176.0	17360
30Mk	- 0.19	321.0	0.77	317.6	312.8	305.9	298.0	30757
5Mu	0.23	27.1	0.80	32.5	36.9	43.3	55.5	4275
10Mu	0.30	95.0	0.39	101.4	110.8	112.2	132.5	11475
20Mu[2]	0.45	230.9	-	239.2	258.6	250.0	286.4	25876
30Mu[3]	0.58	366.6	-	377.0	406.4	387.8	440.5	40284
10Mi	0.21	32.8	0.77	38.0	41.3	47.0	58.5	4670
20Mi	0.17	102.7	0.35	111.6	106.3	109.8	124.4	11187
30Mi	0.38	183.4	0.50	195.7	199.2	201.5	230.6	20605

Table A-4. Rheological parameters of OPC_x_yNSF mixtures (w/b = 0.50)

Mixture		h [Nmm·min]	g [Nmm]	R² [-]	Median T [Nmm] at … [rpm]				FR [Nmm/min]
x	y				20	40	80	120	
-	0.21	0.05	4.6	0.98	5.7	6.4	8.4	10.4	795
20QP	0.18	0.04	1.9	0.99	2.9	3.5	5.4	7.2	495
20TG	0.40	0.07	- 0.1	1.00	1.5	2.6	5.2	8.3	467
20Mk	0.68	0.05	1.5	0.99	2.7	3.3	5.3	7.4	485
20Mu	1.50	1.76	- 7.8	0.95	28.4	63.3	131.5	205.1	11543
20Mi	0.95	0.12	1.5	0.99	4.4	6.3	10.8	16.5	995

[2] Linear extrapolation based on OPC_5Mu and OPC_10Mu values

[3] Linear extrapolation based on OPC_5Mu and OPC_10Mu values

Table A-5. Rheological parameters of OPC_x_yHPEG mixtures (w/b = 0.50)

Mixture		h	g	R^2 [-]	Median T [Nmm] at … [rpm]				FR
x	y	[Nmm·min]	[Nmm]		20	40	80	120	[Nmm/min]
-	0.05	0.05	0.1	0.99	1.4	2.1	4.1	6.6	375
-	0.20	0.03	- 0.5	0.99	0.3	0.7	2.0	3.7	182
10QP	0.04	0.06	0.5	0.99	1.9	2.7	4.8	7.5	440
20QP	0.04	0.05	0.1	0.99	1.3	2.0	3.8	6.1	349
20QP	0.20	0.03	- 0.2	0.98	0.5	0.7	1.8	3.1	160
30QP	0.04	0.04	- 0.2	0.99	0.8	1.3	2.8	4.7	254
10TG	0.07	0.06	- 0.8	0.99	0.8	1.6	3.9	6.9	307
20TG	0.07	0.09	- 0.3	0.99	1.7	2.9	6.0	10.0	484
20TG	0.20	0.06	- 0.9	0.99	0.4	1.2	3.2	5.9	370
30TG	0.07	0.10	- 1.3	0.98	1.3	2.7	6.2	11.4	462
20Mk	0.19	0.07	5.9	0.99	7.6	8.3	10.8	14.1	988
20Mk	0.20	0.05	7.0	0.95	8.2	8.6	10.6	12.7	1047
10Mu	0.16	0.33	- 8.3	0.85	1.5	4.1	13.1	32.7	916
20Mu	0.16	1.09	- 26.5	0.72	4.5	14.5	44.1	107.0	4384
20Mu	0.20	0.83	- 23.3	0.70	2.2	7.5	27.1	79.0	2911
10Mi	0.37	0.05	- 0.8	0.99	0.4	1.1	3.0	5.3	265
20Mi	0.20	0.20	21.8	0.77	27.3	29.7	35.3	46.8	3510
20Mi	0.37	0.13	0.8	0.94	4.5	5.7	9.9	17.0	953
30Mi	0.37	0.44	79.8	0.62	91.9	97.1	108.6	134.1	10859

Table A-6. Rheological parameters of OPC_x_yamphMPEG mixtures (w/b = 0.50)

Mixture		h	g	R^2 [-]	Median T [Nmm] at … [rpm]				FR
x	y	[Nmm·min]	[Nmm]		20	40	80	120	[Nmm/min]
-	0.06	0.05	1.9	0.97	3.4	3.6	5.9	8.6	550
-	0.20	0.03	- 0.5	0.99	0.3	0.7	2.0	3.6	180
20QP	0.04	0.05	0.7	0.99	1.9	2.4	4.2	6.4	386
20TG	0.08	0.10	1.0	0.98	3.6	4.6	8.0	12.8	751
20TG	0.20	0.06	- 0.9	0.99	0.4	1.2	3.3	5.9	289
20Mk	0.19	0.07	11.8	0.79	14.4	14.0	15.9	20.7	1615
20Mk	0.20	0.07	11.7	0.79	14.4	14.0	15.8	20.5	1603
20Mu	0.20	1.98	- 30.2	0.72	19.6	48.6	116.7	215.5	10634
20Mu	0.21	1.98	- 30.4	0.72	18.2	45.4	112.4	209.3	10224
20Mi	0.20	0.22	42.2	0.78	48.3	50.7	56.7	69.3	5657
20Mi	0.41	0.13	0.0	0.96	3.6	4.8	8.0	12.8	758

Table A-7. Rheological parameters of PLC_x reference mixtures (w/b = 0.50)

Mixture x	h [Nmm·min]	g [Nmm]	R^2 [-]	Median T [Nmm] at … [rpm]				FR [Nmm/min]
				20	40	80	120	
-	0.10	9.5	0.98	11.9	13.3	16.9	21.6	1627
10TG	0.11	13.7	0.98	16.2	17.9	21.5	26.7	2097
20TG	0.15	19.2	0.91	22.6	25.1	29.7	36.9	2908
30TG	0.16	22.3	0.95	25.6	28.7	33.7	41.1	3288
10Mk	0.05	67.3	0.92	67.8	69.8	72.0	73.6	7123
20Mk	0.24	77.5	0.85	81.8	87.7	96.5	106.0	9428
30Mk	- 0.32	397.2	0.66	391.3	381.5	375.8	357.8	37547
5Mu	0.26	41.8	0.80	47.2	52.6	60.3	72.7	5916
10Mu	0.43	107.8	0.77	113.7	128.1	141.5	158.9	13820
20Mu[4]	0.77	239.8	-	246.9	279.2	303.9	331.2	29626
30Mu[5]	1.11	371.8	-	379.7	430.1	466.3	503.7	45426
10Mi	0.16	40.2	0.84	43.9	46.6	51.0	59.2	5060
20Mi	0.20	86.3	0.67	92.4	93.7	99.0	110.9	9911
30Mi	0.37	198.0	0.63	208.8	213.4	217.5	243.4	22059

Table A-8. Rheological parameters of PLC_x_yNSF mixtures (w/b = 0.50)

Mixture		h [Nmm·min]	g [Nmm]	R^2 [-]	Median T [Nmm] at … [rpm]				FR [Nmm/min]
x	y				20	40	80	120	
-	0.24	0.03	5.6	0.85	6.3	6.9	8.5	9.7	805
20TG	0.50	0.08	1.1	1.00	2.9	4.2	7.2	10.6	656
20Mk	0.77	0.05	1.1	1.00	2.2	2.9	4.9	7.0	448
20Mu	1.50	0.74	- 11.5	0.86	7.5	17.8	38.9	79.1	3750
20Mi	0.97	0.12	3.6	0.99	6.6	8.2	12.7	18.6	1194

Table A-9. Rheological parameters of PLC_x_yHPEG mixtures (w/b = 0.50)

Mixture		h [Nmm·min]	g [Nmm]	R^2 [-]	Median T [Nmm] at … [rpm]				FR [Nmm/min]
x	y				20	40	80	120	
-	0.06	0.05	1.5	0.99	2.9	3.6	5.5	8.1	519
-	0.20	0.03	- 0.6	0.99	0.3	0.7	2.0	3.7	180
20TG	0.08	0.09	2.5	0.98	4.8	5.9	9.1	13.5	860
20TG	0.20	0.05	- 0.9	0.99	0.4	1.1	3.0	5.5	267
20Mk	0.20	0.04	13.8	0.90	15.1	15.3	17.1	19.3	1681
20Mu	0.16	1.15	- 10.4	0.74	21.0	32.8	67.3	130.0	6488
20Mu	0.20	1.00	- 23.7	0.77	4.7	13.5	41.5	94.9	4008
20Mi	0.20	0.23	41.4	0.66	47.6	50.5	56.5	68.9	5628
20Mi	0.40	0.10	- 0.7	0.98	2.1	3.3	6.9	12.0	634

[4] Linear extrapolation based on PLC_5Mu and PLC_10Mu values

[5] Linear extrapolation based on PLC_5Mu and PLC_10Mu values

Table A-10. Rheological parameters of PLC_x_yamphMPEG mixtures (w/b = 0.50)

Mixture		h [Nmm·min]	g [Nmm]	R^2 [-]	Median T [Nmm] at … [rpm]				FR [Nmm/min]
x	y				20	40	80	120	
-	0.07	0.05	2.8	0.99	4.1	4.8	6.7	9.3	640
-	0.20	0.03	- 0.5	1.00	0.3	0.7	2.0	3.6	179
20TG	0.08	0.08	0.5	0.99	2.5	3.5	6.5	10.3	597
20TG	0.20	0.05	- 0.8	0.99	0.4	1.0	2.9	5.2	253
20Mk	0.20	0.07	17.2	0.79	21.0	22.2	21.6	26.0	2258
20Mk	0.21	0.06	17.2	0.79	19.6	18.8	20.2	23.3	2034
20Mu	0.18	2.04	45.7	0.76	85.6	135.4	193.5	291.8	18496
20Mu	0.20	1.67	43.4	0.70	83.5	110.8	159.8	245.9	15469
20Mi	0.20	0.28	61.2	0.68	69.0	72.1	79.2	95.7	7935
20Mi	0.42	0.11	3.4	0.91	7.1	6.7	10.4	16.7	1021

9.4 Appendix A4: Calculated efficiency of superplasticizers

The reduction in yield stress factor, viscosity factor and torque by the addition of superplasticizer is expressed as efficiency, as published in the first and third journal paper. This section includes the calculated efficiency of all mixtures tested. The efficiency in OPC mixtures with w/b = 0.45 and w/b = 0.50 is shown in Table A-11 and Table A-12, respectively. For PLC mixtures, it is shown with metaphyllosilicates and TG in Table A-13 and with the other calcined common clays in Table A-14.

The following abbreviations are used in the tables of this section:

Abbreviation	Definition
g	Yield stress factor [Nmm]
h	Viscosity factor [Nmm·min]
T	Torque [Nmm]
g,red	Reduction in yield stress factor
h,red	Reduction in viscosity factor
T,red	Reduction in torque

Table A-11. Efficiency of superplasticizers in OPC°_x_y mixtures (w/b = 0.45)

Mixture	Difference in … [%] compared to reference mixture (0 %)			Efficiency in … [%/0.01% bwob]			
	g	h	T	g,red	h,red	T,red	**Total**
OPC°_0.14Mg-LS	55.5	38.3	50.7	4.0	2.7	3.6	**10.3**
OPC°_0.15Na-LS	44.9	46.4	44.7	3.0	3.1	3.0	**9.1**
OPC°_20CT_ 0.45Mg-LS	99.1	4.2	77.7	2.2	0.1	1.7	**4.0**
OPC°_20CT_0.47Na-LS	91.9	9.9	73.4	1.9	0.2	1.6	**3.7**
OPC°_20Mk_ 0.69Mg-LS	103.1	- 24.6	90.7	1.5	(- 0.4)	1.3	**2.8**
OPC°_20Mk_0.82Na-LS	101.9	- 13.5	90.6	1.2	(- 0.2)	1.1	**2.3**

Table A-12. Efficiency of superplasticizers in OPC_x_y mixtures (w/b = 0.50)

Mixture	Difference in … [%] compared to reference mixture (0 %)			Efficiency in … [%/0.01% bwob]			
	g	h	T	g,red	h,red	T,red	**Total**
OPC_0.21NSF	27.5	39.8	32.4	1.3	1.9	1.5	**4.7**
OPC_0.05HPEG	97.7	32.6	71.4	19.5	6.5	14.3	**40.3**
OPC_0.20HPEG	108.6	55.4	87.0	5.4	2.8	4.3	**12.5**
OPC_0.06amphMPEG	70.9	31.7	54.6	11.8	5.3	9.1	**26.2**
OPC_0.20amphMPEG	108.4	56.3	87.3	5.4	2.8	4.4	**12.6**
OPC_10QP_0.04HPEG	87.7	34.4	60.5	21.9	8.6	15.1	**45.6**
OPC_20QP_0.18NSF	46.8	38.2	42.2	2.6	2.1	2.3	**7.0**
OPC_20QP_0.04HPEG	96.3	31.2	62.4	24.1	7.8	15.6	**47.5**
OPC_20QP_0.20HPEG	106.5	61.9	83.3	5.3	3.1	4.2	**12.6**
OPC_20QP_ 0.04amphMPEG	80.0	35.0	56.6	20.0	8.8	14.1	**42.9**
OPC_30QP_0.04HPEG	110.8	29.2	62.0	27.7	7.3	15.5	**50.5**
OPC_10TG_0.07HPEG	109.8	37.1	80.0	15.7	5.3	11.4	**32.4**
OPC_20TG_0.40NSF	100.7	49.1	84.7	2.5	1.2	2.1	**5.8**
OPC_20TG_0.07HPEG	101.9	37.7	82.1	14.6	5.4	11.7	**31.7**
OPC_20TG_0.20HPEG	105.3	58.8	91.0	5.3	2.9	4.5	**12.7**
OPC_20TG_ 0.08amphMPEG	94.1	29.6	74.2	11.8	3.7	9.3	**24.8**
OPC_20TG_ 0.20amphMPEG	105.2	59.1	90.9	5.3	2.9	4.5	**12.7**
OPC_30TG_0.07HPEG	106.0	45.9	85.5	15.1	6.6	12.2	**33.9**
OPC_20Mk_0.68NSF	99.1	13.9	97.3	1.5	0.2	1.4	**3.1**
OPC_20Mk_0.19HPEG	96.5	- 19.9	94.1	5.1	(- 1.1)	4.9	**10.0**
OPC_20Mk_0.20HPEG	95.9	15.7	94.2	4.8	0.8	4.7	**10.3**
OPC_20Mk_ 0.19amphMPEG	93.0	- 27.5	90.6	4.9	(- 1.4)	4.8	**9.7**
OPC_20Mk_ 0.20amphMPEG	93.1	- 26.5	90.7	4.6	(- 1.3)	4.5	**9.1**
OPC_10Mu_0.16HPEG	108.7	- 10.0	89.6	6.8	(- 0.6)	5.6	**12.4**
OPC_20Mu_1.50NSF	103.4	- 294.4	59.9	0.7	(- 2.0)	0.4	**1.1**
OPC_20Mu_0.16HPEG	111.5	- 144.8	84.4	7.0	(- 9.0)	5.3	**12.3**
OPC_20Mu_0.20HPEG	110.1	- 86.7	89.4	5.5	(- 4.3)	4.5	**10.0**
OPC_20Mu_ 0.21amphMPEG	113.1	- 342.8	62.8	5.4	(- 16.3)	3.0	**8.4**
OPC_20Mu_ 0.20amphMPEG	113.2	- 343.4	64.2	5.7	(- 17.2)	3.2	**8.9**
OPC_10Mi_0.37HPEG	102.5	75.9	93.9	2.8	2.0	2.5	**7.3**
OPC_20Mi_0.95NSF	98.5	28.3	83.0	1.0	0.3	0.9	**2.2**
OPC_20Mi_0.20HPEG	78.8	23.0	36.1	3.9	1.1	1.8	**6.8**
OPC_20Mi_0.37HPEG	99.2	- 157.6	83.4	2.7	(- 4.3)	2.3	**5.0**
OPC_20Mi_0.20amphMPEG	58.9	- 28.6	- 4.1	2.9	(- 1.4)	(- 0.2)	**2.9**
OPC_20Mi_0.41amphMPEG	100.0	22.5	86.9	2.4	0.5	2.1	**5.1**
OPC_30Mi_0.37HPEG	56.5	- 17.0	48.1	1.5	(- 0.5)	1.3	**2.8**

Table A-13. Efficiency of superplasticizers in PLC_x_y mixtures (w/b = 0.50)

Mixture	Difference in … [%] compared to reference mixture (0 %)			Efficiency in … [%/0.01% bwob]			
	g	h	T	g,red	h,red	T,red	**Total**
PLC_0.24NSF	40.8	66.0	50.0	1.7	2.7	2.1	**6.5**
PLC_0.06HPEG	83.7	46.2	69.7	13.9	7.7	11.6	**33.2**
PLC_0.20HPEG	106.0	65.0	90.7	5.3	3.2	4.5	**13.0**
PLC_0.07amphMPEG	70.6	46.5	61.6	10.1	6.6	8.8	**25.5**
PLC_0.20amphMPEG	105.4	66.2	90.8	5.3	3.3	4.5	**13.1**
PLC_20TG_0.50NSF	94.2	45.9	79.4	1.9	0.9	1.6	**4.4**
PLC_20TG_0.08HPEG	87.0	37.6	72.0	10.9	4.7	9.0	**24.6**
PLC_20TG_0.20HPEG	104.8	63.5	92.2	5.2	3.2	4.6	**13.0**
PLC_20TG_0.08amphMPEG	97.3	44.8	81.3	12.2	5.6	10.2	**28.0**
PLC_20TG_0.20amphMPEG	104.2	66.0	92.6	5.2	3.3	4.6	**13.1**
PLC_20Mk_0.77NSF	98.6	79.2	95.5	1.3	1.0	1.2	**3.5**
PLC_20Mk_0.20HPEG	82.2	81.0	82.0	4.1	4.0	4.1	**12.2**
PLC_20Mk_0.20amphMPEG	77.8	71.0	75.5	3.9	3.5	3.8	**11.2**
PLC_20Mk_0.21amphMPEG	77.8	75.8	77.9	3.7	3.6	3.7	**11.0**
PLC_20Mu_1.50NSF	104.8	2.9	88.5	0.7	0.0	0.6	**1.3**
PLC_20Mu_0.16HPEG	104.3	- 50.3	79.6	6.5	(- 3.1)	5.0	**11.5**
PLC_20Mu_0.20HPEG	109.9	- 30.5	87.7	5.5	(- 1.5)	4.4	**9.9**
PLC_20Mu_0.18amphMPEG	80.9	- 165.3	41.3	4.5	(- 9.2)	2.3	**6.8**
PLC_20Mu_0.20amphMPEG	81.9	- 117.4	49.9	4.1	(- 5.9)	2.5	**6.6**
PLC_20Mi_0.97NSF	95.8	38.3	88.6	1.0	0.4	0.9	**2.3**
PLC_20Mi_0.20HPEG	52.1	- 12.6	43.8	2.6	(- 0.6)	2.2	**4.8**
PLC_20Mi_0.40HPEG	100.9	47.6	94.1	2.5	1.3	2.3	**6.1**
PLC_20Mi_0.20amphMPEG	29.1	- 40.5	20.5	1.5	(- 2.0)	1.0	**2.5**
PLC_20Mi_0.42amphMPEG	96.1	45.8	89.9	2.3	1.1	2.1	**5.5**

Table A-14. Efficiency of superplasticizers in PLC*_x_y mixtures (w/b = 0.50 if not noted otherwise)

Mixture	Difference in … [%] compared to reference mixture (0 %)			Efficiency in … [%/0.01% bwob]			
	g	h	T	g,red	h,red	T,red	**Total**
PLC*_0.05HPEG (w/b = 0.40)	60.9	11.5	47.6	12.2	2.3	9.5	**24.0**
PLC*_0.05IPEG1 (w/b = 0.40)	33.6	- 23.1	18.5	6.2	(- 4.6)	3.7	**9.9**
PLC*_0.05IPEG2 (w/b = 0.40)	61.8	0.0	45.1	12.4	0.0	9.0	**21.4**
PLC*_0.05HPEG	65.9	13.2	47.7	13.2	3.3	9.5	**26.0**
PLC*_0.05IPEG1	- 89.3	- 8.3	- 56.3	(- 17.9)	(- 1.7)	(- 11.3)	**0.0**
PLC*_0.10IPEG1	86.1	25.0	74.7	8.6	2.5	6.5	**17.6**
PLC*_0.20IPEG1	103.5	33.3	90.0	5.2	1.7	4.0	**10.9**
PLC*_0.05IPEG2	75.9	33.3	60.5	15.2	6.7	12.1	**34.0**
PLC*_0.10IPEG2	101.1	41.7	80.0	10.1	4.3	8.0	**22.4**
PLC*_0.20IPEG2	104.5	66.7	89.3	5.2	3.3	4.5	**13.0**
PLC*_30MURR_0.05HPEG	73.4	8.3	54.0	14.7	1.7	10.8	**27.2**
PLC*_30MURR_0.05IPEG1	67.5	8.3	49.6	13.5	1.7	9.9	**25.1**
PLC*_30MURR_0.10IPEG1	90.0	8.3	64.5	9.0	0.8	6.4	**16.2**
PLC*_30MURR_0.20IPEG1	104.1	33.3	81.5	5.2	1.7	4.1	**11.0**
PLC*_30MURR_0.05IPEG2	69.7	- 25.0	40.8	13.9	(- 5.0)	8.2	**22.1**
PLC*_30MURR_0.10IPEG2	97.3	33.3	75.3	9.7	3.3	7.5	**20.5**
PLC*_30AC_0.05HPEG	67.6	10.0	48.5	13.5	2.0	9.7	**25.2**
PLC*_30AC_0.05IPEG1	68.9	10.0	52.1	13.8	2.0	10.4	**26.2**
PLC*_30AC_0.10IPEG1	88.7	20.0	68.3	8.9	2.0	6.8	**17.7**
PLC*_30AC_0.20IPEG1	99.8	40.0	82.0	5.0	2.0	4.1	**11.1**
PLC*_30AC_0.05IPEG2	78.7	20.0	60.4	15.7	4.0	12.1	**31.8**
PLC*_30AC_0.10IPEG2	92.6	40.0	75.5	9.3	4.0	7.5	**20.8**
PLC*_30AC_0.20IPEG2	102.0	50.0	87.8	5.1	2.5	4.4	**12.0**
PLC*_30KUP_0.05HPEG (w/b = 0.40)	16.2	- 14.7	10.8	3.2	(- 2.9)	2.2	**5.4**
PLC*_30KUP_0.05IPEG1 (w/b = 0.40)	29.2	- 17.6	20.5	5.8	(- 3.5)	4.1	**9.9**
PLC*_30KUP_0.05IPEG2 (w/b = 0.40)	6.5	1.5	4.7	1.3	0.3	0.9	**2.5**
PLC*_30KUP_0.05HPEG	66.5	- 11.1	48.0	13.3	(- 2.2)	9.6	**22.9**
PLC*_30KUP_0.05IPEG1	40.8	- 25.9	24.9	8.2	(- 5.2)	5.0	**13.2**
PLC*_30KUP_0.10IPEG1	66.3	33.3	58.2	6.6	3.3	5.8	**15.7**
PLC*_30KUP_0.05IPEG2	75.4	- 44.4	46.6	15.1	(- 8.9)	9.3	**24.4**
PLC*_30KUP_0.10IPEG2	95.6	22.2	78.3	9.6	2.2	7.8	**19.6**
PLC*_30KUP_0.20IPEG2	104.5	44.4	90.3	5.2	2.2	4.5	**11.9**
PLC*_30RKUP_0.05HPEG	70.3	0.0	61.3	14.1	0.0	12.2	**26.3**
PLC*_30RKUP_0.05IPEG1	46.8	- 17.6	38.2	9.3	(- 3.5)	7.6	**16.9**
PLC*_30RKUP_0.10IPEG1	80.2	17.6	71.7	8.0	1.8	7.2	**17.0**
PLC*_30RKUP_0.20IPEG1	98.5	47.1	91.7	4.9	2.3	4.6	**11.8**
PLC*_30RKUP_0.05IPEG2	67.6	- 5.9	58.1	13.5	(- 1.2)	11.6	**25.1**
PLC*_30RKUP_0.10IPEG2	96.6	41.2	89.3	9.7	4.1	8.9	**22.7**
PLC*_30RKUP_0.20IPEG2	100.6	70.6	96.1	5.0	3.5	4.8	**13.3**
PLC*_30FUP_0.05HPEG	52.9	13.3	48.5	10.6	2.7	9.7	**23.0**
PLC*_30FUP_0.05IPEG1	45.2	26.7	42.9	9.0	5.3	8.6	**22.9**
PLC*_30FUP_0.10IPEG1	64.9	33.3	61.7	6.5	3.3	6.2	**16.0**
PLC*_30FUP_0.20IPEG1	89.1	33.3	82.6	4.5	1.7	4.1	**10.3**
PLC*_30FUP_0.05IPEG2	61.0	26.7	57.4	12.2	5.3	11.5	**29.0**
PLC*_30FUP_0.10IPEG2	80.7	26.7	74.4	8.0	2.7	7.4	**18.1**
PLC*_30FUP_0.20IPEG2	93.7	46.7	88.1	4.7	2.3	4.4	**11.4**

9.5 Appendix A5: Comparison of linear Bingham fits with modified Bingham and Herschel-Bulkley fits applied to CCBC pastes

Those mixtures, that show a R^2 value < 0.90 (0.95) with the linear Bingham fit, are analyzed with non-linear models, namely modified Bingham fit[6] and Herschel-Bulkley fit[7]. The yield stress factor according to linear Bingham model is compared with parameters of modified Bingham fit in Table A-15 to Table A-19 and with parameters of Herschel-Bulkley fit in Table A-20 to Table A-24. The mixtures with metaphyllosilicates, QP and TG have been analyzed by using the whole torque curve with approximately 9,400 data points. Later on, the mixtures with calcined common clays have been analyzed by using the median torque at the chosen rotational speeds (v = 120, 80, 40 and 20 rpm). The use of these four data points, in turn, resulted in significantly higher R^2 values compared to the initial analysis. In order to compare all mixtures, this section includes the analysis of the above mentioned mixtures by considering also their median torques instead of the whole torque curve.

The following abbreviations / symbols are used in the tables of this section:

Abbreviation	Definition
c	Second order term of the modified Bingham equation
g	Yield stress factor of the linear Bingham fit
K	Consistency factor according to Herschel-Bulkley fit
μ	Linear term of the modified Bingham equation
n	Consistency/flow index according to Herschel-Bulkley fit
τ_0	Yield stress according to modified Bingham or Herschel-Bulkley fit
x	Replacement level [wt%] and type of metaphyllosilicate/calcined common clay (plus dosage [%bwob] and type of superplasticizer if added)

[6] Yahia, A. and K.H. Khayat, *Analytical models for estimating yield stress of high-performance pseudoplastic grout.* Cement and Concrete Research, 2001. **31**(5): p. 731-738.

[7] Hackley, V.A. and C.F. Ferraris, *Guide to Rheological Nomenclature - Measurements in Ceramic Particulate Systems*. 2001, National Institute of Standards and Technology (NIST): Gaithersburg, Maryland, USA. p. III, 29.

Table A-15. Comparison of linear Bingham and modified Bingham fits for OPC_x mixtures with $R^2 < 0.90$ for linear Bingham model equation (note: the whole flow curve was considered for these mixtures)

Mixture x	Yield stress factor according to linear Bingham fit		Parameters derived from modified Bingham fit			
	g [Nmm]	R^2 [-]	τ_0 [Nmm]	μ [Nmm min]	c [Nmm min²]	R^2 [-]
30TG	21.3	0.85	**25.1**	0.040	$1.03 \cdot 10^{-3}$	0.87
20Mk	**169.3**	0.77	167.5	0.126	$-4.64 \cdot 10^{-4}$	0.79
20Mk_ 0.19amphMPEG	11.8	0.79	**15.5**	- 0.073	$9.73 \cdot 10^{-4}$	0.85
20Mk_ 0.20amphMPEG	11.7	0.79	**15.3**	- 0.068	$7.54 \cdot 10^{-4}$	0.86
30Mk	**321.0**	0.77	**321.4**	- 0.206	$9.83 \cdot 10^{-5}$	0.77
5Mu	27.1	0.80	**31.1**	0.076	$1.05 \cdot 10^{-3}$	0.81
10Mu	95.0	0.39	**104.1**	- 0.051	$2.38 \cdot 10^{-3}$	0.40
10Mi	32.8	0.77	**36.9**	- 0.287	$1.65 \cdot 10^{-3}$	0.87
20Mi	102.7	0.35	**118.4**	- 0.446	$4.14 \cdot 10^{-3}$	0.44
20Mi_0.20HPEG	21.8	0.77	**27.2**	- 0.009	$1.43 \cdot 10^{-3}$	0.78
20Mi_0.20amphMPEG	42.2	0.78	**48.5**	- 0.025	$1.65 \cdot 10^{-3}$	0.80
30Mi	183.4	0.50	**204.5**	- 0.453	$5.57 \cdot 10^{-3}$	0.54

Table A-16. Comparison of linear Bingham and modified Bingham fits for OPC_x mixtures (considers the median torques at 120, 80, 40 and 20 rpm)

Mixture x	Yield stress factor according to linear Bingham fit		Parameters derived from modified Bingham fit			
	g [Nmm]	R^2 [-]	τ_0 [Nmm]	μ [Nmm min]	c [Nmm min²]	R^2 [-]
30TG	21.6	0.97	**25.1**	0.043	$1.00 \cdot 10^{-3}$	1.00
20Mk	**162.2**	0.59	153.9	0.429	$-2.42 \cdot 10^{-3}$	0.92
20Mk_ 0.19amphMPEG	12.1	0.85	**15.5**	- 0.073	$9.73 \cdot 10^{-4}$	1.00
20Mk_ 0.20amphMPEG	12.0	0.88	**15.3**	- 0.068	$7.54 \cdot 10^{-4}$	1.00
30Mk	**321.0**	1.00	**321.4**	- 0.206	$1.00 \cdot 10^{-4}$	1.00
5Mu	27.5	0.98	**31.0**	0.082	$1.00 \cdot 10^{-3}$	0.99
10Mu	96.2	0.88	**103.5**	- 0.023	$2.10 \cdot 10^{-3}$	0.92
10Mi	33.2	0.97	**32.3**	0.033	$1.20 \cdot 10^{-3}$	0.99
20Mi	104.1	0.59	**118.5**	- 0.449	$4.17 \cdot 10^{-3}$	0.99
20Mi_0.20HPEG	22.3	0.96	**27.1**	- 0.007	$1.41 \cdot 10^{-3}$	1.00
20Mi_0.20amphMPEG	42.8	0.95	**48.4**	- 0.022	$1.63 \cdot 10^{-3}$	1.00
30Mi	185.6	0.80	**204.3**	- 0.436	$5.40 \cdot 10^{-3}$	0.97

Table A-17. Comparison of linear Bingham and modified Bingham fits for PLC mixtures with $R^2 < 0.90$ for linear Bingham model equation (note: the whole flow curve was considered for these mixtures)

Mixture x	Yield stress factor according to linear Bingham fit		Parameters derived from modified Bingham fit			
	g [Nmm]	R^2 [-]	τ_0 [Nmm]	μ [Nmm min]	c [Nmm min²]	R^2 [-]
0.24NSF	**5.6**	0.85	5.4	0.044	$-6.94 \cdot 10^{-5}$	0.85
20Mk	**77.5**	0.85	77.1	0.255	$-4.64 \cdot 10^{-4}$	0.85
20Mk_0.20amphMPEG	17.2	0.79	**20.9**	- 0.087	$9.66 \cdot 10^{-4}$	0.89
20Mk_0.21amphMPEG	17.2	0.79	**20.8**	-0.080	$8.97 \cdot 10^{-4}$	0.88
30Mk	**397.2**	0.66	392.6	- 0.141	$-1.22 \cdot 10^{-3}$	0.66
5Mu	41.7	0.80	**44.4**	0.150	$7.09 \cdot 10^{-4}$	0.80
10Mu	**107.7**	0.77	104.6	0.552	$-8.36 \cdot 10^{-4}$	0.77
20Mu_ 0.18amphMPEG	45.7	0.76	**63.0**	1.35	$4.56 \cdot 10^{-3}$	0.76
10Mi	40.2	0.84	**43.1**	0.043	$7.59 \cdot 10^{-4}$	0.85
20Mi	86.3	0.67	**93.3**	- 0.072	$1.83 \cdot 10^{-3}$	0.69
20Mi_0.20HPEG	41.4	0.66	**47.7**	- 0.008	$1.53 \cdot 10^{-3}$	0.67
20Mi_0.20amphMPEG	61.2	0.68	**69.8**	- 0.056	$2.27 \cdot 10^{-3}$	0.70
30Mi	198.0	0.63	**216.6**	- 0.289	$4.40 \cdot 10^{-3}$	0.67

Table A-18. Comparison of linear Bingham and modified Bingham fits for PLC mixtures (considers the median torques at 120, 80, 40 and 20 rpm)

Mixture x	Yield stress factor according to linear Bingham fit		Parameters derived from modified Bingham fit			
	g [Nmm]	R^2 [-]	τ_0 [Nmm]	μ [Nmm min]	c [Nmm min²]	R^2 [-]
0.24NSF	**5.6**	0.99	5.4	0.043	$-6.06 \cdot 10^{-5}$	0.99
20Mk	**77.5**	1.00	76.8	0.265	$-1.89 \cdot 10^{-4}$	1.00
20Mk_0.20amphMPEG	17.9	0.83	**20.5**	- 0.065	$7.47 \cdot 10^{-4}$	0.99
20Mk_0.21amphMPEG	17.8	0.85	**20.4**	- 0.058	$6.89 \cdot 10^{-4}$	0.99
30Mk	**396.8**	0.96	393.0	- 0.158	$-1.10 \cdot 10^{-3}$	0.96
5Mu	42.0	0.99	**44.4**	0.153	$7.00 \cdot 10^{-4}$	0.99
10Mu	**107.6**	0.98	104.4	0.560	$-9.00 \cdot 10^{-4}$	0.99
20Mu_ 0.18amphMPEG	47.6	0.99	**61.3**	1.422	$4.00 \cdot 10^{-3}$	0.99
10Mi	40.5	0.98	**43.0**	0.047	$7.00 \cdot 10^{-4}$	1.00
20Mi	87.0	0.93	**93.2**	- 0.070	$1.81 \cdot 10^{-3}$	1.00
20Mi_0.20HPEG	42.3	0.96				
20Mi_0.20amphMPEG	62.0	0.94	**69.7**	- 0.052	$2.23 \cdot 10^{-3}$	1.00
30Mi	199.7	0.86	**214.3**	- 0.273	$4.30 \cdot 10^{-3}$	0.97

Table A-19. Comparison of linear Bingham and modified Bingham fits for PLC* mixtures with $R^2 < 0.95$ for Bingham model equation (considers the median torques at 120, 80, 40 and 20 rpm)

Mixture x	Yield stress factor according to linear Bingham fit		Parameters derived from modified Bingham fit			
	g [Nmm]	R^2 [-]	τ_0 [Nmm]	μ [Nmm min]	c [Nmm min²]	R^2 [-]
0.05IPEG1	22.0	0.58	**34.1**	- 0.350	$3.2 \cdot 10^{-3}$	1.00
30KUP	49.4	0.93	**56.2**	0.003	$1.5 \cdot 10^{-3}$	1.00
30RKUP_0.05HPEG	19.8	0.94	**24.9**	- 0.030	$1.3 \cdot 10^{-3}$	0.99
30RKUP_0.05IPEG1	35.6	0.94	**41.7**	- 0.035	$1.6 \cdot 10^{-3}$	0.99
30RKUP_0.05IPEG2	21.7	0.94	**27.3**	- 0.045	$1.5 \cdot 10^{-3}$	0.99
30FUP	71.4	0.94	**76.2**	- 0.038	$1.2 \cdot 10^{-3}$	0.99
30FUP_0.05HPEG	33.6	0.94	**37.8**	- 0.037	$1.1 \cdot 10^{-3}$	1.00
30FUP_0.05IPEG1	39.1	0.91	**43.4**	- 0.056	$1.1 \cdot 10^{-3}$	1.00
30FUP_0.05IPEG2	27.8	0.92	**31.8**	- 0.053	$1.1 \cdot 10^{-3}$	1.00
30FUP_0.10IPEG1	25.0	0.85	**28.9**	- 0.094	$1.3 \cdot 10^{-3}$	1.00
30FUP_0.10IPEG2	13.9	0.90	**18.5**	- 0.069	$1.2 \cdot 10^{-3}$	0.99

Table A-20. Comparison of linear Bingham and Herschel-Bulkley fits for OPC_x mixtures with $R^2 < 0.90$ for linear Bingham model equation (note: the whole flow curve was considered for these mixtures)

Mixture x	Yield stress factor according to linear Bingham fit		Parameters according to Herschel-Bulkley equation			
	g [Nmm]	R^2 [-]	τ_0 [Nmm]	K	n	R^2 [-]
30TG	21.3	0.85	**25.7**	0.003	1.79	0.87
20Mk	**169.3**	0.77	137.4	24.14	0.10	0.79
20Mk_0.19amphMPEG	11.8	0.79	**14.3**	5.80E-7	3.39	0.85
20Mk_0.20amphMPEG	11.7	0.79	**14.1**	7.58E-7	3.21	0.83
30Mk	**321.0**	0.77	Not applicable			
5Mu	27.1	0.80	**32.0**	0.008	1.65	0.80
10Mu	95.0	0.39	**104.8**	3.37E-5	2.84	0.41
10Mi	32.8	0.77	**37.8**	0.003	1.87	0.81
20Mi	102.7	0.35	**108.3**	1.01E-8	4.42	0.43
20Mi_0.20HPEG	21.8	0.77	**27.2**	8.23E-4	2.10	0.78
20Mi_0.20amphMPEG	42.2	0.78	**48.3**	5.73	2.19	0.80
30Mi	183.4	0.50	**196.3**	3.72E-7	3.83	0.55

Table A-21. Comparison of linear Bingham and Herschel-Bulkley fits for OPC_x mixtures (considers the median torques at 120, 80, 40 and 20 rpm)

Mixture x	Yield stress factor according to linear Bingham fit		Parameters according to Herschel-Bulkley equation			
	g [Nmm]	R^2 [-]	τ_0 [Nmm]	K	n	R^2 [-]
30TG	21.6	0.97	**25.6**	0.004	1.77	0.99
20Mk	**162.2**	0.59	Not applicable[8]			
20Mk_0.19amphMPEG	12.1	0.85	**14.3**	6.05E-7	3.38	0.99
20Mk_0.20amphMPEG	12.0	0.88	**14.0**	5.58E-7	3.29	1.00
30Mk	**321.0**	1.00	Not applicable			
5Mu	27.5	0.98	**31.9**	0.01	1.63	0.99
10Mu	96.2	0.88	**104.6**	6.49E-5	2.71	0.93
10Mi	33.2	0.97	**37.8**	0.003	1.87	0.99
20Mi	104.1	0.59	**108.8**	5.22E-12	6.00	0.92
20Mi_0.20HPEG	22.3	0.96	**27.2**	8.77E-4	2.09	1.00
20Mi_0.20amphMPEG	42.8	0.95	**48.2**	6.18E-4	2.18	1.00
30Mi	185.6	0.80	**197.3**	9.78E-10	5.06	0.99

Table A-22. Comparison of linear Bingham and Herschel-Bulkley fits for PLC mixtures with R^2 < 0.90 for linear Bingham model equation (note: the whole flow curve was considered for these mixtures)

Mixture x	Yield stress factor according to linear Bingham fit		Parameters according to Herschel-Bulkley equation			
	g [Nmm]	R^2 [-]	τ_0 [Nmm]	K	n	R^2 [-]
0.24NSF	**5.6**	0.85	5.2	0.09	0.81	0.85
20Mk	**77.5**	0.85	76.2	0.38	0.91	0.85
20Mk_0.20amphMPEG	17.2	0.79	**19.2**	1.58E-8	4.21	0.90
20Mk_0.21amphMPEG	17.2	0.79	**19.2**	1.47E-8	4.11	0.88
30Mk	**397.2**	0.66	Not applicable			
5Mu	41.7	0.80	**45.8**	0.04	1.36	0.80
10Mu	**107.7**	0.77	95.7	2.56	0.67	0.77
20Mu_0.18amphMPEG	45.7	0.76	**69.1**	0.50	1.27	0.76
10Mi	40.2	0.84	**43.6**	0.004	1.71	0.85
20Mi	86.3	0.67	**92.3**	1.09E-4	2.52	0.69
20Mi_0.20HPEG	41.4	0.66	**47.8**	8.92E-4	2.10	0.67
20Mi_0.20amphMPEG	61.2	0.68	**69.3**	3.60E-4	2.34	0.70
30Mi	198.0	0.63	**210.6**	8.63E-7	3.64	0.68

[8] Yield stress output is 0 Nmm, whereas K is in the range of yield stress value as derived from linear Bingham fit

Table A-23. Comparison of linear Bingham and Herschel-Bulkley fits for PLC mixtures (considers the median torques at 120, 80, 40 and 20 rpm)

Mixture x	Yield stress factor according to linear Bingham fit		Parameters according to Herschel-Bulkley equation			
	g [Nmm]	R^2 [-]	τ_0 [Nmm]	K	n	R^2 [-]
0.24NSF	**5.6**	0.99	5.3	0.07	0.85	0.99
20Mk	**77.5**	1.00	75.6	0.46	0.87	1.00
20Mk_0.20amphMPEG	17.9	0.83	**19.2**	6.86E-8	3.74	0.97
20Mk_0.21amphMPEG	17.8	0.85	**19.1**	7.04E-8	3.58	0.98
30Mk	**396.8**	0.96	Not applicable			
5Mu	42.0	0.99	**45.2**	0.05	1.33	0.99
10Mu	**107.6**	0.98	93.2	3.36	0.62	0.99
20Mu_0.18amphMPEG	47.6	0.99	**66.3**	0.64	1.22	0.99
10Mi	40.5	0.98	**43.5**	0.005	1.69	0.99
20Mi	87.0	0.93	**92.3**	1.18E-4	2.50	1.00
20Mi_0.20HPEG	42.3	0.96	**47.5**	0.001	2.04	1.00
20Mi_0.20amphMPEG	62.0	0.94	**69.2**	3.95E-4	2.32	1.00
30Mi	199.7	0.86	**210.6**	6.55E-7	3.70	0.99

Table A-24. Comparison of linear Bingham and Herschel-Bulkley fits for PLC* mixtures with $R^2 < 0.95$ for Bingham model equation (considers the median torques at 120, 80, 40 and 20 rpm)

Mixture x	Yield stress factor according to linear Bingham fit		Parameters according to Herschel-Bulkley equation			
	g [Nmm]	R^2 [-]	τ_0 [Nmm]	K	n	R^2 [-]
0.05IPEG1	22.0	0.58	**26.5**	1.01E-12	6.76	0.94
30KUP	49.4	0.93	**56.4**	0.001	2.05	1.00
30RKUP_0.05HPEG	19.8	0.94	**24.6**	2.30E-4	2.33	1.00
30RKUP_0.05IPEG1	35.6	0.94	**41.5**	2.39E-4	2.36	0.99
30RKUP_0.05IPEG2	21.7	0.94	**26.9**	1.39E-4	2.44	1.00
30FUP	71.4	0.94	**75.7**	1.11E-4	2.45	1.00
30FUP_0.05HPEG	33.6	0.94	**37.4**	8.61E-5	2.47	1.00
30FUP_0.05IPEG1	39.1	0.91	**42.7**	1.55E-5	2.80	1.00
30FUP_0.05IPEG2	27.8	0.92	**31.0**	2.89E-5	2.66	1.00
30FUP_0.10IPEG1	25.0	0.85	**28.3**	2.51	3.62	1.00
30FUP_0.10IPEG2	13.9	0.90	**17.3**	2.99E-5	2.66	0.99

9.6 Appendix A6: Estimation of rheological and physical parameters

Linear equations are derived for the viscosity factor, yield stress factor and flow resistance from measurements on reference mixtures with varying replacement levels (0 – 30 wt%) in order to estimate these parameters regardless of the replacement level used (Table A-25).

Table A-25. Linear equations of reference mixtures for the relationship between replacement level (x) and viscosity factor, yield stress factor and flow resistance, based on the measured values with 0, (5), 10, 20 and 30 wt% replacement level

Mixture	Equation for viscosity factor [Nmm·min]	Equation for yield stress factor [Nmm]	**Equation for flow resistance [Nmm/min]**
OPC_QP	y = - 0.0017x + 0.11 (R^2 = 0.98)	y = 6.228x – 0.14 (R^2 = 0.98)	**y = - 19.68x + 1208 (R^2 = 0.99)**
OPC_Mk	y = 0.0025x + 0.06 (R^2 = 0.25)	y = 10.6240x – 22.51 (R^2 = 0.95)	**y = 1006.30x - 1406 (R^2 = 0.96)**
OPC_Mu	y = 0.0165x + 0.13 (R^2 = 0.99)	y = 11.6965x – 12.47 (R^2 = 0.97)	**y = 1275.78x - 461 (R^2 = 0.98)**
OPC_Mi	y = 0.0077x + 0.10 (R^2 = 0.74)	y = 6.0093x – 8.81 (R^2 = 0.96)	**y = 647.86x - 307 (R^2 = 0.96)**
OPC_TG	y = 0.0028x + 0.09 (R^2 = 0.80)	y = 0.5419x + 5.23 (R^2 = 0.93)	y = 78.97x + 1014 (R^2 = 0.96)
PLC_Mk	y = 0.0085x + 0.05 (R^2 = 0.78)	y = 11.7342x – 38.14 (R^2 = 0.74)	**y = 1100.59x - 2577 (R^2 = 0.78)**
PLC_Mu	y = 0.0336x + 0.10 (R^2 = 1.00)	y = 11.8533x – 4.02 (R^2 = 0.98)	**y = 1436.02x + 183 (R^2 = 0.99)**
PLC_Mi	y = 0.0085x + 0.08 (R^2 = 0.90)	y = 6.1167x – 8.26 (R^2 = 0.91)	**y = 661.41x - 256 (R^2 = 0.91)**
PLC_TG	y = 0.0022x + 0.097 (R^2 = 0.93)	y = 10.3048x - 15.07 (R^2 = 0.94)	y = 57.88x + 1612.3 (R^2 = 0.97)

In order to compare the estimated flow resistance with the actually measured flow resistance of CCBC pastes with calcined common clays, the mineralogical composition of these common clays is simplified by considering the main phases quartz, kaolinite, muscovite and illite (Table A-26). The common clay MURR is omitted here, as it contains significant amounts of smectite, which is not investigated as pure phase within this thesis.

Table A-26. Simplified mineralogical composition of raw common clays and normalized amount of the (meta)phase present in CCBC at 30 wt% replacement level

Common clay	Normalized to 100 wt% in raw material [wt%]				Normalized amount present in blended cement at 30 wt% replacement level [wt%]			
	Quartz	Kaolinite	Muscovite	Illite	Quartz	Meta-kaolinite	Meta-muscovite	Meta-illite
TG[9]	30	25	22.5	22.5	9	7.5	6.7	6.7
AC	25	28.7	6.3	40	7.5	8.6	1.9	12
KUP	34.7	27.4	37.9	-	10.4	8.2	11.4	-
RKUP	50	46.9	3.1	-	15	14.1	0.9	-
FUP	12.4	76.3	3.1	8.2	3.7	22.9	0.9	2.5

[9] based on Figure 13 in first journal paper (chapter 7.1)

Two approaches are proposed, how to estimate the flow resistance of pastes with calcined common clays from mixtures with pure phases (quartz powder and metaphyllosilicates). The first approach (I) requires the normalized amount of pure phases as present in raw clay, which is multiplied with the flow resistance of CCBC with this pure (meta)phase at a respective replacement level (taken from from Table A-3 and Table A-7). The second approach (II) uses the linear fits from Table A-25, depending on the cement (OPC/PLC) used, and considers the replacement level in the equation. The estimated flow resistance values are provided in Table A-27 and are compared with the measured flow resistance values in Figure A-10.

I. The flow resistance values, as measured with x wt% replacement level[10], are multiplied by the normalized wt% of the respective phase as present in raw clay:

$$FR_{estimated,1}\left[\frac{Nmm}{min}\right] = \frac{m_{Qz}FR_{C\_xQP} + m_K FR_{C\_xMk} + m_M FR_{C\_xMu} + m_I FR_{C\_xMi}}{100\ wt\%}$$

with

$m_{Qz/K/M/I}$ normalized amount of quartz (Qz), kaolinite (K), muscovite (M) and illite (I) as present in raw clay [wt%]

$FR_{C\_xQP/Mk/Mu/Mi}$ flow resistance measured for the respective CCBC [Nmm/min] with

C = type of cement (OPC/PLC)

x = replacement level [wt%]

II. The normalized wt% of the mineral phase, as present in raw clay, is inserted into the respective linear equation and the replacement level is considered.

For the OPC mixtures, the simplified equation is provided:

$$FR_{OPC.estimated,2}\left[\frac{Nmm}{min}\right] = \left(-19.68m_{Qz} + 1006.3m_K + 1275.78m_M + 647.86m_I\right) * \frac{x}{100\ wt\ \%} - 966$$

[10] OPC_30QP values are used due to the absent flow resistance of PLC_30QP and PLC_30Mu values are extrapolated from PLC_5Mu and PLC_10Mu

For the PLC mixtures, the simplified equation is provided:

$$FR_{PLC,estimated,2}\left[\frac{Nmm}{min}\right] = \left(-19.68m_{Qz} + 1100.59m_K + 1436.02m_M + 661.41m_I\right) * \frac{x}{100\ wt\ \%} - 1442$$

with

$m_{Qz/K/M/I}$ amount of quartz (Qz), kaolinite (K), muscovite (M) and illite (I) present in raw clay [wt%]

x replacement level [wt%]

Table A-27. Estimated flow resistance for CCBC pastes (w/b = 0.50)

Mixture	Estimated flow resistance according to approach I [Nmm/min]	Estimated flow resistance according to approach II [Nmm/min]
OPC_10TG	5307	5819
OPC_20TG	12930	12604
OPC_30TG	21567	19389
PLC_10TG	6340	5970
PLC_20TG	11504	13381
PLC_30TG	24748	20793
PLC_30AC	22609	18537
PLC_30KUP	27710	23728
PLC_30RKUP	19314	15084
PLC_30FUP	31939	26640

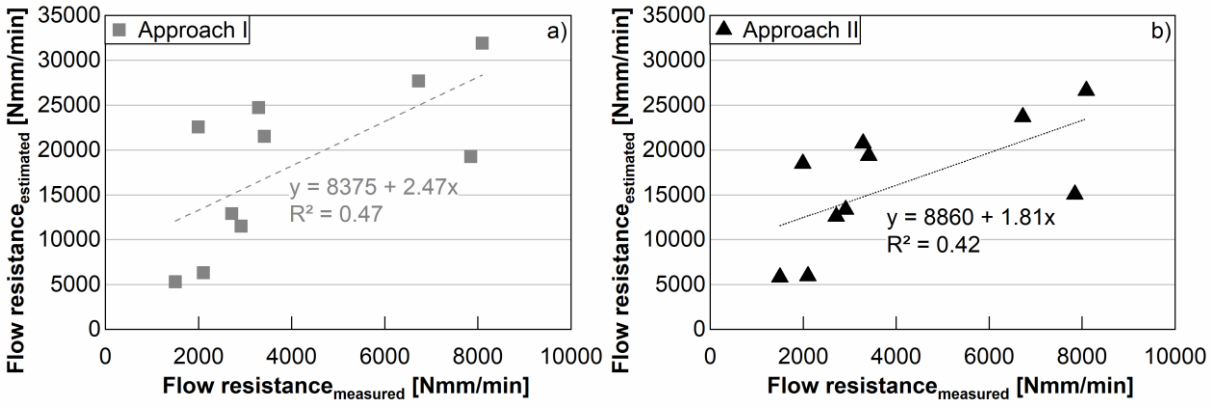

Figure A-10. Comparison of measured and estimated flow resistance values of CCBC pastes with calcined common clays and varying replacement levels according to a) approach I and b) approach II

The specific surface area as the water demand of calcined common clays are both estimated based on their mineralogical composition. The normalized amount of the pure phases, as present in raw clay, is taken from Table A-26 and multiplied with the determined values of the

pure phases. The specific surface area is determined with the BET method, and the water demand is determined according to the Puntke method. These values, such as the measured values of the calcined common clays, are provided in the first and third journal paper. For comparison, Table A-28 compares the estimated and measured specific surface area and water demand of calcined common clays.

Table A-28. Estimated and measured specific surface area and water demand for calcined common clays

Calcined common clay	Specific surface area [m²/g]		Water demand [wt%]	
	Estimated	as determined with BET method	Estimated	as determined according to Puntke method
TG	28.5	3.9	53.1	42.1
AC	43.8	17.2	53.2	28.3
KUP	9.4	6.6	52.4	40.4
RKUP	8.9	7.9	38.6	35.1
FUP	21.7	42.4	53.8	43.6

9.7 Appendix A7: Time-dependent rheological measurements

The torque development over a period of 120 minutes at constant rotational speed is shown for mixtures with varying replacement levels (Figure A-11). Furthermore, the time-dependent torque curves of mixtures with NSF (Figure A-12), HPEG (Figure A-13) and amphMPEG (Figure A-14) have been enlarged for a better identification of the curves at torques < 20 Nmm (50 Nmm). Beside these measurements, the rheological analysis (linear Bingham fit, median torque and flow resistance) is provided for the PLC* mixtures with calcined common clays that have been measured at 5, 30, 50 and 105 minutes after water addition. Mixtures with w/b = 0.40 are found in Table A-29 and Table A-30, those with w/b = 0.50 in Table A-31 to Table A-36.

The following abbreviations are used in the tables of this section:

Abbreviation	Definition
FR	Flow resistance [Nmm/min]
g	Yield stress factor [Nmm]
h	Viscosity factor [Nmm·min]
T	Torque [Nmm]
x	Replacement level [wt%] + metaphyllosilicate/calcined common clay
y	Dosage [%bwob] and type of superplasticizer

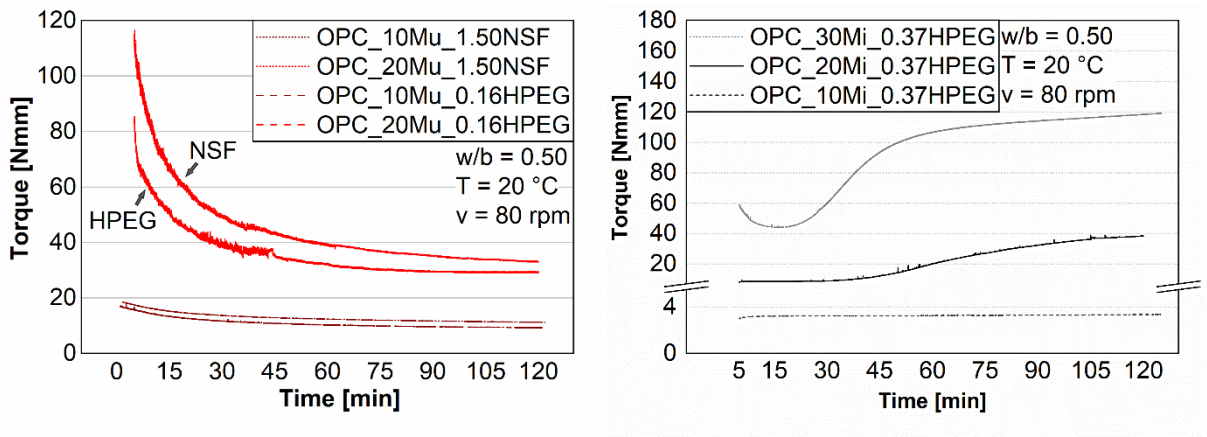

Figure A-11. Time-related torque of CCBC with varying replacement levels (left: OPC mixtures with 10 and 20 wt% Mu and 1.50 %bwob NSF or 0.16 %bwob HPEG, right: OPC mixtures with 10, 20 and 30 wt% Mi and 0.37 %bwob HPEG)

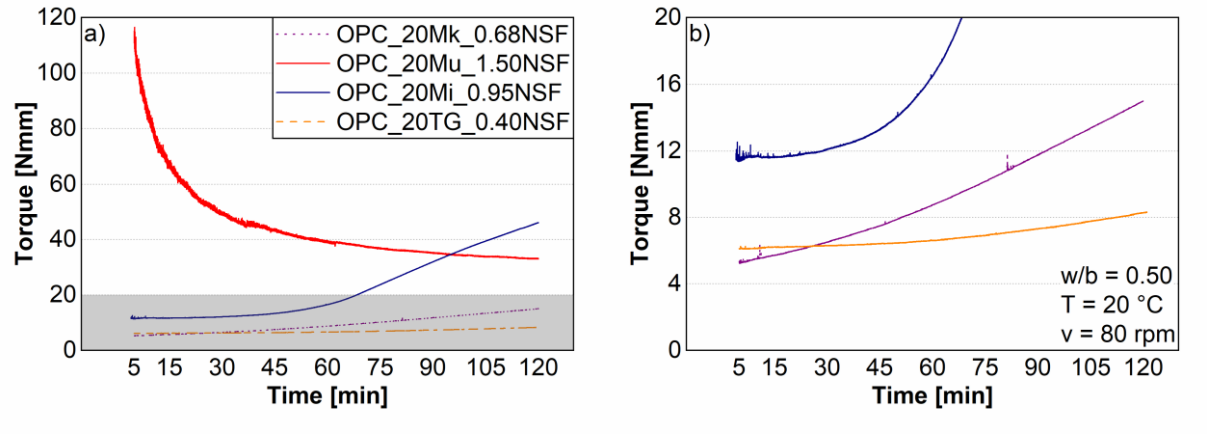

Figure A-12. Time-related torque of CCBCs (a) including thixotropic OPC_20Mu mixture and (b) enlarged for torque range of 0 – 20 Nmm with NSF superplasticizer

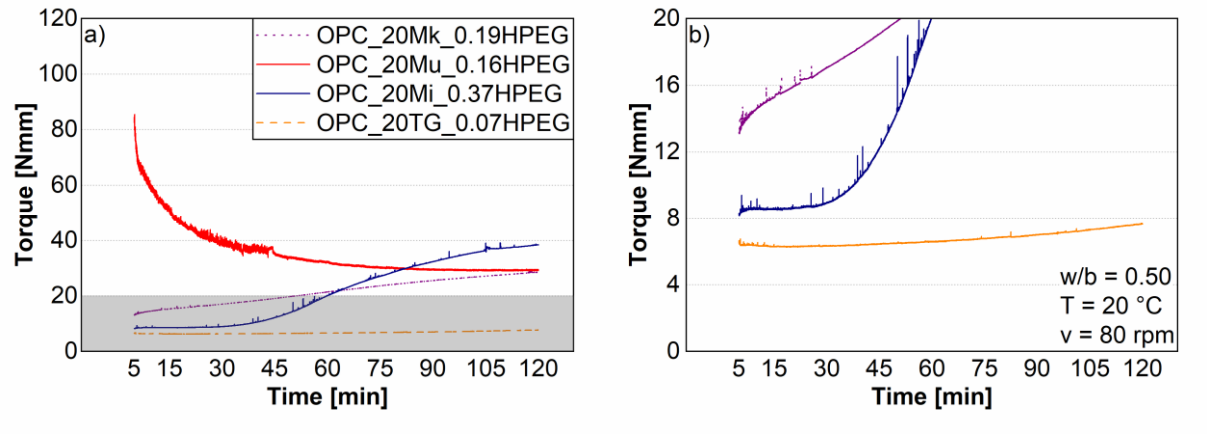

Figure A-13. Time-related torque of CCBCs (a) including thixotropic OPC_20Mu mixture and (b) enlarged for torque range of 0 – 20 Nmm with HPEG superplasticizer

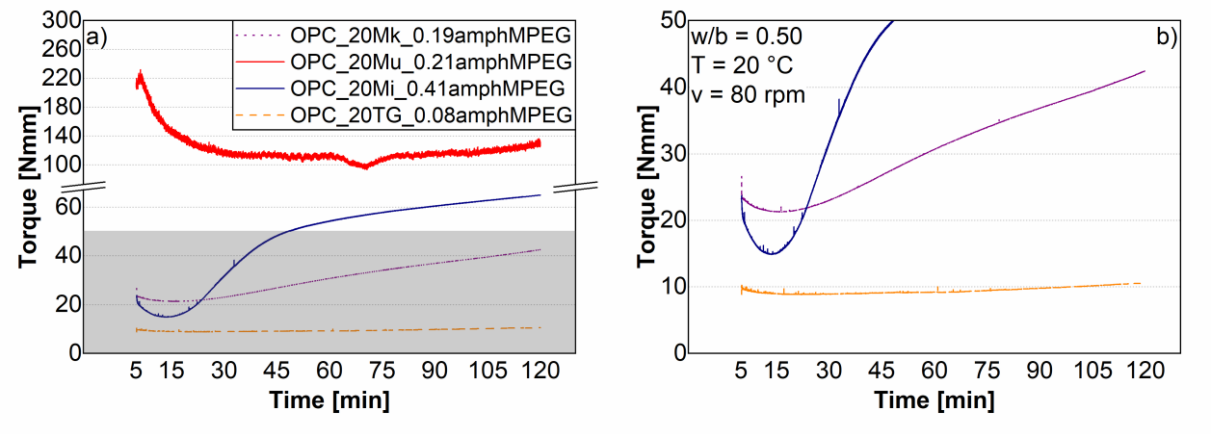

Figure A-14. Time-related torque of CCBCs (a) including thixotropic OPC_20Mu mixture and (b) enlarged for torque range of 0 – 50 Nmm with amphMPEG superplasticizer

Table A-29. Rheological parameters of PLC*_y mixtures (w/b = 0.40)

Mixture	h [Nmm·min]	g [Nmm]	R^2 [-]	Median T [Nmm] at … [rpm] 20	40	80	120	FR [Nmm/min]
ref								
5 min	0.26	42.0	0.80	47.9	52.7	60.0	73.2	5921
30 min	0.21	45.8	0.94	49.9	54.7	61.7	71.0	6027
50 min	0.18	48.4	0.99	51.5	56.2	62.7	69.8	6105
105 min	0.19	48.4	0.97	51.9	56.8	63.3	71.4	6183
0.05HPEG								
5 min	0.23	16.4	0.72	22.7	25.6	31.5	44.9	3153
30 min	0.19	18.2	0.94	22.7	25.7	31.4	40.9	3071
50 min	0.16	18.9	0.99	22.6	25.5	31.1	38.8	3011
105 min	0.19	22.8	0.94	27.1	30.4	36.2	45.4	3539
0.05IPEG1								
5 min	0.32	27.9	0.73	35.9	41.0	49.2	66.9	4895
30 min	0.23	23.4	0.93	28.8	32.7	39.8	51.4	3889
50 min	0.19	21.6	0.98	25.7	29.3	35.6	44.5	3452
105 min	0.16	17.6	0.98	21.2	24.2	29.7	37.3	2875
0.05IPEG2								
5 min	0.26	16.0	0.74	23.0	26.4	33.3	48.3	3321
30 min	0.20	18.2	0.96	22.9	26.3	32.9	42.8	3190
50 min	0.18	18.7	0.99	22.7	25.9	32.1	40.5	3101
105 min	0.31	19.2	0.61	27.8	31.7	38.4	57.4	3912

Table A-30. Rheological parameters of PLC*_30KUP_y mixtures (w/b = 0.40)

Mixture	h [Nmm/min]	g [Nmm]	R^2 [-]	Median T [Nmm] at … [rpm]				FR [Nmm/min]
				20	40	80	120	
ref								
5 min	0.68	197.0	0.38	217.2	222.1	240.6	280.8	24076
30 min	0.42	200.2	0.25	196.4	223.6	252.9	249.0	23769
50 min	0.05	231.3	0.00	233.6	226.8	245.9	236.5	23708
105 min	0.43	251.1	0.09	264.9	267.3	275.5	304.5	27778
0.05HPEG								
5 min	0.78	165.3	0.66	184.7	199.0	214.3	261.0	21607
30 min	0.45	178.1	0.86	187.2	197.3	211.1	232.3	20881
50 min	0.33	188.3	0.93	195.9	200.3	214.2	227.7	21090
105 min	0.46	197.2	0.78	203.9	219.2	233.0	252.3	22983
0.05IPEG1								
5 min	0.80	139.5	0.73	153.3	173.0	206.0	235.0	19665
30 min	0.39	161.6	0.44	158.6	182.6	208.4	206.1	19524
50 min	0.18	177.5	0.10	166.4	194.7	208.2	196.9	19769
105 min	0.71	201.2	0.76	212.3	232.4	260.4	286.0	25229
0.05IPEG2								
5 min	0.67	184.3	0.48	185.2	220.8	247.1	263.2	23624
30 min	0.35	194.2	0.32	191.7	215.2	232.2	234.9	22359
50 min	0.39	188.5	0.29	184.8	206.1	232.8	233.9	22023
105 min	0.38	179.9	0.26	182.9	196.0	220.4	224.1	21008

Table A-31. Rheological parameters of PLC*_y mixtures (w/b = 0.50)

Mixture	h [Nmm·min]	g [Nmm]	R^2 [-]	Median T [Nmm] at … [rpm]				FR [Nmm/min]
				20	40	80	120	
ref								
5 min	0.12	11.6	0.95	14.6	16.4	20.2	26.5	1975
30 min	0.11	11.3	0.99	13.7	15.6	19.2	24.3	1859
50 min	0.10	11.8	1.00	14.0	15.9	19.4	23.9	1869
105 min	0.15	14.1	0.81	18.2	20.2	24.2	32.9	2415
0.05HPEG								
5 min	0.10	3.9	0.92	6.6	7.8	11.0	16.3	1069
30 min	0.10	4.0	0.98	6.4	7.8	11.0	15.7	1052
50 min	0.09	4.0	0.99	6.2	7.6	10.9	15.1	1031
105 min	0.10	5.1	0.97	7.4	8.9	12.2	17.1	1174
0.05IPEG1								
5 min	0.13	22.0	0.24	28.4	25.2	26.7	38.3	2875
30 min	0.12	8.5	0.71	13.1	12.3	15.2	23.5	1578
50 min	0.09	6.4	0.94	9.3	9.4	12.5	17.8	1231
105 min	0.09	3.2	0.98	5.4	6.7	9.8	14.1	930
0.10IPEG1								
5 min	0.09	1.6	0.97	3.7	4.9	7.9	12.0	738
30 min	0.08	0.6	0.98	2.6	3.6	6.4	10.4	597
50 min	0.07	0.3	0.99	2.1	3.1	5.7	9.2	524
105 min	0.07	0.0	0.98	2.0	2.9	5.6	9.3	518
0.20IPEG1								
5 min	0.08	- 0.4	0.99	1.5	2.4	5.1	8.8	469
30 min	0.08	- 0.9	0.98	1.0	2.0	4.6	8.4	422
50 min	0.07	- 0.9	0.99	0.8	1.8	4.3	7.7	387
105 min	0.07	- 1.1	0.99	0.7	1.7	4.3	7.8	386
0.05IPEG2								
5 min	0.08	2.8	0.96	4.8	5.8	8.6	12.5	815
30 min	0.08	2.9	0.99	4.8	5.8	8.7	12.4	817
50 min	0.08	3.0	0.99	4.8	5.9	8.7	12.2	813
105 min	0.09	3.9	0.99	6.0	7.3	10.4	14.5	984
0.10IPEG2								
5 min	0.07	- 0.1	0.99	1.6	2.4	4.8	8.1	443
30 min	0.07	- 0.1	0.98	1.6	2.4	4.8	8.1	445
50 min	0.06	0.0	0.99	1.6	2.5	4.8	7.9	441
105 min	0.07	0.2	0.97	2.1	3.0	5.5	9.3	517
0.20IPEG2								
5 min	0.04	- 0.5	0.99	0.5	1.2	2.8	4.9	251
30 min	0.05	- 0.6	0.97	0.6	1.2	2.9	5.1	259
50 min	0.05	- 0.6	0.99	0.6	1.2	2.9	5.1	261
105 min	0.05	- 0.7	0.98	0.6	1.3	3.1	5.6	279

Table A-32. Rheological parameters of PLC*_30MURR_y mixtures (w/b = 0.50)

Mixture	h [Nmm·min]	g [Nmm]	R^2 [-]	Median T [Nmm] at … [rpm]				FR [Nmm/min]
				20	40	80	120	
ref								
5 min	0.12	14.1	0.94	17.2	19.1	22.7	29.3	2240
30 min	0.12	14.8	0.97	17.5	19.4	23.1	28.9	2260
50 min	0.11	15.3	0.99	17.8	19.7	23.2	28.5	2264
105 min	0.12	18.3	0.97	21.2	23.2	26.9	33.0	2642
0.05HPEG								
5 min	0.11	3.7	0.95	6.4	7.7	11.2	16.5	1076
30 min	0.10	4.1	0.99	6.5	7.8	11.3	16.0	1070
50 min	0.09	4.4	0.99	6.6	7.9	11.3	15.7	1071
105 min	0.10	5.7	0.98	8.1	9.7	13.3	18.1	1267
0.05IPEG1								
5 min	0.11	4.6	0.86	7.3	8.6	12.3	17.6	1174
30 min	0.10	4.5	0.97	6.8	8.3	12.0	16.5	1125
50 min	0.09	4.8	0.99	7.0	8.4	11.8	16.2	1122
105 min	0.10	6.3	0.99	8.8	10.4	14.1	18.9	1341
0.10IPEG1								
5 min	0.11	1.4	0.98	4.1	5.4	9.2	14.4	859
30 min	0.10	1.0	0.98	3.4	4.7	8.2	12.9	760
50 min	0.09	1.0	0.99	3.3	4.5	7.8	12.2	723
105 min	0.09	1.3	0.99	3.6	4.8	8.1	12.6	756
0.20IPEG1								
5 min	0.08	- 0.6	0.99	1.4	2.4	5.2	9.0	473
30 min	0.08	- 1.0	0.98	1.0	2.0	4.6	8.5	426
50 min	0.07	- 0.9	0.99	0.9	1.8	4.4	7.9	400
105 min	0.07	- 0.9	0.98	0.8	1.7	4.1	7.4	373
0.05IPEG2								
5 min	0.15	4.3	0.91	8.0	9.9	14.3	22.0	1390
30 min	0.12	5.0	0.99	8.0	9.8	14.1	20.1	1337
50 min	0.12	5.3	0.99	8.0	9.8	13.9	19.4	1317
105 min	0.12	6.6	0.99	9.5	11.4	15.6	21.3	1488
0.10IPEG2								
5 min	0.08	0.4	0.98	2.5	3.6	6.5	10.7	608
30 min	0.08	0.6	0.99	2.6	3.7	6.6	10.5	610
50 min	0.08	0.8	0.99	2.7	3.7	6.6	10.3	607
105 min	0.08	1.0	0.98	3.1	4.2	7.1	11.1	664

Table A-33. Rheological parameters of PLC*_30AC_y mixtures (w/b = 0.50)

Mixture	h [Nmm·min]	g [Nmm]	R^2 [-]	Median T [Nmm] at … [rpm]				FR [Nmm/min]
				20	40	80	120	
ref								
5 min	0.10	13.2	0.96	15.5	17.1	20.4	25.2	1987
30 min	0.10	14.2	0.97	16.4	18.1	21.2	26.0	2074
50 min	0.09	15.0	0.99	17.1	18.7	21.7	26.2	2124
105 min	0.11	18.0	0.95	20.6	22.5	25.8	31.5	2543
0.05HPEG								
5 min	0.09	4.3	0.96	6.6	7.9	11.1	15.7	1062
30 min	0.09	4.9	0.99	7.0	8.3	11.4	15.6	1088
50 min	0.08	5.5	0.99	7.4	8.7	11.8	15.7	1123
105 min	0.10	7.3	0.95	9.8	11.3	14.6	19.7	1416
0.05IPEG1								
5 min	0.09	4.1	0.96	6.2	7.3	10.4	14.5	990
30 min	0.09	5.3	0.96	7.4	8.7	11.7	15.9	1124
50 min	0.08	5.7	0.96	7.6	9.0	11.9	15.9	1140
105 min	0.09	6.7	0.94	9.0	10.4	13.4	18.2	1302
0.10IPEG1								
5 min	0.08	1.5	0.96	3.4	4.4	7.2	11.0	673
30 min	0.08	1.5	0.97	3.4	4.4	7.1	10.8	666
50 min	0.07	1.9	0.93	3.6	4.6	7.3	10.7	681
105 min	0.09	3.3	0.94	5.5	6.7	9.7	14.2	928
0.20IPEG1								
5 min	0.06	0.0	0.98	1.5	2.2	4.3	7.1	397
30 min	0.06	- 0.2	0.97	1.4	2.1	4.3	7.3	395
50 min	0.06	- 0.2	0.93	1.3	2.0	4.2	7.0	381
105 min	0.06	- 0.2	0.95	1.4	2.2	4.4	7.6	409
0.05IPEG2								
5 min	0.08	2.8	0.96	4.8	5.9	8.7	12.6	826
30 min	0.08	3.1	0.99	5.0	6.1	8.9	12.6	842
50 min	0.08	3.4	0.99	5.2	6.3	9.1	12.6	859
105 min	0.09	5.0	0.97	7.3	8.6	11.7	16.1	1121
0.10IPEG2								
5 min	0.06	1.0	0.95	2.6	3.4	5.6	8.7	524
30 min	0.06	1.2	0.93	2.7	3.6	5.9	8.9	546
50 min	0.06	1.5	0.96	2.9	3.8	6.0	8.9	563
105 min	0.08	2.4	0.86	4.4	5.3	8.0	12.0	762
0.20IPEG2								
5 min	0.04	- 0.3	0.99	0.8	1.4	3.1	5.1	276
30 min	0.05	- 0.3	0.98	0.9	1.5	3.2	5.5	291
50 min	0.05	- 0.2	0.98	1.0	1.5	3.3	5.6	299
105 min	0.05	- 0.0	0.98	1.4	2.0	3.8	6.5	356

Table A-34. Rheological parameters of PLC*_30KUP_y mixtures (w/b = 0.50)

Mixture	h [Nmm·min]	g [Nmm]	R^2 [-]	Median T [Nmm] at … [rpm]				FR [Nmm/min]
				20	40	80	120	
ref								
5 min	0.27	49.4	0.78	56.5	60.2	67.4	82.8	6723
30 min	0.33	49.9	0.60	58.2	63.4	71.0	89.9	7120
50 min	0.21	57.9	0.84	61.2	68.7	73.5	83.8	7288
105 min	0.23	66.3	0.92	70.0	77.2	84.5	94.5	8287
0.05HPEG								
5 min	0.30	16.6	0.68	24.4	28.5	36.0	52.9	3597
30 min	0.21	19.8	0.96	24.6	28.5	35.3	45.5	3422
50 min	0.19	19.8	0.97	24.0	27.3	33.7	42.4	3256
105 min	0.18	23.5	0.96	27.5	31.0	36.9	45.7	3596
0.05IPEG1								
5 min	0.34	29.3	0.70	38.0	43.1	51.3	70.8	5140
30 min	0.22	28.0	0.91	33.2	37.2	43.9	55.3	4310
50 min	0.19	26.4	0.96	30.6	34.1	40.3	49.3	3930
105 min	0.18	25.0	0.88	29.2	32.5	38.1	47.3	3739
0.10IPEG1								
5 min	0.18	16.7	0.84	21.4	23.8	28.8	38.8	2859
30 min	0.14	19.9	0.93	23.2	25.6	30.5	37.3	2966
50 min	0.13	20.6	0.88	23.7	25.7	29.9	36.3	2933
105 min	0.16	22.8	0.86	27.0	29.2	33.7	42.6	3350
0.05IPEG2								
5 min	0.39	12.2	0.54	23.1	27.1	37.3	59.9	3732
30 min	0.36	10.7	0.58	21.6	24.5	30.7	54.6	3274
50 min	0.16	18.2	0.98	21.7	24.4	31.0	37.7	2947
105 min	0.17	19.1	0.97	23.1	26.1	31.8	40.4	3093
0.10IPEG2								
5 min	0.21	2.1	0.86	7.7	10.0	16.0	27.2	1559
30 min	0.17	3.6	0.97	7.9	10.0	15.6	24.0	1485
50 min	0.15	4.1	0.99	8.0	9.9	15.2	22.8	1443
105 min	0.14	4.6	0.97	8.2	10.2	15.2	22.1	1436
0.20IPEG2								
5 min	0.15	- 2.2	0.95	1.6	3.3	7.9	15.5	742
30 min	0.13	- 1.7	0.98	1.5	3.1	7.6	13.9	690
50 min	0.12	- 1.5	0.99	1.4	2.9	7.1	12.9	644
105 min	0.13	- 2.0	0.74	1.4	3.0	7.3	14.2	681

Table A-35. Rheological parameters of PLC*_30RKUP_y mixtures (w/b = 0.50)

Mixture	h [Nmm·min]	g [Nmm]	R^2 [-]	Median T [Nmm] at … [rpm]				FR [Nmm/min]
				20	40	80	120	
ref								
5 min	0.17	66.9	0.73	71.2	74.2	78.5	88.2	7841
30 min	0.13	69.1	0.90	71.9	74.4	78.7	85.2	7805
50 min	0.11	70.8	0.99	72.8	75.5	79.2	83.8	7840
105 min	0.12	70.4	0.96	72.6	75.7	80.0	85.2	7900
0.05HPEG								
5 min	0.17	19.8	0.75	24.5	26.5	30.6	40.5	3071
30 min	0.13	19.6	0.95	22.8	24.7	28.5	35.2	2815
50 min	0.11	19.5	0.99	22.3	24.0	27.8	33.3	2722
105 min	0.12	21.2	0.96	24.2	26.1	30.0	36.2	2952
0.05IPEG1								
5 min	0.20	35.6	0.68	41.1	43.8	48.4	60.5	4870
30 min	0.14	33.7	0.94	36.8	39.3	43.2	50.1	4278
50 min	0.12	31.9	0.98	34.4	36.7	40.3	45.9	3976
105 min	0.13	30.3	0.94	33.3	35.5	39.3	45.9	3889
0.10IPEG1								
5 min	0.14	13.3	0.86	17.0	18.8	22.7	30.6	2256
30 min	0.12	9.9	0.95	13.0	14.4	18.0	24.3	1768
50 min	0.10	8.3	0.97	10.9	12.1	15.3	20.4	1492
105 min	0.12	6.3	0.92	9.3	10.6	14.2	20.6	1395
0.20IPEG1								
5 min	0.09	1.0	0.96	3.3	4.4	7.3	11.8	693
30 min	0.08	0.0	0.98	2.1	3.1	5.9	10.0	552
50 min	0.08	- 0.4	0.99	1.5	2.5	5.1	8.9	473
105 min	0.08	- 0.8	0.98	1.2	2.2	4.9	8.8	448
0.05IPEG2								
5 min	0.18	21.7	0.72	26.7	28.7	32.8	43.6	3312
30 min	0.12	21.8	0.96	24.8	26.6	30.3	36.7	2994
50 min	0.11	21.8	0.99	24.3	26.0	29.6	34.8	2905
105 min	0.11	23.6	0.98	26.3	28.1	31.8	37.4	3127
0.10IPEG2								
5 min	0.10	2.3	0.92	4.9	6.0	9.0	14.3	877
30 min	0.09	2.2	0.98	4.5	5.5	8.5	12.8	804
50 min	0.08	2.4	0.99	4.4	5.4	8.4	12.3	788
105 min	0.10	3.4	0.96	6.0	7.1	10.4	15.5	1003
0.20IPEG2								
5 min	0.05	- 0.4	0.99	1.0	1.7	3.7	6.3	335
30 min	0.06	- 0.6	0.97	0.9	1.6	3.7	6.6	338
50 min	0.06	- 0.6	0.98	0.9	1.6	3.7	6.5	333
105 min	0.06	- 0.6	0.97	1.0	1.8	3.9	7.1	364

Table A-36. Rheological parameters of PLC*_30FUP_y mixtures (w/b = 0.50)

Mixture	h [Nmm·min]	g [Nmm]	R^2 [-]	Median T [Nmm] at … [rpm]				FR [Nmm/min]
				20	40	80	120	
ref								
5 min	0.15	71.4	0.58	75.6	77.2	80.7	89.6	8090
30 min	0.11	80.8	0.70	83.8	85.3	88.3	94.7	8825
50 min	0.08	86.8	0.95	88.5	90.3	93.1	96.9	9258
105 min	0.07	106.1	0.84	107.5	109.5	111.2	115.0	11108
0.05HPEG								
5 min	0.13	33.6	0.73	37.3	38.5	41.6	49.4	4182
30 min	0.08	41.8	0.72	44.3	44.9	47.0	52.0	4708
50 min	0.07	46.7	0.87	48.6	49.3	51.3	55.1	5120
105 min	0.18	52.1	0.44	58.0	59.1	61.7	74.5	6311
0.05IPEG1								
5 min	0.11	39.1	0.58	42.6	43.4	45.9	53.0	4623
30 min	0.08	50.4	0.60	52.5	53.3	56.7	60.5	5604
50 min	0.10	52.0	0.85	54.4	55.9	58.7	64.0	5852
105 min	0.18	54.4	0.48	59.3	61.4	65.2	76.0	6564
0.10IPEG1								
5 min	0.10	25.0	0.71	28.4	28.4	30.3	36.8	3084
30 min	0.08	35.8	0.61	38.0	38.3	41.5	45.1	4092
50 min	0.08	40.4	0.64	42.8	43.0	45.9	50.2	4557
105 min	0.18	43.3	0.56	48.4	50.4	53.8	65.1	5452
0.20IPEG1								
5 min	0.10	7.8	0.90	10.9	11.3	14.4	20.3	1431
30 min	0.07	18.0	0.79	20.4	20.2	21.9	26.3	2215
50 min	0.06	23.5	0.65	25.9	25.5	27.0	31.4	2731
105 min	0.19	26.7	0.43	33.1	33.5	36.5	49.8	3793
0.05IPEG2								
5 min	0.11	27.8	0.61	31.2	31.5	34.4	40.9	3452
30 min	0.08	34.8	0.75	37.2	37.5	39.6	44.3	3967
50 min	0.06	40.5	0.85	42.5	42.8	44.7	48.5	4469
105 min	0.21	56.6	0.76	62.2	65.2	70.5	82.7	7053
0.10IPEG2								
5 min	0.11	13.9	0.73	17.8	17.1	20.9	27.4	2077
30 min	0.07	22.5	0.82	25.0	24.8	26.8	31.3	2690
50 min	0.06	28.1	0.80	30.3	30.3	31.9	35.6	3200
105 min	0.20	37.1	0.41	43.3	44.5	47.7	61.0	4895
0.20IPEG2								
5 min	0.08	4.5	0.96	6.8	7.4	10.2	14.5	987
30 min	0.06	10.2	0.94	12.2	12.2	14.2	17.8	1414
50 min	0.06	13.8	0.89	16.0	15.6	17.4	21.1	1746
105 min	0.15	18.9	0.43	24.1	24.3	26.9	37.5	2795

9.8 Appendix A8: Time-dependent mini slump tests

This appendix section includes the individual values of mini slump tests over a period of 120 minutes, as conducted for mixtures with metaphyllosilicates and calcined Amaltheen clay and different superplasticizers (Table A-37 to Table A-45).

Table A-37. Mini slump values of OPC°_x_yLS mixtures (w/b = 0.45)

Mixture		Mini slump [cm] after … [min]								
x	y	5	15	30	45	60	75	90	105	120
-	-	17	16.5	16	15.5	14.5	14.5	14	13.5	13.5
-	0.14Mg-	23	21.5	20	19.5	19	19	18.5	18.5	18
-	0.15Na-	23.5	21.5	20	19	18.5	18	17.5	17	17
20CT	0.45Mg-	26.5	26.5	26	26	25	24.5	24.5	24	23
20CT	0.47Na-	26.5	25	23.5	21.5	20.5	20.5	19.5	19.5	19
20Mk	0.69Mg-	26.5	26.5	26	26	27	27	27	27	27
20Mk	0.82Na-	26.5	26	26	26	25	25	24.5	24	23

Table A-38. Mini slump values of OPC_x reference mixtures (w/b = 0.50)

Mixture x	Mini slump [cm] after … [min]								
	5	15	30	45	60	75	90	105	120
-	18	19.5	18.5	18.5	18.5	18.5	18.5	18.5	18
20TG	15	15	14.5	14.5	14	14	14	14	14
20Mk	8	-	-	-	-	-	-	-	-
20Mu	8	-	-	-	-	-	-	-	-
20Mi	8	-	-	-	-	-	-	-	-

Table A-39. Mini slump values of OPC_x_yNSF mixtures (w/b = 0.50)

Mixture		Mini slump [cm] after … [min]								
x	y	5	15	30	45	60	75	90	105	120
-	0.21	26	25	23.5	22.5	22.5	22.5	22.5	22	21.5
20TG	0.40	26	26	25.5	25.5	25.5	25	24	24	24
20Mk	0.68	25.5	25.5	25	23	22	20	19	17	16.5
20Mu	1.50	26	26	27.5	28	27.5	27.5	28.5	28	27.5
20Mi	0.95	26	26.5	23.5	18.5	14	10	9	8.5	8

Table A-40. Mini slump values of OPC_x_yHPEG mixtures (w/b = 0.50)

Mixture		Mini slump [cm] after … [min]								
x	y	5	15	30	45	60	75	90	105	120
-	0.05	25	25	24.5	24	24	23.5	23	23.5	23
20TG	0.07	25	25	24	23	22.5	22	22	21	20
20Mk	0.19	25.5	20.5	18.5	18	15.5	13.5	11.5	10	8.5
20Mu	0.16	24.5	26.5	26.5	26	25.5	23.5	23	22.5	22
20Mi	0.37	27	28	23	22.5	22	22	22	21	20

Table A-41. Mini slump values of OPC_x_yamphMPEG mixtures (w/b = 0.50)

Mixture		Mini slump [cm] after … [min]								
x	y	5	15	30	45	60	75	90	105	120
-	0.06	24.5	23.5	23	23	23	23	22	22	21.5
20TG	0.08	22.5	21	20	20	20	19.5	20	19.5	19
20Mk	0.19	25	22	17.5	16	15	13	11.5	9	8
20Mu	0.21	29	30.5	30	28.5	28	27.5	27	25	24
20Mi	0.41	23	21.5	11.5	8	8	8	8	8	8

Table A-42. Mini slump values of PLC_x reference mixtures (w/b = 0.50)

Mixture x	Mini slump [cm] after … [min]								
	5	15	30	45	60	75	90	105	120
-	16	16	14.5	14.5	14.5	14	14.5	14	14
20TG	13	12.5	12	11.5	11	11	11	11	11
20Mk	8	-	-	-	-	-	-	-	-
20Mu	8	-	-	-	-	-	-	-	-
20Mi	8	-	-	-	-	-	-	-	-

Table A-43. Mini slump values of PLC_x_yNSF mixtures (w/b = 0.50)

Mixture		Mini slump [cm] after … [min]								
x	y	5	15	30	45	60	75	90	105	120
-	0.24	25	23	21.5	21	20	20	20	19.5	19
20TG	0.50	29	27.5	26	25.5	25	25	24	23	23
20Mk	0.77	28	25.5	25	23	22	21.5	20	18	17
20Mu	1.50	32	32	30	30	30	30.5	29.5	29.5	29.5
20Mi	0.97	25.5	23	21	17	16	13	10	9	8.5

Table A-44. Mini slump values of PLC_x_yHPEG mixtures (w/b = 0.50)

Mixture		Mini slump [cm] after … [min]								
x	y	5	15	30	45	60	75	90	105	120
-	0.06	26	23.5	22	19	17.5	15.5	12	11	8
20TG	0.08	26	24	23.5	23	23	22	21	21	20
20Mk	0.20	24.5	21	20	18	16.5	13.5	13	11.5	8.5
20Mu	0.16	26	22	18	16	15	13.5	13	11.5	8.5
20Mi	0.40	30.5	28.5	21	16	13	11.5	10	9	8.5

Table A-45. Mini slump values of PLC_x_yamphMPEG mixtures (w/b = 0.50)

Mixture		Mini slump [cm] after … [min]								
x	y	5	15	30	45	60	75	90	105	120
-	0.07	25	22.5	22.5	22.5	22.5	22	21.5	21.5	21
20TG	0.08	26	23.5	23.5	22	21	21	21	19.5	18
20Mk	0.21	24.5	21	19	15	10	9	8	8	8
20Mu	0.18	8	8	8	8	8	8	8	8	8
20Mi	0.42	25.5	15.5	10.5	8	8	8	8	8	8

9.9 Appendix A9: Analysis of isothermal calorimetric measurements

Significant values, such as the heat flow and time at end of dormant period and heat maxima, are summarized in Table A-46 to Table A-61. The heat of hydration is provided for 3, 6, 12, 24 and 48 hours in Table A-62 to Table A-65. At the time, when the dormant period ends, the heat of hydration is set at 0 J/g_{cement} and the heat released before is neglected ('-' in the tables).

Heat flow was recorded in general two times thanks to a low error rate with the isothermal calorimeter used (example given in Figure A-15). However, the measurements of two mixtures (OPC/PLC_20Mu_1.50NSF) revealed strong deviations. In order to compare these mixtures with other CCBC mixtures, they were tested ten times each and the average was formed. Figure A-16 and Figure A-17 show the deviations in heat of hydration and heat flow curves for OPC_20Mu_1.50NSF and PLC_20Mu_1.50NSF, respectively. Significant values for the individual repeats of these mixtures are given in Table A-49 and Table A-54.

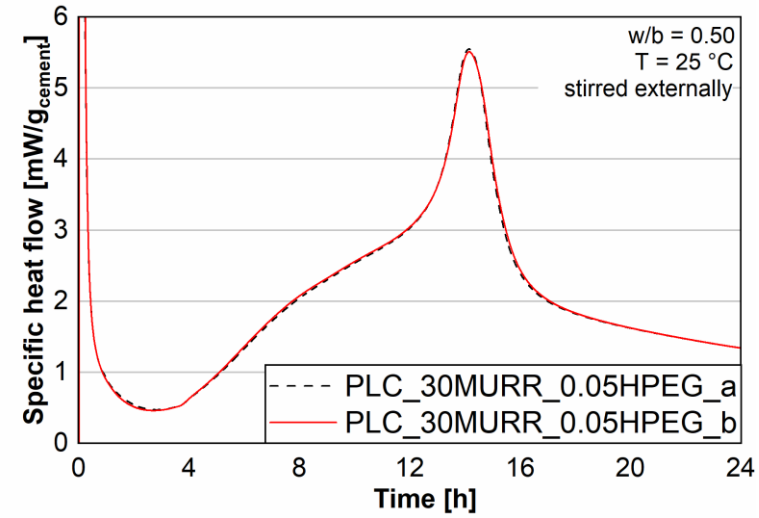

Figure A-15. Heat flow curves of mixture with calcined common clays and PCE (differences between the individual measurements: Q_{min} = 0.01 mW/g_{cement}, t_{min} = 0.11 h, Q_{max2} = 0.04 mW/g_{cement}, t_{max2} = 0.01 h)

The following abbreviations / symbols are used in the tables of this section:

Abbreviation	Definition
Q_{max1}	Heat recorded at the first maximum [mW/g_{cement}]
Q_{max2}	Heat recorded at the only or second maximum [mW/g_{cement}]
Q_{min}	Heat recorded at the end of the dormant period [mW/g_{cement}]
t_{Qmax1}	Time of occurrence of Q_{max1} [h]
t_{Qmax2}	Time of occurrence of Q_{max2} [h]
t_{Qmin}	End of dormant period [h]
x	Replacement level [wt%] and type of metaphyllosilicate/calcined common clay
y	Dosage [%bwob] and type of superplasticizer if added

Table A-46. Significant Q values of OPC°_x_yLS mixtures (w/b = 0.45)

Mixture		Q_{min} [mW/g_{cement}]	$t_{Q,min}$ [h]	Q_{max1} [mW/g_{cement}]	$t_{Q,max1}$ [h]	Q_{max2} [mW/g_{cement}]	$t_{Q,max2}$ [h]
x	y						
-	-	0.39	2.9	2.47	12.1	2.19	16.9
-	0.14Mg-	0.27	3.9	2.40	14.6	2.27	19.0
-	0.15Na-	0.27	3.9	2.38	15.0	2.34	17.9
20CT	-	0.47	3.2	2.23	12.1	2.60 / 3.28	14.9 / 20.3
20CT	0.14Mg-	0.35	3.4	2.17	15.2	2.36	22.3
20CT	0.15Na-	0.35	3.9	2.10	14.7	2.27	22.3
20CT	0.45Mg-	0.09	11.4	-	-	2.51	32.3
20CT	0.47Na-	0.17	12.7	-	-	2.67	32.2
20Mk	0.14Mg-	0.65	3.2	-	-	5.33	13.6
20Mk	-	0.78	2.7	2.92	8.4	6.60	13.0
20Mk	0.15Na-	0.63	3.3	-	-	4.98	14.0
20Mk	0.69Mg-	0.19	10.2	-	-	4.36	26.1
20Mk	0.82Na-	0.14	10.0	-	-	3.25	27.1

Table A-47. Significant Q values of OPC_x reference mixtures (w/b = 0.50)

Mixture x	Q_{min} [mW/g_{cement}]	$t_{Q,min}$ [h]	Q_{max1} [mW/g_{cement}]	$t_{Q,max1}$ [h]	Q_{max2} [mW/g_{cement}]	$t_{Q,max2}$ [h]
-	0.45	2.1	2.83	10.5	2.66	13.7
10TG	0.39	2.4	3.18	11.0	2.58	15.7
20TG	0.55	2.2	3.03	10.5	3.01	13.5
30TG	0.67	2.1	3.10	9.4	4.45	17.4
20Mk	0.86	2.5	-	-	10.58	9.4
30Mk	1.09	2.1	-	-	15.80	7.9
10Mu	0.54	1.8	-	-	3.25	11.4
20Mu	0.64	1.8	-	-	5.91	13.2
30Mu	0.70	1.9	-	-	6.61	12.7
20Mi	1.51	2.5	-	-	16.73	8.2
30Mi	2.22	2.7	-	-	17.74	6.4

Table A-48. Significant Q values of OPC_x_yNSF mixtures (w/b = 0.50)

Mixture		Q_{min} [mW/g_{cement}]	$t_{Q,min}$ [h]	Q_{max1} [mW/g_{cement}]	$t_{Q,max1}$ [h]	Q_{max2} [mW/g_{cement}]	$t_{Q,max2}$ [h]
x	y						
-	0.21	0.40	2.3	3.17	10.3	2.59	14.5
20TG	0.40	0.33	3.6	3.21	12.2	3.13	15.1
20Mk	0.68	0.52	3.2	-	-	13.54	11.7
10Mu	1.50	0.11	11.2	3.14	30.6	3.84	36.0
20Mu	1.50	*0.10*	*12.5*	-	-	*5.72*	*30.8*
30Mu	1.50	0.08	13.3	-	-	6.43	31.9
20Mi	0.95	1.16	3.1	-	-	14.64	9.6

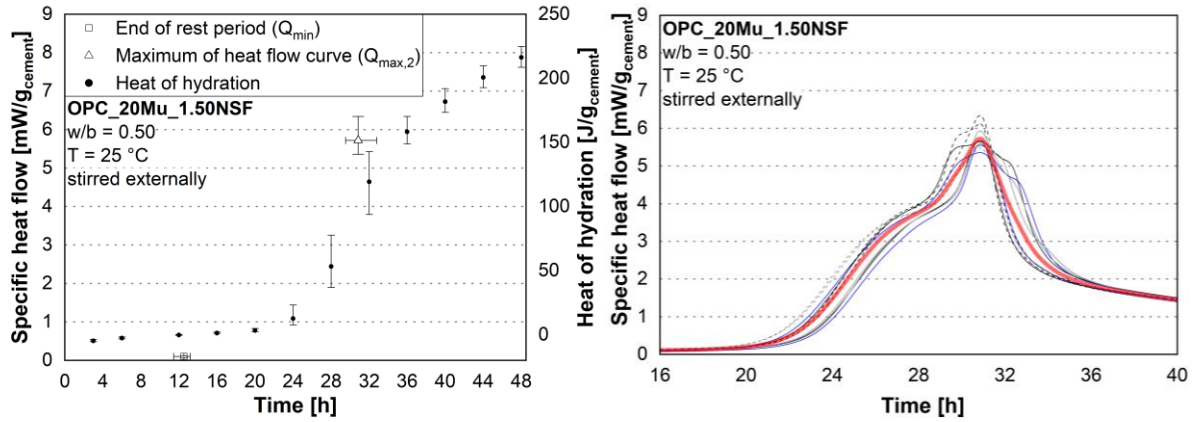

Figure A-16. Deviations of specific heat flow curve and heat of hydration development of OPC_20Mu_1.50NSF

Table A-49. Significant values of OPC_20Mu_1.50NSF repeats (w/b = 0.50)

#	Q_{min} [mW/g$_{cement}$]	$t_{Q,min}$ [h]	Q_{max2} [mW/g$_{cement}$]	$t_{Q,max2}$ [h]	Heat of hydration [J/g$_{cement}$] at … [h]				
					3	6	12	24	48
1	0.10	12.4	5.65	31.1	- 4.8	- 2.7	- 0.1	11.6	216.5
2	0.10	12.7	5.67	31.0	- 4.8	- 2.6	- 0.2	8.5	214.8
3	0.11	11.4	6.12	29.5	- 4.7	- 2.5	0.2	23.2	224.8
4	0.12	12.9	6.34	30.0	- 5.4	- 3.2	- 0.4	17.3	221.9
5	0.11	13.3	5.94	29.6	- 5.1	- 3.0	- 0.5	15.1	218.7
6	0.10	13.0	5.53	30.3	- 5.1	- 3.0	- 0.4	12.2	217.2
7	0.11	12.4	5.58	31.0	- 5.1	- 2.9	- 0.2	16.0	219.6
8	0.11	13.0	5.48	32.8	- 5.0	- 2.9	- 0.4	7.7	211.0
9	0.07	11.9	5.36	32.1	- 3.6	- 1.7	0.0	7.8	210.3
10	0.07	12.2	5.58	30.9	- 3.6	- 1.8	- 0.1	7.6	208.6
$\bar{x}$	**0.10**	**12.5**	**5.73**	**30.8**	**- 4.7**	**- 2.6**	**- 0.2**	**12.7**	**216.3**
$d_{\bar{x}}$	0.01	0.4	0.25	0.8	0.5	0.4	0.2	4.1	4.1

Table A-50. Significant Q values of OPC_x_yHPEG mixtures (w/b = 0.50)

Mixture		Q_{min} [mW/g$_{cement}$]	$t_{Q,min}$ [h]	Q_{max1} [mW/g$_{cement}$]	$t_{Q,max1}$ [h]	Q_{max2} [mW/g$_{cement}$]	$t_{Q,max2}$ [h]
x	y						
-	0.05	0.33	2.8	3.22	11.5	3.22	13.5
-	0.20	0.19	4.8	-	-	3.01	18.0
10TG	0.07	0.38	2.7	3.00	11.9	3.04	14.2
20TG	0.07	0.40	3.0	3.19	12.0	3.23	14.9
20TG	0.20	0.24	5.0	3.06	18.6	3.05	24.2
30TG	0.07	0.54	2.5	2.92	11.4	4.25	18.8
20Mk	0.19	0.59	2.7	-	-	11.28	11.6
20Mk	0.20	0.70	2.7	-	-	8.10	8.9
10Mu	0.16	0.32	3.5	-	-	5.92	17.8
20Mu	0.16	0.40	2.7	-	-	8.50	13.9
20Mu	0.20	0.33	3.5	-	-	7.81	15.6
30Mu	0.16	0.53	2.5	-	-	8.18	13.3
20Mi	0.20	1.26	2.7	-	-	15.37	9.1
20Mi	0.37	1.21	2.9	-	-	13.37	9.6

Table A-51. Significant Q values of OPC_x_yamphMPEG mixtures (w/b = 0.50)

Mixture		Q_{min} [mW/g_{cement}]	$t_{Q,min}$ [h]	Q_{max1} [mW/g_{cement}]	$t_{Q,max1}$ [h]	Q_{max2} [mW/g_{cement}]	$t_{Q,max2}$ [h]
x	y						
-	0.06	0.39	2.5	2.94	11.3	2.89	13.7
-	0.20	0.28	3.3	-	-	3.10	14.3
20TG	0.08	0.48	2.5	2.99	11.5	3.11	14.1
20TG	0.20	0.37	3.2	2.91	12.5	3.09	15.7
20Mk	0.19	0.72	2.5	-	-	9.61	11.3
20Mk	0.20	0.68	2.5	-	-	9.55	11.3
20Mu	0.20	0.51	2.3	-	-	7.58	14.1
20Mu	0.21	0.46	2.4	-	-	7.42	14.1
20Mi	0.20	1.16	3.0	-	-	14.13	9.6
20Mi	0.41	1.07	3.2	-	-	11.80	10.3

Table A-52. Significant Q values of PLC_x reference mixtures (w/b = 0.50)

Mixture x	Q_{min} [mW/g_{cement}]	$t_{Q,min}$ [h]	Q_{max1} [mW/g_{cement}]	$t_{Q,max1}$ [h]	Q_{max2} [mW/g_{cement}]	$t_{Q,max2}$ [h]
-	0.47	2.0	2.65	8.2	2.97	10.3
20TG	0.57	2.1	2.63	7.9	3.00	10.0
30TG	0.62	2.0	-	-	5.60	14.8
20Mk	0.85	2.1	-	-	12.41	7.7
30Mk	1.14	2.3	-	-	10.95	6.4
20Mu	0.67	2.0	-	-	5.27	12.9
30Mu	1.14	2.3	-	-	10.95	6.4
20Mi	1.28	2.4	-	-	12.92	8.2
30Mi	1.95	2.8	-	-	13.17	6.1

Table A-53. Significant Q values of PLC_x_yNSF mixtures (w/b = 0.50)

Mixture		Q_{min} [mW/g_{cement}]	$t_{Q,min}$ [h]	Q_{max1} [mW/g_{cement}]	$t_{Q,max1}$ [h]	Q_{max2} [mW/g_{cement}]	$t_{Q,max2}$ [h]
x	y						
-	0.24	0.42	2.2	2.60	9.4	2.79	11.3
20TG	0.50	0.41	3.1	-	-	5.52	15.8
20Mk	0.77	0.57	3.7	-	-	8.47	11.3
20Mu	1.50	*0.07*	*14.0*	-	-	*3.85*	*36.3*
20Mi	0.97	0.94	4.0	-	-	14.19	9.8

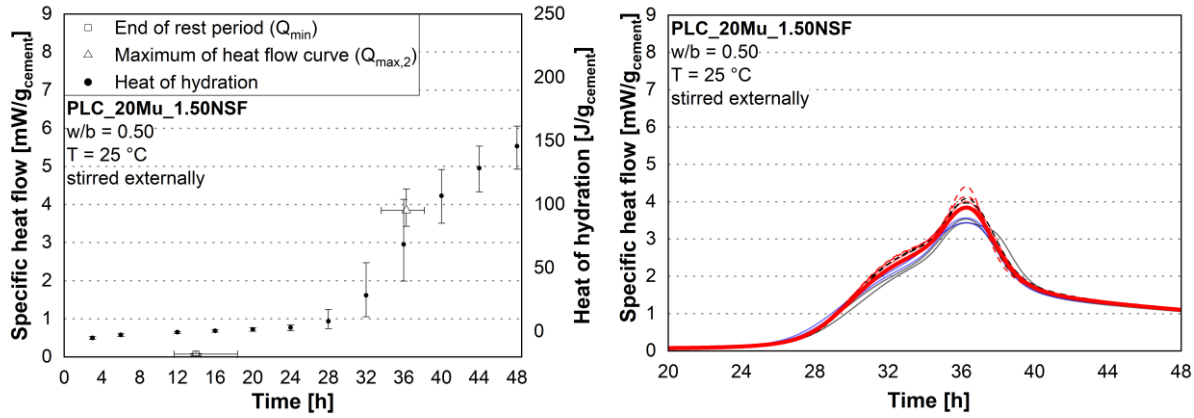

Figure A-17. Deviations of specific heat flow curve and heat of hydration development of PLC_20Mu_1.50NSF

Table A-54. Significant values of PLC_20Mu_1.50NSF repeats (w/b = 0.50)

#	Q_{min} [mW/g$_{cement}$]	$t_{Q,min}$ [h]	Q_{max2} [mW/g$_{cement}$]	$t_{Q,max2}$ [h]	Heat of hydration [J/g$_{cement}$] at … [h]				
					3	6	12	24	48
1	0.03	18.4	3.54	38.2	- 4.0	- 2.0	- 0.6	0.7	127.8
2	0.07	18.0	3.43	36.8	- 6.3	- 3.9	- 1.6	1.9	136.3
3	0.05	14.0	3.87	37.9	- 4.8	- 2.5	- 0.4	2.2	140.3
4	0.07	13.5	4.01	37.3	- 5.3	- 2.9	- 0.4	3.1	146.7
5	0.06	14.4	3.56	37.7	- 5.4	- 3.0	- 0.6	2.7	134.8
6	0.06	14.2	3.44	37.3	- 5.0	- 2.7	- 0.5	2.6	139.4
7	0.08	12.0	4.09	34.9	- 4.7	- 2.3	0.0	4.4	156.0
8	0.09	11.7	3.97	34.6	- 4.9	- 1.8	0.1	4.6	158.3
9	0.07	11.8	4.14	34.3	- 4.6	- 2.2	0.0	4.2	158.2
10	0.08	11.7	4.41	33.6	- 4.8	- 2.3	0.1	5.1	161.7
$\bar{x}$	**0.07**	**14.0**	**3.85**	**36.3**	**- 5.0**	**- 2.6**	**- 0.4**	**3.2**	**145.9**
$d_{\bar{x}}$	0.01	1.8	0.28	1.5	0.4	0.4	0.4	1.1	10.2

Table A-55. Significant Q values of PLC_x_yHPEG mixtures (w/b = 0.50)

Mixture		Q_{min} [mW/g$_{cement}$]	$t_{Q,min}$ [h]	Q_{max1} [mW/g$_{cement}$]	$t_{Q,max1}$ [h]	Q_{max2} [mW/g$_{cement}$]	$t_{Q,max2}$ [h]
x	y						
-	0.06	0.39	2.3	2.58	8.7	3.03	10.7
-	0.20	0.23	4.2	-	-	2.80	18.2
20TG	0.08	0.44	2.7	-	-	6.71	14.3
20TG	0.20	0.29	4.5	3.29	18.2	2.51	22.0
20Mk	0.20	0.70	2.7	-	-	8.10	8.9
20Mu	0.16	0.51	2.3	-	-	8.56	10.0
20Mu	0.20	0.38	3.4	-	-	6.47	14.4
20Mi	0.20	1.14	2.6	-	-	13.41	8.6
20Mi	0.40	1.07	2.9	-	-	10.77	9.0

Table A-56. Significant Q values of PLC_x_yamphMPEG mixtures (w/b = 0.50)

Mixture		Q_{min} [mW/g_{cement}]	$t_{Q,min}$ [h]	Q_{max1} [mW/g_{cement}]	$t_{Q,max1}$ [h]	Q_{max2} [mW/g_{cement}]	$t_{Q,max2}$ [h]
x	y						
-	0.07	0.42	2.2	2.57	8.2	3.26	10.3
-	0.20	0.33	2.7	-	-	3.90	13.9
20TG	0.08	0.51	2.3	2.48	8.1	2.94	10.2
20TG	0.20	0.43	2.7	-	-	5.61	14.1
20Mk	0.20	0.75	2.4	-	-	9.89	8.7
20Mk	0.21	0.72	2.5	-	-	9.67	8.9
20Mu	0.18	0.59	2.0	-	-	10.23	9.4
20Mu	0.20	0.53	2.3	-	-	9.18	10.2
20Mi	0.20	1.11	3.0	-	-	14.89	7.5
20Mi	0.42	1.05	3.2	-	-	13.17	6.1

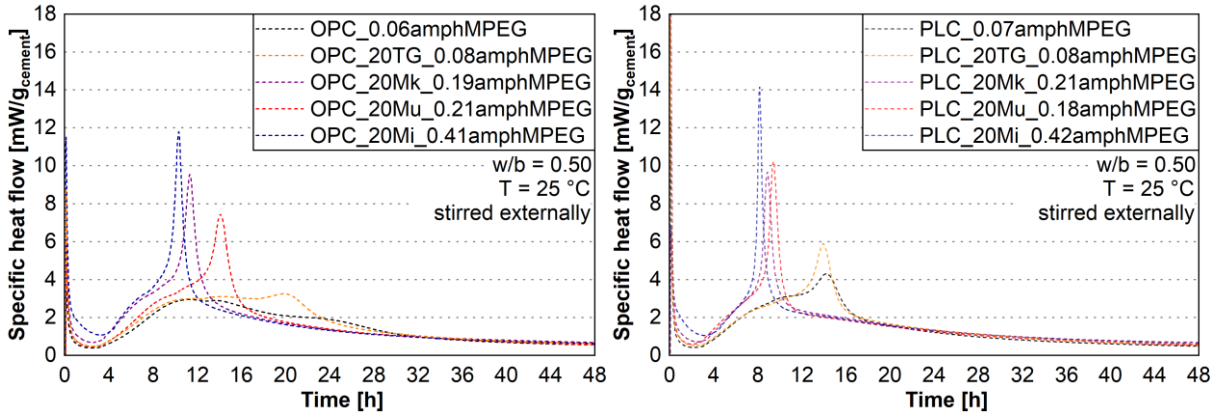

Figure A-18. Heat flow of OPC_x (left) and PLC_x (right) mixtures with varying dosages of amphMPEG

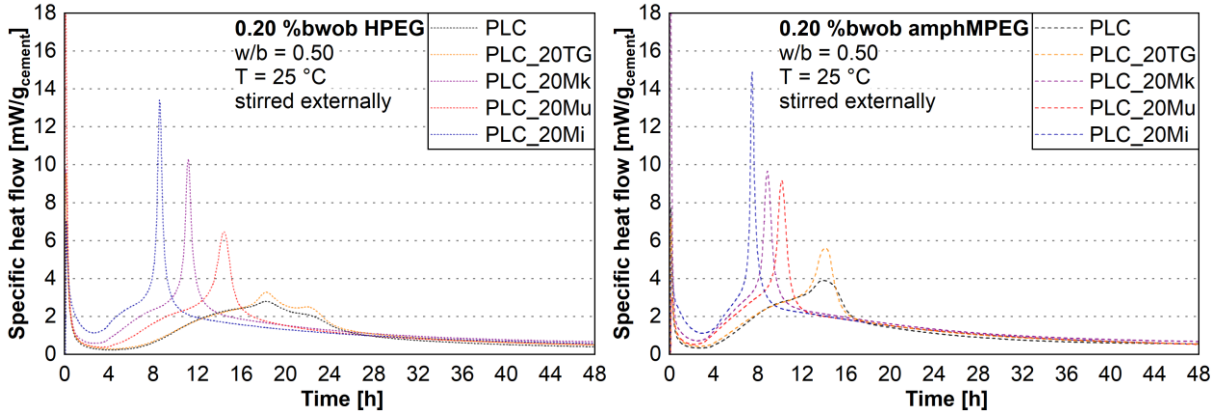

Figure A-19. Heat flow of PLC_x mixtures with 0.20 %bwob HPEG (left) and amphMPEG (right)

Table A-57. Significant Q values of PLC*_x_y mixtures (w/b = 0.40)

Mixture		Q_{min} [mW/g_{cement}]	$t_{Q,min}$ [h]	Q_{max1} [mW/g_{cement}]	$t_{Q,max1}$ [h]	Q_{max2} [mW/g_{cement}]	$t_{Q,max2}$ [h]
x	y						
-	-	0.37	2.4	2.69	10.9	2.61	15.5
-	0.05HPEG	0.35	2.4	2.80	10.7	3.03	15.1
-	0.05IPEG1	0.32	2.6	2.66	11.7	2.56	16.4
-	0.05IPEG2	0.32	2.5	2.71	11.7	2.76	16.1
30KUP	-	0.49	2.7	-	-	5.70	11.9
30KUP	0.05HPEG	0.44	2.6	-	-	5.54	12.0
30KUP	0.05IPEG1	0.43	2.9	-	-	5.24	12.5
30KUP	0.05IPEG2	0.44	2.9	-	-	5.16	12.5

Table A-58. Significant Q values of PLC*_x reference mixtures (w/b = 0.50)

Mixture x	Q_{min} [mW/g_{cement}]	$t_{Q,min}$ [h]	Q_{max1} [mW/g_{cement}]	$t_{Q,max1}$ [h]	Q_{max2} [mW/g_{cement}]	$t_{Q,max2}$ [h]
-	0.37	2.5	2.72	11.8	2.72	17.4
30AC	0.90	3.0	-	-	6.40	13.8
30KUP	0.50	2.7	-	-	5.85	12.8
30RKUP	0.65	3.1	-	-	7.83	10.8
30FUP	1.24	2.8	-	-	10.39	8.0
30MURR	0.53	2.9	-	-	4.94	14.8

Table A-59. Significant Q values of PLC*_x_0.05HPEG mixtures (w/b = 0.50)

Mixture x	Q_{min} [mW/g_{cement}]	$t_{Q,min}$ [h]	Q_{max1} [mW/g_{cement}]	$t_{Q,max1}$ [h]	Q_{max2} [mW/g_{cement}]	$t_{Q,max2}$ [h]
-	0.34	2.7	-	-	3.45	15.9
30AC	0.75	2.5	-	-	9.68	13.0
30KUP	0.43	2.9	-	-	5.60	13.0
30RKUP	0.59	3.2	-	-	7.10	11.3
30FUP	1.12	2.9	-	-	9.17	8.2
30MURR	0.46	2.7	-	-	5.53	14.2

Table A-60. Significant Q values of PLC*_x_yIPEG1 mixtures (w/b = 0.50)

Mixture		Q_{min} [mW/g_{cement}]	$t_{Q,min}$ [h]	Q_{max1} [mW/g_{cement}]	$t_{Q,max1}$ [h]	Q_{max2} [mW/g_{cement}]	$t_{Q,max2}$ [h]
x	y						
-	0.05	0.30	2.8	2.68	13.4	2.91	17.7
	0.10	0.26	3.2	-	-	3.76	17.5
	0.20	0.19	3.9	-	-	5.55	18.2
30AC	0.05	0.82	3.1	-	-	6.35	14.2
	0.10	0.59	3.1	-	-	5.36	16.3
	0.20	0.45	3.8	-	-	6.31	16.4
30KUP	0.05	0.48	3.1	-	-	5.64	12.8
30RKUP	0.05	0.65	3.4	-	-	7.53	11.2
30FUP	0.05	1.15	2.9	-	-	9.26	8.2
	0.10	1.12	3.0	-	-	9.70	8.5
	0.20	1.05	3.1	-	-	8.30	8.5
30MURR	0.05	0.49	3.2	-	-	4.60	15.6

Table A-61. Significant Q values of PLC*_x_yIPEG2 mixtures (w/b = 0.50)

Mixture		Q_{min} [mW/g_{cement}]	$t_{Q,min}$ [h]	Q_{max1} [mW/g_{cement}]	$t_{Q,max1}$ [h]	Q_{max2} [mW/g_{cement}]	$t_{Q,max2}$ [h]
x	y						
-	0.05	0.31	2.9	-	-	3.18	17.2
	0.10	0.25	3.1	-	-	4.86	16.1
	0.20	0.20	3.7	-	-	4.26	18.9
30AC	0.05	0.68	3.0	-	-	6.00	14.8
	0.10	0.56	3.0	-	-	5.60	16.0
	0.20	0.46	3.7	-	-	5.95	16.0
30KUP	0.05	0.47	3.3	-	-	5.66	13.1
30RKUP	0.05	0.60	3.3	-	-	7.30	11.4
30FUP	0.05	1.13	3.0	-	-	8.79	8.2
	0.10	1.10	2.9	-	-	9.03	8.5
	0.20	1.02	3.1	-	-	8.07	8.3
30MURR	0.05	0.44	2.8	-	-	4.91	15.1

Table A-62. Heat of hydration at selected times for OPC°_x_y mixtures (w/b = 0.45)

Mixture	Heat of hydration [J/g_{cement}] at …				
	3 h	6 h	12 h	24 h	48 h
OPC°	0.1	6.7	48.2	136.0	211.2
OPC°_0.14Mg-LS	- 0.9	2.6	28.7	124.7	213.1
OPC°_0.15Na-LS	- 1.0	2.5	27.4	123.6	210.1
OPC°_20CT	- 0.4	6.1	42.0	150.7	224.6
OPC°_20CT_0.14Mg-LS	- 0.5	4.1	32.4	129.1	215.4
OPC°_20CT_0.45Mg-LS	- 4.8	- 2.3	0.2	16.1	152.1
OPC°_20CT_0.15Na-LS	- 1.2	3.1	27.5	124.1	212.8
OPC°_20CT_0.47Na-LS	- 8.9	- 4.9	- 0.4	14.5	145.5
OPC°_20Mk	0.9	17.2	84.1	186.8	260.6
OPC°_20Mk_0.14Mg-LS	- 0.6	9.2	56.3	154.7	227.4
OPC°_20Mk_0.69Mg-LS	- 6.2	- 3.1	1.3	45.6	198.6
OPC°_20Mk_0.15Na-LS	- 0.7	8.3	54.4	156.7	230.8
OPC°_20Mk_0.82Na-LS	- 4.8	- 2.3	1.1	29.2	168.1

Table A-63. Heat of hydration at selected times for OPC_x_y mixtures

Mixture	Heat of hydration [J/g_{cement}] at …				
	3 h	6 h	12 h	24 h	48 h
OPC	1.4	12.0	65.1	154.7	234.1
OPC_0.21NSF	1.1	10.6	68.9	161.7	243.9
OPC_0.05HPEG	0.2	6.4	57.6	172.4	247.1
OPC_0.20HPEG	-	0.9	10.1	115.0	217.0
OPC_0.06amphMPEG	0.8	9.2	61.1	163.4	244.6
OPC_0.20amphMPEG	-	3.7	39.6	151.7	235.1
OPC_10TG	0.9	10.1	67.5	168.4	264.8
OPC_20TG	1.7	14.7	73.3	187.7	272.7
OPC_30TG	2.2	19.6	83.3	213.8	295.1
OPC_20TG_0.40NSF	-	4.0	50.3	185.5	275.4
OPC_10TG_0.07HPEG	0.4	7.8	57.5	178.0	260.0
OPC_20TG_0.07HPEG	0.1	6.7	55.7	190.2	275.2
OPC_20TG_0.20HPEG	-	0.9	12.3	127.0	242.4
OPC_30TG_0.07HPEG	1.0	12.3	67.0	198.3	284.6
OPC_20TG_0.08amphMPEG	0.8	11.2	65.9	190.4	273.3
OPC_20TG_0.20amphMPEG	-	5.3	47.2	176.5	257.9
OPC_20Mk	1.7	27.1	133.3	214.3	289.2
OPC_30Mk	3.8	36.7	141.8	215.5	298.6
OPC_20Mk_0.68NSF	-	9.8	112.1	206.3	288.1
OPC_20Mk_0.19HPEG	0.7	14.9	111.8	203.6	283.9
OPC_20Mk_0.20HPEG	0.7	14.6	89.8	168.4	252.8
OPC_20Mk_0.19amphMPEG	1.4	19.3	119.9	217.8	301.3
OPC_20Mk_0.20amphMPEG	1.2	17.9	114.7	205.7	285.1
OPC_10Mu	2.7	19.2	84.7	194.8	266.0
OPC_20Mu	3.3	33.7	106.2	211.7	281.3
OPC_30Mu	3.1	25.5	103.5	201.2	267.0
OPC_10Mu_1.50NSF	-	-	0.3	7.1	197.9
OPC_20Mu_1.50NSF	-	-	-	12.7	216.3
OPC_30Mu_1.50NSF	-	-	-	9.5	250.3
OPC_10Mu_0.16HPEG	-	4.1	48.0	186.4	266.9
OPC_20Mu_0.16HPEG	0.4	8.7	72.6	197.3	275.4
OPC_20Mu_0.20HPEG	-	5.4	45.9	149.0	214.5
OPC_30Mu_0.16HPEG	0.9	13.5	79.4	196.5	276.0
OPC_20Mu_0.20amphMPEG	1.0	11.6	75.2	198.9	273.9
OPC_20Mu_0.21amphMPEG	0.4	9.5	63.2	180.4	259.6
OPC_20Mi	2.7	36.9	147.5	220.0	290.1
OPC_30Mi	22.7	68.4	164.4	238.7	316.1
OPC_20Mi_0.95NSF	-	23.7	133.2	205.1	275.3
OPC_20Mi_0.20HPEG	1.5	28.6	135.3	207.3	276.2
OPC_20Mi_0.37HPEG	0.4	24.9	133.0	208.8	281.9
OPC_20Mi_0.20amphMPEG	0.0	21.2	126.7	205.8	280.5
OPC_20Mi_0.41amphMPEG	-	16.8	119.9	202.8	279.0

Table A-64. Heat of hydration at selected times for PLC_x_y mixtures

Mixture	Heat of hydration [J/g_{cement}] at …				
	3 h	6 h	12 h	24 h	48 h
PLC	1.9	15.8	74.1	168.9	230.4
PLC_0.24NSF	1.2	12.2	64.7	164.5	229.2
PLC_0.06HPEG	1.0	11.6	67.3	166.8	230.0
PLC_0.20HPEG	-	1.7	22.3	120.6	180.5
PLC_0.07amphMPEG	1.3	13.1	71.4	170.4	234.6
PLC_0.20amphMPEG	0.3	7.6	58.2	150.4	212.5
PLC_20TG	2.0	16.6	76.6	184.2	256.8
PLC_30TG	2.4	18.9	77.9	189.5	264.6
PLC_20TG_0.50NSF	-	7.5	56.0	169.1	247.9
PLC_20TG_0.08HPEG	0.5	9.6	61.0	173.5	248.8
PLC_20TG_0.20HPEG	-	1.8	23.4	128.7	198.5
PLC_20TG_0.08amphMPEG	1.3	13.9	71.5	179.3	253.5
PLC_20TG_0.20amphMPEG	0.5	9.2	60.5	162.8	231.9
PLC_20Mk	3.1	28.4	116.9	192.5	267.5
PLC_30Mk	3.2	33.2	110.1	186.5	280.8
PLC_20Mk_0.77NSF	-	6.6	81.3	162.7	247.6
PLC_20Mk_0.20HPEG	0.7	14.6	89.8	168.4	252.8
PLC_20Mk_0.20amphMPEG	1.6	19.4	124.3	191.2	278.3
PLC_20Mk_0.21amphMPEG	1.2	17.8	101.4	178.9	257.5
PLC_20Mu	2.7	20.3	83.4	170.6	233.8
PLC_30Mu	1.9	18.2	78.9	161.6	221.8
PLC_20Mu_1.50NSF	-	-	-	3.2	145.9
PLC_20Mu_0.16HPEG	1.3	15.2	96.6	171.6	243.2
PLC_20Mu_0.20HPEG	-	5.4	45.9	149.0	214.5
PLC_20Mu_0.18amphMPEG	2.3	20.2	107.5	180.7	251.1
PLC_20Mu_0.20amphMPEG	1.5	16.1	100.4	174.0	244.9
PLC_20Mi	2.6	28.2	114.3	176.5	242.6
PLC_30Mi	1.2	38.3	103.1	167.1	241.2
PLC_20Mi_0.97NSF	-	8.8	93.5	168.7	246.5
PLC_20Mi_0.20HPEG	1.6	21.6	102.9	166.0	234.8
PLC_20Mi_0.40HPEG	0.4	17.7	95.7	158.3	226.1
PLC_20Mi_0.20amphMPEG	0.0	19.5	103.2	176.1	246.9
PLC_20Mi_0.42amphMPEG	-	16.0	99.7	174.6	250.3

Table A-65. Heat of hydration at selected times for PLC*_x_y mixtures (w/b = 0.50 if not noted otherwise)

Mixture	Heat of hydration [J/g_{cement}] at …				
	3 h	6 h	12 h	24 h	48 h
PLC* (w/b = 0.40)	1.0	10.7	61.4	149.4	204.6
PLC*_0.05HPEG (w/b = 0.40)	0.8	9.8	61.1	151.7	208.5
PLC*_0.05IPEG1 (w/b = 0.40)	0.5	7.6	53.8	145.5	202.5
PLC*_0.05IPEG2 (w/b = 0.40)	0.6	7.9	54.6	147.6	205.0
PLC*	0.7	9.3	57.6	152.2	214.1
PLC*_0.05HPEG	0.4	8.0	55.1	153.8	218.6
PLC*_0.05IPEG1	0.2	6.3	48.5	147.1	210.9
PLC*_0.10IPEG1	-	4.1	39.7	148.2	218.5
PLC*_0.20IPEG1	-	1.6	19.3	137.3	217.9
PLC*_0.05IPEG2	0.1	6.3	48.7	149.4	215.7
PLC*_0.10IPEG2	-	4.3	41.5	153.8	224.2
PLC*_0.20IPEG2	-	1.8	17.5	130.5	206.7
PLC*_30AC	0.1	13.4	62.1	165.7	244.4
PLC*_30AC_0.05HPEG	1.2	16.7	76.0	182.1	259.1
PLC*_30AC_0.05IPEG1	-	11.7	57.5	160.4	240.0
PLC*_30AC_0.10IPEG1	-	9.3	52.6	161.4	241.9
PLC*_30AC_0.20IPEG1	-	4.3	38.2	151.5	235.1
PLC*_30AC_0.05IPEG2	0.0	11.0	57.7	163.9	242.6
PLC*_30AC_0.10IPEG2	0.0	8.9	51.6	160.3	240.7
PLC*_30AC_0.20IPEG2	-	4.6	38.7	148.1	229.9
PLC*_30KUP (w/b = 0.40)	0.6	10.4	73.7	158.2	231.7
PLC*_30KUP_0.05HPEG (w/b = 0.40)	0.6	9.1	66.9	153.3	228.9
PLC*_30KUP_0.05IPEG1 (w/b = 0.40)	0.1	7.7	59.6	149.0	221.4
PLC*_30KUP_0.05IPEG2 (w/b = 0.40)	0.1	7.8	58.8	148.5	223.2
PLC*_30KUP	0.5	9.8	62.7	157.1	234.8
PLC*_30KUP_0.05HPEG	0.1	7.7	55.6	152.1	230.3
PLC*_30KUP_0.05IPEG1	-	7.5	54.7	149.3	228.9
PLC*_30KUP_0.05IPEG2	-	6.8	52.4	148.9	229.0
PLC*_30RKUP	-	11.1	85.4	160.7	244.2
PLC*_30RKUP_0.05HPEG	-	9.4	78.2	155.9	239.1
PLC*_30RKUP_0.05IPEG1	-	8.9	78.6	156.0	239.1
PLC*_30RKUP_0.05IPEG2	-	8.8	76.7	156.5	240.8
PLC*_30FUP	0.9	20.9	98.2	165.0	248.0
PLC*_30FUP_0.05HPEG	0.3	17.4	91.3	157.7	241.0
PLC*_30FUP_0.05IPEG1	0.3	17.8	92.8	157.9	239.4
PLC*_30FUP_0.10IPEG1	0.1	17.2	94.3	160.9	245.3
PLC*_30FUP_0.20IPEG1	-	15.1	89.1	155.4	240.9
PLC*_30FUP_0.05IPEG2	0.0	17.1	91.3	158.6	242.9
PLC*_30FUP_0.10IPEG2	0.3	17.0	93.1	160.1	244.1
PLC*_30FUP_0.20IPEG2	-	15.3	88.9	155.2	247.7
PLC*_30MURR	0.1	9.8	59.0	161.6	235.3
PLC*_30MURR_0.05HPEG	0.4	9.3	58.3	163.3	240.7
PLC*_30MURR_0.05IPEG1	-	7.6	51.5	156.5	231.8
PLC*_30MURR_0.05IPEG2	0.3	8.3	54.3	161.1	237.2

9.10 Appendix A10: In situ XRD plots

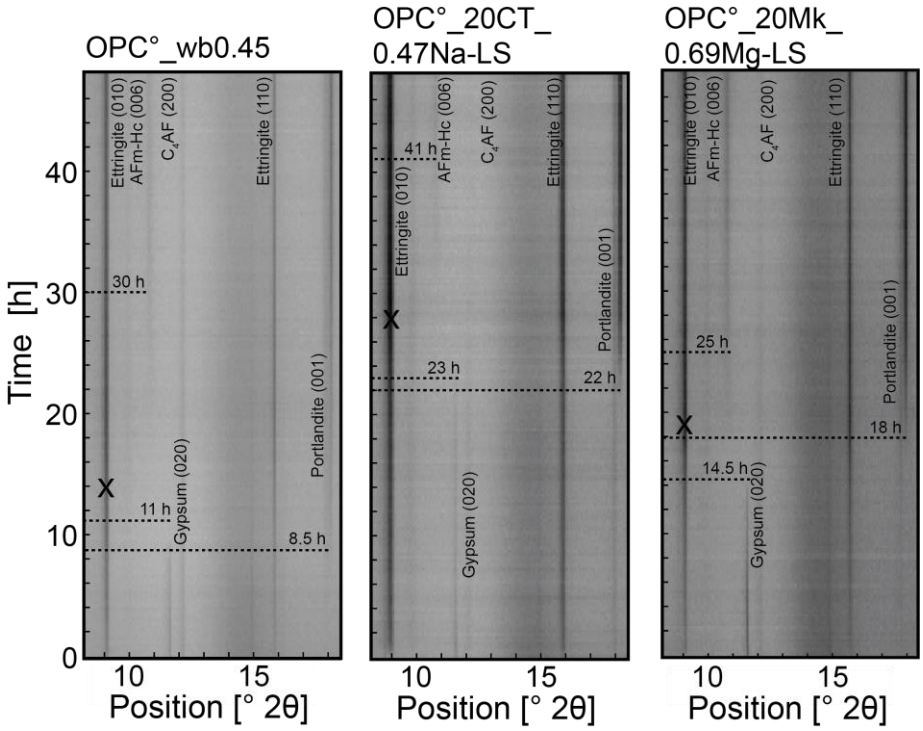

Figure A-20. In situ XRD plots from 8 to 18.5 °2θ for selected mixtures with lignosulfonates (X = time of maximum ettringite peak; w/b = 0.45)

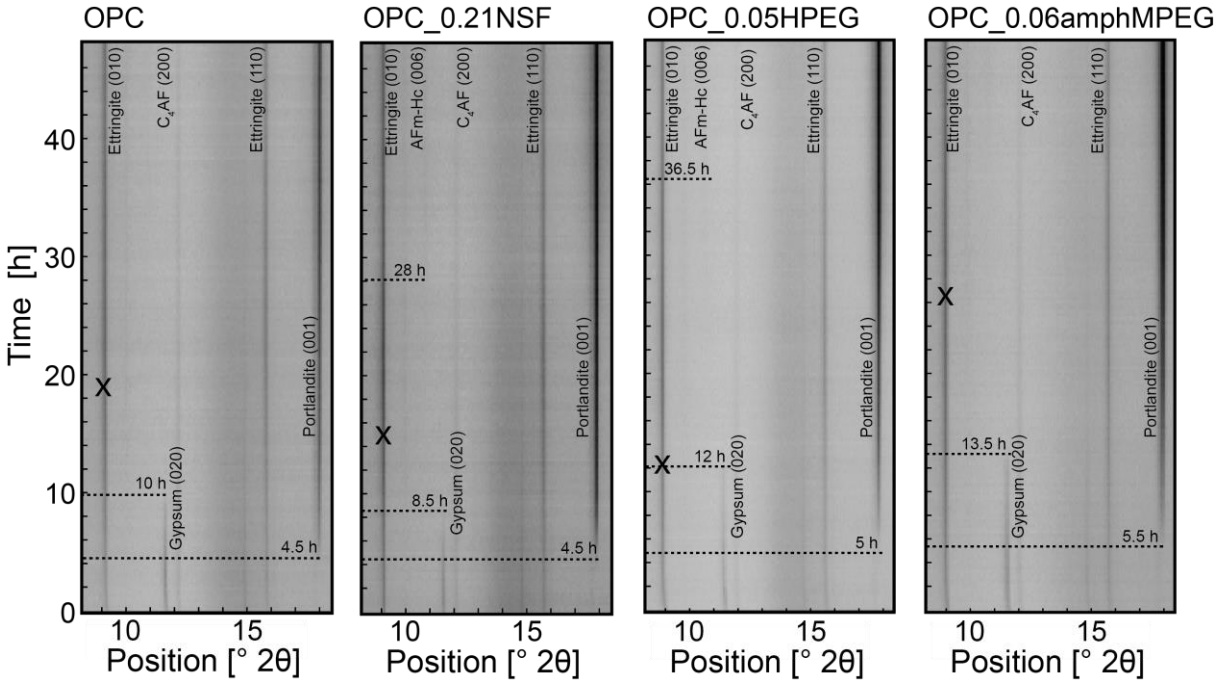

Figure A-21. In situ XRD plots from 8 to 18.5 °2θ for OPC mixtures (X = time of maximum ettringite peak, w/b = 0.50)

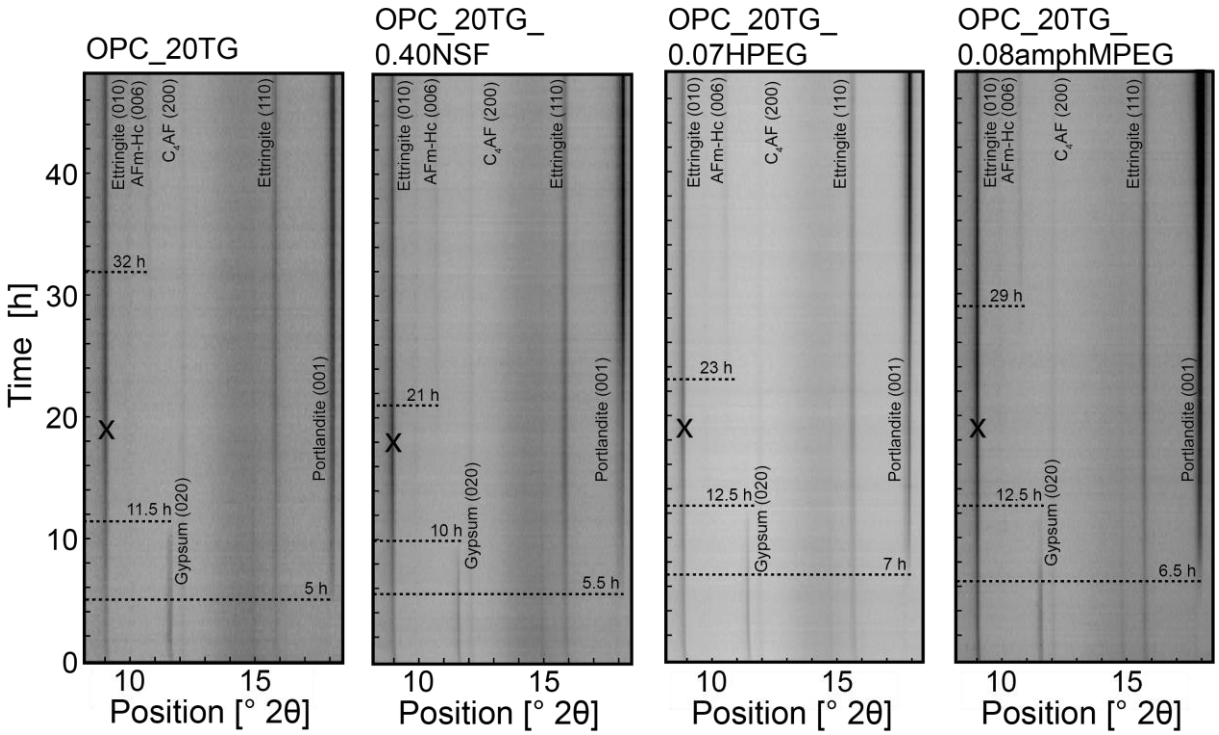

Figure A-22. In situ XRD plots from 8 to 18.5 °2θ for OPC_20TG mixtures (X = time of maximum ettringite peak)

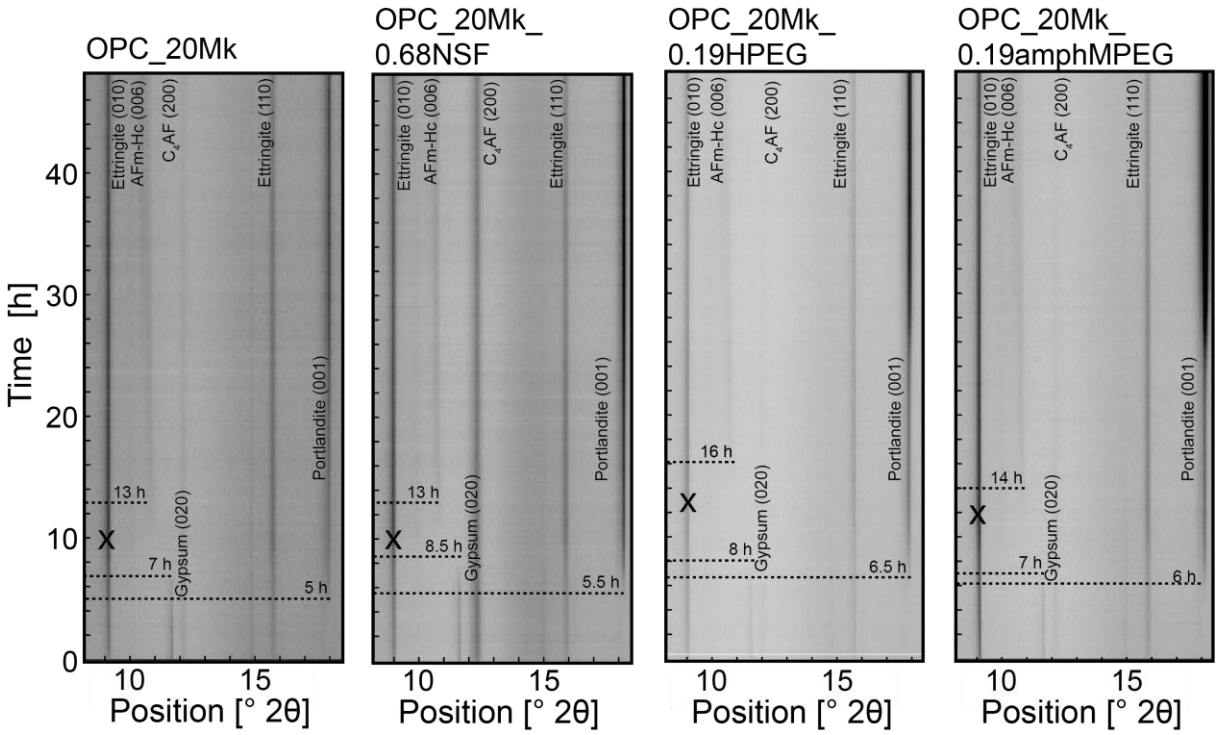

Figure A-23. In situ XRD plots from 8 to 18.5 °2θ for OPC_20Mk mixtures (X = time of maximum ettringite peak)

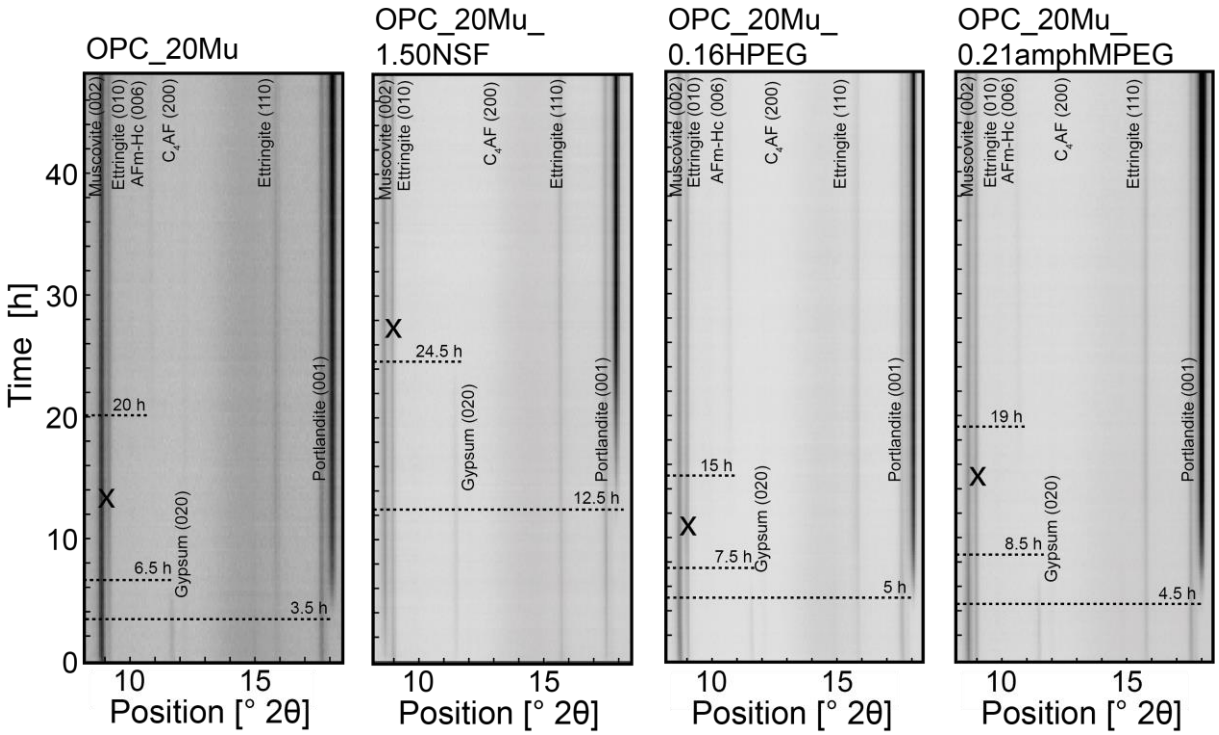

Figure A-24. In situ XRD plots from 8 to 18.5 °2θ for OPC_20Mu mixtures (X = time of maximum ettringite peak)

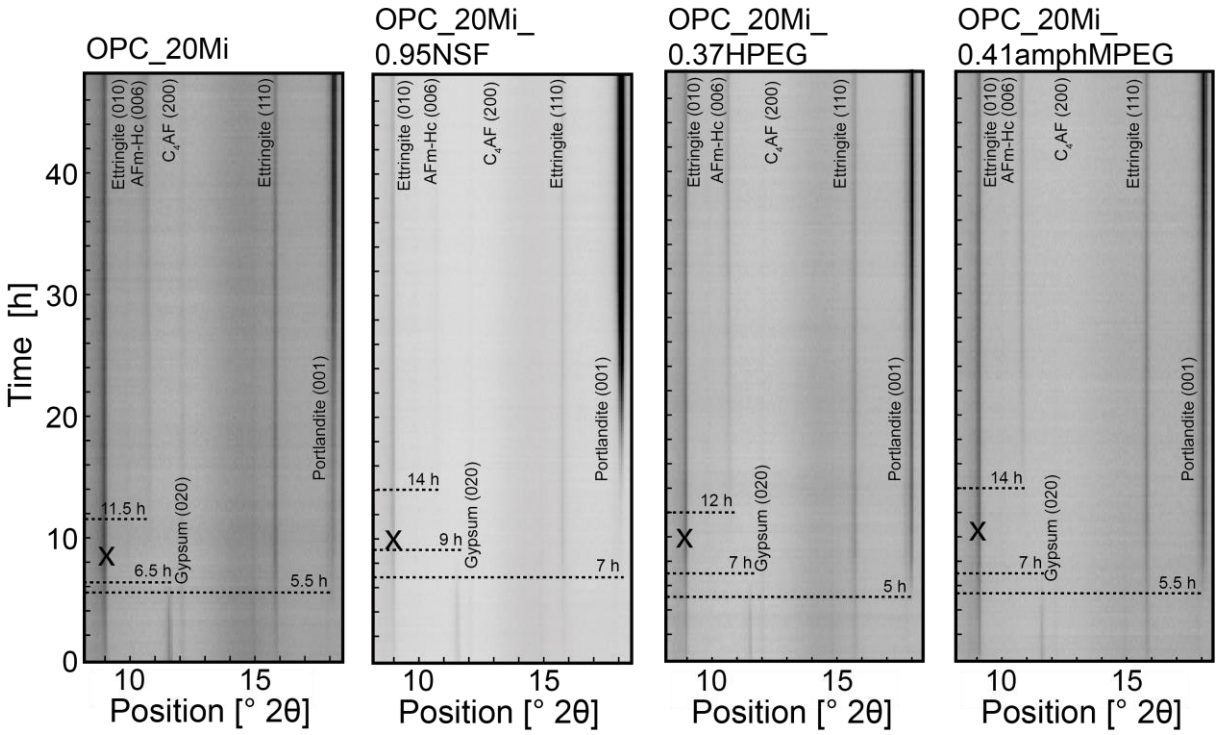

Figure A-25. In situ XRD plots from 8 to 18.5 °2θ for OPC_20Mi mixtures (X = time of maximum ettringite peak)

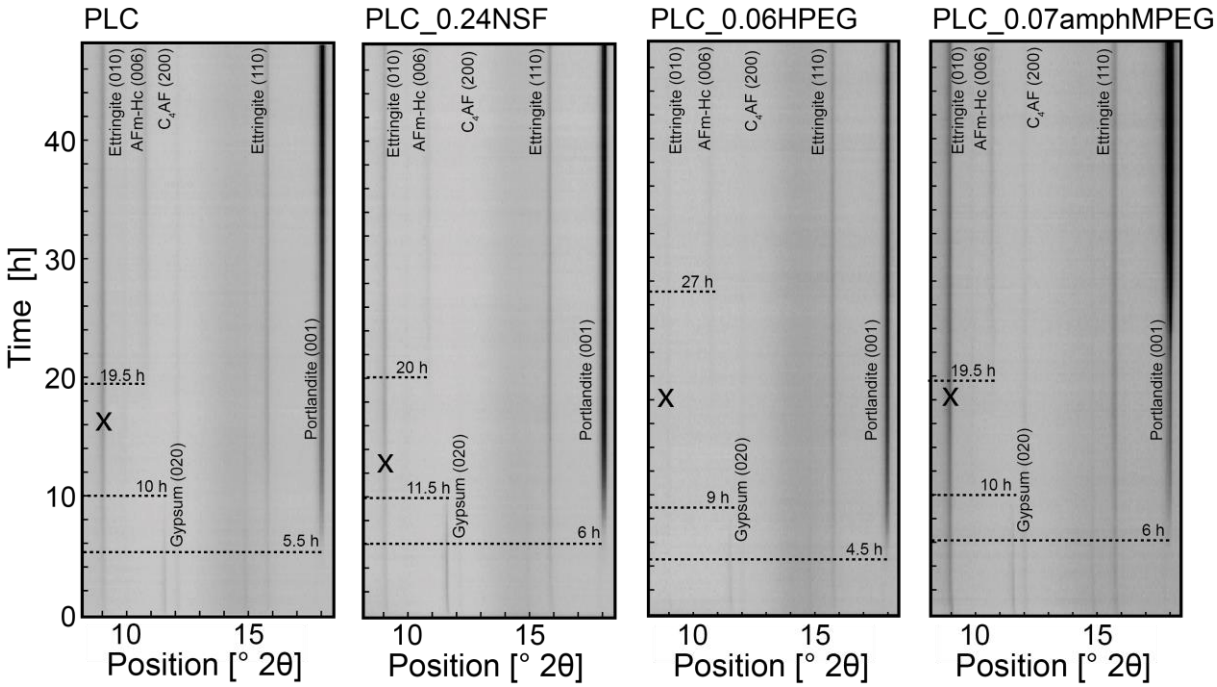

Figure A-26. In situ XRD plots from 8 to 18.5 °2θ for PLC mixtures (X = time of maximum ettringite peak)

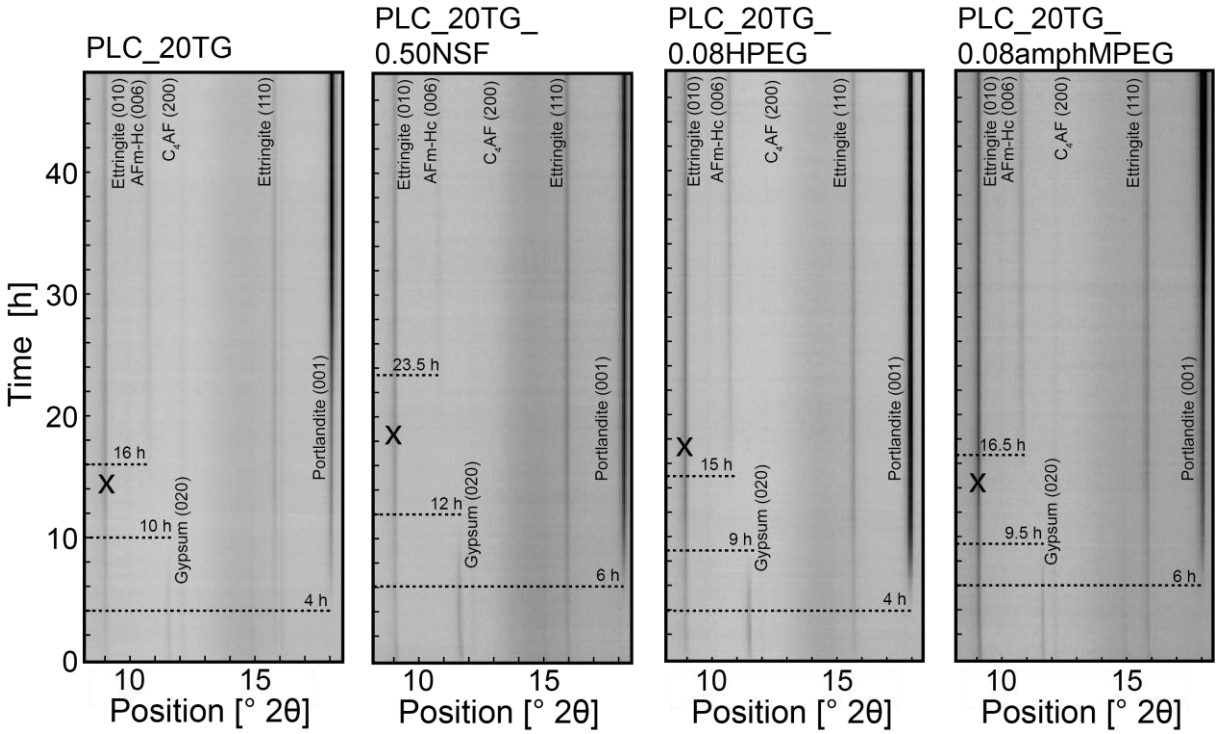

Figure A-27. In situ XRD plots from 8 to 18.5 °2θ for PLC_20TG mixtures (X = time of maximum ettringite peak)

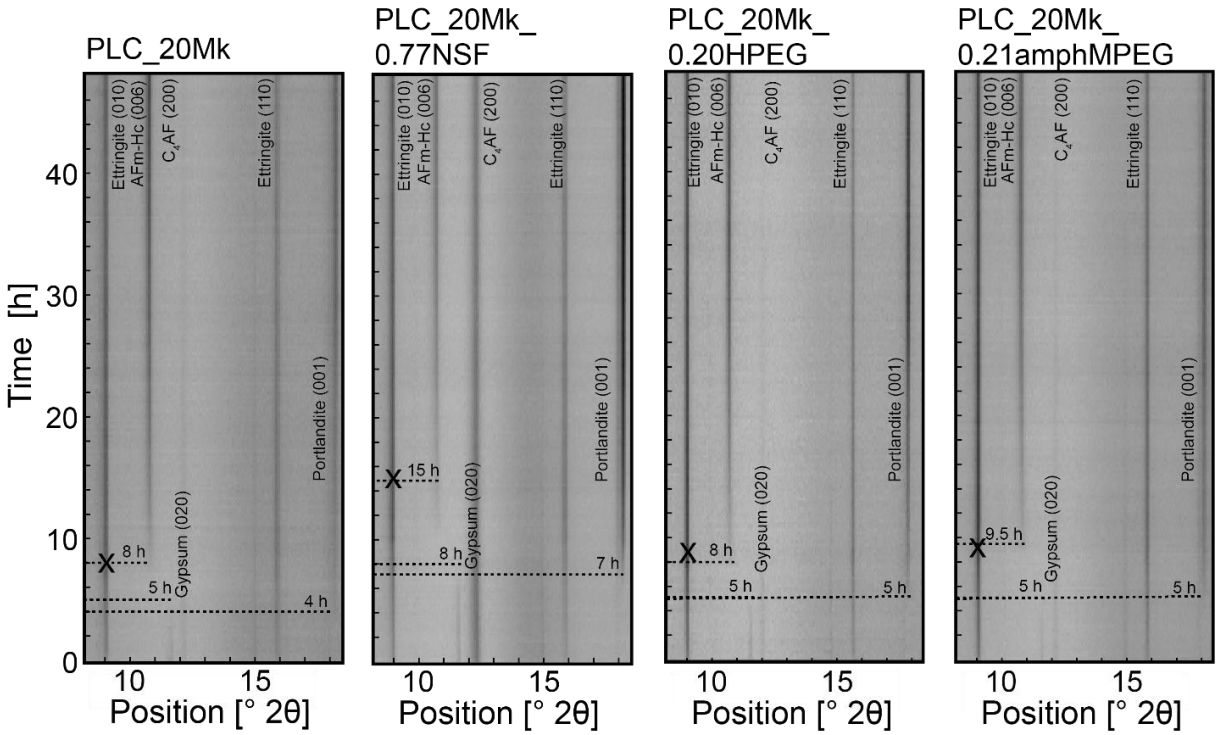

Figure A-28. In situ XRD plots from 8 to 18.5 °2θ for PLC_20Mk mixtures (X = time of maximum ettringite peak)

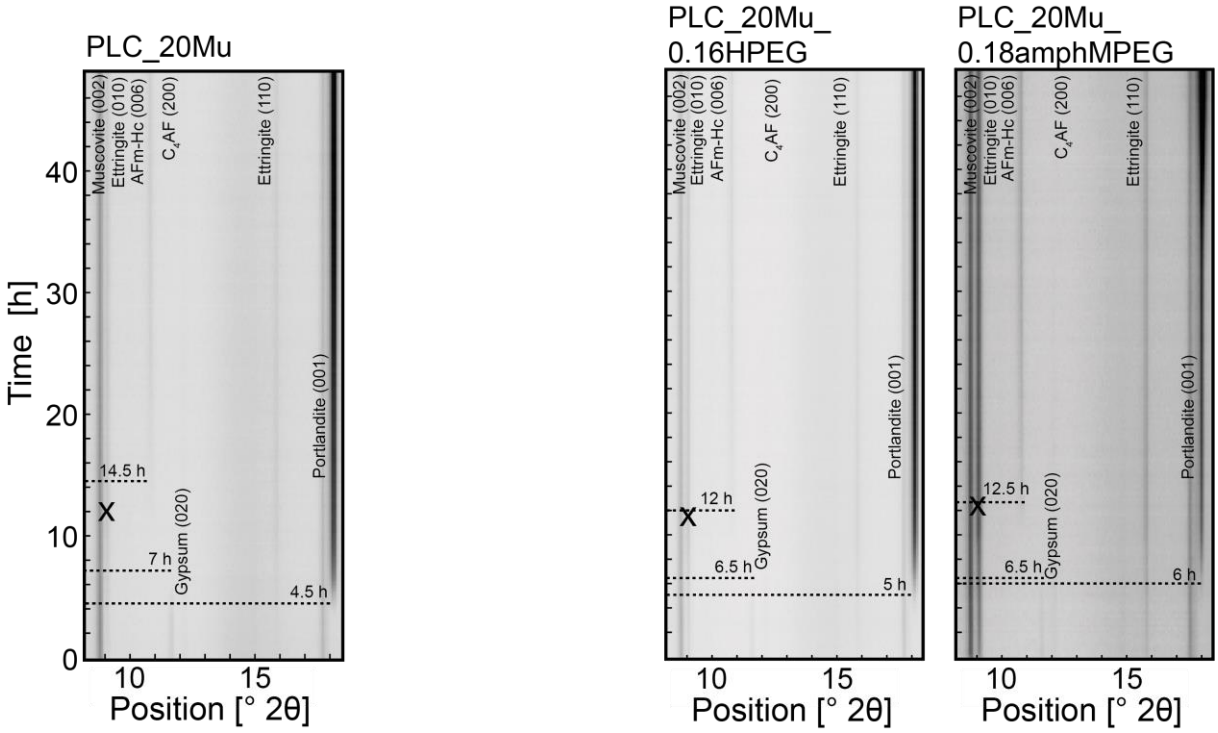

Figure A-29. In situ XRD plots from 8 to 18.5 °2θ for PLC_20Mu mixtures (X = time of maximum ettringite peak)

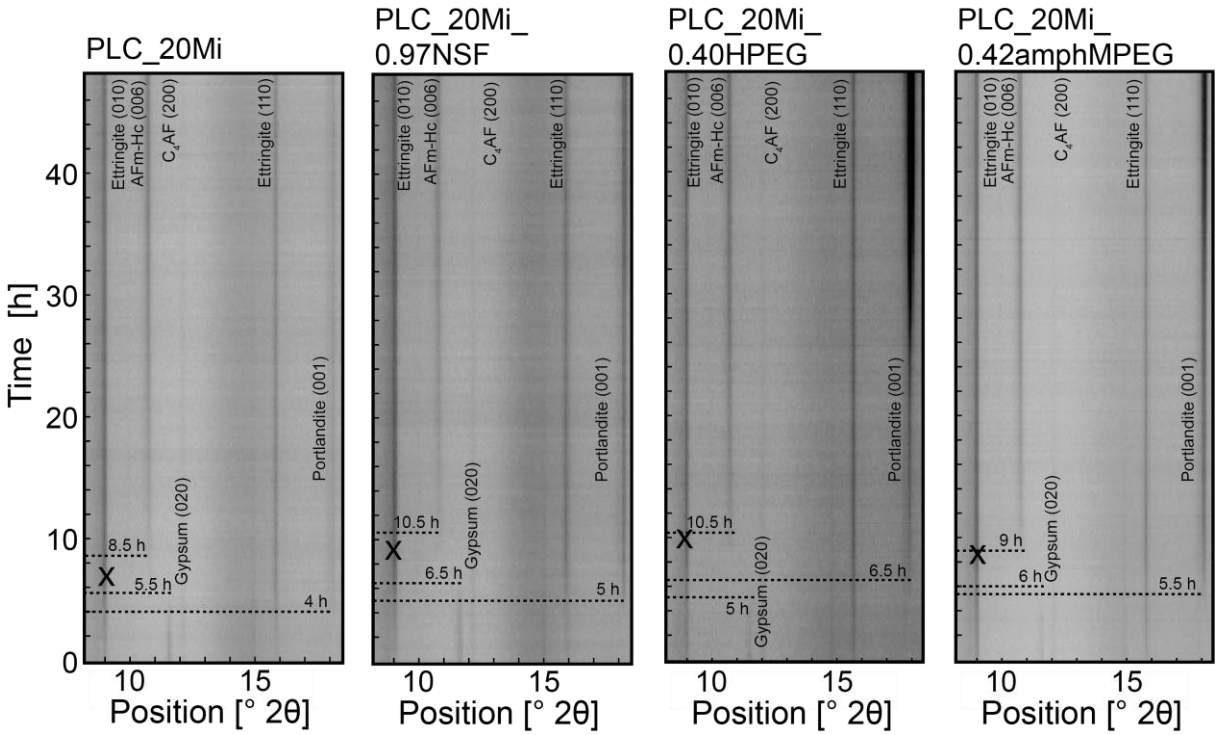

Figure A-30. In situ XRD plots from 8 to 18.5 °2θ for PLC_20Mi mixtures (X = time of maximum ettringite peak)

9.11 Appendix A11: Authorship contribution statement

List of all contributing authors in alphabetical order:

- Dr.-Ing. Nancy Beuntner (NB)
- Isabel Dürr, M.Sc. (ID)
- Matthias Maier, M.Sc. (MM)
- Univ.-Prof. Dr. Johann Plank (JP)
- Marlene Schmid, M.Sc. (MS)
- Ricarda Sposito, M.Sc. (RS)
- Univ.-Prof. Dr.-Ing. Karl-Christian Thienel (CT)

Title of publication	(Co-)Authors	Conceptualization	Methodology	Validation	Investigation	Data curation	Writing – original draft	Writing – review / editing	Supervision
Rheology, setting and hydration of calcined clay blended cements in interaction with PCE-based superplasticisers	RS	70	80	80	100	100	100	0	0
	NB	20	10	10	0	0	0	50	20
	CT	10	10	10	0	0	0	50	80
Characteristics of components in calcined clays and their influence on the efficiency of superplasticizers	RS	70	80	80	100	100	100	0	0
	NB	20	10	10	0	0	0	50	10
	CT	10	10	10	0	0	0	50	90
Physical and mineralogical properties of calcined common clays as SCM and their impact on flow resistance and demand for superplasticizer	RS	70	70	70	80	90	100	0	0
	MM	20	20	10	20	10	0	50	0
	NB	10	10	10	0	0	0	25	30
	CT	0	0	10	0	0	0	25	70
Evaluation of zeta potential of calcined clays and time-dependent flowability of blended cements with customized polycarboxylate-based superplasticizers	RS	70	50	70	80	90	100	0	0
	MM	20	40	10	20	10	0	50	0
	NB	10	10	10	0	0	0	25	30
	CT	0	0	10	0	0	0	25	70
Lignosulfonates in cementitious systems blended with calcined clays	RS	80	70	60	50	90	100	0	0
	ID	10	20	30	50	10	0	0	0
	CT	10	10	10	0	0	0	100	100
Early hydration behavior of blended cementitious systems containing calcined clays and superplasticizer	RS	80	70	70	70	90	100	0	0
	MS	0	10	10	20	0	0	20	0
	NB	10	10	0	0	0	0	20	5
	SS	0	0	10	10	10	0	10	0
	JP	0	0	0	0	0	0	0	5
	CT	10	10	10	0	0	0	50	90

An approach to the rheological behavior of cementitious systems blended with calcined clays and superplasticizers	RS	80	70	70	60	100	100	0	0
	MS	0	10	10	40	0	0	50	0
	JP	0	10	10	0	0	0	10	20
	CT	20	10	10	0	0	0	40	80
Feasability study on PCE based superplasticizers in calcined clay blended cements with focus on the type of phyllosilicate	RS	70	50	70	80	90	100	0	0
	MM	20	40	10	20	10	0	50	0
	NB	10	10	10	0	0	0	25	30
	CT	0	0	10	0	0	0	25	70

9.12 Appendix A12: List of papers

- **Peer-reviewed journal articles:**

Cordoba, G., **Sposito, R.**, Köberl, M., Zito, S., Beuntner, N., Tironi, A., Thienel, K.-Ch., Irassar, E. F. (2022). “Chloride migration and long-term natural carbonation on concretes with calcined clays: A study of calcined clays in Argentina,” Case Studies in Construction Materials, Vol. 17, e01190.

Muhammad, A., Thienel, K.-Ch. & **Sposito, R.** (2022). “Suitability of Clinker Replacement by a Calcined Common Clay in Self-Consolidating Mortar – Impact on Rheology and Early Age Properties,” Minerals, Vol. 12, Issue 5, 625.

Tironi, A., **Sposito, R.**, Cordoba, G., Zito, S., Rahhal, V., Thienel, K.-Ch., Irassar, E. F. (2022). “Influence of different calcined clays on the water transport performance of concretes,” Magazine of Concrete Research, Vol. 74 (14), pp. 702 – 714.

Sposito, R., Maier, M., Beuntner, N. & Thienel, K.-Ch. (2022) “Physical and mineralogical properties of calcined common clays and their impact on flow resistance and superplasticizer demand,” Cement and Concrete Research, Vol. 154, 106743

Maier, M., **Sposito, R.**, Beuntner, N. & Thienel, K.-Ch. (2022*)* “Particle characteristics of calcined clays and limestone and their impact on the early hydration and sulfate demand of blended cement,” Cement and Concrete Research, Vol. 154, 106736

Muhammad, A., Thienel, K.-Ch. & **Sposito, R.** (2021). “Suitabiliy of blending rice husk ash and calcined clay for the production of self-compacting concrete: a review”, Materials, Vol. 14, Issue 21, 6252

Sposito, R., Maier, M., Beuntner, N. & Thienel, K.-Ch. (2021). “Evaluation of zeta potential of calcined clays and time-dependent flowability of blended cement with customized polycarboxy-late-based superplasticizers,” Construction and Building Materials, Vol. 308, 125061

Tironi, A., **Sposito, R.,** Cordoba, G., Zito, S. V., Rahhal, V. F., Thienel, K.-Ch., Irassar, E. F. (2021). “Influence of different calcined clays to the water transport performance of concretes,” Magazine of Concrete Research, 2100031

Sposito, R., Beuntner, N. & Thienel, K.-Ch. (2020). “Characteristics of components in calcined clays and their influence on the efficiency of superplasticizers,” Cement and Concrete Composites, Vol. 110, 103594

Sposito, R., Beuntner, N. & Thienel, K.-Ch. (2020). “Rheology, setting and hydration of calcined clay blended cements in interaction with PCE-based superplasticisers,” Magazine of Concrete Research, Vol. 73, No. 15, pp. 785-797

Cordoba, G., Zito, S. V., **Sposito, R.**, Rahhal, V. F., Tironi, A., Thienel, K.-Ch. & Irassar E. F. (2020). “Concretes with calcined clay and calcined shale: workability, mechanical and transport properties,” Journal of Materials in Civil Engineering, Vol. 32, No. 8, pp. 040202241-11

Beuntner, N., **Sposito, R.** & Thienel, K.-Ch. (2019). “Potential of Calcined Mixed-Layer Clays as Pozzolans in Concrete,” ACI Materials Journal, Vol. 116, No. 4, pp. 19-29

Gmür, R., Thienel, K.-Ch. & Beuntner, N. (2016). “Influence of aging conditions upon the properties of calcined clay and its performance as supplementary cementitious material,” Cement and Concrete Composites, Vol. 72, pp. 114-124

- **Peer-reviewed conference contributions:**

Sposito, R., Maier, M., Beuntner, N. & Thienel, K.-Ch. (2022). “Feasability study on PCE based superplasticizers in calcined clay blended cements with focus on the type of phyllosilicate,” in 13th International Conference on Superplasticizers and Other Chemical Admixtures in Concrete, American Concrete Institute, Milan, Italy

Sposito, R., Schmid, M., Plank, J. & Thienel, K.-Ch. (2021). “An approach to the rheological behavior of cementitious systems blended with calcined clays and superplasticizers,” in ACI-SP 349 11th International Conference on Cementitious Materials and Alternative Binders for Sustainable Concrete, American Concrete Institute, online, pp. 659-685

Schmid, M., **Sposito, R.**, Thienel, K.-Ch. & Plank, J. (2019). “Effectiveness of Chemically Different Superplasticizers in Calcined Clay Blended Cements,” in Calcined Clays for Sustainable Concrete – Proceedings of the 3rd International Conference on Calcined Clays for Sustainable Concrete, Parashar, A., Singh, L., and Rao D., G., Editors, Springer, Singapore, pp. 201-209

Schmid, M., **Sposito, R.**, Thienel, K.-Ch. & Plank, J. (2019). “Novel zwitterionic PCE superplasticizers for calcined clays and their application in calcined clay blended cements,” in 15th International Congress on the Chemistry of Cement, Gemrich, J., Editor, Research Institute of Binding Materials Prague, Prague, Czech Republic, 8 pp.

Sposito, R., Schmid, M., Beuntner, N., Scherb, S., Plank, J. & Thienel, K.-Ch. (2019). “Early hydration behavior of blended cementitious systems containing calcined clays and superplasticizer,” in 15th International Congress on the Chemistry of Cement, Gemrich, J., Editor, Research Institute of Binding Materials Prague, Prague, Czech Republic, 10 pp.

Schmid, M., **Sposito, R.**, Thienel, K.-Ch. & Plank, J. (2019). “The shear-thickening effect of meta muscovite as SCM and its influence on the rheological properties of ecologically optimized cementitious systems,” in 2nd International RILEM Conference on Rheology and Processing of Construction Materials (RheoCon2), Mechtcherine, V., Editor, Springer, Dresden, Germany

Sposito, R., Dürr, I. & Thienel, K.-Ch. (2018). “Lignosulfonates in cementitious systems blended with calcined clays,” in ACI SP 326 – 2nd International Workshop on Durability and Sustainability of Concrete Structures, Falikman, V., et al., Editors, American Concrete Institute, Moscow, Russia, pp. 10.1-10.10

- **Other publications:**

Sposito, R., Maier, M., Cordoba, G., Scherb, S., Tironi, A., Beuntner, N., Neißer-Deiters, A., Irassar E. F., Thienel, K.-Ch. (2022). “Transferability from Pure Metaphases to Calcined

Common Clays – New Insights into Particle Properties and Prediction Models," in International Conference on Calcined Clays for Sustainable Concrete, M. Sharma, et al., Lausanne, Schweiz, pp. 110 – 111.

Maier, M., Scherb, S., **Sposito, R.**, Beuntner, N., Thienel, K.-Ch. (2022). "Parameters Influencing the Aluminate Clinker Reaction in Presence of Calcined Clay: Implications from Model Systems and Blended Cements," in International Conference on Calcined Clays for Sustainable Concrete, M. Sharma, et al., Lausanne, Schweiz, pp. 112 - 113.

Beuntner, N., **Sposito, R.** (2020). "Reduction of CO_2 emissions by means of calcined clays – a challenge for concrete technology? (CO_2-Reduzierung durch calcinierte Tone – eine betontechnologische Herausforderung?)," in 64th BetonTage, Walther, H.-J., Editor, Bauverlag, Neu-Ulm, Germany, p. 21

Schmid, M., **Sposito, R.**, Thienel, K.-Ch. & Plank, J. (2020). "Новые цвиттер-ионные поликарбоксилатные суперпластификаторы для цементов с добавками прокаленных глин (Novel zwitterionic PCE superplasticizers for calcined clays and their application in calcined clay blended cements)," in Цемент и его применение (Cement and its Application), pp. 1-4

Cordoba, G., Zito, S. V., **Sposito, R.**, Rahhal, V., Beuntner, N., Thienel, K.-Ch., Tironi, A., & Irassar E. F. (2020). "Durabilidad de Hormigones con Arcillas Calcinadas: Comparación de una Illita y un Caolín de Bajo Grado," in IX Congreso Internacional de la Asociación Argentina de Tecnología del Hormigón (AATH), 23ª Reunión Técnica de la AATH, Facultad de Ingeniería Universidad Nacional del Centro de la Provincia de Buenos Aires y AATH, Olavarría, Argentina, pp. 327-334

Zito, S. V., Cordoba, G., **Sposito, R.**, Rahhal, V., Thienel, K.-Ch., Irassar E. F. & Tironi, A. (2019). "Hormigones elaborados con arcillas calcinadas: studio de difusión de cloruros," in Joncier 4as Jornadas Nacionales de Investigación Cerámica, Facultad de Ingeniería Universidad Nacional del Centro de la Provincia de Buenos Aires y AATH, Rosario, Sante Fe, Argentina, p. 43

Zito, S. V., Cordoba, G., **Sposito, R.**, Tironi, A., Rahhal, V., Thienel, K.-Ch. & Irassar E. F. (2018). "Arcillas calcinadas como material cementíceo suplementario en hormigones," in VIII Congreso Internacional de la Asociación Argentina de Tecnología del Hormigón (AATH), 22ª Reunión Técnica de la AATH, Facultad de Ingeniería Universidad Nacional del Centro de la Provincia de Buenos Aires y AATH, Olavarría, Argentina, pp. 89-96

Schmid, M., **Sposito, R.**, Thienel, K.-Ch. & Plank, J. (2018). "Novel Zwitterionic Superplasticizers for Cements Blended with Calcined Clays," in 20. Internationale Baustofftagung (ibausil), Fischer, H.-B., and Volke, A., Editors, F.A. Finger-Institut für Baustoffkunde der Bauhaus-Universität Weimar, Weimar, Germany, pp. 842-849

Sposito, R., Beuntner, N., Thienel, K.-Ch., Schmid, M. & Plank, J. (2018). "Calcinierte Tone als innovativer Zementersatzstoff und ihre Wechselwirkungen mit Fließmitteln in Zementleim," in 4. Grazer Betonkolloquium, Tue, Nguyen V., Editor. Graz, Austria, pp. 185-192

Thienel, K.-Ch. & **Sposito, R.** (2017). "Effects of Specimen Shape, Size, Age and Curing on Compressive Strength Values Obtained for Structural Lightweight Concrete," ALITinform: Cement. Concrete. Dry Mixtures, Vol. 47, No. 2-3, pp. 26-46

Cordoba, G. P., Zito, S. V., **Sposito, R.**, Tironi, A., Rahhal, V. F., Thienel, K.-Ch. & Irassar E. F. (2017). "Caracterización física de arcillas calcinadas para su empleo como material cementicio suplementario en hormigones," in JIM 2017 – 6º Encuentro de Jóvenes Investigadores en Ciencia y Tecnología de Materiales, Buenos Aires, Argentina, 4 pp.